GRAPHENE

Graphene is the thinnest known material: a sheet of carbon atoms arranged in hexagonal cells only a single atom thick, and yet stronger than diamond.

Since it was experimentally isolated in 2004, it has been the object of intense theoretical and experimental research. It has potentially significant applications in nanotechnology, 'beyond-silicon' electronics, solid-state realization of high-energy physics phenomena and as a prototype membrane that could revolutionize soft-matter and two-dimensional physics.

In this book, leading graphene research theorist Mikhail I. Katsnelson systematically presents the basic concepts of graphene physics. Topics covered include Berry's phase, topologically protected zero modes, Klein tunnelling, vacuum reconstruction near supercritical charges and deformation-induced gauge fields. The book also contains an introduction to the theory of flexible membranes relevant to graphene physics and a detailed discussion of electronic transport, optical properties, magnetism and spintronics. Standard undergraduate-level knowledge of quantum and statistical physics and solid-state theory is assumed.

This is an important textbook for graduate students in nanoscience and nanotechnology, and an excellent introduction to the fast-growing field of graphene science for physicists and materials-science researchers working in related areas.

MIKHAIL I. KATSNELSON is a Professor and Head of the Theory of Condensed Matter group at the Institute for Molecules and Materials, Radboud University, in the Netherlands. His fields of expertise are magnetism, electronic structure and quantum many-body theory, and, after the discovery of graphene, he became one of the leaders in this new field. Professor Katsnelson is the author of several books, including *Quantum Solid State Physics* (with S. V. Vonsovsky, Springer, 1989), and has been awarded a Russian State Prize for young researchers. He has also been honoured as a Knight of the Order of the Dutch Lion.

GRAPHENE

Carbon in Two Dimensions

MIKHAIL I. KATSNELSON
Radboud University, the Netherlands

CAMBRIDGE
UNIVERSITY PRESS

CAMBRIDGE UNIVERSITY PRESS
Cambridge, New York, Melbourne, Madrid, Cape Town,
Singapore, São Paulo, Delhi, Mexico City

Cambridge University Press
The Edinburgh Building, Cambridge CB2 8RU, UK

Published in the United States of America by Cambridge University Press, New York

www.cambridge.org
Information on this title: www.cambridge.org/9780521195409

First published 2012

Printed in the United Kingdom at the University Press, Cambridge

A catalogue record for this publication is available from the British Library

Library of Congress Cataloguing in Publication Data

Katsnel'son, M. I. (Mikhail Iosifovich)
Graphene : carbon in two dimensions / Mikhail I. Katsnelson,
Radboud University, the Netherlands.
pages cm
Includes bibliographical references and index.
ISBN 978 0 521 19540 9
1. Graphene. I. Title.
QD181.C1K29 2012
546′.681 dc23
2011046203

ISBN 978 0 521 19540 9 Hardback

In memory of my teacher Serghey Vonsovsky
and my friend Sasha Trefilov

Contents

Preface

I do not think that I need to explain, in the preface to a book that is all about graphene, what graphene is and why it is important. After the Nobel Prize for physics in 2010, everybody should have heard something about graphene. I do need, however, to explain why I wrote this book and what is special about it.

I hope it will not be considered a disclosure of insider information if I tell you that Andre Geim is a bit sarcastic (especially with theoreticians). Every time I mentioned that I was somewhat busy writing a book on graphene, he always replied 'Go to amazon.com and search for "graphene".' Indeed, there are many books on graphene, many more reviews and infinitely many collections of papers and conference proceedings (well, not really infinitely many ... in the main text I will use the mathematical terminology in a more rigorous way, I promise). Why, nevertheless, has this book been written and why may it be worthwhile for you to read it?

Of course, this is a personal view of the field. I do love it, and it has been my main scientific activity during the last seven years, from 2004 when graphene started to be the subject of intensive and systematic investigations. Luckily, I was involved in this development almost from the very beginning. It was a fantastic experience to watch a whole new world coming into being and to participate in the development of a new language for this new world. I would like to try to share this experience with the readers of this book.

The beauty of graphene is that it demonstrates in the most straightforward way many basic concepts of fundamental physics, from Berry's phase and topologically protected zero modes to strongly interacting fluctuations and scaling laws for two-dimensional systems. It is also a real testbed for relativistic quantum phenomena such as Klein tunnelling or vacuum reconstruction, 'CERN on one's desk'. I was not able to find a book focused on these aspects of graphene, namely on its role in our general physical view of the world. I have tried to write such a book myself. The price is that I have sacrificed all practical aspects of graphene science and technology, so you will not find a single word here about the ways in which graphene is produced, and there is hardly anything about its potential applications. Well, there is a lot of literature on these subjects. Also, I have said very little about the chemistry of graphene, which is an extremely interesting subject in itself. It certainly deserves a separate book, and I am not chemist enough to write it.

The field is very young, and it is not easy to know what will not be out of date in just a couple of years. My choice is clear from the contents of this book. I do believe that it represents the core of graphene physics which will not be essentially modified in the near future. I do not mean that this is *the most interesting* part; moreover, I am sure that there will be impressive progress, at least, in two more directions that are hardly mentioned in the book: in the *many-body* physics of graphene and in our understanding of electron transport near the neutrality point, where the semiclassical Boltzmann equation is obviously inapplicable. I think, however, that it is a bit too early to cover these subjects in a book, since too many things are not yet clear. Also, the mathematical tools required are not as easy as those used in this book, and I think it is unfair to force the reader to learn something technically quite complicated without a deep internal confidence that the results are relevant for the real graphene.

The way the book has been written is how I would teach a course with the title ‘Introduction to the theory of graphene’. I have tried to make a presentation that is reasonably independent of other textbooks. I have included therefore some general issues such as Berry’s phase, the statistical mechanics of fluctuating membranes, a quick overview of itinerant-electron magnetism, a brief discussion of basic nonequilibrium statistical mechanics, etc. The aims were, first, to show the physics of graphene in a more general context and, second, to make the reading easier.

It is very difficult to give an overview of a field that has developed so quickly as has that of graphene. So many papers appear, literally every day, that keeping permanently up to date would be an enterprise in the style of ancient myths, e.g., those of Sisyphus, the Danaïdes and some of the labours of Hercules. I apologise therefore for the lack of many important references. I tried to do my best.

I cannot even list all of the scientific *reviews* on the basic physics of graphene which are available now (let alone reviews of applications and of popular literature). Let me mention at least several of them, in chronological order: Katsnelson (2007a), Geim & Novoselov (2007), Beenakker (2008), Castro Neto *et al.* (2009), Geim (2009), Abergel *et al.* (2010), Vozmediano, Katsnelson & Guinea (2010), Peres (2010), Das Sarma *et al.* (2011), Goerbig (2011) and Kotov *et al.* (2011). There you can find different, complementary views on the field (with the possible exception of the first one). Of course, the Nobel lectures by Geim (2011) and Novoselov (2011) are especially strongly recommended. In particular, the lecture by Andre Geim contains a brilliant presentation of the prehistory and history of graphene research, so I do not need to discuss these, unavoidably controversial, issues in my book.

I am very grateful to Andre Geim and Kostya Novoselov, who involved me in this wonderful field before it became fashionable (otherwise I would probably never have dared to join such a brilliant company). I am especially grateful to Andre for regular and long phone conversations; when you have to discuss a theory using just words, without formulas and diagrams, and cannot even make faces, after several years it does improve your understanding of theoretical physics.

It is impossible to thank all my other collaborators in the field of graphene in a short preface, as well as other colleagues with whom I have had fruitful discussions. I have to thank, first of all, Annalisa Fasolino, Paco Guinea, Sasha Lichtenstein and Tim Wehling for especially close and intensive collaboration. I am very grateful to the former and current members of our group in Nijmegen working on graphene: Misha Akhukov, Danil Boukhvalov, Jan Los, Koen Reijnders, Rafa Roldán, Timur Tudorovskiy, Shengjun Yuan and Kostya Zakharchenko, and to my other collaborators and coauthors, especially Mark Auslender, Eduardo Castro, Hans De Raedt, Olle Eriksson, Misha Fogler, Jos Giesbers, Leonya Levitov, Tony Low, Jan Kees Maan, Hector Ochoa, Marco Polini, Sasha Rudenko, Mark van Schilfgaarde, Andrey Shytov, Alyosha Tsvelik, Maria Vozmediano, Oleg Yazyev and Uli Zeitler.

I am grateful to the Faculty of Science of Radboud University and the Institute for Molecules and Materials for making available to me the time and resources for research and writing.

I am very grateful to Marina Katsnelson and Timur Tudorovskiy for their invaluable help with the preparation of the manuscript and for their critical reading. I am grateful to many colleagues for permission to reproduce figures from their papers and for providing some of the original figures used in the book. I am especially grateful to Annalisa Fasolino for the wonderful picture which is used for the cover.

Of course, the role of my wife Marina in this book amounts to much more than her help with the manuscript. You cannot succeed in such a long and demanding task without support from your family. I am very grateful for her understanding and full support.

The book is dedicated to the memory of two people who were very close to me, my teacher Serghey Vonsovsky (1910 1998) and my friend Sasha Trefilov (1951 2003). I worked with them for about twenty years, and they had a decisive influence on the formation of my scientific taste and my scientific style. I thought many times during these last seven years how sad it is that I cannot discuss with them some new interesting physics about graphene. Also, in a more technical sense, I would not have been able to write this book without the experience of writing my previous books, Vonsovsky & Katsnelson (1989) and Katsnelson & Trefilov (2002).

1

The electronic structure of ideal graphene

1.1 The carbon atom

Carbon is the sixth element in the Periodic Table. It has two stable isotopes, ^{12}C (98.9% of natural carbon) with nuclear spin $I = 0$ and, thus, nuclear magnetic moment $\mu_n = 0$, and ^{13}C (1.1% of natural carbon) with $I = \frac{1}{2}$ and $\mu_n = 0.7024\mu_N$ (μ_N is the nuclear magneton), see Radzig & Smirnov (1985). Like most of the chemical elements, it originates from nucleosynthesis in stars (for a review, see the Nobel lecture by Fowler (1984)). Actually, it plays a crucial role in the chemical evolution of the Universe.

The stars of the first generation produced energy only by proton proton chain reaction, which results in the synthesis of one α-particle (nucleus ^{4}He) from four protons, p. Further nuclear fusion reactions might lead to the formation of either of the isotopes ^{5}He and ^{5}Li ($p + \alpha$ collisions) or of ^{8}Be ($\alpha + \alpha$ collisions); however, all these nuclei are very unstable. As was first realized by F. Hoyle, the chemical evolution does not stop at helium only due to a lucky coincidence the nucleus ^{12}C has an energy level close enough to the energy of three α-particles, thus, the *triple* fusion reaction $3\alpha \rightarrow {}^{12}\mathrm{C}$, being resonant, has a high enough probability. This opens up a way to overcome the mass gap (the absence of stable isotopes with masses 5 and 8) and provides the prerequisites for nucleosynthesis up to the most stable nucleus, ^{56}Fe; heavier elements are synthesized in supernova explosions.

The reaction $3\alpha \rightarrow {}^{12}\mathrm{C}$ is the main source of energy for red giants. Carbon plays also an essential role in nuclear reactions in stars of the main sequence (heavier than the Sun) via the so-called CNO cycle.

The carbon atom has six electrons, two of them forming a closed $1s^2$ shell (helium shell) and four filling 2s and 2p states. The ground-state atomic configuration is $2s^2\,2p^2$, with the total spin $S = 1$, total orbital moment $L = 1$ and total angular moment $J = 0$ (the ground-state multiplet $^3P_0$). The first excited state, with a $J=1$, $^3P_1$ multiplet, has the energy 16.4 cm$^{-1} \approx 2$ meV (Radzig & Smirnov, 1985), which gives an estimate of the strength of the spin–orbit coupling in the carbon atom. The lowest-energy state, with configuration $2s^1\,2p^3$, has the energy 33 735.2 cm$^{-1} \approx 4.2$ eV (Radzig & Smirnov, 1985), so this is the promotion energy for exciting a 2s electron into a 2p state. At first sight, this would mean that carbon should always be divalent, due to there being two 2p electrons while the 2s electrons are chemically quite inert. This conclusion is, however, wrong. Normally, carbon is tetravalent, due to a formation of hybridized sp electron states, according to the concept of 'resonance' developed by L. Pauling (Pauling, 1960; Eyring, Walter & Kimball, 1946).

When atoms form molecules or solids the total energy decreases due to overlap of the electron wave functions at various sites and formation of molecular orbitals (in molecules), or energy bands (in solids); for a compact introduction to chemical bonding in solids, see Section 1.7 in Vonsovsky & Katsnelson (1989). This energy gain can be sufficient to provide the energy which is necessary to promote a 2s electron into a 2p state in the carbon atom.

In order to maximize the energy gained during the formation of a covalent bond, the overlap of the wave functions with those at neighbouring atoms should also be maximal. This is possible if the neighbouring atoms are situated in such directions from the central atoms that the atomic wave functions take on maximum values. The larger these values are the stronger the bond is. There are four basis functions corresponding to the spherical harmonics

$$\begin{aligned} Y_{0,0}(\vartheta,\varphi) &= \frac{1}{\sqrt{4\pi}}, \\ Y_{1,0}(\vartheta,\varphi) &= i\sqrt{\frac{3}{4\pi}}\cos\vartheta, \\ Y_{1,\pm1}(\vartheta,\varphi) &= \mp i\sqrt{\frac{3}{8\pi}}\sin\vartheta\,\exp(\pm i\varphi), \end{aligned} \tag{1.1}$$

where ϑ and φ are polar angles. Rather than take the functions $Y_{1,m}(\vartheta,\varphi)$ to be the basis functions, it is more convenient to choose their orthonormalized linear combinations of the form

$$\begin{aligned} \frac{i}{\sqrt{2}}[Y_{1,1}(\vartheta,\varphi) - Y_{1,-1}(\vartheta,\varphi)] &= \sqrt{\frac{3}{4\pi}}\sin\vartheta\,\cos\varphi, \\ \frac{i}{\sqrt{2}}[Y_{1,1}(\vartheta,\varphi) + Y_{1,-1}(\vartheta,\varphi)] &= \sqrt{\frac{3}{4\pi}}\sin\vartheta\,\sin\varphi, \\ iY_{1,0}(\vartheta,\varphi) &= \sqrt{\frac{3}{4\pi}}\cos\vartheta, \end{aligned} \tag{1.2}$$

which are transformed under rotations as the Cartesian coordinates x, y and z, respectively. Recall that the radial components of the s and p functions in the simplest approximation are equal in magnitude and may be omitted, together with the constant factor $1/\sqrt{4\pi}$, which is not important here. Then the angular dependence of the four basis functions which we will introduce in lieu of $Y_{\mathrm{l,m}}(\vartheta, \varphi)$ can be represented as

$$\begin{gathered} |s\rangle = 1, \\ |x\rangle = \sqrt{3}\sin\vartheta\,\cos\varphi, \qquad |y\rangle = \sqrt{3}\sin\vartheta\,\sin\varphi, \qquad |z\rangle = \sqrt{3}\cos\vartheta. \end{gathered} \tag{1.3}$$

We now seek linear combinations of the functions (1.3) that will ensure maximum overlap with the functions of the adjacent atoms. This requires that the value of $\alpha = \max\limits_{\vartheta,\varphi} \psi$ be a maximum. With the normalization that we have chosen, $\alpha = 1$ for the s states and $\alpha = \sqrt{3}$ for the p functions of $|x\rangle$, $|y\rangle$ and $|z\rangle$. We then represent the function $|\psi\rangle$ as

$$|\psi\rangle = a|s\rangle + b_1|x\rangle + b_2|y\rangle + b_3|z\rangle, \tag{1.4}$$

where a and b_i are real-valued coefficients that satisfy the normalization condition

$$a^2 + b_1^2 + b_2^2 + b_3^2 = 1. \tag{1.5}$$

The function $|\psi\rangle$, then, is normalized in the same way as (1.3). This follows from their mutual orthogonality,

$$\int do|\psi(\vartheta, \varphi)|^2 \equiv \langle\psi|\psi\rangle = a^2\langle s|s\rangle + b_1^2\langle x|x\rangle + b_2^2\langle y|y\rangle + b_3^2\langle z|z\rangle = 4\pi,$$

with do being an element of solid angle. For the time being, the orientation of the axes in our case is arbitrary.

Let us assume that in one of the functions ψ, for which α is a maximum, this maximum value is reached in the direction along the diagonal of the cube (1, 1, 1), with the carbon atom at its centre and with the coordinate axes parallel to its edges (Fig. 1.1). Then $b_1 = b_2 = b_3 = b$. The (1, 1, 1) direction is given by angles ϑ and φ such that

$$\sin\varphi = \cos\varphi = \frac{1}{\sqrt{2}}, \qquad \cos\vartheta = \frac{1}{\sqrt{3}}, \qquad \sin\vartheta = \sqrt{\frac{2}{3}},$$

so that

$$|x\rangle = |y\rangle = |z\rangle = 1.$$

In addition,

$$\alpha = a + 3b = a + \sqrt{3(1 \quad a^2)}, \tag{1.6}$$

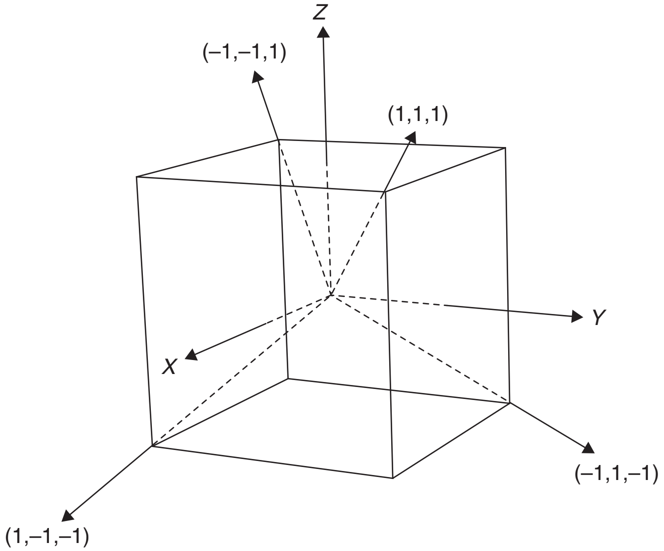

Fig. 1.1. Directions of sp^3 chemical bonds of the carbon atom.

where we have used the conditions (1.3). The maximum of α as a function of a is reached for $a=\frac{1}{2}$ and is equal to 2. The quantity b in this case is equal to $\frac{1}{2}$. Thus the first orbital with maximum values along the coordinate axes that we have chosen is of the form

$$|1\rangle = \frac{1}{2}(|s\rangle + |x\rangle + |y\rangle + |z\rangle). \tag{1.7}$$

It can be readily shown that the functions

$$\begin{aligned} |2\rangle &= \frac{1}{2}(|s\rangle + |x\rangle - |y\rangle - |z\rangle), \\ |3\rangle &= \frac{1}{2}(|s\rangle - |x\rangle + |y\rangle - |z\rangle), \\ |4\rangle &= \frac{1}{2}(|s\rangle - |x\rangle - |y\rangle + |z\rangle) \end{aligned} \tag{1.8}$$

correspond to the same value $\alpha = 2$. The functions $|i\rangle$ (i = 1, 2, 3, 4) are mutually orthogonal. They take on their maximum values along the (1, 1, 1), (1, 1, 1), (1, 1, 1) and (1, 1, 1) axes, i.e., along the axes of the tetrahedron, and, therefore, the maximum gain in chemical-bonding energy corresponds to the tetrahedral environment of the carbon atom. In spite of being qualitative, the treatment that we have performed above nevertheless explains the character of the crystal structure of the Periodic Table group-IV elements (diamond-type lattice, Fig. 1.2) as well as the shape of the methane molecule, which is very close to being tetrahedral.

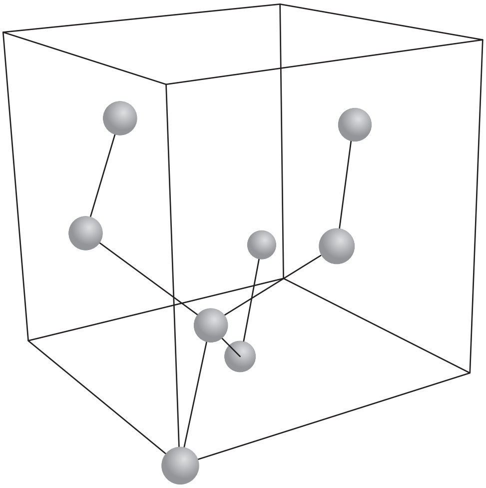

Fig. 1.2. Chemical bonds in the diamond structure.

The wave functions (1.7) and (1.8) correspond to a so-called sp^3 state of the carbon atom, for which all chemical bonds are equivalent. Another option is that *three* sp electrons form hybrid covalent bonds whereas one p electron has a special destiny, being distributed throughout the whole molecule (benzene) or the whole crystal (graphite or graphene). If one repeats the consideration above for a smaller basis including only functions $|s\rangle$, $|x\rangle$ and $|y\rangle$ one finds the following functions corresponding to the maximum overlap (Eyring, Walter & Kimball, 1946):

$$\begin{aligned} |1\rangle &= \frac{1}{\sqrt{3}}(|s\rangle + \sqrt{2}|x\rangle), \\ |2\rangle &= \frac{1}{\sqrt{3}}|s\rangle \quad \frac{1}{\sqrt{6}}|x\rangle + \frac{1}{\sqrt{2}}|y\rangle, \\ |3\rangle &= \frac{1}{\sqrt{3}}|s\rangle \quad \frac{1}{\sqrt{6}}|x\rangle \quad \frac{1}{\sqrt{2}}|y\rangle. \end{aligned} \tag{1.9}$$

The corresponding orbits have maxima in the xy-plane separated by angles of 120°. There are called σ *bonds*. The last electron with the p orbital perpendicular to the plane ($|z\rangle$ function) forms a π *bond*. This state (sp^2) is therefore characterized by threefold coordination of carbon atoms, in contrast with fourfold coordination for the sp^3 state. This is the case of *graphite* (Fig. 1.3).

1.2 π States in graphene

Graphene has a honeycomb crystal lattice as shown in Fig. 1.4(a). The Bravais lattice is triangular, with the lattice vectors

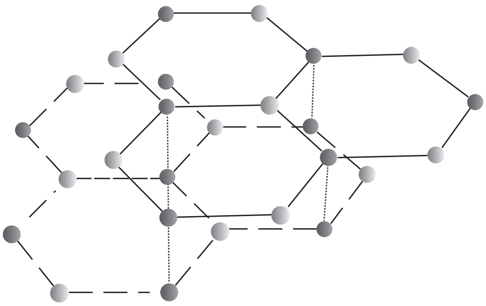

Fig. 1.3. The structure of graphite. Carbon atoms belonging to two different sublattices are shown as black and light grey.

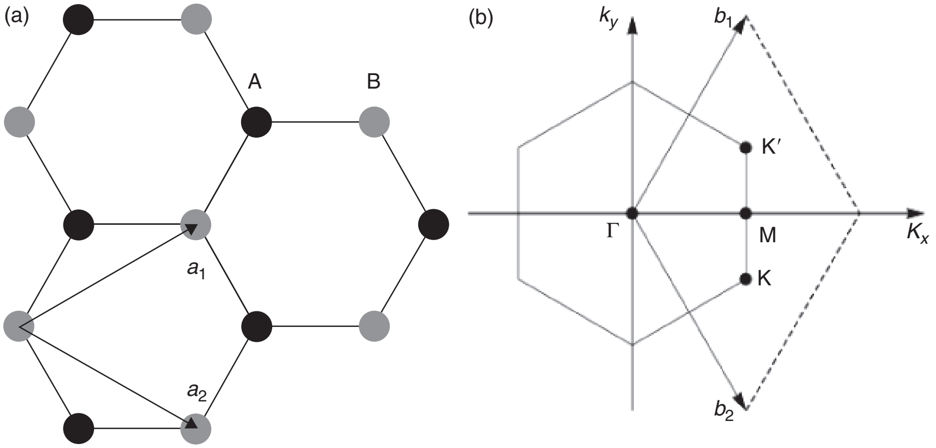

Fig. 1.4. (a) A honeycomb lattice, subblattices A and B are shown as black and grey. (b) Reciprocal lattice vectors and some special points in the Brillouin zone.

$$\vec{a}_1 = \frac{a}{2}(3, \sqrt{3}), \qquad \vec{a}_2 = \frac{a}{2}(3, -\sqrt{3}), \tag{1.10}$$

where $a \approx 1.42$ Å is the nearest-neighbour distance. It corresponds to a so-called conjugated carbon–carbon bond (like in benzene) intermediate between a single bond and a double bond, with lengths $r_1 \approx 1.54$ Å and $r_2 \approx 1.31$ Å, respectively.

The honeycomb lattice contains two atoms per elementary cell. They belong to two sublattices, A and B, each atom from sublattice A being surrounded by three atoms from sublattice B, and vice versa (a bipartite lattice). The nearest-neighbour vectors are

$$\vec{\delta}_1 = \frac{a}{2}\left(1, \sqrt{3}\right), \qquad \vec{\delta}_2 = \frac{a}{2}\left(1, -\sqrt{3}\right), \qquad \vec{\delta}_3 = a(-1, 0). \tag{1.11}$$

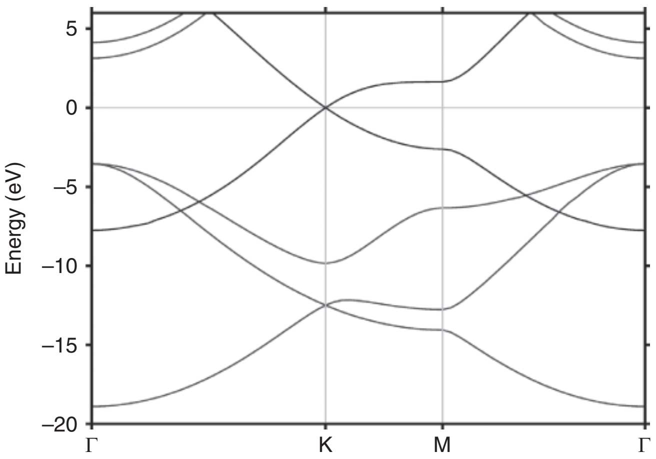

Fig. 1.5. The band structure of graphene (reproduced with permission from Boukhvalov, Katsnelson & Lichtenstein, 2008).

The reciprocal lattice is also triangular, with the lattice vectors

$$\vec{b}_1 = \frac{2\pi}{3a}\left(1, \sqrt{3}\right), \qquad \vec{b}_2 = \frac{2\pi}{3a}\left(1, \quad \sqrt{3}\right). \tag{1.12}$$

The Brillouin zone is presented in Fig. 1.4(b). Special high-symmetry points K, K′ and M are shown there, with the wave vectors

$$\vec{K}' = \left(\frac{2\pi}{3a}, \frac{2\pi}{3\sqrt{3}a}\right), \qquad \vec{K} = \left(\frac{2\pi}{3a}, \quad \frac{2\pi}{3\sqrt{3}a}\right), \qquad \vec{M} = \left(\frac{2\pi}{3a}, 0\right). \tag{1.13}$$

The electronic structures of graphene and graphite are discussed in detail in Bassani & Pastori Parravicini (1975). In Fig. 1.5 we show a recent computational result for graphene. The sp^2 hybridized states (σ states) form occupied and empty bands with a huge gap, whereas π states form a single band, with a conical self-crossing point in K (the same point, by symmetry, exists also in K′). This conical point is a characteristic of the peculiar electronic structure of graphene and the origin of its unique electronic properties. It was first obtained by Wallace (1947) in the framework of a simple tight-binding model. Further this model was developed by McClure (1957) and Slonczewski & Weiss (1958).

Let us start, following Wallace (1947), with the nearest-neighbour approximation for the π states only, with the hopping parameter t. The basis of electron states contains two π states belonging to the atoms from sublattices A and B. In the nearest-neighbour approximation, there are no hopping processes within the sublattices; hopping occurs only between them. The tight-binding Hamiltonian is therefore described by the 2 × 2 matrix

$$\hat{H}(\vec{k}) = \begin{pmatrix} 0 & tS(\vec{k}) \\ tS^*(\vec{k}) & 0 \end{pmatrix}, \tag{1.14}$$

where $\vec{k}$ is the wave vector and

$$S(\vec{k}) = \sum_{\vec{\delta}} e^{i\vec{k}\vec{\delta}} = 2\exp\left(\frac{ik_x a}{2}\right)\cos\left(\frac{k_y a\sqrt{3}}{2}\right) + \exp(\quad ik_x a). \tag{1.15}$$

The energy is, therefore,

$$E(\vec{k}) = \pm t|S(\vec{k})| = \pm t\sqrt{3 + f(\vec{k})}, \tag{1.16}$$

where

$$f(\vec{k}) = 2\cos\left(\sqrt{3}k_y a\right) + 4\cos\left(\frac{\sqrt{3}}{2}k_y a\right)\cos\left(\frac{3}{2}k_x a\right). \tag{1.17}$$

One can see immediately that $S(\vec{K}) = S(\vec{K}') = 0$, which means band crossing. On expanding the Hamiltonian near these points one finds

$$\begin{aligned} \hat{H}_{K'}(\vec{q}) &\approx \frac{3at}{2}\begin{pmatrix} 0 & \alpha(q_x + iq_y) \\ \alpha^*(q_x \quad iq_y) & 0 \end{pmatrix}, \\ \hat{H}_K(\vec{q}) &\approx \frac{3at}{2}\begin{pmatrix} 0 & \alpha^*(q_x \quad iq_y) \\ \alpha(q_x + iq_y) & 0 \end{pmatrix}, \end{aligned} \tag{1.18}$$

where $\alpha = e^{5i\pi/6}$, with $\vec{q} = \vec{k} \quad \vec{K}$ and $\vec{k} \quad \vec{K}'$, respectively. The phase $5\pi/6$ can be excluded by a unitary transformation of the basis functions. Thus, the effective Hamiltonians near the points K and K′ take the form

$$\hat{H}_{K,K'}(\vec{q}) = hv\begin{pmatrix} 0 & q_x \mp iq_y \\ q_x \pm iq_y & 0 \end{pmatrix}, \tag{1.19}$$

where

$$v = \frac{3a|t|}{2} \tag{1.20}$$

is the electron velocity at the conical points. The possible negative sign of t can be excluded by an additional phase shift by $\quad\pi$.

On taking into account the next-nearest-neighbour hopping t', one finds, instead of Eq. (1.16),

$$E(\vec{k}) = \pm t|S(\vec{k})| + t'f(\vec{k}) = \pm t\sqrt{3 + f(\vec{k})} + t'f(\vec{k}). \tag{1.21}$$

The second term breaks the electron hole symmetry, shifting the conical point from $E = 0$ to $E = \quad 3t'$, but it does not change the behaviour of

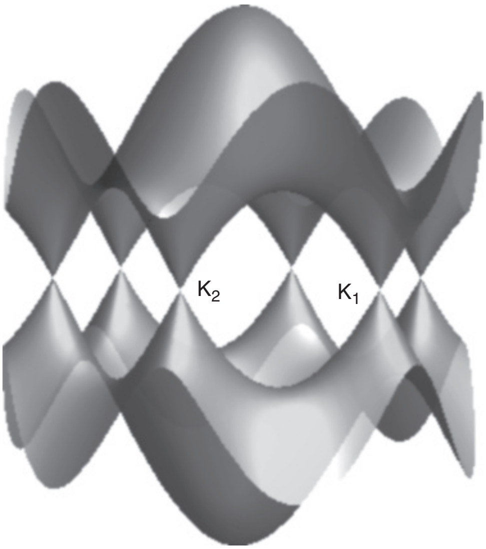

Fig. 1.6. The electron energy spectrum of graphene in the nearest-neighbour approximation.

the Hamiltonian near the conical points. Actually, this behaviour is symmetry-protected (and even topologically protected), as we will see in the next section.

The points K and K′ differ by the reciprocal lattice vector $\vec{b} = \vec{b}_1 \quad \vec{b}_2$, so the point K′ is equivalent to K. To show this explicitly, it is convenient sometimes to use a larger unit cell in the reciprocal space, with six conical points. The spectrum (1.16) in this representation is shown in Fig. 1.6.

The parameters of the effective tight-binding model can be found by fitting the results of first-principles electronic-structure calculations. According to Reich *et al.* (2002), the first three hopping parameters are $t = \quad 2.97$ eV, $t' = \quad 0.073$ eV and $t'' = \quad 0.33$ eV. The smallness of t' means that the electron hole symmetry of the spectrum is very accurate not only in the vicinity of the conical points but also throughout the whole Brillouin zone.

There are saddle points of the electron energy spectrum at M (see Figs. 1.5 and 1.6), with Van Hove singularities in the electron density of states, $\delta N(E) \propto \quad \ln|E \quad E_M|$ (Bassani & Pastori Parravicini, 1975). The positions of these singularities are

$$E_M \quad = t + t' \quad 3t'' \approx \quad 2.05\,\text{eV}$$

and

$$E_{M+} = \quad t + t' + 3t'' \approx 1.91\,\text{eV}.$$

1.3 Massless Dirac fermions in graphene

Undoped graphene has a Fermi energy coinciding with the energy at the conical points, with a completely filled valence band, an empty conduction band and no band gap in between. This means that, from the point of view of a general band theory, graphene is an example of a *gapless semiconductor* (Tsidilkovskii, 1996). Three-dimensional crystals, such as HgTe and α-Sn (grey tin) are known to be gapless semiconductors. What makes graphene unique is not the gapless state itself but the very special, chiral nature of the electron states, as well as the high degree of electron hole symmetry.

For any realistic doping, the Fermi energy is close to the energy at the conical point, $|E_F| \ll |t|$. To construct an effective model describing electron and hole states in this regime one needs to expand the effective Hamiltonian near one of the special points K and K′ and then make the replacements

$$q_x \to \quad i\frac{\partial}{\partial x}, \qquad q_y \to \quad i\frac{\partial}{\partial y},$$

which corresponds to the effective mass approximation, or $\vec{k}\cdot\vec{p}$ perturbation theory (Tsidilkovskii, 1982; Vonsovsky & Katsnelson, 1989). From Eq. (1.19), one has

$$\hat{H}_K = \quad ihv\vec{\sigma}\nabla, \tag{1.22}$$

$$\hat{H}_{K'} = \hat{H}_K^T, \tag{1.23}$$

where

$$\sigma_0 = \begin{pmatrix} 1 & 0 \\ 0 & 1 \end{pmatrix}, \quad \sigma_x = \begin{pmatrix} 0 & 1 \\ 1 & 0 \end{pmatrix}, \quad \sigma_y = \begin{pmatrix} 0 & i \\ i & 0 \end{pmatrix}, \quad \sigma_z = \begin{pmatrix} 1 & 0 \\ 0 & 1 \end{pmatrix} \tag{1.24}$$

are Pauli matrices (only x- and y-components enter Eq. (1.22)) and T denotes a transposed matrix. A complete low-energy Hamiltonian consists of 4×4 matrices taking into account both two sublattices and two conical points (in terms of semiconductor physics, two valleys).

In the basis

$$\Psi = \begin{pmatrix} \psi_{KA} \\ \psi_{KB} \\ \psi_{K'A} \\ \psi_{K'B} \end{pmatrix}, \tag{1.25}$$

where ψ_{KA} means a component of the electron wave function corresponding to valley K and sublattice A, the Hamiltonian is a 2×2 block supermatrix,

$$\hat{H} = \begin{pmatrix} \hat{H}_K & 0 \\ 0 & \hat{H}_{K'} \end{pmatrix}. \tag{1.26}$$

Sometimes it is more convenient to choose the basis as

$$\Psi = \begin{pmatrix} \psi_{\mathrm{KA}} \\ \psi_{\mathrm{KB}} \\ \psi_{\mathrm{K'B}} \\ \psi_{\mathrm{K'A}} \end{pmatrix} \tag{1.27}$$

(Aleiner & Efetov, 2006; Akhmerov & Beenakker, 2008; Basko, 2008), then the Hamiltonian (1.26) takes the most symmetric form

$$\hat{H} = \quad ihv\tau_0 \otimes \vec{\sigma}\,\nabla, \tag{1.28}$$

where τ_0 is the unit matrix in valley indices (we will use different notations for the same Pauli matrices acting on different indices, namely, $\vec{\sigma}$ in the sublattice space and $\vec{\tau}$ in the valley space).

For the case of an ideal graphene the valleys are decoupled. If we add some inhomogeneities (external electric and magnetic fields, disorder, etc.) that are smooth at the atomic scale the valleys remain independent, since the Fourier component of external potential with the *Umklapp* wave vector $\vec{b}$ is very small, and intervalley scattering is improbable. We will deal mainly with this case. However, one should keep in mind that any sharp (atomic-scale) inhomogeneities, e.g., boundaries, will mix the states from different valleys, see Chapter 5.

The Hamiltonian (1.22) is a two-dimensional analogue of the Dirac Hamiltonian for massless fermions (Bjorken & Drell, 1964; Berestetskii, Lifshitz & Pitaevskii, 1971; Davydov, 1976). Instead of the velocity of light c, there is a parameter $v \approx 10^6\ \mathrm{m\,s}^{\ 1} \approx c/300$ (we will discuss later, in Chapter 2, how this parameter has been found experimentally).

A formal similarity between ultrarelativistic particles (with energy much larger than the rest energy mc^2, such that one can consider the particles as massless) and electrons in graphene makes graphene a playground on which to study various quantum relativistic effects 'CERN on one's desk'. These relations between the physics of graphene and relativistic quantum mechanics will be considered in the next several chapters.

The internal degree of freedom, which is just spin for 'true' Dirac fermions, is the sublattice index in the case of graphene. The Dirac 'spinors' consist here of the components describing the distribution of electrons in sublattices A and B. We will call this quantum number *pseudospin*, so that pseudospin 'up' means sublattice A and pseudospin 'down' means sublattice B. Apart from the pseudospin, there are two more internal degrees of freedom, namely the valley label (sometimes called isospin) and real spin, so, the most general low-energy Hamiltonian of electrons in graphene is an 8×8 matrix.

Spin–orbit coupling leads to a mixture of pseudospin and real spin and to the gap opening (Kane & Mele, 2005b). However, the value of the gap is supposed to be very small, of the order of 10^{-2} K for pristine graphene (Huertas-Hernando, Guinea & Brataas, 2006). The reason is not only the lightness of carbon atoms but also the orientation of orbital moments for π states perpendicular to the graphene plane. Defects can significantly enhance the spin–orbit coupling (Castro Neto & Guinea, 2009) and the corresponding effects are relevant, e.g., for spin relaxation in graphene (Huertas-Hernando, Guinea & Brataas, 2009), but the influence of spin–orbit coupling on the electronic structure is negligible. Henceforth we will neglect these effects, until the very end of the book (see Section 12.4).

For the case of ‘true’ Dirac fermions in three-dimensional space, the Hamiltonian is a 4×4 matrix, due to two projections of spins and two values of a charge degree of freedom — particle versus antiparticle. For the two-dimensional case the latter is not independent of the former. Electrons and holes are just linear combinations of the states from the sublattices A and B. The 2×2 matrix $hv\vec{\sigma}\vec{k}$ (the result of action of the Hamiltonian (1.22) on a plane wave with wave vector $\vec{k}$) is diagonalized by the unitary transformation

$$\hat{U}_{\vec{k}} = \frac{1}{\sqrt{2}}\left(1 + i\vec{m}_{\vec{k}}\vec{\sigma}\right), \tag{1.29}$$

where $\vec{m}_{\vec{k}} = (\cos\phi_{\vec{k}}, -\sin\phi_{\vec{k}})$ and $\phi_{\vec{k}}$ is the polar angle of the vector $\vec{k}(\vec{m}_{\vec{k}} \perp \vec{k})$. The eigenfunctions

$$\psi_{\mathrm{e,h}}^{(\mathrm{K})}(\vec{k}) = \frac{1}{\sqrt{2}}\begin{pmatrix} \exp\left(-i\phi_{\vec{k}}/2\right) \\ \pm\exp\left(i\phi_{\vec{k}}/2\right) \end{pmatrix} \tag{1.30}$$

correspond to electron (e) and hole (h) states, with the energies

$$E_{\mathrm{e,h}} = \pm hvk. \tag{1.31}$$

For the valley K′ the corresponding states (in the basis (1.25)) are

$$\psi_{\mathrm{e,h}}^{(\mathrm{K'})}(\vec{k}) = \frac{1}{\sqrt{2}}\begin{pmatrix} \exp\left(i\phi_{\vec{k}}/2\right) \\ \pm\exp\left(-i\phi_{\vec{k}}/2\right) \end{pmatrix}. \tag{1.32}$$

For the electron (hole) states, by definition,

$$\frac{(\vec{k}\vec{\sigma})}{k}\psi_{\mathrm{e,h}} = \pm\psi_{\mathrm{e,h}}. \tag{1.33}$$

This means that the electrons (holes) in graphene have a definite pseudospin direction, namely parallel (antiparallel) to the direction of motion. Thus, these states are *chiral* (*helical*), as should be the case for massless

Dirac fermions (Bjorken & Drell, 1964). This is of crucial importance for ‘relativistic’ effects, such as Klein tunnelling, which will be considered in Chapter 4.

The Dirac model for electrons in graphene results from the lowest-order expansion of the tight-binding Hamiltonian (1.14) near the conical points. If one takes into account the next, quadratic, term, one finds, instead of the Hamiltonian (1.28) (in the basis (1.27)),

$$\hat{H} = hv\tau_0 \otimes \vec{\sigma}\vec{k} + \mu\tau_z \otimes \left[2\sigma_y k_x k_y \quad \sigma_x\left({k_x}^2 \quad {k_y}^2\right)\right], \tag{1.34}$$

where $\mu = 3a^2t/8$. The additional term in Eq. (1.34) corresponds to a *trigonal warping* (Ando, Nakanishi & Saito, 1988; McCann *et al.*, 2006). Diagonalization of the Hamiltonian (1.34) gives the spectrum $E_{\mathrm{e,h}}(\vec{k}) = \pm\varepsilon(\vec{k})$, where

$$\varepsilon^2(\vec{k}) = h^2v^2k^2 \mp 2hv\mu k^3 \cos\left(3\phi_{\vec{k}}\right) + \mu^2k^4, \tag{1.35}$$

with the signs $\mp$ corresponding to valleys K and K$'$. The dispersion law is no longer isotropic but has threefold symmetry. Importantly, $\varepsilon(\vec{k}) \neq \varepsilon(\quad\vec{k})$, which means that the trigonal warping destroys an effective time-reversal symmetry for a given valley (the property $E(\vec{k}) = E(\quad\vec{k})$ follows from the time-reversal symmetry (Vonsovsky & Katsnelson, 1989)). Of course, for the electron spectrum as a whole, taking into account the two valleys, the symmetry holds:

$$\varepsilon(\vec{k} + \vec{K}) = \varepsilon(\quad\vec{k} \quad \vec{K}). \tag{1.36}$$

At the end of this section we show, following Mañes, Guinea & Vozmediano (2007), that the gapless state with the conical point is symmetry-protected. The proof is very simple and based on consideration of two symmetry operations: time reversal T and inversion I. We will use the basis (1.25) and the extended-Brillouin-zone representation of Fig. 1.6 assuming $\vec{K}' = \quad\vec{K}$. The time reversal changes the sign of the wave vector, or valley,

$$T\psi_{\mathrm{K(A,B)}} = \psi^*_{\mathrm{K(A,B)}} = \psi_{\mathrm{K'(A,B)}}, \tag{1.37}$$

whereas the inversion exchanges also the sublattices:

$$I\psi_{\mathrm{KA}} = \psi_{\mathrm{K'B}}, \qquad I\psi_{\mathrm{KB}} = \psi_{\mathrm{K'A}}. \tag{1.38}$$

Invariance under these symmetries imposes the following conditions for $\hat{H}_{\mathrm{K}}$ and $\hat{H}_{\mathrm{K'}}$:

$$T : H_{\mathrm{K}} = H^*_{\mathrm{K'}} = H_{\mathrm{K}}, \tag{1.39}$$

$$I : H_{\mathrm{K}} = \sigma_x H_{\mathrm{K'}} \sigma_x = H_{\mathrm{K}}. \tag{1.40}$$

Indeed,

$$\sigma_x \begin{pmatrix} a_{11} & a_{12} \\ a_{21} & a_{22} \end{pmatrix} \sigma_x = \begin{pmatrix} a_{22} & a_{21} \\ a_{12} & a_{11} \end{pmatrix}, \tag{1.41}$$

so the operation in (1.40) does exchange the A and B sublattices.

The conditions (1.39) and (1.40) establish relations between the Hamiltonians for the different valleys. If we use both these symmetry transformations we impose restrictions on H_{K} and $H_{\mathrm{K}'}$ separately, e.g.,

$$TI : H_{\mathrm{K}} = \sigma_x H_{\mathrm{K}}^* \sigma_x = H_{\mathrm{K}}. \tag{1.42}$$

If we write the Hamiltonian as

$$H_{\mathrm{K}} = \sum_i \alpha_i \sigma_i$$

one can see immediately that $\alpha_z = 0$, which means the absence of the mass term. Thus, a perturbation that is invariant under T and I can, in principle, shift the conical point (we will see in Chapter 10 that it can indeed be done, by deformations), but cannot open the gap: $(H_{\mathrm{K}})_{11} = (H_{\mathrm{K}})_{22}$ and the bands split by $\pm|H_{12}|$.

If the sublattices are no longer equivalent, then there is no inversion symmetry, the mass term naturally appears and the gap opens. This is, for example, the case of graphene on top of hexagonal boron nitride, h-BN (Giovannetti *et al.*, 2007; Sachs *et al.*, 2011).

1.4 The electronic structure of bilayer graphene

By exfoliation of graphene one can obtain *several* layers of carbon atoms. Bilayer graphene (Novoselov *et al.*, 2006) is especially interesting. Its electronic structure can be understood in the framework of a tight-binding model (McCann & Falko, 2006; McCann, Abergel & Falko, 2007).

The crystal structure of bilayer graphene is shown in Fig. 1.7. Like in graphite, the second carbon layer is rotated by 60° with respect to the first one. In graphite, such a configuration is repeated, which is called *Bernal stacking*. The sublattices A of the two layers lie exactly on top of one another, with a significant hopping parameter γ_1 between them, whereas there are no essential hopping processes between the sublattices B of the two layers. The parameter $\gamma_1 = t_\perp$ is usually taken as 0.4 eV, from data on the electronic structure of graphite (Brandt, Chudinov & Ponomarev, 1988; Dresselhaus & Dresselhaus, 2002), which is an order of magnitude smaller than the nearest-neighbour in-plane hopping parameter $\gamma_0 = t$. The simplest model which takes into account only these processes is described by the Hamiltonian

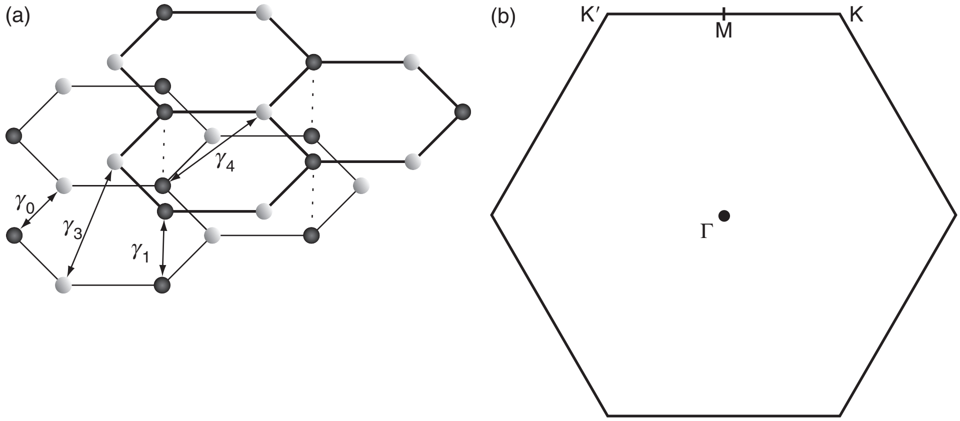

Fig. 1.7. (a) The crystal structure of bilayer graphene; hopping parameters are shown. (b) Special points in the Brillouin zone for the bilayer graphene.

$$\hat{H}(\vec{k}) = \begin{pmatrix} 0 & tS(\vec{k}) & t_\perp & 0 \\ tS^*(\vec{k}) & 0 & 0 & 0 \\ t_\perp & 0 & 0 & tS^*(\vec{k}) \\ 0 & 0 & tS(\vec{k}) & 0 \end{pmatrix} \tag{1.43}$$

with $S(\vec{k})$ from Eq. (1.15). The basis states are ordered in the sequence first layer, sublattice A; first layer, sublattice B; second layer, sublattice A; second layer, sublattice B.

The matrix (1.43) can be easily diagonalized, with four eigenvalues

$$E_i(\vec{k}) = \pm\frac{1}{2}t_\perp \pm \sqrt{\frac{1}{4}t_\perp^2 + t^2|S(\vec{k})|^2} \tag{1.44}$$

with two independent ± signs. The spectrum is shown in Fig. 1.8(a). Two bands touch one another at the points K and K′. Near these points

$$E_{1,2}(\vec{k}) \approx \pm\frac{t^2|S(\vec{k})|^2}{t_\perp} \approx \pm\frac{h^2q^2}{2m^*}, \tag{1.45}$$

where the effective mass is $m^* = |t_\perp|/(2v^2) \approx 0.054m_\mathrm{e}$, where m_e is the mass of a free electron (McCann, Abergel & Falko, 2007). Note that the recent experimental data give a value that is smaller by a factor of two: $m^* \approx 0.028m_\mathrm{e}$ (Mayorov *et al.*, 2011). So, in contrast with the case of a single layer, bilayer graphene turns out to be a gapless semiconductor with *parabolic* band touching. Two other branches $E_{3,4}(\vec{k})$ are separated by a gap $2|t_\perp|$ and are irrelevant for low-energy physics.

If one neglects intervalley scattering and replaces hq_x and hq_y by operators $\hat{p}_x = \quad ih\partial/\partial x$ and $\hat{p}_y = \quad ih\partial/\partial y$ as usual, one can construct the effective

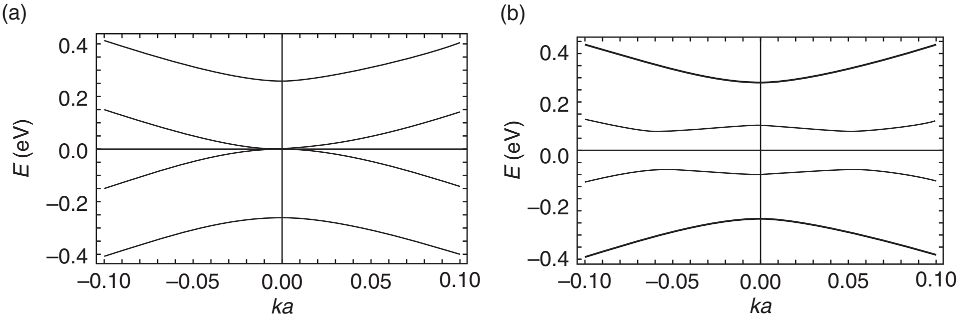

Fig. 1.8. (a) The electronic structure of bilayer graphene within the framework of the simplest model (nearest-neighbour hopping processes only). (b) The same, for the case of biased bilayer graphene (a voltage is applied perpendicular to the layers).

Hamiltonian; for single-layer graphene, this is the Dirac Hamiltonian (1.22). For the case of bilayer graphene, instead, we have (Novoselov *et al.*, 2006; McCann & Falko, 2006)

$$\hat{H}_{\mathrm{K}} = \frac{1}{2m^*}\begin{pmatrix} 0 & \left(\hat{p}_x \quad i\hat{p}_y\right)^2 \\ \left(\hat{p}_x + i\hat{p}_y\right)^2 & 0 \end{pmatrix}. \tag{1.46}$$

This is a new type of quantum-mechanical Hamiltonian that is different both from nonrelativistic (Schrödinger) and from relativistic (Dirac) cases. The eigenstates of this Hamiltonian have very special chiral properties (Novoselov *et al.*, 2006), resulting in a special Landau quantization, special scattering, etc., as will be discussed later. Electron and hole states corresponding to the energies

$$E_{\mathrm{e,h}} = \pm\frac{h^2k^2}{2m^*} \tag{1.47}$$

(cf. Eq. (1.31)) have a form similar to Eq. (1.30), with the replacement $\phi_{\vec{k}} \to 2\phi_{\vec{k}}$:

$$\psi_{\mathrm{e,h}}^{(\mathrm{K})}(\vec{k}) = \frac{1}{\sqrt{2}}\begin{pmatrix} e^{\quad i\phi_{\vec{k}}} \\ \pm e^{i\phi_{\vec{k}}} \end{pmatrix}. \tag{1.48}$$

These are characterized by a helicity property similar to Eq. (1.33):

$$\frac{\left(\vec{k}\vec{\sigma}\right)^2}{k^2}\psi_{\mathrm{e,h}} = \pm\psi_{\mathrm{e,h}}. \tag{1.49}$$

By applying a voltage V perpendicular to the carbon planes one can open a gap in the energy spectrum (McCann & Falko, 2006; Castro *et al.*, 2007, 2010a). In this case, instead of the Hamiltonian (1.43), one has

$$H(\vec{k}) = \begin{pmatrix} V/2 & tS(\vec{k}) & t_\perp & 0 \\ tS^*(\vec{k}) & V/2 & 0 & 0 \\ t_\perp & 0 & V/2 & tS^*(\vec{k}) \\ 0 & 0 & tS(\vec{k}) & V/2 \end{pmatrix} \tag{1.50}$$

and, instead of the eigenvalues (1.44), we obtain

$$E_i^2(\vec{k}) = t^2|S(\vec{k})|^2 + \frac{t_\perp^2}{2} + \frac{V^2}{4} \pm \sqrt{\frac{t_\perp^4}{4} + (t_\perp^2 + V^2)t^2|S(\vec{k})|^2}. \tag{1.51}$$

For the two low-lying bands in the vicinity of the K (or K′) point the spectrum has the ‘Mexican hat’ dispersion

$$E(\vec{k}) \approx \pm\left(\frac{V}{2} \quad \frac{Vh^2v^2}{t_\perp^2}k^2 + \frac{h^4v^4}{t_\perp^2 V}k^4\right), \tag{1.52}$$

where we assume, for simplicity, that $hvk \ll V \ll |t_\perp|$. This expression has a maximum at $k = 0$ and a minimum at $k = V/(\sqrt{2}hv)$ (see Fig. 1.8(b)). The opportunity to tune a gap in bilayer graphene is potentially interesting for applications. It was experimentally confirmed by Castro *et al.* (2007) and Oostinga *et al.* (2008).

Consider now the effect of larger-distance hopping processes, namely hopping between B sublattices ($\gamma_3 \approx 0.3$ eV) (Brandt, Chudinov & Ponomarev, 1988; Dresselhaus & Dresselhaus, 2002). Higher-order terms, such as $\gamma_4 \approx 0.04$ eV, are assumed to be negligible. These processes lead to a qualitative change of the spectrum near the K (K′) point. As was shown by McCann & Falko (2006) and McCann, Abergel & Falko (2007), the effective Hamiltonian (1.46) is modified by γ_3 terms, giving

$$\hat{H}_{\mathrm{K}} = \begin{pmatrix} 0 & \frac{\left(\hat{p}_x - i\hat{p}_y\right)^2}{2m^*} + \frac{3\gamma_3 a}{h}\left(\hat{p}_x + i\hat{p}_y\right) \\ \frac{\left(\hat{p}_x + i\hat{p}_y\right)^2}{2m^*} + \frac{3\gamma_3 a}{h}\left(\hat{p}_x - i\hat{p}_y\right) & 0 \end{pmatrix}, \tag{1.53}$$

with the energy spectrum determined by the equation (assuming that $|\gamma_3| \ll |\gamma_0|$)

$$E^2(\vec{k}) \approx (3\gamma_3 a)^2 k^2 + \frac{3\gamma_3 a h^2 k^3}{m^*}\cos\left(3\phi_{\vec{k}}\right) + \left(\frac{h^2k^2}{2m^*}\right)^2. \tag{1.54}$$

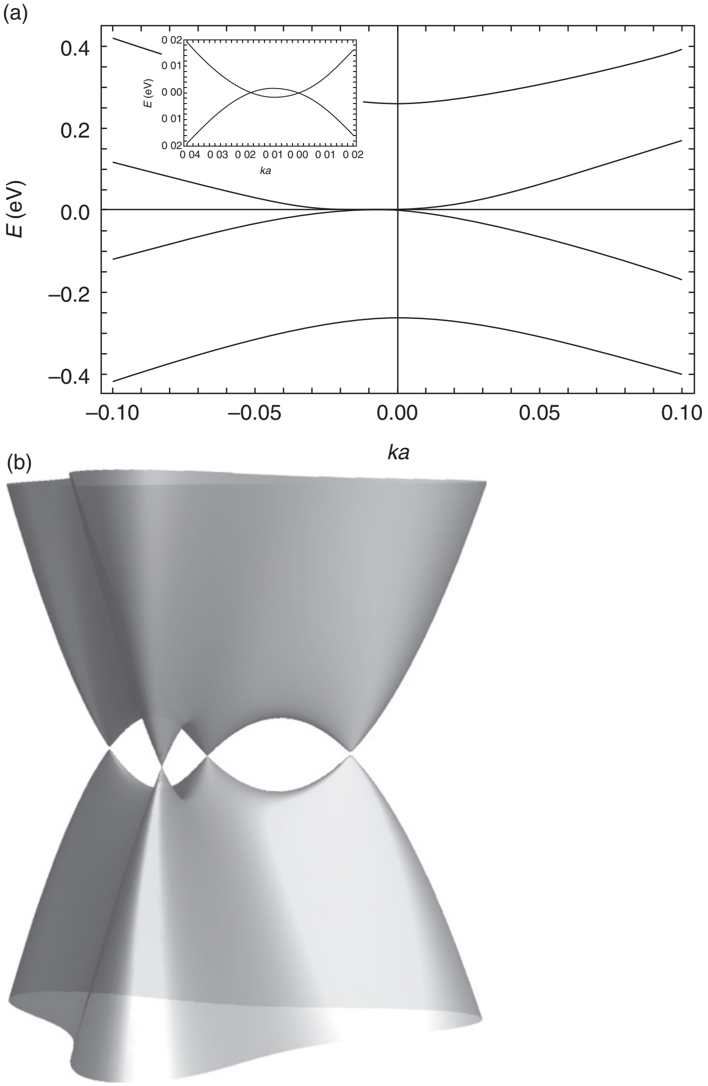

Fig. 1.9. The effect of trigonal warping on the electronic structure of bilayer graphene. (a) A cross-section of the dispersion surface at $\phi_{\vec{k}} = 0$; one can see the asymmetry of the spectrum (cf. Fig. 1.8(a)). (b) A general view of the dispersion surface.

This means that, at small enough wave vectors,

$$ka \leq \left| \frac{\gamma_3 \gamma_1}{{\gamma_0}^2} \right| \sim 10^{\ 2}, \tag{1.55}$$

the parabolic dispersion law (1.47) is replaced by the linear one. The corresponding level of doping when the Fermi wave vector satisfies the conditions (1.55) is estimated as $n < 10^{11}\ \mathrm{cm}^{\ 2}$ (McCann, Abergel & Falko, 2007).

The spectrum (1.54) is shown in Fig. 1.9. The term with $\cos\left(3\phi_{\vec{k}}\right)$ in Eq. (1.53) corresponds to the trigonal warping, which is more important for the bilayer than it is for the single layer: it leads to a reconstruction of isoenergetic lines when k grows. Instead of one point of parabolic touching of the bands at $k = 0$, there are now four conical points at $k = 0$ and $k = 6m^{*}\gamma_3 a/h^2, \cos(3\phi_{\vec{k}}) = \pm 1$, where the signs ± correspond to K and K′ valleys. The merging of four cones into one paraboloid with increasing energy is a particular case of the Lifshitz electronic topological transition associated with a Van Hove singularity of the electron density of states (Lifshitz, Azbel & Kaganov, 1973; Abrikosov, 1988; Vonsovsky & Katsnelson, 1989).

1.5 Multilayer graphene

For the third layer of carbon atoms there are two options: it can be rotated with respect to the second layer either by −60° or by 60°. In the first case, the third layer lies exactly on top of the first layer, with the layer order aba. In the second case, we will denote the structure as abc. In bulk graphite, the most stable state corresponds to Bernal stacking, abab … However, *rhombohedral* graphene with the stacking abcabc … also exists, as does *turbostratic* graphite with an irregular stacking.

Here we consider the evolution of the electronic structure of N-layer graphene with different stacking as N increases (Guinea, Castro Neto & Peres, 2006; Partoens & Peeters, 2006; Koshino & McCann, 2010). First we will discuss the case of Bernal stacking. We will restrict ourselves to considering only the simplest model with parameters $\gamma_0 = t$ and $\gamma_1 = t_\perp$, neglecting all other hopping parameters γ_i. For the case of bilayer graphene this corresponds to the Hamiltonian (1.43).

On introducing the basis functions $\psi_{n,\mathrm{A}}(\vec{k})$ and $\psi_{n,\mathrm{B}}(\vec{k})$ ($n = 1, 2, \ldots, N$ is the number of carbon layers, A and B label sublattices, and $\vec{k}$ is the two-dimensional wave vector in the layer) we can write the Schrödinger equation as

$$\begin{aligned}
E\psi_{2n,\mathrm{A}}(\vec{k}) &= tS(\vec{k})\psi_{2n,\mathrm{B}}(\vec{k}) + t_\perp\left[\psi_{2n-1,\mathrm{A}}(\vec{k}) + \psi_{2n+1,\mathrm{A}}(\vec{k})\right],\\
E\psi_{2n,\mathrm{B}}(\vec{k}) &= tS^{*}(\vec{k})\psi_{2n,\mathrm{A}}(\vec{k}),\\
E\psi_{2n+1,\mathrm{A}}(\vec{k}) &= tS^{*}(\vec{k})\psi_{2n+1,\mathrm{B}}(\vec{k}) + t_\perp\left[\psi_{2n,\mathrm{A}}(\vec{k}) + \psi_{2n+2,\mathrm{A}}(\vec{k})\right],\\
E\psi_{2n+1,\mathrm{B}}(\vec{k}) &= tS(\vec{k})\psi_{2n+1,\mathrm{A}}(\vec{k}).
\end{aligned} \tag{1.56}$$

Excluding the components ψ_{B} from Eqs. (1.56), one can write the equation

$$\left(E - \frac{t^2|S(\vec{k})|^2}{E}\right)\psi_{n,\mathrm{A}}(\vec{k}) = t_\perp\left[\psi_{n+1,\mathrm{A}}(\vec{k}) + \psi_{n-1,\mathrm{A}}(\vec{k})\right]. \tag{1.57}$$

For an infinite sequence of layers (bulk graphite with Bernal stacking) one can try the solutions of Eq. (1.57) as

$$\psi_{n,\mathrm{A}}(\vec{k}) = \psi_{\mathrm{A}}(\vec{k})e^{in\xi}, \tag{1.58}$$

which gives us the energies (Wallace, 1947)

$$E(\vec{k},\xi) = t_\perp \cos\xi \pm \sqrt{t^2|S(\vec{k})|^2 + t_\perp^2\cos^2(\xi)}. \tag{1.59}$$

The parameter ξ can be written as $\xi = 2k_z c$, where k_z is the z-component of the wave vector, c is the interlayer distance and, thus, $2c$ is the lattice period in the z-direction. A more accurate tight-binding model of the electronic structure of graphite taking into account more hoppings γ_i was proposed by McClure (1957) and Slonczewski & Weiss (1958); for reviews, see Dresselhaus & Dresselhaus (2002) and Castro Neto *et al.* (2009).

For the case of N-layer graphene ($n = 1, 2, \ldots, N$) one can still use Eq. (1.57), continuing it for $n = 0$ and $n = N + 1$, but with constraints

$$\psi_{0,\mathrm{A}} = \psi_{N+1,\mathrm{A}} = 0 \tag{1.60}$$

requiring the use of linear combinations of the solutions with ξ and $\ \xi$; since $E(\xi) = E(\ \xi)$ the expression for the energy (1.59) remains the same but ξ is now discrete. Owing to Eq. (1.60) we have

$$\psi_{n,\mathrm{A}} \sim \sin(\xi_p n) \tag{1.61}$$

with

$$\xi_p = \frac{\pi p}{N+1}, \quad p = 1, 2, \ldots, N. \tag{1.62}$$

Equations (1.59) and (1.62) solve formally the problem of the energy spectrum for N-layer graphene with Bernal stacking. For the case of bilayer graphene $\cos\xi_p = \pm\frac{1}{2}$ and we come back to Eq. (1.44). For $N = 3$, there are six solutions with $\cos\xi_p = 0, \pm 1/\sqrt{2}$:

$$E(\vec{k}) = \begin{cases} \pm t|S(\vec{k})|, \\ \pm t_\perp\sqrt{2}/2 \pm \sqrt{t_\perp^2/2 + t^2|S(\vec{k})|^2}. \end{cases} \tag{1.63}$$

We have both conical (like in single-layer graphene) and parabolic (like in bilayer graphene) touching at K and K′ points where $S(\vec{k}) \to 0$.

For rhombohedral stacking (abc), instead of Eq. (1.56), we have the Schrödinger equation in the form

$$\begin{aligned}
E\psi_{1,\mathrm{A}}(\vec{k}) &= tS(\vec{k})\psi_{1,\mathrm{B}}(\vec{k}) + t_\perp\psi_{2,\mathrm{A}}(\vec{k}),\\
E\psi_{1,\mathrm{B}}(\vec{k}) &= tS^*(\vec{k})\psi_{1,\mathrm{A}}(\vec{k}),\\
E\psi_{2,\mathrm{A}}(\vec{k}) &= tS^*(\vec{k})\psi_{2,\mathrm{B}}(\vec{k}) + t_\perp\psi_{1,\mathrm{A}}(\vec{k}),\\
E\psi_{2,\mathrm{B}}(\vec{k}) &= tS(\vec{k})\psi_{2,\mathrm{A}}(\vec{k}) + t_\perp\psi_{3,\mathrm{A}}(\vec{k}),\\
E\psi_{3,\mathrm{A}}(\vec{k}) &= tS(\vec{k})\psi_{3,\mathrm{B}}(\vec{k}) + t_\perp\psi_{2,\mathrm{B}}(\vec{k}),\\
E\psi_{3,\mathrm{B}}(\vec{k}) &= tS^*(\vec{k})\psi_{3,\mathrm{A}}(\vec{k}).
\end{aligned} \tag{1.64}$$

On excluding from Eq. (1.64) $\psi_{1,\mathrm{B}}$ and $\psi_{3,\mathrm{B}}$, one obtains

$$\begin{aligned}
\left(E - \frac{t^2|S(\vec{k})|^2}{E}\right)\psi_{1,\mathrm{A}}(\vec{k}) &= t_\perp\psi_{2,\mathrm{A}}(\vec{k}),\\
\left(E - \frac{t^2|S(\vec{k})|^2}{E}\right)\psi_{3,\mathrm{A}}(\vec{k}) &= t_\perp\psi_{2,\mathrm{B}}(\vec{k}),
\end{aligned} \tag{1.65}$$

so we have just two equations for $\psi_{2,\mathrm{A}}$ and $\psi_{2,\mathrm{B}}$,

$$\begin{aligned}
E\left(1 - \frac{t_\perp^2}{E^2 - t^2|S(\vec{k})|^2}\right)\psi_{2,\mathrm{A}}(\vec{k}) &= tS^*(\vec{k})\psi_{2,\mathrm{B}}(\vec{k}),\\
E\left(1 - \frac{t_\perp^2}{E^2 - t^2|S(\vec{k})|^2}\right)\psi_{2,\mathrm{B}}(\vec{k}) &= tS(\vec{k})\psi_{2,\mathrm{A}}(\vec{k}),
\end{aligned} \tag{1.66}$$

and, finally, the equation for the energy

$$E^2\left(1 + \frac{t_\perp^2}{t^2|S(\vec{k})|^2 - E^2}\right)^2 = t^2|S(\vec{k})|^2. \tag{1.67}$$

Near the K and K′ points when $S(\vec{k}) \to 0$ there is a solution of Eq. (1.67) that behaves as

$$E(\vec{k}) \approx \pm\frac{t^3|S(\vec{k})|^3}{t_\perp^2} \propto \pm q^3, \tag{1.68}$$

where $\vec{q} = \vec{k} - \vec{K}$ or $\vec{k} - \vec{K}'$. So, in trilayer graphene with rhombohedral stacking we have a gapless semiconducting state with *cubic* touching of the conduction and valence bands.

If we have a rhombohedral stacking of N layers (each layer is rotated with respect to the previous one by +60°), the low-lying part of the spectrum behaves, similarly to Eq. (1.68), according to

$$E(\vec{q}) \propto \pm\frac{t^N}{t_\perp^{N-1}}q^N \tag{1.69}$$

(Mañes, Guinea & Vozmediano, 2007).

Effects of γ_i beyond the simplest model were discussed by Koshino & McCann (2010).

To finish this chapter, we calculate the density of states

$$N(E) = 2\int \frac{d^2k}{(2\pi)^2}\delta\left(E - E(\vec{k})\right), \tag{1.70}$$

where integration is over the Brillouin zone of the honeycomb lattice and the factor 2 takes into account spin degeneracy. For small energies $E \to 0$ the contribution to (1.70) comes only from the vicinity of the K and K′ points and $E = E(|\vec{q}\,|)$ depends, to a first approximation (neglecting trigonal warping), only on the modulus of the wave vector. Thus, one gets

$$N(E) = 2{\cdot}2\int_0^\infty \frac{dq\,q}{2\pi}\delta(E - E(\vec{q})) = \frac{2}{\pi}\frac{q(E)}{|dE/dq|}. \tag{1.71}$$

For the case of single-layer graphene, according to Eq. (1.31),

$$N(E) = \frac{2}{\pi}\frac{|E|}{h^2 v^2} \tag{1.72}$$

and the density of states vanishes linearly as $E \to 0$. For bilayer graphene, due to Eq. (1.47),

$$N(E) = \frac{2m^*}{\pi h^2} \tag{1.73}$$

and the density of states is constant. Finally, for the spectrum (1.69) the density of states is divergent at $E \to 0$, $N > 2$:

$$N(E) \propto \frac{1}{|E|^{1-2/N}}. \tag{1.74}$$

At large enough energies the density of states has Van Hove singularities (related to the M point) that are relevant for the optical properties and will be discussed in Chapter 7.

2

Electron states in a magnetic field

2.1 The effective Hamiltonian

The reality of massless Dirac fermions in graphene has been demonstrated by Novoselov *et al.* (2005a) and Zhang *et al.* (2005) using quantized magnetic fields. The discovery of the anomalous (half-integer) quantum Hall effect in these works was the real beginning of the 'graphene boom'. Discussion of the related issues allows us to clarify in the most straightforward way possible the basic properties of charge-carrier states in graphene, such as chirality, Berry's phase, etc. So, it seems natural, both historically and conceptually, to start our consideration of the electronic properties of graphene with a discussion of the effects of the magnetic field.

We proceed with the derivation of the effective Hamiltonian of band electrons in a magnetic field (Peierls, 1933); our presentation will mainly follow Vonsovsky & Katsnelson (1989). It is assumed that the magnetic length

$$l_B = \sqrt{\frac{hc}{|e|B}} \tag{2.1}$$

(B is the magnetic induction) is much larger than the interatomic distance:

$$l_B \gg a, \tag{2.2}$$

which is definitely the case for any experimentally available fields; it would be violated only for $B \gg 10^4$ T.

Another approximation is that we will take into account only π electrons and neglect transitions to other electron bands (e.g., σ bands). Since the distance between π and σ bands is of the order of the π bandwidth (see Fig. 1.5) one can prove that the approximation is justified under the same condition (2.2) (see the discussion of magnetic breakdown at the end of this section). A rigorous theory of the effect of magnetic fields on Bloch states has been developed by

Kohn (1959) and Blount (1962). It is rather cumbersome, and its use for the case of graphene, with its very simple band structure, would obviously be overkill.

The original Hamiltonian is

$$H = \frac{\hat{\vec{\pi}}^2}{2m} + V(\vec{r}), \tag{2.3}$$

where

$$\hat{\vec{\pi}} = \hat{\vec{p}} \quad \frac{e}{c}\vec{A}, \quad \vec{p} = \quad ih\vec{\nabla}, \tag{2.4}$$

$\vec{A}$ is the vector potential,

$$\vec{B} = \vec{\nabla} \times \vec{A}, \tag{2.5}$$

m is the mass of a free electron and $V(\vec{r})$ is a periodic crystal potential. The operators $\hat{\pi}_\alpha$ satisfy the commutation relations

$$\left[\hat{\pi}_x, \hat{\pi}_y\right] = \quad \left[\hat{\pi}_y, \hat{\pi}_x\right] = \frac{ie}{hc}B, \tag{2.6}$$

other commutators being zero (we assume that the magnetic induction is along the z-axis).

We can try a general solution of the Schrödinger equation,

$$H\psi = E\psi, \tag{2.7}$$

as an expansion in the Wannier basis $\varphi_i(\vec{r})$ (we will omit the band label since we will consider only π states):

$$\psi = \sum_i c_i \varphi_i(\vec{r}). \tag{2.8}$$

The Wannier function on state i can be represented as

$$\varphi_i(\vec{r}) = \varphi_0(\vec{r} \quad \vec{R}_i) = \exp\left\{ \quad \frac{i}{h}\vec{R}_i\hat{\vec{p}}\right\}\varphi_0(\vec{r}), \tag{2.9}$$

where φ_0 is the function corresponding to the zero site.

For future use, we have to specify the gauge. Here we will use a radial gauge,

$$\vec{A} = \frac{1}{2}\vec{B} \times \vec{r} = \left(\quad \frac{By}{2}, \frac{Bx}{2}, 0\right). \tag{2.10}$$

Then, instead of the expansions (2.8) and (2.9), it is convenient to choose another basis, namely

$$\begin{aligned} \psi &= \sum_i a_i \tilde{\varphi}_i(\vec{r}), \\ \tilde{\varphi}_i(\vec{r}) &= \exp\left\{ \quad \frac{i}{h}\vec{R}_i\hat{\vec{\Pi}}\right\}\varphi_0(\vec{r}), \end{aligned} \tag{2.11}$$

where

$$\hat{\vec{\Pi}} = \hat{\vec{p}} + \frac{e}{c}\vec{A}. \tag{2.12}$$

The point is that the operators $\hat{\Pi}_\alpha$ commute with $\hat{\pi}_\beta$ and, thus, with the kinetic energy term in Eq. (2.3):

$$\left[\hat{\pi}_\alpha, \hat{\Pi}_\beta\right] = \frac{ieh}{c}\left(\frac{\partial A_\beta}{\partial x_\alpha} + \frac{\partial A_\alpha}{\partial x_\beta}\right) = 0 \tag{2.13}$$

due to Eq. (2.10). Using the identity

$$\exp\left(\hat{A} + \hat{B}\right) = \exp\left(\hat{A}\right)\exp\left(\hat{B}\right)\exp\left(-\frac{1}{2}\left[\hat{A}, \hat{B}\right]\right) \tag{2.14}$$

(assuming $\left[\hat{A}, \left[\hat{A}, \hat{B}\right]\right] = \left[\hat{B}, \left[\hat{A}, \hat{B}\right]\right] = 0$), see Vonsovsky & Katsnelson (1989), one can prove that the operator

$$\exp\left(\frac{i}{h}\vec{R}_i\hat{\vec{\Pi}}\right) = \exp\left\{\frac{ie}{2hc}\left(\vec{R}_i \times \vec{B}\right)\vec{r}\right\}\exp\left\{\frac{i}{h}\vec{R}_i\hat{\vec{p}}\right\} \tag{2.15}$$

commutes also with the potential energy $V(\vec{r})$ due to translational invariance of the crystal:

$$\exp\left\{\frac{i}{h}\vec{R}_i\hat{\vec{p}}\right\}V(\vec{r})\ldots = V\left(\vec{r} + \vec{R}_i\right)\exp\left\{\frac{i}{h}\vec{R}_i\hat{\vec{p}}\right\}\ldots = V(\vec{r})\exp\left\{\frac{i}{h}\vec{R}_i\hat{\vec{p}}\right\}\ldots \tag{2.16}$$

and, thus, the Hamiltonian matrix in the basis (2.12) has the form

$$H_{ij} = \int d\vec{r}\,\varphi_0^*\,(\vec{r})\hat{H}\exp\left(\frac{i}{h}\vec{R}_i\hat{\vec{\Pi}}\right)\exp\left(-\frac{i}{h}\vec{R}_j\hat{\vec{\Pi}}\right)\varphi_0(\vec{r}). \tag{2.17}$$

Using, again, Eq. (2.14) one finds

$$\begin{aligned}
\exp\left(\frac{i}{h}\vec{R}_i\hat{\vec{\Pi}}\right)\exp\left(-\frac{i}{h}\vec{R}_j\hat{\vec{\Pi}}\right) &= \exp\left[\frac{i}{h}\hat{\vec{\Pi}}\left(\vec{R}_i - \vec{R}_j\right)\right]\exp\left\{-\frac{ie}{2hc}\left(\vec{R}_i \times \vec{R}_j\right)\vec{B}\right\} \\
&= \exp\left\{\frac{i}{2hc}\left[\left(\vec{R}_i - \vec{R}_j\right) \times \vec{B}\right]\vec{r}\right\} \\
&\quad \times \exp\left\{-\frac{ie}{2hc}\left(\vec{R}_i \times \vec{R}_j\right)\vec{B}\right\}\exp\left\{\frac{i}{h}\hat{\vec{p}}\left(\vec{R}_i - \vec{R}_j\right)\right\}.
\end{aligned} \tag{2.18}$$

The Wannier functions are localized within a region of extent a few interatomic distances, so, to estimate the various terms in (2.18), one has to assume $r \approx a$ and $\left|\vec{R}_i - \vec{R}_j\right| \approx a$ and take into account Eq. (2.2).

Thus,

$$H_{ij} \approx \exp\left\{ \quad \frac{ie}{2hc}\left(\vec{R}_i \quad \times \vec{R}_j\right)\vec{B}\right\} t_{ij}, \tag{2.19}$$

where $t_{ij} = H_{ij}(\vec{B} = 0)$ is the hopping parameter without a magnetic field. With the same accuracy, one can prove that the basis (2.11) is orthonormal.

Further straightforward transformations (Vonsovsky & Katsnelson, 1989) show that the change of the hopping parameters (2.11) corresponds to a change of the band Hamiltonian $t(\vec{p})$ (where $\vec{p} = h\vec{k}$) by

$$\hat{H}_{\mathrm{eff}} = t\left(\hat{\vec{\pi}}\right) \tag{2.20}$$

and, thus, the Schrödinger equation (2.7) takes the form

$$t\left(\hat{\vec{\pi}}\right)\psi = E\psi. \tag{2.21}$$

Instead of the operators $\hat{\pi}_x$ and $\hat{\pi}_y$ satisfying the commutation relations (2.6), it is convenient to introduce the standard Bose operators $\hat{b}$ and $\hat{b}^+$ by writing

$$\begin{aligned} \hat{\pi}\quad &= \hat{\pi}_x \quad i\hat{\pi}_y = \sqrt{\frac{2|e|hB}{c}}\hat{b}, \\ \hat{\pi}_+ &= \hat{\pi}_x + i\hat{\pi}_y = \sqrt{\frac{2|e|hB}{c}}\hat{b}^+ \end{aligned} \tag{2.22}$$

in such a way that

$$\left[\hat{b}, \hat{b}^+\right] = 1. \tag{2.23}$$

We will see later that this representation is very convenient for the cases of both single-layer and, especially, bilayer graphene.

To finish this section, we should discuss the question of neglected transitions to other bands (magnetic breakdown). If the distance between the bands is of the order of their bandwidth (which is the case for σ and π bands in graphene), the condition (2.2) still suffices to allow us to neglect the transitions. If the gap between the states $\Delta \ll |t|$, the magnetic breakdown can be neglected if

$$\frac{|e|B}{hc} = \frac{1}{l_B^2} \ll \left(\frac{\Delta}{t}\right)^2 \frac{1}{a^2},$$

where we assume that $t \sim h^2/(ma^2)$ (Vonsovsky & Katsnelson, 1989).

Similarly to the derivation of equations for the electron spectrum of a semiconductor with impurities in the effective-mass approximation (Tsidilkovskii, 1982), one can prove that, if the magnetic induction $\vec{B}(x, y)$ is inhomogeneous but the spatial scale of this inhomogeneity is much larger than a, the Hamiltonian (2.20) still works.

2.2 Landau quantization for massless Dirac fermions

Let us apply the general theory to electrons in graphene in the vicinity of the point K. It follows from Eqs. (1.22), (2.20) and (2.22) that the effective Hamiltonian is

$$\hat{H} = v\begin{pmatrix} 0 & \hat{\pi} \\ \hat{\pi}_+ & 0 \end{pmatrix} = \sqrt{\frac{2|e|\hbar Bv^2}{c}}\begin{pmatrix} 0 & \hat{b} \\ \hat{b}^+ & 0 \end{pmatrix} \tag{2.24}$$

and the Schrödinger equation (2.21) for the two-component spinor reads

$$\begin{aligned} \hat{b}\psi_2 &= \varepsilon\psi_1, \\ \hat{b}^+\psi_1 &= \varepsilon\psi_2, \end{aligned} \tag{2.25}$$

where we have introduced a dimensionless quantity ε, such that

$$E = \sqrt{\frac{2|e|\hbar Bv^2}{c}}\varepsilon \equiv \frac{\sqrt{2}\hbar v}{l_B}\varepsilon. \tag{2.26}$$

We assume here that $B > 0$ (magnetic field up). For the second valley K′, ψ_1 and ψ_2 exchange their places in Eq. (2.25).

First, one can see immediately from (2.25) that a zero-energy solution exists with $\psi_1 = 0$, and $\psi_2 \equiv |0\rangle$ is the ground state of a harmonic oscillator:

$$b|0\rangle = 0. \tag{2.27}$$

This solution is 100% polarized in pseudospin; that is, for a given direction of the magnetic field for the valleys K and K′, electrons in this state belong completely to sublattices A and B, respectively, or conversely if the direction of the magnetic field is reversed.

To find the complete energy spectrum, one has to act with the operator $\hat{b}^+$ on the first equation of (2.25), which gives us immediately

$$\hat{b}^+\hat{b}\psi_2 = \varepsilon^2\psi_2 \tag{2.28}$$

with the well-known eigenvalues

$$\varepsilon_n^2 = n = 0,\ 1,\ 2,\ \ldots \tag{2.29}$$

Thus, the eigenenergies of massless Dirac electrons in a uniform magnetic field are given by

$$E_n^{(\pm)} = \pm h\omega_c\sqrt{n}, \tag{2.30}$$

where the quantity

$$h\omega_c = \frac{\sqrt{2}hv}{l_B} = \sqrt{\frac{2h|e|Bv^2}{c}} \tag{2.31}$$

will be called the 'cyclotron quantum'. In the context of condensed-matter physics, this spectrum was first derived by McClure (1956), in his theory of the diamagnetism of graphite. This spectrum is drastically different from that for nonrelativistic electrons with $t(\hat{\vec{\pi}}) = \hat{\vec{\pi}}^2/(2m)$, where (Landau, 1930)

$$\varepsilon_n = h\tilde{\omega}_c\left(n + \frac{1}{2}\right), \quad \tilde{\omega}_c = \frac{|e|B}{mc}. \tag{2.32}$$

Discrete energy levels of two-dimensional electrons in magnetic fields are called *Landau levels*.

First, the spectrum (2.31), in contrast with (2.32), is not equidistant. Second, and more importantly, the zero Landau level ($n = 0$) has zero energy and, due to the electron hole symmetry of the problem, is equally shared by electrons and holes. The states at this level are chiral; that is, they belong to only one sublattice, as was explained above. The existence of the zero Landau level has deep topological reasons and leads to dramatic consequences for the observable properties of graphene, as will be discussed later in this chapter.

To understand better the relations between relativistic and nonrelativistic Landau spectra, let us calculate the Hamiltonian (2.24) squared, taking into account the commutation relations (2.6):

$$\hat{H}^2 = v^2\left(\vec{\sigma}\hat{\vec{\pi}}\right)^2 = v^2\hat{\vec{\pi}}^2 + iv^2\hat{\vec{\sigma}}\left(\hat{\vec{\pi}} \times \hat{\vec{\pi}}\right) = v^2\hat{\vec{\pi}}^2 \quad \frac{v^2 h|e|B}{c}\sigma^z. \tag{2.33}$$

The spectrum of the operator (2.33) can be immediately found from the solution of the nonrelativistic problem if one puts $m = 1/(2v^2)$. Then,

$$E_n^2 = \frac{2h|e|Bv^2}{c}\left(n + \frac{1}{2}\right) \mp \frac{v^2 h|e|B}{c} = \frac{2h|e|Bv^2}{c}\left(n + \frac{1}{2} \mp \frac{1}{2}\right), \tag{2.34}$$

where ± 1 are eigenstates of the operator $\hat{\sigma}^z$. The last term in Eq. (2.33) looks like Zeeman splitting, and the existence of the zero Landau level in these terms results from an exact cancellation of the cyclotron energy and the

Zeeman energy. Actually, for free electrons, for which the same mass is responsible both for the orbital motion and for the internal magnetic moment, the situation is exactly the same:

$$E_{n,\sigma} = \frac{h|e|B}{mc}\left(n + \frac{1}{2}\right) \mp \frac{h|e|B}{2mc}. \tag{2.35}$$

In semiconductors the effective electron mass is usually much smaller than the effective electron mass, and the Zeeman term gives just small corrections to Landau quantization. For the case of graphene, the pseudo-Zeeman term originates also from the orbital motion, namely from hopping processes between neighbouring sites.

To find the eigenfunctions corresponding to the eigenenergies (2.30) one needs to specify a gauge for the vector potential. The choice (2.10) gives us solutions with radial symmetry. It is more convenient, however, to use the Landau gauge

$$\vec{A} = (0, Bx, 0). \tag{2.36}$$

Then Eq. (2.25) takes the form

$$\begin{aligned} \left(\frac{\partial}{\partial x} \quad i\frac{\partial}{\partial y} \quad \frac{x}{l_B^2}\right)\psi_2 &= \frac{iE}{hv}\psi_1, \\ \left(\frac{\partial}{\partial x} + i\frac{\partial}{\partial y} + \frac{x}{l_B^2}\right)\psi_1 &= \frac{iE}{hv}\psi_2. \end{aligned} \tag{2.37}$$

In the gauge (2.36) y is the cyclic coordinate, and the solutions of Eq. (2.37) can be tried in the form

$$\psi_{1,2}(x, y) = \psi_{1,2}(x)\exp\left(ik_y y\right), \tag{2.38}$$

which transforms Eqs. (2.37) into

$$\begin{aligned} \left(\frac{\partial}{\partial x} \quad \frac{x \quad x_0}{l_B^2}\right)\psi_2 &= \frac{iE}{hv}\psi_1, \\ \left(\frac{\partial}{\partial x} + \frac{x \quad x_0}{l_B^2}\right)\psi_1 &= \frac{iE}{hv}\psi_2, \end{aligned} \tag{2.39}$$

where

$$x_0 = l_B^2 k_y \tag{2.40}$$

is the coordinate of the centre of the electron orbit (Landau, 1930). On introducing a dimensionless coordinate

$$X = \frac{\sqrt{2}}{l_B}(x - x_0) \tag{2.41}$$

and a dimensionless energy (2.26), one can transform Eq. (2.37) to

$$\left(\frac{d^2}{dX^2} + \varepsilon^2 + \frac{1}{2} - \frac{X^2}{4}\right)\psi_1(X) = 0, \tag{2.42}$$

$$\psi_2(X) = -\frac{i}{\varepsilon}\left(\frac{d}{dX} + \frac{X}{2}\right)\psi_1(X). \tag{2.43}$$

We assume in the second equation that $\varepsilon \neq 0$, otherwise

$$\begin{aligned} &\psi_1(X) \sim \exp\left(-\frac{X^2}{4}\right), \\ &\psi_2(X) = 0. \end{aligned} \tag{2.44}$$

The only solution of Eq. (2.42) vanishing at $X \to -\infty$ (the second one is exponentially growing) is, with an accuracy to within a constant multiplier,

$$\psi_1(X) = D_{\varepsilon^2}(-X), \tag{2.45}$$

where $D_\nu(X)$ is the Weber function (Whittaker & Watson, 1927) and

$$\psi_2(X) = i\varepsilon D_{\varepsilon^2 - 1}(-X). \tag{2.46}$$

If the sample is not restricted for both $X \to -\infty$ and $X \to \infty$, the solutions (2.45) and (2.46) are normalizable only for integer ε^2, which gives us again the quantization condition (2.29). For an integer index n, the Weber functions

$$D_n(X) = (-1)^n \exp\left(\frac{X^2}{4}\right)\frac{d^n}{dX^n}\exp\left(-\frac{X^2}{2}\right) \tag{2.47}$$

decay as $\exp(-X^2/4)$ for $X \to \pm\infty$.

The energy is not dependent on the quantum number k_y or, equivalently, on the position of the centre of the orbit x_0. This means that the Landau levels (2.30) have a macroscopically large degeneracy g. To calculate it, it is convenient to use a periodic (Born–von Kármán) boundary condition in the y-direction,

$$\psi_{1,2}(x, y) = \psi_{1,2}(x, y + L_y) \tag{2.48}$$

(for large enough samples the density of states does not depend on boundary conditions, Vonsovsky & Katsnelson (1989)). Thus,

$$k_y = \frac{2\pi}{L_y}n, \tag{2.49}$$

where $n = 0, \pm 1, \ldots$ The maximum value of n is determined by the condition that the centre of the orbit should be within the sample: $0 < x_0 < L_x$ (L_x is the width of the sample in the x-direction), or

$$\left|k_y\right| < \frac{L_x}{l_B^2} = \frac{|e|B}{hc} L_x. \tag{2.50}$$

Thus, the total number of solutions is

$$g = \frac{|e|B}{hc}\frac{L_x L_y}{2\pi} = \frac{|e|B}{hc}\frac{A}{2\pi} = \frac{\Phi}{\Phi_0}, \tag{2.51}$$

where $A = L_x L_y$ is the sample area, Φ is the total magnetic flux though the sample and

$$\Phi_0 = \frac{hc}{|e|} \tag{2.52}$$

is the flux quantum. Keeping in mind further applications to graphene, one should multiply the degeneracy (2.51) by a factor of 4, namely a factor of 2 for the two valleys K and K′ and a further factor of 2 for the two spin projections. The latter is possible since the ratio of the Zeeman energy $E_z = |e|hB/(2mc)$ to the cyclotron quantum $h\omega_c$ is always very small (about 0.01 in fields $B \approx 10 \quad 30\,\mathrm{T}$).

2.3 Topological protection of the zero-energy states

The existence of the zero-energy Landau level is the consequence of one of the most important theorems of modern mathematical physics, the Atiyah Singer index theorem (Atiyah & Singer, 1968, 1984). This theorem has important applications in quantum field and superstring theories (Kaku, 1988; Nakahara, 1990). In its simplest version, being applied to the operator

$$\hat{H} = v\hat{\vec{\sigma}}\left(\quad ih\vec{\nabla} \quad \frac{e}{c}\vec{A}(x,y)\right) \tag{2.53}$$

acting on a torus (that is, with periodic boundary conditions both in the y- and in the x-direction), the theorem states that the *index* of this operator is proportional to the total flux, namely

$$\mathrm{index}\left(\hat{H}\right) = N_+ \quad N \quad = \frac{\Phi}{\Phi_0} \tag{2.54}$$

for an inhomogeneous magnetic field as well as for a homogeneous one. Here N_+ is the number of solutions with zero energy and positive chirality,

$$\hat{H}\psi_1 = 0, \qquad \psi_2 = 0, \tag{2.55}$$

and N_- is the number of solutions with zero energy and negative chiraity,

$$\psi_1 = 0, \qquad \hat{H}\psi_2 = 0. \tag{2.56}$$

For the case of a homogeneous magnetic field, $N_+ = g$ is given by Eq. (2.51) and $N_- = 0$. Strictly speaking, we did not consider the case of a torus; instead we considered periodic boundary conditions in the y-direction only; the case of a torus is analysed by Tenjinbayashi, Igarashi & Fujiwara (2007), and the result for the number of zero modes is the same. A simplified (in comparison with the general case) formal discussion of the Atiyah–Singer theorem for the Hamiltonian (2.53) can be found in Katsnelson & Prokhorova (2008).

The index theorem tells us that the zero-energy Landau level is topologically protected; that is, it is robust with respect to possible inhomogeneities of the magnetic field (Novoselov *et al.*, 2005a; Katsnelson, 2007a). This statement is important for real graphene since the effective magnetic field there *should* be inhomogeneous due to the effect of so-called *ripples*, as will be discussed in Chapter 10.

The simplest way (at least for physicists) to understand the robustness of zero-energy modes is to construct explicitly the solutions for zero-energy states in an inhomogeneous magnetic field. This was done by Aharonov & Casher (1979) for the case of an infinite sample with the magnetic flux Φ localized in a restricted region.

Let us assume, first, that the vector potential satisfies the condition

$$\vec{\nabla}\vec{A} = 0; \tag{2.57}$$

otherwise, one can always use the gauge transformation

$$\vec{A} \to \vec{A} + \vec{\nabla}\chi, \qquad \psi \to \psi \exp\left(\frac{ie}{hc}\chi\right), \tag{2.58}$$

choosing χ to provide Eq. (2.57). Thus, one can introduce a scalar 'potential' $\varphi(x, y)$ such that

$$A_x = \frac{\partial\varphi}{\partial x}, \qquad A_y = \frac{\partial\varphi}{\partial y} \tag{2.59}$$

and, due to Eq. (2.5),

$$B = \nabla^2\varphi. \tag{2.60}$$

Then, the equations (2.55) and (2.56) can be written in the form

$$\left(\frac{\partial}{\partial x} + i\sigma\frac{\partial}{\partial y} + \frac{ie}{hc}\frac{\partial\varphi}{\partial x} + \frac{\sigma e}{hc}\frac{\partial\varphi}{\partial y}\right)\psi_{1,2} = 0, \tag{2.61}$$

where $\sigma = 1$ and $\;1$ for ψ_1 and ψ_2, respectively. The potential φ can be excluded by the substitution

$$\psi_{1,2} = \exp\left(\;\frac{\sigma e}{hc}\varphi\right) f_{1,2}, \tag{2.62}$$

which transforms Eq. (2.61) into the equation

$$\left(\frac{\partial}{\partial x} + i\sigma\frac{\partial}{\partial y}\right) f_{1,2} = 0. \tag{2.63}$$

This means that f_1 and f_2 are analytic and complex-conjugated analytic entire functions of $z = x + iy$, respectively.

The equation (2.60) has a solution

$$\varphi(\vec{r}) = \int d\vec{r}\,' G(\vec{r}, \vec{r}\,') B(\vec{r}\,'), \tag{2.64}$$

where

$$G(\vec{r}, \vec{r}\,') = \frac{1}{2\pi} \ln\left(\frac{|\vec{r} \;\; \vec{r}\,'|}{r_0}\right) \tag{2.65}$$

is the Green function of the Laplace operator in two dimensions (Jackson, 1962), where r_0 is an arbitrary constant. At $r \to \infty$

$$\varphi(r) \approx \frac{\Phi}{2\pi} \ln\left(\frac{r}{r_0}\right) \tag{2.66}$$

and

$$\psi_{1,2}(r) = \left(\frac{r_0}{r}\right)^{\frac{\sigma e \Phi}{2\pi\hbar c}} f_{1,2}(\vec{r}), \tag{2.67}$$

where

$$\Phi = \int d\vec{r}\, \vec{B}(\vec{r}) \tag{2.68}$$

is the total magnetic flux. Since the entire function $f(z)$ cannot go to zero in all directions at infinity, ψ_i can be normalizable only assuming that $\sigma e \Phi > 0$; that is, zero-energy solutions can exist only for one (pseudo)spin direction, depending on the sign of the total flux.

Let us count now how many independent solutions of Eq. (2.63) we have. As a basis, we can choose just polynomials searching the solutions of the form

$$f_1(z) = z^j \tag{2.69}$$

(to be specific, we consider the case $e\Phi > 0$), where $j = 0, 1, 2, \ldots$ One can see from Eq. (2.67) that the solution is integrable with the square only assuming that $j < N$, where N is the integer part of

$$\frac{e\Phi}{2\pi hc} = \frac{\Phi}{\Phi_0}.$$

Thus, the number of the states with zero energy for one (pseudo)spin projection is equal to N, and there are no such solutions for another spin projection. This agrees with Eq. (2.54).

2.4 Semiclassical quantization conditions and Berry's phase

The exact spectrum (2.30) of Dirac electrons in a uniform magnetic field B seems to be in a contradiction with the Lifshitz Onsager semiclassical quantization condition (Lifshitz, Azbel & Kaganov, 1973; Abrikosov, 1988; Vonsovsky & Katsnelson, 1989)

$$S(E_n) = \frac{2\pi|e|B}{hc}\left(n + \frac{1}{2}\right), \tag{2.70}$$

where $S(E_n)$ is the area of k-space inside the line determined by the equation

$$E(k_x, k_y) = E_n. \tag{2.71}$$

For massless Dirac electrons this is just a circle of radius $k(E) = E/(hv)$, and

$$S(E) = \pi\frac{E^2}{(hv)^2}, \tag{2.72}$$

so the term with $\frac{1}{2}$ in Eq. (2.70) should not exist. Strictly speaking, the semiclassical condition (2.70) is valid only for highly excited states, $n \gg 1$; however, for these states it should give us not only the leading, but also the subleading, term correctly, which is not the case now.

The replacement $n \to n + \frac{1}{2}$ follows from the existence of two turning points for a classical periodic orbit; in a more general case, it is related to the so-called Keller Maslov index. The simplest way to derive it is probably by using the saddle-point approximation in the path-integral formulation of quantum mechanics (Schulman, 1981). It turns out that the case of electrons in single-layer (as well as in bilayer, see below) graphene is very special, and, for Dirac fermions, the correct semiclassical condition is

$$S(E_n) = \frac{2\pi|e|B}{hc}n, \tag{2.73}$$

which gives us, together with Eq. (2.72), the *exact* spectrum (2.30), including the existence of a zero mode at $n = 0$. Of course, in general, we are not always so lucky, and for the case of bilayer graphene (Section 2.5) the situation is different.

The mystery of the missing term $\frac{1}{2}$ is a good way to introduce one of the deepest concepts of modern quantum mechanics, namely Berry's (or the geometrical) phase (Berry, 1984; Schapere & Wilczek, 1989).

Let us start with the following simple observation. If we rotate the $\vec{k}$ vector by the angle 2π, the wave functions (1.30) change sign:

$$\psi_{\mathrm{e,h}}\left(\phi_{\vec{k}} = 2\pi\right) = \quad \psi_{e,h}\left(\phi_{\vec{k}} = 0\right). \tag{2.74}$$

This is not surprising when rotating spin $\frac{1}{2}$ in spin space, but we are talking about rotations in real physical space, and our 'spin' is just a label for sublattices! This property (2.74) has a deep geometrical and topological meaning.

Berry (1984) considered a general adiabatic evolution of a quantum system. To be specific, we will apply these ideas to the evolution of electron states in $\vec{k}$ space (Zak, 1989; Chang & Niu, 2008).

The Bloch states

$$\psi_{n\vec{k}}(\vec{r}) = u_{n\vec{k}}(\vec{r})\exp\left(i\vec{k}\vec{r}\right), \tag{2.75}$$

where $u_{n\vec{k}}(\vec{r})$ is the Bloch amplitude periodic in the real space, evolve under the action of external electric and magnetic fields. If they are time-independent, or their time dependence is slow in comparison with typical electron times of the order of h/W (W is the bandwidth), this evolution is mainly within the same band n, with an exponentially small probability of interband transitions (electric or magnetic breakdown) (Vonsovsky & Katsnelson, 1989).

By substituting Eq. (2.75) into the Schrödinger equation one can derive the equation for the Bloch amplitude with a slowly varying wave vector $\vec{k}(t)$,

$$ih\frac{\partial|u(t)\rangle}{\partial t} = \hat{H}_{\mathrm{eff}}\left(\vec{k}(t)\right)|u(t)\rangle \tag{2.76}$$

(an explicit form of the Hamiltonian H_{eff} is not essential here). The time-dependent band states $|n\vec{k}\rangle$ satisfy a *stationary* Schrödinger equation

$$\hat{H}_{\mathrm{eff}}\left(\vec{k}\right)\left|n,\vec{k}\right\rangle = E_n\left(\vec{k}\right)\left|n,\vec{k}\right\rangle, \tag{2.77}$$

where $\left|n\vec{k}\right\rangle = u_{n\vec{k}}(\vec{r})$. Neglecting interband transitions, one can try the solution of Eq. (2.76) with an initial condition

$$|u(0)\rangle = \left|n,\vec{k}(0)\right\rangle \tag{2.78}$$

as

$$|u(t)\rangle = |u(0)\rangle \exp\left\{ \quad \frac{i}{h}\int_0^t dt'\, E_n\left(\vec{k}(t')\right)\right\} \exp\{i\gamma_n(t)\}\left|n, \vec{k}(t)\right\rangle. \tag{2.79}$$

On substituting Eq. (2.79) into Eq. (2.76), one finds

$$\frac{\partial \gamma_n(t)}{\partial t} = i\left\langle n, \vec{k}(t)\right|\vec{\nabla}_{\vec{k}}\left|n, \vec{k}(t)\right\rangle \frac{d\vec{k}(t)}{dt}. \tag{2.80}$$

If we consider a periodic motion $\vec{k}(\tau) = \vec{k}(0)$, then, on integrating Eq. (2.80) over the period of motion τ, one finds for the *Berry phase*

$$\gamma_n = i\oint_C d\vec{k}\left\langle n, \vec{k}\right|\vec{\nabla}_{\vec{k}}\left|n, \vec{k}\right\rangle, \tag{2.81}$$

where C is a line drawn by the end of the vector $\vec{k}(t)$. For nondegenerate bands, it is obvious that $\gamma_n = 0$. However, this is not the case for a degenerate spectrum and, in particular, for the case in which conical points exist, like in graphene.

Using Stokes' theorem, Eq. (2.81) can be written in terms of the surface integral over the area, restricted by the contour C:

$$\gamma_n(C) = \quad \mathrm{Im}\int d\vec{S}\cdot\vec{\nabla}_{\vec{k}} \times \left\langle n, \vec{k}\right|\vec{\nabla}_{\vec{k}}\left|n, \vec{k}\right\rangle = \quad \mathrm{Im}\int d\vec{S}\left\langle \vec{\nabla}_{\vec{k}} n\right| \times \left|\vec{\nabla}_{\vec{k}} n\right\rangle \tag{2.82}$$

with obvious notations, e.g., $\left|\vec{\nabla}_{\vec{k}} n\right\rangle = \vec{\nabla}_{\vec{k}}\left|n, \vec{k}\right\rangle$.

To demonstrate explicitly the role of crossing points of the energy spectrum (such as the conical points in graphene), we introduce, following Berry (1984), the summation over a complete set of eigenstates $|m\rangle$:

$$\left\langle \vec{\nabla}_{\vec{k}} n\right| \times \left|\vec{\nabla}_{\vec{k}} n\right\rangle = \sum_m \left\langle \vec{\nabla}_{\vec{k}} n \,\middle|\, m\right\rangle \times \left\langle m \,\middle|\, \vec{\nabla}_{\vec{k}} n\right\rangle. \tag{2.83}$$

The term with $m = n$ in Eq. (2.83) is obviously zero and can be omitted since, due to the normalization condition $\langle n|n\rangle = 1$, $\left\langle \vec{\nabla}_{\vec{k}} n\middle| n\right\rangle = \quad \left\langle n\middle|\vec{\nabla}_{\vec{k}} n\right\rangle$. On differentiating Eq. (2.77) with respect to $\vec{k}$ one has

$$\vec{\nabla}_{\vec{k}}\hat{H}_{\mathrm{eff}}|n\rangle + \left(\hat{H}_{\mathrm{eff}} \quad E_n\right)\left|\vec{\nabla}_{\vec{k}} n\right\rangle = \vec{\nabla}_k E_n|n\rangle. \tag{2.84}$$

On multiplying Eq. (2.84) by $\langle m|$ from the left and taking into account that $\langle m|n\rangle = 0$ at $m \neq n$, one finds

$$\left\langle m \middle| \vec{\nabla}_{\vec{k}} n \right\rangle = \frac{\left\langle m \middle| \vec{\nabla}_{\vec{k}} \hat{H}_{\text{eff}} \middle| n \right\rangle}{E_n \quad E_m}. \tag{2.85}$$

Finally, by substituting Eq. (2.85) into Eq. (2.83) we derive the following expression for the Berry phase:

$$\gamma_n(C) = \quad \int d\vec{S}\, \vec{V}_n\left(\vec{k}\right), \tag{2.86}$$

where

$$\vec{V}_n = \operatorname{Im} \sum_{m/n} \frac{\langle n|\vec{\nabla}_{\vec{k}} \hat{H}_{\text{eff}}\,|m\rangle \times \langle m|\vec{\nabla}_{\vec{k}} \hat{H}_{\text{eff}}|n\rangle}{(E_m \quad E_n)^2}.$$

Suppose we have two neighbouring bands described by the effective Hamiltonian

$$\hat{H}_{\text{eff}} = \frac{1}{2} \vec{R}\left(\vec{k}\right) \vec{\sigma} \tag{2.87}$$

with the eigenenergies

$$E_{\pm}\left(\vec{k}\right) = \pm \frac{1}{2} \left| R\left(\vec{k}\right) \right|. \tag{2.88}$$

We can make the following replacements of variables in the integral (2.86): $\vec{k} \to \vec{R}$, $d\vec{S} \to d\vec{S}_{\vec{R}}$ and $\vec{\nabla}_{\vec{k}} \to \vec{\nabla}_{\vec{R}}$.

After that the calculations are trivial:

$$\gamma_{\pm}(C) = \mp \int d\vec{S}_{\vec{R}}\, \vec{V}\left(\vec{R}\right), \tag{2.89}$$

where

$$\vec{V}\left(\vec{R}\right) = \frac{\vec{R}}{2R^3},$$

which is nothing other than the electric flux through the contour C created by the charge $\frac{1}{2}$ at the point $\vec{R} = 0$. The answer is obvious:

$$\gamma_{\pm}(C) = \mp \frac{1}{2} \Omega(C), \tag{2.90}$$

where $\Omega(C)$ is the solid angle of the contour (Fig. 2.1).

For the case of massless Dirac fermions $\vec{R}\left(\vec{k}\right) \sim \vec{k}$ is the two-dimensional vector (k_x, k_y), and the solid angle is 2π, so the Berry phase is

$$\gamma_{\pm} = \mp \pi, \tag{2.91}$$

in agreement with Eq. (2.74).

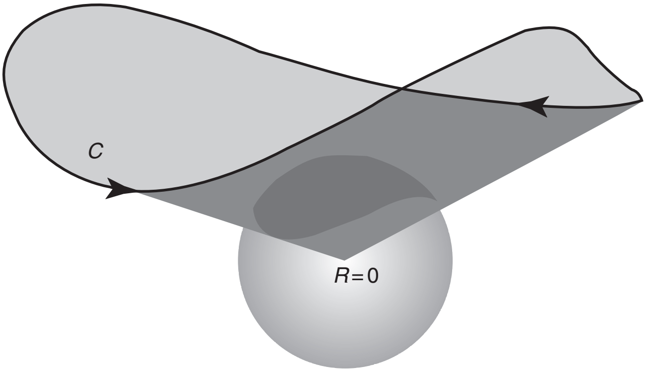

Fig. 2.1. The derivation of Berry's phase (Eq. (2.90)).

As was demonstrated by Kuratsuji & Iida (1985), the Berry phase enters the semiclassical quantization condition. Their approach was based on the path-integral formalism (Schulman, 1981). Here we will present in the simplest way just a general idea of the derivation. Instead of $\vec{k}(t)$ we will consider a general set of slowly varying with time (adiabatic) variables $\vec{x}(t)$.

Let us consider a periodic process with $x_i(\tau) = x_i(0)$. We are interested in calculating the evolution operator

$$\hat{K}(\tau) = \hat{T}\exp\left\{-\frac{i}{h}\int_0^{\tau} dt\,\hat{H}[x_i(t)]\right\}, \tag{2.92}$$

where $\hat{H}$ is the Hamiltonian dependent on $\vec{x}(t)$ and $\hat{T}$ is the time-ordering operator. To calculate the expression (2.92) via a path integral, one has to discretize the time interval, $t_n = n\varepsilon$, where $n = 0, 1, \ldots, N-1$ and $\varepsilon = T/N$ $(N \to \infty)$:

$$\hat{K}(\tau) = \mathrm{Tr}\left\{\exp\left[-\frac{i\varepsilon}{h}\hat{H}(t_0)\right]\exp\left[-\frac{i\varepsilon}{h}\hat{H}(t_1)\right]\ldots\exp\left[-\frac{i\varepsilon}{h}\hat{H}(t_{N-1})\right]\right\}. \tag{2.93}$$

In the adiabatic approximation, the evolution involves only the transitions between the same states of the Hamiltonian:

$$\hat{K}(\tau) = \sum_n \langle n(t_0)|\exp\left[-\frac{i\varepsilon}{h}\hat{H}(t_0)\right]|n(t_1)\rangle\langle n(t_1)|\exp\left[-\frac{i\varepsilon}{h}\hat{H}(t_1)\right]|n(t_2)\rangle$$
$$\ldots\langle n(t_{N-1})|\exp\left[-\frac{i\varepsilon}{h}\hat{H}(t_{N-1})\right]|n(t)\rangle. \tag{2.94}$$

At $\varepsilon \to 0$, the overlap integral

$$\begin{aligned}\left\langle n(t) \middle| n(t+\varepsilon) \right\rangle &\approx \left\langle n(t) \middle| n(t) \right\rangle + \varepsilon \frac{d\vec{x}}{dt} \left\langle n(t) \middle| \vec{\nabla}_{\vec{x}} n(t) \right\rangle \\ &= 1 + \varepsilon \frac{d\vec{x}}{dt} \left\langle n(t) \middle| \vec{\nabla}_{\vec{x}} n(t) \right\rangle \\ &\approx \exp\left[\varepsilon \frac{d\vec{x}}{dt} \left\langle n(t) \middle| \vec{\nabla}_{\vec{x}} n(t) \right\rangle \right] \end{aligned} \qquad (2.95)$$

and each term in $\langle n| \dots |n\rangle$ in Eq. (2.94), apart from the standard dynamical contribution, has an additional phase factor

$$\prod_{n\ 0}^{N\ 1} \langle n(t_n)|n(t_{n+1})\rangle = \exp\left[\int_0^{\tau} dt \frac{d\vec{x}}{dt} \left\langle n \middle| \vec{\nabla}_{\vec{x}} n \right\rangle \right] = \exp[i\gamma_n(C)] \qquad (2.96)$$

(cf. Eq. (2.81)), which leads to the change of the effective action of the system $S \to S + \hbar\gamma$. On repeating a standard derivation of the semiclassical quantization condition, one can see that $n + \frac{1}{2}$ is replaced by $n + \frac{1}{2}\quad \gamma/(2\pi)$. In particular, for Bloch electrons in a magnetic field, instead of Eq. (2.70), one has

$$S(E_n) = \frac{2\pi|e|B}{\hbar c}\left(n + \frac{1}{2}\quad \frac{\gamma}{2\pi}\right) \qquad (2.97)$$

(Mikitik & Sharlai, 1999). For $\gamma = \pi$ one has the quantization condition (2.73).

Again, we see that anomalous quantization of Landau levels for the case of graphene is related to the nontrivial topological properties of a system with a conical point in its energy spectrum.

2.5 Landau levels in bilayer graphene

Consider now the case of bilayer graphene (Novoselov *et al.*, 2006; McCann & Falko, 2006; McCann, Abergel & Falko, 2007; Falko, 2008).

Let us start with the simplest Hamiltonian (1.46), which means intermediate energies

$$\gamma_3^2 \frac{|t_\perp|}{t^2} \ll |E| \ll |t_\perp|. \qquad (2.98)$$

At lower energies (cf. Eq. (1.55)) trigonal warping terms in the Hamiltonian (1.53) become important and at higher energies all four bands (1.44) become relevant. For realistic parameters, this means energies of the order of tens of meV. Later we will consider a more general case.

On combining Eq. (1.46) with Eqs. (2.20) and (2.22) we find the Hamiltonian for the case of a uniform magnetic field:

$$\hat{H} = h\omega_{\mathrm{c}}^{*} \begin{pmatrix} 0 & \hat{b}^2 \\ (\hat{b}^{+})^2 & 0 \end{pmatrix}, \tag{2.99}$$

where

$$\omega_{\mathrm{c}}^{*} = \frac{|e|B}{m^{*}c} \tag{2.100}$$

is the cyclotron frequency for nonrelativistic electrons with effective mass m^{*}. Then, instead of Eq. (2.25) for single-layer graphene, one has the Schrödinger equation

$$\begin{aligned} \hat{b}^2 \psi_2 &= \varepsilon \psi_1, \\ \left(\hat{b}^{+}\right)^2 \psi_1 &= \varepsilon \psi_2, \end{aligned} \tag{2.101}$$

where the dimensionless energy ε is introduced now by writing

$$E = h\omega_{\mathrm{c}}^{*}\, \varepsilon. \tag{2.102}$$

Again, for the case of valley K′ one has to exchange ψ_1 and ψ_2.

First, one can see immediately from Eq. (2.102) that there are zero modes with $\varepsilon = 0$ and $\psi_2 = 0$, and their number is twice as great as for the case of a single layer. Indeed, both the states of the harmonic oscillator with $n = 0$ and those with $n = 1$ satisfy the equation $\hat{b}^2|\psi\rangle = 0$:

$$\hat{b}|0\rangle = 0, \qquad \hat{b}^2|1\rangle = \hat{b}\left(\hat{b}|1\rangle\right) = \hat{b}|0\rangle = 0. \tag{2.103}$$

On multiplying the first of the equations (2.101) by $\left(\hat{b}^{+}\right)^2$ from the left, one finds

$$\left(\hat{b}^{+}\right)^2 \hat{b}^2 \psi_1 = \varepsilon^2 \psi_1. \tag{2.104}$$

Since

$$\left(\hat{b}^{+}\right)^2 \hat{b}^2 = \left(\hat{b}^{+}\hat{b}\right)\left(\hat{b}^{+}\hat{b} - 1\right) \tag{2.105}$$

we have immediately the spectrum

$$E_{\nu} = \pm h\omega_{\mathrm{c}}^{*} \sqrt{n(n-1)} \tag{2.106}$$

with $n = 0, 1, 2, \ldots$

The counting of the degeneracy of Landau levels (2.106) can be done in exactly the same way as in Section 2.2, and one finds, instead of Eq. (2.51),

$$g_n = \frac{\Phi}{\Phi_0}, \quad n \geq 2, \tag{2.107}$$

and

$$g_0 = \frac{2\Phi}{\Phi_0} \tag{2.108}$$

(the latter follows from the fact that the zero and first levels are degenerate, Eq. (2.103)).

One can prove that Eq. (2.108) follows from the Atiyah Singer index theorem and remains correct if the magnetic field is inhomogeneous (Katsnelson & Prokhorova, 2008). This fact is quite simple and follows from the property that the index of a product of operators equals the sum of their indices. An explicit construction of zero modes for the Hamiltonian (2.99) that is similar to the Aharonov Casher construction for the case of the Dirac equation (see Section 2.3) was done by Kailasvuori (2009).

For $n \gg 1$, the spectrum (2.106) is described by the expression

$$|E_n| \approx h\omega_c^* \left(n \quad \frac{1}{2}\right), \tag{2.109}$$

in agreement with the semiclassical quantization condition

$$S(E_n) = \frac{2\pi|e|B}{hc}\left(n \quad \frac{1}{2}\right). \tag{2.110}$$

It follows from the general quantization law (2.97) assuming that the Berry phase

$$\gamma = 2\pi. \tag{2.111}$$

This is indeed the case (Novoselov *et al.*, 2006; McCann & Falko, 2006). The Hamiltonian (1.46) has the form (2.87) with

$$\left(R_x, R_y\right) \sim \left(k_x^2 \quad k_y^2, 2k_x k_y\right)$$

or

$$\left(R_x + iR_y\right) \sim \left(k_x + ik_y\right)^2. \tag{2.112}$$

It is clear, therefore, that when the vector $\vec{k}$ runs over the closed loop the vector $\vec{R}$ runs over the same loop twice, and the Berry phase should be twice as large as for the case of a single layer. Actually, the Berry phase and the index are proportional; they are both related to the winding number of the vector $\vec{R}$ in the Hamiltonian (Katsnelson & Prokhorova, 2008). For the case of a rhombohedral N-layer system (1.69) the number of zero modes is equal to $N\,\Phi/\Phi_0$ and the Berry phase is $\gamma = N\pi$.

2.6 The case of bilayer graphene: trigonal warping effects

Consider now the case of small energies,

$$|E| \sim \gamma_3^2 \frac{|t_\perp|}{t^2}. \tag{2.113}$$

Thus, the effects of trigonal warping should be taken into account, and one has to proceed with the Hamiltonian (1.53). Instead of the Hamiltonian (2.99) we have for the case of a uniform magnetic field

$$\hat{H} = h\omega_c^* \begin{pmatrix} 0 & \hat{b}^2 + \alpha\hat{b}^+ \\ (\hat{b}^+)^2 + \alpha\hat{b} & 0 \end{pmatrix}, \tag{2.114}$$

where

$$\alpha = \frac{3\gamma_3 a m^*}{h^2} \sqrt{\frac{2hc}{|e|B}} \tag{2.115}$$

is a dimensionless parameter characterizing the role of trigonal warping. The Schrödinger equation (2.101) is modified to the form

$$\begin{aligned} \left(\hat{b}^2 + \alpha\hat{b}^+\right)\psi_2 &= \varepsilon\psi_1, \\ \left((\hat{b}^+)^2 + \alpha\hat{b}\right)\psi_1 &= \varepsilon\psi_2. \end{aligned} \tag{2.116}$$

First, let us consider zero modes with $\varepsilon = 0$ and $\psi_1 = 0$. Taking into account that in dimensionless coordinates, (2.40) and (2.41),

$$\begin{aligned} \hat{b} &= i\left(\frac{\partial}{\partial X} + \frac{X}{2}\right), \\ \hat{b}^+ &= i\left(\frac{\partial}{\partial X} - \frac{X}{2}\right), \end{aligned} \tag{2.117}$$

the first of the equations (2.116) for $\varepsilon = 0$ reads

$$\frac{d^2\psi_2}{dX^2} + (X + i\alpha)\frac{d\psi_2}{dX} + \left(\frac{1}{2} + \frac{X^2}{4} - \frac{iX\alpha}{2}\right)\psi_2 = 0. \tag{2.118}$$

The substitution

$$\psi_2(X) = \exp\left(-\frac{X^2}{4} - \frac{i\alpha}{2}X\right)\varphi(X) \tag{2.119}$$

eliminates the first derivative $\partial/\partial X$ in Eq. (2.118), so

$$\frac{\partial^2}{\partial X^2}\varphi + \left(\frac{\alpha^2}{4} - iX\alpha\right)\varphi = 0. \tag{2.120}$$

At $\alpha = 0$ there are two independent solutions of Eq. (2.120), $\varphi_0 = 1$ and $\varphi_1 = X$. For finite α there are still two solutions, and they can be expressed in terms of Bessel functions of order $\pm\frac{1}{3}$ (Whittaker & Watson, 1927). Anyway, both of the solutions (2.119) vanish at $X \to \pm\infty$ due to the factor $\exp(-X^2/4)$ and, therefore, the number of zero modes remains the same at $\alpha \neq 0$. Obviously, the second of the equations (2.116) has no normalizable solutions at $\varepsilon = 0$. These results are not surprising; they are related to a general statement that index(H) is determined solely by the terms with the highest order of derivatives (Katsnelson & Prokhorova, 2008).

To consider the effects of the trigonal warping on other Landau levels one has to square the Hamiltonian (2.114) or just act by the operator $\left((\hat{b}^+)^2 + \alpha\hat{b}\right)$ from the left on the first equation of Eq. (2.116). The result is

$$\hat{L}\psi_2 = \varepsilon^2\psi_2, \tag{2.121}$$

where

$$\hat{L} = \left(\hat{b}^+\hat{b}\right)^2 - \left(1 - \alpha^2\right)\hat{b}^+\hat{b} + \alpha\left(\hat{b}^3 + (\hat{b}^+)^3\right).$$

Using a standard perturbation theory in α one can find a strange result: only the level with $n = 2$ has corrections of the order of α^2,

$$\varepsilon_2{}^2 = 2 - \frac{\alpha^2}{3}, \tag{2.122}$$

whereas the leading corrections to the levels with $n > 2$ are proportional to α^4 and positive.

To understand qualitatively the opposite case of a very large α (or very weak magnetic fields), it is convenient to use the semiclassical approximation (Dresselhaus, 1974). In this regime, one can consider energy levels belonging independently to each of four cones of the spectrum (see Fig. 1.9). The energy level with $n = 2$ tends to zero at $\alpha \to \infty$ since one more zero mode should appear for three independent (in this limit) side cones: the zero mode corresponding to the central cone is associated (for a given direction of the magnetic field) with another valley.

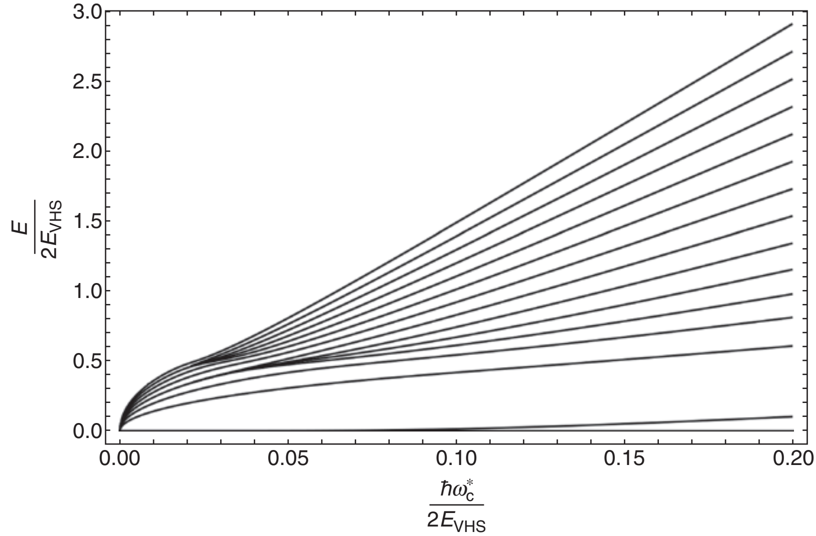

Fig. 2.2. The energy spectrum for bilayer graphene in a magnetic field, with the trigonal warping effects taken into account. Here $h\omega_c^*$ is the cyclotron quantum and E_{VHS} is the energy of the Van Hove singularity at the merging of four conical legs.

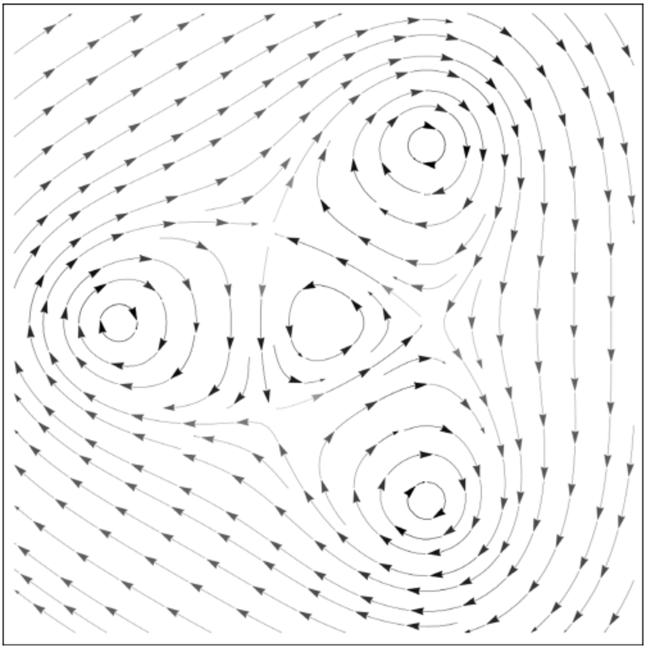

Fig. 2.3. The distribution of the Berry vector potential in bilayer graphene, with the trigonal warping effects taken into account.

For intermediate α the equations (2.116) can be solved numerically (McCann & Falko, 2006; Mayorov *et al.*, 2011). The results are shown in Fig. 2.2.

Finally, we analyse the effects of trigonal warping on the Berry phase. One can demonstrate by a straightforward calculation (Mikitik & Sharlai, 2008) that each of the three side conical points contributes π to the Berry phase and the central one contributes $-\pi$, so the total Berry phase is $3\pi - \pi = 2\pi$, in agreement with Eq. (2.111). One can also see straightforwardly that the winding number of the transformation

$$\left(R_x + iR_y\right) \sim \left(k_x + ik_y\right)^2 + \alpha\left(k_x - ik_y\right) \tag{2.123}$$

is the same (two) as for Eq. (2.112).

The distribution of the Berry 'vector potential' $\vec{\Omega}\left(\vec{k}\right) = -i\langle n|\vec{\nabla}_{\vec{k}}|n\rangle$ demonstrating singularities at four conical points is shown in Fig. 2.3.

2.7 A unified description of single-layer and bilayer graphene

Consider now the case of magnetic fields large enough that

$$|E| \geq |t_\perp|. \tag{2.124}$$

At these energies, a parabolic dispersion transforms to a conical one. Neglecting the trigonal warping and using Eqs. (2.20) and (1.43), one has the 4 × 4 Hamiltonian

$$\hat{H} = \begin{pmatrix} 0 & v\hat{\pi}_+ & t_\perp & 0 \\ v\hat{\pi}_- & 0 & 0 & 0 \\ t_\perp & 0 & 0 & v\hat{\pi}_- \\ 0 & 0 & v\hat{\pi}_+ & 0 \end{pmatrix}. \tag{2.125}$$

Using the operator (2.22) and dimensionless units (2.26) and introducing the notation

$$t_\perp = \Gamma\sqrt{\frac{2|e|hBv^2}{c}}, \tag{2.126}$$

one can represent the Schrödinger equation with the Hamiltonian (2.125) as

$$\begin{aligned} \hat{b}\psi_2 + \Gamma\psi_3 &= \varepsilon\psi_1, \\ \hat{b}^+\psi_1 &= \varepsilon\psi_2, \\ \Gamma\psi_1 + \hat{b}^+\psi_4 &= \varepsilon\psi_3, \\ \hat{b}\psi_3 &= \varepsilon\psi_4. \end{aligned} \tag{2.127}$$

On excluding ψ_4 and ψ_2 from Eqs. (2.127), one obtains

$$\begin{aligned}
&\frac{1}{\varepsilon}\hat{b}\hat{b}^{+}\psi_1 + \Gamma\psi_3 = \varepsilon\psi_1,\\
&\Gamma\psi_1 + \frac{1}{\varepsilon}\hat{b}^{+}\hat{b}\psi_3 = \varepsilon\psi_3.
\end{aligned} \tag{2.128}$$

One can see that ψ_i are eigenfunctions of the operator $\hat{n} = \hat{b}^{+}\hat{b}$ whose eigenstates are $n = 0, 1, 2, \ldots$ On replacing $\hat{b}^{+}\hat{b}$ by n and $\hat{b}\hat{b}^{+}$ by $n + 1$ in Eq. (2.128) we find the eigenenergies ε_n as

$$\varepsilon_n^2 = \frac{\Gamma^2 + 2n + 1}{2} \pm \sqrt{\left(\frac{\Gamma^2 + 2n + 1}{2}\right)^2 \quad n(n+1)}. \tag{2.129}$$

This formula (Pereira, Peeters & Vasilopoulos, 2007) gives a unified description of Landau levels for the cases both of single-layer and of bilayer graphene (without trigonal warping effects). On putting $\Gamma = 0$ we come to the case of two independent layers, with

$$\varepsilon_n^2 = n + \frac{1}{2} \pm \frac{1}{2}, \tag{2.130}$$

which exactly coincides with Eq. (2.34). For large Γ (the case of relatively low energies, Eq. (2.98)) we have

$$\varepsilon_{n1}^2 = \frac{n(n+1)}{\Gamma^2} \tag{2.131}$$

and

$$\varepsilon_{n2}^2 = \Gamma^2 + 2n + 1. \tag{2.132}$$

Equation (2.131) gives the Landau levels for low-lying bands in the parabolic approximation (1.46). The energies

$$\varepsilon_{n2} \approx \pm\left[\Gamma + \frac{1}{\Gamma}\left(n + \frac{1}{2}\right)\right] \tag{2.133}$$

following from Eq. (2.132) are nothing other than the Landau levels for two-gapped bands in the parabolic approximation.

The condition $\Gamma \approx 1$ for which nonparabolic band effects in the Landau-level spectrum of bilayer graphene become very important corresponds to magnetic fields of the order of

$$B_c \approx \frac{2}{9}\left(\frac{t_\perp}{t}\right)^2 \frac{hc}{|e|a^2} \approx 70\,\mathrm{T},$$

which is too high to be attained in present-day experiments. However, even in fields of 20 30 T the effects of nonparabolicity should be quite noticeable.

2.8 Magnetic oscillations in single-layer graphene

Magneto-oscillation effects in quantized magnetic fields make possible one of the most efficient ways to probe the electron-energy spectra of metals and semiconductors (Schoenberg, 1984). The basis idea of the oscillations is quite simple: since most of the properties are dependent on what happens in the close vicinity of the Fermi level, whenever, on changing the magnetic induction or chemical potential μ, one of the Landau levels coincides with the Fermi energy, the properties should have some anomalies that repeat periodically as a function of the inverse magnetic field (the latter follows from the semiclassical quantization condition (2.97), $\Delta n \sim (1/B)\Delta E$). These anomalies are smeared by temperature and disorder so, to observe the oscillations, one needs, generally speaking, low temperatures and clean enough samples. It was the observation of magneto-oscillation effects (Novoselov *et al.*, 2005a; Zhang *et al.*, 2005) which demonstrated the massless Dirac behaviour of charge carriers in graphene. Experimentally, oscillations of the conductivity (the Shubnikov de Haas effect) were studied first; it is more difficult (but quite possible, see later in this section) to observe the oscillations of thermodynamic properties, e.g., magnetization (the de Haas van Alphen effect) in a single layer of atoms. However, physics of these two effects is just the same, but theoretical treatment of thermodynamic properties can be done in a more clear and rigorous way. Here we will consider, following Sharapov, Gusynin & Beck (2004), de Haas van Alphen magnetic oscillations for two-dimensional Dirac fermions, i.e., for single-layer graphene.

The standard expression for the thermodynamic potential of the grand canonical ensemble for noninteracting fermions with energies E_λ is (Landau & Lifshitz, 1980)

$$\Omega = -T\sum_{\lambda}\left[1+\exp\left(\frac{\mu - E_\lambda}{T}\right)\right] = -T\int_{\infty}^{\infty} d\varepsilon\, N(\varepsilon)\ln\left[1+\exp\left(\frac{\mu-\varepsilon}{T}\right)\right], \quad (2.134)$$

where

$$N(\varepsilon) = \sum_{\lambda}\delta(\varepsilon \quad E_\lambda) \quad (2.135)$$

is the density of states. However, one should be careful at this point since statistical mechanics assumes that the energy spectrum is bounded from below, which is not the case for the Dirac equation. One can either use a complete tight-binding Hamiltonian, where the spectrum is bound, and analyse carefully the limit of the continuum model, or just write the answer from considerations of relativistic invariance (Cangemi & Dunne, 1996). The correct relativistic answer is

$$\Omega = \quad T\int_{\infty}^{\infty} d\varepsilon\, N(\varepsilon)\ln\left[2\cosh\left(\frac{\varepsilon \quad \mu}{2T}\right)\right], \tag{2.136}$$

which differs from Eq. (2.134) by the term

$$\Delta\Omega = \frac{1}{2}\int_{\infty}^{\infty} d\varepsilon\, N(\varepsilon)(\varepsilon \quad \mu). \tag{2.137}$$

This term is, in general, infinite and temperature-independent. If the spectrum is symmetric, namely $N(\quad\varepsilon) = N(\varepsilon)$ (which is necessary for relativistic invariant theories), and the chemical potential is chosen in such a way that $\mu = 0$ for the half-filled case (all hole states are occupied and all electron states are empty), then the correction (2.137) vanishes in that situation.

The expression (2.136) is still not well defined, but its derivatives with respect to μ, temperature and magnetic field are convergent. For example, the compressibility is proportional to the 'thermodynamic density of states'

$$D(\mu) = \frac{\partial n}{\partial \mu} = \quad \frac{\partial^2 \Omega}{\partial \mu^2} = \int_{\infty}^{\infty} d\varepsilon\, N(\varepsilon)\left(\quad \frac{\partial f(\varepsilon)}{\partial \varepsilon}\right), \tag{2.138}$$

where $f(\varepsilon)$ is the Fermi function,

$$\frac{\partial f(\varepsilon)}{\partial \varepsilon} = \frac{1}{4T\cosh^2\left(\frac{\varepsilon \quad \mu}{2T}\right)}, \tag{2.139}$$

and this expression is certainly well defined, with the difference between Eqs. (2.134) and (2.136) becoming irrelevant. The quantity (2.138) is directly measurable as the *quantum capacitance* (John, Castro & Pulfrey, 2004); for the case of graphene, see Ponomarenko *et al.* (2010).

At zero temperature, the expression (2.138) is just a sum of delta-functional contributions:

$$D_{T\quad 0}(\mu) = 4\frac{\Phi}{\Phi_0}\left[\delta(E) + \sum_{\nu \quad 1}^{\infty} \delta\left(E \quad h\omega_c\sqrt{\nu}\right) + \delta\left(E + h\omega_c\sqrt{\nu}\right)\right] \tag{2.140}$$

(see Eqs. (2.30), (2.31) and (2.51); we have taken into account a factor of 4 due to the valley and spin degeneracy). Using the identities

$$\delta(E - x) + \delta(E + x) = 2|E|\delta\left(E^2 - x^2\right), \tag{2.141}$$

$$\delta(E) = \frac{d\Theta(E)}{dE} \tag{2.142}$$

($\Theta(x > 0) = 1$, $\Theta(x < 0) = 0$ is the step function) and

$$\sum_{n=1}^{\infty}\Theta(a - xn) = \Theta(a)\left[-\frac{1}{2} + \frac{a}{x} + \sum_{k=1}^{\infty}\frac{\sin\left(2\pi k\frac{a}{x}\right)}{\pi k}\right], \tag{2.143}$$

one can find the closed expression

$$D_{T=0}(\mu) = 4\frac{\Phi}{\Phi_0}\,\mathrm{sgn}(\mu)\frac{d}{d\mu}\left\{\frac{\mu^2}{\varepsilon_c^2} + \frac{1}{\pi}\tan^{-1}\left[\cot\left(\frac{2\pi\mu^2}{\varepsilon_c^2}\right)\right]\right\}, \tag{2.144}$$

where $\varepsilon_c = h\omega_c$ (Sharapov, Gusynin & Beck, 2004). Equation (2.143) is the partial case of the Poisson summation formula

$$\sum_{n=-\infty}^{\infty}\delta(x - n) = \sum_{k=-\infty}^{\infty}\exp(2\pi ikx) \tag{2.145}$$

and, thus,

$$\sum_{n=1}^{\infty} f(n) = \sum_{k=-\infty}^{\infty}\int_{a}^{\infty} dx f(x)\exp(2\pi ikx) \tag{2.146}$$

($0 < a < 1$) for any $f(x)$, and the identity

$$\sum_{n=1}^{\infty}\frac{\sin(\pi nx)}{n} = \tan^{-1}\left(\frac{\sin(\pi x)}{1 - \cos(\pi x)}\right) \tag{2.147}$$

is used when deriving (2.144).

To consider the case of finite temperatures, it is convenient to use the expansion of $-\partial f(E)/\partial E$ into the Fourier integral:

$$-\frac{\partial f(E)}{\partial E} = \int_{-\infty}^{\infty}\frac{dt}{2\pi}\exp[i(\mu - E)t]R(t), \tag{2.148}$$

where

$$R(t) = \frac{\pi T t}{\sinh[(\pi T t)]}. \tag{2.149}$$

On substituting Eq. (2.148), together with Eqs. (2.141) and (2.142), into the definition (2.138) one finds

$$D(\mu) = 4\frac{\Phi}{\pi\Phi_0}\iint dE\,dt\,R(t)\exp[i(\mu - E)t]|E|\left[\frac{1}{\varepsilon_c^2} + \frac{2}{\varepsilon_c^2}\sum_{k=1}^{\infty}\cos\left(2\pi k\frac{E^2}{\varepsilon_c^2}\right)\right]. \tag{2.150}$$

The sum over k describes oscillations of the thermodynamic density of states. To proceed further, one can use the saddle-point method (or 'the method of steepest descent') for integrals of strongly oscillating functions (Fedoryuk, 1977). The procedure is the following. If we have a multidimensional integral

$$I(\lambda\ ) = \int d^n x f(x)\exp(i\lambda\Phi(x)) \tag{2.151}$$

with a large parameter λ, then the main contribution follows from the stationary point x_0 of the phase $\Phi(x)$, where

$$\frac{\partial\Phi}{\partial x_k} = 0, \tag{2.152}$$

since the oscillations are weakest in the vicinity of these points. On expanding $\Phi(x)$ near x_0,

$$\Phi(x) \approx \Phi(x_0) + \frac{1}{2}\sum_{kl}\left(\frac{\partial^2\Phi}{\partial x_k\,\partial x_l}\right)_0 (x_k \quad x_{k_0})(x_l \quad x_{l_0}), \tag{2.153}$$

one finds

$$I(\lambda) \approx f(x_0)\frac{(2\pi)^{n/2}}{\prod_k(\quad i\mu_k)^{1/2}}\exp[i\lambda\Phi(x_0)], \tag{2.154}$$

where μ_k are eigenvalues of the matrix

$$\left(\frac{\partial^2\Phi}{\partial x_k\,\partial x_l}\right).$$

If there is more than one stationary point their contributions are just summed up.

The oscillating part of the expression (2.150) can be estimated by this method, choosing

$$\Phi(E,t) = (\mu - E)t \pm \frac{2\pi k E^2}{\varepsilon_c^2}, \tag{2.155}$$

which gives us immediately

$$\begin{aligned} E_0 &= \mu, \\ t_0 &= \mp \frac{4\pi k \mu}{\varepsilon_c^2}. \end{aligned} \tag{2.156}$$

Finally, one obtains

$$D_{\text{osc}}(\mu) \approx \frac{8A|\mu|}{\pi h^2 v^2} \sum_{k=1}^{\infty} \frac{zk}{\sinh(zk)} \cos\left(\frac{\pi k c \mu^2}{h|e|Bv^2}\right), \tag{2.157}$$

where

$$z = \frac{2\pi^2 Tc|\mu|}{h|e|Bv^2} \tag{2.158}$$

and A is the sample area. A formal condition of applicability of the saddle-point method is that the resulting oscillations are fast enough; that is, the argument of the cosine in Eq. (2.157) is much larger than 1.

Disorder will broaden Landau levels and smear the delta-functional peaks in the density of states suppressing the oscillations. This effect too can be taken into account (Sharapov, Gusynin & Beck, 2004; Ponomarenko *et al.*, 2010).

A general semiclassical consideration for an arbitrary energy dispersion law (the Lifshitz–Kosevich theory; see Lifshitz, Azbel & Kaganov (1973) and Abrikosov (1988)) leads to a similar temperature dependence of the oscillations, with

$$z = \frac{2\pi^2 Tcm^*}{h|e|B}, \tag{2.159}$$

where

$$m^* = \frac{1}{2\pi} \frac{\partial S(E)}{\partial E}\bigg|_{E=\mu} \tag{2.160}$$

is the effective cyclotron mass. For the massless Dirac fermions

$$m^* = \frac{|\mu|}{v^2}, \tag{2.161}$$

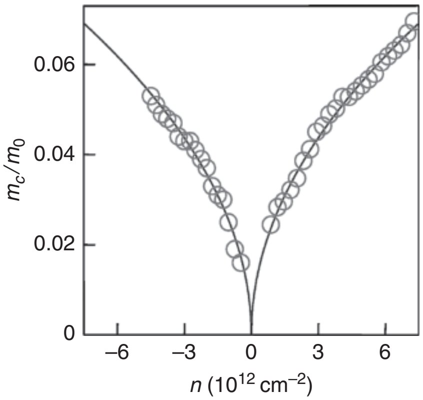

Fig. 2.4. The concentration dependence of the cyclotron mass for charge carriers in single-layer graphene; m_0 is the free-electron mass (reproduced with permission from Novoselov *et al.*, 2005a).

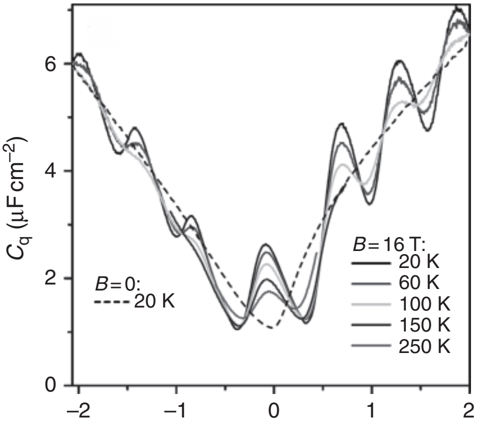

Fig. 2.5. Magnetic oscillations of the quantum capacitance (thermodynamic density of states) as a function of the gate voltage (which is proportional to the charge carrier concentration), for the magnetic field $B = 16$ T and various temperatures (reproduced with permission from Ponomarenko *et al.*, 2010).

which is nothing other than the famous Einstein relation $E = mc^2$ with a replacement of c by v. For two-dimensional systems, $S = \pi k_F^2 \propto n$, where n is the charge-carrier concentration, and, thus, for massless Dirac fermions one can expect

$$m^* \sim \sqrt{n}. \tag{2.162}$$

The experimental observation of this dependence (Novoselov *et al.*, 2005a; Zhang *et al.*, 2005) was the first demonstration of the reality of massless Dirac fermions in graphene (see Fig. 2.4). This gives us also a value

$v \approx 10^6\,\mathrm{m\,s}^{\ 1} \approx c/300$. Note that what was measured experimentally in these works was the conductivity, not $D(\mu)$, but the temperature dependence should be the same. Oscillations of $D(\mu)$ were measured later via quantum capacitance (Ponomarenko *et al.*, 2010). They are well pronounced even at room temperature (see Fig. 2.5); their broadening is determined by disorder effects.

2.9 The anomalous quantum Hall effect in single-layer and bilayer graphene

The anomalous character of the quantum Hall effect in single-layer (Novoselov *et al.*, 2005a; Zhang *et al.*, 2005) and bilayer (Novoselov *et al.*, 2006) graphene is probably the most striking demonstration of the unusual nature of the charge carriers therein. We do not need to present here a real introduction to the theory of the quantum Hall effect in general (see Prange & Girvin, 1987). However, it would seem useful to provide some basic information, to emphasise the relation to the Berry phase and the existence of topologically protected zero modes.

If we consider the motion of electrons in the crossed magnetic ($\vec{B}$) and electric ($\vec{E}$) fields, the Lorentz force acting on an electron moving with a velocity $\vec{v}$ is

$$\vec{F} = e\left(\vec{E} + \frac{1}{c}\vec{v} \times \vec{B}\right). \tag{2.163}$$

In the crossed fields, $\vec{B}||Oz$ and $\vec{E}||Oy$, this will result in a steady drift of the electrons along the x-axis with a velocity of

$$v_x = c\frac{E}{B}. \tag{2.164}$$

This effect results in the appearance of an off-diagonal (Hall) conductivity proportional to the total electron concentration and inversely proportional to the magnetic field:

$$\sigma_{xy} = \frac{nec}{B}. \tag{2.165}$$

The standard theory of the quantum Hall effect assumes that all the states between Landau levels are localized due to disorder (Anderson localization), see Fig. 2.6. This means that, if the Fermi energy lies between the Landau levels, then only the states belonging to the occupied Landau levels contribute to transport and the Hall conductivity is merely proportional to the number of occupied levels N:

$$\sigma_{xy} = N g_s g_v \frac{\Phi}{\Phi_0}\frac{1}{A}\frac{nec}{B} = g_s g_v N \frac{e^2}{h}, \tag{2.166}$$

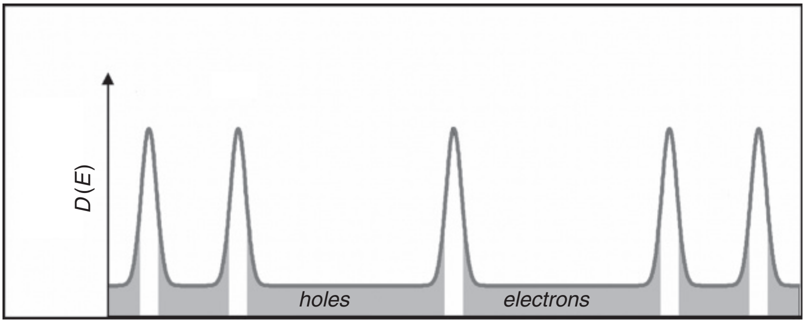

Fig. 2.6. A sketch of the density of states under quantum-Hall-effect conditions in graphene. The zero-energy Landau level separates electron and hole states and is equally shared by electrons and holes. Regions of localized and extended states are shown in grey and white, respectively.

where g_s and g_v are the spin and valley degeneracy factors (for graphene $g_s = g_v = 2$) and we take into account Eq. (2.51) for the number of states per Landau level. Thus, the Hall conductivity should have plateaux as a function of the electron concentration: it remains constant and integer (in the units of e^2/h per valley per spin) when we pass from one occupied Landau level to the next one.

However, in the case of graphene the zero-energy Landau level is equally shared by electrons and holes. This means that when counting only electrons ($\mu > 0$) or only holes ($\mu < 0$) it contains half as many states as do all other Landau levels. Thus, instead of Eq. (2.166), one has

$$\sigma_{xy} = g_s g_v \left(N + \frac{1}{2} \right) \frac{e^2}{h} \tag{2.167}$$

(Novoselov *et al.*, 2005a; Zhang *et al.*, 2005; Schakel, 1991; Gusynin & Sharapov, 2005; Castro Neto, Guinea & Peres, 2006). This is exactly the behaviour observed experimentally (the *half-integer quantum Hall effect*). For the case of bilayer graphene, the zero-energy level contains twice as many states as for single-layer graphene, and the quantum Hall effect is integer, but, in contrast with the case of a conventional electron gas, there is no plateau at zero Fermi energy (Novoselov *et al.*, 2006). These two cases are shown in Fig. 2.7. Thus, the anomalous quantum Hall effect in graphene is related to the existence of zero-energy modes and, thus, to the Atiyah Singer theorem.

Further understanding of geometrical and topological aspects of the anomalies can be attained within an approach developed by Thouless *et al.* (1982); see also Kohmoto (1985, 1989). The main observation is that the Hall conductivity can be represented in a form very similar to that for the Berry

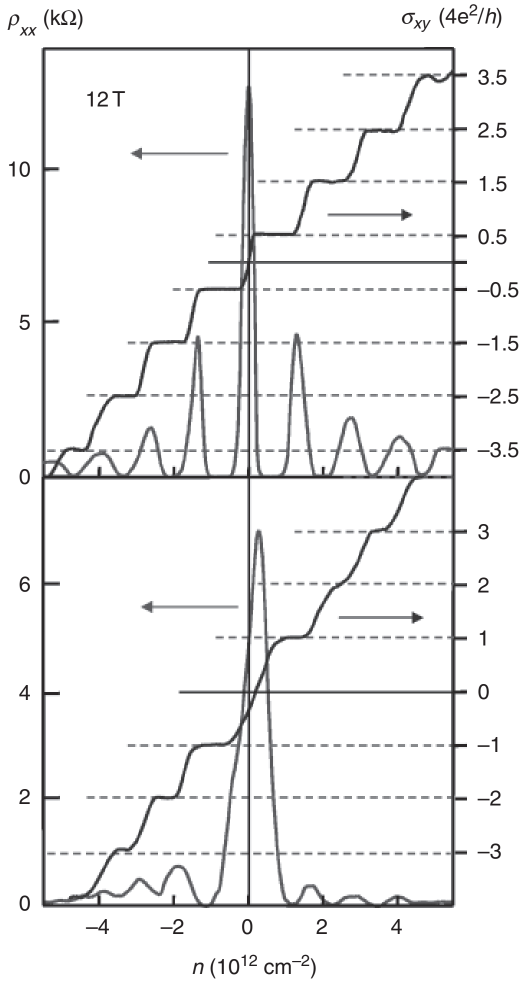

Fig. 2.7. The resistivity and Hall conductivity as functions of the charge-carrier concentration in single-layer (top) and bilayer (bottom) graphene (reproduced with permission from Novoselov *et al.*, 2005a (top) and Novoselov, 2006 (bottom)).

phase. Actually, the work by Thouless *et al.* (1982) was done before that by Berry (1984); the relation under discussion has been emphasized by Simon (1983).

Let us consider, again, a general two-dimensional electron system in a periodic potential plus uniform magnetic field (Section 2.1). One can prove that, if the flux per elementary cell is rational (in units of the flux quantum), the eigenstates of this problem can be rigorously characterized by the wave vector $\vec{k}$ and considered as Bloch states in some supercell (for a formal discussion, see Kohmoto, 1985). We will label them as $|\lambda\rangle = \left|n, \vec{k}\right\rangle$, where n is the band index.

We will use a linear response theory leading to a so-called Kubo formula (Kubo, 1957). The Hall effect was first considered in this way by Kubo, Hasegawa & Hashitsume (1959); for a detailed derivation and discussions, see Ishihara (1971) and Zubarev (1974). For the single-electron case it can be essentially simplified.

Let A be a one-electron operator that can be represented in a secondary quantized form as

$$\hat{A} = \sum_{12} A_{12} \hat{c}_1^+ \hat{c}_2 \tag{2.168}$$

(the numerical indices will label here electron states in some basis; $\hat{c}_i^+$ and $\hat{c}_i$ are fermionic creation and annihilation operators). Thus, its average over an arbitrary state is

$$\langle \hat{A} \rangle = \sum_{12} A_{12} \langle \hat{c}_1^+ \hat{c}_2 \rangle = T_2\left(\hat{A}\hat{\rho}\right), \tag{2.169}$$

where

$$\rho_{21} = \langle \hat{c}_1^+ \hat{c}_2 \rangle \tag{2.170}$$

is the single-electron density matrix. For noninteracting electrons, the Hamiltonian of the system has the same form:

$$\hat{H} = \sum_{12} H_{12} \hat{c}_1^+ \hat{c}_2, \tag{2.171}$$

and, using the commutation relation

$$\left[\hat{c}_1^+ \hat{c}_2, \hat{c}_3^+ \hat{c}_4\right] = \delta_{23} \hat{c}_1^+ \hat{c}_4 \quad \delta_{14} \hat{c}_3^+ \hat{c}_2, \tag{2.172}$$

one can prove that the density matrix $\hat{\rho}$ satisfies the communication relations

$$ih \frac{\partial \hat{\rho}}{\partial t} = \left[\hat{H}, \hat{\rho}\right], \tag{2.173}$$

where the matrix multiplication is performed in the single-particle space, e.g.,

$$\left(\hat{H}\hat{\rho}\right)_{12} = \sum_{3} H_{13} \rho_{32}. \tag{2.174}$$

Let $\hat{H}(t) = \hat{H}_0 + \hat{V}(t)$, where $\hat{H}_0$ is diagonal (E_i are its eigenenergies) and $\hat{V}(t)$ is a small perturbation depending on time as $\exp(\quad i\omega t + \delta t)|_{\delta \to +0}$. Then, the correction to the density matrix, $\hat{\rho}' \exp(\quad i\omega t + \delta t)$, is given by the expression (see Vonsovsky & Katsnelson, 1989)

$$\rho'_{12} = \frac{f_1 \quad f_2}{E_2 \quad E_1 + h(\omega + i\delta)} V_{12}, \tag{2.175}$$

where $f_i = f(E_i)$ is the Fermi function and the perturbation of an observable A is $\delta A \exp(\quad i\omega t + \delta t)$, where

$$\delta A = \mathrm{Tr}\left(\hat{A}\hat{\rho}'\right) = \sum_{12} \frac{f_1 \quad f_2}{E_2 \quad E_1 + h(\omega + i\delta)} V_{12} A_{21}. \tag{2.176}$$

To calculate the Hall conductivity one has to consider a perturbation

$$V = \quad e\vec{r}\vec{E}, \tag{2.177}$$

where $\vec{E}$ is the electric field, the coordinate operator is

$$\vec{r} = i\,\vec{\nabla}_{\vec{k}} \tag{2.178}$$

(see Vonsovsky & Katsnelson, 1989) and the current operator is

$$\hat{\vec{j}} = e\frac{d\hat{\vec{r}}}{dt} = \frac{ie}{h}\left[\hat{H}, \hat{\vec{r}}\right]. \tag{2.179}$$

Using the identity (2.84) and restricting ourselves to the static case only ($\omega = \eta = 0$), one finds, for the case $T = 0$,

$$\sigma_{\mathrm{H}} = \frac{2e^2}{Ah} \mathrm{Im} \int \frac{d\vec{k}}{(2\pi)^2} \sum_{E_m < \mu} \sum_{E_n > \mu} \frac{\langle m|\partial H/\partial k_x|n\rangle\langle n|\partial H/\partial k_y|m\rangle}{(E_n \quad E_m)^2}, \tag{2.180}$$

where the integral is taken over the Brillouin zone of the magnetic supercell. This is exactly the same expression as in Eq. (2.86), and, thus, as in Eq. (2.82). Using Stokes' theorem one can represent Eq. (2.180) as a contour integral over the boundary of the Brillouin zone:

$$\sigma_{\mathrm{H}} = \frac{e^2}{2\pi h} \mathrm{Im} \sum_n^{occ} \oint d\vec{k} \langle n|\vec{\nabla}_{\vec{k}}|n\rangle, \tag{2.181}$$

where the sum is taken over all occupied bands. The contour integral gives us the change of the phase of the state $|n\rangle$ when rotating by 2π in $\vec{k}$-space. If all the states are topologically trivial (i.e., there is no Berry phase) all these changes should be integer (in the units of 2π), and, thus, Eq. (2.181) gives us the quantization of the Hall conductivity (2.166). In the case of graphene, the Berry phase π should be added, which changes the quantization condition to Eq. (2.167).

The real situation is more complicated since the consideration by Thouless *et al.* (1982) does not take into account disorder effects, in particular, Anderson localization, which are actually crucial for a proper understanding of the quantum Hall effect. A more complete mathematical theory requires the use of noncommutative geometry (Bellissard, van Elst & Schulz-Balders, 1994) and is too complicated to review here. Keeping in mind the case of graphene, it was demonstrated by Ostrovsky, Gornyi & Mirlin (2008) that, actually, the quantum Hall effect can be either anomalous (half-integer) or normal (integer) depending on the type of disorder. Short-range scatterers induce a strong mixture of the states from different valleys and restore the ordinary (integer) quantum Hall effect. Of course, this is beyond the 'Dirac' physics which is valid assuming that the valleys are essentially independent.

The cyclotron quantum (2.31) in graphene is much higher than in most semiconductors. The energy gap between the Landau levels with $n=0$ and $n=1$ is $\Delta E \approx 2800$ K for the largest currently available permanent magnetic fields, $B=45$ T ($\Delta E \approx 1800$ K for $B=20$ T). This makes graphene a unique system exhibiting the quantum Hall effect at room temperature (Novoselov *et al.*, 2007).

Here we discuss only the background to quantum Hall physics in graphene. The real situation is much more complicated, both theoretically (involving the role of disorder and electron electron interactions) and experimentally (Zhang *et al.*, 2006; Jiang *et al.*, 2007b; Giesbers *et al.*, 2007; Checkelsky, Li & Ong, 2008; Giesbers *et al.*, 2009). In particular, at high enough magnetic fields the spin and, probably, valley degeneracies are destroyed and additional plateaux appear, in addition to the fact that the gap opens at $n=0$. The nature of these phenomena is still controversial. Last, but not least, the fractional quantum Hall effect has been observed for freely suspended graphene samples (Du *et al.*, 2009; Bolotin *et al.*, 2009). This is an essentially many-body phenomenon (Prange & Girvin, 1987). We will come back to the physics of the quantum Hall effect in graphene many times in this book.

2.10 Effects of smooth disorder and an external electric field on the Landau levels

In reality, all Landau levels are broadened due to disorder. If the latter can be described by a scalar potential $V(x, y)$ that is smooth and weak enough the result will be just a modulation of the Landau levels by this potential,

$$E_\nu(x, y) \approx E_\nu + V(x, y) \tag{2.182}$$

(Prange & Girvin, 1987). The weakness means that

$$|V(x, y)| \ll h\omega_c \tag{2.183}$$

and the smoothness means that a typical spatial scale of $V(x,y)$ is large in comparison with the magnetic length (2.1). The calculations for the case of graphene are especially simple and transparent if one assumes a one-dimensional modulation, such that V is dependent only on the y-coordinate (Katsnelson & Novoselov, 2007). Thus, instead of Eq. (2.37) one has

$$\begin{aligned}
\left(\frac{\partial}{\partial x} - \frac{x}{l_B^2} - i\frac{\partial}{\partial y}\right)\psi_2 &= \frac{iE}{hv}\psi_1 - \frac{iV(y)}{hv}\psi_1, \\
\left(\frac{\partial}{\partial x} + \frac{x}{l_B^2} + i\frac{\partial}{\partial y}\right)\psi_1 &= \frac{iE}{hv}\psi_2 - \frac{iV(y)}{hv}\psi_2.
\end{aligned} \tag{2.184}$$

We can try the solutions of Eq. (2.184) as an expansion in the basis of the solutions (2.45) of the unperturbed problem ($V=0$):

$$\psi_i(x,y) = \sum_{n=0}^{\infty} \int_{-\infty}^{\infty} \frac{dk_y}{2\pi} c_n^{(i)}(k_y) \exp(ik_y y) A_n D_n\left(\frac{\sqrt{2}(x - l_B^2 k_y)}{l_B}\right), \tag{2.185}$$

where A_n is the normalization factor (the basis functions are supposed to be normalized with respect to unity).

After straightforward calculations, one obtains a set of equations for the expansion coefficients $c_n^{(i)}(k_y)$:

$$\begin{aligned}
-\frac{\sqrt{2}}{l_B}(1-\delta_{n,0})c_n^{(2)}(k_y) &= \frac{iE}{hv}c_n^{(1)}(k_y) - \frac{i}{hv}\sum_{n'=0}^{\infty}\int_{-\infty}^{\infty}\frac{dq_y}{2\pi}v(k_y-q_y)c_{n'}^{(1)}(q_y)\langle n,k_y|n',q_y\rangle, \\
\frac{\sqrt{2}}{l_B}(1+n)c_n^{(1)}(k_y) &= \frac{iE}{hv}c_n^{(2)}(k_y) - \frac{i}{hv}\sum_{n'=0}^{\infty}\int_{-\infty}^{\infty}\frac{dq_y}{2\pi}v(k_y-q_y)c_{n'}^{(2)}(q_y)\langle n,k_y|n',q_y\rangle,
\end{aligned} \tag{2.186}$$

where $v(q)$ is a Fourier component of $V(y)$,

$$\langle n,k_y|n',q_y\rangle = A_n A_{n'} \int_{-\infty}^{\infty} dx\, D_n\left(\frac{\sqrt{2}(x-l_B^2 k_y)}{l_B}\right) D_{n'}\left(\frac{\sqrt{2}(x-l_B^2 q_y)}{l_B}\right). \tag{2.187}$$

If the potential is smooth and weak enough, one can use the adiabatic approximation and neglect the terms with $n' \neq n$ in Eq. (2.186) describing transitions between the Landau levels. Then,

$$\begin{aligned}(1-\delta_{n,0})\tilde{c}_n^{(2)}(k_y) &= i\varepsilon c_n^{(1)}(k_y) - i\int_{-\infty}^{\infty}\frac{dq_y}{2\pi}v(k_y-q_y)\langle n,k_y|n,q_y\rangle c_n^{(1)}(q_y),\\ nc_n^{(1)}(k_y) &= i\varepsilon\tilde{c}_n^{(2)}(k_y) - i\int_{-\infty}^{\infty}\frac{dq_y}{2\pi}v(k_y-q_y)\langle n,k_y|n,q_y\rangle \tilde{c}_n^{(2)}(q_y),\end{aligned} \tag{2.188}$$

where $\tilde{c}_n^{(2)} = c_{n-1}^{(2)}$ and we use a dimensionless energy (2.26). For $n=0$, the components 1 and 2 are decoupled and we have

$$\varepsilon c(k_y) = \int_{-\infty}^{\infty}\frac{dq_y}{2\pi}v(k_y-q_y)\exp\left[-\frac{l_B^2}{4}(k_y-q_y)^2\right]c(q_y), \tag{2.189}$$

where c is either $c_0^{(1)}$ or $\tilde{c}_0^{(2)}$ and we calculate explicitly $\langle 0,k_y|0,q_y\rangle$.

Coming back to real space,

$$c(k_y) = \int_{-\infty}^{\infty}dy\exp(-ik_yy)c(k_y), \tag{2.190}$$

one can transform Eq. (2.189) to the form

$$(\varepsilon - \tilde{V}(y))c(y) = 0, \tag{2.191}$$

where

$$\begin{aligned}\tilde{V}(y) &= \frac{1}{\hbar\omega_c}\int_{-\infty}^{\infty}\frac{dq_y}{2\pi}v(q_y)\exp\left[-\frac{l_B^2}{4}\left(q_y^2+iq_yy\right)\right]\\ &= \frac{1}{\hbar\omega_c}\int_{-\infty}^{\infty}dy'\,V(y')\frac{1}{\sqrt{\pi}l_B}\exp\left[-\frac{(y-y')^2}{l_B^2}\right]\end{aligned} \tag{2.192}$$

is a convolution of the potential $V(y)$ with the ground-state probability density of a harmonic oscillator. If the potential is smooth in comparison with l_B, then $\tilde{V}(y) \approx V(y)$.

Equation (2.191) has solutions

$$\begin{aligned}c(y) &= \delta(y-Y),\\ \varepsilon &= \tilde{V}(Y),\end{aligned} \tag{2.193}$$

which means that the zero-energy Landau level broadens via just a modulation by the scalar potential. However, a random *vector* potential does not broaden the zero-energy level, due to the index theorem (Section 2.3). All other Landau levels are broadened both by scalar and by vector potentials. For a scalar potential only, one has in general

$$E_n(Y) \pm \frac{h v_{\mathrm{F}}}{l_B} \sqrt{2n} = V(Y). \tag{2.194}$$

There is some experimental evidence that the zero-energy Landau levels in graphene are narrower than the other ones (Giesbers *et al.*, 2007). The most natural explanation is that there exist random pseudomagnetic fields in graphene due to ripples (corrugations) (Morozov *et al.*, 2006). The origin of these pseudomagnetic fields will be discussed later, in Chapter 10.

For the case of a constant electric field E,

$$V(x) = \quad eEx, \tag{2.195}$$

the problem has a beautiful exact solution that is based on relativistic invariance of the Dirac equation (Lukose, Shankar & Baskaran, 2007). The Lorentz transformation

$$y' = \frac{y \quad \beta v t}{\sqrt{1 \quad \beta^2}}, \qquad t' = \frac{t \quad \beta y / v}{\sqrt{1 \quad \beta^2}} \tag{2.196}$$

corresponding to the coordinate system moving with the velocity βv, with $\beta < 1$ (we remind the reader that for our Dirac equation v plays the role of the velocity of light), changes the electric field $\vec{E} || Oy$ and magnetic field $\vec{B} || Oz$ according to

$$E' = \frac{E \quad \beta \frac{vB}{c}}{\sqrt{1 \quad \beta^2}}, \qquad \frac{vB'}{c} = \frac{\frac{vB}{c} \quad \beta E}{\sqrt{1 \quad \beta^2}} \tag{2.197}$$

(Jackson, 1962). This means that, if the electric field is weak enough,

$$E < \frac{v}{c} B, \tag{2.198}$$

it can be excluded by the Lorentz transformation with

$$\beta^* = \frac{cE}{vB}. \tag{2.199}$$

In the opposite case

$$E > \frac{v}{c} B$$

one can, vice versa, exclude the magnetic field, see Shytov *et al.* (2009).

Thus, the effective magnetic field is

$$B_{\mathrm{eff}} = B\sqrt{1 \quad \beta^{*2}}. \tag{2.200}$$

As a result, the energy spectrum of the problem is (Lukose, Shankar & Baskaran, 2007)

$$E_n\left(k_y\right) = \pm h\omega_{\mathrm{c}}\sqrt{n}\left(1 \quad \beta^{*2}\right)^{3/4} \quad hv\beta^{*}k_y. \tag{2.201}$$

The distances between Landau levels are decreased by the factor $(1 \quad \beta^{*2})^{3/4}$. The last term in Eq. (2.201) (as well as the additional factor $\sqrt{1 \quad \beta^{*2}}$ in the first term) is nothing other than the result of Lorentz transformation of energy and momentum. It transforms the Landau *levels* into Landau *bands*, in qualitative agreement with Eq. (2.194).

3

Quantum transport via evanescent waves

3.1 *Zitterbewegung* as an intrinsic disorder

The Berry phase, the existence of a topologically protected zero-energy level and the anomalous quantum Hall effect are striking manifestations of the peculiar, ‘ultrarelativistic’ character of charge carriers in graphene.

Another amazing property of graphene is the finite minimal conductivity, which is of the order of the conductance quantum e^2/h per valley per spin (Novoselov *et al.*, 2005a; Zhang *et al.*, 2005). Numerous considerations of the conductivity of a two-dimensional massless Dirac fermion gas do give us this value of the minimal conductivity with an accuracy of some factor of the order of one (Fradkin, 1986; Lee, 1993; Ludwig *et al.*, 1994; Nersesyan, Tsvelik & Wenger, 1994; Ziegler, 1998; Shon & Ando, 1998; Gorbar *et al.*, 2002; Yang & Nayak, 2002; Katsnelson, 2006a; Tworzydlo *et al.*, 2006; Ryu *et al.*, 2007).

It is really surprising that in the case of massless two-dimentional Dirac fermions there is a finite conductivity for an *ideal* crystal, that is, in the absence of any scattering processes (Ludwig *et al.*, 1994; Katsnelson, 2006a; Tworzydlo *et al.*, 2006; Ryu *et al.*, 2007). This was first noticed by Ludwig *et al.* (1994) using a quite complicated formalism of conformal field theory (see also a more detailed and complete discussion in Ryu *et al.*, 2007). After the discovery of the minimal conductivity in graphene (Novoselov *et al.*, 2005a; Zhang *et al.*, 2005) I was pushed by my experimentalist colleagues to give a more transparent physical explanation of this fact, which has been done in Katsnelson (2006a) on the basis of the concept of *Zitterbewegung* (Schrödinger, 1930) and the Landauer formula (Beenakker & van Houten, 1991; Blanter & Büttiker, 2000). The latter approach was immediately developed further and used to calculate the shot noise (Tworzydlo *et al.*, 2006), which turns out to be similar to that in *strongly disordered* metals (a 'pseudodiffusive transport'). There are now more theoretical (Prada *et al.*, 2007; Katsnelson & Guinea, 2008; Rycerz, Recher & Wimmer, 2009; Schuessler *et al.*, 2009; Katsnelson, 2010a) and experimental (Miao *et al.*, 2007; Danneau *et al.*, 2008; Mayorov *et al.*, 2011) works studying this regime in the context of graphene. This situation is very special. For a conventional electron gas in semiconductors, in the absence of disorder, the states with definite energy (eigenstates of the Hamiltonian) can be simultaneously the states with definite current (eigenstates of the current operator) and it is the disorder that results in the non-conservation of the current and finite conductivity. In contrast, for the Dirac fermions the current operator does not commute with the Hamiltonian (*'Zitterbewegung'*) which can be considered as a kind of intrinsic disorder (Katsnelson, 2006a; Auslender & Katsnelson, 2007). Therefore, a more detailed understanding of the pseudodiffusive transport in graphene is not only important for physics of graphene devices but also has a great general interest for quantum statistical physics and physical kinetics.

The *Zitterbewegung* is a quantum relativistic phenomenon that was first discussed by Schrödinger as early as in 1930 (Schrödinger, 1930). Only very recently was it observed experimentally for trapped ions (Gerritsma *et al.*, 2010). This phenomenon seems to be important if one wishes to understand qualitatively the peculiarities of electron transport in graphene at small doping (Katsnelson, 2006a; Auslender & Katsnelson, 2007). Other aspects of the *Zitterbewegung* in graphene physics, in particular, possibilities for its direct experimental observation, are discussed by Cserti & Dávid (2006) and Rusin & Zawadzki (2008, 2009). Here we will explain this basic concept for the case of two-dimensional massless Dirac fermions. In a secondary quantized form, the Dirac Hamiltonian reads

$$\hat{H} = v \sum_{\vec{p}} \hat{\Psi}^{+}_{\vec{p}} \sigma \vec{p}\, \hat{\Psi}_{\vec{p}} \tag{3.1}$$

and the corresponding expression for the current operator is

$$\hat{\vec{j}} = ev \sum_{\vec{p}} \hat{\Psi}^{+}_{\vec{p}} \sigma \hat{\Psi}_{\vec{p}} = \sum_{\vec{p}} \hat{\vec{j}}_{\vec{p}}, \tag{3.2}$$

where $\vec{p}$ is the momentum and $\hat{\Psi}^{+}_{\vec{p}} = \left(\hat{\psi}^{+}_{\vec{p}1}, \hat{\psi}^{+}_{\vec{p}2}\right)$ are pseudospinor electron-creation operators. The expression (3.2) follows from Eq. (3.1) and the gauge invariance, which requires (Abrikosov, 1998)

$$\hat{\vec{j}} = \frac{\delta \hat{H}}{\delta \vec{p}}. \tag{3.3}$$

Here we omit spin and valley indices (so, keeping in mind applications to graphene, the results for the conductivity should be multiplied by 4 due to there being two spin projections and two conical points per Brillouin zone). Straightforward calculations give for the time evolution of the electron operators $\Psi(t) = \exp(i\hat{H}t)\Psi\exp(\ \ i\hat{H}t)$ (here we will put $h = 1$)

$$\hat{\Psi}_{\vec{p}}(t) = \frac{1}{2}\left\{\left[\exp(\ \ i\varepsilon_{\vec{p}}t)\right]\left(1 + \frac{\vec{p}\sigma}{p}\right) + \left[\exp(i\varepsilon_{\vec{p}}t)\right]\left(1\ \ \ \frac{\vec{p}\sigma}{p}\right)\right\}\hat{\Psi}_{\vec{p}} \tag{3.4}$$

and for the current operator

$$\begin{aligned}
\hat{\vec{j}}(t) &= \hat{\vec{j}}_0(t) + \hat{\vec{j}}_1(t) + \hat{\vec{j}}_1^{\,+}(t),\\
\hat{\vec{j}}_0(t) &= ev\sum_{\vec{p}}\hat{\Psi}_{\vec{p}}^{+}\frac{\vec{p}(\vec{p}\sigma)}{p^2}\hat{\Psi}_{\vec{p}},\\
\hat{\vec{j}}_1(t) &= \frac{ev}{2}\sum_{\vec{p}}\hat{\Psi}_{\vec{p}}^{+}\left[\sigma\ \ \ \frac{\vec{p}(\vec{p}\sigma)}{p^2} + \frac{i}{p}\sigma\times\vec{p}\right]\hat{\Psi}_{\vec{p}}\exp(2i\varepsilon_{\vec{p}}t),
\end{aligned} \tag{3.5}$$

where $\varepsilon_{\vec{p}} = vp$ is the particle energy. The last term in Eq. (3.5) corresponds to the *Zitterbewegung*.

Its physical interpretation is usually given in terms of the Landau Peierls generalization of the Heisenberg uncertainty principle (Landau & Peierls, 1931; Berestetskii, Lifshitz & Pitaevskii, 1971; Davydov, 1976). Attempts to measure the coordinate of a relativistic particle with a very high accuracy require an amount of energy that is sufficient to create particle antiparticle pairs and, thus, we will inevitably lose our initial particle, being unable to distinguish it from one of the created particles (according to quantum statistics, all the particles are equivalent). This pair creation corresponds to the oscillating terms with frequency $2\varepsilon_{\vec{p}}$ in Eq. (3.5).

In terms of condensed-matter physics, the *Zitterbewegung* is nothing other than a special kind of interband transition with the creation of virtual electron hole pairs. The unitary transformation generated by the operator (1.29) diagonalizes the Hamiltonian and thus introduces electron and hole states with the energies $\pm vp$; after this transformation the oscillating term in Eq. (3.5) obviously corresponds to the interband transitions, e.g.,

$$U_{\vec{p}}^{+}\,j_{\vec{p}}^{x}U_{\vec{p}} = ev\begin{pmatrix} -\cos\phi_{\vec{p}} & -i\sin\phi_{\vec{p}}\exp\left(-i\phi_{\vec{p}}\ \ + 2i\varepsilon_{\vec{p}}t\right)\\ i\sin\phi_{\vec{p}}\exp\left(i\phi_{\vec{p}} - 2i\varepsilon_{\vec{p}}t\right) & \cos\phi_{\vec{p}}\end{pmatrix}. \tag{3.6}$$

To calculate the conductivity $\sigma(\omega)$ one can try first to use the Kubo formula (Kubo, 1957) which reads, for the two-dimensional isotropic case,

$$\sigma(\omega) = \frac{1}{A}\int_0^\infty dt \exp(i\omega t)\int_0^\beta d\lambda \left\langle \hat{\vec{j}}(t \quad i\lambda)\hat{\vec{j}} \right\rangle, \tag{3.7}$$

where $\beta = T^{\quad 1}$ is the inverse temperature and A is the sample area. In the static limit $\omega = 0$, taking into account the Onsager relations and the analyticity of the correlations $\left\langle \hat{\vec{j}}(z)\hat{\vec{j}} \right\rangle$ for $\beta < \mathrm{Im}\ z \leq 0$ (Zubarev, 1974), one has

$$\sigma = \frac{\beta}{2A}\int_{\infty}^{\infty} dt \left\langle \hat{\vec{j}}(t)\hat{\vec{j}} \right\rangle. \tag{3.8}$$

Usually, for ideal crystals, the current operator commutes with the Hamiltonian and thus $\hat{\vec{j}}(t)$ does not depend on time. In that case, due to Eq. (3.7), the frequency-dependent conductivity in the ground state contains only the Drude peak

$$\sigma_{\mathrm{D}}(\omega) = \frac{\pi}{A}\lim_{T\to 0}\frac{\left\langle \hat{\vec{j}}^{2} \right\rangle}{T}\delta(\omega). \tag{3.9}$$

Either the spectral weight of the Drude peak is finite and, thus, the static conductivity is infinite, or it is equal to zero. It is easy to check that for the system under consideration the spectral weight of the Drude peak is proportional to the modulus of the chemical potential $|\mu|$ and thus vanishes at zero doping ($\mu = 0$). It is the *Zitterbewegung*, i.e., the oscillating term $\hat{\vec{j}}_1(t)$, which is responsible for the nontrivial behaviour of the conductivity for zero temperature and zero chemical potential. A straightforward calculation gives the formal result

$$\sigma = \frac{\pi e^2}{h}\int_0^\infty d\varepsilon\, \varepsilon\delta^2(\varepsilon), \tag{3.10}$$

where one delta-function originates from the integration over t in Eq. (3.8) and the second one from the derivative of the Fermi distribution function appearing in the calculation of the average over the product of Fermi operators. Of course, the square of the delta-function is not a well-defined object and thus Eq. (3.10) is meaningless before specification of how one should regularize the delta-functions. After regularization the integral in Eq. (3.10) is finite, but its value depends on the regularization procedure (for a detailed discussion of this uncertainty, see Ryu *et al.*, 2007). Although this derivation cannot give us a correct numerical factor, it opens a new path to qualitative understanding of more complicated situations. For example, the minimal conductivity of the order of e^2/h per channel has been observed experimentally also for bilayer graphene (Novoselov *et al.*, 2006), with an energy spectrum drastically different from that for the single-layer case. Bilayer graphene is a zero-gap semiconductor with *parabolic* touching of the electron and hole bands described by the single-particle Hamiltonian (1.46). The Hamiltonian can be diagonalized by the unitary transformation $U_{\vec{p}}$ with the replacement $\phi_{\vec{p}} \to 2\phi_{\vec{p}}$. Thus, the current operator after the transformation takes the form (3.6) with the replacements $v \to p/m$ and $\exp(-i\phi_{\vec{p}}) \to \exp(-2i\phi_{\vec{p}})$. In contrast with the single-layer case, the density of electron states for the Hamiltonian (1.46) is finite at zero energy but the square of the current is, vice versa, linear in energy. As a result, we have the same estimate as Eq. (3.10).

3.2 The Landauer-formula approach

A deeper understanding of the origin of finite conductivity without charge carriers can be reached using the Landauer-formula approach (Beenakker & van Houten, 1991; Blanter & Büttiker, 2000). Following Katsnelson (2006a) we consider the simplest possible geometry, choosing the sample as a ring of length L_y in the y-direction; we will use the Landauer formula to calculate the conductance in the x-direction (see Fig. 3.1). As we will see, the conductivity turns out to be dependent on the shape of the sample. To have a final transparency we should keep L_x finite. On the other hand, periodic boundary conditions in the y-direction are nonphysical and we have to choose L_y as large as possible in order to weaken their effects. Thus, for the two-dimensional situation one should choose $L_x \ll L_y$.

In the coordinate representation the Dirac equation at zero energy takes the form

$$\begin{aligned} \left(\frac{\partial}{\partial x} + i\frac{\partial}{\partial y}\right)\psi_1 &= 0, \\ \left(\frac{\partial}{\partial x} - i\frac{\partial}{\partial y}\right)\psi_2 &= 0. \end{aligned} \tag{3.11}$$

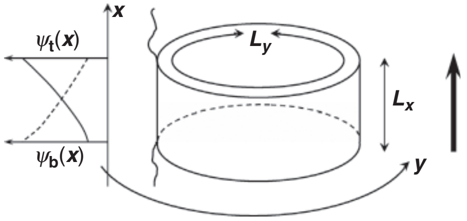

Fig. 3.1. The geometry of the sample. The thick arrow shows the direction of the current. Solid and dashed lines represent wave functions of the edge states localized near the top ($\psi_t(x)$) and bottom ($\psi_b(x)$) of the sample, respectively.

General solutions of these equations are just arbitrary analytic (or complex-conjugated analytic) functions:

$$\begin{aligned}\psi_1 &= \psi_1(x+iy),\\ \psi_2 &= \psi_2(x-iy).\end{aligned} \tag{3.12}$$

Owing to periodicity in the y-direction both wave functions should be proportional to $\exp(ik_y y)$, where $k_y = 2\pi n/L_y$, $n = 0, \pm 1, \pm 2, \ldots$ This means that the dependence on x is also fixed: the wave functions are proportional to $\exp(\pm 2\pi n x/L_y)$. They correspond to the states localized near the bottom and top of the sample (see Fig. 3.1).

To use the Landauer formula, we should introduce boundary conditions at the sample edges ($x = 0$ and $x = L_x$). To be specific, let us assume that the leads are made of doped graphene with the potential $V_0 < 0$ and the Fermi energy $E_F = vk_F = -V_0$. The wave functions in the leads are supposed to have the same y-dependence, namely $\psi_{1,2}(x,y) = \psi_{1,2}(x)\exp(ik_y y)$. Thus, one can try the solution of the Dirac equation in the following form that is consistent with Eq. (1.30):

$$\begin{aligned}\psi_1(x) &= \begin{cases}\exp(ik_x x) + r\exp(-ik_x x), & x < 0,\\ a\exp(k_y x), & 0 < x < L_x,\\ t\exp(ik_x x), & x > L_x,\end{cases}\\ \psi_2(x) &= \begin{cases}\exp(ik_x x + i\phi) - r\exp(-ik_x x - i\phi), & x < 0,\\ b\exp(-k_y x), & 0 < x < L_x,\\ t\exp(ik_x x + i\phi), & x > L_x,\end{cases}\end{aligned} \tag{3.13}$$

where $\sin\phi = k_y/k_\mathrm{F}$ and $k_x = \sqrt{k_\mathrm{F}^2 - k_y^2}$. From the conditions of continuity of the wave functions, one can find the transmission coefficient

$$T_n = \left|t(k_y)\right|^2 = \frac{\cos^2\phi}{\cosh^2(k_y L_x) - \sin^2\phi}. \tag{3.14}$$

Further, one should assume that $k_\mathrm{F} L_x \gg 1$ and put $\phi \cong 0$ in Eq. (3.14), so

$$T_n = \frac{1}{\cosh^2(k_y L_x)}. \tag{3.15}$$

The conductance G (per spin per valley) and Fano factor F of the shot noise (Blanter & Büttiker, 2000) are expressed via the transmission coefficients (3.15):

$$G = \frac{e^2}{h}\sum_{n=-\infty}^{\infty} T_n \tag{3.16}$$

and

$$F = 1 \quad \frac{\sum\limits_{n \quad \infty}^{\infty} T_n^2}{\sum\limits_{n \quad \infty}^{\infty} T_n}. \tag{3.17}$$

Note that in the ballistic regime, where the transmission probability for a given channel is either one or zero, $F = 0$ (the current is noiseless), whereas if all $T_n \ll 1$ (e.g., current through tunnel junctions) $F \approx 1$.

Thus, the trace of the transparency, which is just the conductance (in units of e^2/h), is

$$\mathrm{Tr}\, T = \sum_{n \quad \infty}^{\infty} \frac{1}{\cosh^2\left(k_y L_x\right)} \cong \frac{L_y}{\pi L_x}. \tag{3.18}$$

Assuming that the conductance is equal to $\sigma\, L_y/L_x$ one finds a contribution to the conductivity per spin per valley equal to $e^2/(\pi h)$ (Katsnelson, 2006a; Tworzydlo *et al.*, 2006). This result seems to be confirmed experimentally (Miao *et al.*, 2007; Mayorov *et al.*, 2011). Note also that for the case of nanotubes ($L_x \gg L_y$) one has a conductance e^2/h per channel, in accordance with known results (Tian & Datta, 1994; Chico *et al.*, 1996).

For the Fano factor one has

$$F = \frac{1}{3} \tag{3.19}$$

(Tworzydlo *et al.*, 2006). This result is very far from the ballistic regime and coincides with that for strongly disordered metals (Beenakker & Büttiker, 1992; Nagaev, 1992). This means that, in a sense, the *Zitterbewegung* works as an intrinsic disorder.

Instead of periodic boundary conditions in the y-direction, one can consider closed boundaries with zigzag-type or infinite-mass boundary conditions (we will discuss these later). The result (Tworzydlo *et al.*, 2006) is just a replacement of the allowed values of the wave vectors in Eq. (3.15). One can write, in general (Rycerz, Recher & Wimmer, 2009),

$$k_y(n) = \frac{g\pi(n + \gamma)}{L_y}, \tag{3.20}$$

where $g = 1$ and $\gamma = \frac{1}{2}$ for closed boundary conditions and $g = 2$ and $\gamma = 0$ for periodic boundary conditions. The results (3.18) and (3.19) for the case $L_x \gg L_y$ remain the same.

The case of bilayer graphene (Katsnelson, 2006b; Snyman & Beenakker, 2007; Cserti, Csordás & Dávid, 2007) is more subtle. Even if we neglect the trigonal warping and use the Hamiltonian (1.46), an additional spatial scale

$$l_{\perp} = \frac{hv}{t_{\perp}} \approx 10a \tag{3.21}$$

arises in the problem (Snyman & Beenakker, 2007), and the results for the conductance and the Fano factor depend on the sequence of the limits $L_x/l_{\perp} \to \infty$ and $E_{\mathrm{F}} \to 0$. Moreover, when we cross the energy of trigonal warping and k_F satisfies the inequality (1.55), all four conical points work and the results are changed again (Cserti, Csordás & Dávid, 2007).

3.3 Conformal mapping and Corbino geometry

Thus, electron transport in undoped graphene is due to zero modes of the Dirac operator, which are represented by analytic functions of $z = x + iy$ determined by boundary conditions. For the geometry shown in Fig. 3.1 these functions are just exponents:

$$\psi_{1n}(z) = \exp\left(\frac{2\pi nz}{L_y}\right), \tag{3.22}$$

so a generic wave function inside a graphene flake can be written as

$$\Psi(x,y) \equiv \sum_{n \quad \infty}^{\infty} \left[a_n \begin{pmatrix} \exp\left(\frac{2\pi nz}{L_y}\right) \\ 0 \end{pmatrix} + b_n \begin{pmatrix} 0 \\ \exp\left(\frac{2\pi nz}{L_y}\right) \end{pmatrix} \right], \tag{3.23}$$

where the coefficients a_n and b_n are determined by the boundary conditions. Let the Fermi wavelength in the leads be much smaller than the geometrical lengths of the flake. Then, for most of the modes one can write the boundary conditions assuming normal incidence, $\phi = 0$:

$$\begin{aligned} \psi_{\text{in}} &\equiv \begin{pmatrix} 1 + r \\ 1 \quad r \end{pmatrix}, \\ \psi_{\text{out}} &\equiv \begin{pmatrix} t \\ t \end{pmatrix}, \end{aligned} \tag{3.24}$$

where subscripts ‘in’ and ‘out’ label the values of the wave functions at the boundaries between the leads and the sample. In this approximation it is very easy to solve the problem of electron transport through a graphene quantum dot of arbitrary shape using a conformal mapping of this shape to the strip (Katsnelson & Guinea, 2008; Rycerz, Recher & Wimmer, 2009). For example, the mapping

$$w(z) = R_1 \exp\left(\frac{2\pi z}{L_y}\right) \tag{3.25}$$

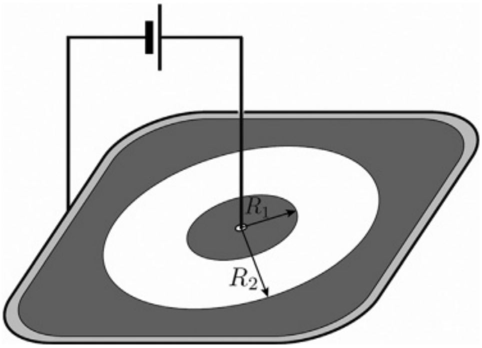

Fig. 3.2. The Corbino geometry: radial electric current in the ring.

with

$$\exp\left(\frac{2\pi L_x}{L_y}\right) = \frac{R_2}{R_1}$$

transforms the rectangular strip $L_x \times L_y$ into a circular ring with inner and outer radii R_1 and R_2, respectively. Indeed, for $z = x + iy$, with $0 < x < L_x$ and $0 < y < L_y$, the transformation (3.25) leads to $0 \leq \arg w < 2\pi$ and $R_1 \leq |w| \leq R_2$. Instead of Eq. (3.23) one can try in this case

$$\Psi(x,y) \equiv \sum_{n \quad \infty}^{\infty} \left[a_n \begin{pmatrix} z^n \\ 0 \end{pmatrix} + b_n \begin{pmatrix} 0 \\ z^n \end{pmatrix} \right]. \tag{3.26}$$

The conformal mapping allows us to find immediately the solution for Corbino geometry where ‘in’ and ‘out’ leads are attached to the inner and outer edges of the ring, respectively (see Fig. 3.2); in this case periodic boundary conditions in the y-direction should naturally be used. Moreover, the solution of the problem for any shape of the flake that is topologically equivalent to the ring can be written automatically in terms of the corresponding conformal mapping (Rycerz, Recher & Wimmer, 2009). Earlier (Katsnelson & Guinea, 2008) this method was applied to the case of graphene quantum dots with thin leads attached.

If we just repeat the derivation of Eq. (3.15) using the boundary conditions (3.24), one can see that

$$\begin{aligned} \cosh(k_y L_x) &= \frac{1}{2}\left[\exp(k_y L_x) + \exp(\quad k_y L_x)\right] \\ &= \frac{1}{2}\left[\frac{\psi_1(x = L_x)}{\psi_1(x = 0)} + \frac{\psi_1(x = 0)}{\psi_1(x = L_x)}\right] \end{aligned} \tag{3.27}$$

and

$$\frac{\psi_1(x=L_x)}{\psi_1(x=0)}=\frac{\psi_2(x=0)}{\psi_2(x=L_x)}. \tag{3.28}$$

Under the conformal mapping (3.25)

$$\frac{\psi_1(x=L_x)}{\psi_1(x=0)}=\exp\left(\frac{2\pi L_x}{L_y}\right)\to\frac{\psi_1(r=R_2)}{\psi_1(r=R_1)}=\frac{R_2}{R_1} \tag{3.29}$$

and the result for the transmission coefficient reads

$$T_n=\frac{4}{\left(\frac{R_2}{R_1}\right)^n+\left(\frac{R_1}{R_2}\right)^n}. \tag{3.30}$$

We should be careful, however, since up to now we have not taken into account the Berry phase π for massless Dirac fermions. When we pass along the circle within the disc we have not periodic but *anti*periodic boundary conditions:

$$\psi_1(|w|,\arg w)=-\psi_1(|w|,\arg w+2\pi), \tag{3.31}$$

which means that n in (3.30) should be replaced by $n+\frac{1}{2}$. Finally, one has (Rycerz, Recher & Wimmer, 2009)

$$T_j=\frac{1}{\cosh^2\left[j\ln\left(\frac{R_2}{R_1}\right)\right]},\quad j=\pm\frac{1}{2},\pm\frac{3}{2},\pm\frac{5}{2},\ldots \tag{3.32}$$

and the summation over integer n in Eqs. (3.16) and (3.17) should be replaced by a summation over half-integer j. For a ring that is thin enough, $|R_2-R_1|\ll R_1$, the result is

$$G\approx\frac{2e^2}{h}\frac{1}{\ln\left(\frac{R_2}{R_1}\right)},\qquad F\approx\frac{1}{3}. \tag{3.33}$$

This agrees with the result (3.18) if we take into account that the thin ring is equivalent to the rectangular strip with $L_x=R_2-R_1$ and $L_y=2\pi R_1$. In the opposite limit $R_1\ll R_2$ one has

$$G\approx\frac{8e^2}{h}\frac{R_1}{R_2},\qquad F\approx 1-G\frac{h}{8e^2}. \tag{3.34}$$

Thus, for zero doping, the conductance of a graphene flake of arbitrary shape can be found without explicit solution of Dirac equation, by a conformal mapping to a rectangle.

3.4 The Aharonov–Bohm effect in undoped graphene

The Aharonov Bohm effect (Aharonov & Bohm, 1959; Olariu & Popescu, 1985) is the shift of interference patterns from different electron trajectories by the magnetic flux through the area between the trajectories. This leads to oscillations of observable quantities such as conductance as a function of the magnetic flux. The Aharonov Bohm effect in graphene has been studied both theoretically (Recher *et al.*, 2007; Jackiw *et al.*, 2009; Wurm *et al.*, 2010; Katsnelson, 2010a; Rycerz, 2010) and experimentally (Russo *et al.*, 2008; Huefner *et al.*, 2009) for the case of a finite doping. It is not clear a priori whether this effect is observable or not in undoped graphene, where the transport is determined by evanescent waves. The analysis of Katsnelson (2010a) and Rycerz (2010) shows that, whereas for the case of very thin rings the Aharonov Bohm oscillations are exponentially small, for a reasonable ratio of radii, such as, e.g., $R_2/R_1 = 5$, the effect is quite observable.

By combining the conformal-mapping technique with a general consideration of zero-energy states for massless Dirac fermions one can derive simple and general rigorous formulas for any graphene flakes topologically equivalent to the ring, avoiding both numerical simulations and explicit solutions of the Schrödinger equation for some particular cases (Katsnelson, 2010a). Note that for the case of a circular ring and a constant magnetic field the problem can be solved exactly for any doping (Rycerz, 2010), but, of course, the mathematics required is much more cumbersome. In the corresponding limits, the results are the same.

The effect of magnetic fields on the states with zero energy can be considered by employing the method of Aharonov & Casher (1979) (see Section 2.3). The general solutions have the form (2.62), where f_1 and f_1 are analytic and complex-conjugated analytic functions. The boundary conditions following from Eq. (3.24) are

$$\begin{aligned} 1 + r &= \psi_+^{(1)}, \\ 1 \quad r &= \psi^{(1)}, \\ t &= \psi_+^{(2)}, \\ t &= \psi^{(2)}, \end{aligned} \tag{3.35}$$

where superscripts 1 and 2 label the boundaries attached to the corresponding leads.

If the boundary of the sample is simply connected, one can always choose $\varphi = 0$ at the boundary and, thus, the magnetic fields disappear from Eqs. (3.35); this fact was used by Schuessler *et al.* (2009) as a very elegant way to prove that a random vector potential has no effect on the value of the minimal conductivity. Further, we will consider a ring where the scalar potential φ is still constant at each boundary but these constants, φ_1 and φ_2, are different. Also, by symmetry (cf. Eq. (3.28)),

$$\frac{f_+^{(2)}}{f_+^{(1)}} = \frac{f_-^{(1)}}{f_-^{(2)}}. \tag{3.36}$$

The answer for the transmission coefficient $T = |t|^2$ for the case of a ring has the form

$$T_j = \frac{1}{\cosh^2\left[(j+a)\ln\left(\frac{R_2}{R_1}\right)\right]}, \tag{3.37}$$

the only difference from Eq. (3.32) being the shift of j by

$$a = \frac{e}{hc}\frac{\varphi_2 - \varphi_1}{\ln\left(\frac{R_2}{R_1}\right)} \tag{3.38}$$

which generalized the corresponding result of Rycerz, Recher & Wimmer (2009) on the case of finite magnetic fields. The conductance G (per spin per valley) and Fano factor of the shot noise F are expressed via the transmission coefficients (3.37) by Eqs. (3.16) and (3.17). To calculate the sums one can use the Poisson summation formula (2.145). On substituting Eq. (3.37) into (3.16) and (3.17) one finds a compact and general answer for the effect of a magnetic field on the transport characteristics:

$$G = \frac{2e^2}{h\ln(R_2/R_1)}\left[1 + 2\sum_{k=1}^{\infty}(-1)^k\cos(2\pi k a)\alpha_k\right], \tag{3.39}$$

$$F = 1 - \frac{2}{3}\left[\frac{1 + 2\sum_{k=1}^{\infty}(-1)^k\cos(2\pi k a)\alpha_k\left(1 + \pi^2k^2/\ln^2\left(\frac{R_2}{R_1}\right)\right)}{1 + 2\sum_{k=1}^{\infty}(-1)^k\cos(2\pi k a)\alpha_k}\right], \tag{3.40}$$

where

$$\alpha_k = \frac{\pi^2 k/\ln\left(\frac{R_2}{R_1}\right)}{\sinh\left(\pi^2 k/\ln\left(\frac{R_2}{R_1}\right)\right)}. \tag{3.41}$$

Equation (2.60) can be solved explicitly for radially symmetric distributions of the magnetic field $B(r)$:

$$\varphi_2 - \varphi_1 = \frac{\Phi}{\Phi_0} \ln\left(\frac{R_2}{R_1}\right) + \int_{R_1}^{R_2} \frac{dr}{r} \int_{R_1}^{r} dr' r' B(r'), \tag{3.42}$$

where Φ is the magnetic flux though the inner ring. In the case of the Aharonov–Bohm effect where the whole magnetic flux is concentrated within the inner ring one has

$$a = \frac{\Phi}{\Phi_0}. \tag{3.43}$$

Owing to the large factor π^2 in the argument of sinh in Eq. (3.41) only the terms with $k = 1$ should be kept in Eqs. (3.36) and (3.37) for all realistic shapes, thus

$$G = G_0 \left[1 - \frac{4\pi^2}{\ln\left(\frac{R_2}{R_1}\right)} \exp\left(- \frac{\pi^2}{\ln\left(\frac{R_2}{R_1}\right)} \right) \cos\left(\frac{e\Phi}{hc}\right) \right], \tag{3.44}$$

$$F = \frac{1}{3} + \frac{8\pi^4}{3\ln^3\left(\frac{R_2}{R_1}\right)} \exp\left(- \frac{\pi^2}{\ln\left(\frac{R_2}{R_1}\right)} \right) \cos\left(\frac{e\Phi}{hc}\right), \tag{3.45}$$

where G_0 is the conductance of the ring without magnetic field (3.33).

Oscillating contributions to G and F are exponentially small for very thin rings but are certainly measurable if the ring is thick enough. For $R_2/R_1 = 5$ their amplitudes are 5.3% and 40%, respectively.

Consider now a generic case with the magnetic field $B = 0$ within the flake. Then, the solution of Eq. (2.60) is a harmonic function, that is, the real or imaginary part of an analytic function. It can be obtained from the solution for the disc by the same conformal transformation as that which we use to solve the Dirac equation. One can see immediately that Eq. (3.35) remains the same. The expressions (3.44) and (3.45) can be rewritten in terms of an experimentally measurable quantity G_0,

$$G = G_0 \left[1 - \frac{4\pi^2}{\beta} \exp\left(- \frac{\pi^2}{\beta} \right) \cos\left(\frac{e\Phi}{hc}\right) \right], \tag{3.46}$$

$$F = \frac{1}{3} + \frac{8\pi^4}{3\beta^3} \exp\left(- \frac{\pi^2}{\beta} \right) \cos\left(\frac{e\Phi}{hc}\right), \tag{3.47}$$

where $\beta = 2e^2/(hG_0)$ and we assume that $\beta \ll \pi^2$.

Thus, conformal transformation (Katsnelson & Guinea, 2008; Rycerz, Recher & Wimmer, 2009) is a powerful tool with which to consider pseudodiffusive transport in undoped graphene flakes of arbitrary shape, not only in the absence of a magnetic field but also in the presence of magnetic fluxes in the system. An experimental study of the Aharonov Bohm oscillations and comparison with the simple expressions (3.46) and (3.47) derived here would be a suitable way to check whether the ballistic (pseudodiffusive) regime is reached or not in a given experimental situation.

To conclude this chapter, we note that undoped graphene is a gapless semiconductor, with a completely filled valence band and an empty conduction band. It is really counterintuitive that in such a situation, at zero temperature, it has a finite conductivity, of the order of the conductance quantum e^2/h. This is one of the most striking consequences of its peculiar 'ultrarelativistic' energy spectrum. Formally, the electron transport in undoped graphene is determined by zero modes of the Dirac operator, which are described by analytic functions with proper boundary conditions. Therefore, the whole power of complex calculus can be used here, just as in classical old-fashioned branches of mathematical physics such as two-dimensional hydrodynamics and electrostatics. These states cannot correspond to the waves propagating through the sample but, rather, are represented by evanescent waves. The transport via evanescent waves in undoped graphene is a completely new variety of electron transport in solids, being drastically different from all types known before (ballistic transport in nanowires and constrictions, diffusive transport in dirty metals, variable-range-hopping transport in Anderson insulators, etc.). Gaining a deeper understanding of these new quantum phenomena would seem to be a very important task.

4

The Klein paradox and chiral tunnelling

4.1 The Klein paradox

Soon after the discovery of the Dirac equation, O. Klein (1929) noticed one of its strange properties which was called afterwards ‘the Klein paradox’. Klein considered the 4 × 4 matrix Dirac equation for a relativistic spin-$\frac{1}{2}$ particle propagating in three-dimensional space. To be closer to our main subject, we will discuss the 2 × 2 matrix equation for a particle propagating in two-dimensional space; the essence of the paradox remains the same. Thus, we will consider the stationary Schrödinger equation

$$\hat{H}\Psi = E\Psi \tag{4.1}$$

with the two-component spinor wave function

$$\Psi = \begin{pmatrix} \psi_1 \\ \psi_2 \end{pmatrix}$$

and the Hamiltonian

$$\hat{H} = \quad ihc\hat{\vec{\sigma}}\nabla + V(x,y)\hat{\mathbf{1}} + mc^2\hat{\sigma}_z. \tag{4.2}$$

Here c is the velocity of light, m is the mass of the particle and $V(x, y)$ is a potential energy; we will write explicitly the identity matrix $\hat{\mathbf{1}}$ to show the spinor structure of the Hamiltonian. Let us consider the one-dimensional case $V = V(x)$ and $\psi_i = \psi_i(x)$ (the latter means normal incidence). Equation (4.1) now takes the form

$$\begin{aligned} ihc\frac{d\psi_2}{dx} &= \left[E \quad mc^2 \quad V(x)\right]\psi_1, \\ ihc\frac{d\psi_1}{dx} &= \left[E + mc^2 \quad V(x)\right]\psi_2. \end{aligned} \tag{4.3}$$

Consider first just a jump of the potential:

$$V(x) = \begin{cases} 0, & x < 0, \\ V_0, & x > 0, \end{cases} \tag{4.4}$$

with a positive V_0.

At the left side of the barrier, the solutions ψ_1 and ψ_2 have x-dependence as exp($\pm ikx$), where the wave vector k satisfies the relativistic dispersion relation $E^2 = (hck)^2 + m^2c^4$, or

$$k = \frac{\sqrt{E^2 \quad m^2c^4}}{hc}. \tag{4.5}$$

The allowed energy values are $E > mc^2$ (electron states) or $E < \quad mc^2$ (hole, or positron, states). To be specific, we will consider the first case. Thus, using Eq. (4.3) with $V = 0$ one finds for the incident wave

$$\Psi_{\text{in}}(x) = \begin{pmatrix} 1 \\ \alpha \end{pmatrix} e^{ikx} \tag{4.6}$$

and for the reflected wave

$$\Psi_{\text{r}}(x) = \begin{pmatrix} 1 \\ \quad \alpha \end{pmatrix} e^{\quad ikx}, \tag{4.7}$$

where

$$\alpha = \sqrt{\frac{E \quad mc^2}{E + mc^2}}. \tag{4.8}$$

We will assume a solution of the general form

$$\Psi(x) = \Psi_{\text{in}}(x) + r\Psi_{\text{r}}(x), \tag{4.9}$$

where r is the reflection coefficient.

At the right side of the barrier, we have the dispersion relation $(E \quad V_0)^2 = h^2c^2q^2 + m^2c^4$ for the new wave vector q. We will consider the case of a potential jump that is strong enough:

$$V_0 > E + mc^2. \tag{4.10}$$

In this case the solution

$$q = \frac{\sqrt{(V_0 \quad E)^2 \quad m^2c^4}}{hc} \tag{4.11}$$

is real and the particle can propagate also on the right side of the barrier. However, this particle belongs to the lower (positron, or hole) continuum; see

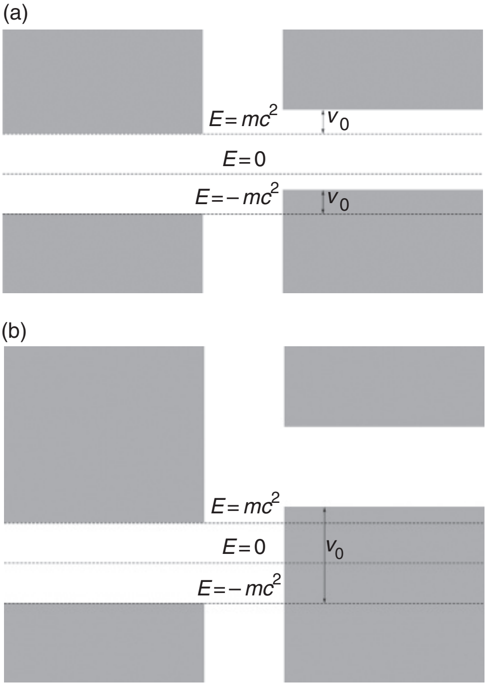

Fig. 4.1. Electron and positron states on the left and right sides of the barrier for the cases $V_0 < 2mc^2$ (a) and $V_0 > 2mc^2$ (b).

Fig. 4.1. It is in this situation that the paradox arises, so we will consider only this case. For smaller values of V_0, one has either the situation of propagating electrons on both sides of the barrier, if $V_0 < E - mc^2$, or evanescent waves at $x > 0$ if $E - mc^2 < V_0 < E + mc^2$ (Fig. 4.1(a)).

On solving the Schrödinger equation (4.3) for $x > 0$ one finds for the transmitted wave

$$\Psi_{\mathrm{t}}(x) = \begin{pmatrix} 1 \\ \frac{1}{\beta} \end{pmatrix} e^{iqx}, \tag{4.12}$$

where

$$\beta = \sqrt{\frac{V_0 - E - mc^2}{V_0 - E + mc^2}}. \tag{4.13}$$

One can find the reflection coefficient r and the transmission coefficient t assuming that the wave function is continuous at $x = 0$, that is,

$$\Psi_{\mathrm{in}} + r\Psi_{\mathrm{r}}|_{x=-0} = t\Psi_{\mathrm{t}}|_{x=+0} \tag{4.14}$$

or

$$\begin{aligned} 1 + r &= t, \\ \alpha(1 - r) &= -\frac{1}{\beta}t. \end{aligned} \tag{4.15}$$

We find straightforwardly

$$r = \frac{1 + \alpha\beta}{\alpha\beta - 1}. \tag{4.16}$$

Since for the case under consideration α and β are real, $0 < \alpha, \beta < 1$, one can see immediately that $r < 0$ and

$$R = |r|^2 = \left(\frac{1 + \alpha\beta}{1 - \alpha\beta}\right)^2 > 1. \tag{4.17}$$

However, R is nothing other than the reflection probability! Indeed, the current density

$$j_x = c\psi^+\sigma_x\Psi = c\left(\psi_1^*\psi_2 + \psi_2^*\psi_1\right) \tag{4.18}$$

has the values $2\alpha c$ and $-2\alpha cR$ for the incident and reflected parts of the wave function (4.9), respectively. Thus, we have the very strange conclusion that, under the condition (4.10), the reflected current is larger than the incident one and the reflection probability is larger than unity. This was initially called the Klein paradox.

Our further discussion will follow Calogeracos & Dombey (1999) and Dombey & Calogeracos (1999). (A rather complete list of references can be found in Greiner & Schramm (2008).)

First, as was noticed by Pauli, there is a problem with the definition of the transmitted wave. For the case (4.10), the group velocity of the particle on the right side of the barrier,

$$v_g = \frac{1}{h}\frac{dE}{dq} = \frac{1}{h}\left(\frac{dq}{dE}\right)^{-1} = \frac{hqc^2}{E - V_0}, \tag{4.19}$$

is opposite to the direction of the wave vector q. This means that, formally speaking, the transmitted wave (4.12) describes the particle propagating to the left (for positive q) since the direction of propagation is determined by the direction of the group velocity, not by the momentum. So, at first sight, the formal paradox disappears (see also Vonsovsky & Svirsky, 1993).

However, it reappears in a more detailed view of the problem. Instead of the infinitely broad barrier (4.4), let us consider the finite one:

$$V(x) = \begin{cases} V_0, & |x| < a, \\ 0, & |x| > a. \end{cases} \tag{4.20}$$

In this situation, there is no problem with the choice of the transmitted wave at the right side, it is just $t\Psi_{\text{in}}$; within the barrier region one has to consider the most general solution, with both parts, proportional to exp $(\pm iqx)$. The calculations are simple and straightforward (see, e.g., Calogeracos & Dombey, 1999; Su, Siu & Chou, 1993) and the results for the reflection and transmission probabilities R and T are

$$R = \frac{\left(1 - \alpha^2\beta^2\right)^2 \sin^2(2qa)}{4\alpha^2\beta^2 + \left(1 - \alpha^2\beta^2\right)^2 \sin^2(2qa)}, \tag{4.21}$$

$$T = \frac{4\alpha^2\beta^2}{4\alpha^2\beta^2 + \left(1 - \alpha^2\beta^2\right)^2 \sin^2(2qa)}. \tag{4.22}$$

There is no formal problem in the sense that $0 < R < 1$, $0 < T < 1$ and $R + T = 1$, as should be the case.

Now, the case of an infinitely broad barrier can be considered from Eqs. (4.21) and (4.22) in the limit $a \to \infty$. We should be careful here, because of fast oscillations. If

$$qa = \frac{N\pi}{2} \tag{4.23}$$

(N is an integer) then $\sin(2qa) = 0$ and we have complete transmission ($R = 0$, $T = 1$). If we just average over the fast oscillations in the limit $a \to \infty$, replacing $\sin^2(2qa)$ by its average value $\frac{1}{2}$, we will find the expressions

$$R_\infty = \frac{\left(1 - \alpha^2\beta^2\right)^2}{8\alpha^2\beta^2 + \left(1 - \alpha^2\beta^2\right)^2}, \qquad T_\infty = \frac{8\alpha^2\beta^2}{8\alpha^2\beta^2 + \left(1 - \alpha^2\beta^2\right)^2}. \tag{4.24}$$

Thus, the paradox reappears in a different form. It is no longer a paradox in a logical or mathematical sense, it is just a physically counterintuitive behaviour.

The well-known tunnelling effect in quantum mechanics assumes that the particle can penetrate through a classically forbidden region with $E < V(x)$ but the probability of the penetration is exponentially small if the barrier is high and broad. In the semiclassical approximation, the transmission of the barrier between classical turning points $x_{1,2}$ satisfying the equation $E = V(x_{1,2})$ can be estimated as (Landau & Lifshitz, 1977)

$$T \sim \exp\left\{ -\frac{2}{h} \int_{x_1}^{x_2} dx \sqrt{2m[V(x) - E]} \right\}, \tag{4.25}$$

where m is the mass of the particle; the motion is supposed to be nonrelativistic. For the relativistic particle under the condition (4.10) the situation is dramatically different: in the limit $a \to \infty$ the penetration probability (4.24) remains finite and, in general, is not small at all. Even for an infinitely high barrier ($V_0 \to \infty$) one has $\beta = 1$ and

$$T_\infty = \frac{E^2 - m^2c^4}{E^2 - \frac{1}{2}m^2c^4}. \tag{4.26}$$

This quantity is of the order of unity if $E - mc^2$ is of the order of mc^2. In the ultrarelativistic limit

$$E \gg mc^2 \tag{4.27}$$

one has $T_\infty \approx 1$. The ability of quantum relativistic particles to penetrate with large enough probabilities through barriers with arbitrarily large height and width is the contemporary formulation of the Klein paradox (Calogeracos & Dombey, 1999).

A hand-waving explanation of the tunnel effect is based on the Heisenberg principle: since one cannot know with arbitrary accuracy both the momentum and the position of a particle at a given instant one cannot accurately separate the total energy into a potential part and a kinetic part. Thus, the kinetic energy can be 'a bit' negative.

In the relativistic regime, there is a much stronger restriction (Landau & Peierls, 1931). One cannot know even the position alone with accuracy better than hc/E. This means that relativistic quantum mechanics cannot be *mechanics*, it can only be field theory (Berestetskii, Lifshitz & Pitaevskii, 1971). It always contains particles and antiparticles, and to measure the position with an accuracy better than hc/E one needs to apply so high an energy that it will create particle–antiparticle pairs. The original particle whose position is supposed to be measured will be lost among the newly born particles.

This consideration is relevant for the Klein paradox since under the condition (4.10) both electron and positron states are explicitly involved.

The standard interpretation of the states with negative energy is based on the Dirac theory of holes (Bjorken & Drell, 1964; Berestetskii, Lifshitz & Pitaevskii, 1971; Davydov, 1976). It is supposed that in the vacuum all the states with negative energy are occupied; antiparticles are the holes in this energy continuum. In the case (4.10) the tunnelling of a relativistic particle happens from a state from the upper energy continuum ($x < 0$) to a state in the lower one ($x > 0$). In this situation the definition of the vacuum should be reconsidered. This reconstruction takes place necessarily when we switch on the potential and pass from the 'normal' situation of small V to the 'paradoxical' case (4.10).

Let us consider the case of a rectangular barrier (4.20) but for arbitrary V. If V is small enough the bound states are formed in the gap, that is, with energies $|E| < mc^2$. A straightforward solution of this problem gives the following equation for the energy of the bound states (Calogeracos & Dombey, 1999):

$$\begin{aligned} \tan(qa) &= \sqrt{\frac{(mc^2 - E)(mc^2 + E + V_0)}{(mc^2 + E)(E + V_0 - mc^2)}}, \\ \tan(qa) &= -\sqrt{\frac{(mc^2 + E)(mc^2 + E + V_0)}{(mc^2 - E)(E + V_0 - mc^2)}}, \end{aligned} \tag{4.28}$$

where

$$q = \frac{\sqrt{(E + V_0)^2 - m^2c^4}}{hc}$$

and we have made the replacement $V_0 \rightarrow -V_0$.

When $qa = \pi/2$ and, thus,

$$V_0 = mc^2 + \sqrt{(mc^2)^2 + \frac{\pi^2 h^2 c^2}{4a^2}}, \tag{4.29}$$

the energy of one of the bound states reaches the boundary of the positron continuum, $E = -mc^2$ (Fig. 4.2). It is energetically favourable now to occupy this state, creating a hole in the negative energy continuum (positron emission). At $qa = \pi$ the next state reaches the continuum, and the vacuum state is reconstructed. This allows us to understand better the nature of the original Klein paradox. Despite the problem that a large enough barrier looks static, actually it is not. One needs to study carefully how this state is reached, and this process involves positron emission by the growing barrier. For a more detailed discussion of the role of the electron positron pairs in the Klein paradox, see Krekora, Su & Grobe (2005). We will come back to this issue later, when discussing supercritical charges in graphene (Chapter 8).

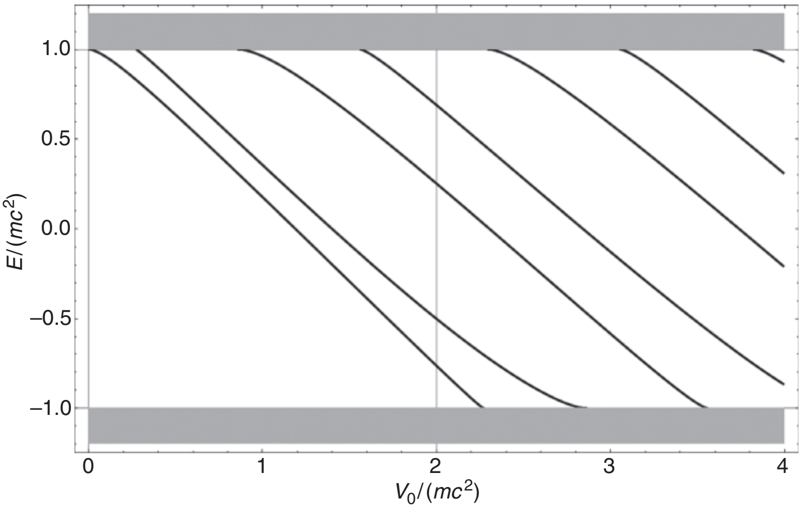

Fig. 4.2. Energies of the bound state found from Eq. (4.28) as functions of the height of the barrier; $a = 2h/(mc)$.

4.2 The massless case: the role of chirality

We are going to discuss the Klein paradox and related issues for the massless Dirac fermions in graphene (Katsnelson, Novoselov & Geim, 2006). The case $m=0$ is very special. If we put $m=0$ in the results (4.21) and (4.22) we will have $T=1$ and $R=0$ for any parameters of the potential (one can see from Eqs. (4.8) and (4.13) that $\alpha=\beta=1$ for $m=0$). This result is not related to a specific choice of the potential barriers (4.20).

For $m=0$, the equations (4.3) can be solved very easily for arbitrary $V(x)$. Let us introduce a variable

$$w = \frac{1}{hc}\int^{x} dx'[E - V(x')]. \tag{4.30}$$

Of course, we have to be careful: this change of variables is possible only for the intervals within which $E > V(x)$ or $E < V(x)$, so dw/dx never vanishes. Therefore, we will use (4.30) separately for each interval between two turning points (and for the intervals between $-\infty$ and the first turning point and between the last turning point and $+\infty$). There are two basic solutions for each such interval:

$$\Psi_{>} = \begin{pmatrix} 1 \\ 1 \end{pmatrix} \exp(i|w|) \tag{4.31}$$

and

$$\Psi_< = \begin{pmatrix} 1 \\ -1 \end{pmatrix} \exp(-i|w|). \tag{4.32}$$

Both components of the spinor should be continuous at the turning points, so one can see immediately that the only way to match the solutions is to choose either $\Psi_>$ or $\Psi_<$ to be zero everywhere. One can never have a combination of incident and reflected waves, since propagation is allowed in one direction only (one has to recall that here we consider only the case of normal incidence; for two-dimensional problems with $\Psi(x, y)$ this is not the case, see the next section).

The point is that a massless Dirac particle can propagate only either along its (pseudo)spin direction or in the opposite direction. The scalar potential proportional to the identity matrix in the Hamiltonian (4.2) does not act on the pseudospin and therefore cannot change the direction of propagation of a massless particle with spin $\frac{1}{2}$ to the opposite.

This property has an analogue in more general two-dimensional and three-dimensional situations with $V = V(x, y)$ or $V = V(x, y, z)$: backscattering is forbidden. This was found long ago for the scattering of ultrarelativistic particles in three dimensions (Yennie, Ravenhall & Wilson, 1954; Berestetskii, Lifshitz & Pitaevskii, 1971). Ando, Nakanishi & Saito (1998) noticed an importance of this property for carbon materials. In particular, the absence of backscattering explains the existence of conducting channels in metallic carbon nanotubes; in a nonrelativistic one-dimensional system an arbitrarily small disorder leads to localization (Lifshitz, Gredeskul & Pastur, 1988), so the conductive state of the nanotubes is not trivial.

The consideration of Ando, Nakanishi & Saito (1998) is very instructive, since it shows explicitly the role of the Berry phase and time-reversal symmetry, but it is quite cumbersome. Here we present a somewhat simplified version of this proof. To this end, we consider the equation (Newton, 1966) for the scattering T-matrix,

$$\hat{T} = \hat{V} + \hat{V}\hat{G}_0\hat{T}, \tag{4.33}$$

where $\hat{V}$ is the scattering potential operator,

$$\hat{G}_0 = \lim_{\delta \to +0} \frac{1}{E - \hat{H}_0 + i\delta} \tag{4.34}$$

is the Green function of the unperturbed Hamiltonian $\hat{H}_0$ and E is the electron energy (we will assume $E > 0$). For more details of this formalism, see Chapter 6. If $\hat{H}_0$ is the Dirac Hamiltonian for massless fermions (1.22), we have

$$\hat{G}_0(\vec{r},\vec{r}') = \int \frac{d\vec{q}}{(2\pi)^2} \hat{G}_0(\vec{q}) \exp[i\vec{q}(\vec{r} - \vec{r}')], \tag{4.35}$$

where

$$\hat{G}_0(\vec{q}) = \frac{1}{E - hv\vec{q}\vec{\sigma} + i\delta} = \frac{1}{hv} \frac{k + \vec{q}\vec{\sigma}}{(k + i\delta)^2 - q^2} \tag{4.36}$$

with $k = E/(hv)$. The probability amplitude of the backscattering can be found by iterations of Eq. (4.33) and is proportional to

$$T\left(-\vec{k},\vec{k}\right) = \left\langle -\vec{k} \middle| V + V\hat{G}V + V\hat{G}V\hat{G}V + \cdots \middle| \vec{k} \right\rangle \equiv T^{(1)} + T^{(2)} + \cdots, \tag{4.37}$$

where $T^{(n)}$ is the contribution proportional to V^n.

Let us assume that $\vec{k}||Ox$ (we can always choose the axes in such a way), then $\left|\vec{k}\right\rangle$ and $\left|-\vec{k}\right\rangle$ have spinor structures

$$\begin{pmatrix} 1 \\ 1 \end{pmatrix} \quad \text{and} \quad \begin{pmatrix} 1 \\ -1 \end{pmatrix},$$

respectively (see Eq. (1.32)). Thus, if $\hat{T}$ is a 2×2 matrix

$$\hat{T} = T_0 + \vec{T}\hat{\vec{\sigma}} \tag{4.38}$$

one has

$$T\left(-\vec{k},\vec{k}\right) \sim \left\langle -\vec{k} \middle| T_z + iT_y \middle| \vec{k} \right\rangle. \tag{4.39}$$

Then, keeping in mind that V is proportional to the identity matrix, one can prove, term by term, that all contributions to $\left\langle -\vec{k} \middle| T_z \middle| \vec{k} \right\rangle$ and $\left\langle -\vec{k} \middle| T_y \middle| \vec{k} \right\rangle$ vanish by symmetry. Actually, this is just because $\vec{T}\left(\vec{k}\right) \sim \vec{k} \,||\, Ox$ one cannot construct from the vectors $\vec{k}$ and $-\vec{k}$ anything with nonzero y- or z-components: for two nonparallel vectors $\vec{k}_1$ and $\vec{k}_2$ one of them has a nonzero y-component, and $\vec{k}_1 \times \vec{k}_2 \,||\, Oz$.

4.3 Klein tunnelling in single-layer graphene

Keeping in mind electrons in quantum electrodynamics, it is not easy to create potential jumps larger than $2mc^2 \approx 1\,\text{MeV}$. Similar phenomena take place in very high electric or gravitational fields (Greiner, Mueller &

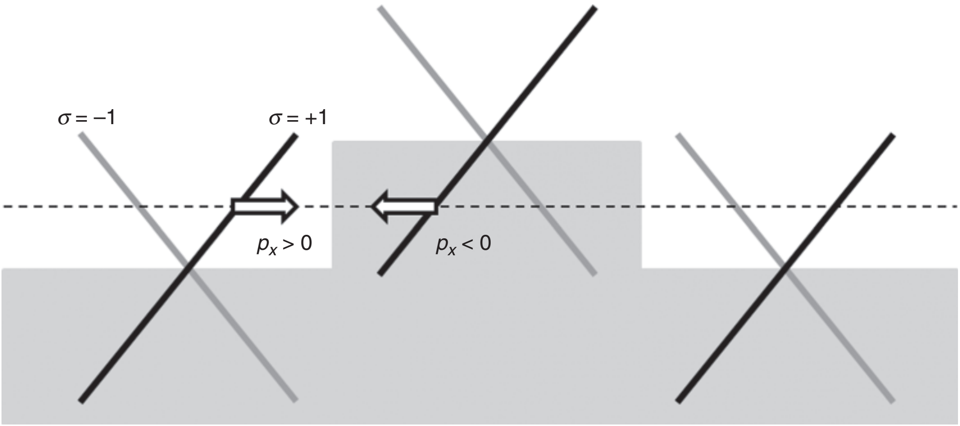

Fig. 4.3. Transformation of an electron to a hole under the potential barrier; the large arrows show directions of momenta assuming that the group velocity is always parallel to the *Ox* axis. Black and grey lines show the dispersion of electronic states with opposite pseudospin projections.

Rafelski, 1985; Grib, Mamaev & Mostepanenko, 1994; for a detailed list of references, see Greiner & Schramm, 2008), but the context is always quite exotic, such as collisions of ultraheavy ions or even black-hole evaporation. There were no experimental data that would require the Klein paradox for their explanation.

It was realized soon after the discovery of graphene that Klein tunnelling (tunnelling of Dirac fermions under the conditions of the Klein paradox) is one of the crucial phenomena for graphene physics and electronics (Katsnelson, Novoselov & Geim, 2006). Soon after the theoretical prediction of Klein tunnelling in graphene, it was confirmed experimentally (Stander, Huard & Goldhaber-Gordon, 2009; Young & Kim, 2009).

In conventional terms of solid-state physics, Klein tunnelling is nothing other than tunnelling through a p n p (or n p n) junction when electrons are transformed into holes and then back to electrons (or vice versa) (Fig. 4.3). As we saw in the previous section, for massless Dirac fermions the transmission at normal incidence is always 100% irrespective of the height and width of the potential barrier. From the point of view of applications, this is very bad news: if one just copies the construction of a silicon transistor it will not work, since it is impossible to lock it. The gap opening is necessary. The good news is that, due to the Klein paradox, the unavoidable inhomogeneities of the electron density in graphene (see Chapter 10) do not lead to localization and, moreover, their effect on the electron mobility is not very great. We will come back to this important issue many times in this book.

Consider now, following Katsnelson, Novoselov & Geim (2006), electron propagation through the barrier (4.20) for an arbitrary angle of incidence φ. The energy $E = hvk$ is supposed to be positive. There is a refraction of the electron wave at the potential jump, and the new angle θ is determined by the conservation of the y-component of the electron momentum (and, thus, of the wave vector):

$$k_y = k \sin\varphi = q_y = q \sin\theta, \tag{4.40}$$

where

$$q = \frac{|E - V_0|}{hv} \tag{4.41}$$

is the length of the wave vector within the barrier. For massless Dirac fermions with energy E propagating at the angle φ to the x-axis the components of the spinor wave functions are related by

$$\psi_2 = \psi_1 \exp(i\varphi)\operatorname{sgn}E \tag{4.42}$$

(see Eq. (1.30)). Thus, the wave function has the following form (cf. Eq. (3.13) for the case of zero energy):

$$\psi_1(x,y) = \begin{cases} [\exp(ik_x x) + r\exp(-ik_x x)]\exp\left(ik_y y\right), & x < -a, \\ [A\exp(iq_x x) + B\exp(-iq_x x)]\exp\left(ik_y y\right), & |x| < a, \\ t\exp\left(ik_x x + ik_y y\right), & x > a, \end{cases} \tag{4.43}$$

$$\psi_2(x,y) = \begin{cases} s[\exp(ik_x x + i\varphi) - r\exp(-ik_x x - i\varphi)]\exp\left(ik_y y\right), & x < -a, \\ s'[A\exp(iq_x x + i\theta) - B\exp(-iq_x x - i\theta)]\exp\left(ik_y y\right), & |x| < a, \\ st\exp\left(ik_x x + ik_y y + i\varphi\right), & x > a, \end{cases} \tag{4.44}$$

where

$$s = \operatorname{sgn}E, \qquad s' = \operatorname{sgn}(E - V_0), \qquad k_x = \cos\varphi, \qquad q_x = q\cos\theta \tag{4.45}$$

and we have taken into account that the reflected particle moves at the angle $\pi - \varphi$, $\exp[i(\pi - \varphi)] = -\exp(-i\varphi)$. The parameters r (the reflection coefficient), t (the transmission coefficient), A and B should be found from the continuity of ψ_1 and ψ_2 at $x = \pm a$. Note that the Klein-paradox situation is

$$ss' = -1 \tag{4.46}$$

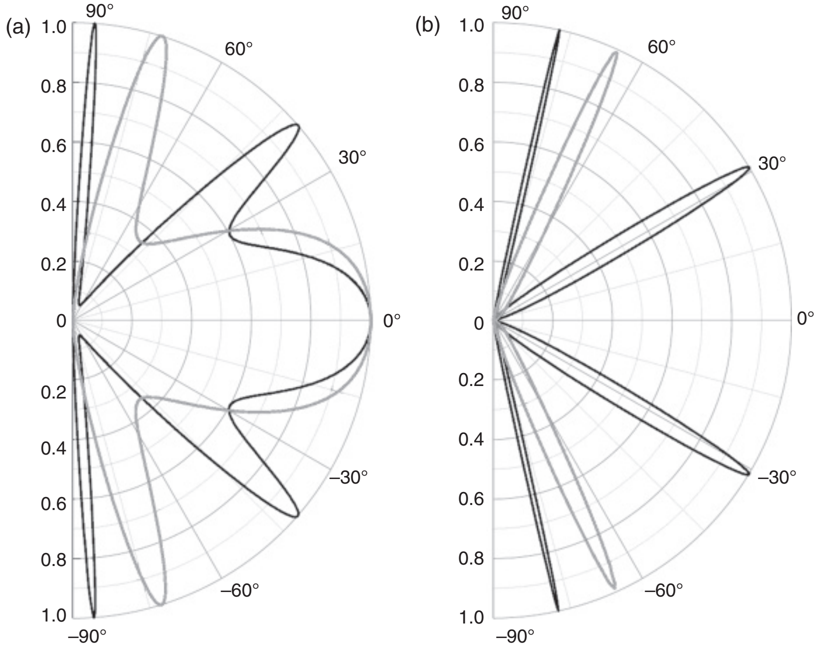

Fig. 4.4. Transmission probabilities through a 100-nm-wide barrier as a function of the angle of incidence for single-layer (a) and bilayer (b) graphene. The electron concentration n outside the barrier is chosen as 0.5×10^{12} cm ^{2} for all cases. Inside the barrier, hole concentrations p are 1×10^{12} and 3×10^{12} cm ^{2} for black and grey curves, respectively (such concentrations are most typical in experiments with graphene). This corresponds to Fermi energies E of incident electrons $\approx$80 and $\approx$17 meV for single-layer and bilayer graphene, respectively. The barrier heights V_0 are (a) 200 and (b) 50 meV (black curves) and (a) 285 and (b) 100 meV (grey curves). (Reproduced with permission from Katsnelson, Novoselov & Geim, 2006.)

(with opposite signs of the energy outside and inside the barrier). As a result, one finds

$$r = 2\exp(i\varphi - 2ik_xa)\sin(2q_xa) \times \frac{\sin\varphi - ss'\sin\theta}{ss'[\exp(-2iq_xa)\cos(\varphi+\theta) + \exp(2iq_xa)\cos(\varphi-\theta)] - 2i\sin(2q_xa)}. \tag{4.47}$$

The transmission probability can be calculated as

$$T = |t|^2 = 1 \quad |r|^2. \tag{4.48}$$

The results are shown in Fig. 4.4. In agreement with the general consideration of the previous section, $r = 0$ at $\varphi = 0$ (this can be seen immediately from Eqs. (4.47) and (4.40)).

There are also additional ‘magic angles’ for which $r = 0$ and one has 100% transmission. They correspond to the condition $\sin(2q_x a) = 0$, or

$$q_x a = \frac{\pi}{2} N, \tag{4.49}$$

where $N = 0, \pm 1, \pm 2, \ldots$ Interestingly, this coincides with the condition (4.23) of complete transmission for the case of nonzero mass. These conditions correspond to the Fabry Pérot resonances in optics (Born & Wolf, 1980). The same resonances can take place for a more general potential $V = V(x)$, as was shown in the semiclassical approximation by Shytov, Rudner & Levitov (2008) (see also Shytov *et al.*, 2009). This issue will be considered in the next section.

4.4 Klein tunnelling for a smooth potential barrier and the effect of magnetic fields

Strictly speaking, the Dirac-cone approximation itself does not work for the case of an atomically sharp potential since it will induce intervalley scattering, which can change the whole physical picture dramatically. The sharp potential jump considered in the previous sections means a sharpness in comparison with the electron wave length $k^{\;\;1}$ but not in comparison with the interatomic distance a. So, the typical spatial scale of the change of potential at the barrier d was assumed to satisfy the condition

$$a \ll d \ll \frac{1}{k}. \tag{4.50}$$

The opposite limit case, that of a very smooth potential,

$$kd \gg 1, \tag{4.51}$$

was first considered by Cheianov and Falko (2006). It turns out that in this case the region of high transmission near $\varphi \approx 0$ is pretty narrow:

$$T(\varphi) = \exp\big(\quad Ckd \sin^2\varphi\big), \tag{4.52}$$

where C is a numerical factor depending on the specific shape of the potential, thus $T(\varphi) \approx 1$ if

$$|\varphi| \leq \frac{1}{\sqrt{kd}} \tag{4.53}$$

(the ‘Klein collimation’). The result (4.52) was obtained there using both the exact solution of the Dirac equation in a constant electric field and the semiclassical approximation. We will present here a simple derivation following Shytov, Gu & Levitov (2007) (see also Shytov *et al.*, 2009).

Let us consider the Schrödinger equation (4.1) with the Hamiltonian (4.2) for the case when

$$V(x) = \quad eEx, \tag{4.54}$$

where E is the electric field. One can use the momentum representation for the coordinate x, $x \leftrightarrow k_x$. Then the coordinate $x \to i\partial/\partial k_x$ and the Schrödinger equation takes the form (with the replacement $c \to v$, keeping in mind the case of graphene)

$$ieE\frac{\partial \Psi}{\partial k_x} = \hat{H}'\Psi, \tag{4.55}$$

where

$$\hat{H}' = hv\vec{k}\vec{\sigma} \quad \varepsilon$$

(here we use the notation ε for the electron energy, in order not to confuse it with the electric field). The equation (4.55) is formally equivalent to the time-dependent Schrödinger equation with a time $t' = \quad hk_x/(eE)$ and the Hamiltonian linearly dependent on the 'time'. This is nothing other than the problem of Landau Zener breakdown, in which the term $hvk_y\sigma_y$ plays the role of the gap in the Hamiltonian. Using the known solution of this problem (Vonsovsky & Katsnelson, 1989) one finds

$$T \approx \exp\left(\quad \frac{\pi hvk_y^2}{|eE|}\right), \tag{4.56}$$

which coincides with Eq. (4.52), keeping in mind that $d \approx hvk/|eE|$.

If we have crossed electric and magnetic fields E and B ($B \,||\, Oz$), one can use the Lorentz transformation, similarly to what was done in Section 2.10 (see Eqs. (2.196) and (2.197)). In the case

$$E > \frac{v}{c}B, \tag{4.57}$$

which is complementary to Eq. (2.198), one can exclude the *magnetic* field, and the electric field E is replaced in Eq. (4.56) by

$$E\sqrt{1 \quad \left(\frac{vB}{cE}\right)^2} = \sqrt{E^2 \quad \left(\frac{vB}{c}\right)^2}$$

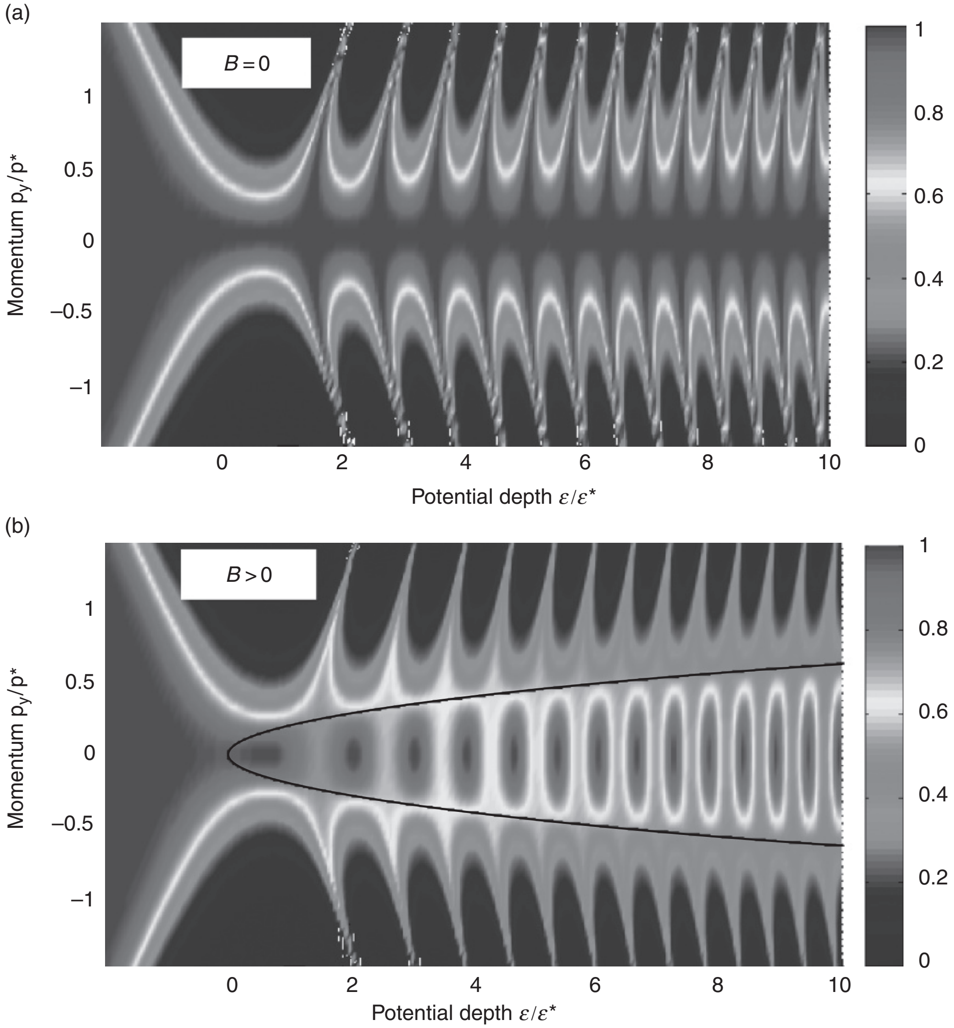

Fig. 4.5. The transmission coefficient, obtained from numerical solution of the Dirac equation with the potential (4.58), plotted as a function of the component of electron momentum p_y and potential depth. At zero magnetic field (a), transmission exhibits fringes with a phase that is nearly independent of p_y. At finite magnetic field (b), the fringe contrast reverses its sign on the parabola (black thin line). Here $\varepsilon^* = \left(ah^2v^2\right)^{1/3}$ and $p^* = \varepsilon^*/v$. (Reproduced with permission from Shytov, Rudner & Levitov (2008)).

(cf. Eq. (2.200)). The effects of disorder on the motion of an electron near a p n junction were considered by Fogler *et al.* (2008).

Shytov, Rudner & Levitov (2008) studied the case of a parabolic potential barrier,

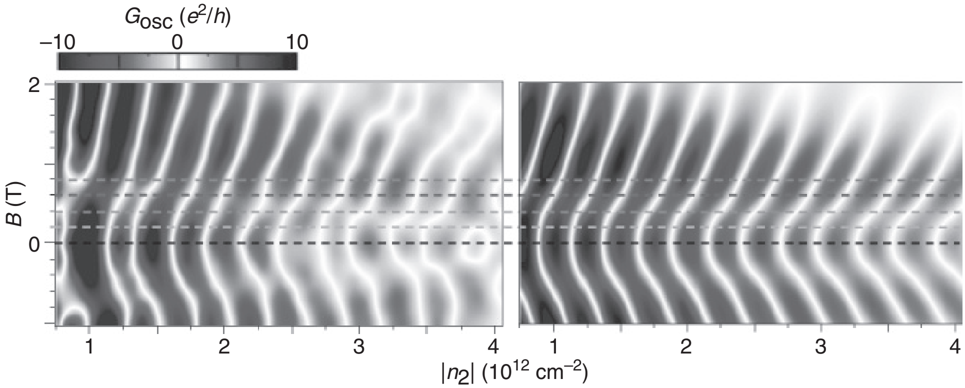

Fig. 4.6. The magnetic-field and density dependences of the conductance of a p–n–p junction in graphene; left and right panels present experimental data and theoretical results, respectively. (Reproduced with permission from Young & Kim, 2009.)

$$V(x) = ax^2 - \varepsilon \tag{4.58}$$

(a, $\varepsilon > 0$), which creates p–n boundaries at

$$x = \pm x_\varepsilon \equiv \pm\sqrt{\frac{\varepsilon}{a}}. \tag{4.59}$$

The magnetic field B is included in the Landau gauge, $A_x = 0$, $A_y = -B_x$. Numerical solution of the Schrödinger equation gives the results shown in Fig. 4.5. One can see that a region of 100% transmission can exist not only for a rectangular barrier (see Eq. (4.49)) but also for a more general potential. At the same time, for *nonsymmetric* potentials, $V(x) \neq V(-x)$, the side resonances with $\varphi \neq 0$ turn out to be suppressed (Tudorovskiy, Reijnders & Katsnelson, 2012). The magnetic field modifies the picture of the transmission in a peculiar way. Oscillations of the conductance through the barrier as a function of the magnetic field were observed by Young & Kim (2009) (Fig. 4.6).

4.5 Negative refraction coefficient and Veselago lenses for electrons in graphene

As was discussed in Section 4.1, the group velocity $\vec{v}_g$ is parallel to the wave vector $\vec{k}$ for particles (electrons) and antiparallel for antiparticles (holes). In the situation of the Klein paradox, the incident and transmitted waves propagate, by definition, in the same direction, and the propagation direction is determined by the group velocity. This means that the wave vectors for these waves are antiparallel. For massless particles with a linear dispersion, the group velocity is

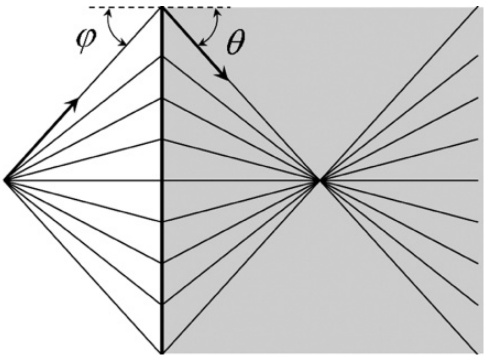

Fig. 4.7. A Veselago lens for the case of a negative refraction index.

$$\vec{v}_{\mathrm{g}} = \pm v \frac{\vec{k}}{k}, \tag{4.60}$$

where the signs + and correspond to electrons and holes, respectively. The incident electron wave has the wave vector $\vec{k} = k(\cos\varphi, \sin\varphi)$ and the group velocity $\vec{v}_{\mathrm{e}} = v(\cos\varphi, \sin\varphi)$. The reflected wave has the wave vector $\vec{k}' = k(\ \cos\varphi, \sin\varphi)$ and the group velocity $\vec{v}_{\mathrm{e}}' = v(\ \cos\varphi, \sin\varphi)$. For the transmitted wave, in the situation of the Klein paradox (or for a p n junction, using conventional semiconductor terminology) the group velocity $\vec{v}_{\mathrm{h}} = v(\cos\theta', \sin\theta')$ and the wave vector $\vec{q} = \ q(\cos\theta', \sin\theta')$, $\cos\theta' > 0$, q is determined by Eq. (4.41) and $\theta' = \ \theta$. The refraction angle θ' is determined by the continuity of the y-component of the wave vector (see Eq. (4.40)), or

$$\frac{\sin\theta'}{\sin\varphi} = \ \frac{k}{q} \equiv n \tag{4.61}$$

with a negative refractive index n. This means that the p n junction in graphene transforms a divergent electron beam into a collimated one, see Fig. 4.7 (Cheianov, Falko & Altshuler, 2007).

In optics such devices are known as Veselago lenses (Veselago, 1968), and materials with negative refractive indices are called left-handed materials, or metamaterials (Pendry, 2004). Creation of such a material for the visual light is not an easy task. For electrons in graphene such a situation can be realized quite easily. For a detailed discussion of the relation between the negative refraction index and the Klein paradox, see Güney & Meyer (2009).

4.6 Klein tunnelling and minimal conductivity

As was stressed in the previous chapter, the existence of a minimal conductivity of the order of e^2/h is one of the striking properties of graphene. We

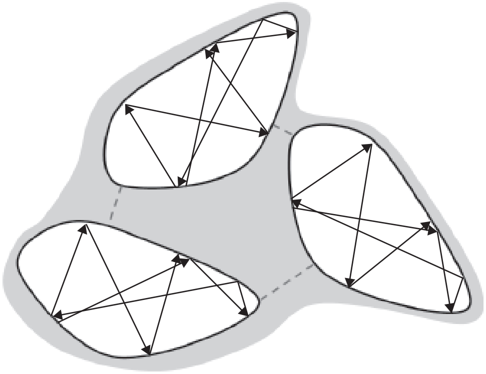

Fig. 4.8. A sketch of electronic states in conventional semiconductors with strong disorder; electrons tunnel, with a small probability, between classically allowed regions.

discussed this from the perspective of pure samples (the ballistic regime). It is instructive to consider the same problem from the opposite perspective of strong disorder (Katsnelson, Novoselov & Geim, 2006).

It is worth recalling first some basic ideas on the electronic structure of strongly disordered systems (Mott, 1974; Mott & Davis, 1979; Shklovskii & Efros, 1984; Lifshitz, Gredeskul & Pastur, 1988). Let us start with the case in which typical fluctuations of the potential energy $V(x, y)$ are much stronger than the kinetic energy T. The electrons are locked into puddles restricted by the equipotential lines $E = V(x, y)$. There is a small probability of tunnelling from one puddle to another, so some electrons are distributed among couples of puddles, fewer electrons among trios of puddles, etc. (Fig. 4.8). On increasing the ratio $|T/V|$ the tunnelling probability increases, and at some point a percolation transition happens (Shklovskii & Efros, 1984), with the formation of an infinite cluster of regions connected by electron tunnelling. This percolation is associated with the Mott Anderson metal insulator transition, although the latter involves more then just percolation, since phase relations between the electron wave functions are also important (Mott & Davis, 1979).

The Klein tunnelling changes the situation dramatically. However small the kinetic energy is (or, equivalently, however high and broad the potential barriers are), the electrons cannot be locked into puddles (Fig. 4.9). Thus, their states cannot be localized.

In the absence of Anderson localization, the minimal conductivity can be estimated via Mott's considerations on the basis of the remark by Ioffe and Regel that for extended states the electron mean free path l cannot be smaller than the electron de Broglie wave length (Mott, 1974; Mott & Davis, 1979). Here we apply this general consideration to graphene.

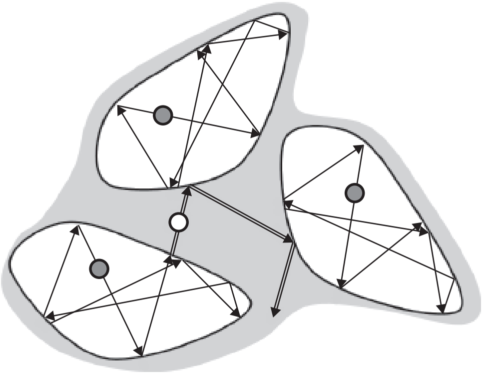

Fig. 4.9. A sketch of electronic states in graphene with strong disorder; due to Klein tunnelling, electrons cannot be locked and penetrate through p–n boundaries, transforming into holes.

Let us start with Einstein's relation between the conductivity σ and the electron diffusion coefficient D,

$$\sigma = e^2 \frac{\partial n}{\partial \mu} D \tag{4.62}$$

(Zubarev, 1974). For a noninteracting degenerate (obeying Fermi statistics) electron gas

$$\frac{\partial n}{\partial \mu} = N(E_{\mathrm{F}}) = \frac{2|E_F|}{\pi \hbar^2 v^2} = \frac{2k_F}{\pi \hbar v} \tag{4.63}$$

(see Eqs. (2.138) and (1.72)). For the two-dimensional case, the diffusion coefficient is

$$D = \frac{1}{2} v^2 \tau, \tag{4.64}$$

where τ is the electron mean-free-path time. On substituting Eqs. (4.63) and (4.64) into (4.62) one finds

$$\sigma = \frac{e^2}{\pi \hbar} k_{\mathrm{F}} l = \frac{2e^2}{h} k_{\mathrm{F}} l, \tag{4.65}$$

where $l = v\tau$ is the mean free path. Assuming that the minimal possible value of $k_{\mathrm{F}} l$ is of the order of unity, we have an estimation for the minimal conductivity of

$$\sigma_{\min} \sim \frac{e^2}{h} \tag{4.66}$$

coinciding, in the order of magnitude, with the ballistic conductivity $e^2/(\pi h)$ per channel (see Eq. (3.18)).

This conclusion is very important, in the light of experimental observation of electron–hole puddles in graphene on a substrate in the vicinity of the neutrality point (Martin *et al.*, 2007). Moreover, it was demonstrated theoretically that the puddles are unavoidable even for freely suspended graphene at room temperature since the inhomogeneities of electron density result from thermal bending fluctuations (Gibertini *et al.*, 2010); this phenomenon will be considered in detail in Chapter 10. It is the Klein tunnelling which protects electron states from localization and makes large-scale inhomogeneities rather irrelevant for electron transport.

The minimal conductivity was analysed in terms of classical percolation by Cheianov *et al.* (2007). It follows from their analysis that the minimal conductivity is of the order of e^2/h if the number of electrons (holes) per puddle is of the order of one.

4.7 Chiral tunnelling in bilayer graphene

To elucidate which features of the anomalous tunnelling in graphene are related to the linear dispersion and which features are related to the pseudospin and chirality of the Dirac spectrum, it is instructive to consider the same problem for bilayer graphene (Katsnelson, Novoselov & Geim, 2006). We will restrict ourselves to the case of moderate electron energies, for which the parabolic approximation (1.46) works. This means that the energies are smaller than that of interlayer hopping, both outside and inside the barrier:

$$|E|, |E - V_0| \ll 2|\gamma_1| \tag{4.67}$$

and, at the same time, the trigonal warping effects are not important,

$$ka,\ qa > \left|\frac{\gamma_3\gamma_1}{\gamma_0^2}\right| \tag{4.68}$$

(cf. Eq. (1.55)), where we assume that the potential barrier has the shape (4.20), and k and q are the wave vectors outside and inside the barrier, respectively:

$$k = \sqrt{\frac{2m^*|E|}{h^2}}, \qquad q = \sqrt{\frac{2m^*|E - V_0|}{h^2}}. \tag{4.69}$$

Assuming that the wave function propagates in the y-direction with the wave-vector component k_y, the two components of the spinor wave function are

$$\begin{aligned} \psi_1(x,y) &= \psi_1(x)\exp\left(ik_y y\right), \\ \psi_2(x,y) &= \psi_2(x)\exp\left(ik_y y\right), \end{aligned} \tag{4.70}$$

where $\psi_i\,(x)$ satisfy the second-order equations

$$\left(\frac{d^2}{dx^2} - k_y^2\right)^2 \psi_i = k^4\psi_i \tag{4.71}$$

outside the barrier and

$$\left(\frac{d^2}{dx^2} - k_y^2\right)^2 \psi_i = q^4\psi_i \tag{4.72}$$

inside it. At the boundaries $x = \pm a$ one has to require that four conditions be fulfilled, namely continuity of ψ_1, ψ_2, $d\psi_1/dx$ and $d\psi_2/dx$. To satisfy them one has to include not only propagating but also evanescent solutions of Eqs. (4.71) and (4.72) but, of course, without the terms growing exponentially at $x \to \pm\infty$.

Let us consider first the case $x < -a$. The two components of the wave function can be found from the equations

$$\begin{aligned} \left(\frac{d}{dx} + k_y\right)^2 \psi_2 &= sk^2\psi_1, \\ \left(\frac{d}{dx} - k_y\right)^2 \psi_1 &= sk^2\psi_2, \end{aligned} \tag{4.73}$$

where $s = \operatorname{sgn} E$ (cf. Eq. (4.45)). Thus, for this region one can try the solutions

$$\begin{aligned} \psi_1(x) &= \alpha_1 \exp(ik_x x) + \beta_1 \exp(-ik_x x) + \gamma_1 \exp(\chi_x x), \\ \psi_2(x) &= s[\alpha_1 \exp(ik_x x + 2i\varphi) + \beta_1 \exp(-ik_x x - 2i\varphi) - \gamma_1 h_1 \exp(\chi_x x)], \end{aligned} \tag{4.74}$$

where φ is the angle of incidence,

$$k_y = k\sin\varphi, \qquad k_x = k\cos\varphi, \tag{4.75}$$

$$\chi_x = \sqrt{k_x^2 + 2k_y^2} = k\sqrt{1 + \sin^2\varphi} \tag{4.76}$$

and

$$h_1 = \left(\sqrt{1 + \sin^2\varphi} - \sin\varphi\right)^2. \tag{4.77}$$

The coefficients α_1, β_1 and γ_1 are the amplitudes of the incident, reflected and evanescent waves, respectively.

For the case $x > a$ there is no reflected wave:

$$\begin{aligned} \psi_1(x) &= \alpha_3 \exp(ik_x x) + \delta_3 \exp(-\chi_x x), \\ \psi_2(x) &= s\left[\alpha_3 \exp(ik_x x + 2i\varphi) - \frac{\delta_3}{h_1} \exp(-\chi_x x)\right]; \end{aligned} \tag{4.78}$$

the phase factor $\exp(2i\varphi)$ follows from Eq. (1.48). Finally, inside the barrier $|x| < a$ one has to use the most general solution with two propagating and two evanescent waves:

$$\begin{aligned} \psi_1(x) &= \alpha_2 \exp(iq_x x) + \beta_2 \exp(-iq_x x) + \gamma_2 \exp(\chi'_x x) + \delta_2 \exp(-\chi'_x x), \\ \psi_2(x) &= s'\Big[\alpha_2 \exp(iq_x x + 2i\theta) + \beta_2 \exp(-iq_x x - 2i\theta) - \gamma_2 h_2 \exp(\chi'_x x) \\ &\qquad - \frac{\delta_2}{h_2} \exp(-\chi'_x x)\Big], \end{aligned} \tag{4.79}$$

where θ is the refraction angle,

$$q_y = q \sin\theta = k_y, \qquad q_x = q\cos\theta, \tag{4.80}$$

$$\chi'_x = q\sqrt{1 + \sin^2\theta}, \tag{4.81}$$

$$h_2 = \left(\sqrt{1 + \sin^2\theta} - \sin\theta\right)^2 \tag{4.82}$$

and $s' = \operatorname{sgn}(E - V_0)$ (cf. Eq. (4.45)). The presence of the evanescent waves is a very interesting feature of bilayer graphene that is dramatically different both from the Dirac case and from the Schrödinger case.

Now we have to find the coefficients α_i, β_i, γ_i and δ_i from eight conditions of continuity of $\psi_i(x)$ and $d\psi_i(x)/dx$ at $x = a$ and $x = -a$. In general, this can be done only numerically. Typical results for the 'Klein' case $ss' = -1$ are shown in Fig. 4.4(b). Similarly to the case of single-layer graphene, there are 'magic angles' with transmission probability equal to unity.

For the case of normal incidence ($\varphi = 0$, $\theta = 0$) the problem can be solved analytically, and the result for the transmission coefficient is

$$t = \frac{\alpha_3}{\alpha_1} = \frac{4ikq \exp(2ika)}{(q + ik)^2 \exp(-2qa) - (q - ik)^2 \exp(2qa)}. \tag{4.83}$$

In contrast with the case of single-layer graphene, $T = |t|^2$ decays exponentially with the height and the width of the barriers, as $\exp(-4qa)$ for $\varphi = 0$.

This illustrates a drastic difference between the cases of chiral scattering with Berry phases π and 2π. For the latter case, the condition (1.49) does not fix the projection of the pseudospin to the direction of the motion (cf. Eq. (1.33)), so the conservation of the chirality does not forbid backscattering.

For the case $a \to \infty$ (which is just a potential step corresponding to a single p n junction) $T = 0$ at $\varphi = 0$, which looks rather counterintuitive: there is a continuum of allowed states after the barrier but the penetration there is forbidden. Furthermore, for a single p n junction with $V_0 \gg E$, the following analytic solution for any φ has been found:

$$T = \frac{E}{V_0} \sin^2(2\varphi), \tag{4.84}$$

which, again, yields $T = 0$ for $\varphi = 0$. This behaviour is in obvious contrast with that of single-layer graphene, where normally incident electrons are always perfectly transmitted.

The perfect reflection (instead of perfect transmission) can be viewed as another incarnation of the Klein paradox, because the effect is again due to the charge-conjugation symmetry. For single-layer graphene, an electron wave function at the barrier interface perfectly matches the corresponding wave function for a hole with the same direction of pseudospin, yielding $T = 1$. In contrast, for bilayer graphene, the charge conjugation requires a propagating electron with wave vector k to transform into a hole with wave vector ik (rather than k), which is an evanescent wave inside a barrier.

For completeness, we compare the results obtained with those from the case of conventional nonrelativistic electrons. If a tunnel barrier contains no electronic states, the difference is obvious: the transmission probability in this case is known to decay exponentially with increasing barrier width and height (Esaki, 1958), so that the tunnel barriers discussed above would reflect electrons completely. However, both graphene systems are gapless, and it is more appropriate to compare them to gapless semiconductors with nonchiral charge carriers (such a situation can be realized in certain heterostructures (Meyer *et al.*, 1995; Teissier *et al.*, 1996)). In this case, we find

$$t = \frac{4k_x q_x \exp(2iq_x a)}{(q_x + k_x)^2 \exp(\;\;2iq_x a) \quad (q_x \quad k_x)^2 \exp(2iq_x a)}, \tag{4.85}$$

where k_x and q_x are the x-components of the wave vector outside and inside the barrier, respectively. Again, similarly to the case of single-layer and bilayer graphene, there are resonance conditions $2q_x\, a = \pi N$, $N = 0, \pm 1, \ldots$, at which the barrier is transparent. For the case of normal incidence ($\varphi = 0$), the

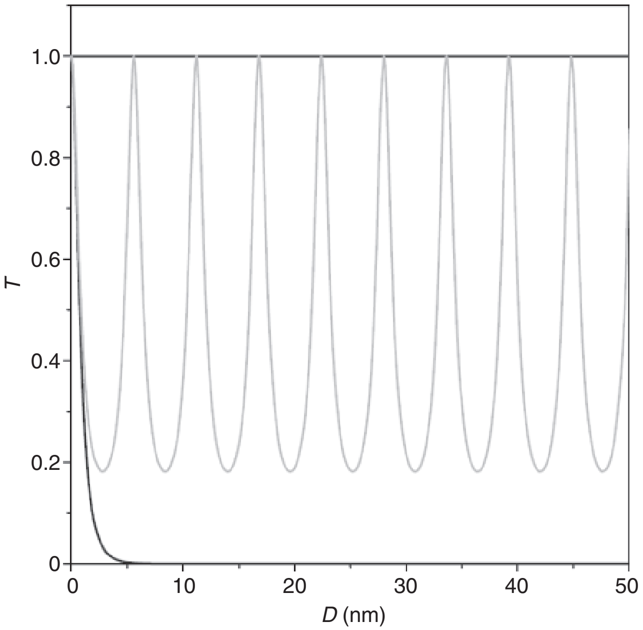

Fig. 4.10. The transmission probability T for normally incident electrons in single-layer and bilayer graphene and in a nonchiral zero-gap semiconductor as a function of the width D of the tunnel barrier. The concentrations of charge carriers are chosen as $n = 0.5 \times 10^{12}$ cm^{-2} and $p = 1 \times 10^{13}$ cm^{-2} outside and inside the barrier, respectively, for all three cases. The transmission probability for bilayer graphene (the lowest line) decays exponentially with the barrier width, even though there are plenty of electronic states inside the barrier. For single-layer graphene it is always 1 (the upper line). For the nonchiral semiconductor it oscillates with the width of the barrier (the intermediate curve). (Reproduced with permission from Katsnelson, Novoselov & Geim, 2006.)

tunnelling coefficient is then an oscillating function of the tunnelling parameters and can exhibit any value from 0 to 1 (see Fig. 4.10). This is in contrast with graphene, for which T is always 1, and bilayer graphene, for which $T = 0$ for sufficiently wide barriers. This makes it clear that the drastic difference among the three cases is essentially due to the different chiralities or pseudospins of the quasiparticles involved rather than any other features of their energy spectra.

The existence of magic angles with 100% transmission for the case of bilayer graphene implies, again, that there is no way to lock the electrons into a restricted region of strongly disordered bilayer graphene. One could therefore expect the existence of a minimal conductivity of the order of e^2/h in this case as well, in agreement with experiment (Novoselov *et al.*, 2006).

To summarize this chapter, the Klein paradox is a key phenomenon for electronic transport in graphene and for graphene-based electronics. On the one hand, it protects high electron mobility in inhomogeneous graphene and prevents Anderson localization. On the other hand, it is an essential obstacle to copying a ‘normal’ transistor based on p n p (or n p n) junctions in conventional semiconductors. Usually, one can easily lock the transistor by applying a voltage to the potential barrier, which is impossible for the cases of both single-layer and bilayer graphene due to the Klein paradox. One needs to open a gap in the electron spectrum. One of the most natural ways to do this is the use of space quantization in graphene nanoribbons and nanoflakes, which will be one of the subjects of the next chapter.

5

Edges, nanoribbons and quantum dots

5.1 The neutrino billiard model

Owing to the Klein paradox, the massless Dirac fermion cannot be confined in a restricted region by any configuration of a purely electrostatic (scalar) potential $V(x, y)$; one needs the gap opening. As discussed in Section 1.3, this requires a violation of the equivalence of the sublattices. Let us consider the Hamiltonian

$$\hat{H} = \quad ihv\vec{\sigma}\nabla + \sigma_z\Delta(x, y), \tag{5.1}$$

where the last term represents a difference of potential energy between the A and B sites (or between (pseudo)spin up and (pseudo)spin down states). With $\Delta =$ constant the energy spectrum of the Hamiltonian (5.1) is

$$E\left(\vec{k}\right) = \pm\sqrt{h^2v^2k^2 + \Delta^2}, \tag{5.2}$$

where $\vec{k}$ is the wave vector and there is the energy gap $2|\Delta|$. For a given energy E, the regions where $|E| < |\Delta(x, y)|$ are classically forbidden; quantum mechanically, the probability of tunnelling to these regions decays exponentially with the distance from the boundary. In particular, one can introduce the boundary condition

$$|\Delta(x, y)| = \pm\infty \tag{5.3}$$

at a line L; thus, only the region D restricted by the line L is allowed for the particle (Fig. 5.1). The line L is parameterized by the length s counted from some initial point:

$$x = x_{\mathrm{L}}(s), \qquad y = y_{\mathrm{L}}(s) \tag{5.4}$$

We will assume

$$\Delta(x, y) = 0 \tag{5.5}$$

within the region D.

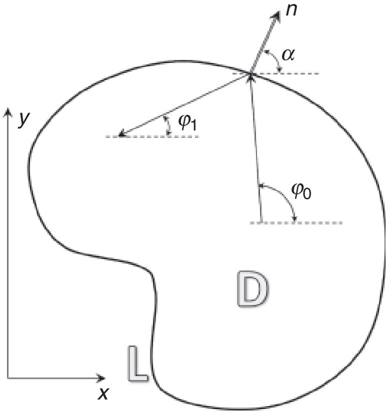

Fig. 5.1. The geometry of a 'neutrino billiard'. The particle moves within the region D restricted by the line L where the infinite-energy gap opens.

This model was considered by Berry & Mondragon (1987) long before the discovery of graphene and was called the 'neutrino billiard' (at that time it was assumed that the neutrino had zero mass). It is not sufficient to describe completely the edge effects and confinement in graphene nanoribbons and nanoflakes: as we will see further the existence of two valleys is of crucial importance, thus, the single Dirac point approximation is not enough. However, it contains already some important physics, so it is convenient to start our consideration with this model.

An important property of the Hamiltonian (5.1) is that it is not invariant under the time-reversal symmetry operation $\hat{T}$. The latter can be represented (Landau & Lifshitz, 1977) as

$$\hat{T} = \hat{U}\hat{K}, \tag{5.6}$$

where

$$\hat{U} = i\hat{\sigma}_y = \begin{pmatrix} 0 & 1 \\ 1 & 0 \end{pmatrix} \tag{5.7}$$

and $\hat{K}$ is the complex conjugation. Under this operation the Hamiltonian $\hat{H}$ (5.1) is transformed into

$$\hat{H}' = \hat{U}\hat{H}^*\hat{U}^+ = \quad ihv\vec{\sigma}\nabla \quad \sigma_z\Delta(x, y) \tag{5.8}$$

and differs from Eq. (5.1) by the sign of Δ. This means that there is no Kramers degeneracy (Landau & Lifshitz, 1977) of the energy levels of the Hamiltonian (5.1). At the same time this means that the energy spectrum is insensitive to the sign of Δ: if

$$\Psi = \begin{pmatrix} \psi_1 \\ \psi_2 \end{pmatrix}$$

is an eigenstate of the Hamiltonian (5.1) with an energy E the function

$$\Psi' = \hat{T}\Psi = \begin{pmatrix} \psi_2^* \\ \psi_1^* \end{pmatrix} \tag{5.9}$$

corresponds to the same eigenvalue E for the Hamiltonian (5.8). Obviously, Ψ' is orthogonal to Ψ since $(\Psi')^* \, \Psi \equiv 0$.

The most general boundary condition for the Hamiltonian (5.1) and (5.5) follows from the requirement that it should be Hermitian (or, equivalently, its energy spectrum should be real). Using the Gauss theorem, one has

$$\begin{aligned} \iint\limits_{D} dx\,dy\left(\Psi^+\hat{H}\Psi \quad \Psi^+\hat{H}^+\Psi\right) &= \quad ih v\iint\limits_{D} dx\,dy[\Psi^+\vec{\sigma}\,\nabla\Psi + (\nabla\Psi^+)\vec{\sigma}\Psi] \\ &= \quad ih v\iint\limits_{D} dx\,dy\,\nabla[\Psi^+\vec{\sigma}\Psi] \\ &= \quad ih\oint\limits_{L} ds\,\vec{n}(s)\vec{j}(s) = 0, \end{aligned} \tag{5.10}$$

where $\vec{n}$ is the unit vector normal to the curve L and $\vec{j} = v\Psi^+\vec{\sigma}\Psi$ is the current density (cf. Eq. (3.2)).

The local boundary condition must ensure that there is no normal current to the boundary at any point. On introducing the angle α such that

$$\vec{n} = (\cos\alpha, \sin\alpha) \tag{5.11}$$

(see Fig. 5.1) one can write this condition as

$$\cos\alpha\ \mathrm{Re}\left(\psi_1^*\psi_2\right) + \sin\alpha\ \mathrm{Im}\left(\psi_1^*\psi_2\right) = 0 \tag{5.12}$$

or, equivalently,

$$\frac{\psi_2}{\psi_1} = iB\exp(i\alpha(s)), \tag{5.13}$$

where $B = B(s)$ is real.

To specify B one can consider first the case of a flat boundary $L \parallel Oy$. One can assume that $\Delta = 0$ at $x < 0$ and $\Delta = \Delta_0 =$ constant at $x > 0$, solve explicitly the Dirac equation as was done in the previous chapter, consider the reflection problem and compare the result for $\psi_2(x = \quad 0)/\psi_1(x = \quad 0)$ with Eq. (5.13) at $\alpha = 0$. One can see that

$$B = \pm 1 \tag{5.14}$$

at $\Delta_0 \to \pm\infty$. We will call Eq. (5.13) with $B = \pm 1$ the *infinite-mass boundary condition* (Berry & Mondragon, 1987).

It is not surprising that this boundary condition is not invariant under the time-reversal operation. Indeed, it follows from Eqs. (5.9) and (5.13) that

$$\frac{\psi_2'}{\psi_1'} = \left(\frac{\psi_1}{\psi_2}\right)^* = iB\exp(i\alpha(s)), \tag{5.15}$$

which differs from Eq. (5.13) by the sign (we have taken into account that $B^2 = 1$).

Confinement of electrons in a finite region leads to a discrete energy spectrum. Consider first the simplest case in which L is just a circle, $r = R$, where we pass to the polar coordinates

$$x = r\cos\varphi, \qquad y = y\sin\varphi. \tag{5.16}$$

In these coordinates,

$$i\vec{\sigma}\nabla = i\begin{pmatrix} 0 & e^{\;i\varphi}\left(\frac{\partial}{\partial r} \quad \frac{i}{r}\frac{\partial}{\partial\varphi}\right) \\ e^{i\varphi}\left(\frac{\partial}{\partial r} + \frac{i}{r}\frac{\partial}{\partial\varphi}\right) & 0 \end{pmatrix} \tag{5.17}$$

and the Schrödinger equation for the state with $E = hvk$ takes the form

$$\begin{aligned} e^{\;i\varphi}\left(\frac{\partial}{\partial r} \quad \frac{i}{r}\frac{\partial}{\partial\varphi}\right)\psi_2 &= ik\psi_1, \\ e^{i\varphi}\left(\frac{\partial}{\partial r} + \frac{i}{r}\frac{\partial}{\partial\varphi}\right)\psi_1 &= ik\psi_2. \end{aligned} \tag{5.18}$$

One can try solutions of Eq. (5.18) of the form

$$\begin{aligned} \psi_1(r,\varphi) &= \psi_1(r)\exp(il\varphi), \\ \psi_2(r,\varphi) &= \psi_2(r)\exp[i(l+1)\varphi], \end{aligned} \tag{5.19}$$

where l is integer. On substituting Eq. (5.19) into Eq. (5.18) one has

$$\begin{aligned} \frac{d\psi_2}{dr} + \frac{l+1}{r}\psi_2 &= ik\psi_1, \\ \frac{d\psi_1}{dr} \quad \frac{l}{r}\psi_1 &= ik\psi_2. \end{aligned} \tag{5.20}$$

By excluding ψ_1 (or ψ_2) from Eq. (5.20) one can find a second-order differential equation for the Bessel functions (Whittaker & Watson, 1927). The solutions regular at $r \to 0$ are

$$\begin{aligned}\psi_1(r) &= J_l(kr),\\ \psi_2(r) &= iJ_{l+1}(kr).\end{aligned} \tag{5.21}$$

The energy spectrum $k = k_{nl}$ can be found from the boundary condition (5.13) keeping in mind that for the circle $\alpha = \varphi$. Thus, the quantization rule for the disc is

$$J_{l+1}(k_{nl}R) = BJ_l(k_{nl}R). \tag{5.22}$$

This leads to a discrete spectrum with a distance between neighbouring energy levels with a given l of

$$\delta_l(E) \cong \frac{\pi hv}{R}. \tag{5.23}$$

The density of states of the whole system is an extensive quantity proportional (in two dimensions) to the system area A. Therefore, the average energy distance (for an arbitrary shape of the billiard, not necessarily for the disc) can be estimated as

$$\delta(E) \approx \frac{1}{N(E)A}, \tag{5.24}$$

where $N(E)$ is the density of states of the Dirac Hamiltonian per unit area:

$$N(E) = \frac{E}{2\pi h^2 v^2} = \frac{k}{2\pi hv}. \tag{5.25}$$

It differs from Eq. (1.72) by a factor of 4 (here we do not take into account the fourfold spin and valley degeneracy for graphene). The semiclassical estimation (5.24) (see Perenboom, Wyder & Meier, 1981; Halperin, 1986; Stöckmann, 2000) is valid at

$$k\sqrt{A} \gg 1. \tag{5.26}$$

For the case of a circular disc Eq. (5.20) gives, taking into account Eqs. (5.23) (5.25),

$$\delta(E) \approx \frac{\delta_l(E)}{kR} \propto \frac{1}{R^2} \quad (kR \gg 1). \tag{5.27}$$

There is an important issue relating to the energy-level distribution in finite systems (Bohr & Mottelson, 1969; Perenboom, Wyder & Meier, 1981; Stöckmann, 2000). In the case of integrable systems with regular classical motion of particles it is supposed that it follows the Poisson statistics. It was shown by Berry & Mondragon (1987) that this is indeed the case for the spectrum determined by Eq. (5.22). For a generic system with chaotic motion level repulsion takes place, and the probability of finding two very close energy levels is strongly suppressed. The main physical statement can be seen just from the two-level quantum-mechanical problem with a 2×2 Hamiltonian, for which the splitting of eigenvalues is

$$\Delta_{1,2} = \sqrt{(H_{11} - H_{22})^2 + 4|H_{12}|^2}. \tag{5.28}$$

If the Hamiltonian matrix is diagonal the probability of degeneracy $\Delta_{1,2} = 0$ is equal to the probability that $H_{11} = H_{22}$; if the matrix is off-diagonal and real, it is the probability that $H_{11} = H_{22}$ and $H_{12} = 0$; if it is not real, it is the probability that $H_{11} = H_{22}$, and Re $H_{12} = 0$ and Im $H_{12} = 0$, which is obviously smaller.

For a generic chaotic system with time-reversal symmetry (this means that there exists the basis in which the Hamiltonian is real) the distribution of the neighbouring levels, $S = \Delta E/\delta(E)$, is given by the Gaussian orthogonal ensemble (GOE), with the probability function

$$P_{\text{GOE}}(S) = \frac{\pi S}{2} \exp\left(-\frac{\pi S^2}{4}\right), \tag{5.29}$$

whereas without time-reversal symmetry we have the Gaussian unitary ensemble (GUE), with

$$P_{\text{GUE}}(S) = \frac{32 S^2}{\pi^2} \exp\left(-\frac{4 S^2}{\pi}\right) \tag{5.30}$$

(Bohr & Mottelson, 1969; Perenboom, Wyder & Meier, 1981; Stöckmann, 2000).

The numeral calculations of Berry & Mondragon (1987) demonstrate that the level distribution for neutrino billiards with chaotic classical motion obeys the GUE statistics (5.30). This is the consequence of violation of the time-reversal symmetry, which was discussed above.

5.2 A generic boundary condition: valley mixing

As was discussed in Chapter 1, charge carriers in graphene can be described in the single Dirac-cone approximation only if all external inhomogeneities are smooth at the atomic scale. The edges of the terminated honeycomb lattice are sharp and can, in general, mix the electron states belonging to different valleys. So, one should use a more general, two-valley Hamiltonian (1.28) (we will use here the representation (1.27)). The current operator (cf. Eq. (3.3)) is

$$\hat{\vec{j}} = \frac{\delta \hat{H}}{\delta \vec{p}} = v \tau_0 \otimes \vec{\sigma}. \tag{5.31}$$

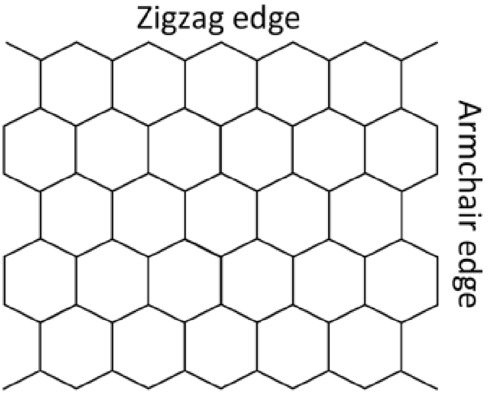

Fig. 5.2. Zigzag and armchair edges of the honeycomb lattice.

The most general restriction on the boundary condition generalizing Eqs. (5.10) and (5.12) in the two-valley case is the absence of the normal component of the current through the boundary,

$$\left\langle\Psi\middle|\vec{n}(s)\hat{\vec{j}}\middle|\Psi\right\rangle = 0, \tag{5.32}$$

at any s.

We will consider, following McCann & Falko (2004) and Akhmerov & Beenakker (2008), the boundary conditions for the abruptly terminated honeycomb lattice, with zero probability of finding an electron outside the graphene flake. The simplest terminations, *zigzag* and *armchair* edges, are shown in Fig. 5.2.

Then the Schrödinger equation inside the flake reads

$$\left[\quad ihv\tau_0 \otimes \vec{\sigma}\,\nabla + hv\hat{M}'\delta(\vec{r} \quad \vec{r}_{\mathrm{B}})\right]\Psi = E\Psi, \tag{5.33}$$

where $\vec{r} = \vec{r}_{\mathrm{B}}(s)$ in the equation of the boundary line L and $\hat{M}'$ is an energy-independent Hermitian matrix. By integrating Eq. (5.33) along an infinitesimal line parallel to the normal $\vec{n}(s)$ to the boundary and taking into account that $\Psi = 0$ outside the flake one finds the boundary condition

$$\hat{A}\Psi = i\hat{M}'\Psi \tag{5.34}$$

at $\vec{r} = \vec{r}_{\mathrm{B}}(s)$, where

$$\hat{A} = \vec{n}\hat{\tau}_0 \otimes \hat{\vec{\sigma}} = \frac{1}{v}\vec{n}\cdot\hat{\vec{j}} \tag{5.35}$$

$\left(\hat{A}^2 = 1\right)$. Equivalently, the condition (5.34) can be represented as

$$\Psi = \hat{M}\Psi \quad (\vec{r} = \vec{r}_{\mathrm{B}}), \tag{5.36}$$

where

$$\hat{M} = i\hat{A}\hat{M}'. \tag{5.37}$$

On iterating Eq. (5.36) one can see that

$$\hat{M}^2 = 1. \tag{5.38}$$

If we require that the Hermitian matrices $\hat{A}$ and $\hat{M}'$ anticommute,

$$\left\{\hat{A}, \hat{M}'\right\} = 0, \tag{5.39}$$

the matrix (5.37) turns out to be Hermitian and, due to Eq. (5.38), also unitary:

$$\hat{M}^+ = \hat{M} = \hat{M}^{-1}. \tag{5.40}$$

It also anticommutes with the matrix $\hat{A}$:

$$\left\{\hat{A}, \hat{M}\right\} = i\hat{A}^2\hat{M}' + i\left(\hat{A}\hat{M}'\right)\hat{A} = 0 \tag{5.41}$$

and the condition (5.32) is satisfied automatically in this case:

$$\Psi^+\hat{A}\Psi = \Psi^+\hat{M}^+\hat{A}\hat{M}\Psi = -\Psi^+\hat{A}\Psi = 0. \tag{5.42}$$

Thus, the boundary condition (5.36) with the most general matrix $\hat{M}$ satisfying the requirements (5.40) and (5.41) seems to be the most general form of the boundary conditions at the edges of terminated graphene flakes.

As was proven by Akhmerov & Beenakker (2008) the most general allowed matrix $\hat{M}$ can be represented as

$$\hat{M} = \sin\Lambda\,\hat{\tau}_0 \otimes \left(\vec{n}_1\hat{\vec{\sigma}}\right) + \cos\Lambda\left(\vec{v}\hat{\vec{\tau}}\right) \otimes \left(\vec{n}_2\hat{\vec{\sigma}}\right), \tag{5.43}$$

where Λ is an arbitrary real number and $\vec{v}$, $\vec{n}_1$ and $\vec{n}_2$ are three-dimensional unit vectors such that $\vec{n}_1$ and $\vec{n}_2$ are mutually orthogonal and also orthogonal to $\vec{n}$ ($\vec{v}$ is arbitrary).

One can assume that the boundary conditions for the graphene flake as a whole should be time-reversal-symmetric. Formally this follows from the fact that the tight-binding Hamiltonian for the honeycomb lattice in real space can be chosen as a *real* matrix. The time-reversal symmetry can be broken by spontaneous valley polarization at the edges or by spin polarization plus spin–orbit coupling. So far, there is no experimental evidence for such phenomena.

On generalizing the definition of the time-reversal operation (5.6) to the case of two valleys one can write

$$\hat{T} = -\hat{\tau}_y \otimes \hat{\sigma}_y \cdot \hat{K}. \tag{5.44}$$

The matrix $\hat{M}$ (5.43) commutes with $\hat{T}$ only at $\Lambda = 0$; thus, for the time-reversal-invariant case

$$\hat{M} = \left(\vec{v}\,\vec{\hat{\tau}}\right) \otimes \left(\vec{m}\,\vec{\hat{\sigma}}\right), \quad \vec{m} \perp \vec{n}. \tag{5.45}$$

Further specification of the boundary conditions can be achieved by assuming the nearest-neighbour approximation (which is actually quite accurate for graphene, see Chapter 1). In this approximation there exist only hopping terms between sublattices, $\hat{H}_{\mathrm{AB}}$, whereas intrasublattice terms vanish: $\hat{H}_{\mathrm{AA}} = \hat{H}_{\mathrm{BB}} = 0$ (see Eq. (1.14)). The Schrödinger equation for the two-component wave function (the components correspond to the sublattices)

$$\begin{aligned} \hat{H}_{\mathrm{AB}}\psi_{\mathrm{A}} &= E\psi_{\mathrm{B}}, \\ \hat{H}^{+}_{\mathrm{AB}}\psi_{\mathrm{B}} &= E\psi_{\mathrm{A}} \end{aligned} \tag{5.46}$$

has a rigorous electron hole symmetry: $\psi_{\mathrm{B}} \to \quad \psi_{\mathrm{B}}$, $E \to \quad E$ transforms the equation to itself. In the limit of small energies $|E| \ll |t|$ this means that the operation $\hat{R} = \tau_z \otimes \sigma_z$ changes the sign of the Hamiltonian

$$\hat{R}\hat{H}\hat{R} = \quad \hat{H} \tag{5.47}$$

or, equivalently (keeping in mind that $\hat{R}^2 = 1$),

$$\left\{\hat{H}, \hat{\tau}_z \otimes \hat{\sigma}_z\right\} = 0. \tag{5.48}$$

This symmetry is an approximate one for real graphene but this approximation is quite good due to the smallness of the second-neighbour hopping, $|t'/t| \approx 0.025$ (see Section 1.2). If we require (5.48), there are only two classes of allowed boundary conditions: (1) $\vec{v} \,||\, Oz, \vec{m} \,||\, Oz$, for which

$$\hat{M} = \pm\hat{\tau}_z \otimes \hat{\sigma}_z; \tag{5.49}$$

and (2) $v_z = m_z = 0$, for which

$$\hat{M} = \left(\cos\varphi\,\hat{\tau}_x + \sin\varphi\,\hat{\tau}_y\right) \otimes \sigma_x \tag{5.50}$$

(we assume that the edge is along the x-axis, $\vec{n} \,||\, Oy$, and, thus, $\vec{m} \,||\, Ox$).

Boundary conditions of the type (5.36) and (5.49) are called *zigzaglike*, whereas those of the type (5.36) and (5.50) are called *armchairlike*, for reasons that will be discussed in the next section. There is an important result (Akhmerov & Beenakker, 2008; Wimmer, Akhmerov & Guinea, 2010) that zigzaglike boundary conditions are generic whereas armchairlike boundary conditions occur only for some exceptional orientation of the edges.

5.3 Boundary conditions for a terminated honeycomb lattice

Here we present, following Akhmerov & Beenakker (2008), a microscopic derivation of the boundary conditions for a terminated honeycomb lattice in the nearest-neighbour approximation. The geometry of our problem is clear from Fig. 5.3. The translation vector along the boundary is

$$\vec{T} = n\vec{R}_1 + m\vec{R}_2, \tag{5.51}$$

where

$$\vec{R}_{1,2} = \frac{a}{2}\left(\sqrt{3}, \mp 1\right) \tag{5.52}$$

are elementary translation vectors and n and m are integers. The number N of missing sites and the number N' of dangling bonds per period are larger than or equal to $n+m$. Figure 5.3(d) shows a *minimal* boundary where $N=N'=n+m$.

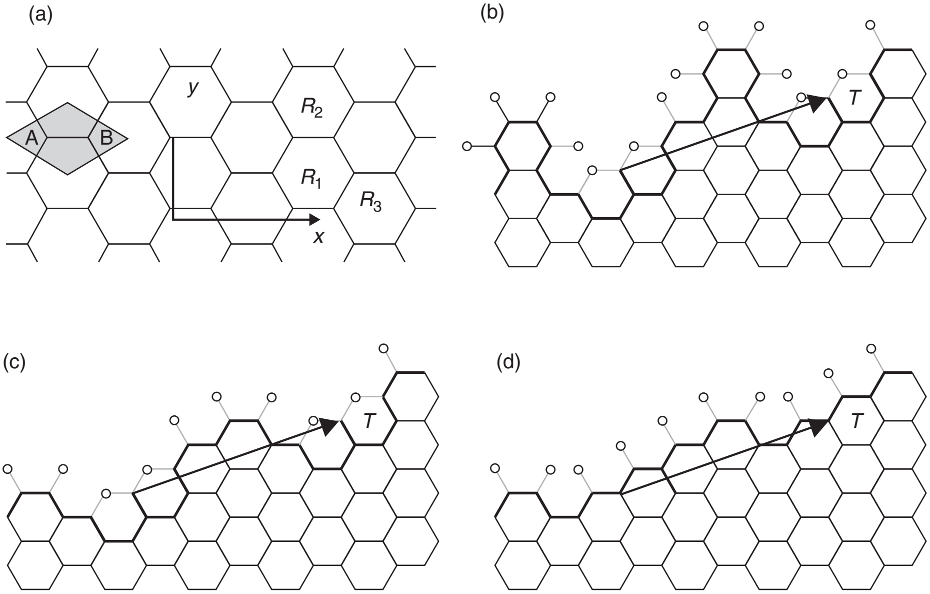

Fig. 5.3. (a) A honeycomb lattice constructed from a unit cell (grey rhombus) containing two atoms (labelled A and B), translated over lattice vectors $\mathbf{R}_1$ and $\mathbf{R}_2$. Panels (b)–(d) show three different periodic boundaries with the same period $\mathbf{T}=n\mathbf{R}_1+m\mathbf{R}_2$. Atoms on the boundary (connected by thick solid lines) have dangling bonds (thin-grey-line segments) to empty neighbouring sites (open circles). The number N of missing sites and the number N' of dangling bonds per period are $n+m$. Panel (d) shows a minimal boundary, for which $N = N' = n + m$. (Reproduced with permission from Akhmerov & Beenakker, 2008.)

The Schrödinger equation for the tight-binding model in the nearest-neighbour approximation reads

$$\begin{aligned} \psi_B(\vec{r}) + \psi_B\left(\vec{r} - \vec{R}_1\right) + \psi_B\left(\vec{r} - \vec{R}_2\right) &= \varepsilon\psi_A(\vec{r}), \\ \psi_A(\vec{r}) + \psi_A\left(\vec{r} + \vec{R}_1\right) + \psi_A\left(\vec{r} + \vec{R}_2\right) &= \varepsilon\psi_B(\vec{r}), \end{aligned} \tag{5.53}$$

where $\varepsilon = E/t$ is the dimensionless energy and subscripts A and B label sublattices.

The angle between the translation vector $\vec{T}$ and the armchair orientation (the direction Ox in Fig. 5.3(a)) is

$$\varphi = \arctan\left(\frac{1}{\sqrt{3}}\frac{n - m}{n + m}\right). \tag{5.54}$$

Owing to symmetry with respect to rotations at ± $\pi/3$ we can restrict ourselves to the case $|\varphi| \leq \pi/6$ only.

The boundary condition is the requirement that the wave function vanishes at the empty sites. One can assume that it depends smoothly on the energy ε. We are interested in the case of small ε (the states close to the Dirac points) and, thus, can put $\varepsilon = 0$ in Eq. (5.53). So, as a first step one can find zero-energy modes for the terminated honeycomb lattice. Owing to the translational invariance along the boundary one can use Bloch's theorem and require that

$$\psi_{A,B}\left(\vec{r} + \vec{T}\right) = e^{ik}\psi_{A,B}(\vec{r}) \tag{5.55}$$

with a real $0 \leq k < 2\pi$.

For the behaviour normal to the boundary, we assume that

$$\psi_{A,B}\left(\vec{r} + \vec{R}_3\right) = \lambda\psi_{A,B}(\vec{r}), \tag{5.56}$$

where $\vec{R}_3 = \vec{R}_1 - \vec{R}_2$ is antiparallel to the y-axis in Fig. 5.3(a). This lattice vector has a nonzero component $a\cos\varphi > a\sqrt{3}/2$ perpendicular to $\vec{T}$. For the states localized at the edge $|\lambda| < 1$ and for propagating states $|\lambda| = 1$; of course, the case $|\lambda| > 1$ is meaningless since the corresponding wave function cannot be normalized. If $|\lambda| < 1$ the solution satisfying Eq. (5.56) has a decay length in the direction normal to $\vec{T}$ of

$$l = -\frac{a\cos\varphi}{\ln|\lambda|}. \tag{5.57}$$

Taking into account that $\vec{R}_1 = \vec{R}_2 + \vec{R}_3$, one can rewrite Eq. (5.53) at $\varepsilon = 0$ as

$$\begin{aligned} \psi_{\mathrm{B}}(\vec{r}) + \psi_{\mathrm{B}}\left(\vec{r} - \vec{R}_2 - \vec{R}_3\right) + \psi_{\mathrm{B}}\left(\vec{r} - \vec{R}_2\right) &= 0, \\ \psi_{\mathrm{A}}(\vec{r}) + \psi_{\mathrm{A}}\left(\vec{r} + \vec{R}_2 + \vec{R}_3\right) + \psi_{\mathrm{A}}\left(\vec{r} + \vec{R}_2\right) &= 0. \end{aligned} \tag{5.58}$$

On substituting Eq. (5.56) into Eq. (5.58) one finds

$$\begin{aligned} \psi_{\mathrm{B}}\left(\vec{r} + \vec{R}_2\right) &= -\frac{1}{1+\lambda}\psi_{\mathrm{B}}(\vec{r}), \\ \psi_{\mathrm{A}}\left(\vec{r} + \vec{R}_2\right) &= -(1+\lambda)\psi_{\mathrm{A}}(\vec{r}). \end{aligned} \tag{5.59}$$

Using Eqs. (5.56) and (5.55) together, we have, for any integer p and q,

$$\begin{aligned} \psi_{\mathrm{B}}\left(\vec{r} + p\vec{R}_2 + q\vec{R}_3\right) &= \lambda^q(-1-\lambda)^{-p}\psi_{\mathrm{B}}(\vec{r}), \\ \psi_{\mathrm{A}}\left(\vec{r} + p\vec{R}_2 + q\vec{R}_3\right) &= \lambda^q(-1-\lambda)^{p}\psi_{\mathrm{A}}(\vec{r}). \end{aligned} \tag{5.60}$$

Now we have to recall the Bloch theorem (5.55) for

$$\vec{T} = n\left(\vec{R}_2 + \vec{R}_3\right) + m\vec{R}_2 = (n+m)\vec{R}_2 + n\vec{R}_3. \tag{5.61}$$

Thus, we have two equations relating k and λ:

$$(-1-\lambda)^{m+n} = e^{ik}\lambda^n \tag{5.62}$$

for the sublattice A and

$$(-1-\lambda)^{m+n} = e^{ik}\lambda^m \tag{5.63}$$

for the sublattice B. One needs to find all solutions λ of Eqs. (5.62) and (5.63) for a given k satisfying the conditions $|\lambda| \le 1$.

A general zero-energy state can be represented as

$$\begin{aligned} \psi_{\mathrm{A}} &= \sum_{p=1}^{M_{\mathrm{A}}} \alpha_p \psi_p, \\ \psi_{\mathrm{B}} &= \sum_{p=1}^{M_{\mathrm{B}}} \alpha'_p \psi'_p, \end{aligned} \tag{5.64}$$

where M_{A} and M_{B} are the numbers of solutions of Eqs. (5.62) and (5.63) within the unit circle, respectively, and ψ_p and ψ'_p are the corresponding eigenstates. The coefficients α_p and α'_p should be chosen in such a way that ψ_{A} and ψ_{B} vanish at missing sites from the sublattices A and B.

The Dirac limit corresponds to the case of small k. Explicit calculations for the case $k = 0$ give the result (Akhmerov and Beenakker, 2008)

$$\begin{aligned} M_{\mathrm{A}} &= \frac{2n+m}{3} + 1, \\ M_{\mathrm{B}} &= \frac{2m+n}{3} + 1. \end{aligned} \tag{5.65}$$

These solutions include also the values

$$\lambda_{\pm} = \exp\left(\pm\frac{2\pi i}{3}\right) \tag{5.66}$$

corresponding to the propagating modes; for all other modes $|\lambda| < 1$, so they are localized at the edge. The corresponding eigenstate is $\exp(\pm i\vec{K}\vec{r})$, with

$$\vec{K} = \frac{4\pi}{3a^2}\vec{R}_3. \tag{5.67}$$

Thus, the general zero-energy mode at $k = 0$ can be represented as

$$\begin{aligned} \psi_{\mathrm{A}} &= \psi_1 \exp\left(i\vec{K}\vec{r}\right) + \psi_4 \exp\left(-i\vec{K}\vec{r}\right) + \sum_{p=1}^{M_{\mathrm{A}}-2} \alpha_p \psi_p, \\ \psi_{\mathrm{B}} &= \psi_2 \exp\left(i\vec{K}\vec{r}\right) + \psi_3 \exp\left(-i\vec{K}\vec{r}\right) + \sum_{p=1}^{M_{\mathrm{B}}-2} \alpha'_p \psi'_p. \end{aligned} \tag{5.68}$$

The four amplitudes $(\psi_1, -i\psi_2, i\psi_3, -\psi_4)$ correspond to the four components of the wave function (1.27) in the Dirac limit; ψ_1 and ψ_2 are associated with the valley K, ψ_3 and ψ_4 with the valley K′.

At the same time, there are N_{A} conditions $\psi_{\mathrm{A}} = 0$ at the missing sites belonging to the sublattice A and N_{B} conditions $\psi_{\mathrm{B}} = 0$ at the missing sites belonging to the sublattice B (N_{A} and N_{B} are the numbers of missing sites belonging to the corresponding sublattice).

For the minimal boundary, $N_{\mathrm{A}} = n$ and $N_{\mathrm{B}} = m$. At the same time, for $n > m$ one has $M_{\mathrm{A}} \leq n$ conditions $\psi_{\mathrm{A}} = 0$ at some sites. The only way to satisfy them is to require that $\psi_{\mathrm{A}} = 0$ on the whole boundary, including $\psi_1 = \psi_4 = 0$. At the same time, $M_{\mathrm{B}} \geq m + 2$, so ψ_2 and ψ_3 remain undetermined.

This corresponds to the zigzag boundary conditions Eq. (5.49), with the minus sign. Similarly, for $n < m$ one has the zigzag boundary conditions with the plus sign. Only at $n = m$ does one have $M_{\mathrm{A}} = M_{\mathrm{B}} = n + 1 > n$ such that one has the same condition for sublattices A and B. All ψ_i are nonzero in this case, with

$$|\psi_1| = |\psi_4|, \qquad |\psi_2| = |\psi_3| \tag{5.69}$$

(armchair boundary conditions (5.50)).

So, at least for the case of minimal edges, one can prove that the armchair boundary conditions are exceptional whereas the zigzag ones are generic. This result seems to be correct also for non-minimal edges, as well as for the case of disorder at the edges (Martin & Blanter, 2009; Wimmer, Akhmerov & Guinea, 2010).

For the case $n > m$, the number of independent zero-energy modes per unit length is

$$\rho = \frac{M_{\mathrm{A}} \quad n}{|\vec{T}|} = \frac{|m \quad n|}{3a\sqrt{n^2 + nm + m^2}} = \frac{2}{3a}|\sin\varphi| \tag{5.70}$$

(Akhmerov & Beenakker, 2008; Wimmer, Akhmerov & Guinea, 2010). At $\varphi = 0$ (armchair boundaries) there are no such states. The existence of the zero-energy modes and the corresponding sharp peak in the density of states at zigzag edges was first found numerically by Nakada *et al.* (1996). It will be analysed in more detail in the next sections.

Akhmerov & Beenakker (2008) have demonstrated that the infinite-mass boundary condition (5.13) with $B = \pm 1$ can be obtained in the limit of an infinite staggered field (difference of on-site energies between sublattices A and B at the edge). The sign of B is determined by the sign of this staggered field.

5.4 Electronic states of graphene nanoribbons

The previous consideration was a bit formal but the result is quite simple. For the case of pure zigzag edges *all* missing atoms belong to sublattice A only (or sublattice B only), thus the corresponding components of the wave function for the two valleys, K and K′, should vanish at the boundary. If the numbers of missing atoms belonging to A and B are not equal, the boundary conditions remain the same, depending on the majority of the atoms: ‘the winner takes all’. Only in the exceptional case in which the numbers of missing atoms from A and B coincide exactly (armchair edges) are all four components of the Dirac spinors finite at the edge, satisfying the two relations (5.69).

If we have a nanoribbon of a constant width L ($|y| \le L/2$) with zigzag edges, one edge corresponds to the missing atoms A and the other to the missing atoms B. The boundary conditions are

$$\begin{aligned} u\left(y = \quad \frac{L}{2}\right) &= 0, \\ v\left(y = \frac{L}{2}\right) &= 0, \end{aligned} \tag{5.71}$$

where u is ψ_1 or ψ_4 and v is ψ_2 or ψ_3. In this case the valleys are decoupled, so in the Dirac approximation we can consider them independently. For the valley K, the Schrödinger equation reads

$$\begin{aligned} \left(\frac{\partial}{\partial x} + i\frac{\partial}{\partial y}\right)u(x,y) &= ikv(x,y), \\ \left(\frac{\partial}{\partial x} - i\frac{\partial}{\partial y}\right)v(x,y) &= iku(x,y), \end{aligned} \tag{5.72}$$

where $k = E/(hv)$. For the valley K$'$, the signs before $\partial/\partial y$ are exchanged. The analytic solution of Eq. (5.72) with the boundary conditions (5.71) has been found by Brey & Fertig (2006).

Let us try the solutions as

$$\begin{aligned} u(x,y) &= \exp(ik_x x)u(y), \\ v(x,y) &= \exp(ik_x y)v(y), \end{aligned} \tag{5.73}$$

where u and v satisfy a system of two linear ordinary differential equations with constant coefficients:

$$\begin{aligned} \left(k_x + \frac{d}{dy}\right)u(y) &= kv(y), \\ \left(k_x - \frac{d}{dy}\right)v(y) &= ku(y). \end{aligned} \tag{5.74}$$

The solution can be tried as

$$\begin{aligned} u(y) &= A\exp(zy) + B\exp(-zy), \\ v(y) &= C\exp(zy) + D\exp(-zy), \end{aligned} \tag{5.75}$$

where

$$z = \sqrt{k_x^2 - k^2} \tag{5.76}$$

can be either real (for evanescent waves) or imaginary (for propagating waves). On substituting Eq. (5.75) into Eq. (5.74) and taking into account Eq. (5.71) one finds a dispersion relation for the waves in the nanoribbon:

$$\varphi(z) = \frac{k_x - z}{k_x + z} = \exp(-2Lz). \tag{5.77}$$

Graphical solution of Eq. (5.77) (Fig. 5.4) shows that a real solution (other than the trivial one, $z = 0$) exists if

$$k_x > \frac{1}{L}. \tag{5.78}$$

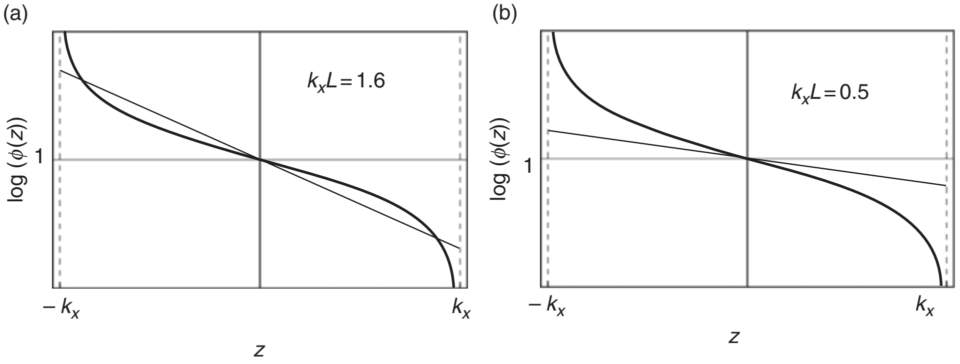

Fig. 5.4. Graphical solution of Eq. (5.77) (the logarithm of both sides is taken). If the condition (5.78) is satisfied there is a nontrivial ($z \neq 0$) solution (a); otherwise, $z = 0$ is the only solution (b).

Indeed, at this condition $\varphi(z) \approx 1 \quad 2z/k_x$ is larger than $\exp(\quad 2Lz) \approx 1 \quad 2\,Lz$ at small z. At the same time, $\varphi(k_x) = 0 < \exp(\quad 2Lk_x)$, thus the curves should cross. Otherwise, there are no solutions.

Equation (5.78) is the condition of existence of the edge state; for the semispace ($L \to \infty$) it always exists, with the decay decrement $z = k_x$, in agreement with the consideration of the previous section. For a finite width L, those states with energies

$$E_\mathrm{s} = \pm hv\sqrt{k_x^2 \quad z^2} \tag{5.79}$$

are linear combinations of the states localized on the left and right edges of the ribbon. There are no solutions at $k_x < 0$, so, for a given valley, these edge states can propagate only in one direction. Conversely, for the valley K′ the solutions exist only for $k_x < 0$. Numerical calculations for honeycomb-lattice nanoribbons (Brey & Fertig, 2006; Peres, Castro Neto & Guinea, 2006) show that these edge states connect the valleys K and K′ (Fig. 5.5).

For the case of purely imaginary $z = ik_y$ Eq. (5.77) can be rewritten as

$$k_x = k_y \cot\left(k_y L\right), \tag{5.80}$$

which gives ‘bulk’ standing waves with discrete values of k_y and energy

$$E_\mathrm{b} = \pm hv\sqrt{k_x^2 + k_y^2}. \tag{5.81}$$

For the case of armchair nanoribbons the amplitudes of the components of wave functions belonging to different valleys are the same but the phases can

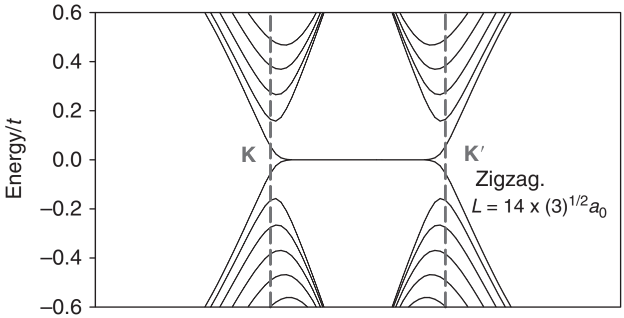

Fig. 5.5. The energy spectrum for zigzag-terminated graphene nanoribbon with 56 atoms per unit cell. (Reproduced with permission from Brey & Fertig, 2006.)

differ (see Eq. (5.69)). A detailed analysis (Brey & Fertig, 2006) results in the following boundary conditions:

$$\begin{aligned} u\left(\;\frac{L}{2}\right) &= u'\left(\;\frac{L}{2}\right), \\ v\left(\;\frac{L}{2}\right) &= v\left(\;\frac{L}{2}\right), \\ u\left(\frac{L}{2}\right) &= \exp(2\pi i v)u'\left(\frac{L}{2}\right), \\ v\left(\frac{L}{2}\right) &= \exp(2\pi i v)v'\left(\frac{L}{2}\right), \end{aligned} \tag{5.82}$$

where the functions with (without) primes correspond to the states from valley K′ (K) and $v = 0, \pm\frac{2}{3}$ depending on the number of rows in the nanoribbons; $v = 0$ if this number is $3p$ (p is an integer) and $v = \pm\frac{2}{3}$ if it is $3p \pm 1$. In this case there are no edge states with real z, the wave functions of the bulk states are very simple, namely

$$u_j(y) = \quad iv_j(y) = \frac{1}{\sqrt{2L}} \exp\left(ik_j y\right), \tag{5.83}$$

$$u_j'(y) = \quad iv_j'(y) = \frac{1}{\sqrt{2L}} \exp\left(\quad ik_j y\right),$$

and k_j is discrete:

$$k_j = \frac{(j+v)\pi}{L}, \quad j = 0, \pm 1, \ldots \tag{5.84}$$

5.5 Conductance quantization in graphene nanoribbons

For the case of zigzag edges, electron motion along the edges is coupled with that in the perpendicular direction, see Eq. (5.80). This coupling leads to interesting consequences for the electron transport in nanoribbons with varying width, such as those with nanoconstrictions (Fig. 5.6).

Let us consider a ribbon with a slowly varying width $L(x)$ assuming that

$$\left|\frac{dL}{dx}\right| \ll 1. \tag{5.85}$$

For simplicity, we will assume mirror symmetry so that the edges correspond to $y = \pm L(x)/2$ (Fig. 5.6). For the case of the Schrödinger equation for conventional nonrelativistic electrons

$$\frac{h^2}{2m}\nabla^2\Psi(x,y) = E\Psi(x,y) \tag{5.86}$$

with boundary conditions

$$\Psi\left(y = \pm\frac{L(x)}{2}\right) = 0 \tag{5.87}$$

(impenetrable walls) the electron states can be considered in the adiabatic approximation (Glazman *et al.*, 1988; Yacoby & Imry, 1990). Owing to the condition (5.87) one can try having the wave function as

$$\Psi(x,y) = \chi(x)\varphi_x(y), \tag{5.88}$$

where

$$\varphi_x(y) = \sqrt{\frac{2}{L(x)}}\sin\left(\frac{\pi n[2y + L(x)]}{L(x)}\right) \tag{5.89}$$

is the standing wave of transverse motion satisfying the boundary condition (5.87) and depending on x as a parameter via $L(x)$. It can be proven (Glazman

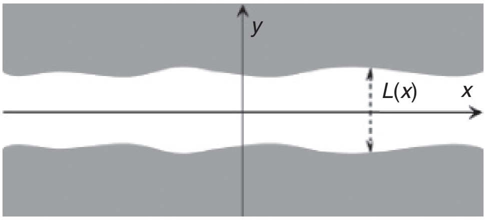

Fig. 5.6. A sketch of a graphene nanoribbon with a smoothly varying width.

et al., 1988; Yacoby & Imry, 1990) that the wave function of longitudinal motion satisfies the Schrödinger equation

$$\frac{d^2\chi_n(x)}{dx^2} + \left(k^2 \quad k_n^2(x)\right)\chi_n(x) = 0, \tag{5.90}$$

where $k^2 = 2mE/h^2$ and

$$k_n(x) = \frac{\pi n}{L(x)}. \tag{5.91}$$

Owing to Eq. (5.85) one can use the semiclassical approximation (Landau & Lifshitz, 1977). At $k > k_n(x)$ the solutions of Eq. (5.90) are propagating waves with an exponentially small probability of reflection, whereas for the classically forbidden regions $k < k_n(x)$ the electron states decay quickly. This means that the electron transport in the adiabatic approximation is determined by the minimal width of the constriction $L_{\min}$: all states with

$$n < \frac{kL_{\min}}{\pi} \tag{5.92}$$

have transmission coefficients close to unity and all states with larger n do not contribute to the electron transmission at all. According to the Landauer formula (see Chapter 3) the conductance in the adiabatic regime should be quantized, with an exponential accuracy of

$$G = \frac{2e^2}{h}n, \tag{5.93}$$

where n is an integer and the factor of 2 is due to spin degeneracy. Each transverse mode corresponds to an independent channel of transmission.

For the case of graphene nanoribbons the situation is more complicated (Katsnelson, 2007b). We will consider here only the case of zigzag boundary conditions, since they are generic for inhomogeneous nanoribbons as discussed above.

Thus, one can solve the equations (5.72) with x-dependent boundary conditions (5.71):

$$\begin{aligned} u\left(x, y = \quad \frac{L(x)}{2}\right) &= 0, \\ v\left(x, y = \frac{L(x)}{2}\right) &= 0. \end{aligned} \tag{5.94}$$

Following Katsnelson (2007b) we expand a general solution in the standing waves with $k_x = 0$. For this case,

$$k_y \equiv k_j = \frac{\pi j}{L}, \quad j = \pm\frac{1}{2}, \pm\frac{3}{2}, \ldots \tag{5.95}$$

(cf. Eq. (5.80)) and the eigenfunctions can be written explicitly:

$$\begin{aligned} u_j(y) &= \frac{1}{\sqrt{L}} \cos\left[k_j\left(y - \frac{L}{2}\right)\right], \\ v_j(y) &= -\frac{1}{\sqrt{L}} \sin\left[k_j\left(y - \frac{L}{2}\right)\right]. \end{aligned} \tag{5.96}$$

Instead of Eq. (5.88) let us use the most general expansion

$$\begin{aligned} u(x,y) &= \sum_j c_j(x) u_j^{(x)}(y), \\ v(x,y) &= \sum_j c_j(x) v_j^{(x)}(y), \end{aligned} \tag{5.97}$$

where $u^{(x)}$ and $v^{(x)}$ are the functions (5.96) with the replacement $L \to L(x)$:

$$\begin{aligned} u_j^{(x)}(y) &= \frac{1}{\sqrt{L(x)}} \cos\left[\pi j\left(\frac{y}{L(x)} - \frac{1}{2}\right)\right], \\ v_j^{(x)}(y) &= -\frac{1}{\sqrt{L(x)}} \sin\left[\pi j\left(\frac{y}{L(x)} - \frac{1}{2}\right)\right]. \end{aligned} \tag{5.98}$$

The functions (5.98) satisfy by construction the boundary conditions. On substituting the expansion (5.97) into Eq. (5.72) and multiplying the first equation by $\langle v_y|$ and the second one by $\langle u_j|$ one finds

$$\begin{aligned} \sum_{j'} \left[\frac{dc_{j'}}{dx}\langle v_j | v_{j'}\rangle + c_{j'}\left\langle v_j \middle| \frac{dv_{j'}}{dx}\right\rangle\right] &= i\sum_{j'} (k - k_{j'}) c_{j'} \langle v_j | u_{j'}\rangle, \\ \sum_{j'} \left[\frac{dc_{j'}}{dx}\langle u_j | u_{j'}\rangle + c_{j'}\left\langle u_j \middle| \frac{du_{j'}}{dx}\right\rangle\right] &= i\sum_{j'} (k - k_{j'}) c_{j'} \langle u_j | v_{j'}\rangle. \end{aligned} \tag{5.99}$$

These equations are formally exact. As a first step to the adiabatic approximation, one should neglect the terms with

$$\left\langle v_j \middle| \frac{dv_{j'}}{dx}\right\rangle \quad \text{and} \quad \left\langle u_j \middle| \frac{du_{j'}}{dx}\right\rangle,$$

which is justified by the smallness of dL/dx, as in the case of nonrelativistic electrons (Yacoby & Imry, 1990).

To proceed further we need to calculate the overlap integrals

$$\langle \phi_1 \mid \phi_2 \rangle = \int_{-L/2}^{L/2} dy\, \phi_1^* \phi_2$$

for different basis functions:

$$\begin{aligned}
\langle u_j | u_{j'} \rangle &= \frac{1}{2}\left(\delta_{jj'} + \delta_{j,-j'}\right),\\
\langle v_j | v_{j'} \rangle &= \frac{1}{2}\left(\delta_{jj'} - \delta_{j,-j'}\right),\\
\langle u_j | v_{j'} \rangle = \langle v_{j'} | u_j \rangle &= \begin{cases} \dfrac{1}{\pi(j'-j)}, & j'-j = 2n+1,\\[2ex] \dfrac{1}{\pi(j'+j)}, & j'-j = 2n, \end{cases}
\end{aligned}\tag{5.100}$$

where n is an integer. On substituting Eq. (5.100) into Eq. (5.99) and neglecting the nonadiabatic terms within the matrix elements of the operator d/dx, we obtain after simple transformations

$$\frac{dc_j(x)}{dx} = -\frac{2i}{\pi}\sum\nolimits_{j'}^{\prime} \frac{k - k_{j'}(x)}{j+j'} c_{j'}(x), \tag{5.101}$$

where the sum is over all j' such that $j'-j$ is even.

Until now we have employed transformations and approximations that are identical to those used in the case of nonrelativistic electrons. However, we still have a coupling between different standing waves, so we cannot prove that the electron transmission through the constriction is adiabatic. To prove this we need one more step, namely a transition from the discrete variable j to a continuous one and a replacement of the sums on the right-hand side of Eq. (5.101) by integrals: $\sum_{j'}^{\prime} \ldots \to \frac{1}{2}P\int dy \ldots$, where P is the symbol of principal value. This step is justified by assuming that $kL \gg 1$, i.e., it is valid only for highly excited states. For low-lying electron standing waves it is difficult to see any way to simplify appreciably the set of equations (5.101) for the coupled states.

For any function $f(z)$ that is analytic in the upper (lower) complex half-plane one has

$$\int_{-\infty}^{\infty} dx\, f(x) \frac{1}{x - x_1 \pm i0} = 0 \tag{5.102}$$

or, equivalently,

$$\int_{-\infty}^{\infty} dx\, f(x) \frac{P}{x - x_1} = \pm i\pi f(x_1). \tag{5.103}$$

Assuming that $c_j(x)$ is analytic in the lower half-plane as a function of the complex variable j one obtains, instead of Eq. (5.101),

$$\frac{dc_j(x)}{dx} = \left[k + k_j(x)\right] c_{-j}(x). \tag{5.104}$$

Similarly, taking into account that $c_{-j}(x)$ is analytic in the upper half-plane as a function of the complex variable j we have

$$\frac{dc_{-j}(x)}{dx} = \left[k_j(x) - k\right] c_j(x). \tag{5.105}$$

Finally, on differentiating Eq. (5.104) with respect to x, neglecting the derivatives of $k_j(x)$ due to the smallness of dL/dx and taking into account Eq. (5.105) we find

$$\frac{d^2 c_j(x)}{dx^2} + \left[k^2 - k_j^2(x)\right] c_j(x) = 0. \tag{5.106}$$

Further analysis completely follows that for the nonrelativistic case. The potential is semiclassical for the case of smoothly varying $L(x)$. Therefore, the transmission coefficient is very close to unity if the electron energy exceeds the energy of the jth level in the narrowest place of the constriction and is exponentially small otherwise. Standard arguments based on the Landauer formula prove the conductance quantization in this situation.

At the same time, for the lowest energy levels the replacement of sums by integrals in Eq. (5.101) cannot be justified and thus the states with different js are in general coupled even for a smooth constriction (Eq. (5.85)). Therefore electron motion along the strip is strongly coupled with that in the perpendicular direction and different electron standing waves are essentially entangled. In this situation there is no general reason to expect sharp jumps and well-defined plateaux in the energy dependence of the conductance. This means that the criterion of the adiabatic approximation is more restrictive for the case of Dirac electrons than it is for nonrelativistic ones. The formal reason is an overlap between components of the wave functions with different pseudospins or, equivalently, between the hole component of the state j and the electron component of the state $j' \neq j$. This conclusion (Katsnelson, 2007b) seems to be confirmed by the numerical simulations of Muños-Rojas *et al.* (2008).

5.6 The band gap in graphene nanoribbons with generic boundary conditions

One has to keep in mind that the terminated honeycomb lattice is a special case of graphene edges. Density-functional calculations show that the reconstructed '5–7' edge (Fig. 5.7) has an energy lower than those both of armchair and of

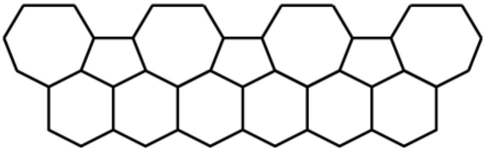

Fig. 5.7. A sketch of a reconstructed 5–7 zigzag edge.

zigzag edges (Koskinen, Malola & Häkkinen, 2008). The reconstruction to this low-energy state requires the overcoming of energy barriers, so the zigzag edges are metastable (Kroes *et al.*, 2011), but under some circumstances it will definitely happen. Zigzag edges are very chemically active, so they will bind hydrogen, oxygen or hydroxyl groups (see, e.g., Boukhvalov & Katsnelson, 2008; Bhandary *et al.*, 2010). Lastly, the density of states peak due to zero-energy modes means ferromagnetic instability (Fujita *et al.*, 1996; Son, Cohen & Louie, 2006a; see also Section 12.3). All of this will substantially modify the boundary conditions. The most general form is given by Eqs. (5.36) and (5.45). It assumes only time-reversal symmetry. Time-reversal symmetry can be broken by ferromagnetic ordering; however, the latter can exist in one-dimensional systems at zero temperature only. At finite temperatures one has, instead, a superparamagnetic state with a finite correlation length ξ, which is just several interatomic distances at room temperature (Yazyev & Katsnelson, 2008). If all essential sizes of the problem (e.g., the width of nanoribbons L) are larger than ξ then the system should be considered time-reversal-invariant.

The most general boundary conditions for the nanoribbons are therefore

$$\begin{aligned} \Psi\left(x, y = \quad \frac{L}{2}\right) &= \left(\vec{v}_1 \cdot \hat{\vec{\tau}}\right) \otimes \left(\vec{n}_1 \cdot \hat{\vec{\sigma}}\right) \Psi\left(x, y = \quad \frac{L}{2}\right), \\ \Psi\left(x, y = \frac{L}{2}\right) &= \left(\vec{v}_2 \cdot \hat{\vec{\tau}}\right) \otimes \left(\vec{n}_2 \cdot \hat{\vec{\sigma}}\right) \Psi\left(x, y = \frac{L}{2}\right), \end{aligned} \tag{5.107}$$

where $\vec{v}_i$ are three-dimensional unit vectors (no restrictions) and $\vec{n}_i$ are three-dimensional unit vectors perpendicular to the y-axis:

$$\begin{aligned} \vec{n}_1 &= (\cos\theta_1, 0, \sin\theta), \\ \vec{n}_2 &= (\cos\theta_2, 0, \sin\theta_2). \end{aligned} \tag{5.108}$$

Valley symmetry implies that only the relative directions of the vectors $\vec{v}_1$ and $\vec{v}_2$ are essential. Thus, the problem is characterized by three angles: θ_1, θ_2 and the angle γ between $\vec{v}_1$ and $\vec{v}_2$.

The most general dispersion relation $E = E(k)$ for the propagating waves

$$\Psi(x, y) \propto \exp(ikx + iqy) \tag{5.109}$$

satisfying the boundary conditions (5.107) has been obtained by Akhmerov & Beenakker (2008). It reads

$$\cos\theta_1\cos\theta_2\left(\cos\omega - \cos^2\Omega\right) + \cos\omega\sin\theta_1\sin\theta_2\sin^2\Omega \\ - \sin\Omega[\sin\Omega\cos\gamma + \sin\omega\sin(\theta_1 - \theta_2)] = 0, \tag{5.110}$$

where

$$\omega^2 = 4L^2\left[\frac{E^2}{h^2v^2} - k^2\right]$$

and

$$\cos\Omega = \frac{hvk}{E}. \tag{5.111}$$

Different solutions of Eq. (5.110) correspond to different standing waves with discrete q_n. Analysis of this equation show that there is a gap in the energy spectrum if $\gamma \neq 0, \pi$ (which means that valleys are coupled at the boundaries) or at $\gamma = \pi$, $\sin\theta_1 \sin\theta_2 > 0$, or at $\gamma = 0$, $\sin\theta_1 \sin\theta_2 < 0$ (Akhmerov & Beenakker, 2008). One can see that the case of zigzag-terminated edges when states with arbitrarily small energy, up to $E = 0$, exist is very exceptional. For generic boundary conditions, the gap is of the order of

$$\Delta \cong \frac{hv}{L}. \tag{5.112}$$

A detailed analysis of the gap, both in a tight-binding model and in realistic density-functional calculations, was carried out by Son, Cohen & Louie (2006b) (see also, e.g., Wassmann *et al.*, 2008).

The gap opening in nanoribbons is very important for applications. It allows one to overcome restrictions due to the Klein tunnelling and build a transistor that can really be locked by a gate voltage (Han *et al.*, 2007; Wang *et al.*, 2008; Han, Brant & Kim, 2010).

5.7 Energy levels in graphene quantum dots

Nanoribbons are restricted in one dimension, therefore their electron spectra consist of bands $E_n(k)$. It is possible to make graphene devices in which electrons are confined in two dimensions — graphene quantum dots (Ponomarenko *et al.*, 2008; Stampfer *et al.*, 2008; Güttinger *et al.*, 2009; Molitor *et al.*, 2010; Zhang *et al.*, 2010). Figure 5.8 (Ponomarenko *et al.*, 2008) shows an example of such a device, together with the voltage dependence of the differential conductance G through the device. Oscillations of

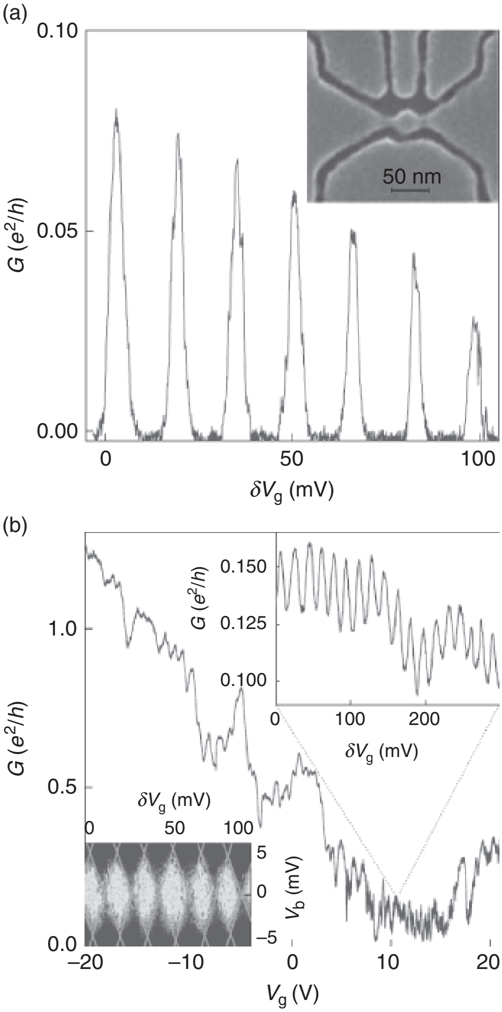

Fig. 5.8. A graphene-based single-electron transistor. The conductance G of a device shown in the insert in the upper right corner is given as a function of the gate voltage, at temperature $T = 0.3\,\mathrm{K}$. Two panels in (b) show the picture with different resolutions. (Reproduced with permission from Ponomarenko *et al.*, 2008.)

G are due to the discreteness of the electron energy spectrum in the dot. First of all, there is a classical electrostatic effect, namely the dependence of the energy on the total charge Q,

$$E_C(Q) = \frac{Q^2}{2C}, \tag{5.113}$$

where C is the capacitance of the dot. When the electron tunnels to the dot or from the dot the charge, Q, is changed by $\pm e$. This effect is known as

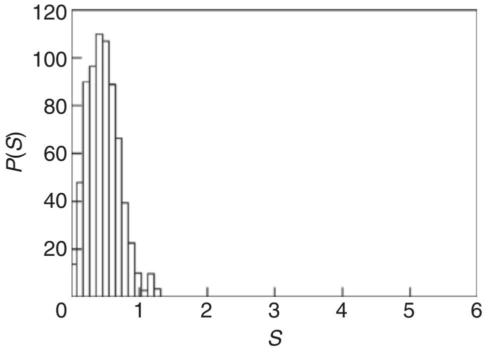

Fig. 5.9. The level-spacing distribution extracted from experimental data on a graphene 40-nm quantum dot. (Reproduced with permission from De Raedt & Katsnelson, 2008.)

Coulomb blockade, see Kouwenhoven, Marcus & McEuen (1997). Apart from this, there is a discreteness of the single-electron energy spectrum superimposed on the Coulomb-blockade peaks. The sharp dependence of G on the gate voltage allows one to use the device as a single-electron transistor (Ponomarenko *et al.*, 2008; Stampfer *et al.*, 2008). The data extracted from the measurements clearly show the effect of level repulsion which was discussed in Section 5.1; this means that the single-electron spectrum of real graphene quantum dots is certainly chaotic (Ponomarenko *et al.*, 2008; De Raedt & Katsnelson, 2008). The function $P(S)$ (cf. Eqs. (5.29) and (5.30)) extracted from the experimental data by Ponomarenko *et al.* (2008) for a 40-nm graphene quantum dot is shown in Fig. 5.9. Its decrease at small S is a manifestation of the level repulsion. At the same time, it is difficult to distinguish between the cases of orthogonal and unitary ensembles. Theoretically, the distinction depends on the probability of intervalley scattering. If it is large enough, then, due to atomic-scale inhomogeneity at the edges, the system is time-reversal-invariant, and one should expect the behaviour typical for the Gaussian orthogonal ensemble, Eq. (5.29). This is obvious already from the fact that, in the absence of a magnetic field, the tight-binding Hamiltonian can be chosen to be real. At the same time, if the inhomogeneities at the edges are smooth enough and intervalley scattering is therefore weak, the situation should be close to the case of a neutrino billiard (Section 5.1) and a unitary ensemble is to be expected. This can indeed be the case, since for chemical passivation of the edges the electronic structure changes smoothly within a rather broad strip near the edges (Boukhvalov & Katsnelson, 2008). Theoretical discussions of the energy-level statistics in graphene quantum dots can be found in Wurm *et al.* (2009), Libisch, Stampfer & Burgdörfer (2009), Wimmer, Akhmerov & Guinea (2010) and Huang, Lai & Grebogi (2010).

5.8 Edge states in magnetic fields and the anomalous quantum Hall effect

Now we can come back to the physics of the half-integer quantum Hall effect discussed in Chapter 2. Our analysis in Section 2.9 was based on the solution of the quantum-mechanical problem for bulk graphene. There is an alternative approach to the quantum Hall effect that is based on the analysis of the edge states of electrons in a magnetic field (Halperin, 1982; MacDonald & Středa, 1984).

Let us start with the classical picture of electron motion in a magnetic field. In two dimensions, the electron orbits are closed circles (Larmor rotation). Depending on the direction of the magnetic field, all electrons in the bulk rotate either clockwise or counterclockwise. However, for the electrons with centres of their orbits close enough to the boundary, reflections form a completely different kind of trajectory, skipping orbits (Fig. 5.10). They possess a magnetic moment opposite to that of the 'bulk' orbits and, actually, exactly compensate for the latter, so that, in agreement with a general theorem, the *classical* system of electrons can be neither paramagnetic nor diamagnetic (Vonsovsky & Katsnelson, 1989). In quantum theory, the skipping orbits are associated with the edge states localized near the boundary and carrying the current. These states are chiral since only one direction of propagation is allowed. Therefore they are protected against localization by disorder; the situation is similar to the Klein tunnelling and forbidden

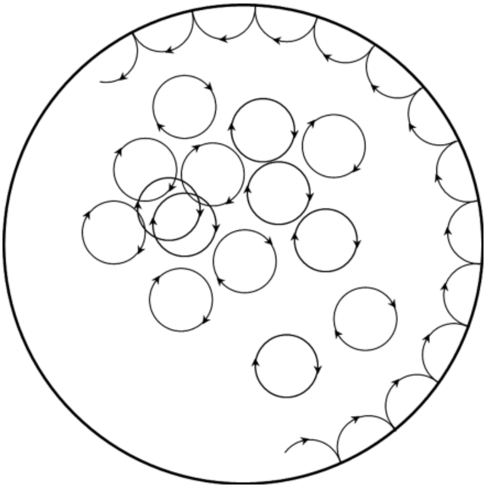

Fig. 5.10. Skipping orbits of electrons due to the combination of Larmor rotation in a magnetic field and reflection from the edges.

back-scattering for massless Dirac fermions (Chapter 4). Simply speaking, there are no other states with the same energy for electrons to be scattered to. Thus, if one assumes that all bulk states are localized there is still a current being carried by the skipping electrons, with a contribution to the conductance of e^2/h per spin (complete transmission). This gives an alternative explanation of the quantum Hall effect (Halperin, 1982).

A topological analysis shows that the number of edge states at the border between a quantum Hall insulator and vacuum is equal to the integer in (2.181) and, thus, 'bulk' and 'edge' approaches to the quantum Hall effect give the same results for σ_{xy} (Hatsugai, 1993; Kellendonk & Schulz-Baldes, 2004; Prodan, 2009).

The counting of the edge states is therefore an alternative way to explain the anomalous ('half-integer') quantum Hall effect in graphene (Abanin, Lee & Levitov, 2006; Hatsugai, Fukui & Aoki, 2006). We will use here the approach of the first of these works, which is based on a solution of the Dirac equation in a magnetic field (the second one uses an analysis of the geometry of the honeycomb lattice).

Let us assume that graphene fills the semispace $x < 0$. The solutions of the Dirac equation for the valley K satisfying the conditions $\psi_i(x) \to 0$ at $x \to -\infty$ are given by Eqs. (2.45) and (2.46),

$$\begin{aligned} \psi_1(X) &= D_n(-X), \\ \psi_2(X) &= i\varepsilon D_{n-1}(-X), \end{aligned} \tag{5.114}$$

where $n = \varepsilon^2$ and X is given by Eqs. (2.40) and (2.41). For the valley K$'$ the results are the same but with the replacement $\psi_1 \to \psi_2'$, $\psi_2 \to -\psi_1'$ (see Eqs. (1.27) and (1.28)), thus,

$$\begin{aligned} \psi_1'(X) &= -i\varepsilon D_{n-1}(-X), \\ \psi_2'(X) &= D_n(-X). \end{aligned} \tag{5.115}$$

The eigenenergy ε can be found from the boundary conditions. For example, for the armchair-terminated edge, one needs to put

$$\begin{aligned} \psi_1(x=0) &= \psi_1'(x=0), \\ \psi_2(x=0) &= \psi_2'(x=0). \end{aligned} \tag{5.116}$$

For the case of zigzag-terminated edges, the valleys are decoupled, and the conditions are

$$\begin{aligned} \psi_1(x=0) &= 0, \\ \psi_1'(x=0) &= 0 \end{aligned} \tag{5.117}$$

(for the zigzag edge with missing A atoms). Then, Eqs. (5.114) and (5.115) give the energy (2.26) depending on the coordinate of the centre of the orbit x_0 (2.40), or, equivalently, on the wave vector k_y along the edge.

It is easier to analyse these solutions after transformation of the original problem to the Schrödinger equation for a double-well potential (Abanin, Lee & Levitov, 2006; Delplace & Montambaux, 2010). The Hamiltonian $\hat{H}^2$ (2.33) can be represented as

$$\hat{H}^2 = \frac{2h|e|Bv^2}{c}\hat{Q}, \tag{5.118}$$

where

$$\hat{Q} = -\frac{1}{2}\frac{d^2}{dx^2} + \frac{1}{2}(x - x_0)^2 - \frac{1}{2}\sigma_z\tau_z,$$

where x and x_0 are in units of the magnetic length l_B and $\sigma_z = +1$ for components corresponding to the sublattice A and $\sigma_z = -1$ for components corresponding to the sublattice B, with $\tau_z = \pm 1$ for the valley K and K′, respectively.

For the case of zigzag edges, the valleys and sublattices are decoupled. The eigenvalues of the operators $\hat{Q}$ for the valleys K and K′ differ by 1. The sublattices are also decoupled, but the edge states for the B sublattice are associated with another edge.

The eigenstates of the problem

$$\hat{Q}\psi(x) = \varepsilon^2\psi(x) \tag{5.119}$$

with the boundary condition (5.117) are the same as the antisymmetric eigenstates for the symmetric potential

$$\hat{Q} = -\frac{1}{2}\frac{d^2}{dx^2} + V(x), \tag{5.120}$$

$$V(x) = \frac{1}{2}(|x| - x_0)^2 \mp \frac{1}{2} \tag{5.121}$$

with $\mp$ signs for the valleys K and K′, respectively (see Fig. 5.11).

If $|x_0| \gg 1$ the potential wells are well separated and the probability of tunnelling between the wells is exponentially small, for

$$\varepsilon^2 \leq \frac{1}{2}x_0^2. \tag{5.122}$$

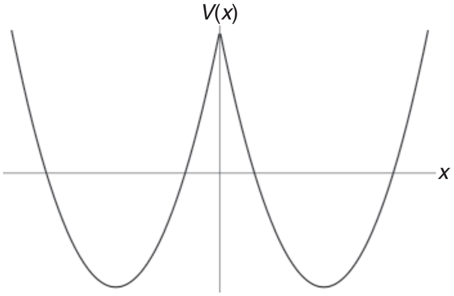

Fig. 5.11. The effective potential (5.121) (for the case of the minus sign).

Then, in zeroth-order approximation, the eigenvalues are the same as for independent walls,

$$\varepsilon_n^2 = n + \frac{1}{2} \mp \frac{1}{2} \tag{5.123}$$

($n = 0, 1, 2, \ldots$). Tunnelling leads to the splitting of each eigenvalue for symmetric and antisymmetric states,

$$\delta\varepsilon_n^2 = \pm\Delta_n \tag{5.124}$$

with

$$\Delta_n \propto \exp\left[-\int_{x_1}^{x_2} dx \sqrt{V(x) - \varepsilon_n{}^2}\right], \tag{5.125}$$

where $x_{1,2}$ are the classical turning points: $V(x_{1,2}) = \varepsilon_n^2$. One needs to choose the plus sign in Eq. (5.124) corresponding to the antisymmetric eigenfunctions.

For the minus sign in Eq. (5.121) (valley K) one has some growing dependence of E_n on the function $|x_0|/l_B$ (the larger $|x_0|$ the smaller the shift) starting from $E = 0$. Starting from the first Landau level, the second valley K′ also contributes, but Δ_n for the same energy corresponds to another value of n ($n \to n - 1$) and, thus, will be different. As a result, we have the picture of the energy levels shown schematically in Fig. 5.12. An almost zero-energy Landau *band* (originating from the zero-energy Landau level for an infinite system) corresponds, for a given edge, to the states from a single valley; the states from the second valley are associated with another edge.

For the case of armchair edges the boundary conditions (5.116) lead to the Schrödinger equation (5.119) and (5.120), but with the potential

$$V(x) = \frac{1}{2}(|x| - x_0)^2 - \frac{1}{2}\operatorname{sgn} x \tag{5.126}$$

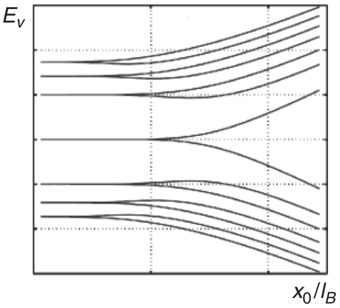

Fig. 5.12. A sketch of the energy spectrum for magnetic edge states.

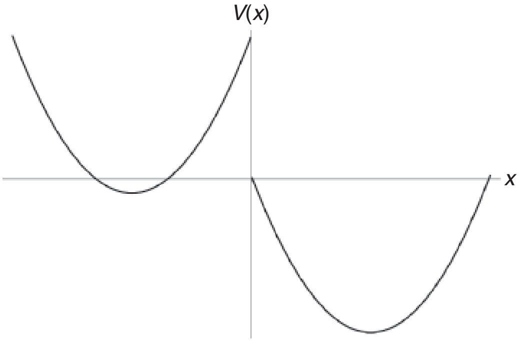

Fig. 5.13. The effective potential (5.126).

(see Fig. 5.13). Indeed, one can define formally

$$\begin{aligned} \psi_1'(x) &\equiv \psi_1(\ \ x), \\ \psi_2'(x) &\equiv \psi_2(\ \ x), \end{aligned} \tag{5.127}$$

so that Eq. (5.116) is nothing other than the condition of continuity of the wave function ψ_1 and its derivative $d\psi_1/dx$ (which is related to ψ_2 by the Dirac equation) at $x = 0$. The qualitative dependence $E_n(x_0/l)$ remains the same as that shown in Fig. 5.12. A more detailed analysis of the problem in the semiclassical approximation was performed by Delplace & Montambaux (2010).

To calculate the Hall conductivity one needs just to count the occupied edge states for a given Fermi energy, with each state contributing e^2/h per spin. One can see immediately from Fig. 5.12 that the lowest-energy Landau band always produces *one* edge electron (for $E > 0$) or hole ($E < 0$) state and all other bands produce two such states. This gives immediately Eq. (2.167) for σ_{xy}, with $g_v = 2$ and $g_s = 1$ (Abanin, Lee & Levitov, 2006).

6

Point defects

6.1 Scattering theory for Dirac electrons

Here we discuss quantum relativistic effects in the electron scattering by a radially symmetric potential $V(r)$. This will give us a feeling for the peculiar properties of charge carriers in *imperfect* graphene, in comparison with the conventional two-dimensional electron gas with impurities (Ando, Fowler & Stern, 1982). Further, we will consider a more realistic model of defects in a honeycomb lattice, beyond the Dirac approximation. In this section we follow the papers by Katsnelson & Novoselov (2007), Hentschel & Guinea (2007), Guinea (2008) and Novikov (2007). It is instructive to compare the scattering theory developed in those works with the two-dimensional scattering theory for the Schrödinger equation (Adhikari, 1986).

Let us start with the equation

$$\left(\quad ihv\hat{\vec{\sigma}}\nabla + V(r)\right)\begin{pmatrix}\psi_1\\ \psi_2\end{pmatrix} = E\begin{pmatrix}\psi_1\\ \psi_2\end{pmatrix}, \tag{6.1}$$

where the potential $V(r)$ is supposed to be isotropic, that is, dependent only on the modulus $r = \sqrt{x^2 + y^2}$. We have to pass to the radial coordinates (see Eqs. (5.16) (5.19)). Then Eq. (6.1) is transformed to the couple of ordinary differential equations

$$\begin{aligned}\frac{dg_l(r)}{dr} \quad \frac{l}{r}g_l(r) \quad \frac{i}{hv}[E \quad V(r)]f_l(r) = 0,\\ \frac{df_l(r)}{dr} + \frac{l+1}{r}f_l(r) \quad \frac{i}{hv}[E \quad V(r)]g_l(r) = 0,\end{aligned} \tag{6.2}$$

where $l = 0, \pm 1, \pm 2, \ldots$ is the angular-momentum quantum number and we try the solution in the following form (cf. Eq. (5.19):

$$\begin{aligned}\psi_1(\vec{r}) &= g_l(r)\exp(il\varphi),\\ \psi_2(\vec{r}) &= f_l(r)\exp(i(l+1)\varphi).\end{aligned} \tag{6.3}$$

To be specific, we will consider further the case of electrons with $E = hvk > 0$.

In two dimensions, the incident electron plane wave has the expansion

$$\exp\left(i\vec{k}\vec{r}\right) = \exp(ikr\cos\varphi) = \sum_{l=-\infty}^{\infty} i^l J_l(kr)\exp(il\varphi), \tag{6.4}$$

where $J_l(z)$ are the Bessel functions (Whittaker & Watson, 1927). At large values of the argument ($kr \gg 1$), they have asymptotics

$$J_l(kr) \cong \sqrt{\frac{2}{\pi kr}}\cos\left(kr - \frac{l\pi}{2} - \frac{\pi}{4}\right). \tag{6.5}$$

The radial Dirac equation (6.2) for free space ($V(r) = 0$) has, for a given l, two independent solutions, which are proportional to the Bessel and Neumann functions, $J_l(kr)$ and $Y_l(kr)$, the latter having the asymptotics ($kr \gg 1$)

$$Y_l(kr) \cong \sqrt{\frac{2}{\pi kr}}\sin\left(kr - \frac{l\pi}{2} - \frac{\pi}{4}\right), \tag{6.6}$$

but the functions $Y_l(kr)$ are divergent at $r \to 0$. Instead, one can use Hankel functions

$$H_l^{(1,2)}(kr) = J_l(kr) \pm iY_l(kr) \tag{6.7}$$

with the asymptotics, at $kr \gg 1$,

$$H_l^{(1,2)}(kr) \cong \sqrt{\frac{2}{\pi kr}}\exp\left[\pm i\left(kr - \frac{l\pi}{2} - \frac{\pi}{4}\right)\right]. \tag{6.8}$$

Thus, the function $H_l^{(1)}$ describes the scattering wave and $H_l^{(2)}$ describes the wave falling at the centre.

If we have a potential of finite radius R ($V(r > R) = 0$), the solution of Eqs. (6.2) at $r > R$ can be represented in the form

$$\begin{aligned} g_l(r) &= A\left[J_l(kr) + t_l H_l^{(1)}(kr)\right], \\ f_l(r) &= iA\left[J_{l+1}(kr) + t_l H_{l+1}^{(1)}(kr)\right], \end{aligned} \tag{6.9}$$

where the terms proportional to Bessel (Hankel) functions describe incident (scattering) waves. The complex factors t_l in Eq. (6.9) are scattering amplitudes.

One can represent them in a more conventional way, via scattering phases δ_l (Newton, 1966; Adhikari, 1986). The latter are determined via the asymptotics of radial solutions at $kr \gg 1$,

$$g_l(kr) \propto \frac{1}{\sqrt{kr}} \cos\left[kr - \frac{l\pi}{2} - \frac{\pi}{4} + \delta_l\right]. \tag{6.10}$$

Taking into account Eqs. (6.5)–(6.8), Eq. (6.10) can be represented as

$$\begin{aligned} g_l(r) &\propto \cos\delta_l\, J_l(kr) - \sin\delta_l\, Y_l(kr) \\ &= \exp(-i\delta_l) \left[J_l(kr) + i\sin\delta_l \exp(i\delta_l) H_l^{(1)}(kr)\right]. \end{aligned} \tag{6.11}$$

On comparing Eqs. (6.9) and (6.11) one finds

$$t_l(k) = i\sin\delta_l(k)\exp[i\delta_l(k)] = \frac{\exp[2i\delta_l(k)] - 1}{2}. \tag{6.12}$$

It follows from Eq. (6.12) that

$$|t_l(k)| \le 1, \tag{6.13}$$

which means, as we will see below, that the scattering current cannot be larger than the incident one.

Let us calculate now the scattering cross-section. For the incident wave propagating along the x-axis we have

$$\Psi^{(0)} = \frac{1}{\sqrt{2}} \begin{pmatrix} 1 \\ 1 \end{pmatrix} \exp(ikx), \tag{6.14}$$

where the numerical factor provides normalization of the incident current:

$$j_x^{(0)} = \left[\Psi^{(0)}\right]^+ \sigma_x \Psi^{(0)} = 1. \tag{6.15}$$

Thus, one can choose $A = 1/\sqrt{2}$ in Eq. (6.9). Taking into account Eqs. (6.9) and (6.8), one finds for the asymptotics of the scattering waves at large distances

$$\Psi_{\text{sc}} \approx \frac{1}{\sqrt{\pi kr}} \exp\left(ikr - \frac{i\pi}{4}\right) \sum_{l=-\infty}^{\infty} t_l \begin{pmatrix} \exp[i(l+1)\varphi] \\ \exp(il\varphi) \end{pmatrix}. \tag{6.16}$$

The current operator in the direction $\vec{n} = \vec{r}/r$ is

$$\hat{j}_n = \vec{n}\hat{\vec{\sigma}} = \begin{pmatrix} 0 & e^{-i\varphi} \\ e^{i\varphi} & 0 \end{pmatrix}, \tag{6.17}$$

which gives us for the scattering current

$$j^{(\text{sc})} = \Psi_{\text{sc}}^+ \hat{j}_n \Psi_{\text{sc}} = \frac{2}{\pi kr} |F(\varphi)|^2, \tag{6.18}$$

where

$$F(\varphi) = \sum_{l=-\infty}^{\infty} t_l \exp(il\varphi). \tag{6.19}$$

Equation (6.18) gives for the differential cross-section

$$\frac{d\sigma}{d\varphi} = \frac{2}{\pi k} |F(\varphi)|^2. \tag{6.20}$$

The Dirac equation (6.2) for the massless case has an important symmetry with respect to the replacement $f \leftrightarrow g$, $l \leftrightarrow -l-1$, which leads to the result

$$t_l(k) = t_{-l-1}(k). \tag{6.21}$$

Taking into account Eq. (6.21), the equation (6.20) can be rewritten in the final form (Katsnelson & Novoselov, 2007)

$$\frac{d\sigma}{d\varphi} = \frac{8}{\pi k} \left| \sum_{l=0}^{\infty} t_l \cos\left[\left(l + \frac{1}{2}\right)\varphi\right] \right|^2. \tag{6.22}$$

It follows immediately from Eq. (6.22) that $d\sigma/d\varphi = 0$ at $\varphi = \pi$, that is, backscattering is absent. This is in agreement with the general considerations of Section 4.2.

If we have a small concentration of point defects, n_{imp}, then, according to the standard semiclassical Boltzmann theory (Ziman, 2001; Shon & Ando, 1998; see also below, Chapter 11), their contribution to the resistivity is

$$\rho = \frac{2}{e^2 v^2 N(E_{\text{F}})} \frac{1}{\tau(k_{\text{F}})}, \tag{6.23}$$

where $\tau(k_{\text{F}})$ is the mean-free-path time and

$$\frac{1}{\tau(k_{\text{F}})} = n_{\text{imp}} v \sigma_{\text{tr}}, \tag{6.24}$$

where

$$\sigma_{\text{tr}} = \int_0^{2\pi} d\varphi \frac{d\sigma}{d\varphi} (1 - \cos\varphi) \tag{6.25}$$

is the *transport cross-section*. The applicability of the semiclassical Boltzmann theory to quantum relativistic particles in graphene is not clear, a priori. This issue will be considered in detail in Chapter 11, and the answer will be that, yes, we can use this theory except in the very close vicinity of the neutrality point, where the minimal conductivity is a purely quantum phenomenon (see Chapter 3). On substituting Eq. (6.20) into Eq. (6.25) one finds

$$\sigma_{\mathrm{tr}} = \frac{4}{k}\sum_{l=0}^{\infty}\sin^2(\delta_l - \delta_{l+1}). \tag{6.26}$$

Note that Eq. (6.23) for the case of graphene coincides with Eq. (4.65), where $l = v\tau(k_{\mathrm{F}})$ is the mean free path.

6.2 Scattering by a region of constant potential

Let us apply a general theory from the previous section to the simplest case of a rectangular potential well (or hump),

$$V(r) = \begin{cases} V_0, & r < R, \\ 0, & r > R. \end{cases} \tag{6.27}$$

Then, the asymptotic expression (6.9) gives us an exact solution for $r > R$. At $r < R$, k should be replaced by

$$q = \frac{E - V_0}{\hbar v} \tag{6.28}$$

and only Bessel functions $J_l(qr)$ are allowed (otherwise, the solution will not be normalizable, due to divergence $Y_l(z) \sim z^{-l}$ at $z \to 0$):

$$\begin{aligned} g_l(r) &= BJ_l(qr), \\ f_l(r) &= iBJ_{l+1}(qr) \end{aligned} \tag{6.29}$$

at $r < R$. One needs to add the conditions of continuity of the functions $g_l(r)$ and $f_l(r)$ at $r = R$. The result is (Katsnelson & Novoselov, 2007; Hentschel & Guinea, 2007)

$$t_l(k) = \frac{J_l(qR)J_{l+1}(kR) - J_l(kR)J_{l+1}(qR)}{H_l^{(1)}(kR)J_{l+1}(qR) - J_l(qR)H_{l+1}^{(1)}(kR)}. \tag{6.30}$$

Let us consider first the case of a short-range potential,

$$kR \ll 1; \tag{6.31}$$

then $q = \ \ V_0/(hv)$ can be considered an energy-independent quantity. At $z \to 0$,

$$J_l(z) \approx \frac{1}{l!}\left(\frac{z}{2}\right)^l,$$
$$H_l^{(1)}(z) \approx \ \ \frac{i}{\pi}\left(\frac{2}{z}\right)^l (l \ \ 1)! \quad (l \neq 0), \tag{6.32}$$
$$H_0^{(1)}(z) \approx \frac{2i}{\pi} \ln z.$$

On substituting Eq. (6.32) into Eq. (6.30), one finds

$$t_l(k) \approx \frac{\pi i}{(l!)^2} \frac{J_{l+1}(qR)}{J_l(qR)} \left(\frac{kR}{2}\right)^{2l+1} \tag{6.33}$$

and, thus, the s-scattering ($l = 0$) dominates,

$$t_0(k) \sim \delta_0(k) \sim kR. \tag{6.34}$$

According to Eq. (6.26),

$$\sigma_{\text{tr}} \sim k \tag{6.35}$$

and the contribution to the resistivity (6.23), (4.65) for the short-range scatterers, can be estimated as

$$\rho \cong \frac{h}{e^2} n_{\text{imp}} R^2. \tag{6.36}$$

We will see later (see the detailed analysis in Chapter 11) that this contribution is negligible.

The results (6.34) and (6.35) are quite clear, keeping in mind an analogy with optics (Born & Wolf, 1980). The dispersion relation for massless Dirac fermions is the same as for photons, but for the latter case we know that obstacles with geometrical sizes much smaller than the wavelength are very inefficient scatterers.

There is a special case, however, if

$$J_0(qR) = 0. \tag{6.37}$$

Then, the expression (6.33) does not work at $l = 0$, and higher-order terms should be taken into account. The result is

$$t_0(k) \cong \frac{\pi i}{2} \frac{1}{\ln(kR)} \tag{6.38}$$

and

$$\sigma_{\mathrm{tr}} = \frac{\pi^2}{k \ln^2(kR)}. \tag{6.39}$$

Therefore, instead of (6.36) we have a much larger contribution to the resistivity (Ostrovsky, Gornyi & Mirlin, 2006; Katsnelson & Novoselov, 2007):

$$\rho \cong \frac{h}{e^2} \frac{n_{\mathrm{imp}}}{n} \frac{1}{\ln^2(k_{\mathrm{F}}R)}, \tag{6.40}$$

where $n = k_{\mathrm{F}}^2/\pi$ is the charge-carrier concentration.

The condition (6.37) corresponds to the case of resonance, for which a virtual bound state in the well lies close to the neutrality point. Later in this chapter we will consider more realistic models of such resonant scatterers, namely vacancies and adatoms. It is interesting to see, however, that the effect exists already in the Dirac approximation.

If we were to repeat the same calculations for a nonrelativistic electron gas (Adhikari, 1986), then, instead of continuity of two components of the spinor wave function at $r = R$, we would have conditions of continuity of the single-component wave function and its derivative. The result is

$$t_l(k) = \frac{\left(\frac{k}{q}\right) J_l(qR) J_{l+1}(kR) \quad J_l(kR) J_{l+1}(qR)}{H_l^{(1)}(kR) J_{l+1}(qR) \quad \left(\frac{k}{q}\right) J_l(qR) H_{l+1}^{(1)}(kR)}, \tag{6.41}$$

where k and q are, again, wave vectors outside and inside the potential region. In this case $t_0(k) \sim 1/\ln(kR)$ (cf. Eq. (6.38)) for general values of the parameters, and the contribution to the resistivity takes the form (6.40). One can say that for the two-dimensional nonrelativistic electron gas *any* potential scattering should be considered resonant. This agrees with the fact that the perturbation theory does not work in such a situation and an arbitrarily weak potential leads to the formation of a bound state (Landau & Lifshitz, 1977).

The opposite limit

$$kR \gg 1 \tag{6.42}$$

is relevant for the problem of electron scattering by clusters of charge impurities (Katsnelson, Guinea & Geim, 2009; see also Chapter 11 of this book). On substituting the asymptotics (6.5) and (6.8) into Eq. (6.30) one finds

$$t_l(k) \approx \frac{1}{2}\left[\exp\left(\frac{2iV_0R}{hv}\right) \quad 1\right]. \tag{6.43}$$

The summation in Eq. (6.19) should be taken up to $|l| \le l_{\max} \approx kR$, thus

$$\frac{d\sigma}{d\varphi} = \frac{2}{\pi k} \sin^2\left(\frac{V_0 R}{hv}\right) \left| \sum_{l=-l_{\max}}^{l_{\max}} e^{il\varphi} \right|^2 = \frac{2}{\pi k} \sin^2\left(\frac{V_0 R}{hv}\right) \frac{\sin^2\left(\frac{(2l_{\max}+1)\varphi}{2}\right)}{\sin^2\left(\frac{\varphi}{2}\right)}. \quad (6.44)$$

The expression (6.44) has sharp maxima at the angles

$$\varphi = \pi \frac{2n+1}{2l_{\max}+1}, \quad n = 0, \pm 1, \ldots,$$

which can be related to periodic classical trajectories of electrons within the potential well (for more details, see Katsnelson, Guinea & Geim, 2009). On substituting Eq. (6.44) into Eq. (6.25) one finds

$$\sigma_{\mathrm{tr}} \cong \frac{4}{k} \sin^2\left(\frac{V_0 R}{hv}\right). \quad (6.45)$$

Interestingly, the cross-section (6.45) is small in comparison with the geometrical size of the potential region R. Indeed, the region is transparent, due to Klein tunnelling. The corresponding contribution to the resistivity is

$$\rho \cong \frac{h}{e^2} \frac{n_{\mathrm{imp}}}{n} \sin^2\left(\frac{V_0 R}{hv}\right). \quad (6.46)$$

Thus, long-range potential scattering leads to a contribution to the resistivity proportional to $1/n$.

6.3 Scattering theory for bilayer graphene in the parabolic-band approximation

We saw in the previous section that the scattering of massless Dirac fermions in graphene (chiral states, a linear dispersion relation) is essentially different from that of nonrelativistic electrons (nonchiral states, a parabolic dispersion relation) in a two-dimensional electron gas. To understand better the role of chirality and of dispersion relations, it is instructive to consider the case of chiral states with a parabolic dispersion relation, that is, the case of bilayer graphene in the parabolic-band approximation (1.46). The corresponding scattering theory was developed by Katsnelson (2007c).

To solve the Schrödinger equation for the Hamiltonian (1.46) with the addition of a radially symmetric potential $V(r)$, one has to use, instead of

Eq. (6.3), the angular dependences of the two components of the spinor wave function,

$$\begin{aligned}\psi_1(\vec{r}) &= g_l(r)\exp(il\varphi),\\ \psi_2(\vec{r}) &= f_l(r)\exp(i(l+2)\varphi),\end{aligned} \tag{6.47}$$

where $l = 0, \pm 1, \ldots$ The radial components satisfy the equations

$$\begin{aligned}\left(\frac{d}{dr} - \frac{l+1}{r}\right)\left(\frac{d}{dr} - \frac{l}{r}\right)g_l &= -\left(k^2 - \frac{2m^* V}{h^2}\right)f_l,\\ \left(\frac{d}{dr} + \frac{l+1}{r}\right)\left(\frac{d}{dr} + \frac{l+2}{r}\right)f_l &= -\left(k^2 - \frac{2m^* V}{h^2}\right)g_l,\end{aligned} \tag{6.48}$$

where, to be specific, we consider the case of electrons with $E = h^2k^2/(2m^*) > 0$.

The problem of scattering for this case is essentially different both from the Dirac theory and from the Schrödinger theory since evanescent waves are unavoidably involved (cf. the discussion of Klein tunnelling for the case of bilayer graphene, Section 4.7). This means that, beyond the radius of action of the potential, Bessel functions of imaginary arguments have to be added to Eq. (6.9). More specifically, we mean the Macdonald function $K_l(kr)$ (Whittaker & Watson, 1927) with the asymptotics

$$K_l(kr) \approx \sqrt{\frac{\pi}{2kr}}\exp(-kr) \tag{6.49}$$

at $kr \gg 1$; the Bessel functions $I_l(kr)$ grow exponentially at large r and cannot be used, due to the normalization condition for the wave function. Thus, one should try for the solution at large distances

$$\begin{aligned}g_l(r) &= A\left[J_l(kr) + t_l H_l^{(1)}(kr) + c_l K_l(kr)\right],\\ f_l(r) &= A\left[J_{l+2}(kr) + t_l H_{l+2}^{(1)}(kr) + c_l K_{l+2}(kr)\right].\end{aligned} \tag{6.50}$$

One can check straightforwardly that the functions (6.50) satisfy the equations (6.48) at $V(r) = 0$ for any A, t_l and c_l.

The terms proportional to $J_l(kr)$ are related to the incident wave (see Eq. (6.4)), those proportional to $H_l^{(1)}(kr)$ to the scattering waves and those proportional to $K_l(kr)$ to the evanescent waves. The coexistence of scattering and evanescent waves at the same energy makes the case of bilayer graphene really peculiar.

The normal component of the current operator

$$\hat{j}_n = \vec{n}\frac{\delta \hat{H}}{h\,\delta\vec{k}}, \tag{6.51}$$

where $\vec{n} = \vec{r}/r$ and $\hat{H}$ is the Hamiltonian (1.46), has the form (cf. Eq. (6.17))

$$\hat{j}_n = \frac{hk}{m^*}\begin{pmatrix} 0 & \exp(-2i\varphi) \\ \exp(2i\varphi) & 0 \end{pmatrix}. \tag{6.52}$$

By calculating, further, the scattering cross-section as in the previous section, we find formally the same expression (6.19) and (6.20) as for the case of single-layer graphene. However, the symmetry properties of Eqs. (6.48) are different. Namely, they are invariant under the replacement $f \leftrightarrow g$, $l \leftrightarrow -l-2$. As a result, instead of Eq. (6.21) we have

$$t_l(k) = t_{-l-2}(k). \tag{6.53}$$

Substituting Eq. (6.53) into Eq. (6.19), we rewrite Eq. (6.20) as

$$\frac{d\sigma}{d\varphi} = \frac{2}{\pi k}\left| t_{-1} + 2\sum_{l=0}^{\infty} t_l \cos[(l+1)\varphi] \right|^2, \tag{6.54}$$

which gives us a general solution of the scattering problem.

To find the scattering amplitudes t_l one needs to specify $V(r)$. For simplicity, we will use the expression (6.27) (a region of constant potential). Then, for the solution of Eqs. (6.48) at $r < R$ that is regular as $r \to 0$ one can try

$$\begin{aligned} g_l(r) &= \alpha_l J_l(qr) + \beta_l I_l(qr), \\ f_l(r) &= \sigma[\alpha_l J_{l+2}(qr) + \beta_l I_{l+2}(qr)], \end{aligned} \tag{6.55}$$

where

$$\begin{aligned} \sigma &= \mathrm{sgn}(E - V_0), \\ q &= \sqrt{\frac{2m^*|E - V_0|}{h^2}}. \end{aligned} \tag{6.56}$$

Equations (6.48) are now satisfied identically, and the coefficients α_l, β_l, t_l and c_l should be found from continuity of $g_l(r)$, $f_l(r)$, $dg_l(r)/dr$ and $df_l(r)/dr$ at $r = R$.

Further, we will consider only the case of a short-range potential, $kR \ll 1$. For the case $l = -1$, taking into account the identities $K_1(z) = K_{-1}(z)$, $I_1(z) = I_1(-z)$, $J_1(z) = -J_{-1}(z)$ and $H_1^{(1)}(z) = -H_{-1}^{(1)}(z)$ one can prove immediately that $c_{-1} = 0$ and

$$t_{-1} \propto (kR)^2. \tag{6.57}$$

Also, taking into account the asymptotics of the Macdonald and Hankel functions for $l > 2$, $z \to 0$ (we need here next-order terms, in comparison with Eq. (6.32)),

$$\begin{aligned} K_l(z) &\approx \frac{1}{2}\left(\frac{2}{z}\right)^l (l-1)! - \frac{1}{2}\left(\frac{2}{z}\right)^{l-2}(l-2)!, \\ H_l^{(1)}(z) &\approx -\frac{i}{\pi}\left(\frac{2}{z}\right)^l (l-1)! - \frac{i}{\pi}\left(\frac{2}{z}\right)^{l-2}(l-2)!, \end{aligned} \tag{6.58}$$

one can prove that for $l \geq 1$ and $kR \to 0$ both t_l and c_l are of the order of $(ka)^{2l}$ or smaller and thus only the s-channel ($l=0$) contributes to the scattering cross-section, so that Eq. (6.54) can be rewritten as

$$\frac{d\sigma}{d\varphi} = \frac{8}{\pi k}|t_0(k)|^2 \cos^2\varphi. \tag{6.59}$$

For single-layer graphene, $d\sigma/d\varphi \sim \cos^2(\varphi/2)$ (see Eq. (6.22)) and backscattering is forbidden. For the case of bilayer graphene there is a strong suppression of the scattering at $\varphi \approx \pi/2$. This reflects a difference of the chiral properties of electron states in these two situations.

For the case $l=0$ the wave functions at $r > R$ (but for $kr \ll 1$), Eqs. (6.50), have the forms

$$\begin{aligned} g_0(r) &= A\left[1 + t_0 + \tau_0 \ln\left(\frac{kr}{2}\right) + \gamma\right] + O\left[(kr)^2 \ln(kr)\right], \\ f_0(r) &= A\left[-\frac{2i}{\pi}t_0 - \tau_0\left(\frac{2}{(kr)^2} - \frac{1}{2}\right)\right] + O\left[(kr)^2 \ln(kr)\right], \end{aligned} \tag{6.60}$$

where $\gamma \approx 0.577\ldots$ is the Euler constant,

$$\tau_0 = \frac{2it_0}{\pi} - c_0. \tag{6.61}$$

It follows from the continuity of $df_0(r)/dr$ at $r = R$ that

$$\tau_0 = \frac{k^2 R^3}{4A}\frac{df_0(r)}{dR} \sim k^2 \tag{6.62}$$

and, thus,

$$\left.\frac{dg_0}{dr}\right|_{r=R} \sim k^2.$$

In the limit $k \to 0$ one has the condition

$$\left.\frac{dg_0}{dr}\right|_{r=R} = 0, \tag{6.63}$$

which gives us a ratio of β_0/α_0. As a result, for $r < R$

$$
\begin{aligned}
g_0(r) &= \alpha_0 \left[J_0(qr) \quad I_0(qr)\frac{J_0'(qR)}{I_0'(qR)} \right], \\
f_0(r) &= \sigma\alpha_0 \left[J_2(qr) \quad I_2(qr)\frac{J_0'(qR)}{I_0'(qR)} \right],
\end{aligned}
\tag{6.64}
$$

where prime means d/dR. Thus, we have two equations for the constant α_0 and A,

$$
\begin{aligned}
g_0(R) &= A(1 + t_0), \\
f_0(R) + \frac{R}{2}\frac{df_0(R)}{dR} &= \quad \frac{2iA}{\pi} t_0,
\end{aligned}
\tag{6.65}
$$

which gives us the final expression for t_0.

It is clear that t_0 does not depend on k in the limit $kR \to 0$. It takes the value with the maximum possible modulus, $t_0 = \quad 1$ (the *unitary limit*), when

$$
\frac{d}{dR}\frac{J_0(qR)}{I_0(qR)} = 0. \tag{6.66}
$$

This behaviour is dramatically different both from that of massless Dirac fermions and from that of conventional nonrelativistic electrons, for which $t_0(k) \to 0$ at $k \to 0$ (either linearly or $\sim 1/|\ln k|$).

As a result, for the case of short-range scattering in bilayer graphene (in the parabolic-band approximation)

$$
\sigma_{\text{tr}} \sim \frac{1}{k} \tag{6.67}
$$

and the corresponding contribution to the resistivity is

$$
\rho \approx \frac{h}{e^2}\frac{n_{\text{imp}}}{n}. \tag{6.68}
$$

Within the perturbation theory, this concentration dependence was obtained by Koshino & Ando (2006).

We will postpone further discussion of these results until Chapter 11, where we will discuss electronic transport in graphene; here we restrict ourselves to the quantum-mechanical problem.

6.4 General theory of defects in a honeycomb lattice

In general, the continuum medium approximation used above is not sufficient for discussing short-range scattering centres in graphene since they induce intervalley transitions (Shon & Ando, 1998). To study these effects, we pass here to consideration of defects in a honeycomb lattice (Peres, Guinea & Castro Neto, 2006; Wehling *et al.*, 2007; Wehling, Katsnelson & Lichtenstein, 2009a; Basko, 2008). We will use the T-matrix formalism which has already been mentioned in Section 4.2 (see Eqs. (4.33) and (4.34)), but here we will present it in a more systematic way (see Lifshitz, Gredeskul & Pastur, 1988; Vonsovsky & Katsnelson, 1989).

Let us consider a general, single-particle Hamiltonian

$$\hat{H} = \hat{H}_0 + \hat{V} \tag{6.69}$$

defined on a crystal lattice, $\hat{H}_0$ being the Hamiltonian of the ideal lattice and $\hat{V}$ the perturbation created by defects. The local density of states at site i is determined by the expression

$$N_i(E) = \langle i|\delta\big(E - \hat{H}\big)|i\rangle, \tag{6.70}$$

which can also be represented as

$$N_i(E) = -\frac{1}{\pi}\operatorname{Im}\hat{G}_{ii}(E), \tag{6.71}$$

where

$$\hat{G}(E) = \lim_{\delta\to+0}\frac{1}{E - \hat{H} + i\delta} \tag{6.72}$$

is the Green function (resolvent) of the operator $\hat{H}$. It follows immediately from Eq. (6.69) that

$$\hat{G}^{-1} = \hat{G}_0^{-1} - \hat{V}, \tag{6.73}$$

where $\hat{G}_0$ is the Green function of the unperturbed problem, Eq. (4.34). By multiplying Eq. (6.73) by operators $\hat{G}$ from the right side and $\hat{G}_0$ from the left side we derive the *Dyson equation*

$$\hat{G}(E) = \hat{G}_0(E) + \hat{G}_0(E)\hat{V}\hat{G}(E). \tag{6.74}$$

Its formal solution can be written as

$$\hat{G}(E) = \hat{G}_0(E)\big[1 - \hat{V}\hat{G}_0(E)\big]^{-1}, \tag{6.75}$$

which is a compact notation for the infinite series

$$\hat{G}(E) = \hat{G}_0(E) + \hat{G}_0(E)\hat{V}\hat{G}_0(E) + \hat{G}_0(E)\hat{V}\hat{G}_0(E)\hat{V}\hat{G}_0(E) + \cdots \tag{6.76}$$

Alternatively, the series (6.76) can be written as

$$\hat{G}(E) = \hat{G}_0(E) + \hat{G}_0(E)\hat{T}(E)\hat{G}_0(E), \tag{6.77}$$

where $\hat{T}$ is the *T-matrix* satisfying Eq. (4.33). Its formal solution can be represented as

$$\hat{T}(E) = \left[1 - \hat{V}\hat{G}_0(E)\right]^{-1}\hat{V}. \tag{6.78}$$

The change of the spectral density can be expressed in terms of the T-matrix. The total density of states

$$N(E) = \mathrm{Tr}\,\delta\left(E - \hat{H}\right) = -\frac{1}{\pi}\,\mathrm{Tr}\,\mathrm{Im}\,\hat{G}(E) \tag{6.79}$$

can be written, due to Eqs. (6.72) and (6.75), as

$$N(E) = \frac{1}{\pi}\frac{\partial}{\partial E}\,\mathrm{Tr\ Im\ ln}\,\hat{G}(E) = \frac{1}{\pi}\frac{\partial}{\partial E}\,\mathrm{Tr\ Im}\left[\ln\hat{G}_0(E) - \ln\left(1 - \hat{V}\hat{G}_0(E)\right)\right] \tag{6.80}$$

since

$$\hat{G}(E) = -\frac{\partial}{\partial E}\ln\hat{G}^{-1}(E). \tag{6.81}$$

At the same time, due to Eq. (6.78),

$$\ln\hat{T}(E) = -\ln\left[1 - \hat{V}\hat{G}_0(E)\right] + \ln\hat{V}, \tag{6.82}$$

the last term being energy-independent. As a result, the change of the density of states due to the perturbation $\hat{V}$ can be presented as

$$\Delta N(E) = N(E) - N_0(E) = \frac{1}{\pi}\frac{\partial}{\partial E}\mathrm{Im\,Tr\ ln}\,\hat{T}(E). \tag{6.83}$$

Finally, using the operator identity

$$\mathrm{Tr\ ln}\,\hat{A} = \ln\det\hat{A}, \tag{6.84}$$

one can represent Eq. (6.83) in the form

$$\Delta N(E) = -\frac{1}{\pi}\,\mathrm{Im}\frac{\partial}{\partial E}\ln\det\left[1 - \hat{G}_0(E)\hat{V}\right], \tag{6.85}$$

which is more convenient for real calculations.

The contribution of point defects to the resistivity can be also expressed in terms of the T-matrix, see Chapter 11.

If the perturbation $\hat{V}$ is localized on one site $i = 0$ only,

$$V_{ij} = V\delta_{i0}\delta_{j0}, \tag{6.86}$$

then one can see, from Eq. (6.78), that the $\hat{T}$-matrix is also localized on the same site:

$$T_{ij}(E) = T_{00}(E)\delta_{i0}\delta_{j0}, \tag{6.87}$$

where

$$T_{00}(E) = \frac{V}{1 - VG_{00}^{(0)}(E)} \tag{6.88}$$

and $G_{00}^{(0)}(E)$ is the matrix element of Green's function for the ideal crystal lattice at site 0. For the lattice without basis,

$$G_{00}^{(0)}(E) = \lim_{\delta\to+0}\sum_{\vec{k}} \frac{1}{E - t\left(\vec{k}\right) + i\delta}. \tag{6.89}$$

However, for the case of a honeycomb lattice the Hamiltonian $\hat{H}_0$ is a 2 × 2 matrix, which has, in the nearest-neighbour approximation, the form (1.14). By inverting the matrix $E - \hat{H}_0$ one finds the Green function $\hat{G}_0$ in the k representation:

$$\hat{G}_0\left(E,\vec{k}\right) = \lim_{\delta\to+0}\frac{1}{(E+i\delta)^2 - \left|t\left(\vec{k}\right)\right|^2}\begin{pmatrix} E & t\left(\vec{k}\right) \\ t^*\left(\vec{k}\right) & E \end{pmatrix}, \tag{6.90}$$

where $t\left(\vec{k}\right) = tS\left(\vec{k}\right)$. Thus, instead of Eq. (6.89) we have, for the on-site Green function,

$$\begin{aligned} G_{00}^{(0)}(E) &= \lim_{\delta\to+0}\sum_{\vec{k}}\frac{E}{(E+i\delta)^2 - \left|t\left(\vec{k}\right)\right|^2} \\ &= \frac{1}{2}\lim_{\delta\to+0}\sum_{\vec{k}}\left(\frac{1}{E+i\delta - \left|t\left(\vec{k}\right)\right|} + \frac{1}{E+i\delta+\left|t\left(\vec{k}\right)\right|}\right), \end{aligned} \tag{6.91}$$

for which it does not matter whether the site 0 belongs to sublattice A or sublattice B. At $|E| \ll |t|$

$$N_0(E) = -\frac{1}{\pi}\,\mathrm{Im}\,G_{00}^{(0)}(E) = \frac{1}{\pi}\frac{|E|}{\hbar^2 v^2} \tag{6.92}$$

(cf. Eq. (1.72); our quantity is smaller by a factor of 2 since here we do not take into account the spin degeneracy). To find the real part of $G_{00}^{(0)}$ one can use Kramers–Kronig relations:

$$\mathrm{Re}\, G_{00}^{(0)}(E) = P \int_{-\infty}^{\infty} dE' \, \frac{N_0(E')}{E - E'}, \tag{6.93}$$

where P is the symbol for the principal value. We can also just guess the answer, keeping in mind that $G_{00}^{(0)}(E)$ is a regular function of energy in the upper complex half-plane.

Notice that $|E| = E \,\mathrm{sgn}\, E = E[1 - 2\theta(-E)]$, where $\theta(x > 0) = 1$, $\theta(x < 0) = 0$ and

$$\theta(-E) = \frac{1}{\pi}\, \mathrm{Im} \ln(E + i\delta).$$

This means that

$$|E| = E - \frac{2}{\pi} E \,\mathrm{Im} \ln(E + i\delta) \tag{6.94}$$

and, thus, the term $|E|$ in $-(1/\pi)\mathrm{Im}\, G_{00}^{(0)}(E)$ corresponds to $2E$ Re $\ln(E + i\delta)$ $= 2E \ln|E|$ in Re $G_{00}^{(0)}(E)$. Taking into account also that

$$G_{00}^{(0)}(E = 0) = 0, \tag{6.95}$$

by symmetry one finds

$$\mathrm{Re} G_{00}^{(0)}(E) \cong \frac{2}{\pi} \frac{E \ln\left(\frac{|E|}{D}\right)}{h^2 v^2}, \tag{6.96}$$

where we introduce within the logarithm a factor D of the order of the bandwidth. For the accurate calculation of this factor, see Basko (2008). A general theory of scattering by short-range defects in graphene, including group-theory analysis, can also be found in that paper.

The contributions of various types of defects to the transport properties will be considered in detail in Chapter 11. Here we will give just some simple estimations, in order to establish relations between this section and the previous ones.

For the case of a weak enough potential V, the scattering rate (6.24) can be estimated, according to the Fermi golden rule, as

$$\frac{1}{\tau(k_F)} = \frac{2\pi}{h} n_{\mathrm{imp}} |V|^2 N_0(E_F). \tag{6.97}$$

For the case of a small concentration of defects but strong scattering, one can prove rigorously (Luttinger & Kohn, 1958) that the potential V should be replaced by the T-matrix:

$$\frac{1}{\tau(k_{\mathrm{F}})} = \frac{2\pi}{h} n_{\mathrm{imp}} |T_{00}(E_{\mathrm{F}})|^2 N_0(E_F) \tag{6.98}$$

(for the case of graphene, see Robinson *et al.*, 2008; Wehling *et al.*, 2010a).

6.5 The case of vacancies

As a specific application of the general theory described above, consider first the case of vacancies (Peres, Guinea & Castro Neto, 2006). Vacancies are not naturally present in graphene, due to their very high formation energy of about 7.5 eV, see Kotakoski, Krasheninnikov & Nordlund (2006). However, they can be created by ion bombardment (Chen *et al.*, 2009).

The simplest way to simulate the vacancy is just to put $V = \infty$ in the expression (6.88), thus making the site $i = 0$ unavailable for electrons. In this case,

$$T_{00}(E) = \quad \frac{1}{G_{00}{}^{(0)}(E)}. \tag{6.99}$$

On substituting Eq. (6.99) into Eq. (6.77) one finds that $G_{00}(E) = 0$, as it should be.

For small energies $|E| \ll D$ one finds from Eqs. (6.96) and (6.99)

$$T_{00}(E) = \quad \frac{\pi h^2 v^2}{E} \frac{1}{2 \ln\left(\frac{|E|}{D}\right) \quad i\pi \operatorname{sgn} E}. \tag{6.100}$$

The change of the density of states, according to Eq. (6.83), is

$$\begin{aligned} \Delta N(E) &= \frac{1}{\pi} \frac{\partial}{\partial E} \operatorname{Im} \ln T_{00}(E) \\ &= \quad \frac{1}{\pi} \frac{\partial}{\partial E} \operatorname{Im} \ln \left[2 \ln\left(\frac{|E|}{\Delta}\right) \quad i\pi \operatorname{sgn} E \right] \approx \quad \frac{2}{|E| \ln^2\left(\frac{D}{|E|}\right)}. \end{aligned} \tag{6.101}$$

This contribution is negative since the vacancy changes the total number of sites in the system by one, thus

$$\int_{\infty}^{\infty} dE \, \Delta N(E) = \quad 1. \tag{6.102}$$

It is singular at $E \to 0$.

By substituting Eq. (6.100) into Eqs. (6.98) and (6.23) one can estimate the vacancy contribution to the momentum relaxation rate and, thus, to the resistivity:

$$\rho \approx \frac{h}{e^2}\frac{n_{\mathrm{imp}}}{n}\frac{1}{\ln^2(k_{\mathrm{F}}a)}, \tag{6.103}$$

coinciding with Eq. (6.40). Thus, the vacancy is a resonant scatterer contributing essentially to the resistivity (Hentschel & Guinea, 2007; Chen *et al.*, 2009).

Qualitatively, this result can be obtained also within the continuum model. Let us consider the Dirac equation for the empty space with the radial wave functions (6.9). Let us assume that the disc $r < R$ is just cut from the sample. To be specific, let us assume boundary conditions of zigzag type, $\psi_{\mathrm{A}} = 0$, that is,

$$g_l(R) = 0 \tag{6.104}$$

(the case $\psi_{\mathrm{B}} = 0$ can be derived just by the replacement $l \rightarrow \quad l \quad 1$, as was explained in Section 6.1). Taking into account the behaviour of Bessel and Hankel functions at $kr \ll 1$ (Eq. 6.32), one finds immediately that

$$t_0(k) = \quad \frac{J_0(kR)}{H_0{}^{(1)}(kR)} \approx \frac{\pi i}{2\ln(kR)}, \tag{6.105}$$

coinciding with Eq. (6.38). As we have seen in Section 6.2 this gives the estimation (6.103) for the resistivity (Hentschel & Guinea, 2007).

Consider now the asymptotics of the perturbed density of states,

$$\Delta N_i(E) = \quad \frac{1}{\pi}\,\mathrm{Im}\left[G_{i0}^{(0)}(E)T_{00}(E)G_{0i}^{(0)}(E)\right] \tag{6.106}$$

(see Eq. (6.77)) at $R_i \rightarrow \infty$. The asymptotics of the Green function

$$G_{i0}^{(0)}(E) = \sum_{\vec{k}} \exp\left(i\vec{k}\vec{R}_i\right) G_0\left(E, \vec{k}\right), \tag{6.107}$$

where $G_0\left(E, \vec{k}\right)$ is defined by Eq. (6.90), is determined by the region of $\vec{k}$ close to one of the conical points, K or K′. For a generic perturbation V the result is (Bena & Kivelson, 2005; Lin, 2005, 2006; Wehling *et al.*, 2007)

$$\Delta N_i(E) \sim \frac{1}{R_i} \tag{6.108}$$

at $|E|R_i/(hv) \gg 1$. For the case of a vacancy ($V = \infty$) we have, instead of Eq. (6.108),

$$\Delta N_i(E) \sim \frac{1}{R_i^2} \tag{6.109}$$

(Pereira *et al.*, 2006).

Finally, consider the case of a finite concentration of vacancies. The singularity of the scattering amplitude, Eqs. (6.100) and (6.105), results in the formation of *mid-gap states*, or *vacancy bands* (Pereira *et al.*, 2006; Yuan, De Raedt & Katsnelson, 2010a, 2010b). Figure 6.1 shows the total density of states (in the small-energy region) obtained numerically for a large (about 10^7 nodes) piece of honeycomb lattice with periodic boundary conditions, with different concentrations of randomly distributed vacancies (Yuan, De Raedt & Katsnelson, 2010a). The vacancy-induced states form a peak at $E = 0$. In the continuum-medium model (see Eq. (6.104)) these states are associated with the edge states at the boundary of the void (Pereira *et al.*, 2006). Note, however, that the latter model is valid only qualitatively since the atomically sharp disorder induces intervalley processes, which should be taken into account (Basko, 2008).

6.6 Adsorbates on graphene

Adsorbed atoms and molecules are probably the most important examples of point defects in the physics of graphene. Owing to the outstanding strength of the carbon honeycomb lattice it is very difficult to introduce any defects into the lattice itself. At the same time, some contamination of graphene is unavoidable. A systematic study of adsorbates on graphene was started by Schedin *et al.* (2007), who discovered an extreme sensitivity of the electric properties of graphene to gaseous impurities; even the adsorption of a single molecule can be detected. The case of NO_2 was studied in detail, both theoretically and experimentally, by Wehling *et al.* (2008b). Optimized structures and electron densities of states for the NO_2 monomer and dimer are shown in Fig. 6.2. One can see that for the latter case (N_2O_4) there is a peak in the density of states that is reminiscent of the vacancy-induced mid-gap states. Chemical functionalization of graphene, leading, in particular, to the derivation of new two-dimensional crystals, such as graphane, CH (Elias *et al.*, 2009), and fluorographene, CF (Nair *et al.*, 2010), starts with chemisorption of the corresponding adatoms or admolecules (for a review, see Boukhvalov & Katsnelson, 2009a). Last but not least, scattering by adatoms and admolecules seems to be one of the most important factors limiting electron mobility in graphene (Wehling *et al.*, 2010a; Ni *et al.*, 2010); for more details, see Chapter 11.

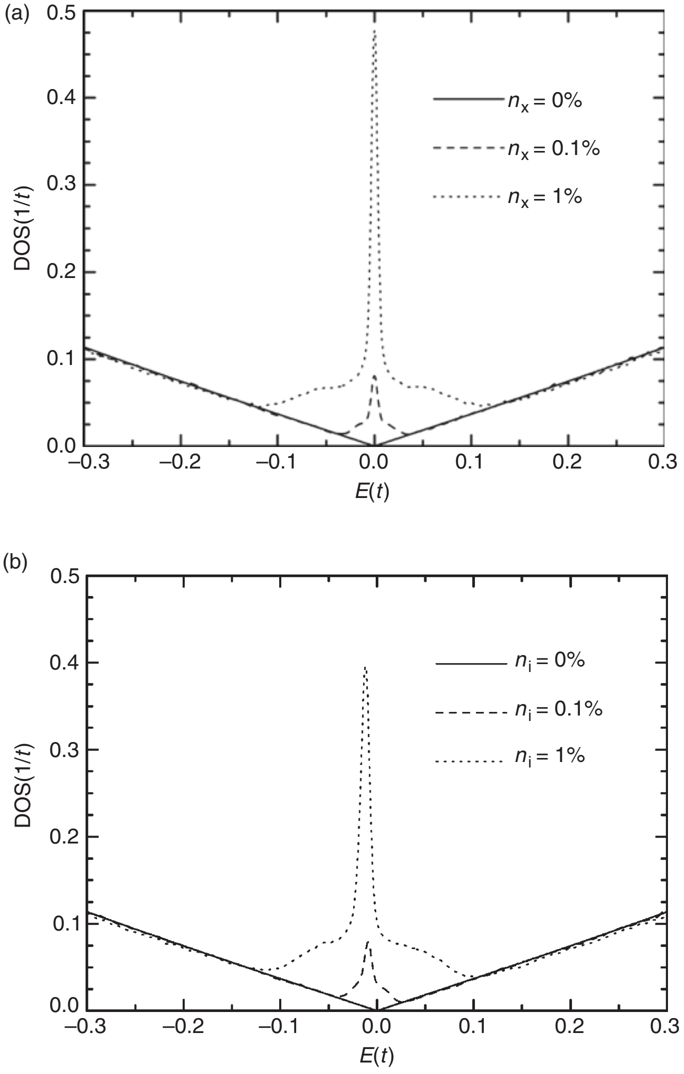

Fig. 6.1. The density of states of graphene with a small concentration of vacancies (a) or hydrogen atoms (that is, adatoms with the parameters (6.114)) (b). Solid lines, pure graphene; dashed lines, 0.1% of defects; dotted lines, 1% of defects. (Reproduced with permission from Yuan, De Raedt & Katsnelson, 2010a.)

The simplest single-electron model describing adsorbates is the hybridization model with the Hamiltonian (Robinson *et al.*, 2008; Wehling *et al.*, 2010a)

$$\hat{H} = \sum_{ij} t_{ij} \hat{c}_i^+ \hat{c}_j + \sum_{ij} \gamma_{ij} \left(\hat{c}_i^+ \hat{d}_j + \hat{d}_j^+ \hat{c}_i \right) + E_\mathrm{d} \sum_i \hat{d}_i^+ \hat{d}_i, \tag{6.110}$$

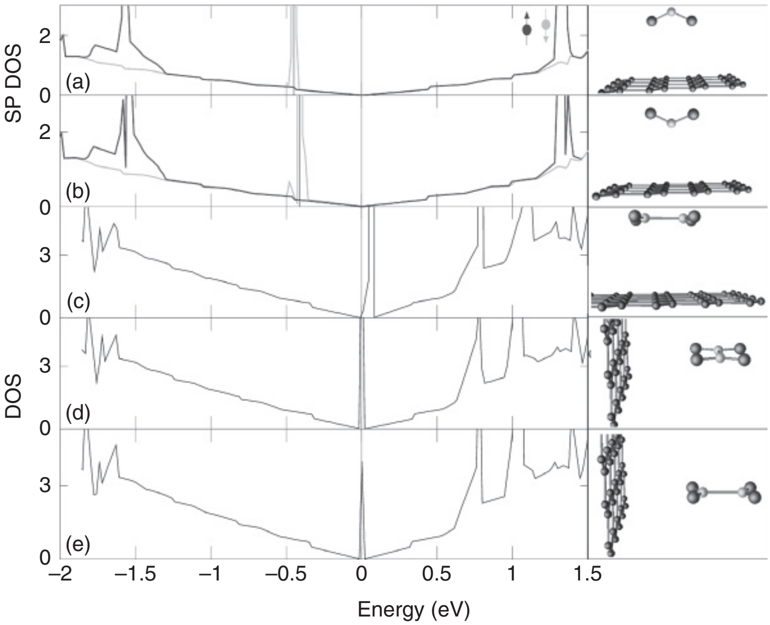

Fig. 6.2. Left: the spin-polarized density of states of graphene with adsorbed NO_2 (the black line is for spin up and the grey line is for spin down), (a) and (b), and the density of states for N_2O_4, (c)–(e), in various adsorption geometries. Right: adsorption geometries obtained from the calculations. (Reproduced with permission from Wehling *et al.*, 2008b.)

where the operators $\hat{c}_i$ and $\hat{d}_i$ annihilate electrons on the ith carbon atom and ith atom of adsorbate, respectively, t_{ij} are the hopping parameters for the carbon honeycomb lattice, E_d is the electron energy for the adsorbate atoms (which are assumed to be identical) and γ_{ij} are hybridization parameters between the ith carbon atom and jth adsorbed atom. The d electron subsystem can be rigorously excluded by projection to c subspace only; the effective Hamiltonian for c electrons has the form (6.69), where $\hat{H}_0$ is the first term on the right-hand side of Eq. (6.110) (the band Hamiltonian for graphene) and $\hat{V}$ is the *energy-dependent* perturbation,

$$V_{ij} = \frac{\sum_l \gamma_{il}\gamma_{lj}}{E - E_\mathrm{d}}. \tag{6.111}$$

If we consider the case of a single adatom ($i = 0$) and assume, for simplicity, that $\gamma_{ij} = \gamma\delta_{ij}$ we pass to the problem (6.86) with

$$V(E) = \frac{\gamma^2}{E - E_\mathrm{d}}. \tag{6.112}$$

Further, we can simply use the theory developed in the previous section.

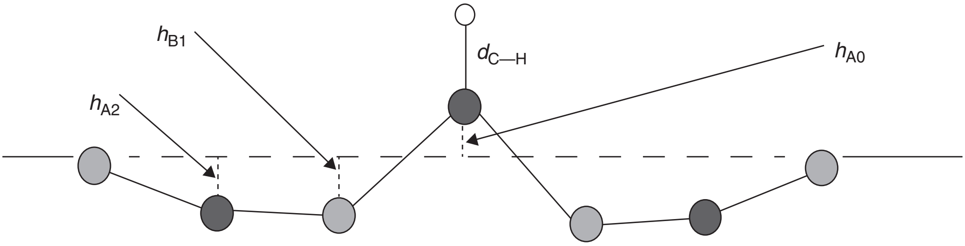

Fig. 6.3. Atomic displacements around a hydrogen atom attached to one of the carbon atoms in graphene. Carbon atoms belonging to sublattices A and B are shown in dark grey and light grey, respectively; $h_{A0} = 0.257$ Å, $h_{B1} = -0.047$ Å, $h_{A2} = -0.036$ Å and $d_{C-H} = 1.22$ Å. (Reproduced with permission from Boukhvalov, Katsnelson & Lichtenstein, 2008.)

If the condition

$$\gamma^2 \gg |E_d||t| \tag{6.113}$$

is satisfied, then, at energies close enough to the Dirac point ($|E| \ll |t|$), the potential (6.112) is very strong, and an adatom is effectively equivalent to a vacancy.

To understand this very important point, let us consider the hydrogen atom as an example. It is attached to one of the carbon atoms, transforming locally its state from sp^2 bonded to sp^3 bonded; distortions make the angles between the bonds and bond lengths locally similar to those in diamond (Boukhvalov, Katsnelson & Lichtenstein, 2008), see Fig. 6.3. This means that the carbon atom bonded with hydrogen is almost unavailable for π electrons, since their energies are locally shifted too strongly. This makes it similar to a vacancy. *Ab initio* calculations (Wehling *et al.*, 2010a) show that the local electronic structure for the case of a hydrogen adatom can be quite accurately fitted by the hybridization model with the parameters

$$\gamma \approx 2|t|, \qquad E_d \approx \frac{|t|}{16}, \tag{6.114}$$

so the inequality (6.113) is satisfied with high precision. This means that hydrogen atoms form mid-gap states, which are, however, slightly shifted with respect to the Dirac point, because $E_d < 0$ (Wehling *et al.*, 2010a; Yuan, De Raedt & Katsnelson, 2010a), see Fig. 6.1.

Interestingly, approximately the same parameters (6.114) describe the case of various organic groups, such as CH_3, C_2H_5 and CH_2OH, attached to carbon atoms via the carbon–carbon chemical bond (Wehling *et al.*, 2010a). One can assume that such bonds can be formed in real graphene with organic contaminants, which, therefore, can be responsible for the appearance of strongly ‘resonant’ scatterers (Wehling *et al.*, 2010a; Ni *et al.*, 2010).

The position of the impurity peak corresponds to the pole of the T-matrix,

$$1 = V(E_{\mathrm{imp}})G_{00}^{(0)}(E_{\mathrm{imp}}) \tag{6.115}$$

(see Eq. (6.88)). With the parameters (6.114) we find $E_{\mathrm{imp}} \approx\ \ 0.03\,\mathrm{eV}$, in agreement with the results of straightforward *ab initio* calculations (Wehling, Katsnelson & Lichtenstein, 2009b). For the case of fluorine, F, and the hydroxyl group, OH, the latter parameters give, respectively, $E_{\mathrm{imp}} \approx\ \ 0.67\,\mathrm{eV}$ and $E_{\mathrm{imp}} \approx\ \ 0.70\,\mathrm{eV}$, so these impurities are weaker scatterers than hydrogen or a vacancy (Wehling, Katsnelson & Lichtenstein, 2009b).

Further discussion will be presented in Chapters 11 and 12, in relation to the effects of adatoms on electronic transport in graphene and their magnetic properties, respectively.

6.7 Scanning tunnelling microscopy of point defects on graphene

Scanning tunnelling microscopy (STM) allows us to probe the electronic properties of conducting materials with atomic-scale spatial resolution (Binnig & Rohrer, 1987). Being a local probe, it is especially suitable for studying the electronic structures of various types of defects and defect-induced features, including many-body effects (Li *et al.*, 1998; Madhavan *et al.*, 1998; Balatsky, Vekhter & Zhu, 2006). In particular, it was used to probe locally vacancies in the top (graphene) layer of graphite (Ugeda *et al.*, 2010) and a magnetic adatom (Co) on graphene (Brar *et al.*, 2011). Here we will discuss some general peculiarities of the STM spectra of graphene (Uchoa *et al.*, 2009; Wehling *et al.*, 2010b; Saha, Paul & Sengupta, 2010).

Assuming that the tunnelling between the sample and the STM tip is weak enough one can derive, to lowest order in the tunnelling amplitude M, the following expression for the current voltage ($I\ \ V$) characteristic (Tersoff & Hamann, 1985; Mahan, 1990):

$$I(V) = \frac{\pi e}{h}\sum_{n\nu\sigma}\left|M_{n\nu}^{\sigma}\right|^2\int dE\,N_n^{\sigma}(E)N_{\nu}^{\sigma}(E\quad eV)[f(E\quad eV)\quad f(E)], \tag{6.116}$$

where $f(E)$ is the Fermi distribution function, σ is the spin projection, Greek (Latin) indices label electron eigenstates for the sample (tip) $\psi_{\nu\sigma}$ and $\psi_{n\sigma}$,

$$M_{n\nu}^{\sigma} = \frac{h^2}{2m}\int d\vec{S}\left(\psi_{n\sigma}^{*}\nabla\psi_{\nu\sigma}\quad \psi_{\nu\sigma}\nabla\psi_{n\sigma}^{*}\right) \tag{6.117}$$

is the current-matrix element, m is the free-electron mass and the surface integral in Eq. (6.117) is taken over arbitrary area between the tip and sample. The spectral densities

$$N_{\nu}^{\sigma}(E) = \quad \frac{1}{\pi} \operatorname{Im} G_{\nu}^{\sigma}(E) \tag{6.118}$$

for the sample and a similar quantity $N_{\nu}^{\sigma}(E)$ for the tip determine the intensity of tunnelling. If one neglects the spin polarization, assumes that the spectral density of the tip is a smooth function and uses a semiclassical approximation (Ukraintsev, 1996) one can demonstrate that, at low enough temperatures ($T \ll |eV|$),

$$\frac{dI}{dV} \propto \quad \frac{1}{\pi} \operatorname{Im} G_{ii}(E = eV), \tag{6.119}$$

where i is the site index for the atom of the sample nearest to the tip. This means that, using STM, one can probe the spatial distribution of the electron density around the defect (see Wehling *et al.*, 2007).

Let us assume that the adatom situated at the site $i = 0$ has a resonant state which can be of single-electron or many-body origin (e.g., the Kondo effect). The expression (6.116) and, thus, (6.119) are correct, anyway, assuming that the tunnelling amplitude M is small enough and the lowest-order perturbation theory in M works (Mahan, 1990).

The resonance at $E = E_{\mathrm{d}}$ is manifested in this situation via two contributions, namely, the direct contribution of d electrons to tunnelling and the contribution of c electrons to the tunnelling, via c d hybridization. This leads to the *Fano (anti)resonance effect* (Madhavan *et al.*, 2001). For simplicity, we can assume that d states are more localized than c states and, thus, only the second effect is important. In this situation, we can use Eq. (6.119), assuming that G is the Green function of c electrons. Its change due to the presence of an impurity is determined by Eq. (6.77). On putting $i = 0$ one finds

$$\begin{aligned}\operatorname{Im}\left[G_{00}(E) \quad G_{00}^{(0)}(E)\right] &= \operatorname{Im}\left\{\left[G_{00}^{(0)}(E)\right]^2 T_{00}(E)\right\} \\ &= \left\{\operatorname{Re}\left[G_{00}^{(0)}(E)\right]^2 \quad \operatorname{Im}\left[G_{00}^{(0)}(E)\right]^2\right\} \operatorname{Im} T_{00}(E) \\ &\quad + 2\left\{\operatorname{Im}\left[G_{00}^{(0)}(E)\right] \operatorname{Re}\left[G_{00}^{(0)}(E)\right]\right\} \operatorname{Re} T_{00}(E).\end{aligned} \tag{6.120}$$

In the case of resonance,

$$T_{00}(E) \sim \frac{1}{E \quad E_{\mathrm{d}} + i\Delta}, \tag{6.121}$$

where Δ is the halfwidth of the resonance, thus

$$\mathrm{Im}\ T_{00}(E) \sim \frac{\Delta}{(E - E_{\mathrm{d}})^2 + \Delta^2} \tag{6.122}$$

has a maximum at $E = E_{\mathrm{d}}$ and

$$\mathrm{Re}\ T_{00}(E) \sim \frac{E - E_{\mathrm{d}}}{(E - E_{\mathrm{d}})^2 + \Delta^2} \tag{6.123}$$

changes sign. Assuming that $G_{00}^{(0)}(E)$ is smoothly dependent on the energy at the energy scale $|E - E_{\mathrm{d}}| \approx \Delta$ and substituting Eqs. (6.120)–(6.123) into Eq. (6.119), one finds

$$\frac{dI}{dV} \propto \frac{q^2 - 1 + 2q\varepsilon'}{1 + \varepsilon'^2}, \tag{6.124}$$

where

$$\varepsilon' = \frac{eV - E_{\mathrm{d}}}{\Delta} \tag{6.125}$$

and the quantity

$$q = -\frac{\mathrm{Re}\ G_{00}^{(0)}(E_{\mathrm{d}})}{\mathrm{Im}\ G_{00}^{(0)}(E_{\mathrm{d}})} \tag{6.126}$$

is called the *Fano asymmetry factor* (which should not be confused with the Fano factor (3.17) – the usual problem when a particular scientist made essential contributions to various fields!). If q is large then the *resonance* should be observed, whereas for small q one will observe rather the *antiresonance* (a dip in dI/dV instead of a peak).

For graphene, due to Eqs. (6.92) and (6.96), the Fano factor at $|E| \ll \Delta$,

$$q = \frac{2}{\pi} \ln\left|\frac{\Delta}{E_{\mathrm{d}}}\right|, \tag{6.127}$$

is very large (Wehling *et al.*, 2010b).

For a more detailed analysis, see Uchoa *et al.* (2009), Wehling *et al.* (2010b) and Saha, Paul & Sengupta (2010).

6.8 Long-range interaction between adatoms on graphene

Consider now the *energetics* of point defects and their clusters. On substituting Eq. (6.83) for the change of the total density of states into the expression for the thermodynamic potential of noninteracting fermions, Eq. (2.134), one finds

$$
\begin{aligned}
\Delta\Omega = &\quad \frac{T}{\pi}\,\mathrm{Im\,Tr}\int_{\infty}^{\infty} dE\,\ln\left[1+\exp\left(\frac{\mu \quad E}{T}\right)\right]\frac{\partial}{\partial E}\ln\,\hat{T}(E)\\
&= \frac{1}{\pi}\,\mathrm{Im\,Tr}\int_{\infty}^{\infty} dE\,f(E)\ln\hat{T}(E)\\
&= \frac{1}{\pi}\,\mathrm{Im}\int_{\infty}^{\infty} dE\,f(E)\ln\det\left[1 \quad \hat{G}_0(E)\hat{V}\right]
\end{aligned}
\qquad (6.128)
$$

(see Eq. (6.85)).

This expression can be used, for example, to study the effects of interactions between impurities. Let us assume that

$$V_{ij} = V_1\delta_{i1}\delta_{j1} + V_2\delta_{i2}\delta_{j2}, \qquad (6.129)$$

which means two defects with local potential at sites $i=1$ and $i=2$ (cf. Eq. (6.86)).

Then,

$$\det\left[1 \quad \hat{G}_0 V\right] = \left[1 \quad \hat{G}^{(0)}_{11}V_1\right]\left[1 \quad \hat{G}^{(0)}_{12}V_2\right] \quad V_1\hat{G}^{(0)}_{12}V_2\hat{G}^{(0)}_{21}. \qquad (6.130)$$

To find the interaction energy one needs to substitute Eq. (6.130) into Eq. (6.128) and subtract the same expression with $\hat{G}^{(0)}_{12}=0$ which corresponds to the case of noninteracting defects. As a result, we obtain

$$\Omega_{\mathrm{int}} = \frac{1}{\pi}\,\mathrm{Im}\int_{\infty}^{\infty} dE\,f(E)\ln\left[1 \quad T^{(0)}_{11}(E)G^{(0)}_{12}(E)T^{(0)}_{22}(E)G^{(0)}_{21}(E)\right], \qquad (6.131)$$

where $T^{(0)}_{ii}(E)$ are the single-site T-matrices (6.88). Keeping in mind that the functions $G^{(0)}(E)$ and $T(E)$ are analytic at $\mathrm{Im}\,E>0$ and that the Fermi function has poles at

$$E = \mu + i\varepsilon_n, \qquad (6.132)$$

where

$$\varepsilon_n = \pi T(2n+1),$$

with the residues $\quad T$ and recalling that

$$\mathrm{Im}\,A(E+i0) = \frac{1}{2i}\left[A(E+i0) \quad A(E \quad i0)\right], \qquad (6.133)$$

one can rewrite the expression (6.131) as

$$\Omega_{\text{int}} = -T \sum_{\varepsilon_n} \ln\left[1 - T_{11}^{(0)}(i\varepsilon_n + \mu) G_{12}^{(0)}(i\varepsilon_n + \mu) T_{22}^{(0)}(i\varepsilon_n + \mu) G_{21}^{(0)}(i\varepsilon_n + \mu)\right] \quad (6.134)$$

(Shytov, Abanin & Levitov, 2009). One can use this expression to calculate the interaction energy for two resonant impurities, such as vacancies or hydrogen adatoms, when Eq. (6.99) can be used for the T-matrix.

To calculate the asymptotics of the interaction energy at large distances one can assume that G_{12} is small and take into account only the first term in the Taylor expansion of Eq. (6.134):

$$\Omega_{\text{int}} \approx T \sum_{\varepsilon_n} T_{11}^{(0)}(i\varepsilon_n + \mu) G_{12}^{(0)}(i\varepsilon_n + \mu) T_{22}^{(0)}(i\varepsilon_n + \mu) G_{21}^{(0)}(i\varepsilon_n + \mu). \quad (6.135)$$

Later we will consider the case of undoped graphene ($\mu = 0$).

Using this expression one can prove that the sign of the interaction is different for impurities belonging to the same sublattice and to a different sublattice. In the latter case, there is *attraction* between the impurities, decaying as

$$U_{\text{AB}}(r) \sim \frac{1}{r \ln(r/a)} \quad (6.136)$$

($r \gg a$), whereas for the former case there is *repulsion*,

$$U_{\text{AA}}(r) \sim \frac{1}{r \ln^2(r/a)} \quad (6.137)$$

This means that the resonant impurities would prefer to sit in different sublattices (Shytov, Abanin & Levitov, 2009). This consideration is valid only at large distances. Interestingly, first-principles electronic-structure calculations (Boukhvalov, Katsnelson & Lichtenstein, 2008; Boukhvalov & Katsnelson, 2009a) show that the same happens for the nearest-neighbour, next-nearest-neighbour, etc. distances: the resonant impurities *always* prefer to sit in different sublattices.

7

Optics and response functions

7.1 Light absorption by Dirac fermions: visualization of the fine-structure constant

In this chapter we will discuss electromagnetic properties of graphene related to electron–photon interaction. The discussion of optical properties related to phonons (infrared adsorption, the Raman effect) will be postponed until Chapter 9.

Massless Dirac fermions in two dimensions have an amazing property: their optical response is universal and expressed only in terms of the fine-structure constant

$$\alpha = \frac{e^2}{\hbar c} \approx \frac{1}{137.036} \tag{7.1}$$

(Ando, Zheng & Suzuura, 2002; Gusynin, Sharapov & Carbotte, 2006; Nair *et al.*, 2008). Experiments on light absorption of graphene can, literally, visualize this fundamental constant (Nair *et al.*, 2008). To see this, let us determine the electric field of the light via the vector potential $\vec{A}(t) = \vec{A}\exp(-i\omega t)$,

$$\vec{E}(t) = -\frac{1}{c}\frac{\partial \vec{A}}{\partial t} = \frac{i\omega}{c}\vec{A}. \tag{7.2}$$

This is more convenient for optics than the representation via the scalar potential, $\vec{E} = -\vec{\nabla}\varphi$, but is, of course, equivalent to it due to gauge invariance. Thus, the Hamiltonian of Dirac electrons in the presence of an electric field is (cf. Eqs. (2.20) and (2.24))

$$\hat{H} = v\vec{\sigma}\left(\hat{\vec{p}} - \frac{e}{c}\vec{A}\right) = \hat{H}_0 + \hat{H}_{\text{int}}, \tag{7.3}$$

where

$$\hat{H}_{\text{int}} = -\frac{ve}{2c}\vec{\sigma}\vec{A} = \frac{iev}{2\omega}\vec{\sigma}\vec{E} \tag{7.4}$$

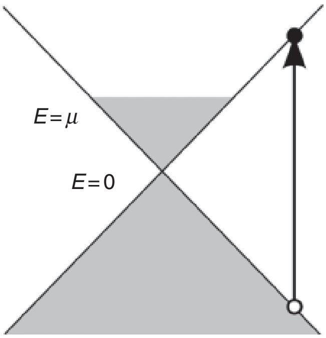

Fig. 7.1. A schematic representation of direct optical transitions in graphene.

is the Hamiltonian of the electron photon interaction. The factor $\frac{1}{2}$ in Eq. (7.4) is necessary since the standard expression for the complex field is

$$\vec{E}(t) = \mathrm{Re}\left[\vec{E}\exp(-i\omega t)\right] = \frac{1}{2}\left[\vec{E}\exp(-i\omega t) + \vec{E}^{*}\exp(i\omega t)\right] \tag{7.5}$$

and we take into account only the first term. This interaction induces transitions from the occupied hole states $\psi_{\mathrm{h}}\left(\vec{k}\right)$ to the empty electron states $\psi_{\mathrm{e}}\left(\vec{k}\right)$ with the same wave vector $\vec{k}$ (see Eq. (1.30)), the intraband transitions being forbidden by the momentum conservation (Fig. 7.1). The matrix element of the Hamiltonian (7.4) is

$$\langle\psi_{\mathrm{h}}|\hat{H}_{\mathrm{int}}|\psi_{\mathrm{e}}\rangle = \frac{ev}{2\omega}\left(E_y\cos\varphi \mp E_x\sin\varphi\right), \tag{7.6}$$

where the $-$ and $+$ signs correspond to K and K′ valleys. It depends only on the polar angle φ of the $\vec{k}$ vector, not on its length. On averaging the square matrix element over φ one finds

$$|M|^2 \equiv \overline{\left|\langle\psi_{\mathrm{h}}|\hat{H}_{\mathrm{int}}|\psi_{\mathrm{e}}\rangle\right|^2} = \frac{e^2v^2}{8\omega^2}\left|\vec{E}\right|^2, \tag{7.7}$$

where we assume that the photon propagates perpendicular to the graphene plane and, thus, the vector $\vec{E} = \left(E_x, E_y, 0\right)$ lies within the plane. The absorption probability per unit time, to the lowest order of perturbation theory, is (Landau & Lifshitz, 1977)

$$P = \frac{2\pi}{\hbar}|M|^2 N\left(\varepsilon = \frac{\hbar\omega}{2}\right), \tag{7.8}$$

where $N(\varepsilon)$ is the density of states (1.72) (we take into account the spin and valley degeneracy) and the energy of the final states is $\hbar\omega/2$ as is obvious from Fig. 7.1. On substituting Eqs. (1.72) and (7.7) into (7.8) we find

$$P = \frac{e^2}{4h^2\omega}\left|\vec{E}\right|^2. \tag{7.9}$$

Thus, the absorption energy per unit time is

$$W_\mathrm{a} = Ph\omega = \frac{e^2}{4h}\left|\vec{E}\right|^2. \tag{7.10}$$

At the same time, the incident energy flux is (Jackson, 1962)

$$W_\mathrm{i} = \frac{c}{4\pi}\left|\vec{E}\right|^2. \tag{7.11}$$

The absorption coefficient is, therefore,

$$\eta = \frac{W_\mathrm{a}}{W_\mathrm{i}} = \frac{\pi e^2}{hc} \approx 2.3\% \tag{7.12}$$

and is universal, assuming that $h\omega > 2|\mu|$. Otherwise, the transitions are forbidden by the Pauli principle (see Fig. 7.1) and $\eta = 0$. For visible light, $h\omega \approx 1 \quad 2\,\mathrm{eV}$ is much higher than the Fermi energy in graphene. Moreover, it is much higher than the energy of electron hopping between layers in multilayer graphene or graphite. Therefore, the absorption for N-layer graphene is just $N\eta$. This behaviour was observed experimentally for single-layer and bilayer graphene (Nair *et al.*, 2008) and for graphite (Kuzmenko *et al.*, 2008). According to Eq. (7.12), graphene is quite transparent. At the same time, one should keep in mind that this is an absorption coefficient of more than 2% *per single atomic layer*, which is a huge value. Thus, the interaction of Dirac electrons with photons is actually very strong.

In the first work (Novoselov *et al.*, 2004) single-layer graphene on $\mathrm{SiO_2}$ was first detected just by the human eye, via a conventional (optical) microscope. It was a lucky coincidence that the contrast due to light absorption in graphene was strongly enhanced by interference phenomena in the $\mathrm{SiO_2}$ layer with appropriate thickness. The optics of the visibility of graphene on a substrate was considered by Blake *et al.* (2007) and Abergel, Russell & Falko (2007).

7.2 The optics of Dirac fermions: the pseudospin precession formalism

The optical properties of Dirac fermions can be studied in a physically transparent way using the equations of motion for the density matrix (Katsnelson, 2008). It has the form (2.173). For the Hamiltonian one can use Eq. (7.3); however, it is more instructive to change the gauge and write

$$\hat{H}_{\text{int}} = \quad e\vec{E}(t)\hat{\vec{r}} = \quad ie\vec{E}(t)\vec{\nabla}_{\vec{k}} \tag{7.13}$$

(see Eq. (2.178)). We will show explicitly that the result (7.12) can be derived within this representation as well. Thus, the equation (2.173) reads

$$ih\frac{\partial\hat{\rho}_{\vec{k}}}{\partial t} = hv\vec{k}\left[\hat{\vec{\sigma}}, \hat{\rho}_{\vec{k}}\right] \quad ie\left(\vec{E}(t)\cdot\vec{\nabla}_{\vec{k}}\right)\hat{\rho}_{\vec{k}}, \tag{7.14}$$

where $\hat{\rho}_{\vec{k}}$ is the 2×2 pseudospin matrix

$$\left(\hat{\rho}_{\vec{k}}\right)_{\alpha\beta} = \left\langle \psi^{+}_{\vec{k}\beta}\psi_{\vec{k}\alpha} \right\rangle \tag{7.15}$$

(cf. Eqs. (2.170) and (3.1)). It can be expanded in Pauli matrices,

$$\hat{\rho}_{\vec{k}} = n_{\vec{k}}\hat{I} + m_{\vec{k}}\hat{\vec{\sigma}}, \tag{7.16}$$

where $\hat{I}$ is the unit 2×2 matrix,

$$n_{\vec{k}} = \frac{1}{2}\,\mathrm{Tr}\,\hat{\rho}_{\vec{k}} \tag{7.17}$$

and

$$\vec{m}_{\vec{k}} = \frac{1}{2}\,\mathrm{Tr}\left(\hat{\vec{\sigma}}\hat{\rho}_{\vec{k}}\right) \tag{7.18}$$

are charge and pseudospin densities (in the $\vec{k}$ representation). On substituting Eq. (7.16) into Eq. (7.14) we find the separated equations for the charge density,

$$\frac{\partial n_{\vec{k}}}{\partial t} = \quad \frac{e}{h}\left(\vec{E}\cdot\vec{\nabla}_{\vec{k}}\right)n_{\vec{k}}, \tag{7.19}$$

and the pseudospin density,

$$\frac{\partial\vec{m}_{\vec{k}}}{\partial t} = 2v\left(\vec{k}\times\vec{m}_{\vec{k}}\right) \quad \frac{e}{h}\left(\vec{E}\cdot\vec{\nabla}_{\vec{k}}\right)\vec{m}_{\vec{k}}. \tag{7.20}$$

To calculate the time-dependent current density

$$\vec{j} = \mathrm{Tr}\left(\hat{\vec{j}}\hat{\rho}\right) = 2ev\sum_{\vec{k}}\vec{m}_{\vec{k}} \tag{7.21}$$

we need only Eq. (7.20). It is rigorous (for noninteracting fermions) and can be used to calculate both linear and nonlinear optical properties. The first term on the right-hand side of Eq. (7.20) is nothing other than precession, with a pseudomagnetic 'field' proportional to $\vec{k}$ acting on the pseudospin degree of freedom. A similar formalism was used by Anderson (1958) as the most physical way to represent the BCS theory of superconductivity.

To calculate the optical conductivity we will use the first-order perturbation in $\vec{E}$, assuming that it has the form $\vec{E}\exp(\quad i\omega t)$, and look for the solution of Eq. (7.20) as

$$\vec{m}_{\vec{k}}(t) = \vec{m}_{\vec{k}}^{(0)} + \delta\vec{m}_{\vec{k}}\exp(\quad i\omega t), \tag{7.22}$$

where

$$\delta\vec{m}_{\vec{k}} \sim \vec{E}.$$

To calculate $\vec{m}_{\vec{k}}^{(0)}$ we use the unitary transformation

$$\begin{aligned} \psi_{\vec{k}1} &= \frac{1}{\sqrt{2}}\left(\xi_{\vec{k}1} + \xi_{\vec{k}2}\right), \\ \psi_{\vec{k}2} &= \frac{\exp\left(i\varphi_{\vec{k}}\right)}{\sqrt{2}}\left(\xi_{\vec{k}1} \quad \xi_{\vec{k}2}\right), \end{aligned} \tag{7.23}$$

diagonalizing the Hamiltonian $\hat{H}_0$,

$$\hat{H}_0 = \sum_{\vec{k}} hvk\left(\xi_{\vec{k}2}^{+}\xi_{\vec{k}2} \quad \xi_{\vec{k}1}^{+}\xi_{\vec{k}1}\right). \tag{7.24}$$

So $\xi_{\vec{k}1}$ and $\xi_{\vec{k}2}$ are annihilation operators for holes and electrons, respectively. At equilibrium,

$$\left\langle \xi_{\vec{k}i}^{+}\xi_{\vec{k}i} \right\rangle = f_{\vec{k}i} \tag{7.25}$$

are Fermi distribution functions depending on the energies $\mp hvk$. We obtain

$$\vec{m}_{\vec{k}}^{(0)} = \frac{\vec{k}}{2k}\left(f_{\vec{k}1} \quad f_{\vec{k}2}\right). \tag{7.26}$$

Equation (7.20) takes the form

$$\omega\,\delta\vec{m}_{\vec{k}} = 2v\left(\vec{k}\times\delta\vec{m}_{\vec{k}}\right) \quad \frac{e}{h}\left(\vec{E}\cdot\vec{\nabla}_{\vec{k}}\right)\vec{m}_{\vec{k}}^{(0)}. \tag{7.27}$$

Since the vector (7.26) lies in the xy-plane the component δm^z is not coupled to the electric field and can be found from Eq. (7.27):

$$\delta m_{\vec{k}}^{z} = \frac{2v}{\omega}\left(k_x\,\delta m_{\vec{k}}^{y} \quad k_y\,\delta m_{\vec{k}}^{x}\right). \tag{7.28}$$

Using Eq. (7.28) to exclude δm^z from the equations for δm^x and δm^y we find

$$\begin{aligned}\left(\omega^2 - 4v^2k_y^2\right)\delta m_{\vec{k}}^x + 4v^2k_xk_y\,\delta m_{\vec{k}}^y &= -\frac{ie\omega}{h}E\frac{\partial m_{\vec{k}}^{x(0)}}{\partial k_x},\\ 4v^2k_xk_y\delta m_{\vec{k}}^x + \left(\omega^2 - 4v^2k_x^2\right)\delta m_{\vec{k}}^y &= -\frac{ie\omega}{h}E\frac{\partial m_{\vec{k}}^{y(0)}}{\partial k_x},\end{aligned} \tag{7.29}$$

where we have chosen the direction of the x-axis along the electric field. By solving Eq. (7.29) and calculating the current along the x-axis as

$$j_x = 2ev\sum_{\vec{k}}\delta m_{\vec{k}}^x = \sigma(\omega)E \tag{7.30}$$

we obtain the following expression for the optical conductivity:

$$\sigma(\omega) = -\frac{8ie^2v^3}{h\omega}\sum_{\vec{k}}\frac{k_y}{\omega^2 - 4v^2k^2}\left(k_y\frac{\partial m_{\vec{k}}^{x(0)}}{\partial k_x} - k_x\frac{\partial m_{\vec{k}}^{y(0)}}{\partial k_x}\right). \tag{7.31}$$

On substituting Eq. (7.26) into Eq. (7.31) we find

$$\begin{aligned}\sigma(\omega) &= -\frac{4ie^2v^3}{h\omega}\sum_{\vec{k}}\frac{k_y^2}{\omega^2 - 4v^2k^2}\frac{1}{k}\left(f_{\vec{k}1} - f_{\vec{k}2}\right)\\ &= -\frac{2ie^2v^3}{h\omega}\sum_{\vec{k}}\frac{k\left(f_{\vec{k}1} - f_{\vec{k}2}\right)}{\omega^2 - 4v^2k^2}.\end{aligned} \tag{7.32}$$

As is usual in calculations of response functions, one should make the replacements $\omega \to \omega + i\delta$ in Eq. (7.32) and $\delta \to +0$ at the end of the calculations (Zubarev, 1974).

To calculate Re $\sigma(\omega)$, one needs to make the replacement

$$\begin{aligned}\frac{1}{\omega^2 - 4v^2k^2} \to \operatorname{Im}\frac{1}{(\omega + i\delta)^2 - 4v^2k^2} &= -\pi i\delta\left(\omega^2 - 4v^2k^2\right)\\ &= -\frac{\pi i\delta(\omega - 2vk)}{4vk}.\end{aligned} \tag{7.33}$$

So,

$$\begin{aligned}\operatorname{Re}\sigma(\omega) &= \frac{\pi e^2v^2}{2h\omega}\sum_{\vec{k}}\left(f_{\vec{k}1} - f_{\vec{k}2}\right)\delta(\omega - 2vk)\\ &= \frac{e^2}{16h}\left[f\left(\varepsilon = -\frac{h\omega}{2}\right) - f\left(\varepsilon = \frac{h\omega}{2}\right)\right].\end{aligned} \tag{7.34}$$

This is the conductivity per valley per spin. On multiplying the result by 4 and setting the temperature to zero one has

$$\operatorname{Re}\sigma(\omega) = \begin{cases} 0, & \omega < 2|\mu|, \\ \dfrac{e^2}{4h}, & \omega > 2|\mu|. \end{cases} \tag{7.35}$$

This expression corresponds exactly to the absorption coefficient (7.12).

It is important to stress that the universal optical conductivity

$$\sigma_0 = \frac{e^2}{4h} = \frac{\pi e^2}{2h} \tag{7.36}$$

is of the order of, but not equal to, the static ballistic conductivity

$$\sigma_{\mathrm{B}} = \frac{4e^2}{\pi h} \tag{7.37}$$

(see Eq. (3.18)). This is not surprising since we saw in Chapter 3 that limits $\omega \to 0$, $\mu \to 0$, $T \to 0$, etc. do not necessarily commute with one another, as different ways to regularize the ill-posed expression (3.10).

The imaginary part of the conductivity can be restored from Eq. (7.35) via the Kramers Kronig relations. The result is (see, e.g., Stauber, Peres & Geim, 2008)

$$\operatorname{Im}\sigma(\omega) = \frac{\sigma_0}{\pi}\left(\frac{4\mu}{h\omega} \quad \ln\left|\frac{h\omega + 2\mu}{h\omega \quad 2\mu}\right|\right). \tag{7.38}$$

At $\mu \to 0$, Im $\sigma(\omega) \to 0$ for any frequency.

7.3 The absence of many-body corrections to the universal optical conductivity

Experimental data obtained by Nair *et al.* (2008) agree, to within a few per cent, with the theoretical value (7.12) (or, equivalently, (7.35)), which is, actually, a problem. As we will see below, the electron electron interaction in graphene is not small, and earlier considerations (Herbut, Juričić & Vafek, 2008; Fritz *et al.*, 2008) predicted a rather strong renormalization of the optical conductivity, of the order of $1/\ln|t/(h\omega)|$. Here we present, following Katsnelson (2008), some arguments based on the phenomenological Fermi-liquid theory stating that, actually, many-body corrections to $\sigma(\omega)$ for Dirac fermions are absent. This seems to be confirmed by the following first-principles GW (G is the Green function and W is the dynamically screened interaction) calculations (Yang *et al.*, 2009) and a more detailed many-body analysis (Mishchenko, 2008; Sheehy & Schmalian, 2009; de Juan, Grushin & Vozmediano, 2010). Later, the absence of correlation corrections to the optical conductivity of electrons on the honeycomb lattice was proved rigorously for the case of a weak enough, short-range inter-electron interaction (Giuliani, Mastropietro & Porta, 2011).

The equation of motion for the density matrix can be naturally modified to the kinetic equation for quasiparticles within the framework of Landau Fermi-liquid theory (Landau, 1956; Platzman & Wolf, 1973; Vonsovsky & Katsnelson, 1989). Assuming

$$\hat{\rho} = \hat{\rho}^{(0)} + \delta\hat{\rho}\exp(-i\omega t) \tag{7.39}$$

(cf. Eq. (7.22)), one can write, instead of Eq. (7.14),

$$h\omega\,\delta\hat{\rho}_{\vec{k}} = hv\vec{k}\left[\hat{\vec{\sigma}}, \delta\hat{\rho}_{\vec{k}}\right] - ie\left(\vec{E}\cdot\vec{\nabla}_{\vec{k}}\right)\hat{\rho}^{(0)}_{\vec{k}} + \left[\delta\hat{H}_{\vec{k}}, \hat{\rho}^{(0)}_{\vec{k}}\right], \tag{7.40}$$

where the last term contains the change of the Hamiltonian $\delta\hat{H}$ due to the change of the density matrix. In the spirit of Landau theory it is due to the interaction between quasiparticles characterized by some matrix $\hat{F}$:

$$\delta\hat{H}_{\vec{k}} = \sum_{\vec{k}'}\hat{F}_{\vec{k}\vec{k}'}\,\delta\hat{\rho}_{\vec{k}'}. \tag{7.41}$$

Equation (7.41) generalizes the standard Landau theory to the case of a *matrix* distribution function for the quasiparticles.

The (pseudo)spinor structure of the matrix $\hat{F}$ can be found by invoking symmetry considerations. First, it should be rotationally invariant in the two-dimensional space. Second, as was discussed in Chapter 1 (see Eq. (1.42)), the Hamiltonian $\delta\hat{H}$ and, thus, the matrix $\hat{F}$ cannot contain the $\hat{\sigma}_z$ matrix (this follows from the inversion and time-reversal symmetries). Third, it should vanish at $\vec{k}, \vec{k}' \to 0$, together with $\hat{H}_0\left(\vec{k}\right)$. The most general expression satisfying these requirements is

$$\begin{aligned}\hat{F}_{\vec{k}\vec{k}'} = {} & A\left(\left|\vec{k}-\vec{k}'\right|\right)I\otimes I' + B\left(\left|\vec{k}-\vec{k}'\right|\right)\left(\vec{k}\cdot\hat{\vec{\sigma}}\right)\otimes\left(\vec{k}'\cdot\hat{\vec{\sigma}}'\right) \\ & + C\left(\left|\vec{k}-\vec{k}'\right|\right)(\vec{k}\cdot\vec{k}')(\hat{\sigma}_x\otimes\hat{\sigma}'_x + \hat{\sigma}_y\otimes\hat{\sigma}'_y).\end{aligned} \tag{7.42}$$

The long-range Coulomb (Hartree) interaction singular at $\left|\vec{k}-\vec{k}'\right| \to 0$ (see Chapter 8) contributes to the function A only, whereas the functions B and C are supposed to be smooth and tend to become constants as $\left|\vec{k}-\vec{k}'\right| \to 0$.

By substituting Eqs. (7.41) and (7.42) into Eq. (7.40) we derive, instead of Eq. (7.29),

$$\begin{aligned}
\omega^2\,\delta m^x_{\vec{k}} - 4v^2k_y^2\,\delta\tilde{m}^x_{\vec{k}} + 4v^2k_xk_y\,\delta\tilde{m}^y_{\vec{k}} &= -\frac{ie\omega}{h}E\frac{\partial m^{x(0)}_{\vec{k}}}{\partial k_x},\\
4v^2k_xk_y\,\delta\tilde{m}^x_{\vec{k}} + \omega^2\,\delta m^y_{\vec{k}} - 4v^2k_x^2\,\delta\tilde{m}^y_{\vec{k}} &= -\frac{ie\omega}{h}E\frac{\partial m^{y(0)}_{\vec{k}}}{\partial k_x},
\end{aligned} \tag{7.43}$$

where $\delta\vec{\tilde{m}} = \delta\vec{m} + \vec{\Delta}$, and the term

$$\vec{\Delta}_{\vec{k}} = \frac{1}{vk}\sum_{\vec{k}'}\left[B_{\vec{k}\vec{k}'}\vec{k}\left(\vec{k}'\delta\vec{m}_{\vec{k}'}\right) + C_{\vec{k}\vec{k}'}\left(\vec{k}\cdot\vec{k}'\right)\delta\vec{m}_{\vec{k}'}\right] \tag{7.44}$$

contains all correlation effects. Also, we have an additional correlation contribution to the current density,

$$j_x^{\text{corr}} = \frac{\delta\hat{H}_{\vec{k}}}{\delta k_x} = \sum_{\vec{k}}\frac{\delta\hat{F}_{\vec{k}\vec{k}'}}{\delta k_x}\,\delta\hat{\rho}_{\vec{k}'}, \tag{7.45}$$

which can, after some straightforward manipulations, be rewritten as

$$j_x^{\text{corr}} = 8e^2v^3\sum_{\vec{k}}\frac{k_y}{\omega^2 - 4\omega^2k^2}\left(k_y\Delta^x_{\vec{k}} - k_x\Delta^y_{\vec{k}}\right). \tag{7.46}$$

The remaining work is just direct analysis of the corrections term by term, which shows that they all vanish by symmetry after the integration over $\vec{k}$ and $\vec{k}'$ (Katsnelson, 2008).

7.4 The magneto-optics of Dirac fermions

Consider now the case of Dirac fermions in a magnetic field. Instead of momentum $\vec{k}$ the eigenstates of the unperturbed problem, $|n\rangle$, are characterized by the Landau band index n and the coordinate of the Landau orbit x_0 (see Section 2.2). This does not lead to any difficulties since the optical conductivity, as well as any response functions, can easily be written in an arbitrary basis. The general formalism has already been presented in Section 2.9 (see Eq. (2.175) and below). We will use the Hamiltonian (2.177) with the electric field (7.5) and calculate the induced electric current, $\frac{1}{2}\left[\vec{j}\exp(i\omega t) + \vec{j}^*\exp(-i\omega t)\right]$, assuming that

$$\vec{j} = \hat{\sigma}(\omega)\vec{E} \tag{7.47}$$

(in this section, $\vec{j}$ is the *electric* current operator).

Then, using Eqs. (2.176) and (2.177), we find

$$\sigma_{\alpha\beta}(\omega) = e\sum_{mn}\frac{f_m - f_n}{E_n - E_m - h(\omega + i\delta)}\langle n|j_\alpha|m\rangle\langle m|r_\beta|n\rangle. \tag{7.48}$$

We will consider here only the case of finite ω, thus, the term with $m = n$ does not contribute to Eq. (7.48). Keeping in mind Eq. (2.179), we find

$$\langle m|j_\alpha|n\rangle = \frac{ie}{h}\langle m|r_\alpha|n\rangle(E_m - E_n). \tag{7.49}$$

On substituting Eq. (7.49) into Eq. (7.48), taking into account that

$$\frac{1}{E_n - E_m - h(\omega + i\delta)}\frac{1}{E_m - E_n} = -\frac{1}{h\omega}\left(\frac{1}{E_n - E_m - h(\omega + i\delta)} - \frac{1}{E_m - E_n}\right), \tag{7.50}$$

we obtain

$$\sigma_{\alpha\beta}(\omega) = \frac{i}{\omega}\left[\Pi_{\alpha\beta}(\omega) - \Pi_{\alpha\beta}(0)\right], \tag{7.51}$$

where

$$\Pi_{\alpha\beta}(\omega) = \sum_{mn}\frac{f_m - f_n}{E_n - E_m - h(\omega + i\delta)}\langle n|j_\alpha|m\rangle\langle m|j_\beta|n\rangle. \tag{7.52}$$

In particular, for the quantity Re $\sigma_{xx}(\omega)$ determining the absorption of electromagnetic waves we have

$$\text{Re }\sigma_{xx}(\omega) = \frac{\pi}{\omega}\sum_{mn}(f_m - f_n)|\langle n|j_x|m\rangle|^2\delta(E_n - E_m - h\omega). \tag{7.53}$$

For the Dirac electrons $j_x = e\sigma_x$. Without a magnetic field this gives us immediately the result (7.34). In the presence of a magnetic field, we have to use as the basis functions m and n the solutions of the Landau problem (2.45) and (2.46). They are dependent on the Landau indices and on k_y (see Eqs. (2.40) and (2.41)). Obviously, the matrix elements $\langle n|\sigma_x|m\rangle$ are diagonal in k_y. Since the functions $D_n(X)$ are orthogonal, one can see immediately that the allowed transitions are $n \rightarrow n \pm 1$ and $n \rightarrow -(n \pm 1)$ only and, thus, the expression (7.53) describes absorption peaks at

$$h\omega = |E_n| \pm |E_{n+1}|, \tag{7.54}$$

or at $\omega = \omega_c\left(\sqrt{p} + 1 \pm \sqrt{p}\right)$, where $p = 0, 1, 2, \ldots$ The complete expression can be found in Gusynin, Sharapov & Carbotte (2007a, 2009).

This absorption has been observed experimentally (Sadowski *et al.*, 2006; Jiang *et al.*, 2007a; Witowski *et al.*, 2010). The results are in agreement with Eq. (7.54). This effect can be used as an alternative method by which to measure the Fermi velocity v in graphene.

Another interesting magneto-optical effect is the polarization rotation of propagating light in the magnetic field, that is, the Faraday effect (Landau & Lifshitz, 1984). The rotation angle is proportional to $\mathrm{Re}\,\sigma_{xy}$, which has absorption peaks at the same frequencies (7.54) as $\mathrm{Re}\,\sigma_{xx}$ (for the theory of the Faraday effect in graphene, see Fialkovsky & Vassilevich, 2009). Near the resonances, the rotation is very large, as was observed experimentally by Crassee *et al.* (2011). This giant Faraday effect is potentially interesting for applications.

7.5 Optical properties of graphene beyond the Dirac approximation

Consider now the theory of optical conductivity for a honeycomb lattice, beyond the Dirac cone approximation, so that it can be used at $h\omega \geq |t|$ as well (Gusynin, Sharapov & Carbotte, 2007b; Stauber, Peres & Geim, 2008). We will start with the expression (2.20) for the Hamiltonian of band electrons in the presence of a vector potential; in the single-band approximation it works also for the time-dependent vector potential $\vec{A}(t)$.

In particular, in the nearest-neighbour approximation the Hamiltonian has the form

$$\hat{H}\left(\vec{k}\right) = \begin{pmatrix} 0 & tS\left(\vec{k} \quad \frac{e\vec{A}}{hc}\right) \\ tS^{*}\left(\vec{k} \quad \frac{e\vec{A}}{hc}\right) & 0 \end{pmatrix} \tag{7.55}$$

(cf. Eqs. (1.14) and (1.15)). To calculate the linear response, we need to expand the right-hand side of Eq. (7.55) up to *second* order in $\vec{A}$. Indeed, the electric current operator

$$\hat{\vec{j}} = c\frac{\delta \hat{H}}{\delta \vec{A}} \tag{7.56}$$

has paramagnetic (p) and diamagnetic (d) components,

$$\hat{j}_\alpha = \hat{j}_\alpha^{(\mathrm{p})} + \hat{j}_\alpha^{(\mathrm{d})}, \tag{7.57}$$

where

$$\hat{\vec{j}}_{\alpha}^{(\mathrm{p})} = c\left(\frac{\delta \hat{H}}{\delta \vec{A}_{\alpha}}\right)_{\vec{A}\quad 0} \tag{7.58}$$

and

$$\hat{\vec{j}}_{\alpha}^{(\mathrm{d})} = \frac{1}{2}c^{2}\sum_{\beta}\left(\frac{\delta^{2}\hat{H}}{\delta \vec{A}_{\alpha}\,\delta \vec{A}_{\beta}}\right)_{\vec{A}\quad 0} A_{\beta}. \tag{7.59}$$

When calculating the average current density to linear order in $\vec{A}$,

$$j_{\alpha} = \mathrm{Tr}\left(\hat{j}_{\alpha}^{(\mathrm{p})}\hat{\rho}'\right) + \mathrm{Tr}\left(\hat{j}_{\alpha}^{(\mathrm{d})}\hat{\rho}_{0}\right), \tag{7.60}$$

both terms contribute to the conductivity. Further calculations are quite straightforward (Gusynin, Sharapov & Carbotte, 2007b; Stauber, Peres & Geim, 2008). We will present here the expressions for $\mathrm{Re}\,\sigma_{xx}(\omega) = \mathrm{Re}\,\sigma(\omega)$ only:

$$\begin{aligned}\mathrm{Re}\ \sigma(\omega) = D\delta(\omega) + \frac{\pi t^{2}e^{2}a^{2}}{8h^{3}\omega A_{0}}\sum_{\vec{k}}F\left(\vec{k}\right)\left(f_{\vec{k}1}\quad f_{\vec{k}2}\right)\\ \times\left[\delta\left(\omega\quad \varepsilon\left(\vec{k}\right)\right)\quad \delta\left(\omega + \varepsilon\left(\vec{k}\right)\right)\right],\end{aligned} \tag{7.61}$$

where the first term originates from $j^{(\mathrm{d})}$, the Drude weight is

$$D = \quad \frac{e^{2}a^{2}}{3h^{2}A_{0}}\sum_{\vec{k}}\varepsilon\left(\vec{k}\right)\left(f_{\vec{k}1}\quad f_{\vec{k}2}\right), \tag{7.62}$$

$\varepsilon\left(\vec{k}\right) = t\left|S\left(\vec{k}\right)\right|$ $(t > 0)$, $f_{\vec{k}1,2}$ are given by Eq. (7.25), $A_{0} = 3\sqrt{3}a^{2}/2$ is the area

of the unit cell and

$$F\left(\vec{k}\right) = 18\quad 4\left|S\left(\vec{k}\right)\right|^{2} + 18\frac{\left[\mathrm{Re}\ S\left(\vec{k}\right)\right]^{2}\quad \left[\mathrm{Im}\ S\left(\vec{k}\right)\right]^{2}}{\left|S\left(\vec{k}\right)\right|^{2}}. \tag{7.63}$$

The optical conductivity (7.61) at $\omega \neq 0$ is proportional to the density of states

$$N(E) = \sum_{\vec{k}}\delta\left(|E|\quad \varepsilon\left(\vec{k}\right)\right) \tag{7.64}$$

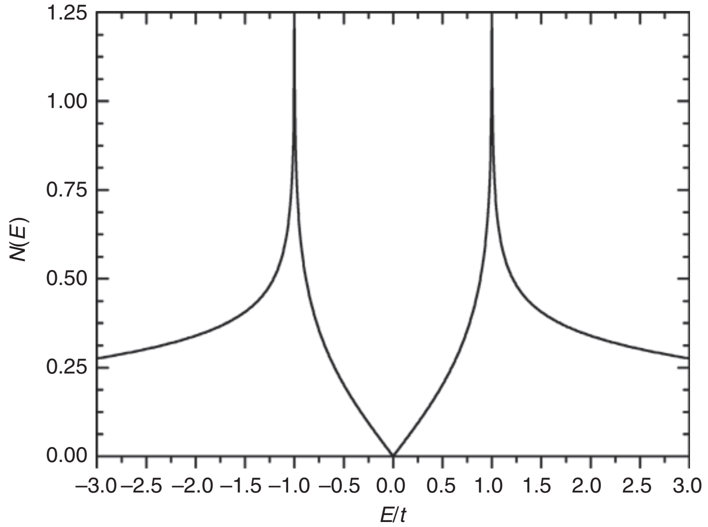

Fig. 7.2. The density of states (7.66). The logarithmic divergences at $E = \pm t$ are Van Hove singularities.

(it differs by a factor of 2 from Eq. (1.70)). It can be analytically expressed (Hobson & Nierenberg, 1953) in terms of the elliptic integral

$$K(m) = \int_0^{\pi/2} \frac{d\varphi}{\sqrt{1 - m\sin^2\varphi}}, \tag{7.65}$$

namely

$$N(|E|) = \frac{2|E|}{\pi^2 t^2} \begin{cases} \dfrac{1}{\sqrt{\varphi(|E|/t)}} K\left(\dfrac{4|E|/t}{\varphi(|E|/t)}\right), & 0 < |E| < t, \\ \dfrac{1}{\sqrt{4|E|/t}} K\left(\dfrac{\varphi(|E|/t)}{4|E|/t}\right), & t < |E| < 3t, \end{cases} \tag{7.66}$$

where

$$\varphi(x) = (1 + x)^2 - \frac{\left(x^2 - 1\right)^2}{4}. \tag{7.67}$$

This function is shown in Fig. 7.2. It has logarithmic divergences at $E = \pm t$ corresponding to Van Hove singularities in the electron density of states.

At $0 < \hbar\omega < t$ the optical conductivity (7.61) coincides with Eq. (7.35). The corrections are (Stauber, Peres & Geim, 2008)

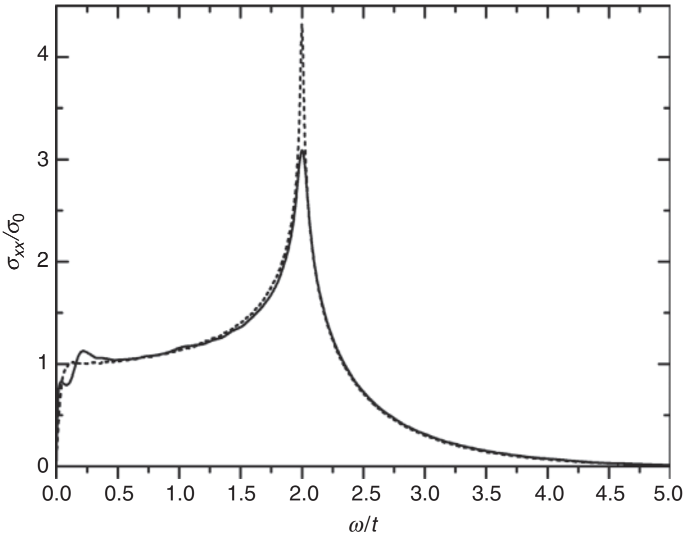

Fig. 7.3. The frequency dependence of Re $\sigma_{xx}(\omega)$ for an ideal honeycomb lattice in the nearest-neighbour approximation (dashed line) and for one with 1% of vacancies, randomly distributed (solid line); σ_0 is given by Eq. (7.36). (Reproduced with permission from Yuan, De Raedt & Katsnelson, 2010a.)

$$\sigma(\omega) \approx \frac{\sigma_0}{2}\left(\tanh\left(\frac{\hbar\omega + 2\mu}{4T}\right) + \tanh\left(\frac{\hbar\omega - 2\mu}{4T}\right)\right)\left[1 + \frac{(\hbar\omega)^2}{36t^2}\right]. \tag{7.68}$$

The curve for the whole interval is shown in Fig. 7.3 (Yuan, De Raedt & Katsnelson, 2010a). One can see a singularity at $\hbar\omega = 2t$; however, a moderate disorder (such as 1% of vacancies or resonant impurities) smears it essentially.

For the case of bilayer graphene we have a Van Hove singularity at low energy, due to trigonal warping and the merging of four Dirac ones to give one paraboloid (see Section 1.4). Also, the gap can be made to open in that case by applying a bias between the layers. Experimentally, these effects on the infrared optics of bilayer graphene have been studied by Kuzmenko *et al.* (2009).

7.6 The dielectric function of Dirac fermions

Now we will consider the response function for an *inhomogeneous* external perturbation,

$$V_{\mathrm{ext}}(\vec{r}, t) = \sum_{\vec{k}} \Psi^{+}_{\vec{k}} \hat{V}^{\mathrm{ext}}_{\vec{q}} \Psi_{\vec{k}+\vec{q}} \exp(i\vec{q}\vec{r} - i\omega t), \tag{7.69}$$

where $\Psi^{+}_{\vec{k}} = (\psi^{+}_{\vec{k}1}, \psi^{+}_{\vec{k}2})$ is the spinor creation operator, $\hat{V}^{\text{ext}}_{\vec{q}}$ is a generic 2×2 matrix and $\vec{q}$ is the wave vector of the inhomogeneity. We need to pass to electron- and hole-creation operators (7.23). The result is

$$\Psi^{+}_{\vec{k}} \hat{V}^{\text{ext}}_{\vec{q}} \Psi_{\vec{k}+\vec{q}} = \Xi^{+}_{\vec{k}} \hat{U}_{\vec{q}} \Xi_{\vec{k}+\vec{q}}, \tag{7.70}$$

where $\Xi^{+}_{\vec{k}} = \left(\xi^{+}_{\vec{k}1}, \xi^{+}_{\vec{k},2}\right)$ and

$$\hat{U}_{\vec{q}} = \frac{1}{2} \begin{pmatrix} 1 & \exp\left(\ \ i\varphi_{\vec{k}+\vec{q}}\right) \\ 1 & \exp\left(\ \ i\varphi_{\vec{k}+\vec{q}}\right) \end{pmatrix} \hat{V}^{\text{ext}}_{\vec{q}} \begin{pmatrix} 1 & 1 \\ \exp\left(i\varphi_{\vec{k}}\right) & \exp\left(i\varphi_{\vec{k}}\right) \end{pmatrix}. \tag{7.71}$$

Then, the perturbation of the density matrix (2.175) is the operator $\hat{\rho}' \exp(i\vec{q}\vec{r}\ \ \ i\omega t)$ with the matrix elements (in the ξ representation)

$$\hat{\rho}'_{\vec{k}+\vec{q},i,\vec{k},j} = \frac{f_{\vec{k},j}\ \ \ f_{\vec{k}+\vec{q},i}}{E_{\vec{k},j}\ \ \ E_{\vec{k}+\vec{q},i}\ \ \ h(\omega + i\delta)} \left(\hat{U}_{\vec{q}}\right)_{ij} \tag{7.72}$$

and the perturbation of the operator

$$\hat{J} = \sum_{\vec{k}\vec{q}} \Psi^{+}_{\vec{k}} \hat{J}_{\vec{q}} \Psi_{\vec{k}+\overleftarrow{q}} \equiv \sum_{\vec{k}\vec{q}} \Xi^{+}_{\vec{k}} \hat{\hat{J}}_{\vec{q}} \Psi_{\vec{k}+\vec{q}} \tag{7.73}$$

is

$$\delta J_{\vec{q}} = \operatorname{Tr}\left(\hat{J}\hat{\rho}'\right) = \sum_{\vec{k}} \frac{f_{\vec{k},j}\ \ \ f_{\vec{k}+\vec{q},i}}{E_{\vec{k},j}\ \ \ E_{\vec{k}+\vec{q},i}\ \ \ h(\omega + i\delta)} \left(\hat{U}_{\vec{q}}\right)_{ij} \left(\hat{\hat{J}}_{\vec{q}}\right)_{ji}. \tag{7.74}$$

Consider first the case of a scalar potential and the density operator $\hat{J} = \hat{n}$; in that case both $\hat{V}^{\text{ext}}_{\vec{q}}$ and $\hat{J}_{\vec{q}}$ are proportional to the unit matrix. We obtain

$$\delta n_{\vec{q}\omega} = \ \ \ \Pi(\vec{q}, \omega) \hat{V}^{\text{ext}}_{\vec{q}\omega}, \tag{7.75}$$

where

$$\Pi(\vec{q}, \omega) = g_{\text{s}} g_{\text{v}} \sum_{\vec{k}} \sum_{s,s'\ \ \ \pm} \lambda_{ss'}\left(\vec{k}, \vec{q}\right) \frac{f\left[sE\left(\vec{k}\right)\right]\ \ \ f\left[s'E\left(\vec{k}+\vec{q}\right)\right]}{s'E\left(\vec{k}+\vec{q}\right)\ \ \ sE\left(\vec{k}\right) + h(\omega + i\delta)} \tag{7.76}$$

is the *polarization operator*, $E\left(\vec{k}\right) = hvk$,

$$\lambda_{ss'}\left(\vec{k}, \vec{q}\right) = \frac{1}{2}\left(1 + ss'\frac{k + q\cos\varphi}{\left|\vec{k}+\vec{q}\right|}\right), \tag{7.77}$$

φ is the angle between $\vec{k}$ and $\vec{q}$ and the factors $g_s = 2$ and $g_v = 2$ take into account spin and valley degeneracy (Ando, 2006; Wunsch *et al.*, 2006; Hwang & Das Sarma, 2007).

Perturbation of the electron density will induce perturbation of the potential,

$$V_{\vec{q}\omega}^{\text{ind}} = v_C(q)\delta n_{\vec{q}\omega}, \tag{7.78}$$

where

$$v_C(q) = \frac{2\pi e^2}{q\varepsilon_{\text{ext}}} \tag{7.79}$$

is the Fourier component of the Coulomb interaction

$$v_C(r) = \frac{e^2}{r\varepsilon_{\text{ext}}} \tag{7.80}$$

in two dimensions and ε_{ext} is the external dielectric constant (e.g., due to screening by a substrate). The total potential perturbation is

$$V_{\vec{q}\omega} = V_{\vec{q}\omega}^{\text{ext}} + V_{\vec{q}\omega}^{\text{ind}} = \frac{V_{\vec{q}\omega}^{\text{ext}}}{\varepsilon(\vec{q},\omega)}. \tag{7.81}$$

The last equality in Eq. (7.81) defines the *dielectric function* $\varepsilon(\vec{q},\omega)$. Within the *random-phase approximation* (RPA) it is assumed that, for a system of *interacting* fermions, the induced density has formally the same expression as for the *non*interacting fermions, (7.75) and (7.76), but with the replacement $V^{\text{ext}} \to V$ in Eq. (7.75). This means that the interaction effects are taken into account via a self-consistent mean field (Vonsovsky & Katsnelson, 1989). As a result,

$$\varepsilon(\vec{q},\omega) = 1 + v_C(q)\Pi(q,\omega). \tag{7.82}$$

If we take into account also the external screening the total dielectric function is

$$\varepsilon_{\text{tot}}(q,\omega) = \varepsilon_{\text{ext}}\varepsilon(q,\omega) = \varepsilon_{\text{ext}} + \frac{2\pi e^2}{q}\Pi(q,\omega). \tag{7.83}$$

In the case when graphene lies between two subspaces with dielectric constants ε_1 and ε_2, one has (Landau & Lifshitz, 1984)

$$\varepsilon_{\text{ext}} = \frac{\varepsilon_1 + \varepsilon_2}{2}. \tag{7.84}$$

For the two most popular substrates, SiO_2 and BN, $\varepsilon_2 \approx 4$, so, assuming $\varepsilon_1 = 1$ (vacuum, or air), one has $\varepsilon_{\text{ext}} \approx 2.5$.

Consider first the case of undoped graphene ($\mu = 0$) at zero temperature. Then, only interband transitions ($s = +$ and $s' = \quad$ or vice versa) contribute to Eq. (7.76) and

$$\Pi_0(q,\omega) = \frac{g_s g_v}{h}\sum_{\vec{k}}\left(1 \quad \frac{(k + q\cos\varphi)}{\left|\vec{k}+\vec{q}\right|}\right)\frac{v\left(k + \left|\vec{k}+\vec{q}\right|\right)}{v^2\left(k + \left|\vec{k}+\vec{q}\right|\right)^2 \quad (\omega + i\delta)^2}. \tag{7.85}$$

As the next step, we calculate $\operatorname{Im}\Pi_0\,(q,\,\omega)$. It contains $\delta\left[v\left(k + \left|\vec{k}+\vec{q}\right| \quad \omega\right)\right]$, which allows us to calculate the integral (first, in ω and then in k) in a quite elementary manner. The result is

$$\operatorname{Im}\Pi_0(q,\omega) = \frac{g_s g_v}{16h}\frac{q^2}{\sqrt{\omega^2 \quad v^2q^2}}\theta(\omega \quad vq), \tag{7.86}$$

where $\theta(x > 0) = 1$, $\theta(x < 0) = 0$ is the step function. Noticing that the analytic function $1/\sqrt{z + i\delta}$ is purely imaginary at real $z < 0$ and purely real at real $z > 0$, one can do analytic continuation immediately, thus having

$$\operatorname{Re}\Pi_0(q,\omega) = \frac{g_s g_v}{h}\frac{q^2}{\sqrt{v^2q^2 \quad \omega^2}}\theta(vq \quad \omega). \tag{7.87}$$

On combining Eqs. (7.86) and (7.87) we have a very simple answer:

$$\Pi_0(q,\omega) = \frac{g_s g_v}{16h}\frac{q^2}{\sqrt{v^2q^2 \quad (\omega + i\delta)^2}}. \tag{7.88}$$

(Gonzáles, Guinea & Vozmediano, 1999).

At $\omega = 0$, $\Pi_0(q,\,\omega) \sim q$ and the dielectric function $\varepsilon(q)$ is actually not dependent on q:

$$\varepsilon = \varepsilon_{\text{ext}} + \frac{\pi e^2}{2hv}. \tag{7.89}$$

For graphene,

$$\alpha = \frac{e^2}{hv} \approx 2.2 \tag{7.90}$$

and the second term on the right-hand side of Eq. (7.89) is about 3.5.

Within the RPA, this result is exact, and high-energy states cannot change the value of $\varepsilon(q = 0)$. Indeed, for arbitrary band structure with the Bloch states $\left|m\vec{k}\right\rangle$, one has (Vonsovsky & Katsnelson, 1989)

$$\Pi(\vec{q},\omega = 0) = 2\sum_{mn}\sum_{\vec{k}}\frac{f_{n,\vec{k}} \quad f_{m,\vec{k}+\vec{q}}}{E_{m,\vec{k}+\vec{q}} \quad E_{n,\vec{k}}}\left|\left\langle n,\vec{k}\middle|m,\vec{k}+\vec{q}\right\rangle\right|^2 \tag{7.91}$$

(the factor of 2 is due to spin degeneracy).

Let us exclude the Dirac point, considering the case when (at $T = 0$) we have completely occupied and completely empty bands and some gap in between. Then Eq. (7.91) can be rewritten as

$$\Pi(\vec{q}, \omega = 0) = 4 \sum_{n}^{\text{occ}} \sum_{m}^{\text{empty}} \frac{1}{E_{m,\vec{k}+\vec{q}} \quad E_{n,\vec{k}}} \left| \left\langle n, \vec{k} \middle| m, \vec{k} + \vec{q} \right\rangle \right|^2, \tag{7.92}$$

which is obviously proportional to q^2 at $q \to 0$. More explicitly, on writing

$$\left| m, \vec{k} + \vec{q} \right\rangle \approx \left(1 + \vec{q}\, \vec{\nabla}_{\vec{k}} \right) \left| m, \vec{k} \right\rangle \tag{7.93}$$

and using Eq. (2.85) one finds for $\vec{q} \to 0$

$$\Pi(\vec{q}, \omega = 0) = \sum_{\alpha\beta} C_{\alpha\beta} q_\alpha q_\beta, \tag{7.94}$$

where

$$C_{\alpha\beta} = 4 \sum_{n}^{\text{occ}} \sum_{m}^{\text{empty}} \frac{1}{\left(E_{m,\vec{k}} \quad E_{n,\vec{k}} \right)^3} \left\langle m, \vec{k} \middle| \frac{\partial \hat{H}}{\partial k_\alpha} \middle| n, \vec{k} \right\rangle \left\langle n, \vec{k} \middle| \frac{\partial \hat{H}}{\partial k_\beta} \middle| m, \vec{k} \right\rangle \tag{7.95}$$

is some finite tensor. Since $v_c(q) \sim 1/q$ we have, in two dimensions, $\varepsilon(q \to 0, \omega = 0) = 1$ for any gapped state. This means that only the region close to the Dirac point contributes to this quantity. Note that first-principles *GW* calculations do indeed give results quite similar to those obtained by use of Eq. (7.89) (Schilfgaarde & Katsnelson, 2011).

Consider now the case of doped graphene (to be specific, we put $\mu > 0$, i.e., the case of electron doping). The calculations are quite cumbersome but straightforward. The result is (Wunsch *et al.*, 2006; Hwang & Das Sarma, 2007)

$$\Pi(q, \omega) = \Pi_0(q, \omega) + \Pi_1(q, \omega),$$

with

$$\begin{aligned} \Pi_1(q, \omega) = {} & \frac{g_s g_v \mu}{2\pi h^2 v^2} - \frac{g_s g_v q^2}{16\pi h \sqrt{\omega^2 - v^2 q^2}} \\ & \times \left\{ G\left(\frac{h\omega + 2\mu}{hvq} \right) - \theta\left(\frac{2\mu - h\omega}{hvq} - 1 \right) \left[G\left(\frac{2\mu - h\omega}{hvq} \right) - i\pi \right] \right. \\ & \left. - \theta\left(\frac{h\omega - 2\mu}{hvq} + 1 \right) G\left(\frac{h\omega - 2\mu}{hvq} \right) \right\}, \end{aligned} \tag{7.96}$$

where

$$G(x) = x\sqrt{x^2 - 1} - \ln\left(x + \sqrt{x^2 - 1}\right). \tag{7.97}$$

For generalization of this expression to the case of gapped graphene, see Pyatkovskiy (2009).

Now we will consider different partial cases of this general expression. Keeping in mind the case of graphene, we will put $g_s = g_v = 2$.

7.7 Static screening

We start with the case $\omega = 0$. The result is (Gorbar *et al.*, 2002; Ando, 2006; Wunsch *et al.*, 2006; Hwang & Das Sarma, 2007)

$$\Pi(q,0) = \frac{2k_F}{\pi h v} \times \begin{cases} 1, & q < 2k_F, \\ 1 - \frac{1}{2}\sqrt{1 - \left(\frac{2k_F}{q}\right)^2} + \frac{q}{4k_F}\cos^{-1}\left(\frac{2k_F}{q}\right), & q > 2k_F. \end{cases} \tag{7.98}$$

Interestingly, at $q < 2k_F$, $\Pi(q,0) = \text{constant}$, due to cancellation of the q dependence in the (formally) μ-dependent contribution

$$\Pi_+(q,0) = \frac{2k_F}{\pi h v}\left(1 - \frac{\pi q}{8k_F}\right) \tag{7.99}$$

and the contribution for the undoped case (see Eq. (7.88)),

$$\Pi_0(q,0) = \frac{q}{4hv}. \tag{7.100}$$

It is instructive to compare Eq. (7.98) with that for a conventional, nonrelativistic two-dimensional electron gas (Stern, 1967):

$$\Pi(q,0) = N(E_F) \times \begin{cases} 1, & q < 2k_F, \\ 1 - \sqrt{1 - \left(\frac{2k_F}{q}\right)^2}, & q > 2k_F. \end{cases} \tag{7.101}$$

In both cases, the polarization operator is constant at $q < 2k_F$. At the same time, the behaviour at $q > 2k_F$ is essentially different. For the nonrelativistic case $\Pi(q, \omega)$ decays with increasing q, as $1/q^2$ at $q \to \infty$, whereas for the case of massless Dirac fermions $\Pi(q, 0)$ *increases* linearly with increasing q, due to the contribution (7.100). The behaviour of expressions (7.98) and (7.101) at $q \to 2k_F$ is also essentially different. Whereas for the nonrelativistic electron gas $\delta\Pi(q,0) \sim \sqrt{q - 2k_F}$, with a divergent derivative, for the case of graphene the singularity is weaker, $\delta\Pi(q, 0) \sim (q - 2k_F)^{3/2}$.

The result for small q corresponds to the *Thomas–Fermi approximation* (Nomura & MacDonald, 2006; Katsnelson, 2006c). The latter (Lieb, 1981) assumes that the perturbation $V(\vec{r})$ is smooth enough that its effect on the electron density

$$n(\mu) = \int_0^\mu dE\, N(E) \tag{7.102}$$

can be taken into account just by making the replacement $n(\mu) \to n[\mu - V(\vec{r})]$. This means that the potential just shifts locally the maximum band energy $E_F(\vec{r})$, such that

$$E_F(\vec{r}) + V(\vec{r}) = \mu. \tag{7.103}$$

The self-consistent equation for the total potential, which is similar to Eq. (7.81), reads

$$V(\vec{r}) = V_{\text{ext}}(\vec{r}) + \frac{e^2}{\varepsilon_{\text{ext}}} \int d\vec{r}\,' \frac{n_{\text{int}}(\vec{r}\,')}{|\vec{r} - \vec{r}\,'|}, \tag{7.104}$$

where

$$n_{\text{int}}(\vec{r}) = n[\mu - V(\vec{r})] - n(\mu) \tag{7.105}$$

is the induced change of the electron density. Assuming that the perturbation V is small, one can expand (7.105) as follows:

$$n_{\text{int}}(\vec{r}) \approx -\frac{\partial n}{\partial \mu} V(\vec{r}) = -N(E_F) V(\vec{r}), \tag{7.106}$$

where the last identity assumes $T = 0$ (cf. Eq. (2.138)).

On Fourier-transforming Eq. (7.104) and comparing the result with Eq. (7.81) one finds

$$\varepsilon(q, 0) = \varepsilon_{\text{ext}} + \frac{2\pi e^2 N(E_F)}{q} = \varepsilon_{\text{ext}} \left(1 + \frac{\kappa}{q}\right), \tag{7.107}$$

where

$$\kappa = \frac{4e^2 |\mu|}{\varepsilon_{\text{ext}} h^2 v^2} \tag{7.108}$$

is the *inverse Thomas–Fermi screening radius*. This result coincides exactly with Eqs. (7.98) and (7.101) at $q < 2k_F$. Thus, for a two-dimensional electron gas, the nonrelativistic and ultrarelativistic versions of Thomas–Fermi theory both give exactly the same result as does the RPA for static screening with $q < 2k_F$. For a three-dimensional electron gas the situation is different (Vonsovsky & Katsnelson, 1989).

Consider now the real-space effects of static screening. If the external potential $V^{\text{ext}}(r)$ is radially symmetric, with the Fourier component V_q^{ext} depending only on the modulus q, the expression for the total potential is

$$V(r) = \int \frac{d\vec{q}}{(2\pi)^2} \exp(i\vec{q}\vec{r}) \frac{V_q^{\text{ext}}}{\varepsilon(q,0)} = \int_0^\infty \frac{dq\, q}{2\pi} J_0(qr) \frac{V_q^{\text{ext}}}{\varepsilon(q,0)}. \tag{7.109}$$

At $r \to \infty$, there are two important contributions to the integral (7.109), from the region of small q (to compensate for large r in the argument of the Bessel function) and from the region $q = 2k_F$, where $\varepsilon(q, 0)$ has a singularity in $\Pi(q, \omega)$ (7.98). In the three-dimensional case the first contribution decays exponentially at $r \to \infty$, whereas the second oscillates and decays as $\cos(2k_F r)/r^3$, being what is called a Friedel oscillation (Vonsovsky & Katsnelson, 1989). In the two-dimensional case, the situation is different since the Thomas Fermi (small-q) contribution decays also as $1/r^3$ (Katsnelson, 2006c; Wunsch *et al.*, 2006). As a result, the asymptotics of the induced density around the point defect is (Wunsch *et al.*, 2006)

$$n_{\text{ind}}(r) \sim \frac{\alpha + \beta \cos(2k_F r)}{r^3}, \tag{7.110}$$

with some parameters α and β dependent on k_F and on the potential.

In a nonrelativistic electron gas in two dimensions, $n_{\text{ind}}(r) \sim \cos(2k_F r)/r^2$ since the singularity in $\Pi(q, \omega)$ at $q \to 2k_F$ is stronger. In graphene, the Thomas Fermi and Friedel contributions to the induced density around point defects are comparable at $r \to \infty$.

The first-principles GW results for the dielectric function $\varepsilon(q, 0)$ of graphene (Schilfgaarde & Katsnelson, 2011) show that the Dirac approximation works for $q \leq 0.05\,\text{Å}\ \ ^{1}$; at $q \approx 0.1\,\text{Å}\ \ ^{1}$ the polarization operator approximately halves in comparison with the value (7.100).

7.8 Plasmons

Let us consider now the opposite limiting case,

$$\omega \gg vq. \tag{7.111}$$

The polarization operator (7.96) in the limit of small q takes the form

$$\Pi(q \to 0, \omega) = \frac{q^2}{2\pi h\omega} \left[\frac{i\pi}{2} \theta(h\omega \quad 2\mu) \quad \frac{2\mu}{h\omega} + \frac{1}{2} \ln \left| \frac{h\omega + 2\mu}{h\omega \quad 2\mu} \right| \right]. \tag{7.112}$$

At $h\omega > 2\mu$ it has an imaginary part that is at least comparable to the real part, so the equation

$$\varepsilon(q, \omega) = 0 \tag{7.113}$$

which determines the spectrum of plasma oscillations (Platzman & Wolf, 1973; Vonsovsky & Katsnelson, 1989) has no real solutions. In the opposite limit

$$h\omega \ll 2\mu \tag{7.114}$$

one has

$$\Pi(q \to 0, \omega) \approx \frac{\mu q^2}{\pi (h\omega)^2} \tag{7.115}$$

and the solution of Eq. (7.113) is

$$\omega = \sqrt{\frac{2e^2\mu}{h^3 \varepsilon_{\text{ext}}}} q. \tag{7.116}$$

At $q \to 0$, the expression (7.116) obviously satisfies the condition (7.114).

The existence of the low-frequency plasmon mode with the dispersion $\omega \sim \sqrt{q}$ is a general property of a two-dimensional electron gas (Ando, Fowler & Stern, 1982). However, the dependence of the plasmon dispersion relation on the electron density n is different: for graphene, due to Eq. (7.116), $\omega \sim n^{1/4} q^{1/2}$, whereas for the nonrelativistic case $\omega \sim n^{1/2} q^{1/2}$.

Outside the region $qv < \omega < 2\mu$ $\Pi(q, \omega)$ has a large imaginary part and the plasmon is essentially damped. This is a partial case of Landau damping due to a decay into incoherent electron hole excitations (Vonsovsky & Katsnelson, 1989). It was argued, however, by Gangadharaiah, Farid & Mishchenko (2008) that higher-order correlation effects, beyond the RPA, can change the situation, leading to a well-defined plasmon mode with $\omega < qv$, even at $\mu = 0$.

Beyond the Dirac approximation, there are two important physical mechanisms that can lead to additional plasmon modes. First, there is Coulomb interaction between electrons from different valleys, resulting in the appearance of intervalley plasmons, with a linear dispersion law $\omega \sim q$ (Tudorovskiy & Mikhailov, 2010). Second, there is a Van Hove singularity in the optical conductivity at $\omega = 2t$ (see Section 7.5), because of which high-energy ‘optical’ plasmons arise (Stauber, Schliemann & Peres, 2010; Hill, Mikhailov & Ziegler, 2009; Yuan, Roldán & Katsnelson, 2011).

7.9 Transverse response functions and diamagnetic susceptibility

Similarly to the previous sections, one can consider the response of electrons in graphene to a vector potential (Principi, Polini & Vignale, 2009). One needs just to choose $\hat{V}_q^{\text{ext}} = \hat{\vec{\sigma}}$ in Eq. (7.70). In general, instead of the polarization operator (7.76) we introduce a set of response functions

$$\Pi_{\alpha\beta}(\vec{q},\omega) = g_s g_v \sum_{\vec{k}} \sum_{s,s'=\pm} \lambda_{ss'}^{\alpha\beta}\left(\vec{k},\vec{q}\right) \frac{f\left[sE\left(\vec{k}\right)\right] - f\left[s'E\left(\vec{k}+\vec{q}\right)\right]}{s'E\left(\vec{k}+\vec{q}\right) - sE\left(\vec{k}\right) + h(\omega + i\delta)}, \quad (7.117)$$

where

$$\lambda_{ss'}^{\alpha\beta}\left(\vec{k},\vec{q}\right) = \left\langle \psi_s\left(\vec{k}\right)\middle|\sigma_\alpha\middle|\psi_{s'}\left(\vec{k}+\vec{q}\right)\right\rangle\left\langle \psi_{s'}\left(\vec{k}+\vec{q}\right)\middle|\sigma_\beta\middle|\psi_s\left(\vec{k}\right)\right\rangle, \quad (7.118)$$

in which $\psi_s\left(\vec{k}\right)$ are electron and hole wave functions (1.30). The density density response function is, in this notation, Π_{00}, where $\sigma_0 = I$. For example,

$$\lambda_{ss'}^{xx}\left(\vec{k},\vec{q}\right) = \frac{1 + ss' \cos\left(\varphi_{\vec{k}} + \varphi_{\vec{k}+\vec{q}}\right)}{2}. \quad (7.119)$$

For the response function determining the current in the x-direction induced by the vector potential in the x-direction ($\hat{j}_x = v\hat{\sigma}_x$)

$$j_{\vec{q}\omega}^x = \frac{e^2 v^2}{c} \Pi_{xx}(\vec{q},\omega) A_{\vec{q},\omega}^x. \quad (7.120)$$

When calculating this quantity we are faced with an important problem showing that sometimes one needs to be very careful when using the Dirac approximation. Let us put $\omega = 0$ and express the vector potential in terms of an external magnetic field $\vec{B} = \vec{\nabla} \times \vec{A} = (0, 0, B(x,y))$:

$$B_{\vec{q}} = \frac{i}{q_y} A_q^x. \quad (7.121)$$

Phenomenologically, the magnetic field induces a magnetization $\vec{M} = (0, 0, M(x,y))$ proportional to the magnetic field

$$M_{\vec{q}} = \chi(\vec{q}) B_{\vec{q}} \quad (7.122)$$

and the current

$$\vec{j} = c\,\vec{\nabla} \times \vec{M} \quad (7.123)$$

(Jackson, 1962; Landau & Lifshitz, 1984), or, equivalently,

$$j_{\vec{q}}^x = icq_y M_{\vec{q}}. \quad (7.124)$$

On substituting Eqs. (7.121) (7.123) into Eq. (7.120) one finds

$$\Pi_{xx}(\vec{q}) = \frac{q_y^2 c^2}{v^2 e^2} \chi(\vec{q}) \quad (7.125)$$

and, obviously, $\Pi_{xx}(\vec{q}=0)=0$. Physically, this means that, due to the gauge invariance, a *constant* vector potential cannot induce any physical response.

However, on substituting Eq. (7.119) into Eq. (7.117) we have, even at $\mu=0$, a divergent integral over $\left|\vec{k}\right|$. On introducing by hand a cut-off $\left|\vec{k}\right| \le k_{\max}$ we find the result (Principi, Polini & Vignale, 2009)

$$\Pi_{xx}(\vec{q}) = \quad g_s g_v \frac{k_{\max}}{4\pi h v}, \tag{7.126}$$

which is finite and, moreover, tends to infinity at $k_{\max} \to \infty$. This is a pathological property of our model, reflecting the fact that by introducing the cut-off we break the gauge invariance $\vec{k} \to \vec{k} \quad e\vec{A}/(hc)$. The contribution (7.126) should be just subtracted from the answer.

By calculating $\Pi_{xx}(q_y, 0)$ at small q_y and using Eq. (7.125) we find the magnetic susceptibility describing the effect of the magnetic field on the orbital motion of electrons:

$$\chi = \quad \frac{g_s g_v}{24\pi} \frac{e^2 v^2}{c^2} \frac{1}{T\cosh^2[\mu/(2T)]} = \quad \frac{g_s g_v}{6\pi} \frac{e^2 v^2}{c^2} \delta(\mu), \tag{7.127}$$

where the last equality assumes the limit $T \to 0$. This expression was first obtained by McClure (1956) by differentiation of the thermodynamic potential (2.134) with respect to the magnetic field (see also Sharma, Johnson & McClure, 1974; Safran & DiSalvo, 1979; Koshino & Ando, 2007, 2010).

The result (7.127) is really unusual. It means that at zero temperature and finite doping the orbital susceptibility of graphene within the Dirac model should be zero! Usually, the contribution of the orbital motion of electrons to the magnetic susceptibility is diamagnetic (Landau Peierls diamagnetism), but here we have an exact cancellation of intraband and interband contributions; for a general discussion of these contributions, see Wilson (1965). In multilayer graphene and graphite, there is no cancellation but, rather, a strong diamagnetism (Sharma, Johnson & McClure, 1974; Koshino & Ando, 2010).

As a result, the orbital magnetism of electrons in single-layer doped graphene is completely determined by electron electron interactions (Principi *et al.*, 2010). Using perturbation theory one can find that the resulting effect is paramagnetic ($\chi > 0$), with

$$\chi = g_s g_v \frac{e^2 v^2}{c^2} \frac{e^2}{h v \varepsilon_{\text{ext}}} \frac{\Lambda}{E_F}, \tag{7.128}$$

where Λ is a function of the interaction constant, of the order of $10\ ^{2}$ (Principi *et al.*, 2010).

Other nontrivial manifestations of the electron electron interactions will be considered in the next chapter.

8

The Coulomb problem

8.1 Scattering of Dirac fermions by point charges

Now we come back to the problem of scattering of Dirac electrons by a radially symmetric potential $V(r)$ considered in Section 6.1. The case of a Coulomb potential

$$V(r) = -\frac{Ze^2}{\varepsilon_{\text{ext}} r} \equiv -\frac{hv\beta}{r} \tag{8.1}$$

deserves a special consideration for reasons that will be clarified in this chapter. Here ε_{ext} is the dielectric constant due to substrate and other external factors and

$$\beta = \frac{Ze^2}{\varepsilon_{\text{ext}} hv} \tag{8.2}$$

is the dimensionless interaction strength (the sign is chosen such that positive β corresponds to attraction). This problem has been considered for the case of two-dimensional massless Dirac equations by Shytov, Katsnelson & Levitov (2007a, 2007b), Pereira, Nilsson & Castro Neto (2007) and Novikov (2007). Here we will follow the works by Shytov, Katsnelson and Levitov.

Instead of using the general expression (5.19) it is convenient to try the solution of the Coulomb problem in the form

$$\Psi(r,\varphi) = \begin{pmatrix} w_+(r) + w_-(r) \\ [w_+(r) - w_-(r)]\exp(i\varphi) \end{pmatrix} r^{s-1/2} \exp\left[i\left(m - \frac{1}{2}\right)\varphi\right] \exp(ikr), \tag{8.3}$$

where m is half-integer,

$$m = \pm\frac{1}{2}, \pm\frac{3}{2}, \ldots \tag{8.4}$$

and the parameters k and s should be found from the behaviour of solutions at large and small r, respectively. For the potential (8.1), we find

$$s = \sqrt{m^2 - \beta^2}, \qquad k = -\frac{E}{\hbar v}, \tag{8.5}$$

where E is the energy. On substituting Eqs. (8.1) and (8.3) into the Dirac equation (6.1) we find, instead of Eq. (6.2),

$$\begin{aligned} r\frac{dw_+}{dr} + (s - i\beta + 2ikr)w_+ - mw_- &= 0, \\ r\frac{dw_-}{dr} + (s + i\beta)w_- - mw_+ &= 0. \end{aligned} \tag{8.6}$$

Note that s can be either real (if $|m| > |\beta|$) or imaginary (if $|m| < |\beta|$); the behaviours of solutions in these two cases are essentially different, as will be discussed later.

Using the second of Eqs. (8.6) one can express w_+ in terms of w_- and substitute it into the first equation. Then, after introducing a new independent variable

$$z = -2ikr, \tag{8.7}$$

one has a confluent hypergeometric equation, or Kummer's equation (Abramowitz & Stegun, 1964)

$$z\frac{d^2w_-}{dz^2} + (c - z)\frac{dw_-}{dz} - aw_- = 0, \tag{8.8}$$

where

$$c = 2s + 1, \qquad a = s + i\beta. \tag{8.9}$$

Its general solution has the form

$$w_-(z) = A\,{}_1F_1(a, c; z) + Bz^{1-c}\,{}_1F_1(a - c + 1, 2 - c; z), \tag{8.10}$$

where A and B are arbitrary constants and

$${}_1F_1(a, c; z) = \frac{\Gamma(c)}{\Gamma(a)} \sum_{n=0}^{\infty} \frac{\Gamma(a+n)}{\Gamma(c+n)} \frac{z^n}{n!} \tag{8.11}$$

is the confluent hypergeometric function (${}_1F_1(a, c; 0) = 1$).

We will start with the case of real s, that is, $|m| > |\beta|$. Then, only the first term in Eq. (8.10) is regular at $r = 0$ and is therefore allowed, thus

$$w_-(z) = A\,{}_1F_1(s + i\beta, 2s + 1; z). \tag{8.12}$$

Using the identity

$$z\frac{d}{dz}\,{}_1F_1(a,c;z) = a[{}_1F_1(a+1,c;z) - {}_1F_1(a,c;z)] \tag{8.13}$$

one finds from Eq. (8.6)

$$w_+(z) = A\frac{s+i\beta}{m}\,{}_1F_1(s+1+i\beta, 2s+1; z). \tag{8.14}$$

Equations (8.12) and (8.14) give us a formal solution of our problem. Using the asymptotic expression (Abramowitz & Stegun, 1964)

$${}_1F_1(a,c;z) \approx \frac{\Gamma(c)}{\Gamma(c-a)}(-z)^{-a} + \frac{\Gamma(c)}{\Gamma(a)}\exp(z)z^{a-c} \tag{8.15}$$

for $|z| \gg 1$, one finds for $kr \gg 1$

$$\begin{aligned} w_-(r) &= \frac{\lambda\exp[-i\beta\ln(2kr)]}{(2kr)^s}, \\ w_+(r) &= \frac{\lambda^*\exp[i\beta\ln(2kr)]\exp(-2ikr)}{(2kr)^s}, \end{aligned} \tag{8.16}$$

where λ is a constant dependent on m and β but not on k. It follows from Eqs. (8.16) that w_- and w_+ represent scattered and incident waves, respectively (we have to recall our definition of k (8.5); E is assumed to be positive). Their ratio gives us the scattering phases $\delta_m(k)$ (cf. Eq. (6.11)):

$$\begin{aligned} \frac{w_-(r)}{w_+(r)} &= \exp[2i\delta_m(k) + 2ikr], \\ \delta_m(k) &= -\beta\ln(2kr) + \arg\lambda. \end{aligned} \tag{8.17}$$

The logarithmic dependence in Eq. (8.17) is typical for the phases coming from the $1/r$ Coulomb tail of the potential (Landau & Lifshitz, 1977). Since this contribution does not depend on m it does not affect the angular dependence of the scattering current, giving just an irrelevant factor $|\exp[-i\beta\ \ln(2kr)]|^2 = 1$. The relevant scattering phases are arg λ. Its explicit dependence on m and β is not important for us; it suffices to know that they are k-independent. From the general expression for the transport cross-section (6.26) one can see immediately that for the Coulomb scattering

$$\sigma_{\text{tr}} \sim \frac{1}{k}, \tag{8.18}$$

which gives us for the contribution of Coulomb impurities to the resistivity (cf. Section 6.2)

$$\rho \approx \frac{h}{e^2}\frac{n_{\mathrm{imp}}}{n}. \tag{8.19}$$

This contribution is much larger (by a factor of $(n_{\mathrm{imp}}R^2)^{-1}$) than that of short-range scatterers (Eq. (6.36)) and corresponds, at least qualitatively, to the experimentally observed V-shape of the dependence of the conductivity on the electron concentration (Novoselov *et al.*, 2005a). It is not surprising therefore that charge impurities were suggested initially to be the main factor limiting electron mobility in graphene (Nomura & MacDonald, 2006; Ando, 2006; Adam *et al.*, 2007). The real situation is probably much more complicated and will be discussed in Chapter 11. It is clear, anyway, that long-range scattering potentials deserve special attention in the case of graphene. However, screening effects are important and should be taken into account, as will be discussed later.

Consider now the case $|\beta| > |m|$ where $s = i\gamma$,

$$\gamma = \sqrt{\beta^2 - m^2}. \tag{8.20}$$

Then both terms in Eq. (8.10) are formally allowed:

$$w_-(z) = A\,{}_1F_1(i(\gamma+\beta),\ 1+2i\gamma; z) + Bz^{-2i\gamma}\,{}_1F_1(i(\beta-\gamma),\ 1-2i\gamma; z). \tag{8.21}$$

This means that the Dirac equation with the potential (8.1) for large enough $|\beta|$ is ill-defined. To find a solution, one needs to add some boundary conditions at small but finite r.

For $|kr| \ll 1$,

$$w_-(z) \approx A + B\exp(-\pi\gamma)\exp[-2i\gamma\ln(2kr)]. \tag{8.22}$$

The solution $w_+(z)$ corresponding to Eq. (8.21) is

$$\begin{aligned} w_+(z) = {} & iA\frac{\gamma+\beta}{m}\,{}_1F_1(1+i\gamma+i\beta,\ 1+2i\gamma; z) \\ & + iB\frac{\beta-\gamma}{m}z^{-2i\gamma}\,{}_1F_1(1+i\beta-i\gamma,\ 1+2i\gamma; z). \end{aligned} \tag{8.23}$$

Its asymptotics at $|kr| \ll 1$ is

$$w_+(z) \approx iA\frac{\gamma+\beta}{m} + iB\frac{\beta-\gamma}{m}\exp(-\pi\gamma)\exp[-2i\gamma\ \ln(2kr)]. \tag{8.24}$$

To be specific, let us use 'zigzag' boundary conditions $\psi_2(r) = 0$ at some cut-off radius $r = r_0$, which means (see Eq. (8.3))

$$w_-(r_0) = w_+(r_0). \tag{8.25}$$

By substituting Eqs. (8.22) and (8.24) into Eq. (8.25) one can find the ratio B/A and then use it to find the ratio $w_-(r)/w_+(r)$ at $|kr| \gg 1$ and the scattering phases (see Eq. (8.17)). The result is (Shytov, Katsnelson & Levitov, 2007b)

$$\exp[2i\delta_m(k)] = \exp[\pi i|m|]\frac{z + \exp[2i\chi(k)]}{1 + z^* \exp[2i\chi(k)]}, \tag{8.26}$$

where

$$z = \frac{\exp(\pi\gamma)}{\eta}\frac{\Gamma(1+2i\gamma)}{\Gamma(1-2i\gamma)}\frac{\Gamma(1-i\gamma+i\beta)}{\Gamma(1+i\gamma+i\beta)} \tag{8.27}$$

and

$$\chi(k) = \gamma\ln(2kr_0) + \arctan\left(\frac{1+\eta}{1-\eta}\right), \tag{8.28}$$

with

$$\eta = \sqrt{\frac{\beta-\gamma}{\beta+\gamma}}. \tag{8.29}$$

The factor $\exp[2i\chi(k)]$ oscillates rapidly at $kr_0 \ll 1$. This conclusion does not depend on a specific choice of the boundary condition (8.25); for a generic boundary condition the first (logarithmic) term in Eq. (8.28) will be the same.

The expressions (8.26)–(8.29) have a very interesting property: they describe the existence of *quasilocalized states* (Shytov, Katsnelson & Levitov, 2007b). For *localized* states the wave function is described by a single real exponent, $\exp(-\kappa r)$ $(\kappa > 0)$, at $r \to \infty$, which means the absence of a scattering wave. Considering $\delta_m(k)$ as a function of the complex variable k and taking into account the condition (8.17), one can write the equation for the bound state as

$$\exp[2i\delta_m(k)] = 0 \tag{8.30}$$

for $k < 0$ and

$$\exp[-2i\delta_m(k)] = 0 \tag{8.31}$$

for $k > 0$. To be specific, let us consider the first case, $E < 0$. Then, Eq. (8.30) is equivalent to

$$\exp[2i\chi(k)] = -z, \tag{8.32}$$

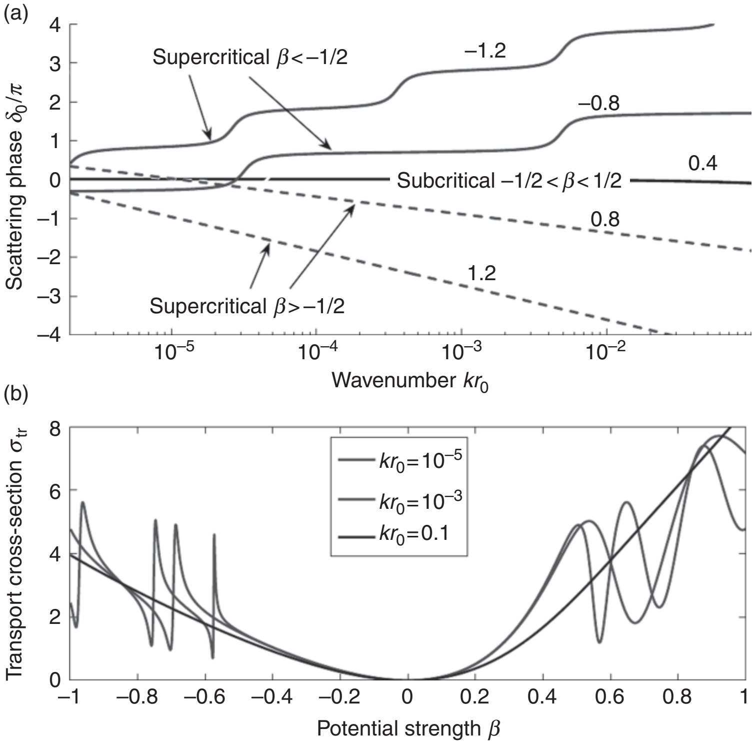

Fig. 8.1. (a) The scattering phase for $m=\frac{1}{2}$ at negative energy $E=-h\nu k<0$. The kinks correspond to quasilocalized states trapped by the impurity potential for supercritical β. (b) The transport cross-section as a function of the potential strength; the quasilocalized states are seen as Fano resonances. (Reproduced with permission from Shytov, Katsnelson & Levitov, 2007b.)

which, taking into account Eq. (8.28), reads

$$\ln(2k_n r_0) = \quad \frac{i}{2\gamma}\ln z \quad \frac{1}{2\gamma}\ln\arctan\left(\frac{1+\eta}{1 \quad \eta}\right) \quad \frac{\pi n}{\gamma}, \tag{8.33}$$

where n is an integer. For small γ, that is, near the threshold $|\beta|\cong|m|$, Eq. (8.33) describes the series of quasilocalized states corresponding to positive n (for negative n, $kr_0\gg 1$, which contradicts our choice of the parameter r_0 as a small cut-off). The k values have an imaginary part, due the term $[i/(2\gamma)]\ln|z|$ in Eq. (8.33). Keeping in mind that

$$\ln|\Gamma(1+i\beta)| = \frac{1}{2}\ln[\Gamma(1+i\beta)\Gamma(1 \quad i\beta)] = \frac{1}{2}\ln\left(\frac{\pi\beta}{\sinh(\pi\beta)}\right), \tag{8.34}$$

one finds

$$k_n = c\exp\left[\quad \frac{\pi n}{\gamma} \quad i\lambda\right], \tag{8.35}$$

where

$$\lambda = \frac{\pi}{1 - \exp(-2\pi\beta)} \tag{8.36}$$

and the prefactor c is of the order of r_0^{-1}. The corresponding energies $E_n = -hvk_n$ have an imaginary part, due to the factor λ; however, it is small:

$$\frac{\operatorname{Im} E_n}{\operatorname{Re} E_n} = \frac{\pi}{\exp(2\pi\beta) - 1}. \tag{8.37}$$

The minimal value of β corresponds to $|\beta| = \frac{1}{2}$, and the right-hand side of Eq. (8.37) is about 0.14. This means that the imaginary part is relatively small and the resonances are narrow. The resonances correspond to jumps in the scattering phases and sharp anomalies in the transport scattering cross-section (6.26). The corresponding numerical data are shown in Fig. 8.1 (Shytov, Katsnelson & Levitov, 2007b). One can see typical Fano resonances (see Section 6.7), as one would expect for quasilocalized states within a continuum spectrum.

8.2 Relativistic collapse for supercritical charges

Our consideration up to now has been rather formal. To understand the physical meaning of the quasilocalized states considered in the previous section we will use a simple semiclassical consideration (Shytov, Katsnelson & Levitov, 2007b; Shytov *et al.*, 2009). It turns out that these states are related to the phenomenon of *relativistic collapse*, or fall of electrons into the centre for superheavy nuclei (Pomeranchuk & Smorodinsky, 1945). This provides us with a new interesting connection between the physics of graphene and high-energy physics.

To gain some insight into the problem let us start with a hand-waving derivation of the size of atoms using the Heisenberg uncertainty principle. If an electron is confined within a spatial region of radius R its typical momentum is of the order of

$$p \approx \frac{h}{R}. \tag{8.38}$$

For nonrelativistic particles with mass m, the kinetic energy is $p^2/(2m)$, and the total energy of the electron, taking into account its attraction to the nucleus, can be estimated as

$$E(R) \approx \frac{h^2}{2mR^2} - \frac{Ze^2}{R} \tag{8.39}$$

with a minimum at

$$R_0 = \frac{h^2}{mZe^2} \tag{8.40}$$

which is nothing other than the Bohr radius. For a relativistic particle we have, instead of Eq. (8.39),

$$E(R) \approx \sqrt{\left(\frac{hc}{R}\right)^2 + (mc^2)^2} \quad \frac{Ze^2}{R}. \tag{8.41}$$

The minimum condition

$$\left(\frac{\partial E}{\partial R}\right)_{R \quad R_0} = 0$$

gives us the equation

$$1 + \left(\frac{mcR_0}{h}\right)^2 = \left(\frac{hc}{Ze^2}\right)^2, \tag{8.42}$$

which has a solution only for

$$Z < Z_c = \frac{hc}{e^2} = \frac{1}{\alpha} \approx 137. \tag{8.43}$$

For $Z > Z_c$, the energy (8.41) decays monotonically with R, decreasing from $E_\infty = mc^2$ at $R \to \infty$ to $E = \quad \infty$ at $R = 0$. This means that the electron falls into the centre.

Speaking more formally, the Dirac equation for a point charge $Z > Z_c$ is ill-defined and has no unique solutions, without introducing some additional boundary conditions at small R, similarly to what we did in the previous section. The wave function has infinitely many oscillations at $r \to 0$ (cf. Eqs. (8.22) and (8.24)), and some of the solutions for the energies (Berestetskii, Lifshitz & Pitaevskii, 1971; Bjorken & Drell, 1964)

$$E_{n,j} = \frac{mc^2}{\sqrt{1 + \frac{(Z\alpha)^2}{\left(n \quad |j| + \sqrt{j^2 \quad (Z\alpha)^2}\right)^2}}} \tag{8.44}$$

($n = 0, 1, 2, \ldots, j = \pm 1, \pm 2, \ldots$) become non-real, which means that the Hamiltonian is not a proper Hermitian operator.

If we draw the positions of the energy levels as a function of $\zeta = Z\alpha$ one can see that at $\zeta = 1$ the energy of the 1s state goes to zero, and the gap between

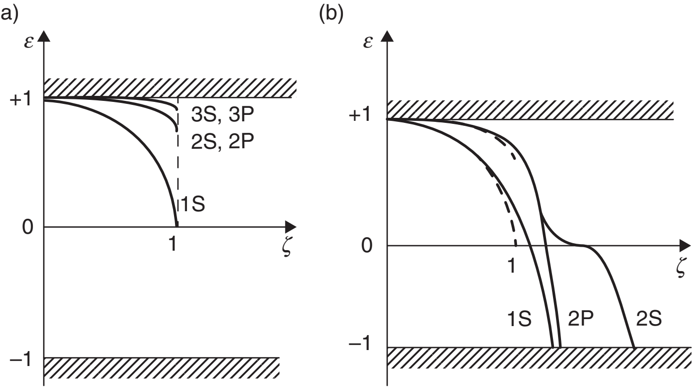

Fig. 8.2. (a) Energy levels of superheavy atoms (in units of mc^2) obtained from the Dirac equation for the Coulomb potential as a function of the coupling constant $\zeta = Z\alpha$. (b) The same, but taking into account the effects of the finite size of atomic nuclei. The critical value of Z is shifted from $Z_c = \alpha^{-1} \approx 137$ to $Z_c \approx 170$ (Zel'dovich & Popov, 1972).

electron and positron states disappears. In this situation one could expect vacuum reconstruction, with the creation of electron positron pairs from vacuum (Pomeranchuk & Smorodinsky, 1945; Zel'dovich & Popov, 1972; Greiner, Mueller & Rafelski, 1985; Grib, Mamaev & Mostepanenko, 1994); cf. our discussion of the Klein paradox in Section 4.1. The scheme of the energy levels (Zel'dovich & Popov, 1972) is shown in Fig. 8.2.

Taking into account the finite size of atomic nuclei $R = R_n$ and assuming a parabolic potential at $r < R_n$, as should be the case for a uniformly charged sphere, one finds a larger value for the critical radius, $Z_c \approx 170$ (Zel'dovich & Popov, 1972), which is still far beyond the charge of the heaviest known element. One can hope to observe this very interesting effect in collisions of two heavy ions with $Z < Z_c$, but in this case the critical value of total Z is even larger. Therefore, this effect of 'relativistic collapse' of superheavy atoms has not been observed, thus far.

In the case of graphene, we have the Fermi velocity $v \approx c/300$, instead of the velocity of light, and the critical value Z_c should be of the order of one, which makes this effect observable (Shytov, Katsnelson & Levitov, 2007a, 2007b; Pereira, Nilsson & Castro Neto, 2007). Actually, some manifestations have been discussed already in the previous section, such as the Fano resonances in the transport scattering cross-section shown in Fig. 8.1 (Shytov, Katsnelson & Levitov, 2007b). Strong oscillations of the local density of states for the supercritically charged impurities observable in principle by STM could be considered another manifestation (Shytov, Katsnelson & Levitov, 2007a).

Strictly speaking, the massless case $m=0$ relevant for graphene deserves special consideration. We saw in the previous section that relatively narrow resonances occur in the continuum spectrum. To understand better their origin it is instructive to consider the problem semiclassically.

For ultrarelativistic particles with the Hamiltonian

$$H(\vec{p}, r) = v|\vec{p}| \quad \frac{Ze^2}{r} \tag{8.45}$$

one can introduce the radial momentum p_r and angular momentum $p_\varphi = M$, which is an integral of motion since the Hamiltonian (8.45) does not depend on φ. One can find from the energy-conservation condition $H=E$ that

$$p_r^2 = \frac{1}{v^2}\left(E + \frac{Ze^2}{r}\right)^2 \quad \frac{M^2}{r^2} \tag{8.46}$$

and the classically allowed regions are determined by the condition $p_r^2 > 0$. If M is large enough,

$$M > M_c = \frac{Ze^2}{v}, \tag{8.47}$$

the particle can propagate from $r=0$ to $r=\infty$. At $M < M_c$ the situation is different, and we have two classically allowed regions, $0 < r < r_1$ and $r > r_2$, separated by a potential barrier, where

$$r_{1,2} = \frac{Ze^2 \mp Mv}{|E|}. \tag{8.48}$$

If we were to neglect the tunnelling through the classically forbidden region, we could use the semiclassical quantization condition (Bohr Sommerfeld condition) for the inner well:

$$\int_0^{r_1} dr\, p_r = \pi h(n + \mu), \tag{8.49}$$

where $n=0, 1, 2, \ldots$ and μ is a factor of the order of unity, cf. Section 2.4 (Landau & Lifshitz, 1977).

One can see, however, that the integral on the left-hand side of Eq. (8.49) is logarithmically divergent at the lower limits, and a cut-off at $r = r_0 \ll r_1$ should be introduced. This divergence reflects the fall towards the centre discussed above. After that we will find from the corrected version of Eq. (8.49)

$$E_n \approx -C\frac{hv}{r_0}\exp\left[-\frac{\pi h n}{\sqrt{M_{\mathrm{c}}^2-M^2}}\right] \tag{8.50}$$

with a factor $C \approx 1$, in very good agreement with the positions of quasilocalized levels found from the exact solution, Eq. (8.35).

Owing to the Klein tunnelling through the classically forbidden region, the lifetime in the inner well is finite, which leads to the appearance of the imaginary part of the energy,

$$\frac{\Gamma_n}{|E_n|} \approx \exp\left(-\frac{2S}{h}\right), \tag{8.51}$$

$$S = \int_{r_1}^{r_2} dr\,|p_r(r)| \tag{8.52}$$

(Landau & Lifshitz, 1977). The explicit calculation gives us the answer

$$S = \pi\left(M_{\mathrm{c}} - \sqrt{M_{\mathrm{c}}^2-M^2}\right). \tag{8.53}$$

At the threshold, $M = M_{\mathrm{c}}$, this gives us a result that differs from the exact one (8.37) only by the replacement

$$\frac{1}{\exp(2\pi\beta)-1} \to \exp(-2\pi\beta). \tag{8.54}$$

The resonances are narrow, and the quasilocalized states are long-lived, because of the numerical smallness $\exp(-\pi) \approx 0.04$ — an interesting example of a small *numerical* parameter for a coupling constant of the order of one!

8.3 Nonlinear screening of charge impurities

Up to now, we have not taken into account electron–electron interactions. However, they are essential in our problem. The Coulomb potential (8.1) induces some redistribution of the electron density, $n_{\mathrm{ind}}(\vec{r})$, which will create an additional potential

$$V_{\mathrm{ind}}(\vec{r}) = \frac{e^2}{\varepsilon_{\mathrm{ext}}}\int d\vec{r}'\,\frac{n_{\mathrm{ind}}(\vec{r}')}{|\vec{r}-\vec{r}'|} + V_{\mathrm{xc}}(\vec{r}), \tag{8.55}$$

where the first term is the Hartree potential and the second one is the exchange–correlation potential. In the simplest approximation the latter can be neglected, and we restrict ourselves to this approximation. The density-functional approach taking into account V_{xc} for the case of massless Dirac fermions was developed by Polini *et al.* (2008) and Rossi & Das Sarma (2008) (see also Brey & Fertig, 2009; Fogler, 2009; Gibertini *et al.*, 2010).

We will focus on the case of undoped graphene (chemical potential $\mu = 0$). In this situation the radial dependence of $n_{\mathrm{ind}}(r')$ can be written just from dimensional analysis. There is no way to construct any length from the parameters of the potential (Ze^2) and of the electron spectrum (the Fermi velocity v); the only relevant characteristic, β, given in (8.2), is dimensionless. At the same time, $n_{\mathrm{ind}}(r)$ has a dimensionality of inverse length squared. The most general expression is

$$n_{\mathrm{ind}}(r) = A(\beta)\delta(\vec{r}) + \frac{B(\beta)}{r^2}, \tag{8.56}$$

with the dimensionless A and B. The physical roles of these two terms are dramatically different. The term proportional to $A(\beta)$ is nothing other than the renormalization of the point charge:

$$\frac{Z}{\varepsilon_{\mathrm{ext}}} \to \quad \frac{Z}{\varepsilon_{\mathrm{ext}}} + A(\beta). \tag{8.57}$$

At the same time, phenomenologically, the answer should be $\quad Ze^2/\varepsilon$, where ε is the total dielectric constant (7.89), thus

$$A(\beta) = Z\left(\frac{1}{\varepsilon} \quad \frac{1}{\varepsilon_{\mathrm{ext}}}\right). \tag{8.58}$$

Therefore, the first term on the right-hand side of Eq. (8.56) describes nothing but *linear* screening, that is, the renormalization of the dielectric constant.

The second term gives a logarithmically divergent contribution to the total charge:

$$Q_{\mathrm{ind}} = \int d\vec{r}'\, n_{\mathrm{ind}}(\vec{r}') \approx 2\pi B(\beta) \ln\left(\frac{r_{\max}}{r_{\min}}\right), \tag{8.59}$$

where $r_{\max}$ and $r_{\min}$ are the upper and lower limits of the integration. The obvious choice for $r_{\min}$ is the lattice constant a, since at such small distances the Dirac model is not applicable. As for $r_{\max}$, it is of the order of the sample length L. The appearance of such contributions proportional to large $\ln(L/a)$ should have very important consequences.

Let us consider first the case of small Z. The linear-response problem was considered in Chapter 7, and no logarithms appeared. Owing to electron hole symmetry, $Q_{\mathrm{ind}}(Z)$ should be an odd function:

$$Q_{\mathrm{ind}}(\quad Z) = \quad Q_{\mathrm{ind}}(Z), \tag{8.60}$$

which means that, at small Z, B can be represented as

$$B(Z) = B_3 Z^3 + B_5 Z^5 + \cdots . \tag{8.61}$$

Straightforward calculations show that $B_3 = 0$ (Ostrovsky, Gornyi & Mirlin, 2006; Biswas, Sachdev & Son, 2007). Later in this section we will show in a nonperturbative way that $B = 0$ at $Z < Z_c$ (Shytov, Katsnelson & Levitov, 2007a).

To consider the opposite limit of large Z one can use the Thomas–Fermi approximation (Katsnelson, 2006c). For the case of atoms one can prove that it is asymptotically exact at $Z \to \infty$ (Lieb, 1981). Within this approximation (Landau & Lifshitz, 1977; Lieb, 1981; Vonsovsky & Katsnelson, 1989) the effect of the total potential

$$V(\vec{r}) = -\frac{Ze^2}{r} + V_{\text{ind}}(\vec{r}) \tag{8.62}$$

on the electron density dependent on the chemical potential, $n(\mu)$, is purely local,

$$n_{\text{ind}}(\vec{r}) = n[\mu - V(r)] - n(\mu), \tag{8.63}$$

and the term V_{xc} in Eq. (8.55) can be neglected. The linearized version of this approximation for the doped case was discussed in Section 7.7.

As a result,

$$V_{\text{ind}}(\vec{r}) = \frac{e^2}{\varepsilon_{\text{ext}}} \int d\vec{r}' \, \frac{n[\mu - V(\vec{r}')] - n(\mu)}{|\vec{r} - \vec{r}'|}. \tag{8.64}$$

For the case of graphene,

$$n(\mu) = \int_0^{\mu} dE \, N(E) = \frac{\mu|\mu|}{\pi h^2 v^2} \tag{8.65}$$

(see Eq. (1.72)).

Let us start with the undoped case ($\mu = 0$). Then, on substituting Eqs. (8.62) and (8.65) into Eq. (8.64) and integrating over angles (it is obvious that $V(\vec{r})$ and $n_{\text{ind}}(\vec{r})$ depend only on $|\vec{r}| = r$), one finds the integral equation (Katsnelson, 2006c)

$$F(r) = Z - \frac{2q}{\pi} \int_0^{\infty} \frac{dr'}{r'} \frac{r}{r + r'} K\left(\frac{2\sqrt{rr'}}{r + r'} \right) F(r') |F(r')|, \tag{8.66}$$

where F is related to V by the expression

$$V(\vec{r}) = \quad \frac{e^2}{\varepsilon_{\mathrm{ext}} r} F(r), \tag{8.67}$$

$K(m)$ is the elliptic integral (7.65) and

$$q = 2\left(\frac{e^2}{\varepsilon_{\mathrm{ext}} hv}\right)^2. \tag{8.68}$$

We will see below that, actually, the integral on the right-hand side of Eq. (8.66) is divergent at $r=0$; the reason is the inapplicability of the Dirac model at $r \leq a$. Therefore, we need to introduce a cut-off at $r' \approx a$, as was discussed above. The exact value of a is not relevant, given the logarithmic accuracy.

To proceed further, we make a replacement of variables in Eq. (8.66), $r' = r \exp(t)$, and introduce the notation $\tilde{F}(\ln r) = F(r)$. As a result, Eq. (8.66) takes the form

$$\tilde{F}(x) = Z \quad q \int_{\ln a}^{x} dt\, \tilde{F}(t)\left|\tilde{F}(t)\right| \quad q \int_{\infty}^{\infty} dt\, \tilde{F}(x+t)\left|\tilde{F}(x+t)\right|\varphi(t), \tag{8.69}$$

where

$$\varphi(t) = \frac{2}{\pi}\frac{K\left(1/\cosh\left(\frac{t}{2}\right)\right)}{1+\exp t} \quad \theta(\ \ t), \tag{8.70}$$

with $\theta(x>0)=1$, $\theta(x<0)=0$. The function $\varphi(t)$ decays exponentially at $t \to \pm\infty$ and has a logarithmic divergence at $t=0$ (see Fig. 8.3). For large x, the last term in Eq. (8.69) can be neglected:

$$\tilde{F}(x) = Z \quad q \int_{\ln a}^{x} dt\, \tilde{F}(t)\left|\tilde{F}(t)\right|. \tag{8.71}$$

This integral equation is equivalent to the differential one:

$$\frac{d\tilde{F}(x)}{dx} = \quad q\tilde{F}(x)\left|\tilde{F}(x)\right|, \tag{8.72}$$

with the initial condition $\tilde{F}(0) = Z$. The solution is

$$F(r) = \frac{Z}{1+|Z|q\ln\left(\frac{r}{a}\right)}, \tag{8.73}$$

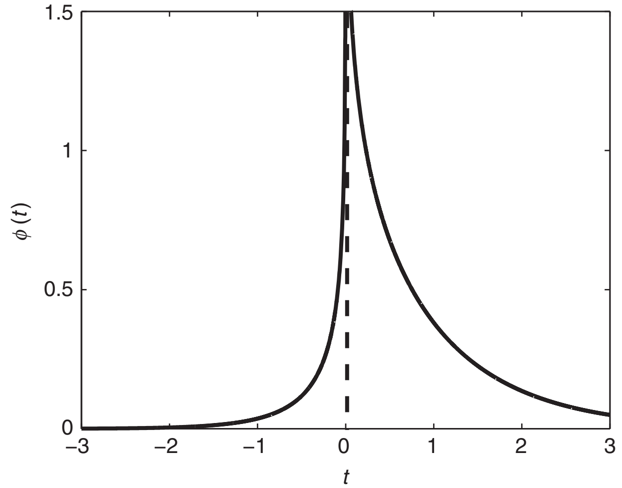

Fig. 8.3. A graph of the function $\varphi(t)$ in (8.70).

which corresponds to a very strong (logarithmic) screening of the effective charge at $r \gg a$:

$$Z_{\text{eff}}(r) = Z + Q_{\text{ind}} \approx \frac{Z_{\text{eff}}(r)}{q \ln\left(\frac{r}{a}\right)}. \tag{8.74}$$

If we were to expand Eq. (8.73) formally in Z, the leading term in Q_{ind} would be

$$Q_{\text{ind}} \approx \quad Z|Z|q \ln\left(\frac{r_{\max}}{r_{\min}}\right) \tag{8.75}$$

which does not have the form (8.61) (but, of course, satisfies the condition (8.60)). However, as we will see, the expression (8.73) is correct only for $|Z| \gg 1$.

If we took the expression (8.73) literally, it would lead to the conclusion that any charge is completely screened by the vacuum of two-dimensional massless Dirac electrons (Katsnelson, 2006c). The situation is reminiscent of 'charge nullification' in quantum electrodynamics (Landau & Pomeranchuk, 1955; Landau, Abrikosov & Khalatnikov, 1956; Migdal, 1977), which was considered (especially by the Landau school) as a fundamental difficulty of quantum field theory in general. Actually, complete nullification occurs neither in quantum electrodynamics nor in graphene. We will see that in the latter case the screening is stopped at the value $Z = Z_c$ (Shytov, Katsnelson & Levitov, 2007a).

The simplest way to demonstrate this is to use arguments based on the Friedel sum rule (Friedel, 1952; Vonsovsky & Katsnelson, 1989); its generalization to the case of the Dirac equation has been proposed by Lin (2005, 2006). According to the sum rule, the total induced charge is related to the phase scattering at the Fermi surface,

$$Q_{\text{int}} = \quad \frac{4}{\pi}\sum_{m}\delta_m(k_{\text{F}}), \tag{8.76}$$

where the minus sign corresponds to that in Eq. (8.5) and we introduce the factor of 4 (valley degeneracy multiplied by spin degeneracy) keeping in mind applications to graphene. We are interested in the limit $k_{\text{F}} \to 0$, which, however, requires some careful treatment for the supercritical charges ($|\beta| > \beta_{\text{c}}$), due to the term ln $(2kr_0)$ in Eq. (8.28). This is, actually, the same logarithmic divergence as in Eq. (8.59), so we will see immediately that the B term in Eq. (8.56) arises naturally at $|\beta| > \beta_{\text{c}}$ (but is equal to zero at $|\beta| < \beta_{\text{c}}$, as has already been mentioned). For the r-dependent term one can estimate, with logarithmic accuracy,

$$Q_{\text{int}}(r) \approx \quad \frac{4}{\pi}\sum_{m}\delta_m\left(k \sim \frac{1}{\mathrm{r}}\right) = \quad \frac{4}{\pi}\sum_{m}\gamma_m \ln\left(\frac{r}{a}\right), \tag{8.77}$$

where the sum is taken over all $|m| < |\beta|$.

Thus, we have the following expression for the logarithmically dependent term in Eq. (8.56):

$$B(\beta) = \quad \frac{2}{\pi^2}\beta \sum_{|m| \, < \, |\beta|} \sqrt{\beta^2 \quad m^2}. \tag{8.78}$$

To proceed further one can use the renormalization group (RG) method, in its simplest form of the 'poor man's scaling' (Anderson, 1970). Let us find the dimensionless charge β self-consistently:

$$\beta(r) = \frac{e^2}{\varepsilon_{\text{ext}} + hv}(Z + Q_{\text{ind}}(r)) = \beta_0\left(Z + 2\pi B \ln\left(\frac{r}{a}\right)\right), \tag{8.79}$$

where β_0 is the bare value (8.2). The differential RG equation for the effective coupling constant reads

$$\frac{d\beta}{d\ln r} = 2\pi\beta_0 B(\beta) = \quad \frac{4e^2\beta}{\pi\varepsilon_{\text{ext}}hv}\sum_{|m| < |\beta|}\sqrt{\beta^2 \quad m^2}. \tag{8.80}$$

Equation (8.80) describes the flow of effective charge from its initial value $\beta(r \approx a) = \beta_0$ to a smaller screened value. The flow stops, however, when $|\beta\,(r)|$ reaches the critical value $\beta_{\text{c}} = \frac{1}{2}$ since $B(|\beta| < \beta_{\text{c}}) = 0$. It happens at a finite screening radius r^* determined by the condition

$$\frac{1}{2\pi|\beta_0|}\int_{\beta_c}^{|\beta|}\frac{d|\beta|}{B(\beta)} = \ln\left(\frac{r^*}{a}\right). \tag{8.81}$$

For the case of $\frac{1}{2} < |\beta_0| < \frac{3}{2}$, for which only one term (with $|m| = \frac{1}{2}$) contributes to $B(\beta)$, the integration can be carried out explicitly:

$$r^* = a\exp\left[\frac{\pi\varepsilon_{\text{ext}}\hbar v}{4e^2}\cosh^{-1}(2\beta_0)\right]. \tag{8.82}$$

This means that the supercritical charge in graphene is surrounded by a cloud of electron–hole pairs (created from the vacuum) of finite radius r^*. For distances $r > r^*$ the supercritical charge looks like the critical one. In our simple theory this critical charge corresponds to $|\beta_c| = \frac{1}{2}$; however, one should keep in mind that a more accurate consideration of electron–electron interactions can renormalize this value. Note also that taking into account the A term (8.58) will lead to the replacement $\varepsilon_{\text{ext}} \to \varepsilon$ in Eqs. (8.80) and (8.82).

Anyway, it is natural to expect that $|\beta_c|$ is of the order of one. Thus, due to the condition $v \ll c$, the rich and interesting physics of the supercritical charge and vacuum reconstruction, which is hardly reachable for superheavy nuclei, can play an important role in graphene.

To finish this section, let us establish the relations between the Thomas–Fermi approximation and our RG treatment. If we assume that $|Z| \gg 1$ and $|\beta|$ is *much* larger than the critical value, the sum in Eq. (8.78) can be replaced by the integral

$$\sum_{|m|<|\beta|}\sqrt{\beta^2 - m^2} \approx \int_{-|\beta|}^{|\beta|} dm\sqrt{\beta^2 - m^2} = \frac{\pi\beta^2}{2}, \tag{8.83}$$

and Eq. (8.80) coincides with Eq. (8.72), with the solution (8.73). Thus, the Thomas–Fermi approximation works at $Z \to \infty$, as one would naturally expect.

8.4 Inter-electron Coulomb interaction and renormalization of the Fermi velocity

As discussed in Chapter 7, electron–electron interaction in graphene is not weak, the effective coupling constant being of the order of one. This makes the problem of a many-body description of graphene very complicated. Also, experimental evidence of many-body effects in graphene (except in the quantum Hall regime) still remains very poor. For these two reasons, it seems to be a bit early to discuss in detail the correlation effects in graphene. However, one of the predictions, namely, a concentration-dependent renormalization of the Fermi velocity (González, Guinea & Vozmediano, 1994) is based on relatively simple Hartee–Fock calculations and should be reliable, at least, qualitatively. Very recently, this effect was confirmed experimentally (Elias *et al.*, 2011). It demonstrates the importance of the long-range character of inter-electron Coulomb interactions and, therefore, will be considered in this chapter.

The Hamiltonian of the Coulomb interaction reads

$$\hat{H}_C = \frac{e^2}{2}\sum_{\alpha,\beta}\iint d\vec{r}\,d\vec{r}\,'\,\frac{\hat{\psi}_\alpha^+(\vec{r})\hat{\psi}_\alpha(\vec{r})\hat{\psi}_\beta^+(\vec{r}\,')\hat{\psi}_\beta(\vec{r}\,')}{|\vec{r}-\vec{r}\,'|}, \tag{8.84}$$

where $\hat{\psi}_\alpha(\vec{r})$ is the electron annihilation operator at the point $\vec{r}$, α is an intrinsic quantum number (e.g., a set of spin-projection, sublattice and valley labels). The Hartree–Fock approximation corresponds to the replacement

$$\hat{\psi}_1^+\hat{\psi}_2\hat{\psi}_3^+\hat{\psi}_4 \to \left\langle\hat{\psi}_1^+\hat{\psi}_2\right\rangle\hat{\psi}_3^+\hat{\psi}_4 + \left\langle\hat{\psi}_1^+\hat{\psi}_4\right\rangle\hat{\psi}_2\hat{\psi}_3^+ = \rho_{21}\hat{\psi}_3^+\hat{\psi}_4 + \rho_{41}\hat{\psi}_2\hat{\psi}_3^+, \tag{8.85}$$

which means a consideration of electron–electron interactions at the mean-field level (Landau & Lifshitz, 1977; Vonsovsky & Katsnelson, 1989). The coupling with

$$\sum_\alpha \left\langle\hat{\psi}_\alpha^+(\vec{r})\hat{\psi}_\alpha(\vec{r})\right\rangle = n(\vec{r}) \tag{8.86}$$

corresponds to Hartree (electrostatic) terms and, within the model of a homogeneous electron gas, is exactly compensated for by the interactions with ionic charge density, due to the electroneutrality of the system. The Fock contribution survives:

$$\hat{H}_F = -e^2\sum_{\alpha,\beta}\int d\vec{r}\,d\vec{r}\,'\,\frac{\left\langle\hat{\psi}_\alpha^+(\vec{r})\hat{\psi}_\beta(\vec{r}\,')\right\rangle\hat{\psi}_\beta^+(\vec{r}\,')\hat{\psi}_\alpha(\vec{r})}{|\vec{r}-\vec{r}\,'|}. \tag{8.87}$$

Owing to the translational invariance of the system,

$$\left\langle\hat{\psi}_\alpha^+(\vec{r})\hat{\psi}_\beta(\vec{r}\,')\right\rangle = \sum_{\vec{k}}\rho_{\beta\alpha}\left(\vec{k}\right)\exp\left[i\vec{k}(\vec{r}-\vec{r}\,')\right], \tag{8.88}$$

where

$$\rho_{\beta\alpha}\left(\vec{k}\right) = \left\langle\hat{\psi}_{\vec{k}\alpha}^+\hat{\psi}_{\vec{k}\beta}\right\rangle \tag{8.89}$$

(cf. Chapter 7, where we used this single-particle density matrix many times). If we apply this assumption to graphene, this means that we neglect inter-valley Coulomb interaction. The corresponding terms contain '*Umklapp* processes' with $\hat{\rho}\left(\vec{k}, \vec{k} \pm \vec{g}\right)$, where $\vec{g} = \vec{K} - \vec{K}'$ is the vector connecting the valleys. This approximation will be discussed later.

On substituting Eq. (8.88) into Eq. (8.87) we will have an additional term in the single-electron Hamiltonian,

$$\hat{H}_{\mathrm{F}} = \sum_{\vec{k}} \sum_{\alpha,\chi} \hat{\psi}_{\alpha}^{+}\left(\vec{k}\right) h_{\alpha\beta}\left(\vec{k}\right) \hat{\psi}_{\beta}\left(\vec{k}\right), \tag{8.90}$$

where

$$h_{\alpha\beta}\left(\vec{k}\right) = -2\pi e^2 \sum_{\vec{k}'} \frac{\rho_{\alpha\beta}\left(\vec{k}'\right)}{\left|\vec{k} - \vec{k}'\right|}. \tag{8.91}$$

If we consider the electron–electron interaction effects by applying a perturbation theory, the corrections to the energies of electrons and holes are nothing other than the matrix elements of $\hat{h}\left(\vec{k}\right)$ in the corresponding basis. The explicit calculation for the undoped case (which is similar to that in Sections 7.2 and 7.6) gives us the following result:

$$\delta E_{\mathrm{e,h}}\left(\vec{k}\right) = \pm \sum_{\vec{k}'} \frac{2\pi e^2}{\left|\vec{k} - \vec{k}'\right|} \frac{1}{2}\left(1 \pm \frac{\vec{k}\vec{k}'}{kk'}\right). \tag{8.92}$$

The integral in Eq. (8.92) is logarithmically divergent at the upper limit and has to be cut at $k_{\mathrm{c}} \approx 1/a$, due to the inapplicability of the Dirac approximation. It contains the term $\pm h\, \delta v_{\mathrm{F}}(k) k$, where

$$\delta v_{\mathrm{F}}(k) = \frac{e^2}{4h} \ln\left(\frac{k_{\mathrm{c}}}{k}\right), \tag{8.93}$$

which is logarithmically divergent at $k \to 0$. This means that, strictly speaking, the Dirac cones near the neutrality point are not exactly cones.

For the case of doped graphene, the divergence at $k \to 0$ is cut at $k \approx k_{\mathrm{F}}$, which results in a logarithmic dependence of the Fermi velocity on the electron concentration:

$$\delta v_{\mathrm{F}} \approx \frac{e^2}{4h} \ln\left(\frac{1}{k_{\mathrm{F}} a}\right). \tag{8.94}$$

If we take into account the screening of the Coulomb interaction by the environment plus virtual electron hole transitions, the expression (8.94) is replaced by

$$\delta v_{\mathrm{F}} \approx \frac{e^2}{4\hbar\varepsilon} \ln\left(\frac{1}{k_{\mathrm{F}} a}\right), \tag{8.95}$$

with ε given by Eq. (7.89). This seems to be in agreement with the experimental data published by Elias *et al.* (2011).

Note that, if we took into account the intervalley Coulomb interaction, the Fourier component $1/\left|\vec{k} - \vec{k}'\right|$ in Eq. (8.92) would be replaced by a constant,

$$\frac{1}{\left|\vec{k} - \vec{k}' + \vec{g}\right|} \approx \frac{1}{g}.$$

This interaction does not lead to any singularities and, therefore, can be neglected.

The situation becomes more complicated and interesting if we take into account *dynamical* screening of the Coulomb interaction (see Eqs. (7.81), (7.82) and (7.88)). As was shown by González, Guinea & Vozmediano (1999), this leads to the damping of electron states proportional to $|E|$, in contrast with the typical Fermi-liquid E^2 behaviour. This means that graphene in the vicinity of the neutrality point should be a *marginal Fermi liquid*, with ill-defined quasiparticles. Currently, it is not clear how this result will be changed on going beyond the perturbation theory.

There is also a huge theoretical literature discussing various types of instabilities in single-layer and bilayer graphene, due to electron electron interaction (exciton condensation, spin liquid, nematic order, charge-density waves, etc.). The issue is extremely interesting, but so controversial that even a selection of references would be too subjective. Let us hope that the situation will be clarified in the very near future.

9

Crystal lattice dynamics, structure and thermodynamics

9.1 Phonon spectra of graphene

Phonon spectra of two-dimensional and quasi-two-dimensional crystals have some peculiar features that were first analysed by Lifshitz (1952) (see also Belenkii, Salaev & Suleimanov, 1988; Kosevich, 1999). To explain them we first recall a general description of the phonon spectra in crystals (Kosevich, 1999; Katsnelson & Trefilov, 2002).

Let the coordinates of the nuclei be

$$\vec{R}_{nj} = \vec{R}_{nj}^{(0)} + \vec{u}_{nj}, \tag{9.1}$$

where $\left\{ \vec{R}_{nj}^{(0)} \right\}$ form a crystal lattice, n labels elementary cells (or sites of the corresponding Bravais lattice), $j = 1, 2, \ldots, \nu$ labels the atoms within elementary cell (or sublattices) and $\vec{u}_{nj}$ are displacements. Further, we will use the notation

$$\vec{R}_{nj}^{(0)} = \vec{r}_n + \vec{\rho}_j, \tag{9.2}$$

where $\vec{r}_n$ are translation vectors and $\vec{\rho}_j$ are basis vectors ($\vec{\rho}_1 \equiv 0$).

The main assumption of the standard theory of crystal lattices is the smallness of average atomic displacements in comparison with the interatomic distance d:

$$\left\langle \vec{u}_{nj}^2 \right\rangle \ll d^2. \tag{9.3}$$

According to Eq. (9.3) one can expand the potential energy $V\left(\left\{ \vec{R}_{nj} \right\} \right)$ in terms of atomic displacements and take into account only the lowest, second-order, term (the linear term obviously vanishes due to mechanical equilibrium conditions):

$$V\left(\left\{ \vec{R}_{nj} \right\} \right) = V\left(\left\{ \vec{R}_{nj}^{(0)} \right\} \right) + \frac{1}{2} \sum_{\substack{nn' \\ ij \\ \alpha\beta}} A_{ni,n'j}^{\alpha\beta} u_{ni}^{\alpha} u_{n'j}^{\beta}, \tag{9.4}$$

where

$$A^{\alpha\beta}_{ni,n'j} = \left(\frac{\partial^2 V}{\partial u^{\alpha}_{ni}\partial u^{\beta}_{n'j}}\right)_{\vec{u}\ \ 0} \tag{9.5}$$

is the *force-constant matrix*. Equation (9.4) defines the *harmonic approximation*.

The classical equations of motion for the potential energy (9.4) read

$$M_i \frac{d^2 u^{(\alpha)}_{ni}}{dt^2} = \quad \sum_{n'j\beta} A^{\alpha\beta}_{ni,n'j} u^{\beta}_{n'j}. \tag{9.6}$$

By looking for solutions of the form $u^{\alpha}_{ni}(t) \sim \exp(\quad i\omega t)$ and using translational symmetry one can prove that the square eigenfrequencies of the problem, $\omega^2 = \omega^2_{\xi}(\vec{q})$, are eigenvalues of the *dynamical matrix*

$$D^{\alpha\beta}_{ij}(\vec{q}) = \sum_n \frac{A^{\alpha\beta}_{0i,nj}}{\sqrt{M_i M_j}} \exp(i\vec{q}\vec{r}_n). \tag{9.7}$$

Here $\vec{q}$ is the phonon wave vector running over the Brillouin zone and $\xi = 1, 2, \ldots, 3\nu$ is the phonon branch label.

After quantization of the classical problem one can prove that in the harmonic approximation the Hamiltonian of the system is

$$\hat{H}_0 = \sum_{\lambda} h\omega_{\lambda}\left(\hat{b}^{+}_{\lambda}\hat{b}_{\lambda} + \frac{1}{2}\right), \tag{9.8}$$

where $\lambda = (\vec{q}, \xi)$ are phonon quantum numbers, $\hat{b}^{+}_{\lambda}$ and $\hat{b}_{\lambda}$ are canonical Bose creation and annihilation operators and the atomic displacement operator is expressed in terms of $\hat{b}^{+}_{\lambda}$ and $\hat{b}_{\lambda}$ as

$$\hat{\vec{u}}_{nj} = \sum_{\lambda} \sqrt{\frac{h}{2N_0 M_j \omega_{\lambda}}}\left(\hat{b}_{\lambda} + \hat{b}^{+}{}_{\lambda}\right)\vec{e}_j(\lambda)\exp(i\vec{q}\vec{r}_n). \tag{9.9}$$

Here N_0 is the number of elementary cells, $(\ \ \lambda) \equiv (\ \ \vec{q}, \xi)$ and $\vec{e}_j(\lambda)$ are polarization vectors, that is, unit eigenvectors of the dynamical matrix.

There are important restrictions on the force-constant matrix, due to the translational invariance of the problem. If we were to move all nuclei of the crystal by the same displacement vector $\vec{u}$ no force would act on any atom. This means, due to Eq. (9.6), that

$$\sum_{nj} A^{\alpha\beta}_{0i,nj} = 0. \tag{9.10}$$

It follows from the condition (9.10) that in three-dimensional space there are three *acoustic* modes, with $\omega_\xi^2(\vec{q} \to 0) \to 0$ ($\xi = 1, 2, 3$) and $3(\nu - 1)$ *optical* modes, with finite $\omega_\xi^2(\vec{q} \to 0)$. The acoustic modes for small $\vec{q}$ correspond to coherent displacements of all atoms in the elementary cell by the same vector $\vec{u}_j \equiv \vec{u}$, whereas optical modes at $\vec{q} = 0$ correspond to the motion of atoms within the elementary cells with the fixed inertia centre:

$$\sum_j M_j \vec{u}_j(\vec{q} = 0) = 0. \tag{9.11}$$

Keeping in mind graphene, we will assume further that $M_j = M$ is the mass of the carbon atom. Owing to mirror symmetry in the graphene plane, it is obvious that

$$\hat{A}^{xz} = \hat{A}^{yz} = 0 \tag{9.12}$$

and, thus, the modes with polarization along the z-direction are rigorously separated, within the harmonic approximation, from the modes polarized in the graphene xy-plane. Also, taking into account that the two sublattices A and B are equivalent, one can see that

$$D_{11}^{\alpha\beta} = D_{22}^{\alpha\beta} \tag{9.13}$$

and, due to Eqs. (9.7) and (9.10),

$$D_{12}^{\alpha\beta}(\vec{q} = 0) + D_{11}^{\alpha\beta}(\vec{q} = 0) = 0. \tag{9.14}$$

Therefore, there are *six* phonon branches in graphene, namely the following.

(1) The acoustic flexural mode ZA ($\vec{u} \parallel Oz$) with the frequencies

$$\omega_{\mathrm{ZA}}^2(\vec{q}) = D_{11}^{zz}(\vec{q}) + D_{12}^{zz}(\vec{q}). \tag{9.15}$$

(2) The optical flexural mode ZO ($\vec{u} \parallel Oz$) with the frequencies

$$\omega_{\mathrm{ZO}}^2(\vec{q}) = D_{11}^{zz}(\vec{q}) - D_{12}^{zz}(\vec{q}). \tag{9.16}$$

(3), (4) Two acoustic in-plane modes, with $\omega^2(\vec{q})$ equal to eigenvalues of the 2×2 matrix

$$D_{11}^{\alpha\beta}(\vec{q}) + D_{12}^{\alpha\beta}(\vec{q}) \quad (\alpha, \beta = x, y).$$

(5), (6) Two optical in-plane modes, with $\omega^2(\vec{q})$ equal to eigenvalues of the 2×2 matrix

$$D_{11}^{\alpha\beta}(\vec{q}) - D_{12}^{\alpha\beta}(\vec{q}) \quad (\alpha, \beta = x, y).$$

If the two-dimensional wave vector $\vec{q}$ lies in symmetric directions, branches (3) (6) can be divided into longitudinal ($\vec{e}\|\vec{q}$) and transverse ($\vec{e}\perp\vec{q}$) modes; for a generic $\vec{q}$ this classification is not possible.

Because of the conditions (9.14) one can assume that for acoustic modes $\omega^2 \sim q^2$ at $\vec{q} \to 0$ and this is, in general, true. However, for the ZA mode q^2 terms also disappear, and $\omega^2_{\mathrm{ZA}}(q) \sim q^4$ (Lifshitz, 1952). This follows from the *rotational invariance* of the system. Indeed, instead of uniform translation $\vec{u}_n =$ constant let us use *uniform rotation*

$$\vec{u}_{nj} = \delta\vec{\varphi} \times \vec{R}^{(0)}_{nj}, \tag{9.17}$$

where $\delta\vec{\varphi}$ is the rotation angle. This should also not lead to the appearance of any forces or torques acting on the atoms. If $\delta\vec{\varphi}$ lies in the xy-plane, $\vec{u}_{nj}\|Oz$ and, additionally to the conditions (9.10), we will have

$$\sum_{nj} A^{zz}_{0i,nj} r^{\alpha}_{n} r^{\beta}_{n} = 0 \tag{9.18}$$

(α, $\beta = x$, y). It follows immediately from Eq. (9.18) and the definition of the dynamical matrix in (9.7) that

$$\frac{\partial^2}{\partial q_\alpha \, \partial q_\beta} \left[D^{zz}_{11}(\vec{q}) + D^{zz}_{12}(\vec{q}) \right] \big|_{\vec{q} \quad 0} = 0 \tag{9.19}$$

and, thus, the expansion of the right-hand side of Eq. (9.15) starts with terms of the order of q^4; therefore,

$$\omega_{\mathrm{ZA}}(q) \sim q^2 \tag{9.20}$$

at $\vec{q} \to 0$. In the next section we will derive this result by means of phenomenological elasticity theory.

There is no way, up to now, to measure phonon dispersion in graphene experimentally since the number of atoms in graphene flakes is insufficient for inelastic neutron-scattering experiments. It can be calculated using the density-functional method (Mounet & Marzari, 2005) or some semi-empirical interatomic potential. The results are quite similar. Later in this chapter we will frequently discuss the results of atomistic simulations obtained using the so-called long-range carbon-bond order potential (LCBOPII) (Los & Fasolino, 2003; Los *et al.*, 2005). Therefore we show in Fig. 9.1 the phonon spectra calculated within the same model (Karssemeijer & Fasolino, 2011). One can clearly see the six branches of the phonons listed above.

Let us consider now the case of finite temperatures. In the harmonic approximation, the mean-square atomic displacement is (Kosevich, 1999; Katsnelson & Trefilov, 2002)

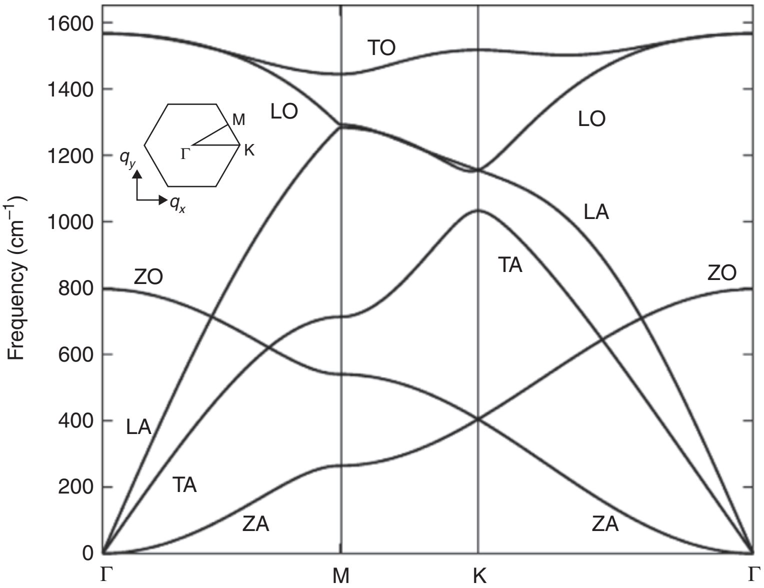

Fig. 9.1. Phonon spectra of graphene. (Reproduced with permission from Karssemeijer and Fasolino, 2011.)

$$\left\langle u_{nj}^{\alpha} u_{nj}^{\beta} \right\rangle = \sum_{\lambda} \frac{h}{2N_0 M_j \omega_\lambda} \left(e_{nj}^{\alpha}\right)^{*} \left(e_{nj}^{\beta}\right) \coth\left(\frac{h\omega_\lambda}{2T}\right). \tag{9.21}$$

For in-plane deformations ($\alpha = \beta = x$ or y) at any finite temperature the integral (9.21) is logarithmically divergent due to the contribution of acoustic branches with $\omega \sim q$ at $\vec{q} \to 0$. This divergence is cut at minimal $q_{\min} \sim L^{\ 1}$ (L is the sample size), thus

$$\left\langle x_{nj}^2 \right\rangle = \left\langle y_{nj}^2 \right\rangle \approx \frac{T}{2\pi M c_{\mathrm{s}}^2} \ln\left(\frac{L}{d}\right), \tag{9.22}$$

where c_{s} is the average sound velocity (Peierls, 1934, 1935; Landau, 1937; Landau & Lifshitz, 1980). This led Landau and Peierls to the conclusion that two-dimensional crystals cannot exist. Strictly speaking, this means just the inapplicability of the harmonic approximation, due to violation of the condition (9.3). However, a more rigorous treatment does confirm this conclusion (Mermin, 1968), as a partial case of the *Mermin Wagner theorem* (Mermin & Wagner, 1966; Ruelle, 1999). This means that the definition of graphene as a 'two-dimensional crystal' requires a detailed and careful discussion, which is one of the main aims of this chapter.

For $\alpha = z$, the situation is even worse, due to the much stronger divergence of ZA phonons, Eq. (9.20). One can see from Eq. (9.21) that

$$\left\langle h_{nj}^2 \right\rangle \sim T \sum_q \frac{1}{q^4} \sim \frac{T}{E_{\text{at}}} L^2, \tag{9.23}$$

where E_{at} is of the order of the cohesive energy. Henceforth we will use the notation $h = u^z$, assuming that $\vec{u} = (u^x, u^y)$ is a two-dimensional vector only.

Before going any further it is important to derive the key results (9.20) and (9.23) from a different point of view.

9.2 The theory of elasticity for thin plates

In this section we present the general equations of the phenomenological elasticity theory, with applications to thin plates (Landau & Lifshitz, 1970; Timoshenko & Woinowsky-Krieger, 1959). This is a necessary preparatory step before we can discuss the unique mechanical properties of graphene (Booth *et al.*, 2008; Lee *et al.*, 2008). Also, it gives us a deeper insight into the properties of flexural phonons.

Let us consider a D-dimensional ($D = 2$ or 3) deformed medium. The particles which had original coordinates x_α are transformed to the position

$$x'_\alpha = x_\alpha + u_\alpha\left(\{x_\beta\}\right). \tag{9.24}$$

The metrics, that is, the distance between infinitesimally distant points, being Pythagorean,

$$dl^2 = dx_\alpha \, dx_\alpha \tag{9.25}$$

(we assume a summation over repeated tensor indices) is changed to

$$dl'^2 = dx'_\alpha \, dx'_\alpha = \frac{\partial x'_\alpha}{\partial x_\beta} \frac{\partial x'_\alpha}{\partial x_\gamma} \, dx_\beta \, dx_\gamma = dl^2 + 2u_{\alpha\beta} \, dx_\alpha \, dx_\beta, \tag{9.26}$$

where

$$u_{\alpha\beta} = \frac{1}{2}\left(\frac{\partial u_\alpha}{\partial x_\beta} + \frac{\partial u_\beta}{\partial x_\alpha} + \frac{\partial u_\gamma}{\partial x_\alpha}\frac{\partial u_\gamma}{\partial x_\beta}\right) \tag{9.27}$$

is a so-called *deformation tensor*. It is assumed, in the elasticity theory, that the free energy of a deformed medium is a functional of the deformation tensor $F = F\left[u_{\alpha\beta}\right]$.

By definition, the equilibrium state without external forces corresponds to $u_{\alpha\beta} = 0$.

There are two types of external forces resulting in the deformation. First, there are bulk forces acting on each atom of the medium, such as gravitational and electric forces. Their volume density is assumed to be $f_\alpha^{(v)}(\vec{r})$. Second, there are mechanical forces, due to contact with various bodies; they act on the surface only. The hydrostatic pressure P is an example; it leads to the total force

$$\vec{f} = \oint d\vec{S}\, P, \tag{9.28}$$

where $d\vec{S}$ is the (vector) element of the surface area. In a more general case in which also shear forces are allowed Eq. (9.28) is generalized as

$$f_\alpha = \oint dS_\beta\, \sigma_{\alpha\beta}, \tag{9.29}$$

where $\sigma_{\alpha\beta}$ is called the *stress tensor*. Using the Gauss theorem, Eq. (9.29) can be represented as an integral over the volume

$$f_\alpha = \int d^D x\, \frac{\partial \sigma_{\alpha\beta}}{\partial x_\beta}. \tag{9.30}$$

Thus, the condition of local equilibrium can be written as

$$\frac{\partial \sigma_{\alpha\beta}}{\partial x_\beta} + f_\alpha^{(v)} = 0. \tag{9.31}$$

One can prove (Landau & Lifshitz, 1970) that, due to the condition of absence of internal torques, the stress tensor is symmetric:

$$\sigma_{\alpha\beta} = \sigma_{\beta\alpha}. \tag{9.32}$$

Interestingly, this condition is violated in ferromagnetic media, due to gyromagnetic effects (Vlasov & Ishmukhametov, 1964), but we will not consider that case here.

The stress tensor creates deformations that are linear in the stress (Hooke's law). In the approximation of an isotropic elastic medium the relation is determined by two *Lamé constants*, λ and μ:

$$\sigma_{\alpha\beta} = \lambda \delta_{\alpha\beta} u_{\gamma\gamma} + 2\mu u_{\alpha\beta}. \tag{9.33}$$

It is obvious that for small enough deformations $|u_{\alpha\beta}| \ll 1$ the renormalization of the local volume is determined by $u_{\gamma\gamma} = \operatorname{Tr} \hat{u}$:

$$\frac{dV'}{dV} = \det\left(\frac{\partial x'_\alpha}{\partial x_\beta}\right) \approx 1 + u_{\gamma\gamma}. \tag{9.34}$$

This component of the deformation tensor is called *dilatation*. The traceless component,

$$u'_{\alpha\beta} = u_{\alpha\beta} \quad \frac{1}{D} \delta_{\alpha\beta} u_{\gamma\gamma}, \tag{9.35}$$

is called *shear deformation*. Hooke's law (9.33) can be rewritten as

$$\sigma_{\alpha\beta} = B\delta_{\alpha\beta}u_{\gamma\gamma} + 2\mu\left(u_{\alpha\beta} - \frac{1}{D}\delta_{\alpha\beta}u_{\gamma\gamma}\right), \tag{9.36}$$

where

$$B = \lambda + \frac{2\mu}{D} \tag{9.37}$$

is the bulk modulus and μ has the meaning of a shear modulus of the system under consideration.

On substituting Eq. (9.33) into Eq. (9.31) we find the equilibrium conditions for the case $f_\alpha^{(v)} = 0$:

$$\frac{\partial}{\partial x_\alpha}\left(\lambda u_{\gamma\gamma}\right) + 2\frac{\partial}{\partial x_\beta}\left(\mu u_{\alpha\beta}\right) = 0. \tag{9.38}$$

Equation (9.38) corresponds to the extremum of the free energy

$$F = \frac{1}{2}\int d^D x\left[\lambda(u_{\alpha\alpha})^2 + 2\mu u_{\alpha\beta}u_{\alpha\beta}\right]. \tag{9.39}$$

Thermodynamic stability requires

$$B > 0, \qquad \mu > 0, \tag{9.40}$$

which is obvious if one considers pure dilatation and pure shear deformation. The inversion of Eq. (9.36) gives us

$$u_{\alpha\beta} = \frac{1}{D^2 B}\delta_{\alpha\beta}\sigma_{\gamma\gamma} + \frac{1}{2\mu}\left(\sigma_{\alpha\beta} - \frac{1}{D}\delta_{\alpha\beta}\sigma_{\gamma\gamma}\right). \tag{9.41}$$

If we apply a uniaxial uniform stress ($\sigma_{xx} = p$ and other components are equal to zero) we can find from Eq. (9.41) that

$$u_{xx} = \frac{p}{Y}, \qquad u_{yy} = -\nu u_{xx}, \tag{9.42}$$

where Y is called *Young's modulus* and ν is the *Poisson ratio* determining the change of sizes in directions perpendicular to the stress. For $D = 3$ one has

$$\begin{aligned} Y &= \frac{9B\mu}{3B+\mu}, \\ \nu &= \frac{1}{2}\frac{3B - 2\mu}{3B+\mu} \end{aligned} \tag{9.43}$$

and, due to Eq. (9.40),

$$1 < \nu < \frac{1}{2}. \tag{9.44}$$

For most solids $\nu > 0$, which means a constriction of the body in the perpendicular direction. For $D = 2$

$$\begin{aligned} Y &= \frac{4B\mu}{B+\mu}, \\ \nu &= \frac{B \quad \mu}{B+\mu}. \end{aligned} \tag{9.45}$$

Now, after recalling these basic definitions of elasticity theory, let us consider the case of a thin plate (its thickness Δ is much smaller than the typical size, L, in the x- and y-directions). We start with the case of small deformations, for which the last, nonlinear, term in the definition (9.27) can be neglected. If we assume that no forces act on the surfaces of the plate, it should be, according to Eq. (9.29), the case that

$$\sigma_{\alpha\beta} n_\beta = 0, \tag{9.46}$$

where $\vec{n}$ is the unit normal to the surface. For the equation of the surface

$$z = h(x, y) \tag{9.47}$$

the components of the normal are

$$\begin{aligned} n_x &= \quad \frac{\partial h}{\partial x} \frac{1}{\sqrt{1 + |\nabla h|^2}}, \\ n_y &= \quad \frac{\partial h}{\partial y} \frac{1}{\sqrt{1 + |\nabla h|^2}}, \\ n_z &= \frac{1}{\sqrt{1 + |\nabla h|^2}}, \end{aligned} \tag{9.48}$$

where

$$\nabla h = \left(\frac{\partial h}{\partial x}, \frac{\partial h}{\partial y} \right)$$

is a two-dimensional gradient (see any textbook on differential geometry, e.g. DoCarmo, 1976; Coxeter, 1989). If $|\nabla h| \ll 1$, the normal is parallel to the z-axis, and Eq. (9.46) reads

$$\sigma_{xz} = \sigma_{yz} = \sigma_{zz} = 0. \tag{9.49}$$

The conditions (9.49) should be satisfied for both surfaces of the plate and, since the plate is thin, should be valid also within the plane. Taking into account Eq. (9.33) and the definitions (9.43), one finds

$$\frac{\partial u_x}{\partial z} = -\frac{\partial u_z}{\partial x}, \qquad \frac{\partial u_y}{\partial z} = -\frac{\partial u_z}{\partial y} \tag{9.50}$$

and

$$u_{zz} = -\frac{\nu}{1-\nu}\left(\frac{\partial u_x}{\partial x} + \frac{\partial u_y}{\partial y}\right). \tag{9.51}$$

Assuming $u_z = h(x, y)$ to be z-independent within the plane, one finds from Eq. (9.50)

$$u_x = -z\frac{\partial h}{\partial x}, \qquad u_y = -z\frac{\partial h}{\partial y} \tag{9.52}$$

and the components of the deformation tensor are

$$\begin{gathered} u_{xx} = -z\frac{\partial^2 h}{\partial x^2}, \qquad u_{yy} = -z\frac{\partial^2 h}{\partial y^2}, \qquad u_{xy} = -z\frac{\partial^2 h}{\partial x \, \partial y}, \\ u_{xz} = u_{yz} = 0, \qquad u_{zz} = z\left(\frac{\partial^2 h}{\partial x^2} + \frac{\partial^2 h}{\partial y^2}\right)\frac{\nu}{1-\nu}. \end{gathered} \tag{9.53}$$

On substituting Eqs. (9.53) into Eq. (9.39) and integrating explicitly over $|z| < \Delta/2$ (Δ is the plate thickness) one finds for the energy of bending deformation

$$F_{\mathrm{b}} = \frac{Y\Delta^3}{24(1-\nu^2)}\int d^2x \left\{ \left(\nabla^2 h\right)^2 + 2(1-\nu)\left[\left(\frac{\partial^2 h}{\partial x \, \partial y}\right)^2 - \frac{\partial^2 h}{\partial x^2}\frac{\partial^2 h}{\partial y^2}\right]\right\}, \tag{9.54}$$

where

$$\nabla^2 = \frac{\partial^2}{\partial x^2} + \frac{\partial^2}{\partial y^2} \tag{9.55}$$

is the two-dimensional Laplacian. The last term in Eq. (9.54),

$$\det\left(\frac{\partial^2 h}{\partial x_i \, \partial x_j}\right),$$

is proportional to the Gaussian curvature K of the deformed surface (DoCarmo, 1976; Coxeter, 1989); for more details see below. It can be represented as a total derivative:

$$2\det\left(\frac{\partial^2 f}{\partial x_i\,\partial x_j}\right) = \quad \varepsilon_{im}\varepsilon_{jm}\frac{\partial^2}{\partial x_m\,\partial x_n}\left(\frac{\partial f}{\partial x_i}\frac{\partial f}{\partial x_j}\right) \tag{9.56}$$

($\hat{\varepsilon}$ is the unit asymmetric 2×2 matrix) and, thus, leads to some integral over the edges of the membrane. It therefore has no effect on the equations of motion. Alternatively, one can refer to the Gauss Bonnet theorem (DoCarmo, 1976; Coxeter, 1989) that $\int dS\,K$ is a topological invariant that is not changed during smooth deformations. Thus, the bending energy (9.54) can be represented as

$$F_{\mathrm{b}} = \frac{\kappa}{2}\int d^2x\left(\nabla^2 h\right)^2, \tag{9.57}$$

where

$$\kappa = \frac{Y\Delta^3}{24(1\quad \nu^2)}. \tag{9.58}$$

If we add the kinetic energy

$$T = \frac{1}{2}\int d^2x\,\rho\left(\frac{\partial\vec{u}}{\partial t}\right)^2 \approx \frac{1}{2}\int d^2x\,\rho\left(\frac{\partial h}{\partial t}\right)^2 \tag{9.59}$$

(ρ is the mass density) and write the Lagrangian $L = T \quad F_{\mathrm{b}}$ and the corresponding equations of motion

$$\frac{\partial}{\partial t}\left(\rho\frac{\partial h}{\partial t}\right) \quad \nabla^2\left(\kappa\,\nabla^2 h\right)^2 = 0, \tag{9.60}$$

then we find for the frequencies of the bending waves

$$\omega^2 = \frac{\kappa}{\rho}q^4, \tag{9.61}$$

in agreement with Eq. (9.20). The quantity κ is called the *bending rigidity*.

Our consideration up to now has not taken into account the energy of in-plane deformations. To take them into account one needs to add the energy (9.39), where $\alpha, \beta = x, y$. One can neglect in the definition (9.27) the nonlinear terms

$$\frac{\partial u_x}{\partial x_\alpha}\frac{\partial u_x}{\partial x_\beta} \quad \text{and} \quad \frac{\partial u_y}{\partial x_\alpha}\frac{\partial u_y}{\partial x_\beta}$$

but one should keep the nonlinearities

$$\frac{\partial h}{\partial x_\alpha}\frac{\partial h}{\partial x_\beta}$$

since, as we will see, they can be comparable to $\partial u_\alpha/\partial x_\beta$ (further, $\vec{u} = \left(u_x, u_y\right)$ is the *two-dimensional* vector):

$$u_{\alpha\beta} = \frac{1}{2}\left(\frac{\partial u_\alpha}{\partial x_\beta} + \frac{\partial u_\beta}{\partial x_\alpha} + \frac{\partial h}{\partial x_\alpha}\frac{\partial h}{\partial x_\beta}\right). \tag{9.62}$$

The total deformation energy is

$$F = \frac{1}{2}\int d^2x\left\{\kappa\left(\nabla^2 h\right)^2 + \lambda(u_{\alpha\alpha})^2 + 2\mu u_{\alpha\beta}u_{\alpha\beta}\right\}, \tag{9.63}$$

where

$$\lambda = \lambda_3\Delta, \qquad \mu = \mu_3\Delta \tag{9.64}$$

are the *two-dimensional* Lamé constants (henceforth we will write two-dimensional parameters λ, μ, B, Y and σ without subscripts and the corresponding three-dimensional parameters with the subscript 3). The equations for equilibrium deformations of the plate can be found by minimization of the functional (9.63), plus interactions with external forces. After rather cumbersome transformations (Landau & Lifshitz, 1970; Timoshenko & Woinovsky-Krieger, 1959) one finds

$$\kappa\nabla^4 h \quad \left[\frac{\partial^2\chi}{\partial y^2}\frac{\partial^2 h}{\partial x^2} + \frac{\partial^2\chi}{\partial x^2}\frac{\partial^2 h}{\partial y^2} \quad 2\frac{\partial^2\chi}{\partial x\,\partial y}\frac{\partial^2 h}{\partial x\,\partial y}\right] = P, \tag{9.65}$$

$$\nabla^4\chi + Y\left[\frac{\partial^2 h}{\partial x^2}\frac{\partial^2 h}{\partial y^2} \quad \left(\frac{\partial^2 h}{\partial x\,\partial y}\right)^2\right] = 0, \tag{9.66}$$

where P is the density of external forces (per unit area) and χ is the potential for the stress tensor:

$$\sigma_{xx} = \frac{\partial^2\chi}{\partial y^2}\Delta, \qquad \sigma_{xy} = \quad \frac{\partial^2\chi}{\partial x\,\partial y}\Delta, \qquad \sigma_{yy} = \frac{\partial^2\chi}{\partial x^2}\Delta. \tag{9.67}$$

These equations (the *Föppl equations*) are essentially nonlinear, and their solution is, in general, a difficult task. One can, however, estimate the deformation for the situation when $|h| \gg \Delta$, the only one which is relevant for graphene, where Δ is of the order of interatomic distance. The first term in Eq. (9.65) is smaller in this situation than the second one and can be neglected (Landau & Lifshitz, 1970). This means that the bending rigidity κ is irrelevant, and it is in-plane deformation and the corresponding Young modulus which determine the resistance to the external force. Dimensional analysis of Eqs. (9.65) and (9.66) gives us a typical value of the deformation:

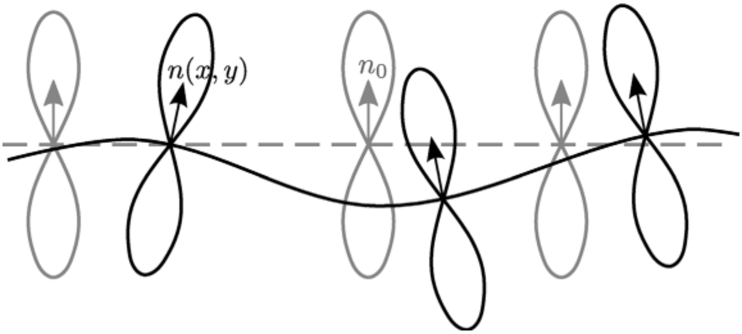

Fig. 9.2. The orientation of normals and the directions of electron orbitals in a fluctuating membrane (black) and in its ground state (grey).

$$h \sim \left(\frac{L^4 P}{Y}\right)^{1/3}. \tag{9.68}$$

For example, for a circular plate of radius R with a clamped edge and uniform P, the deformation at the centre is (Timoshenko & Woinovsky-Krieger, 1959)

$$h_0 \approx 0.662 R \left(\frac{RP}{Y}\right)^{1/3}. \tag{9.69}$$

Estimations show also that linear and nonlinear terms in the deformation tensor (9.62) are, in general, of the same order of magnitude.

Graphene is an extremely strong material (the real values of the constants κ, B and μ will be discussed later in this chapter). Also, being almost defect-free, it can keep a deformation as high as, at least, 10% 15% (Kim *et al.*, 2009). Therefore, for typical flake sizes of the order of 10 to 100 μm, a flake can bear a weight of the order of billions of times its own weight (Booth *et al.*, 2008).

There is another way to derive Eq. (9.57), which starts from the model of a membrane as an infinitely thin plate, that is, a single flexible surface (Nelson, Piran & Weinberg, 2004). It is natural to assume that the energy of a deformed membrane depends on the mutual orientation of normals to the surface at the neighbouring points which determines the orientation of electron orbitals, etc. (Fig. 9.2). If we discretize (e.g., triangulate) the surface, we can write the corresponding free energy as

$$F_{\mathrm{b}} = \tilde{\kappa} \sum_{\langle ij \rangle} \left(1 \quad \vec{n}_i \vec{n}_j\right), \tag{9.70}$$

where $\tilde{\kappa} > 0$, $\vec{n}_i$ is the normal to the ith triangle and the sum is taken over the neighbouring triangles. The bending energy (9.70) is counted from the flat state with all $\vec{n}_i \parallel Oz$. Since

$$1 \quad \vec{n}_i\vec{n}_j = \frac{1}{2}\left(\vec{n}_i \quad \vec{n}_j\right)^2 \tag{9.71}$$

in the continuum limit it will be transformed to the invariant quantity

$$\frac{\partial n_\alpha}{\partial x_\beta}\frac{\partial n_\alpha}{\partial x_\beta}$$

and

$$F_\mathrm{b} = \frac{\kappa}{2}\int d^2x \, \frac{\partial n_\alpha}{\partial x_\beta}\frac{\partial n_\alpha}{\partial x_\beta} \tag{9.72}$$

with $\kappa \propto \tilde{\kappa}$. On substituting Eq. (9.48) into Eq. (9.72) and keeping only the lowest-order terms in $\partial h/\partial x_\alpha$ we have

$$F_\mathrm{b} = \frac{\kappa}{2}\int d^2x \left[\left(\nabla^2 h\right)^2 \quad 2\det\left(\frac{\partial h}{\partial x_i}\frac{\partial h}{\partial x_j}\right)\right]. \tag{9.73}$$

The last term, which is proportional to the Gaussian curvature, can be skipped for the reasons discussed above, and we have the expression (9.57).

One more view of Eq. (9.57) is based on the Helfrich model of liquid membranes (Helfrich, 1973; Jones, 2002). The deformation energy in this model is written in terms of the mean curvature H and Gaussian curvature K of the surface:

$$F = \frac{\kappa}{2}\int dS\, H^2 + \kappa' \int dS\, K, \tag{9.74}$$

where, due to the Gauss Bonnet theorem, the second term is important only for processes during which the topology is changed (e.g., the merging of two vesicles). The first term is known also in mathematics as the Willmore functional; for some recent discussions see Taimanov (2006) and Manyuhina *et al.* (2010). For a general surface defined by Eq. (9.47) one has (DoCarmo, 1976)

$$dS = dx\, dy\sqrt{1 + |\nabla h|^2}, \tag{9.75}$$

$$K = \frac{1}{\left[1 + |\nabla h|^2\right]^2}\left[\frac{\partial^2 h}{\partial x^2}\frac{\partial^2 h}{\partial y^2} \quad \left(\frac{\partial^2 h}{\partial x\,\partial y}\right)^2\right], \tag{9.76}$$

$$H = \frac{1}{\left[1 + |\nabla h|^2\right]^{3/2}}\left\{\left[1 + \left(\frac{\partial h}{\partial x}\right)^2\right]\frac{\partial^2 h}{\partial y^2} + \left[1 + \left(\frac{\partial h}{\partial y}\right)^2\right]\frac{\partial^2 h}{\partial x^2} - 2\frac{\partial^2 h}{\partial x\,\partial y}\frac{\partial h}{\partial x}\frac{\partial h}{\partial y}\right\}. \tag{9.77}$$

Keeping only the lowest-order terms in $|\nabla h|$, we have

$$H \approx \nabla^2 h \tag{9.78}$$

and, thus, Eq. (9.74) is equivalent to Eq. (9.57).

9.3 The statistical mechanics of flexible membranes

The expressions (9.62) and (9.63) provide a background for the statistical mechanics of crystalline membranes at finite temperatures (Nelson & Peliti, 1987; Aronovitz & Lubensky, 1988; Abraham & Nelson, 1990; Le Doussal & Radzihovsky, 1992; Nelson, Piran & Weinberg, 2004). Henceforth we will consider only the classical regime, assuming that $\vec{u}(\vec{r})$ and $h(\vec{r})$ are static fields fluctuating in space. Thus, the partition function is determined by a functional integral

$$Z = \int D\vec{u}(\vec{r})Dh(\vec{r})\exp\{-\beta F[\vec{u}(\vec{r}), h(\vec{r})]\}, \tag{9.79}$$

where $\beta = T^{-1}$ is the inverse temperature and the free energy F (9.63) plays the role of the Hamiltonian. The nonlinear term in Eq. (9.62) couples the two fields, making the theory highly nontrivial — at least as nontrivial as the famous problem of critical behaviour (Wilson & Kogut, 1974; Ma, 1976).

If we neglect this term, the Hamiltonian (9.63) is split into two independent Hamiltonians for the free fields. In the $\vec{q}$ representation, it reads

$$F_0 = \frac{\kappa}{2}\sum_{\vec{q}} q^4 |h_{\vec{q}}|^2 + \frac{1}{2}\sum_{\vec{q}} \left[\mu q^2 |\vec{u}_{\vec{q}}|^2 + (\lambda + \mu)\left(\vec{q}\cdot\vec{u}_{\vec{q}}\right)^2\right], \tag{9.80}$$

where $h_{\vec{q}}$ and $\vec{u}_{\vec{q}}$ are Fourier components of $h(\vec{r})$ and $\vec{u}(\vec{r})$, respectively. The correlation functions for the free fields can be found immediately using the properties of Gaussian functional integrals (Wilson & Kogut, 1974; Ma, 1976; Faddeev & Slavnov, 1980):

$$G_0(\vec{q}) = \left\langle |h_{\vec{q}}|^2 \right\rangle_0 = \frac{T}{\kappa q^4}, \tag{9.81}$$

$$D_0^{\alpha\beta}(\vec{q}) = \left\langle u_{\alpha\vec{q}}^* u_{\beta\vec{q}} \right\rangle_0 = P_{\alpha\beta}(\vec{q})\frac{T}{(\lambda + 2\mu)q^2} + \left[\delta_{\alpha\beta} - P_{\alpha\beta}(\vec{q})\right]\frac{1}{\mu q^2}, \tag{9.82}$$

where $\langle \ldots \rangle_0$ means averaging with the Hamiltonian F_0 and

$$P_{\alpha\beta}(\vec{q}) = \frac{q_\alpha q_\beta}{q^2} \tag{9.83}$$

is the projection operator on the $\vec{q}$ vector. Note that the normal normal correlation function is related to $\left\langle \left|h_{\vec{q}}\right|^2 \right\rangle$ by

$$\langle \vec{n}_{\vec{q}} \vec{n}_{\ \vec{q}} \rangle = q^2 \left\langle \left|h_{\vec{q}}\right|^2 \right\rangle, \tag{9.84}$$

as follows from Eq. (9.48). On substituting Eq. (9.81) into Eq. (9.84) we find

$$\langle \vec{n}_{\vec{q}} \vec{n}_{\ \vec{q}} \rangle = \frac{T}{\kappa q^2}. \tag{9.85}$$

However, the approximation (9.81) turns out not to be satisfactory. It does not describe a flat membrane. Indeed, the membrane is more or less flat if the correlation function

$$\langle \vec{n}_0 \vec{n}_{\vec{R}} \rangle = \sum_{\vec{q}} \left\langle \left|\vec{n}_{\vec{q}}\right|^2 \right\rangle \exp\left(i\vec{q}\vec{R}\right) \tag{9.86}$$

tends to a constant at $R \to \infty$ (normals at large distances have, on average, the same direction). Instead, substitution of Eq. (9.85) into (9.86) leads to a logarithmically divergent integral. Moreover, the mean-square out-of-plane displacement

$$\langle h^2 \rangle = \sum_{\vec{q}} \left\langle \left|h_{\vec{q}}\right|^2 \right\rangle \tag{9.87}$$

after the cut-off at $q_{\min} \sim L^{\ 1}$ gives the result

$$\langle h^2 \rangle \sim \frac{T}{\kappa} L^2 \tag{9.88}$$

(cf. Eq. (9.23)), which means that the membrane is crumpled (on average, it has all three dimensions of the order of L).

Similarly, the in-plane square deformation

$$\langle \vec{u}^2 \rangle = \sum_{\vec{q}} \left\langle \left|\vec{u}_{\vec{q}}\right|^2 \right\rangle \tag{9.89}$$

is logarithmically divergent, as in Eq. (9.22). Thus, we conclude, again, that the statistical mechanics of two-dimensional systems cannot be based on the harmonic approximation, or approximation of free fields.

The nonlinear term

$$\frac{\partial h}{\partial x_\alpha} \frac{\partial h}{\partial x_\beta}$$

in Eq. (9.62) after substitution into Eq. (9.63) results in a coupling of two fields. The integral over $\vec{u}(\vec{r})$ in Eq. (9.79) remains Gaussian and can be calculated rigorously, using the well-known rule (Wilson & Kogut, 1974; Faddeev & Slavnov, 1980)

$$\frac{\int D\vec{u}\exp\left(-\frac{1}{2}\vec{u}\hat{L}\vec{u}-\vec{f}\vec{u}\right)}{\int D\vec{u}\exp\left(-\frac{1}{2}\vec{u}\hat{L}\vec{u}\right)}=\exp\left(\frac{1}{2}\vec{f}\hat{L}^{-1}\vec{f}\right). \tag{9.90}$$

As a result, the partition function (9.79) can be represented as

$$Z=\int Dh(\vec{r})\exp\{-\beta\Phi[h(\vec{r})]\}, \tag{9.91}$$

with the Hamiltonian Φ depending on the out-of-plane deformations only:

$$\Phi=\frac{1}{2}\sum_{\vec{q}}\kappa q^4\left|h_{\vec{q}}\right|^2+\frac{Y}{8}\sum_{\vec{q}\vec{k}\vec{k}'}R\left(\vec{k},\vec{k}',\vec{q}\right)\left(h_{\vec{k}}h_{\vec{q}-\vec{k}}\right)\left(h_{\vec{k}'}h_{-\vec{q}-\vec{k}'}\right) \tag{9.92}$$

where Y is the two-dimensional Young modulus (9.45) and

$$R\left(\vec{k},\vec{k}',\vec{q}\right)=\frac{\left(\vec{q}\times\vec{k}\right)^2\left(\vec{q}\times\vec{k}'\right)^2}{q^4}. \tag{9.93}$$

The term proportional to h^4 in Eq. (9.92) describes anharmonic effects, or self-interaction of the field $h(\vec{r})$, and Y plays the role of the coupling constant.

Thus, we have the problem of interacting fluctuations where the low-q contribution is dominant, which is reminiscent of the problem of a critical point. The difference is that for two-dimensional systems we have such a critical situation at *any* finite temperature.

The correlation function $G(\vec{q})=\left\langle\left|h_{\vec{q}}\right|^2\right\rangle$ satisfies the *Dyson equation*

$$G^{-1}(\vec{q})=G_0^{-1}(\vec{q})+\Sigma(\vec{q}), \tag{9.94}$$

where $G_0(\vec{q})$ is given by Eq. (9.81) and the *self-energy* $\Sigma(\vec{q})$ can be calculated using perturbation theory in Y via, e.g., Feynman diagrams. We can introduce the *renormalized bending rigidity* $\kappa_{\mathrm{R}}(q)$ by writing

$$G(q)=\frac{T}{\kappa_{\mathrm{R}}(q)q^4} \tag{9.95}$$

and discuss this quantity. The first-order correction gives us (Nelson & Peliti, 1987)

$$\delta\kappa(q)=\kappa_{\mathrm{R}}(q)-\kappa=\frac{TY}{\kappa}\sum_{\vec{k}}\frac{1}{\left|\vec{q}+\vec{k}\right|^4}\left[\frac{\left(\vec{q}\times\vec{k}\right)^2}{q^2}\right]^2. \tag{9.96}$$

On calculating the integral over $\vec{k}$ we find

$$\delta\kappa(q) = \frac{3TY}{8\pi\kappa q^2}. \tag{9.97}$$

At

$$q \leq q^* = \sqrt{\frac{3TY}{8\pi\kappa}} \tag{9.98}$$

the correction (9.97) is equal to the bare value of κ or larger than κ, and the perturbation theory is obviously not applicable. The value q^* plays the same role as the 'Ginzburg criterion' (Landau & Lifshitz, 1980; Ma, 1976) in the theory of critical phenomena: below q^* the effects of interactions between fluctuations dominate.

The increase of bending rigidity with increasing temperature has a simple physical explanation. It is known, for the case of a corrugated plate, that corrugations of height $h \gg \Delta$ (Δ is the thickness of the plate) should increase its effective rigidity by a factor $(h/\Delta)^2$ (Briassoulis, 1986; Peng, Liew & Kitipornchai, 2007). Taking into account Eq. (9.88) (with $L \to 1/q$) and $\Delta \approx a$, we will have an estimation like Eq. (9.97).

Note that in the theory of liquid membranes, where the Hamiltonian is given by Eq. (9.74) and the in-plane deformations $\vec{u}$ are not relevant, there is also a divergent anharmonic correction to κ_R (q), due to higher-order (nonlinear) terms in the expression (9.77) for the mean curvature (Peliti & Leibler, 1985):

$$\delta\kappa \approx \frac{3T}{4\pi} \ln\left(\frac{1}{qa}\right). \tag{9.99}$$

This term has the opposite sign in comparison with that for a crystalline membrane (9.97) and is much smaller than the latter. Thus, the Hamiltonian (9.92) takes into account the *main* nonlinearities, and 'liquid' anharmonicities are not relevant for crystalline membranes.

In the next sections we will discuss how to solve this problem and what the real behaviour of fluctuations with $q \leq q^*$ is.

9.4 Scaling properties of membranes and intrinsic ripples in graphene

In situations in which one has strongly interacting long-wavelength fluctuations, scaling considerations are extremely useful (Wilson & Kogut, 1974; Ma, 1976; Patashinskii & Pokrovskii, 1979). Let us assume that the behaviour of the renormalized bending rigidity at small q is determined by some exponent η:

$$\kappa_{\mathrm{R}}(q) \sim q^{-\eta}, \tag{9.100}$$

which means

$$G(q) = \left\langle \left| \vec{h}_{\vec{q}} \right|^2 \right\rangle = \frac{A}{q^{4-\eta} q_0^{\eta}}. \tag{9.101}$$

Here we introduce a parameter

$$q_0 = \sqrt{\frac{Y}{\kappa}} \tag{9.102}$$

of the order of a^{-1} to make A dimensionless. One can assume also a renormalization of effective Lamé constants:

$$\lambda_{\mathrm{R}}(q),\ \mu_{\mathrm{R}}(q) \sim q^{\eta_u}, \tag{9.103}$$

which means

$$D^{\alpha\beta}(\vec{q}) = \left\langle u^*_{\alpha\vec{q}} u_{\beta\vec{q}} \right\rangle \sim \frac{1}{q^{2+\eta_u}}. \tag{9.104}$$

Finally, instead of Eq. (9.88) we assume

$$\left\langle h^2 \right\rangle \sim L^{2\zeta}. \tag{9.105}$$

The values η, η_u and ζ are similar to *critical exponents* in the theory of critical phenomena. They are not independent (Aronovitz & Lubensky, 1988).

First, it is easy to express ζ in terms of η. Substituting Eq. (9.101) into Eq. (9.87) and introducing, as usual, a cut-off at $q_{\min} \sim L^{-1}$ we have

$$\zeta = 1 - \frac{\eta}{2}. \tag{9.106}$$

If $\eta > 1$, $\zeta < 1$ and the membrane remains flat (in the sense that its effective thickness, $\sqrt{\langle h^2 \rangle}$, is much smaller than L at $L \to \infty$). Also, in the correlation function (9.86), due to Eqs. (9.84) and (9.101), there is no divergence from the region of small q:

$$\left\langle \vec{n}_{\vec{q}} \vec{n}_{-\vec{q}} \right\rangle \sim \frac{1}{q^{2-\eta}} \tag{9.107}$$

is an integrable singularity.

The relation between η_u and η has been derived by Aronovitz & Lubensky (1988) using quite complicated tools, such as the renormalization group and Ward identities in Feynman-diagram technique. Its meaning is, however, rather elementary and related to the requirement that the deformation tensor has the correct structure (9.62) under the renormalization. This means that the correlation functions of $\partial u_\alpha / \partial x_\beta$ and

$$\frac{\partial h}{\partial x_\alpha}\frac{\partial h}{\partial x_\beta}$$

should have the same exponents. The first one follows immediately from Eq. (9.104):

$$\Gamma_1(\vec{q}) = \left\langle \left(\frac{\partial u_\alpha}{\partial x_\beta}\right)_{\vec{q}} \left(\frac{\partial u_\alpha}{\partial x_\beta}\right)_{\vec{q}} \right\rangle = q^2 D^{\alpha\alpha}(\vec{q}) \sim q^{\;\;\eta_u}. \tag{9.108}$$

For the second one we have a convolution:

$$\begin{aligned}\Gamma_2(\vec{q}) &= \left\langle \left(\frac{\partial h}{\partial x_\alpha}\frac{\partial h}{\partial x_\beta}\right)_{\vec{q}} \left(\frac{\partial h}{\partial x_\alpha}\frac{\partial h}{\partial x_\beta}\right)_{\vec{q}} \right\rangle \\ &= \sum_{\vec{k}_1 \vec{k}_2} k_{1\alpha}\left(q_\beta \quad k_{1\beta}\right) k_{2\alpha}\left(q_\beta + k_{2\beta}\right) \left\langle h_{\;\;\vec{k}_1} h_{\;\vec{q}\;\;\vec{k}_1} h_{\;\;\vec{k}_2} h_{\vec{q}+\vec{k}_2} \right\rangle.\end{aligned} \tag{9.109}$$

For free fields we have Wick's theorem, and

$$\langle h_1 h_2 h_3 h_4 \rangle = \langle h_1 h_2 \rangle \langle h_3 h_4 \rangle + \langle h_1 h_3 \rangle \langle h_2 h_4 \rangle + \langle h_1 h_4 \rangle \langle h_2 h_3 \rangle. \tag{9.110}$$

For interacting fields this is no longer the case, and we have some irreducible averages (cumulants). It is supposed in the scaling theory that the scaling properties of these cumulants are the same as those for the 'reducible' terms (Patashinskii & Pokrovskii, 1979) and, thus, one can use Eq. (9.110) to calculate the exponents. On substituting Eq. (9.110) into Eq. (9.109) one obtains

$$\Gamma_2(\vec{q}) \sim \sum_{\vec{k}} k^2 \left(\vec{q} \quad \vec{k}\right)^2 G\left(\vec{k}\right) G\left(\vec{k} \quad \vec{q}\right). \tag{9.111}$$

Finally, on substituting Eq. (9.101) into Eq. (9.111) we have

$$\Gamma_2(\vec{q}) \sim \frac{1}{q^{2 \quad 2\eta}}. \tag{9.112}$$

On comparing Eq. (9.112) with Eq. (9.108), we arrive at the result

$$\eta_u = 2 \quad 2\eta. \tag{9.113}$$

This exponent is positive if $0 < \eta < 1$ (we will see later that this is the case). This means that, due to interactions between out-of-plane and in-plane phonons, the former become harder but the latter become softer.

The temperature dependence of the constant A in Eq. (9.101) can be found from the assumption that q^* in (9.98) is the only relevant wave vector in the theory and that Eqs. (9.81) and (9.101) should match at $q \approx q^*$. The result is (Katsnelson, 2010b):

$$A = \alpha \left(\frac{T}{\kappa} \right)^{\zeta}, \tag{9.114}$$

where α is a dimensionless factor of the order of one.

Before discussing how to calculate the exponent η it is worth returning to the Mermin Wagner theorem about the impossibility of long-range crystal order in two-dimensional systems at finite temperatures.

The true manifestation of long-range order is the existence of delta-functional (Bragg) peaks in diffraction experiments; see, e.g., the discussion in Irkhin & Katsnelson (1986). The scattering intensity is proportional to the static structural factor

$$S(\vec{q}) = \sum_{nn'} \sum_{jj'} \left\langle \exp\left[i\vec{q}\left(\vec{R}_{nj} \quad \vec{R}_{n'j'} \right) \right] \right\rangle. \tag{9.115}$$

Using Eqs. (9.1) and (9.2) the expression (9.115) can be rewritten as

$$S(\vec{q}) = \sum_{nn'} \exp[i\vec{q}(\vec{r}_n \quad \vec{r}_{n'})] \sum_{jj'} \exp\left[i\vec{q}\left(\vec{\rho}_j \quad \vec{\rho}_{j'} \right) \right] W_{nj,n'j'}, \tag{9.116}$$

where

$$W_{nj,n'j'} = \left\langle \exp\left[i\vec{q}(\vec{u}_{nj} \quad \vec{u}_{n'j'}) \right] \right\rangle. \tag{9.117}$$

Equations (9.115) and (9.117) are written for the classical case in which $\vec{u}_{nj}$ are not operators but just classical vectors; for a more detailed discussion of the scattering problem in crystal lattices, see Vonsovsky & Katsnelson (1989) and Katsnelson & Trefilov (2002).

In conventional three-dimensional crystals, one can assume that the displacements $\vec{u}_{nj}$ and $\vec{u}_{n'j'}$ are not correlated, and

$$W_{nj,n'j'} = \left\langle \exp\left(i\vec{q}\vec{u}_{nj} \right) \right\rangle \left\langle \exp\left(\quad i\vec{q}\vec{u}_{n'j'} \right) \right\rangle \equiv m_j(\vec{q}) m^*_{j'}(\vec{q}) \tag{9.118}$$

when $|\vec{r}_n \quad \vec{r}_{n'}| \to \infty$; here $m_j(\vec{q})$ are Debye Waller factors that are independent of n due to translational invariance. Therefore, for $\vec{q} = \vec{g}$ (reciprocal lattice vectors), where $\exp(i\vec{q}\vec{r}_n) = 1$, the contribution to $S(\vec{q})$ is proportional to N_0^2, whereas for a generic $\vec{q}$ it is of the order of N_0. The Bragg peaks at $\vec{q} = \vec{g}$ are, therefore, sharp; thermal fluctuations decrease their intensity (by the Debye Waller factor) but do not broaden the peaks. The observation of such sharp

Bragg peaks is an experimental manifestation of the existence of long-range crystal order. In the two-dimensional case, the correlation functions of atomic displacements do not vanish at $|\vec{r}_n - \vec{r}_{n'}| \to \infty$. Indeed, in the continuum limit $\vec{u}_{nj} \to (\vec{u}(\vec{r}), h(\vec{r}))$, where $\vec{u}$ is already a two-dimensional vector, and

$$\left\langle [h(\vec{r}) - h(\vec{r}\,')]^2 \right\rangle = 2\sum_{\vec{q}} \left\langle |h_{\vec{q}}|^2 \right\rangle \{1 - \exp[i\vec{q}(\vec{r} - \vec{r}\,')]\} \sim |\vec{r} - \vec{r}\,'|^{2\zeta}, \quad (9.119)$$

$$\left\langle [\vec{u}(\vec{r}) - \vec{u}(\vec{r}\,')]^2 \right\rangle = 2\sum_{\vec{q}} \left\langle |\vec{u}_{\vec{q}}|^2 \right\rangle \{1 - \exp[i\vec{q}(\vec{r} - \vec{r}\,')]\} \sim |\vec{r} - \vec{r}\,'|^{\eta_u} \quad (9.120)$$

after substitutions of Eqs. (9.101) and (9.103) (Abraham & Nelson, 1990). This means that the approximation (9.118) does not work.

To estimate the structural factor near the Bragg peak, $\vec{q} = \vec{g} + \delta\vec{q}$, we can use the identity

$$\langle e^c \rangle = \exp\left[\frac{1}{2}\langle c^2 \rangle\right] \quad (9.121)$$

for the correlation function (9.117). Strictly speaking, it follows from Wick's theorem and, therefore, is exact only in the harmonic approximation (Vonsovsky & Katsnelson, 1989) but, as was discussed above, should give us correct scaling properties. Therefore,

$$W_{nj,n'j'} \sim \exp\left[-\alpha_1 g_{\|}^2 |\vec{r} - \vec{r}\,'|^{\eta_u} - \alpha_2 (\delta\vec{q}_{\perp})^2 |\vec{r} - \vec{r}\,'|^{2\zeta}\right], \quad (9.122)$$

where $\vec{q}_{\|}$ and $\vec{q}_{\perp}$ are components of the scattering vector parallel and perpendicular to the crystal plane and we take into account that $\vec{g}_{\perp} = 0$.

On substituting Eq. (9.122) into Eq. (9.116) one can see that the sum over n' at a given n is convergent, and $S(\vec{q} = \vec{g}) \sim N_0$. Thus, instead of a delta-functional Bragg peak (in the thermodynamic limit) we have a sharp maximum of finite width at $\delta\vec{q} \to 0$ (Abraham & Nelson, 1990). This means that, rigorously speaking, the statement that two-dimensional crystals cannot exist at finite temperatures (Peierls, 1934, 1935; Landau, 1937) is correct. However, the structural factor still can have *very* sharp maxima at $\vec{q} = \vec{g}$ and the crystal lattice can be restored from the positions of these maxima. In this (restricted) sense, two-dimensional crystals do exist, and graphene is a prototype example of them.

It was found experimentally by electron diffraction, namely by transmission electron microscopy, that freely suspended graphene at room temperature is rippled, that is, exhibits corrugations in the out-of-plane direction (Meyer *et al.*, 2007a, 2007b). The existence of these intrinsic, thermally induced,

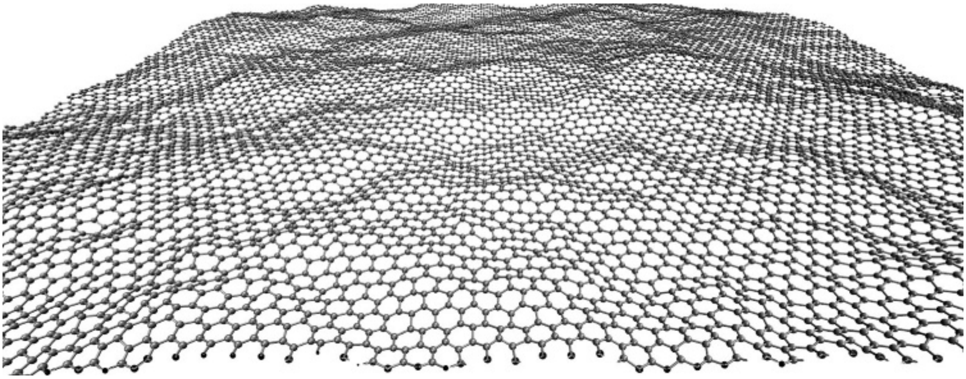

Fig. 9.3. A typical atomic configuration (from atomistic Monte Carlo simulations) for graphene at room temperature (courtesy of A. Fasolino).

ripples in graphene has been confirmed by atomistic Monte Carlo simulations that use the potential LCBOPII mentioned already in Section 9.1 (Fasolino, Los & Katsnelson, 2007). A typical snapshot is shown in Fig. 9.3. Further detailed studies of the correlation function $G(q)$ by such simulations have been performed for single-layer graphene by Los *et al.* (2009) and Zakharchenko *et al.* (2010b) and for bilayer graphene by Zakharchenko *et al.* (2010a). Some of the results are shown in Fig. 9.4 (together with the results of the self-consistent screening approximation, which will be discussed in the next section). Here we show and discuss only the data for $T = 300\,\text{K}$.

At some intermediate value of q, roughly between $0.1\,\text{Å}^{-1}$ and $1\,\text{Å}^{-1}$, the correlation function $G(q)$ follows the harmonic approximation (9.81). From the slope of this dependence one can extract $\kappa \approx 1.1\,\text{eV}$, which means that graphene at room temperature should be considered a rather hard membrane ($\kappa/T \approx 40$). For $q > 1\,\text{Å}^{-1}$ the continuum-medium approximation does not work, and $G(q)$ increases due to closeness to the Bragg peak. At $q \approx q^* \approx 0.2\,\text{Å}^{-1}$ there is a crossover to the behaviour described by Eq. (9.101), with

$$\eta \approx 0.85. \tag{9.123}$$

This value is quite close to that predicted by functional renormalization-group analysis of the model (9.92) (Kownacki & Mouhanna, 2009). Thus, both the continuum model and atomistic simulations predict a rather broad, power-law distribution of intrinsic ripples in graphene, without any dominant spatial scale. Ripples in graphene on a substrate will be discussed in Chapter 11, in relation to scattering mechanisms involved in electron transport.

Other evidence for thermally introduced ripples and their effects on thermodynamic properties will be considered in Section 9.6.

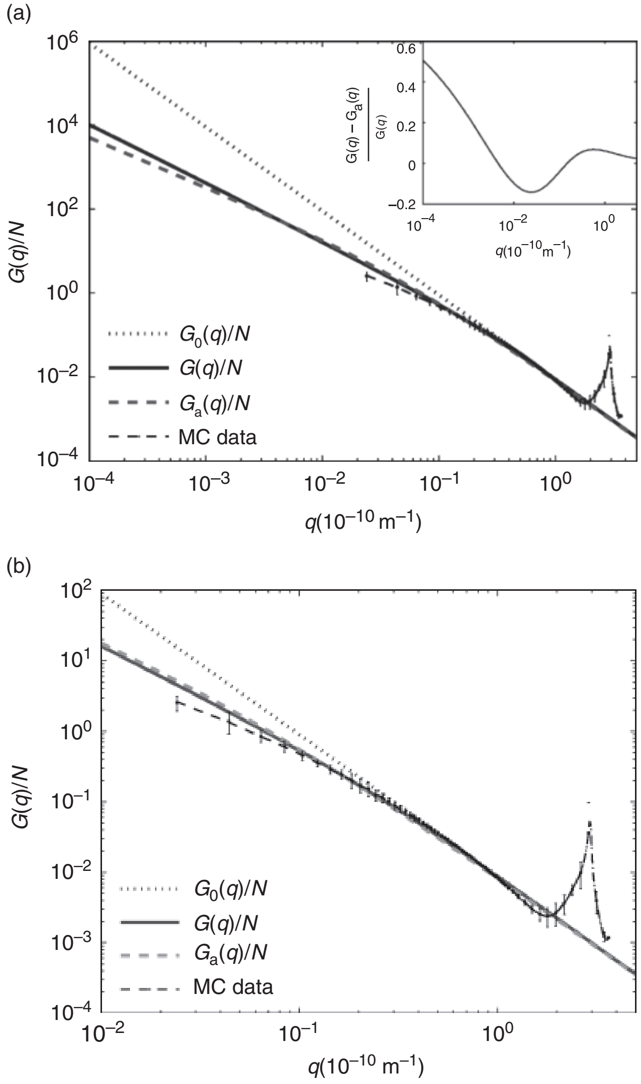

Fig. 9.4. The correlation function $G(q)$ found from numerical solution of the SCSA equations, together with the data of atomistic Monte Carlo (MC) simulations, with the bare Green function (9.81) and with the interpolation formula (9.143). Panels (a) and (b) are changed by the scale; the insert in panel (a) shows the accuracy of the interpolation (9.143). (Reproduced with permission from Zakharchenko *et al.*, 2010b.)

One needs to make one important comment about the model (9.63) (or, equivalently, (9.92)). In this model of a so-called *phantom membrane* there is a phase transition at $T \approx \kappa$ to a crumpled phase (Nelson, Piran & Weinberg, 2004). There are some arguments, however, in favour of the view that this transition is suppressed, and the low-temperature (quasi-)flat phase is stabilized at any temperature if one adds a condition of avoided self-crossing (short-range repulsion forces). It is assumed also that the scaling properties of the (quasi-)flat phase are the same for 'phantom' and 'real' membranes (Nelson, Piran & Weinberg, 2004). Anyway, the regime $T \approx \kappa \approx 10^4\,\mathrm{K}$ is obviously not reachable for graphene. What happens with graphene with increasing temperature will be discussed in Section 9.6.

To finish this section let us discuss the case of bilayer graphene. Intrinsic ripples in bilayer graphene were observed experimentally (Meyer *et al.*, 2007b) and studied theoretically (Zakharchenko *et al.*, 2010b). The main difference from the case of single-layer graphene can be seen even at the level of the harmonic approximation for the bilayer membrane. Instead of Eq. (9.57) (or (9.73)) we have

$$F_{\mathrm{b}} = \frac{1}{2}\int d^2x\left[\kappa\left(\nabla^2 h_1\right)^2 + \kappa\left(\nabla^2 h_2\right)^2 + 2\gamma(\delta h)^2\right], \tag{9.124}$$

where h_1 and h_2 are out-of-plane deformations in each plane, κ is the bending rigidity per layer,

$$\delta h = h_1 - h_2 \tag{9.125}$$

and γ describes a relatively weak van der Waals interaction between the layers. By introducing an average displacement

$$h = \frac{h_1 + h_2}{2} \tag{9.126}$$

one can rewrite Eq. (9.124) as

$$F_{\mathrm{b}} = \frac{1}{2}\int d^2x\left[2\kappa\left(\nabla^2 h\right)^2 + \frac{\kappa}{2}\left(\nabla^2\,\delta h\right)^2 + 2\gamma(\delta h)^2\right] \tag{9.127}$$

and thus we have, in the harmonic approximation, instead of Eq. (9.81)

$$\left\langle \left|h_q\right|^2 \right\rangle = \frac{T}{2\kappa q^4}, \tag{9.128}$$

$$\left\langle \left|\delta h_q\right|^2 \right\rangle = \frac{T}{\frac{1}{2}\kappa q^4 + 2\gamma}. \tag{9.129}$$

Atomistic simulations (Zakharchenko *et al.*, 2010a) give, at room temperature, $\gamma \approx 0.025\,\mathrm{eV\,Å^4}$. At

$$q < q_{\mathrm{c}} = \sqrt[4]{\frac{4\gamma}{\kappa}} \tag{9.130}$$

the correlation function (9.129) goes to a constant. In this regime, a bilayer behaves like a single membrane with bending rigidity twice as large as that for a single layer (see Eq. (9.128)). At $q > q_c$ the layers fluctuate more or less independently. The simulations (Zakharchenko *et al.*, 2010a) qualitatively confirm this simple picture; the wave length of fluctuations at which the crossover happens is about $2\pi/q^* \approx 2$ nm (at room temperature).

9.5 The self-consistent screening approximation

There are several ways to calculate the exponent η analytically, with reasonable accuracy. The simplest approximation is to rewrite Eq. (9.96) in a self-consistent way:

$$\kappa_{\mathrm{R}}(q) = \kappa + TY \sum_{\vec{k}} \frac{1}{\kappa_{\mathrm{R}}\left(\left|\vec{k}+\vec{q}\right|\right)\left|\vec{k}+\vec{q}\right|^4} \left[\frac{\left(\vec{q}\times\vec{k}\right)^2}{q^2k^2}\right]^2, \qquad (9.131)$$

assuming that the Young modulus Y is not renormalized (Nelson & Peliti, 1987). On substituting Eq. (9.100) into Eq. (9.131) we find $-\eta = \eta - 2$, or $\eta = 1$.

A more accurate result is given by the *self-consistent screening approximation* (SCSA) (Le Doussal & Radzihovsky, 1992; see also Xing *et al.*, 2003; Gazit, 2009; Zakharchenko *et al.*, 2010b; Roldán *et al.*, 2011).

The Hamiltonian (9.92) describes the self-interaction of a classical field $h(\vec{r})$ with the momentum-dependent interaction vertex $YR\left(\vec{k},\vec{k}',\vec{q}\right)$. To consider the effects of the interaction one can use a Feynman-diagram technique similar to that used in the theory of critical phenomena (Wilson & Kogut, 1974; Ma, 1976). The basic elements are the Green function $G(\vec{q})$ (solid thick line, in contrast with the solid thin line for $G_0(\vec{q})$) and the interaction vertex (a dot), see Fig. 9.5(a). The exact and bare Green functions are related by the Dyson equation (9.94), where, in the lowest order of the perturbation theory, the self-energy $\Sigma\left(\vec{k}\right)$ is given by the diagram shown in Fig. 9.5(b). Its analytic expresion corresponds to Eq. (9.96). The next step corresponds to the replacement of $G_0(\vec{q})$ by $G(\vec{q})$ (Fig. 9.5(c)), which corresponds to the equation (9.131) and gives $\eta = 1$ as discussed above.

The SCSA corresponds to the summation of 'ladder' diagrams shown in Fig. 9.5(d). This infinite summation is just a geometric progression, with the result

$$1 + \hat{A} + \hat{A}^2 + \cdots = \frac{1}{1 - \hat{A}}. \qquad (9.132)$$

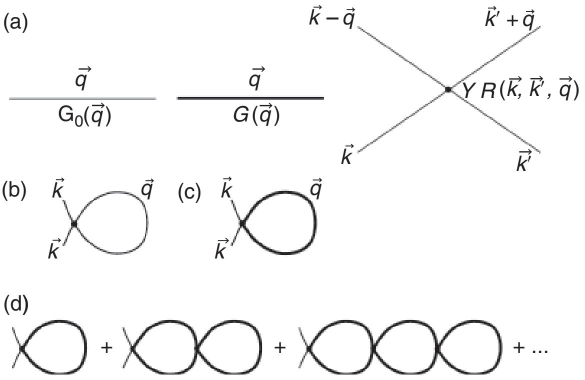

Fig. 9.5. (a) Basic elements of the diagram technique (see the text). (b) The lowest-order perturbation expression for the self-energy corresponding to Eq. (9.96). (c) The self-consistent version of the previous diagram corresponding to Eq. (9.131). (d) The diagram summation equivalent to the SCSA.

The answer is

$$\Sigma(\vec{q}) = 2\int \frac{d^2\vec{k}}{(2\pi)^2} Y_{\text{eff}}\left(\vec{k}\right)\left[\frac{\left(\vec{q}\times\vec{k}\right)^2}{k^2}\right]^2 G\left(\vec{k}-\vec{q}\right), \tag{9.133}$$

where

$$Y_{\text{eff}}\left(\vec{k}\right) = \frac{Y}{1+3YI\left(\vec{k}\right)}, \tag{9.134}$$

$$I\left(\vec{k}\right) = \frac{1}{8}\int \frac{d^2\vec{p}}{(2\pi)^2} p^2\left|\vec{k}-\vec{p}\right|^2 G(\vec{p})G\left(\vec{k}-\vec{p}\right). \tag{9.135}$$

Equations (9.134) and (9.135) describe renormalization of the Young modulus as a result of summation of the infinite series of diagrams according to Eq. (9.132).

Of course, the summation shown in Fig. 9.5(d) is not exact. This approximation was introduced by Bray (1974) in the context of the theory of critical phenomena for an n-component order parameter. It can be justified rigorously if $n \gg 1$. In our problem, the number of components of the field $h(\vec{r})$ is $n = 1$; therefore, the applicability of the SCSA is not clear. The reasonable agreement with the Monte Carlo simulations (Zakharchenko *et al.*, 2010b; see Fig. 9.4) and an explicit analysis of the higher-order diagrams (Gazit, 2009) justify it as a reasonable, relatively simple, approximation in the theory of fluctuating membranes.

Let us consider Eqs. (9.133)–(9.135) in the limit of small q, assuming that $\Sigma(q) \gg G_0^{-1}(q)$ and using Eq. (9.101) for the Green function. Thus,

$$I\left(\vec{k}\right) = \frac{A^2}{8q_0^{2\eta}} \int \frac{d^2\vec{p}}{(2\pi)^2} \frac{1}{p^{2-\eta}\left|\vec{p}-\vec{k}\right|^{2-\eta}} = \frac{A^2}{q_0^{2\eta}} \frac{1}{k^{2-2\eta}} I_1(\eta), \tag{9.136}$$

where

$$I_1(\eta) = \frac{1}{8} \int \frac{d^2\vec{x}}{(2\pi)^2} \frac{1}{x^{2-\eta}|\vec{x}-\vec{x}_0|^{2-\eta}} \tag{9.137}$$

and $\vec{x}_0 = (1, 0)$. The expression (9.136) diverges at $k \to 0$ and, therefore, one can neglect 1 in the denominator of Eq. (9.134), assuming

$$Y_{\text{eff}}\left(\vec{k}\right) \approx \frac{1}{3I\left(\vec{k}\right)} = \frac{q_0^{2\eta}}{A^2} \frac{k^{2-2\eta}}{3I_1(\eta)}. \tag{9.138}$$

On substituting Eq. (9.138) into Eq. (9.133) we have

$$\frac{q^{4-\eta} q_0^{\eta}}{A} = \frac{2q_0^{\eta} q^{4-\eta}}{3AI_1(\eta)} I_2(\eta), \tag{9.139}$$

where

$$I_2(\eta) = \int \frac{d^2\vec{x}}{(2\pi)^2} \frac{x^{2-2\eta}(\vec{x} \times \vec{x}_0)^4}{|\vec{x}-\vec{x}_0|^{4-\eta}}. \tag{9.140}$$

Equation (9.139) is satisfied at arbitrary A, and η can be found from the equation

$$I_1(\eta) = \frac{2}{3} I_2(\eta). \tag{9.141}$$

The integrals I_1 and I_2 can be expressed via a Γ-function and calculated explicitly (Le Doussal & Radzihovsky, 1992; Gazit, 2009). The answer is

$$\eta = \frac{4}{1+\sqrt{15}} \approx 0.821, \tag{9.142}$$

which is not far from the more accurate value $\eta \approx 0.85$ discussed in the previous section (Eq. (9.123)).

To find $G(q)$ for the whole range of q one needs to solve Eqs. (9.133)–(9.135) numerically (Zakharchenko *et al.*, 2010b). The results shown in Fig. 9.4 are in reasonable agreement with the Monte Carlo simulations.

Keeping in mind possible applications, it is worth mentioning that $G(q)$ for all q can be approximated as an interpolation between the high-q limit (9.81) and the low-q limit (9.101) and (9.114):

$$G_a^{-1}(q) = \frac{\kappa q^4}{T} + \left(\frac{\kappa}{T}\right)^{1-\eta/2} \frac{q_0^\eta q^{4-\eta}}{\alpha} \tag{9.143}$$

for some numerical factor α. This fitting is also shown in Fig. 9.4.

The SCSA can be used also to consider the effects of an external stress $\sigma_{\alpha\beta}^{\mathrm{ext}}$ on the properties of membranes (Roldán *et al.*, 2011). The former can be described as an additional term in Eq. (9.63):

$$F = \frac{1}{2}\int d^2x \left\{ \kappa\left(\nabla^2 h\right)^2 + \lambda(u_{\alpha\alpha})^2 + 2\mu u_{\alpha\beta}u_{\alpha\beta} + \sigma_{\alpha\beta}^{\mathrm{ext}} u_{\alpha\beta} \right\}, \tag{9.144}$$

where

$$\sigma_{\alpha\beta}^{\mathrm{ext}} = \lambda\delta_{\alpha\beta}u_{\gamma\gamma}^{\mathrm{ext}} + 2\mu u_{\alpha\beta}^{\mathrm{ext}} \tag{9.145}$$

can be expressed in terms of an *external* strain tensor $u_{\alpha\beta}^{\mathrm{ext}}$. By substituting Eq. (9.62) into Eq. (9.144) one can see that, in the harmonic approximation, the bare Green function (9.81) is modified as follows:

$$G_0(\vec{q}) = \frac{T}{q^2\left(\kappa q^2 + \lambda u_{\alpha\alpha}^{\mathrm{ext}} + 2\mu u_{\alpha\beta}^{\mathrm{ext}} q_\alpha q_\beta / |\vec{q}|^2\right)}. \tag{9.146}$$

Assuming for simplicity the case of isotropic external deformation,

$$u_{\alpha\beta}^{\mathrm{ext}} = u\delta_{\alpha\beta}, \tag{9.147}$$

we have

$$G_0(\vec{q}) = \frac{T}{q^2[\kappa q^2 + 2(\lambda+\mu)u]}, \tag{9.148}$$

where we consider only the case of expansion ($u > 0$); the effect of compression on the membrane is actually very complicated (Sharon *et al.*, 2002; Cerda & Mahadevan, 2003; Moldovan & Golubović, 1999; Brau *et al.*, 2011). One can see that flexural fluctuations are suppressed by the strain at

$$q < q_u = q_0 u^{1/2} \tag{9.149}$$

(see Eq. (9.102)). If $q_u \geq q^*$, that is,

$$u \geq 0.1\frac{T}{\kappa} \tag{9.150}$$

(see Eq. (9.98)), the anharmonic effects are assumed to be strongly suppressed, and the harmonic approximation (9.148) should work up to $q \to 0$. Numerical solutions of the SCSA equations show that actually it happens even earlier, and even deformations $u \approx 10^{\;4}\;\;10^{\;3}$ can completely suppress the anharmonic effects for the case of graphene at room temperature (Roldán *et al.*, 2011). This conclusion will be important for our discussion of the transport properties of freely suspended graphene flakes in Chapter 11.

9.6 Thermodynamic and other thermal properties of graphene

The existence of the soft acoustic flexural (ZA) mode (9.15) and the related tendency to intrinsic ripple formation is crucial to the thermodynamic properties of graphene, first of all, to its thermal expansion.

In the quasiharmonic approximation the lattice thermodynamic properties are assumed to be described by harmonic expressions but with phonon frequencies ω_λ dependent on the lattice constant. In this approximation, the thermal expansion coefficient

$$\alpha_p = \frac{1}{\Omega}\left(\frac{\partial \Omega}{\partial T}\right)_p \tag{9.151}$$

(where Ω is the volume for three-dimensional crystals and area for two-dimensional ones; p is the pressure) is given by the Grüneisen law (Vonsovsky & Katsnelson, 1989; Katsnelson & Trefilov, 2002)

$$\alpha_p = \frac{\gamma C_V(T)}{\Omega B_T}, \tag{9.152}$$

where B_T is the isothermal bulk modulus,

$$C_V(T) = \sum_\lambda C_\lambda, \tag{9.153}$$

where

$$C_\lambda = \left(\frac{h\omega_\lambda}{T}\right)^2 \frac{\exp\left(\frac{h\omega_\lambda}{T}\right)}{\left[\exp\left(\frac{h\omega_\lambda}{T}\right)\quad 1\right]^2} \tag{9.154}$$

is the constant-volume heat capacity in the harmonic approximation, and

$$\gamma = \frac{\sum_\lambda \gamma_\lambda C_\lambda}{\sum_\lambda C_\lambda} \tag{9.155}$$

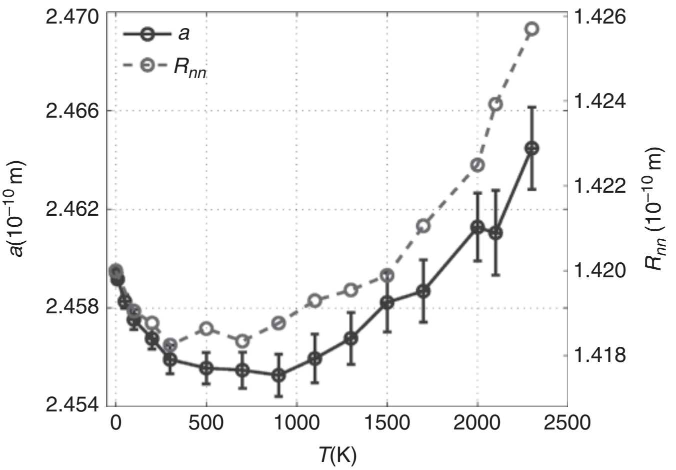

Fig. 9.6. The temperature dependence of the lattice parameter *a* (solid line) and the nearest-neighbour distance R_{nn} multiplied by $\sqrt{3}$ (dashed line) in single-layer graphene. (Reproduced with permission from Zakharchenko, Katsnelson & Fasolino, 2009.)

is the *macroscopic Grüneisen parameter*, where

$$\gamma_\lambda = \frac{\partial \ln \omega_\lambda}{\partial \ln \Omega} \tag{9.156}$$

are *microscopic Grüneisen parameters.*

Graphite is known to have a negative thermal expansion coefficient up to 700 K (Steward, Cook & Kellert, 1960). This behaviour has been explained, in terms of the Grüneisen law, by Mounet & Marzari (2005) via density-functional calculations of ω_λ and γ_λ. It turns out that the Grüneisen parameters γ_λ are negative, both in graphene and in graphite, for ZA phonons over the whole Brillouin zone. The theory explained the change in sign of α_p at $T \approx 700$ K for the case of graphite and predicted that $\alpha_p < 0$ at all temperatures for the case of graphene. Negative thermal expansion of graphene at room temperature and slightly above has been confirmed experimentally by Bao *et al.* (2009). The linear thermal expansion coefficient at these temperatures was about $10\ ^{5}\mathrm{K}\ ^{1}$, a very large negative value. According to the quasiharmonic theory of Mounet & Marzari (2005), it was supposed to be more or less constant up to temperatures of the order of at least 2000 K.

However, straightforward Monte Carlo atomistic simulation with the LCBOPII potential not assuming the quasiharmonic approximation (Zakharchenko, Katsnelson & Fasolino, 2009) gave an essentially different result (Fig. 9.6). One can see that, according to this calculation, α_p is supposed to change sign at $T \approx 700\ \ 900$ K. Very recently, it was confirmed experimentally

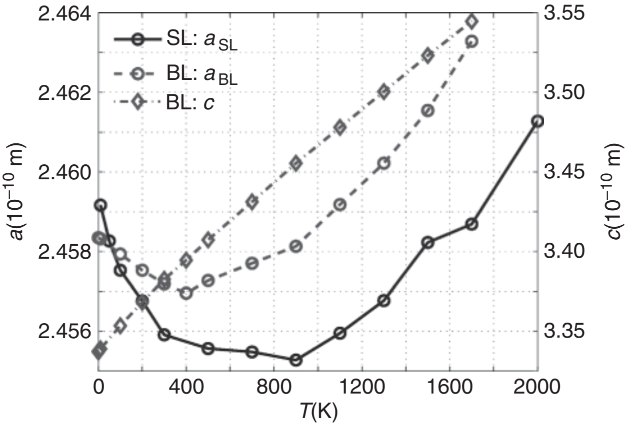

Fig. 9.7. Temperature dependences of the lattice constant a for single-layer (SL) and bilayer (BL) graphene and of the interlayer distance c in interlayer graphene. (Reproduced with permission from Zakharchenko *et al.*, 2010a.)

that α_p, while remaining negative, decreases in modulus with increasing temperature up to 400 K (Yoon, Son & Cheong, 2011). This temperature dependence of $\alpha_p(T)$, beyond the quasiharmonic approximation, is a true anharmonic effect.

Interestingly, the lattice constant a and the average nearest-neighbour distance R_{nn} exhibit different temperature dependences (see Fig. 9.6), whereas for a flat honeycomb lattice $a = \sqrt{3}R_{nn}$. These deviations clearly show that graphene at finite temperatures is not flat, due to the intrinsic ripples.

Similar calculations for the case of bilayer graphene have been performed by Zakharchenko *et al.* (2010a). The results (Fig. 9.7) show that the change of sign of da/dT happens at lower temperatures than for the case of single-layer graphene and that in this sense bilayer graphene should be similar to graphite. The thermal expansion perpendicular to the graphene plane turns out to be positive, $dc/dT > 0$.

The Lamé constants λ and μ have also been found from atomistic simulations (Zakharchenko, Katsnelson & Fasolino, 2009). The room-temperature values of the elastic constants are

$$\mu \approx 10\,\mathrm{eV}\,\mathrm{\mathring{A}}^{\;\;2}, \qquad B \approx 12\,\mathrm{eV}\,\mathrm{\mathring{A}}^{\;\;2}, \qquad \nu \approx 0.12. \tag{9.157}$$

The calculated Young modulus (9.45) lies within the error bars of the experimental value $Y \approx 340 \pm 50\,\mathrm{N\,m}^{\;\;1}$ (Lee *et al.*, 2008). Note that, per atomic layer, it is an order of magnitude higher than that of steel.

One can see that the Poisson ratio in graphene is quite small, ≈ 0.1, which means that $B \approx \mu$ and $\lambda \ll \mu$. According to the simulations

(Zakharchenko, Katsnelson & Fasolino, 2009) v decreases further with increasing temperature and becomes negative at high enough temperatures. Interestingly, the scaling theory of fluctuating membranes predicts that, due to renormalizations of $\lambda_R(q)$ and $\mu_R(q)$, at small q the Poisson ratio should be negative, tending to $\frac{1}{3}$ at $q \to 0$ (Nelson, Piran & Weinberg, 2004). Maybe atomistic simulations for finite-sized crystallites give a feeling for this tendency.

Another high-temperature anharmonic effect is the growth of the heat capacity with the temperature beyond the Dulong Petit value $3R$,

$$C_V(T) = 3R\left(1 + \frac{T}{E_0}\right) \tag{9.158}$$

(Katsnelson & Trefilov, 2002). The atomistic simulations (Zakharchenko, Katsnelson & Fasolino, 2009) confirm this behaviour, with $E_0 \approx 1.3\,\text{eV}$.

Probably the most interesting thermal property of graphene, in view of potential applications, is its extraordinarily high thermal conductivity (Balandin *et al.*, 2008; Ghosh *et al.*, 2010; Balandin, 2011). Usually, solids with high thermal conductivity are metals, and the thermal conductivity is determined by conduction electrons whereas the phonon contribution is negligible (for a general theory of phonon thermal conductivity, see Ziman, 2001). Carbon materials (diamond, nanotubes and graphene) are exceptional. Their thermal conductivity, being of phonon origin, can be higher than for any metal (for a review, see Balandin, 2011). The very general reason is the high phonon group velocity, due to the very strong chemical bonding and the relatively low mass of the carbon nucleus. Currently, graphene has the largest thermal conductivity among all known materials (Balandin *et al.*, 2008). The theory of this thermal conductivity was considered in Ghosh *et al.* (2010). It is a complicated phenomenon, which is not yet fully understood (in particular, the role of flexural phonons needs to be clarified). Its practical importance is related to the problem of heat removal in the electronics industry.

At high enough temperature, graphene is destroyed. This process was studied by atomistic Monte Carlo simulations in Zakharchenko *et al.* (2011). In these simulations the destruction was observed at about 4900 K, which makes graphene probably the most refractory material. The word ‘destruction’ is used instead of ‘melting’ to stress that it is a rather peculiar process leading to the formation of carbon chains, with these chains being strongly entangled and forming something like a polymer melt, rather than a simple liquid (Fig. 9.8).

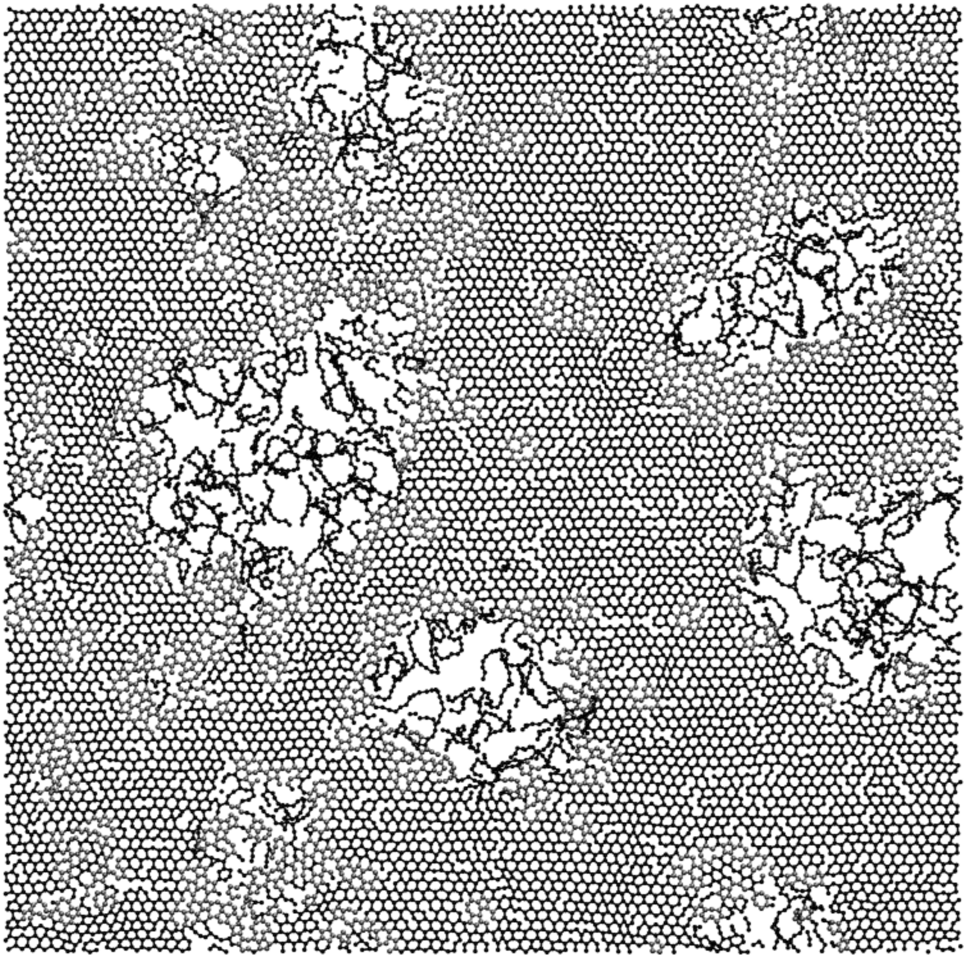

Fig. 9.8. A typical atomic configuration of graphene at $T = 5000\,\mathrm{K}$ from atomistic Monte Carlo simulations (courtesy of K. Zakharchenko).

9.7 Raman spectra of graphene

The main experimental tool allowing us to study phonon spectra throughout the Brillouin zone is inelastic neutron scattering (Vonsovsky & Katsnelson, 1989; Katsnelson & Trefilov, 2002). Unfortunately, this method is not applicable (up to now) to graphene because it requires rather massive samples. Optical tools such as infrared and Raman spectroscopy provide us with information only about phonons at some special points of the Brillouin zone. However, even this information is of crucial importance. Raman spectroscopy is one of the main techniques used in graphene physics (Ferrari *et al.*, 2006; for a review see Malard *et al.*, 2009). Here we discuss some basic ideas about Raman spectra of graphene.

The Raman effect is inelastic light scattering; ‘inelastic’ means that the frequency of the scattered light, ω', is not equal to that of the incident light, ω (Raman, 1928; Raman & Krishnan, 1928; Landsberg & Mandelstam, 1928). Its quantum explanation is based on the Kramers–Heisenberg formula for the light-scattering cross-section (Berestetskii, Lifshitz & Pitaevskii, 1971)

$$\frac{d\sigma}{do'} = \frac{\omega\omega'^3}{h^2c^4}\left|\sum_n\left\{\frac{\left(\vec{d}_{fn}\vec{e}'^*\right)\left(\vec{d}_{ni}\vec{e}\right)}{\omega_{ni}-\omega-i\delta} + \frac{\left(\vec{d}_{fn}\vec{e}\right)\left(\vec{d}_{ni}\vec{e}'^*\right)}{\omega_{ni}+\omega-i\delta}\right\}\right|^2_{\delta\to+0}, \tag{9.159}$$

where do' is the element of solid angle of scattering light, $\vec{e}$ and $\vec{e}'$ are photon polarization vectors for incident and scattered light, respectively, $|f\rangle$ and $|i\rangle$ are the final and initial states of the scattering system, respectively, $|n\rangle$ is its intermediate state, $\vec{d}_{mn}$ are matrix elements of the electric dipole momentum operator,

$$\omega_{ni} = \frac{E_n - E_i}{h} \tag{9.160}$$

and, due to the energy-conservation law,

$$\omega' = \omega + \frac{E_i - E_f}{h}. \tag{9.161}$$

The general expression (9.159) can be applied both to elastic ($\omega = \omega'$) and to inelastic ($\omega \neq \omega'$) cases; we will be interested here in the latter.

The electric dipole moment can be represented as a sum of contributions from electrons and nuclei (phonons):

$$\vec{d} = \vec{d}^{(\mathrm{e})} + \vec{d}^{(\mathrm{ph})}. \tag{9.162}$$

Correspondingly, we have the electron Raman effect when the state $|n\rangle$ corresponds to some electron excitation in the system and the phonon Raman effect when $|n\rangle$ differs from $|i\rangle$ by the creation or annihilation of a phonon with frequency ω_λ. In the latter case,

$$\omega' = \omega \pm \omega_\lambda, \tag{9.163}$$

where the + and − signs correspond to annihilation and creation of the phonon, respectively. Keeping in mind that for visual light the wave vector of a photon is much smaller than the inverse interatomic distance $1/a$ and bearing in mind also the momentum-conservation law, one can conclude that in crystals only phonons at the Γ point ($\vec{q} = 0$) can normally be probed, to leading order of perturbation, by the Raman effect. As we will see, this is not the case for graphene, however.

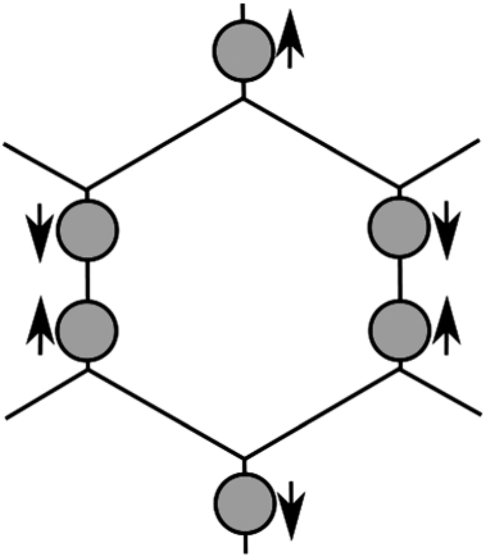

Fig. 9.9. Atomic displacements for a Raman-active optical phonon at the Γ point.

There are selection rules determining whether a given optical phonon can be Raman-active (that is, it contributes to the Raman scattering) or infrared-active (that is, it contributes to absorption of the photon), or both. In general, such analysis requires the use of group theory (Heine, 1960).

For the case of graphene, at the Γ point there are the infrared-active ZO mode and a doubly-degenerate Raman-active optical mode with deformations lying in the plane (see Fig. 9.1). The latter corresponds to the so-called E_g (*g* for *gerade*) representation of the point group of the honeycomb lattice. The atomic displacements for this mode are shown in Fig. 9.9 (the mode is doubly degenerate since there are two equivalent, mutually perpendicular, directions of the displacements). Therefore, one could expect a single line with the frequency $\omega_\lambda = |\omega' \quad \omega|$ equal to that of $\omega_{\mathrm{LO}}(\vec{q} = 0) \approx 1580\,\mathrm{cm}^{\ 1}$. Indeed, this line was observed long ago in graphite (Tuinstra & Koenig, 1970). It is called usually the *G peak*. However, the Raman spectra of graphite are characterized by the second sharp and intensive feature in Fig. 9.11 (Nemanich & Solin, 1977, 1979), which is usually called the *2D peak* in the literature on graphene. (In the literature on nanotubes and in the review by Malard *et al.* (2009), it is called the *G′peak*.) It was interpreted from the very beginning as *a two-phonon peak*; a detailed theory has been proposed by Thomsen & Reich, 2000; Maultzsch, Reich & Thomsen, 2004). The basic idea is that in this case the intermediate state $|n\rangle$ in Eq. (9.159) is a combined electron phonon excitation.

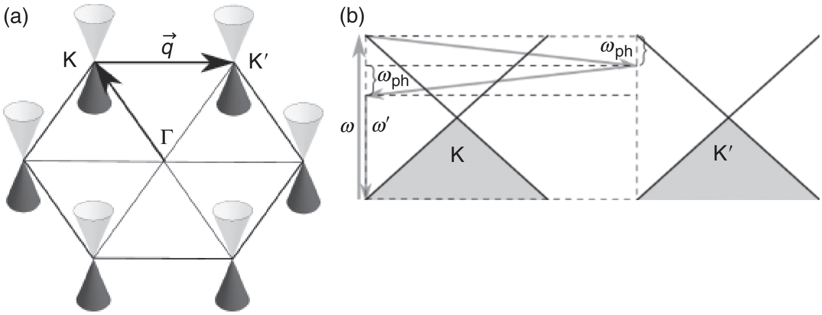

Fig. 9.10. The origin of the 2D Raman peak. (a) The scheme of momentum conservation. (b) The scheme of the energy transfer (see the text).

The basic physics originates from the existence of two valleys, K and K′; the vector $\vec{q}$ connecting K and K′ is equivalent to the vector ΓK (Fig. 9.10(a)). Therefore, the process is allowed when (i) an incident photon initiates a transition from hole to electron bands at the K point, the electron energy being E_0; (ii) the excited electron is transferred from K to K′, emitting a phonon with $\vec{q} = \vec{K}$ and frequency ω_0; (iii) it is transferred back to K′, emitting a second phonon, with $\vec{q} = \quad \vec{K}$ and the frequency ω_0; and (iv) the scattered photon is emitted from the state with $E_n = E_0 \quad 2h\omega_0$ (Fig. 9.10(b)). In this case $\omega' = \omega \quad 2\omega_0$. This is a higher-order process in the *electron phonon* coupling; however, this does not give any additional smallness since the process is resonant: the electron bands in K and K′ are identical, and we know that, for the case of perturbation of *degenerate* energy levels, the effect of the perturbation has no smallness (Landau & Lifshitz, 1977). In the electron photon interaction this is a second-order process, as is a normal Raman effect; therefore, its probability can be comparable to that of single-phonon Raman scattering.

Actually, there are several types of phonons at the K point (see Fig. 9.1); both electrons and phonons have dispersion, so the 2D peak at $\approx 2700\,\mathrm{cm}^{\quad 1}$ is not a single line, but a band (see the high-frequency peak in Fig. 9.11). Detailed study of its shape provides information about phonon dispersion near the K point (Mafra *et al.*, 2007). A theoretical analysis of the electron phonon coupling which is responsible for the 2D peak for various modes has been done by Jiang *et al.* (2005), within a tight-binding model, and by Park *et al.* (2008) using density-functional calculations. The electron phonon coupling is essentially different for different modes. Also, effects of destructive interference between contributions to the double resonance should be taken into account (Maultzsch, Reich & Thomsen, 2004). As a result of all these factors, the main contribution originates from TO phonons along the

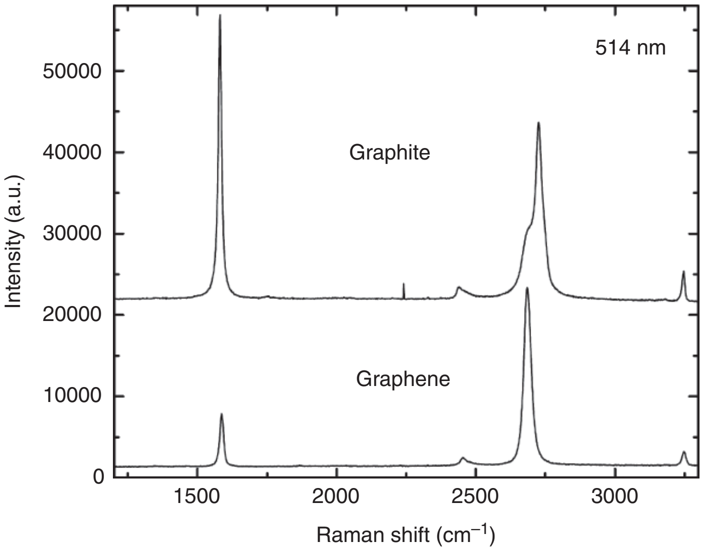

Fig. 9.11. The Raman spectra of graphite and graphene. The wavelength of the incident light is 514 nm. (Reproduced with permission from Ferrari *et al.*, 2006.)

K M direction (Mafra *et al.*, 2007). There is also a satellite line (at smaller frequencies), which originates from the processes with one TO phonon and one LA phonon involved (Mafra *et al.*, 2007).

There is a noticeable shift in position of Raman peaks between graphene and graphite (Ferrari *et al.*, 2006), see Fig. 9.11. Moreover, one can easily distinguish single-layer, bilayer, …, N-layer graphene (up to $N \approx 5$) by Raman spectroscopy, which makes it a very suitable tool for the identification of graphene.

If some defects are present, one of the phonon-induced scattering processes responsible for the 2D peak can be replaced by *elastic* scattering by the defects (the *D peak*, with the frequency $|\omega' \quad \omega| \approx \omega_0$). ‘Resonant’ impurities that change locally the sp^2 state of carbon atoms to sp^3, such as hydrogen, fluorine and C C chemical bonds (see Section 6.6), give the main contribution to the origin of this peak, and its intensity can be used to estimate the concentration of such locally modified sp^3 centres in graphene (Elias *et al.*, 2009; Nair *et al.*, 2010; Ni *et al.*, 2010).

We hope these examples suffice to illustrate the importance of Raman spectroscopy in graphene physics and chemistry.

To summarize, in this chapter we have considered some of the peculiarities of the structural state, dynamics and thermodynamics of graphene. The consequences of these peculiarities for the electronic properties of graphene will be considered in the next two chapters.

10

Gauge fields and strain engineering

10.1 Strain-induced pseudomagnetic fields

We saw in the previous chapter that graphene at finite temperatures is unavoidably corrugated. As a result, in any real atomic configuration the three bonds of each atom with its neighbours are no longer equivalent; see a snapshot from Monte Carlo simulations by Fasolino, Los & Katsnelson (2007), Fig. 10.1. Apart from atomically sharp inhomogeneities, there is a large-scale, macroscopic nonequivalence which survives in a continuum-medium description of graphene and is described in terms of the deformation tensor $u_{\alpha\beta}$.

Let us assume that the hopping parameters t_1, t_2 and t_3 are different throughout the whole sample and repeat the tight-binding derivation of the Dirac Hamiltonian (Chapter 1). As a result, instead of Eq. (1.22) we find the following effective Hamiltonian near the K point (Suzuura & Ando, 2002; Sasaki, Kawazoe & Saito, 2005; Katsnelson & Novoselov, 2007):

$$\hat{H} = \vec{\sigma}\left(-i\hbar v\vec{\nabla} - \vec{A}\right), \tag{10.1}$$

where

$$\begin{aligned} A_x &= \frac{\sqrt{3}}{2}(t_3 - t_2), \\ A_y &= \frac{1}{2}(t_2 + t_3 - 2t_1) \end{aligned} \tag{10.2}$$

play the role of components of the vector potential. Thus, the difference in t_1, t_2 and t_3 shifts the Dirac conical point in some random direction. It does not produce a mass term proportional to σ_z since the sublattices remain equivalent. The field $\vec{A}$ is a typical *gauge field* similar to the vector potential in electrodynamics. It was discussed first in the context of electron–phonon

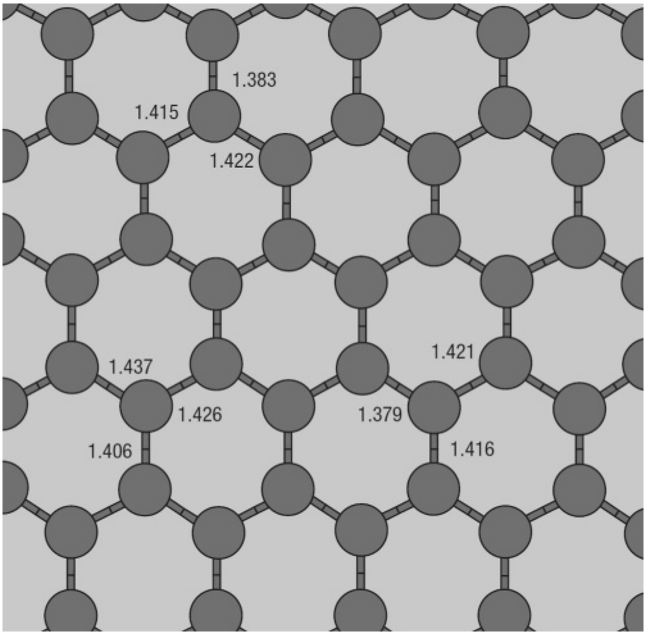

Fig. 10.1. A snapshot of a typical atomic configuration in atomistic Monte Carlo simulations of graphene at $T = 300$ K; the number indicates the bond length (Å). (Reproduced with permission from Fasolino, Los & Katsnelson, 2007.)

interaction in carbon nanotubes (Suzuura & Ando, 2002; Sasaki, Kawazoe & Saito, 2005) and then introduced in the physics of graphene by Morozov *et al.* (2006) and Morpurgo & Guinea (2006) as a mechanism suppressing weak (anti)localization. Note that the vector potential $\vec{A}$ in Eq. (10.1) has the dimension of energy; in conventional units, it should be written as $(ev/c)\vec{A}$.

In the weakly deformed lattice, assuming that the atomic displacements $\vec{u}$ are small in comparison with the interatomic distance a, the length of the nearest-neighbour vectors $\vec{\rho}_i$ will be changed by the quantity

$$\delta a_i = \sqrt{(\vec{\rho}_i + \vec{u}_i \quad \vec{u}_0)^2 \quad a} \approx \frac{\vec{\rho}_i(\vec{u}_i \quad \vec{u}_0)}{a}, \tag{10.3}$$

where $\vec{u}_i$ and $\vec{u}_0$ are displacement vectors for the corresponding atoms and we take into account that $|\vec{\rho}_i| = a$. As a result, the new hopping integrals will be

$$t_i \approx t \quad \frac{\beta t}{a^2}\vec{\rho}_i(\vec{u}_i \quad \vec{u}_0), \tag{10.4}$$

where

$$\beta = \quad \frac{\partial \ln t}{\partial \ln a} \tag{10.5}$$

is the *electron Grüneisen parameter* describing the dependence of the nearest-neighbour hopping integral on the interatomic distance. This value lies in the interval $\beta \approx 2 \quad 3$ (Heeger *et al.*, 1988; Vozmediano, Katsnelson & Guinea, 2010). In the continuum limit (elasticity theory)

$$(\vec{u}_i \quad \vec{u}_0) \sim (\vec{\rho}_i \nabla)\vec{u}(\vec{r}) \tag{10.6}$$

and, thus,

$$\begin{aligned} A_x &= c\frac{\beta t}{a}\left(u_{xx} \quad u_{yy}\right), \\ A_y &= \quad c\frac{2\beta t}{a}u_{xy} \end{aligned} \tag{10.7}$$

(Suzuura & Ando, 2002; Mañes, 2007), where c is a numerical factor depending on the detailed model of chemical bonding. In particular, one should take into account that the nearest-neighbour hopping parameter depends not only on the interatomic distance but also on the angles. Keeping in mind an uncertainty in the value of β, we will put $c = 1$ from now on.

Thus, the two components of the vector potential are proportional to the two *shear* components of the deformation tensor. On general symmetry grounds, strains should also lead to a scalar potential proportional to dilatation (Suzuura & Ando, 2002; Mañes, 2007):

$$V(\vec{r}) = g\left(u_{xx} + u_{yy}\right). \tag{10.8}$$

It originates from a redistribution of electron density under the deformation. A naïve estimation would be to assume that it should be of the order of the bandwidth, $g \approx 20\,\text{eV}$ (Ono & Sugihara, 1966; Sugihara, 1983; Suzuura & Ando, 2002). Recent density-functional calculations for single-layer graphene give a much smaller value, $g \approx 4\,\text{eV}$ (Choi, Jhi & Son, 2010). However, these two values are not actually in contradiction since the density functional takes into account the effect of electron screening, which should lead to a replacement $g \to g/\varepsilon$. Taking into account that for undoped single-layer graphene $\varepsilon \approx 4.5$ (see Eq. (7.89)), we see that *screened* $g \approx 4\,\text{eV}$ corresponds to unscreened $g_0 \approx 18\,\text{eV}$. This value seems to be in agreement with experimental data on electron mobility in freely suspended graphene (Castro *et al.*, 2010b); for more details, see Chapter 11.

Within the framework of the Dirac approximation, a uniform strain cannot open a gap in the spectrum, but leads just to a shift of conical points. However, if the strain is very strong and t_1, t_2 and t_3 are *essentially* different, the gap can be opened. As was shown by Hasegawa *et al.* (2006), there is no gap if the 'triangular inequalities'

$$|t_{l_1} - t_{l_2}| \leq |t_{l_3}| \leq |t_{l_1} + t_{l_2}| \tag{10.9}$$

are satisfied, where (l_1, l_2, l_3) is a permutation of (1, 2, 3). This issue was later studied in more detail within the framework of the tight-binding model (Pereira, Castro Neto & Peres, 2009; Pellegrino, Angilella & Pucci, 2010; Cocco, Cadelano & Colombo, 2010). According to the last of these papers, the minimum shear deformation that leads to the gap opening is about 16%. This is in principle possible in graphene without its destruction (Lee *et al.*, 2008). Henceforth we restrict ourselves to the case of smaller deformations, for which the linear approximation (10.4) is applicable. We can see in this chapter that this already provides very rich and interesting physics, with the prospect of important applications.

If the strain is not uniform the vector potential (10.7) creates, in general, a *pseudomagnetic field* (in normal units)

$$\frac{evB}{c} = \frac{\partial A_y}{\partial x} - \frac{\partial A_x}{\partial y}. \tag{10.10}$$

It is important to stress that the pseudomagnetic field acting on electrons from the valley K′ is exactly opposite to that acting on electrons from the valley K:

$$B_{\mathrm{K}} = -B_{\mathrm{K}'}. \tag{10.11}$$

This follows from explicit calculations and is obvious from the time-reversal symmetry: deformations cannot break it for the honeycomb lattice as a whole. However, if we have only smooth deformations and no scattering processes between the valleys, the electrons in a non-uniformly strained graphene will behave as if the time-reversal symmetry were broken (Morozov *et al.*, 2006; Morpurgo & Guinea, 2006). This has very important consequences for the physics of the quantum Hall effect, weak localization, etc. as will be discussed in this chapter.

10.2 Pseudomagnetic fields of frozen ripples

As the first example we consider the pseudomagnetic field created by a frozen ripple. This means that we substitute Eq. (9.62) for the deformation tensor into Eqs. (10.7) and (10.10) and take into account only the last term,

$$u_{\alpha\beta} = \frac{1}{2}\frac{\partial h}{\partial x_\alpha}\frac{\partial h}{\partial x_\beta}. \tag{10.12}$$

The effects of in-plane relaxation will be taken into account in the next section.

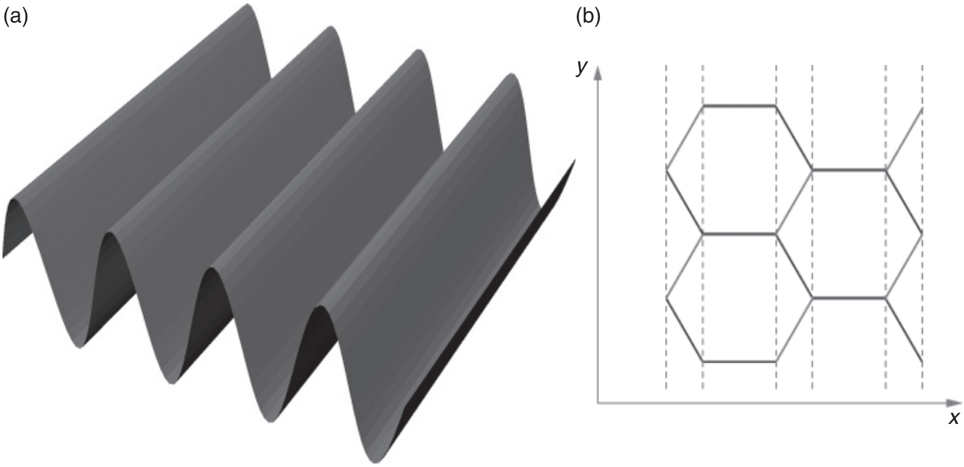

Fig. 10.2. (a) A sketch of the sinusoidal ripple. (b) Atomic rows of a honeycomb lattice. (Reproduced with permission from Guinea, Katsnelson & Vozmediano, 2008.)

Thus, the amplitude of the pseudomagnetic field can be estimated as

$$B \approx \frac{hc}{e}\frac{ah^2}{R^3}, \tag{10.13}$$

where h is the typical height of the ripple and R is its radius (Morozov *et al.*, 2006). This field can be as large as 1 T, for typical sizes of the ripples observed in exfoliated graphene (Morozov *et al.*, 2006).

To perform some quantitave analysis, let us start with the case of the simple sinusoidal deformation shown in Fig. 10.2 (Guinea, Katsnelson & Vozmediano, 2008). We will assume a modulation along the x-axis, $t_{ij} \equiv t_{ij}(x)$. Thus, the problem is effectively one-dimensional and k_y remains a good quantum number. One can consider hopping parameters between the rows (see Fig. 10.2, right panel) that are equal to t (for horizontal bonds) and

$$2t\cos\left(k_y\frac{\sqrt{3}a}{2}\right)$$

for other bonds.

If we assume a modulation of the hopping parameters,

$$t(x) = t + \delta t(x), \tag{10.14}$$

then the two hoppings are renormalized as

$$\begin{aligned} t &\to t(x), \\ 2t\cos\varphi &\to \sqrt{t^2(x)\cos^2\varphi + [\delta t(x)]^2\sin^2\varphi}, \end{aligned} \tag{10.15}$$

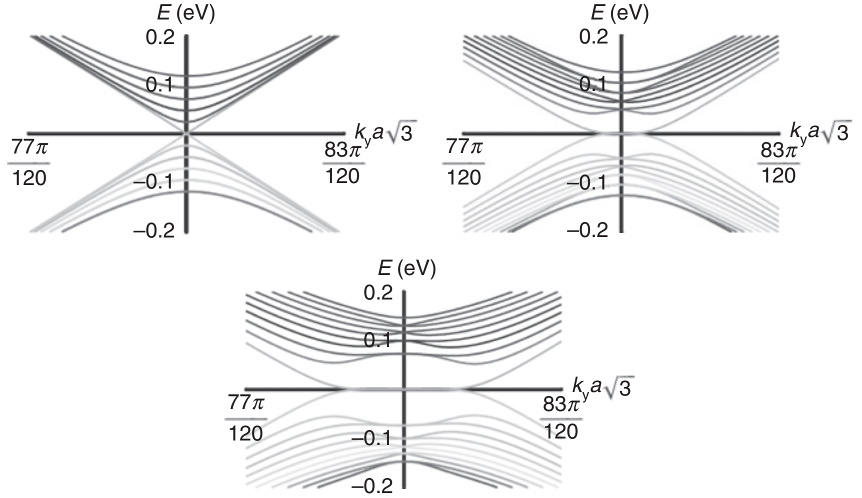

Fig. 10.3. Low-energy states induced by the ripple shown in Fig. 10.2. The average hopping is 3 eV. The width of the ripple is $1200a = 168$ nm. The modulations of the hopping $\delta t/t$ are 0, 0.02 and 0.04 (from left to right). (Reproduced with permission from Guinea, Katsnelson & Vozmediano, 2008.)

where $\varphi = k_y\sqrt{3}a/2$. Let us assume

$$\delta t(x) = \delta t \sin\left(\frac{2\pi x}{l}\right), \tag{10.16}$$

where l is the period of modulation. The electron spectrum has been calculated numerically for a strip with periodic boundary conditions; the results are shown in Fig. 10.3 (Guinea, Katsnelson & Vozmediano, 2008).

The most important result is the appearance of a dispersionless zero-energy mode, its phase volume growths with increasing $\delta t/t$. This is related to the topologically protected zero-energy Landau level in an *inhomogeneous* magnetic field for the Dirac equation (Section 2.3). There are also some features that are reminiscent of other Landau levels, but they are essentially dispersive which changes the situation dramatically from the case of a real magnetic field (but see Section 10.4). The real magnetic field B can be included in the calculations via the replacement

$$k_y \to k_y + \frac{eB}{hc}x. \tag{10.17}$$

The results are shown in Fig. 10.4 (Guinea, Katsnelson & Vozmediano, 2008). Two important features of these results should be mentioned. First, the combination of the pseudomagnetic field due to rippling and a real magnetic field leads to a broadening of all Landau levels *except* the zero-energy one; this is a consequence of the topological protection of the zero-energy Landau level. Second, due to

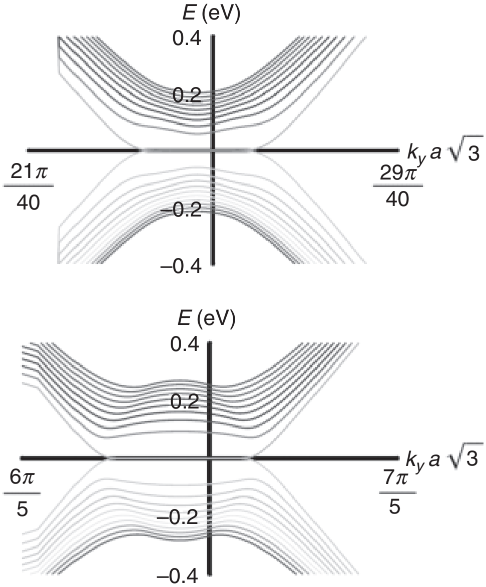

Fig. 10.4. The same as in Fig. 10.3 ($\delta t/t = 0.04$) but with a magnetic field of $B = 10\,\mathrm{T}$. Upper panel, K value; lower panel, K′ value. (Reproduced with permission from Guinea, Katsnelson & Vozmediano, 2008.)

Eq. (10.11) for the pseudomagnetic field the effective total fields acting on electrons from the valleys K and K′ are different, which results in a *valley polarization*. One can clearly see in Fig. 10.4 that the phase space of the dispersionless zero-energy level for the valley K′ is larger than that for the valley K.

The first of these conclusions seem to be relevant for the interpretation of some of the peculiarities of the quantum Hall effect in graphene (Giesbers *et al.*, 2007). The activation gaps for the quantum Hall plateau at $\nu = 2$ and $\nu = 6$ have been extracted from the temperature dependences of the resistivity $\rho_{xx}(T)$. Their dependences on the magnetic field are presented in Fig. 10.5. In the ideal case they would follow $\sqrt{B}$ dependences (see Eqs. (2.30) and (2.31)). However, due to disorder there are deviations from this law and the stronger the disorder the higher the magnetic field at which the $\sqrt{B}$ law is restored. One can see that, for $\nu = 2$, for which the zero-energy Landau level is involved, it happens much earlier than it does for $\nu = 6$. This was explained by Giesbers *et al.* (2007) by postulating that random pseudomagnetic fields created by ripples (Morozov *et al.*, 2006) contribute essentially to the broadening of all Landau levels *except* the zero-energy one, due to its topological protection (Novoselov *et al.*, 2005a; Katsnelson, 2007a). The same situation should occur also for the case of bilayer graphene (Katsnelson & Prokhorova, 2008).

The electronic structure of the frozen sinusoidal ripple has been studied by Wehling *et al.* (2008a) by carrying out density-functional calculations.

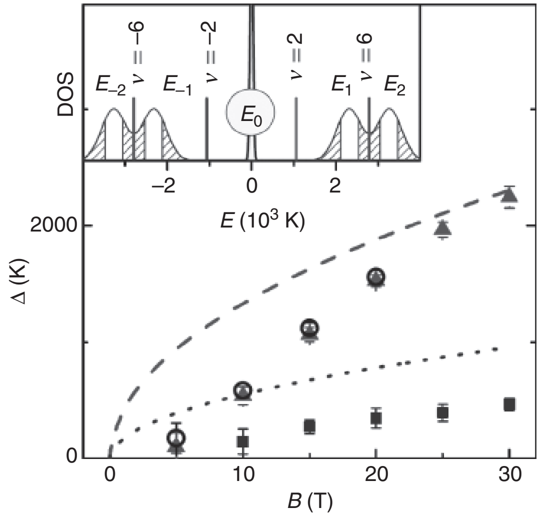

Fig. 10.5. Energy gaps 2Δ between two Landau levels extracted from the temperature dependence of the resistivity ρ_{xx} as a function of the magnetic field for $\nu = +2$ (full triangles), $\nu = -2$ (open circles) and $\nu = +6$ (full squares). The dashed and dotted lines are the theoretically expected energy gaps for sharp Landau levels. The inset shows schematically the density of states for a sharp zero-energy Landau level and broadened higher Landau levels for electrons and holes at $B = 30$ T. Extended states are represented by the white areas, localized states by the dashed areas. (Reproduced with permission from Giesbers *et al.*, 2007.)

These calculations confirm the qualitative predictions of the tight-binding model concerning the existence of zero-energy states. A schematic view of the ripple is shown in Fig. 10.6 and the results for the width of the dispersionless zero-energy mode are illustrated in Fig. 10.7. This qualitative agreement is not trivial since the tight-binding model takes into account neither next-nearest-neighbour hopping nor the *electrostatic* potential (10.8). The reason why the latter is not relevant here will be clear later (see Section 10.6).

The calculations by Wehling *et al.* (2008a) demonstrate a complete sublattice polarization for the zero-energy pseudo-Landau states. This follows from Eq. (10.11): in contrast with the usual quantum Hall effect (Sections 2.2 and 2.3), the solutions for both valleys belong to the same sublattice.

It was shown by Wehling *et al.* (2008a) that, if in-plane relaxation of atoms is allowed, the dispersionless zero-energy mode disappears for the geometry under consideration. The reason for this behaviour will be discussed in the next section.

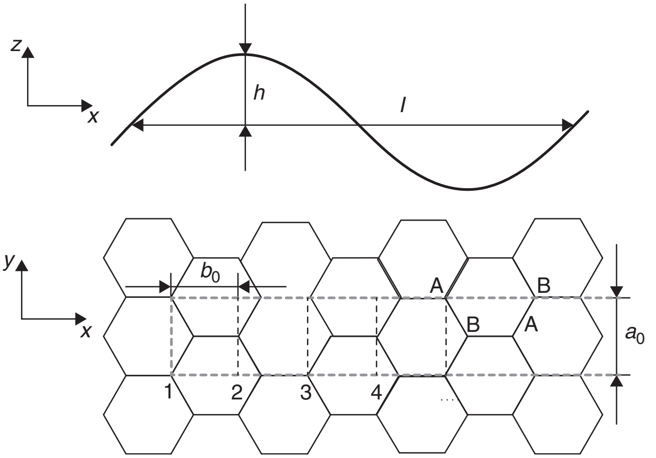

Fig. 10.6. Schematic top and side views of the ripple used in the electronic structure calculations by Wehling *et al.* (2008a).

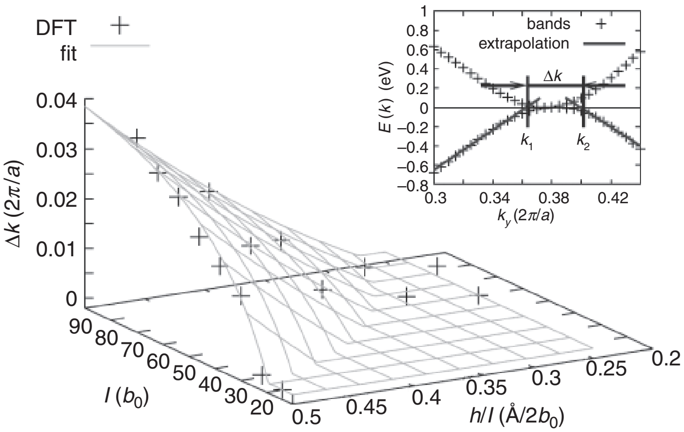

Fig. 10.7. Pseudo-Landau-level extension obtained from the density-functional calculations (DFT) by Wehling *et al.* (2008a). The definition of Δk is clear from the inset; the parameters h and l are defined in Fig. 10.6. Crosses show the fit to the expression $a\Delta k/(2\pi) = A_1(h/l)^2 - A_2/l$ with some constants A_i (courtesy of T. Wehling).

10.3 Pseudomagnetic fields of ripples: the effect of in-plane relaxation

Let us assume a fixed distribution of out-of-plane deformation $h(x, y)$. If in-plane relaxation is allowed, the in-plane deformations u_x and u_y should be found from the minimum of the total energy (9.63) and excluded (Wehling *et al.*, 2008a; Guinea, Horovitz & Le Doussal, 2008). It is convenient to use the complex-number notation, $z = x + iy$, $z^* = x \quad iy$,

$$\begin{aligned} \partial &= \frac{\partial}{\partial z} = \frac{1}{2}\left(\frac{\partial}{\partial x} \quad i\frac{\partial}{\partial y}\right), \\ \partial^* &= \frac{\partial}{\partial z^*} = \frac{1}{2}\left(\frac{\partial}{\partial x} + i\frac{\partial}{\partial y}\right), \\ \nabla^2 &= 4\,\partial\partial^* \end{aligned} \tag{10.18}$$

and

$$\begin{aligned} u(z, z^*) &= u_x \quad iu_y, \\ A(z, z^*) &= A_x \quad iA_y. \end{aligned} \tag{10.19}$$

We will express the deformation tensor via A using Eq. (10.7). As a result, the free energy (9.63) can be rewritten as (Wehling *et al.*, 2008a)

$$\begin{aligned} F &= \int d^2z \Big\{ 8\kappa(\partial\partial^* h)^2 + (\lambda+\mu)\left[\frac{1}{2}(\partial^* u + \partial^* u) + \partial h\,\partial^* h\right] \\ &\qquad + \mu\left[\partial u + (\partial h)^2\right]\left[\partial^* u^* + (\partial^* h)^2\right]\Big\} \\ &= \int d^2z \Big\{ 8\kappa(\partial\partial^* h)^2 + \frac{\mu a^2}{\beta^2 t^2} A A^* \\ &\qquad + (\lambda+\mu)\left[\frac{a}{2\beta t}\frac{1}{\partial\partial^*}\left(\partial^{*2} A + \partial^2 A^*\right) + \frac{1}{\partial\partial^*} R[h]^2\right]\Big\}, \end{aligned} \tag{10.20}$$

where

$$R[h] = \partial^2 h\,\partial^{*2} h \quad (\partial\partial^* h)^2 = \frac{\partial(\partial h, \partial^* h)}{\partial(z, z^*)} \tag{10.21}$$

is proportional to the Gaussian curvature of the surface. On minimizing Eq. (10.20) for a given $h(z, z^*)$ one finds

$$A = \quad \frac{\beta t}{a}\frac{\lambda+\mu}{\lambda+2\mu}\frac{\partial^2}{\partial\partial^*} R, \tag{10.22}$$

$$\frac{evB}{c} = \frac{i\beta t}{a}\frac{\lambda+\mu}{\lambda+2\mu}\frac{\partial^3 \quad \partial^{*3}}{(\partial\partial^*)^2} R. \tag{10.23}$$

One can see from Eqs. (10.22) and (10.23) that for the case of a free membrane both the pseudomagnetic field and the vector potential vanish identically if h depends only on one Cartesian coordinate, which means $R \equiv 0$. This is not so, as we will see in Section 10.5, if the membrane is under strain, in which case an additional term should be added to Eq. (10.20).

This explains the disappearance of zero-energy states created by a frozen sinusoidal ripple under relaxation mentioned at the end of the previous section.

If we induce the field

$$f_{\alpha\beta}(\vec r) = \frac{\partial h}{\partial x_\alpha}\frac{\partial h}{\partial x_\beta} \tag{10.24}$$

and its Fourier component

$$f_{\alpha\beta}\left(\vec k\right) = -\sum_{\vec k_1} k_{1\alpha}\left(k_\beta - k_{1\beta}\right) h_{\vec k_1} h_{\vec k - \vec k_1} \tag{10.25}$$

then the symbolic expression (10.23) can be represented in an explicit form (Guinea, Horovitz & Le Doussal, 2008)

$$\frac{eB\left(\vec k\right)}{hc} = ik_y \frac{3k_x^2 - k_y^2}{k^4}\frac{\beta}{a}\frac{\lambda+\mu}{\lambda+2\mu}\left[k_y^2 f_{xx}\left(\vec k\right) + k_x^2 f_{yy}\left(\vec k\right) - 2k_x k_y f_{xy}\left(\vec k\right)\right]. \tag{10.26}$$

This gives us a formal solution of the problem.

Importantly, Eqs. (10.23) and (10.26) reflect the trigonal symmetry of the problem: if we have an isotropic ripple, $h = h(r)$, and thus $R = R(r)$, the pseudomagnetic field will have an angular dependence

$$B(r,\varphi) = \sin(3\phi)B_0(r), \tag{10.27}$$

where ϕ is the polar angle (Wehling *et al.*, 2008a).

In the next chapter, when discussing electron scattering by the ripples we will be interested in the correlation functions of vector and scalar potentials created by the intrinsic ripples. They are proportional to

$$\begin{aligned} F_{\alpha\beta,\gamma\delta}(\vec q) &= \left\langle f_{\alpha\beta}(\vec q) f_{\gamma\delta}(-\vec q)\right\rangle \\ &= \sum_{\vec q_1 \vec q_2} q_{1\alpha}\left(q_{1\beta} - q_\beta\right) q_{2\gamma}\left(q_{2\gamma} + q_\delta\right)\left\langle h_{\vec q_1} h_{\vec q - \vec q_1} h_{-\vec q_2} h_{-\vec q - \vec q_2}\right\rangle. \end{aligned} \tag{10.28}$$

To estimate the correlation function on the right-hand side of Eq. (10.28) one can use Wick's theorem (9.110) and the results of Section 9.4. The answer is (Katsnelson, 2010b)

$$F(\vec q) \sim \begin{cases} \left(\dfrac{T}{\kappa}\right)^2 \dfrac{\ln q/q^*}{q^2}, & q > q^*, \\ \left(\dfrac{T}{\kappa}\right)^{2-\eta} \dfrac{1}{q_0^{2\eta} q^{2-2\eta}}, & q < q^*, \end{cases} \tag{10.29}$$

where q^* is the crossover wave vector (9.98). This means that the correlation function of the vector potential is singular at $q \to 0$. At the same time, the correlation function

$$\left\langle \left| B_{\vec{q}} \right|^2 \right\rangle \sim q^2 \left\langle \left| A_{\vec{q}} \right|^2 \right\rangle \tag{10.30}$$

tends to zero at $q \to 0$. Similarly to Eq. (10.27) in real space, it has the angular dependence $\sin^2(3\varphi_{\vec{q}})$, where $\varphi_{\vec{q}}$ is the polar angle of the vector $\vec{q}$ (Guinea, Horovitz & Le Doussal, 2008).

10.4 The zero-field quantum Hall effect by strain engineering

In the previous sections we discussed the gauge fields created by ripples, which are almost unavoidable in graphene. However, one can use Eqs. (10.7) and (10.10) to create intentionally a magnetic field with the desired properties, to manipulate the electronic structure of graphene via ‘strain engineering’. First of all, let us consider an opportunity to create a uniform, or almost uniform, pseudomagnetic field and thus realize Landau quantization and the quantum Hall regime without a real magnetic field (Guinea, Katsnelson & Geim, 2010; Guinea *et al.*, 2010).

Let us consider the simplest case of plane geometry, where $h = 0$ and the strain tensor is created by the u-field only. Within linear two-dimensional elasticity theory the general solution for the strain tensor can be written in terms of two arbitrary analytic functions $g(z)$ and $k(z)$, namely

$$\sigma_{xx} = \frac{\partial^2 f}{\partial y^2}, \qquad \sigma_{yy} = \frac{\partial^2 f}{\partial x^2}, \qquad \sigma_{xy} = \quad \frac{\partial^2 f}{\partial x \, \partial y}, \tag{10.31}$$

where

$$f(x, y) = \mathrm{Re}[z^* g(z) + k(z)] \tag{10.32}$$

(Landau & Lifshitz, 1970; Vozmediano, Katsnelson & Guinea, 2010). For a purely shear deformation, $\sigma_{xx} = \quad \sigma_{yy}$, which means that $g(z) = 0$. Thus, the components of the vector potential which are expressed in terms of stress as

$$\begin{aligned} A_x &= \frac{c\beta t}{a\mu}\left(\sigma_{xx} \quad \sigma_{yy}\right), \\ A_y &= \quad \frac{2c\beta t}{a\mu}\sigma_{xy} \end{aligned} \tag{10.33}$$

are proportional to the real and imaginary parts of $d^2 k(z)/dz^2$, respectively, and

$$B \sim \operatorname{Im} \frac{d^3 k(z)}{dz^3}. \tag{10.34}$$

A pure shear deformation that leads to a uniform pseudomagnetic field is

$$k(z) = Az^3 \tag{10.35}$$

(A is a constant). The general deformation (including dilatation) which leads to a uniform pseudomagnetic field is determined by the function

$$f(z) = Az^3 + Bz^* z^2 \tag{10.36}$$

(A and B are constants). It corresponds to the strain tensor linearly dependent on coordinates,

$$u_{\alpha\beta} = \frac{u}{L} x_\alpha e_\beta, \tag{10.37}$$

where u is a typical stress, L is the sample size and $\vec{e}$ is an arbitrary unit vector. The effective pseudomagnetic field is associated with a magnetic length

$$\frac{1}{l_B^2} = \frac{eB}{\hbar c} \approx \frac{\beta u}{aL}. \tag{10.38}$$

For $u = 10^{-2}$ and $L \approx 10\,\mu\text{m}$ we obtain $l_B \approx 0.2\,\mu\text{m}$, which corresponds to a magnetic field of about 0.3 T. Actually, much higher deformations and, thus, much higher pseudomagnetic fields can be created in graphene.

In reality, the stress can be applied only normally to the boundary of a sample. Let the boundary have an equation in polar coordinates $r = r(\varphi)$, with the normal vector $(n_x(\varphi), n_y(\varphi))$. The condition that the applied forces are normal to the boundary means that

$$\begin{aligned} \sigma_{xx} n_x + \sigma_{xy} n_y &= a(\varphi) n_x, \\ \sigma_{xy} n_x + \sigma_{yy} n_y &= a(\varphi) n_y \end{aligned} \tag{10.39}$$

with some unknown function $a(\varphi)$. These equations have a solution if

$$(\sigma_{xx} - a)(\sigma_{yy} - a) - \sigma_{xy}^2 = 0. \tag{10.40}$$

At the same time, the general solution (10.31) and (10.32) can be written, with a proper choice of coordinates, as

$$\begin{aligned} \sigma_{xx} = -\sigma_{yy} &= Ay, \\ \sigma_{xy} &= Ax. \end{aligned} \tag{10.41}$$

On substituting Eq. (10.41) into Eq. (10.40) we find

$$a(\varphi) = \pm A r(\varphi). \tag{10.42}$$

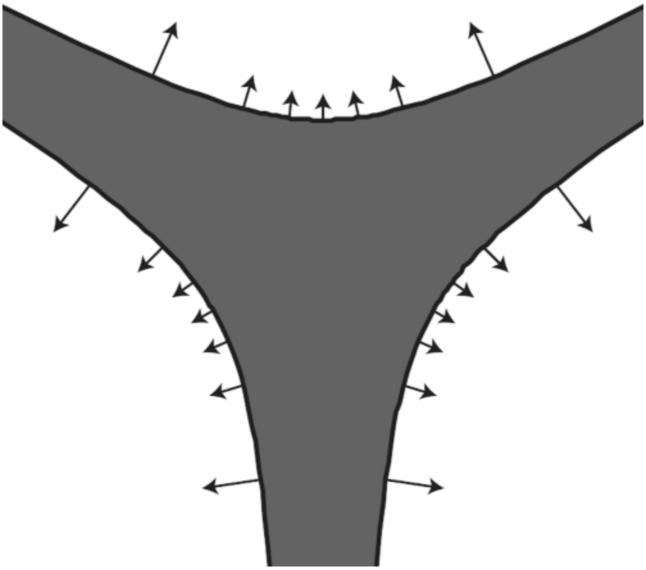

Fig. 10.8. The shape given by Eq. (10.46) with normal stress given by Eqs. (10.41) and (10.42). (Reproduced with permission from Guinea, Katsnelson & Geim, 2010.)

It follows from Eq. (10.39) that

$$\frac{n_x}{n_y} = \frac{\pm r + y}{x} = \frac{\pm 1 + \sin\varphi}{\cos\varphi} \tag{10.43}$$

and, at the same time,

$$\frac{n_x}{n_y} = \frac{dy}{dx}. \tag{10.44}$$

Coming back to the polar coordinates, we find the following equation for the required shape:

$$\frac{d\ln r}{d\varphi} = \frac{\sin\varphi \mp \cos(2\varphi)}{\cos\varphi \pm \sin(2\varphi)}, \tag{10.45}$$

with the solution

$$r(\varphi) = \frac{\text{constant}}{[(\cos(\varphi/2) \mp \sin(\varphi/2))(\pm 1 + 2\sin\varphi)]^{2/3}} \tag{10.46}$$

(Guinea, Katsnelson & Geim, 2010). This shape is shown in Fig. 10.8. It is the only one which allows us to have an exactly uniform pseudomagnetic field.

Fortunately, numerical solutions of the equations of the theory of elasticity show that it is not difficult to have a *quasi*-uniform pseudomagnetic field in much more general and more realistic situations; what is really important is to

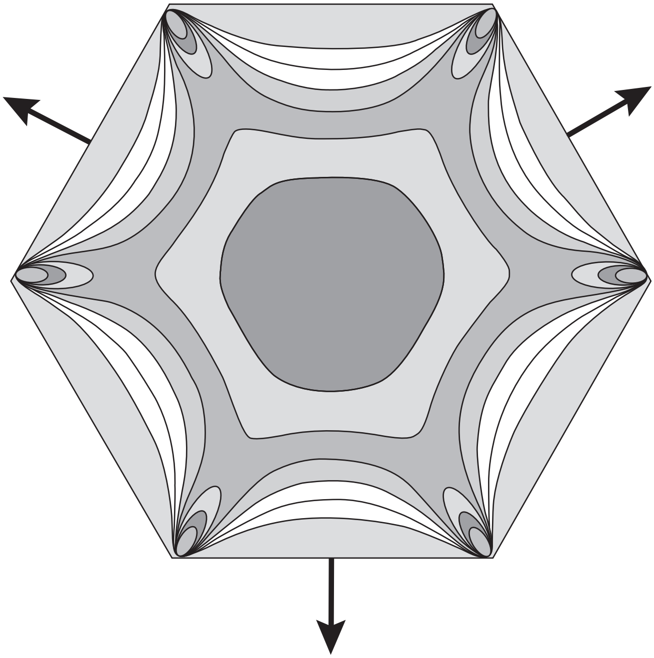

Fig. 10.9. A pseudomagnetic field in a hexagon of a size 1.4 μm that is strained by the forces applied to three sides. The maximum strain of 20% creates an effective field of about 10 T at the hexagon's centre. The counters correspond to 8, 6, 4, 2, 0 and –2 T, from inside to outside. (Reproduced with permission from Guinea, Katsnelson & Geim, 2010.)

keep the trigonal symmetry of the stress (Guinea, Katsnelson & Geim, 2010; Guinea *et al.*, 2010). One can show also that the presence of dilatation and, thus, of an electrostatic potential (10.8) does not affect the results (Guinea *et al.*, 2010). As an example, we present here the results obtained by Guinea, Katsnelson & Geim (2010) for a hexagonal flake with external forces applied to three edges (Fig. 10.9). One can see that the value of the pseudomagnetic field in the central part of the flake is uniform to high accuracy. As a result, the density of states averaged over the central region clearly exhibits pronounced Landau levels (Fig.10.10).

It was suggested by Guinea, Katsnelson & Geim (2010) that one should use electron Raman scattering to observe the Landau levels created by strain. Soon after that, this effect was observed by scanning tunnelling microscopy for graphene bubbles on a platinum surface (Levy *et al.*, 2010). It is significant that these bubbles have a shape with trigonal symmetry. The value of the pseudomagnetic field created by spontaneous deformation in these bubbles was estimated by Levy *et al.* (2010) to be approximately 300 T, which is much higher than any real magnetic field attainable to date.

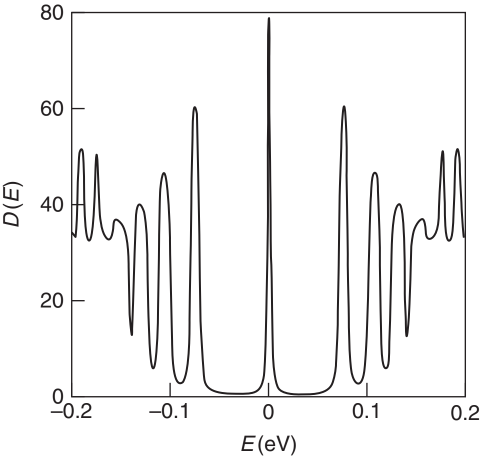

Fig. 10.10. The average density of states in the central region of diameter 0.5 μm for the hexagon shown in Fig. 10.9. (Reproduced with permission from Guinea, Katsnelson & Geim, 2010.)

Owing to the condition (10.11), the system as a whole remains time-reversal-invariant, and, due to the Onsager relations (Zubarev, 1974), one should have $\sigma_{xy} = 0$ (here σ is the conductivity, not the stress!). In terms of edge states (Section 5.8) this results from the existence of two counter-propagating edge states, from values K and K′, without total charge transfer. This situation can be described as a 'valley quantum Hall effect' analogous to the spin quantum Hall effect (Kane & Mele, 2005a, 2005b). Inhomogeneities at the edges will lead to a scattering between the valleys; however, one can show that, due to the smallness of the parameter a/l_B, the mixture of the counter-propagating edge states can be very small (Guinea, Katsnelson & Geim, 2010).

10.5 The pseudo-Aharonov–Bohm effect and transport gap in suspended graphene

As the next example, we consider the pseudomagnetic field arising in a freely suspended graphene membrane (Fogler, Guinea & Katsnelson, 2008). If it is charged, with the electron density n, the electrostatic pressure acts on the membrane (Jackson, 1962),

$$p = \frac{2\pi e^2}{\varepsilon} n^2, \tag{10.47}$$

where ε is the dielectric constant. Under this pressure, the membrane will be bent (Fig. 10.11), with the equation of equilibrium

$$\kappa \frac{d^4 h(x)}{dx^4} \quad \tau \frac{d^2 h}{dx^2} = p, \tag{10.48}$$

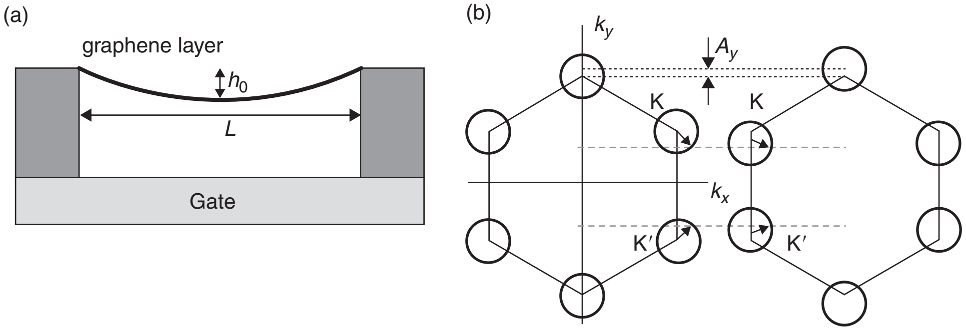

Fig. 10.11. (a) A sketch of the model of a suspended graphene membrane under consideration (see the text). (b) Fermi-circle positions in the Brillouin zone in the leads (left) and in the suspended region (right). (Reproduced with permission from Fogler, Guinea & Katsnelson, 2008.)

where τ is the external strain (this follows from the minimization of the total energy (9.144) in the presence of an external strain, $\sigma_{xx}^{\text{ext}} = \tau$, and u_{xx} is given by Eq. (10.12)). If we assume that the membrane is supported at $x = \pm L/2$ then the solution of Eq. (10.48) satisfying the boundary conditions is (Timoshenko & Woinowsky-Krieger, 1959)

$$h(x) = \frac{pL^4}{16u^4\kappa}\left[\frac{\cosh(2ux/L)}{\cosh u} - 1\right] + \frac{pL^2\left(L^2/4 - x^2\right)}{8u^2\kappa}, \tag{10.49}$$

$$u^2 = \frac{\tau l^2}{4\kappa}. \tag{10.50}$$

The strain has to be found self-consistently, as

$$\tau = \tau_0 + Y \int_{-L/2}^{L/2} dx\, u_{xx} = \tau_0 + \frac{Y}{2L} \int_{-L/2}^{L/2} dx \left(\frac{dh}{dx}\right)^2, \tag{10.51}$$

where τ_0 is an external strain of non-electrostatic origin. First we will assume, for simplicity, that $\tau_0 = 0$ and

$$n \gg \sqrt{\frac{\varepsilon\kappa}{e^2L^3}}, \tag{10.52}$$

which gives us $u \gg 1$. In this regime only the last term on the right-hand side of Eq. (10.49) survives, and the profile $h(x)$ is represented by a simple parabola:

$$h(x) = h_0\left(1 - \frac{4x^2}{L^2}\right), \tag{10.53}$$

where

$$h_0 = \left(\frac{3\pi}{64}\frac{e^2}{\varepsilon Y}n^2L^4\right)^{1/3} \tag{10.54}$$

and

$$\tau = \frac{pL^2}{8h_0} = \frac{\pi e^2 n^2 L}{4\varepsilon h_0}. \tag{10.55}$$

The deformation u_{xx} creates the vector potential. Its effect is largest if the zigzag direction is along the y-axis (this means a change of coordinates in comparison with Eq. (10.7)), thus

$$A_x = 0, \qquad A_y = \pm\frac{\beta t}{a}u_{xx}, \tag{10.56}$$

where the signs ± correspond to the valleys K and K′, respectively. Thus, the conical points will be shifted, inside the membrane, in the y-direction (see Fig. 10.11(b)). If this shift is larger than the Fermi wave vector k_{F}, that is,

$$k_{\mathrm{F}} < \frac{|A_y|}{hv}, \tag{10.57}$$

the matching of wave functions in the leads and in the membrane becomes impossible, and the transport though the membrane will be totally suppressed; that is, the transport gap will be open. Here we assume, for simplicity, that the concentrations of charge carriers for the leads and membrane are the same.

To proceed further, let us replace the deformation u_{xx} in Eq. (10.56) by its average value,

$$u_{xx} = \frac{\tau}{Y}. \tag{10.58}$$

Thus, taking into account Eqs. (10.54) (10.56), we have an estimation

$$\frac{|A_y|}{hv} \approx \left(\frac{e^2}{Y\varepsilon}\right)^{2/3} n^{4/3}L\ ^{1/3} \approx \frac{a^2 n^{4/3}L\ ^{1/3}}{\varepsilon^{2/3}}. \tag{10.59}$$

Keeping in mind that $k_{\mathrm{F}} \sim n^{1/2}$, we see that, if all of the strain is purely electrostatic, the condition (10.57) is not satisfied and the gap never opens. However, it can be open (and will certainly be open, if n is small enough) if $\tau_0 \neq 0$ in Eq. (10.51). This gap opening is an effect of the vector potential itself, not of the pseudomagnetic field, and takes place even if the vector potential is constant: $A_y = \text{constant}$, $B = 0$. Therefore, it can be considered to be an analogue of the Aharonov Bohm effect for pseudomagnetic fields.

The scattering problem can be solved exactly if one assumes, for simplicity, $A_y = \text{constant}$. The calculations are absolutely similar to those in Chapters 3 and 4. We assume (as has already been mentioned) that we have the same value of k_F in the leads and in the membrane. This means that the y-component of the wave vector in the leads is

$$k_y = k_\mathrm{F} \sin \varphi \tag{10.60}$$

(φ is the incidence angle) and within the membrane it is replaced by

$$k_y \to k_y \quad q \equiv k_y \quad \frac{A_y}{hv}. \tag{10.61}$$

The transmission coefficient is (Fogler, Guinea & Katsnelson, 2008)

$$T(k_y) = \frac{k_1^2 k_2^2}{k_1^2 k_2^2 + k_\mathrm{F}^2 q^2 \sin^2(k_2 L)}, \tag{10.62}$$

where

$$\begin{aligned} k_1 &= \sqrt{k_\mathrm{F}^2 \quad k_y^2} = k_\mathrm{F} \cos \varphi, \\ k_2 &= \sqrt{k_\mathrm{F}^2 \quad (k_y \quad q)^2}. \end{aligned} \tag{10.63}$$

The total conductance can be calculated, using the Landauer formula, as

$$G = \frac{4e^2}{h} W \int_{k_\mathrm{F}}^{k_\mathrm{F}} \frac{dk_y}{2\pi} T(k_y), \tag{10.64}$$

where W is the width of the membrane.

Pereira and Castro Neto (2009) have suggested that one could use this effect for *strain engineering*: by applying some external strain distribution to graphene one can create a desirable distribution of the vector potential and thereby manipulate the electronic transport through graphene. This type of strain engineering is different from that considered in the previous section since no real gaps due to Landau quantization are required, *transport* gaps due to the 'pseudo-Aharonov Bohm effect' suffice.

10.6 Gap opening by combination of strain and electric field

Let us consider now the case of *coexistence* of pseudomagnetic fields and electrostatic potential. We will assume that all these perturbations are smooth and therefore the intervalley scattering can be neglected. Thus, the Hamiltonian of the system is

$$\hat{H} = \hat{H}_0 + \hat{H}_A + \hat{H}_V, \tag{10.65}$$

where

$$\begin{aligned}\hat{H} &= \quad ih v \hat{\vec{\sigma}}\,\vec{\nabla},\\ \hat{H}_A &= \quad \hat{\sigma}_x A_x(\vec{r}) \quad \hat{\sigma}_y A_y(\vec{r}),\\ \hat{H}_V &= V(\vec{r}).\end{aligned}$$

We will assume that both perturbations are weak and use the perturbation theory for the Green function:

$$\hat{G} = \frac{1}{E \quad \hat{H} + i\delta} \tag{10.66}$$

(cf. Sections 4.2 and 6.4). We can formally write the answer via the Dyson equation,

$$\hat{G} = \frac{1}{E \quad \hat{H}_0 \quad \hat{\Sigma}(E)}, \tag{10.67}$$

where $\hat{\Sigma}(E)$ is the self-energy operator, which can be written as a perturbation series

$$\hat{\Sigma}(E) = \hat{H}_A + \hat{H}_V + \left(\hat{H}_A + \hat{H}_V\right)\hat{G}_0\left(\hat{H}_A + \hat{H}_V\right) + \cdots, \tag{10.68}$$

where $\hat{G}_0$ is the Green function of the Hamiltonian $\hat{H}_0$, Eqs. (4.35) and (4.36). Both $\hat{G}_0$ and $\hat{H}_A$ contain terms proportional to $\hat{\sigma}_x$ and $\hat{\sigma}_y$, and their product can generate $\hat{\sigma}_z$, that is, the mass term:

$$\hat{\sigma}_x\hat{\sigma}_y = \quad \hat{\sigma}_y\hat{\sigma}_x = i\hat{\sigma}_z. \tag{10.69}$$

In the lowest order, such terms originate from the term linear in $\hat{H}_A$ and linear in $\hat{G}_0$. It is also linear in $\hat{H}_V$. This cross-term has the form

$$\begin{aligned}\hat{\vec{\Sigma}}_0(E) &= \hat{H}_V \frac{1}{E \quad \hat{H}_0 + i\delta}\hat{H}_A + \hat{H}_A \frac{1}{E \quad \hat{H}_0 + i\delta}\hat{H}_V\\ &= \hat{H}_V\left(E \quad \hat{H}_0\right)\frac{1}{(E+i\delta)^2 \quad \hat{H}_0^2}\hat{H}_A\\ &\quad + \hat{H}_A\left(E \quad \hat{H}_0\right)\frac{1}{(E+i\delta)^2 \quad \hat{H}_0^2}\hat{H}_V.\end{aligned} \tag{10.70}$$

Perturbatively, the correction to the effective Hamiltonian is $\hat{\Sigma}\left(\vec{k},\vec{k},E\right)$ (the self-energy depends on two wave vectors since the Hamiltonian (10.65) is not translationally invariant but we need only terms diagonal in $\vec{k}$). The second-order correction containing the mass term is

$$\hat{\Sigma}^{(2)}\left(\vec{k},\vec{k},E\right) = \sum_{\vec{k}'} \hat{W}_{\vec{k}\quad\vec{k}'}\hat{G}_0\left(\vec{k}',E\right)\hat{W}_{\vec{k}'\quad\vec{k}}, \tag{10.71}$$

where

$$\hat{W}_{\vec{q}} = V_{\vec{q}} + \hat{\vec{\sigma}}\vec{A}_{\vec{q}} \tag{10.72}$$

and $\hat{G}_0$ is given by Eq. (4.36). We are interested in the gap opening at the neutrality point and thus should put $E=0$. By substituting Eq. (4.36) into Eq. (10.71) we find

$$\hat{\Sigma}^{(2)}\left(\vec{k},\vec{k},0\right) = \frac{1}{hv}\sum_{\vec{q}} \hat{W}_{\vec{k}-\vec{q}} \frac{\vec{q}\hat{\vec{\sigma}}}{q^2} \hat{W}_{\vec{q}-\vec{k}}. \tag{10.73}$$

Since

$$\hat{W}\hat{\sigma}_\alpha = V\hat{\sigma}_\alpha + A^\alpha + i\varepsilon_{\beta\alpha\gamma}A^\beta\hat{\sigma}_\gamma \tag{10.74}$$

the expression (10.73) contains the gap term, $\Delta\hat{\sigma}_z$, where

$$\Delta_{\vec{k}} = \frac{2}{hv}\sum_{\vec{q}} \frac{\mathrm{Im}\left[V_{\vec{k}-\vec{q}}\left(q_x A^y_{\vec{q}-\vec{k}} - q_y A^x_{\vec{q}-\vec{k}}\right)\right]}{q^2}. \tag{10.75}$$

At $\vec{k}=0$, it can be expressed in terms of the Fourier component of the pseudomagnetic field,

$$B_{\vec{k}} = k_x A^y_{\vec{k}} - k_y A^x_{\vec{k}}, \tag{10.76}$$

namely

$$\Delta_{\vec{k}=0} = \frac{2}{hv}\sum_{\vec{q}} \frac{\mathrm{Im}\left[V_{-\vec{q}}B_{\vec{q}}\right]}{q^2} \tag{10.77}$$

(Low, Guinea & Katsnelson, 2011).

Before discussing this expression we derive an important result for $\partial\hat{\Sigma}/\partial E$. It follows from Eqs. (10.73) and (4.36) that

$$\left.\frac{\partial\Sigma^{(2)}\left(\vec{k},\vec{k},E\right)}{\partial E}\right|_{E=0} = \sum_{\vec{q}} \frac{\hat{W}_{\vec{k}-\vec{q}}\hat{W}_{\vec{q}-\vec{k}}}{(hvq)^2}. \tag{10.78}$$

The integral (10.78) contains an infrared divergence at $q \to 0$, which should be cut, at some $q_{\min}$. The result is

$$\left.\frac{\partial\Sigma^{(2)}\left(\vec{k},\vec{k},E\right)}{\partial E}\right|_{E=0} \approx \frac{|\ln(q_{\min}a)|}{2\pi(hv)^2}\hat{W}_{\vec{k}}\hat{W}_{-\vec{k}}. \tag{10.79}$$

This divergence is very important for the theory of electron transport in graphene, as will be discussed in the next chapter.

It follows from Eq. (10.77) that the gap is determined by correlations between the electrostatic potential and the pseudomagnetic field. Let us characterize these correlations by a parameter

$$C = \lim_{\vec{k} \to 0} (BV)_{\vec{k}}, \tag{10.80}$$

which has the dimension of energy. It is roughly given by the value of the electrostatic potential times the number of flux quanta of the pseudomagnetic field over the region where the field and the electrostatic potential are correlated. The gap can be estimated, according to Eq. (10.77), as

$$\Delta \approx C |\ln(q_{\min} a)|. \tag{10.81}$$

The minimal value of q in pure graphene is determined by the gap itself,

$$q_{\min} \approx \frac{\Delta}{hv}, \tag{10.82}$$

so Eq. (10.81) is an equation for Δ. In dirty samples, the cut-off is determined by disorder.

Since the ripples create both an electrostatic potential and a vector potential it is natural to ask whether this effect can result in gap opening or not. To check this, we will use the expression for the deformation tensor created by ripples with the in-plane relaxation taken into account (Guinea, Horowitz & Le Doussal, 2008):

$$u_{\alpha\beta}\left(\vec{k}\right) = \left[\frac{\left|\vec{k}\right|^2}{2}\delta_{\alpha\beta} \quad \frac{\lambda+\mu}{\lambda+2\mu}k_\alpha k_\beta\right] \frac{k_x^2 f_{yy}\left(\vec{k}\right) + k_y^2 f_{xx}\left(\vec{k}\right) \quad 2k_x k_y f_{xy}\left(\vec{k}\right)}{\left|\vec{k}\right|^4} \tag{10.83}$$

(cf. Eq. (10.26) for the magnetic field). On substituting Eqs. (10.83), (10.7) and (10.8) into Eq. (10.77) we obtain (Low, Guinea & Katsnelson, 2011)

$$\Delta = g_1 \frac{\beta}{\alpha} \frac{\mu(\lambda+\mu)}{(\lambda+2\mu)^2} \sum_{\vec{k}} \frac{\left| k_x^2 f_{yy}\left(\vec{k}\right) + k_y^2 f_{xx}\left(\vec{k}\right) \quad 2k_x k_y f_{xy}\left(\vec{k}\right)\right|^2}{\left|\vec{k}\right|^4} \cos\left(3\varphi_{\vec{k}}\right), \tag{10.84}$$

where $\varphi_{\vec{k}}$ is the polar angle of the vector $\vec{k}$. This expression is zero since on making the replacement $\vec{k} \to \quad \vec{k}$ the cosine changes sign ($\varphi_{\quad \vec{k}} = \pi + \varphi_{\vec{k}}$) and $f_{\alpha\beta}(\quad \vec{k}) = f_{\alpha\beta}{}^*(\vec{k})$ (since the expression (10.24) is real). This means that, while the scalar and vector potentials originate from the same deformations, the gap is not open. To achieve gap opening one needs to apply an inhomogeneous electrostatic potential, *together* with strains. Some specific devices of such a kind were considered by Low, Guinea & Katsnelson (2011). Under some quite realistic assumptions about parameters of the devices, a gap of the order of 0.1 eV can reasonably be expected. In general, this direction in strain engineering looks quite promising.

In this chapter we have considered only the simplest gauge field, that is, a pseudomagnetic one, which can be created by smooth deformations. Topological defects in graphene such as dislocations and disclinations can create *non-Abelian* gauge fields acting on two valleys. This issue and more formal aspects of gauge fields in graphene are reviewed by Vozmediano, Katsnelson & Guinea (2010).

11

Scattering mechanisms and transport properties

11.1 The semiclassical Boltzmann equation and limits of its applicability

The conventional theory of electronic transport in metals and semiconductors (Ziman, 2001) is based on the *Boltzmann equation* (or kinetic equation) for the *distribution function* $f\left(\vec{k}, \vec{r}, t\right)$, which is nothing other than a probability density in the single-electron phase space (instead of the canonical variables $\vec{p}$ and $\vec{r}$ we will use $\vec{k}$ and $\vec{r}$, $\vec{k} = \vec{p}/h$). It has the form (Ziman, 2001; Abrikosov, 1988; Vonsovsky & Katsnelson, 1989; Lifshitz, Azbel & Kaganov, 1973)

$$\frac{\partial f}{\partial t} + \dot{\vec{k}} \nabla_{\vec{k}} f + \dot{\vec{r}} \nabla_{\vec{r}} f = I_{\vec{k}}[f], \tag{11.1}$$

where $\dot{\vec{k}}$ and $\dot{\vec{r}}$ are determined by the canonical equations of motion

$$h\dot{\vec{k}} = e\left(\vec{E} + \frac{1}{c}\vec{v}_{\vec{k}} \times \vec{B}\right), \tag{11.2}$$

$$\dot{\vec{r}} = \vec{v}_{\vec{k}} = \frac{1}{h}\frac{\partial \varepsilon\left(\vec{k}\right)}{\partial \vec{k}}, \tag{11.3}$$

where $\varepsilon\left(\vec{k}\right)$ is the band dispersion and $\vec{E}$ and $\vec{B}$ are the electric and magnetic fields. The right-hand side of Eq. (11.1) is called the *collision integral.* If we neglect electron electron scattering processes and assume that there is only elastic scattering by some external (with respect to the electron subsystem) sources the collision integral takes the form

$$I_{\vec{k}}[f] = \sum_{\vec{k}'} w\left(\vec{k}, \vec{k}'\right)\left[f_{\vec{k}'}\left(1 - f_{\vec{k}}\right) - f_{\vec{k}}\left(1 - f_{\vec{k}'}\right)\right] = \sum_{\vec{k}'} w\left(\vec{k}, \vec{k}'\right)\left(f_{\vec{k}'} - f_{\vec{k}}\right), \tag{11.4}$$

where $w\left(\vec{k}, \vec{k}'\right)$ is the quantum-mechanical scattering probability and the factors (1 f) in Eq. (11.4) take into account the Pauli principle forbidding scattering into occupied states. One can see, however, that these factors are not essential. If the scattering Hamiltonian has the form

$$\hat{H}' = \sum_{\vec{k}\vec{k}'} V_{\vec{k}\vec{k}'} \hat{c}^{+}_{\vec{k}} \hat{c}_{\vec{k}'} \tag{11.5}$$

then, in the Born approximation, according to ‘Fermi’s golden rule’,

$$w\left(\vec{k}, \vec{k}'\right) = \frac{2\pi}{h} \left\langle \left| V_{\vec{k}\vec{k}'} \right|^2 \right\rangle \delta\left(\varepsilon_{\vec{k}} - \varepsilon_{\vec{k}'}\right) \tag{11.6}$$

(angular brackets denote the average over the states of the scatterers). Note that in this approximation $w(\vec{k}, \vec{k}') = w(\vec{k}', \vec{k})$, which is already taken into account in Eq. (11.4). For simplicity, we omit spin indices and do not take into account summation over them; otherwise, the right-hand side of Eq. (11.4) should be multiplied by 2, the spin degeneracy factor.

We will consider here only a linear response, assuming that the external electric field $\vec{E}$ is small enough. Then,

$$f_{\vec{k}}(\vec{r}, t) = f_0\left(\varepsilon_{\vec{k}}\right) + \delta f_{\vec{k}}(\vec{r}, t), \tag{11.7}$$

where $f_0(\varepsilon)$ is the Fermi–Dirac distribution function, and we need to take into account only linear terms in Eq. (11.1). Then, the collision integral is

$$I_{\vec{k}}[f] = \sum_{\vec{k}'} w\left(\vec{k}, \vec{k}'\right)\left(\delta f_{\vec{k}'} - \delta f_{\vec{k}}\right). \tag{11.8}$$

The current and the perturbation of the electron charge density can be calculated as

$$\vec{j}(\vec{r}, t) = e \sum_{\vec{k}} \vec{v}_{\vec{k}} \delta f_{\vec{k}}, \tag{11.9}$$

$$\delta\rho(\vec{r}, t) = e \sum_{\vec{k}} \delta f_{\vec{k}}. \tag{11.10}$$

The rigorous quantum-mechanical derivation of the Boltzmann equation from fundamental physical laws, that is, from the Schrödinger equation, is a very complicated problem. It is part of the general problem of the derivation of statistical physics and of macroscopic irreversibility (the Boltzmann equation is irreversible; that is, it has no time-reversal symmetry, whereas the Schrödinger equation does have time-reversal symmetry), see, e.g., Zubarev (1974), Ishihara (1971) and Balescu (1975). For the particular case of elastic scattering with randomly distributed impurities,

$$V(\vec{r}) = \sum_i u\left(\vec{r} - \vec{R}_i\right) \tag{11.11}$$

($\vec{R}_i$ are their positions), the problem was solved by Kohn & Luttinger (1957). The idea was the following. First, the Schrödinger equation is equivalent to the equation (2.173) for the density matrix

$$\rho_{\vec{k},\vec{k}'} = \left\langle \hat{c}^{+}_{\vec{k}'} \hat{c}_{\vec{k}} \right\rangle \tag{11.12}$$

(cf. Eq. (2.170)). For the case of a spatially uniform system,

$$f_{\vec{k}} = \rho_{\vec{k},\vec{k}}. \tag{11.13}$$

One can prove that, if V is weak enough, the off-diagonal terms of the density matrix (11.12) are small in comparison with the diagonal ones, with the latter satisfying the Boltzmann equation (11.1) and (11.4) and (11.6). Assuming a random distribution of the impurities, one has

$$\left\langle \left| V_{\vec{k}\vec{k}'} \right|^2 \right\rangle = n_{\text{imp}} \left| u_{\vec{k} - \vec{k}'} \right|^2, \tag{11.14}$$

where n_{imp} is the impurity concentration. Luttinger & Kohn (1958) proved that if n_{imp} is small one can repeat the whole derivation without assuming the smallness of potential u, and Eqs. (11.1), (11.4) and (11.6) remain correct, but with replacement of the potential $\hat{u}$ by the single-site $\hat{T}$-matrix:

$$\left\langle \left| V_{\vec{k}\vec{k}'} \right|^2 \right\rangle = n_{\text{imp}} \left| T_{\vec{k}\vec{k}'}\left(E = \varepsilon_{\vec{k}}\right) \right|^2. \tag{11.15}$$

This result has already been mentioned and used in Chapter 6.

If neither the potential nor the concentration of the defects is small, the Boltzmann equation is, in general, incorrect. For example, it does not take into account the effects of Anderson localization which are crucially important for *strongly* disordered systems (Lifshitz, Gredeskul & Pastur, 1988; Mott, 1974; Mott & Davis, 1979; Shklovskii & Efros, 1984).

Some general and powerful tools with which to derive kinetic equations, such as Kadanoff–Baym nonequilibrium Green functions and the Keldysh diagram technique for their calculation (Kadanoff & Baym, 1962; Keldysh, 1964; Rammer & Smith, 1986; Wagner, 1991; Kamenev & Levchenko, 2009) and the nonequilibrium statistical operator (NSO) method and similar approaches (Zubarev, 1974; Kalashnikov & Auslender, 1979; Akhiezer & Peletminskii, 1981; Luzzi, Vasconcellos & Ramos, 2000; Kuzemsky, 2005) were developed thereafter. They are all based on the idea of a *coarse-grained* description. If the disorder is weak (due to either weakness of the scattering potential or smallness of the concentration of defects) the off-diagonal elements of the density matrix have a very fast dynamics in comparison with that of the diagonal ones and can be eliminated. On time scales much larger than typical electron times (e.g., $h/|t|$, where t is the hopping integral) the dynamics of the whole system can be described by a small number of degrees of freedom (we have N_0 diagonal elements (11.13) and N_0^2 elements of the total density matrix (11.12)). If there are no small parameters in the problem under consideration the coarse-grained approach cannot be justified and one needs other methods (see, e.g., Efetov, 1997; Evers & Mirlin, 2008).

Above we discussed the case of a spatially uniform system. If we have inhomogeneities on an atomic scale and no small parameters, the kinetic equation does not work. For the case of smooth enough inhomogeneities the Boltzmann equation (11.1) can be justified for the *Wigner distribution function*

$$f_{\vec{k}}(\vec{r},t) = \int d\vec{\xi} \exp\left(-i\vec{k}\vec{\xi}\right)\rho\left(\vec{r}+\frac{\vec{\xi}}{2},\vec{r}-\frac{\vec{\xi}}{2};t\right), \tag{11.16}$$

where $\rho(\vec{r},\vec{r}') = \left\langle \hat{\psi}^{+}(\vec{r}')\hat{\psi}(\vec{r})\right\rangle$ is the density matrix in the coordinate representation (Kadanoff & Baym, 1962). Henceforth we will not consider the inhomogeneous case. We also restrict ourselves to the case of dc transport with a time-independent $\vec{E}$. Therefore, the terms with $\partial/\partial t$ and $\nabla_{\vec{r}}$ in Eq. (11.1) can be neglected.

For the case of graphene, the applicability of the Boltzmann equation is not obvious. In the standard theory of electron transport in solids, the current operator commutes with the unperturbed Hamiltonian $\hat{H}_0$, thus we start with states that have simultaneously well-defined values of energy and well-defined values of momentum. The perturbation $\hat{H}'$ does not commute with the current operator, leading to scattering between these states. For the Dirac Hamiltonian (3.1) the current operator (3.2) does *not* commute with it (*Zitterbewegung*, see Chapter 3). At the same time, for the case of a scalar potential

$$\hat{H}' = \sum_{\vec{k}\vec{k}'} \hat{\psi}^{+}_{\vec{k}} V_{\vec{k}\vec{k}'} \hat{\psi}_{\vec{k}'} \tag{11.17}$$

the current operator commutes with $\hat{H}'$. It is not at all clear how important this huge formal difference can be. Also, it is not clear when interband scattering processes can be neglected; thus, at least, instead of the scalar quantity (11.13) one needs to consider the matrix (7.15) in pseudospin space. If we have atomically sharp scattering, also the valley index should be taken into account, but we will not consider that case here. The *matrix* Boltzmann equation for the case of graphene has been derived by Auslender & Katsnelson

(2007) (see also Kailasvuori & Lüffe, 2010; Trushin *et al.*, 2010). They used the NSO approach; Kailasvuori & Lüffe (2010) used the Keldysh diagram technique and discussed the relation between these two approaches.

The corresponding derivations are rather complicated and cumbersome, but the physical results are quite clear. Here we present therefore only the general idea and the answers.

First, let us diagonalize the Dirac Hamiltonian by the transformation (7.23) to the form (7.24). The scattering operator (11.5) takes the form

$$\hat{H}' = \sum_{\vec{k}\vec{k}'} \hat{\Xi}^+_{\vec{k}} V'_{\vec{k}\vec{k}'} \hat{\Xi}_{\vec{k}'}, \tag{11.18}$$

where $\hat{\Xi}^+_{\vec{k}} = \left(\hat{\xi}^+_{\vec{k}1}, \hat{\xi}^+_{\vec{k}2}\right)$ and

$$V_{\vec{k}\vec{k}'} \to V'_{\vec{k}\vec{k}'} = \frac{1}{2} V_{\vec{k}\vec{k}'} \begin{pmatrix} 1 + \exp\left[i\left(\varphi_{\vec{k}'} - \varphi_{\vec{k}}\right)\right] & 1 - \exp\left[i\left(\varphi_{\vec{k}'} - \varphi_{\vec{k}}\right)\right] \\ 1 - \exp\left[i\left(\varphi_{\vec{k}} - \varphi_{\vec{k}'}\right)\right] & 1 + \exp\left[i\left(\varphi_{\vec{k}'} - \varphi_{\vec{k}}\right)\right] \end{pmatrix}. \tag{11.19}$$

It contains both diagonal and nondiagonal elements. In the NSO method one needs first to postulate the set of 'coarse-grained' variables for which a closed set of equations of motion is assumed to exist. In our case, this is the 2 × 2 density matrix $\left\langle \hat{\Xi}^+_{\vec{k}} \hat{\Xi}_{\vec{k}} \right\rangle$ or, equivalently,

$$\begin{aligned} D_{\vec{k}} &= \left\langle \hat{\xi}^+_{\vec{k}1} \hat{\xi}_{\vec{k}1} \right\rangle + \left\langle \hat{\xi}^+_{\vec{k}2} \hat{\xi}_{\vec{k}2} \right\rangle \quad 1, \\ N_{\vec{k}} &= \left\langle \hat{\xi}^+_{\vec{k}1} \hat{\xi}_{\vec{k}1} \right\rangle + 1 \quad \left\langle \hat{\xi}^+_{\vec{k}2} \hat{\xi}_{\vec{k}2} \right\rangle, \\ g_{\vec{k}} &= \left\langle \hat{\xi}^+_{\vec{k}1} \hat{\xi}_{\vec{k}2} \right\rangle = \left\langle \hat{\xi}^+_{\vec{k}2} \hat{\xi}_{\vec{k}1} \right\rangle^*. \end{aligned} \tag{11.20}$$

Note that the function $g_{\vec{k}}$ is complex. The generalized Boltzmann equation to second order in V reads (Auslender & Katsnelson, 2007)

$$\frac{\partial D_{\vec{k}}}{\partial t} + \frac{eE}{h}\frac{\partial D_{\vec{k}}}{\partial k_x} = \quad \frac{2\pi}{h} \sum_{\vec{q}} \left| V_{\vec{k},\vec{q}} \right|^2 \cos^2\left(\frac{\varphi_{\vec{k}} \quad \varphi_{\vec{q}}}{2}\right) \delta\left(\varepsilon_{\vec{k}} \quad \varepsilon_{\vec{q}}\right)\left(D_{\vec{k}} \quad D_{\vec{q}}\right), \tag{11.21}$$

$$\begin{aligned} &\frac{\partial N_{\vec{k}}}{\partial t} + eE\frac{\partial N_{\vec{k}}}{\partial k_x} \quad \frac{2eE \sin\varphi_{\vec{k}}}{hk} \operatorname{Im} g_{\vec{k}} \\ &\quad = \frac{2\pi}{h} \sum_{\vec{q}} \left| V_{\vec{k},\vec{q}} \right|^2 \left\{ \frac{1}{\pi} \sin\left(\varphi_{\vec{k}} \quad \varphi_{\vec{q}}\right) \operatorname{Re} g_{\vec{q}} \left(\frac{1}{\varepsilon_{\vec{q}} + \varepsilon_{\vec{k}}} + \frac{1}{\varepsilon_{\vec{q}} \quad \varepsilon_{\vec{k}}} \right) \right. \\ &\qquad \left. \left[\cos^2\left(\frac{\varphi_{\vec{k}} \quad \varphi_{\vec{q}}}{2}\right)\left(N_{\vec{k}} \quad N_{\vec{q}}\right) + \sin\left(\varphi_{\vec{k}} \quad \varphi_{\vec{q}}\right) \operatorname{Im} g_{\vec{q}}\right] \right\} \delta\left(\varepsilon_{\vec{k}} \quad \varepsilon_{\vec{q}}\right), \end{aligned} \tag{11.22}$$

$$
\begin{aligned}
&\frac{\partial g_{\vec{k}}}{\partial t} - 2ivkg_{\vec{k}} + \frac{eE}{h}\frac{\partial g_{\vec{k}}}{\partial k_x} + \frac{iE}{2hk}\left(N_{\vec{k}} - 1\right)\sin\varphi_{\vec{k}} \\
&= \frac{\pi}{h}\sum_{\vec{q}}\left|V_{\vec{k},\vec{q}}\right|^2\left\{ -\frac{i}{2}\sin\left(\varphi_{\vec{k}} - \varphi_{\vec{q}}\right)D_{\vec{q}}\left[\delta\left(\varepsilon_{\vec{k}} - \varepsilon_{\vec{q}}\right) + \frac{i}{\pi}\frac{1}{\varepsilon_{\vec{k}} - \varepsilon_{\vec{q}}}\right]\right. \\
&\qquad + 2\cos^2\left(\frac{\varphi_{\vec{k}} - \varphi_{\vec{q}}}{2}\right)\left[\left(g_{\vec{k}} - g_{\vec{q}}\right)\delta\left(\varepsilon_{\vec{k}} - \varepsilon_{\vec{q}}\right) + \frac{i}{\pi}\frac{g_{\vec{k}} + g_{\vec{q}}}{\varepsilon_{\vec{k}} - \varepsilon_{\vec{q}}}\right] \\
&\qquad \left. + \frac{1}{2\pi}\frac{N_{\vec{q}}}{\varepsilon_{\vec{k}} + \varepsilon_{\vec{q}}}\sin\left(\varphi_{\vec{k}} - \varphi_{\vec{q}}\right) - \frac{2i}{\pi}\frac{g_{\vec{k}} + g^*_{\vec{q}}}{\varepsilon_{\vec{k}} + \varepsilon_{\vec{q}}}\sin^2\left(\frac{\varphi_{\vec{k}} - \varphi_{\vec{q}}}{2}\right)\right\},
\end{aligned}
\tag{11.23}
$$

where $\varepsilon_{\vec{k}} = hvk$ and the electric field E is supposed to be directed along the x-axis. The current is expressed in terms of these functions as

$$
j_x = ev\sum_{\vec{q}}\left(N_{\vec{q}}\cos\varphi_{\vec{q}} + 2\sin\varphi_{\vec{q}}\operatorname{Im}g_{\vec{q}}\right). \tag{11.24}
$$

The equation (11.21) is decoupled from Eqs. (11.22) and (11.23) and is formally equivalent to the usual Boltzmann equation (11.1), (11.4) and (11.6), but the other two equations have an essentially different structure. The most important difference is that the 'collision integral' contains now not only 'dissipative' terms with $\delta\left(\varepsilon_{\vec{k}} - \varepsilon_{\vec{q}}\right)$ but also 'reactive' terms with $1/(\varepsilon_{\vec{k}} \pm \varepsilon_{\vec{q}})$. These terms are associated with virtual interband transitions, that is, with *Zitterbewegung* (see Chapter 3). As a result, the linearized kinetic equations are singular, and their solutions contain logarithmic divergences at small enough chemical potential μ and temperature T. For the case of the contact potential, $V_{\vec{k},\vec{q}} = \text{constant}$, these integral equations can be solved exactly (Auslender & Katsnelson, 2007).

First, let us neglect off-diagonal terms, that is, $g_{\vec{k}}$. Then we will have the standard Boltzmann equation for the Dirac fermions and the corresponding expression for the resistivity (6.23) with the inverse Drude mean-free-path time (Shon & Ando, 1998)

$$
\begin{aligned}
\frac{1}{\tau_{\vec{k}}} &= \frac{\pi}{h}\sum_{\vec{q}}\left|V_{\vec{k},\vec{q}}\right|^2\sin^2\left(\varphi_{\vec{k}} - \varphi_{\vec{q}}\right)\delta\left(\varepsilon_{\vec{k}} - \varepsilon_{\vec{q}}\right) \\
&= \frac{\pi\varepsilon_{\vec{k}}}{(2\pi hv)^2}n_{\text{imp}}\int_0^{2\pi}d\varphi\left|u\left(2k\sin\left(\frac{\varphi}{2}\right)\right)\right|^2\sin^2\varphi,
\end{aligned}
\tag{11.25}
$$

where $u(q)$ is the Fourier component of $u(r)$ from Eq. (11.11).

If we now find the off-diagonal terms of the density matrix, $g_{\vec{k}}$, by iterations we will see that they have a smallness in the parameter

$$\lambda = \frac{h}{|\varepsilon_{\mathrm{F}}|\tau(k_{\mathrm{F}})} \sim \frac{e^2 \rho_{\mathrm{B}}}{h} \tag{11.26}$$

where ρ_{B} is the resistivity (6.23) and (11.25) calculated by applying the ordinary semiclassical Boltzmann equation. If we go closer to the neutrality point the off-diagonal terms are divergent. For the case of the contact potential the exact solution of the integral equations mentioned above gives a typical energy scale (Auslender & Katsnelson, 2007)

$$\varepsilon_{\mathrm{K}} = W \exp\left(\quad \frac{\pi h}{e^2 \rho_{\mathrm{B}}} \right), \tag{11.27}$$

where W is a cut-off energy of the order of the bandwidth. The conventional Boltzmann equation is valid if

$$|\varepsilon_{\mathrm{F}}|, T \gg \varepsilon_{\mathrm{K}}. \tag{11.28}$$

The subscript K in Eq. (11.27) refers to Kondo, due to a formal similarity between the energy scale discussed here and the Kondo effect in the scattering of electrons in metals by a magnetic impurity (Kondo, 1964; Hewson, 1993). In that case, due to spin-flip processes involved in the scattering a resonant singlet state is formed ('Kondo resonance'), which, being considered perturbatively, leads to logarithmic corrections in the temperature dependences of various physical quantities. It is important that the spin-up and spin-down states of the impurities are degenerate. A magnetic field kills this degeneracy and suppresses the Kondo effect. The scattering potential (11.19) contains off-diagonal matrix elements between electron and hole bands. At $\mu = 0$, these bands are degenerate, and an analogue of the Kondo effect arises, making the standard Born approximation insufficient. A finite chemical potential μ plays the same role as the magnetic field in the Kondo effect. The condition (11.28) guarantees that all singularities are suppressed. One can see that this is equivalent to the condition

$$\lambda \ll 1, \tag{11.29}$$

which is the desired criterion of applicability of the standard semiclassical Boltzmann theory. In the vicinity of the neutrality point we are in the 'strong-coupling' regime. Note that Eqs. (11.21) (11.23) are probably insufficient in this case. As was emphasized above, in the situation without any smallness of disorder other methods have to be applied. They will be briefly discussed later in this chapter (Section 11.6). The main role of the approach considered here is that it justifies the use of the standard Boltzmann equation under the condition (11.29).

Note that these ‘Kondo’ logarithms are related to the divergence of $\partial\Sigma/\partial E$ at the neutrality point, Eq. (10.79). From another point of view and in a different context (Dirac fermions in d-wave superconductors) these logarithms were discussed by Lee (1993), Nersesyan, Tsvelik & Wenger (1994) and Ziegler (1998).

Thus, not too close to the neutrality point, namely at

$$\sigma = \frac{1}{\rho} \gg \frac{e^2}{h}, \tag{11.30}$$

the interband transitions are negligible. If we assume, to be specific, that the Fermi energy lies in the electron band then only the (1, 1) matrix element of the current operator and that of the scattering potential are relevant:

$$\left(j_{\vec{k}x}\right)_{1,1} = ev\cos\varphi_{\vec{k}}, \tag{11.31}$$

$$\left(V'_{\vec{k}\vec{k}'}\right)_{1,1} = V_{\vec{k}\vec{k}'}\frac{1+\exp\left[i\left(\varphi_{\vec{k}'}-\varphi_{\vec{k}}\right)\right]}{2}. \tag{11.32}$$

Let us consider the most general form of the scattering potential $V_{\vec{k}\vec{k}'}$ in Eq. (11.17):

$$V_{\vec{k}\vec{k}'} = V^{(0)}_{\vec{k}\vec{k}'} + \vec{V}_{\vec{k}\vec{k}'}\vec{\sigma}. \tag{11.33}$$

Then, the effective scattering potential will be

$$\begin{aligned} V^{\text{eff}}_{\vec{k}\vec{k}'} &= \left(V'_{\vec{k}\vec{k}'}\right)_{1,1} \\ &= V^{(0)}_{\vec{k}\vec{k}'}\frac{1+\exp\left[i\left(\varphi_{\vec{k}'}-\varphi_{\vec{k}}\right)\right]}{2} + V^{z}_{\vec{k}\vec{k}'}\frac{1-\exp\left[i\left(\varphi_{\vec{k}'}-\varphi_{\vec{k}}\right)\right]}{2} \\ &\quad + \left(V^{x}_{\vec{k}\vec{k}'} + iV^{y}_{\vec{k}\vec{k}'}\right)\exp\left(-i\varphi_{\vec{k}}\right) + \left(V^{x}_{\vec{k}\vec{k}'} - iV^{y}_{\vec{k}\vec{k}'}\right)\exp\left(i\varphi_{\vec{k}'}\right). \end{aligned} \tag{11.34}$$

Thus, under the condition (11.30) we have a single-band problem with the unperturbed Hamiltonian

$$\hat{H}_0 = \sum_{\vec{k}} hvk\hat{\xi}^{+}_{\vec{k}}\hat{\xi}_{\vec{k}}, \tag{11.35}$$

current operator

$$\hat{j}_x = \sum_{\vec{k}} ev\cos\varphi_{\vec{k}}\,\hat{\xi}^{+}_{\vec{k}}\hat{\xi}_{\vec{k}} \tag{11.36}$$

and scattering operator

$$\hat{H}_0 = \sum_{\vec{k}} V^{\mathrm{eff}}_{\vec{k}\vec{k}'} \hat{\xi}^{+}_{\vec{k}} \hat{\xi}_{\vec{k}'}, \tag{11.37}$$

where we will omit the label '1' for electron operators. In the next section we will present a convenient and general tool by means of which to find the resistivity in this problem.

11.2 The Kubo–Nakano–Mori formula for resistivity

In general, the linearized Boltzmann equation is an integral equation that can be solved exactly only in some special cases (e.g., for contact interaction $u\left(\vec{r}\quad \vec{R}_1\right)$ in Eq. (11.11)). Usually, a variational approach (Ziman, 2001) is used. However, within the Born approximation there is a more straightforward way to calculate transport properties. It is based on the use of the *Kubo Nakano Mori* formula (Kubo, 1957; Nakano, 1957; Mori, 1965) for the resistivity. It gives exactly the same result as the solution of Boltzmann equation by the variational approach but in a technically simpler way. Since this method seems not to be well known in graphene community, we will present it here following Mori (1965). It will allow us also to illustrate the idea of coarse graining, which is fundamental for the nonequilibrium statistical mechanics which was discussed preliminarily in the previous section.

Let us start with the Kubo formula (3.7) for σ_{xx}. It can be rewritten as

$$\sigma_{xx}(\omega) = \beta \int_0^\infty dt \exp(i\omega t) \left(\hat{j}_x(t), \hat{j}_x \right), \tag{11.38}$$

where

$$\left(\hat{A}, \hat{B}\right) = \frac{1}{\beta} \int_0^\beta d\lambda \left\langle \exp\left(\lambda \hat{H}\right) \hat{A} \exp\left(\quad \lambda \hat{H}\right) \hat{B}^{+} \right\rangle. \tag{11.39}$$

$\hat{H}$ is the Hamiltonian of the system and we put the area of the sample equal to one. Importantly, if we consider *operators* $\{\hat{A}\}$ as *vectors* in some linear space, Eq. (11.39) determines the *scalar product* in this space and satisfies all of the axioms of the scalar product.

The operator equation of motion is

$$\frac{d\hat{A}(t)}{dt} = i\hat{L}\hat{A}(t), \tag{11.40}$$

where

$$\hat{L}\hat{A} \equiv \left[\hat{H},\hat{A}\right] \tag{11.41}$$

is the *Liouville (super)operator*. 'Super' means that it acts as an operator in the vector space of quantum-mechanical Hermitian operators. Here we put $h = 1$ for simplicity.

Let us assume that $\{\hat{A}\}$ form a set of operators such that their dynamics is closed, that is, $\{\langle\hat{A}(t)\rangle\}$ at any time t is determined by initial conditions $\{\langle\hat{A}(0)\rangle\} \equiv \{\langle\hat{A}\rangle\}$. This implies the coarse-grained dynamics. A technical advantage of Mori's approach is that we use far fewer operators than in the kinetic equation, just current operators, but with almost the same accuracy.

Since Eq. (11.39) defines the scalar product in our vector space, one can introduce a *projection operator* of any set of operators $\{\hat{G}\}$ on the initial set $\{\hat{A}\}$:

$$\hat{P}_0\hat{G} = \left(\hat{G},\hat{A}\right)\cdot\left(\hat{A},\hat{A}\right)^{-1}\cdot\hat{A}, \tag{11.42}$$

where the dot denotes the matrix product, e.g.,

$$\left[(\hat{G},\hat{A})\cdot\hat{A}\right]_i = \sum_j \left(G_i,\hat{A}_j\right)\hat{A}_j \tag{11.43}$$

and i and j label operators within the set $\{\hat{A}\}$. Thus, $\hat{A}$(t) can be represented as a sum of 'projective' and 'perpendicular' components with respect to $\{\hat{A}\}$:

$$\hat{A}(t) = \Xi_0(t)\hat{A} + \hat{A}'(t), \tag{11.44}$$

where

$$\Xi_0(t) = \left(\hat{A}(t),\hat{A}\right)\cdot\left(\hat{A},\hat{A}\right)^{-1} \tag{11.45}$$

and

$$\hat{A}'(t) = \left(1 - \hat{P}_0\right)\hat{A}(t). \tag{11.46}$$

Next, we can derive the equation of motion for $\hat{A}'$. Acting by $\left(1 - \hat{P}_0\right)$ on Eq. (11.40) we find

$$\frac{d\hat{A}'(t)}{dt} - i\hat{L}_1\hat{A}'(t) = \Xi_0(t)\hat{f}_1, \tag{11.47}$$

where

$$\hat{L}_1 = \left(1 - \hat{P}_0\right)\hat{L}, \tag{11.48}$$

$$\hat{f}_1 = i\hat{L}_1\hat{A}. \tag{11.49}$$

It has the formal solution

$$\hat{A}'(t) = \int_0^t ds\, \Xi_0(s)\hat{f}_1(t - s), \tag{11.50}$$

where we take into account that $\hat{A}'(0) = 0$ and

$$\hat{f}_1(t) = \exp\left(i\hat{L}_1 t\right)\hat{f}_1. \tag{11.51}$$

Equation (11.50) represents a convolution. On taking the Laplace transform

$$\hat{A}(z) = \int_0^\infty dt \exp(-zt)\hat{A}(t) \tag{11.52}$$

we find

$$\hat{A}(z) = \Xi_0(z)\cdot\left[\hat{A} + \hat{f}_1(z)\right]. \tag{11.53}$$

As the next step we have to repeat the procedure for $\hat{f}_1$. It satisfies the equation of motion

$$\frac{d\hat{f}_1}{dt} = i\hat{L}_1\hat{f}_1. \tag{11.54}$$

We can reproduce it as

$$\hat{f}_1(t) = \Xi_1(t)\cdot\hat{f}_1 + \hat{f}_1'(t), \tag{11.55}$$

where

$$\Xi_1(t) = \left(\hat{f}_1(t), \hat{f}_1\right)\cdot\left(\hat{f}_1, \hat{f}_1\right)^{-1} \tag{11.56}$$

and

$$\hat{f}_1'(t) = \left(1 - \hat{P}_1\right)\hat{f}_1(t), \tag{11.57}$$

where $\hat{P}_1$ is the projection operator onto $\left\{\hat{f}_1\right\}$. Further, we will have for the Laplace transform,

$$\hat{f}_1(z) = \Xi_1(z)\cdot\left[\hat{f}_1 + \hat{f}_2(z)\right], \tag{11.58}$$

which is similar to Eq. (11.53) and where

$$\hat{f}_2(t) = \exp\left(i\hat{L}_2 t\right)i\hat{L}_2\hat{f}_1, \tag{11.59}$$

$$\hat{L}_2 = \left(1 - \hat{P}_1\right)\hat{L}_1. \tag{11.60}$$

Treating $\hat{f}_2$ in a similar way, we introduce a new object $\hat{f}_3$, etc., so that we will have a set of quantities $\left\{\hat{f}_j(t)\right\}$ $\left(\hat{f}_0 = \hat{A}\right)$ defined iteratively as

$$\hat{f}_j(t) = \exp\left(i\hat{L}_j t\right) i\hat{L}_j \hat{f}_{j-1}, \tag{11.61}$$

where

$$\hat{L}_j = \left(1 - \hat{P}_{j-1}\right)\hat{L}_{j-1}, \qquad \hat{L}_0 = \hat{L} \tag{11.62}$$

and $\hat{P}_j$ is the projection operator onto $\left\{\hat{f}_j\right\}$. The Laplace transforms of $\hat{f}_j$ satisfy the chain of equations

$$\hat{f}_j(z) = \Xi_j(z)\cdot\left[\hat{f}_j + \hat{f}_{j+1}(z)\right]. \tag{11.63}$$

As a result, we derive a *continued-fraction* representation of the correlators (Mori, 1965):

$$\Xi_0(z) = \frac{1}{z - i\omega_0 - \Delta_0^2 \Xi_1(z)}, \tag{11.64}$$

$$\Xi_1(z) = \frac{1}{z - i\omega_1 - \Delta_1^2 \Xi_2(z)} \tag{11.65}$$

etc., where

$$i\omega_j = \left(\dot{f}_j, f_j\right)\cdot\left(f_j, f_j\right)^{-1}, \tag{11.66}$$

$$\Delta_j^2 = \left(f_j, f_j\right)\cdot\left(f_{j-1}, f_{j-1}\right)^{-1}. \tag{11.67}$$

Let us apply this general scheme to the conductivity. We have to choose as the first step $\hat{A} = \left(\hat{j}_x, \hat{j}_y\right)$. Next, we have to calculate ω_0. This can easily be done using the identity

$$\begin{aligned}
\left(\dot{\hat{A}}, \hat{B}\right) &= \frac{i}{\beta}\int_0^\beta d\lambda \left\langle \exp\left(\lambda\hat{H}\right)\left[\hat{H}, \hat{A}\right]\exp\left(-\lambda\hat{H}\right)\hat{B}^+\right\rangle \\
&= \frac{i}{\beta}\int_0^\beta d\lambda \frac{d}{d\lambda}\left\langle \exp\left(\lambda\hat{H}\right)\hat{A}\exp\left(-\lambda\hat{H}\right)\hat{B}^+\right\rangle \\
&= \frac{i}{\beta}\left[\left\langle \exp\left(\beta\hat{H}\right)\hat{A}\exp\left(-\beta\hat{H}\right)\hat{B}^+\right\rangle - \left\langle \hat{A}\hat{B}^+\right\rangle\right] \\
&= \frac{i}{\beta}\left\langle\left[\hat{B}^+, \hat{A}\right]\right\rangle,
\end{aligned} \tag{11.68}$$

where we take into account that

$$\langle\hat{A}\rangle = \mathrm{Tr}\left[\exp(\quad\beta\hat{H})\hat{A}\right]/Z \tag{11.69}$$

and implement the cyclic permutation under the trace symbol.

In the absence of a magnetic field, the average values of all of the commutators of the current operator are zero (in particular, $\langle\hat{\sigma}_z\rangle = 0$), so one can conclude that $\omega_0 = 0$. Also, one can conclude by symmetry arguments that

$$\left(j_\alpha, j_\beta\right) = \delta_{\alpha\beta}(j_x, j_x). \tag{11.70}$$

Let us stop the procedure at the first step, neglecting $\hat{f}_2$ and all higher-order terms. Then, the result for the conductivity (11.38) will be

$$\sigma_{xx}(\omega) = \frac{\beta(j_x, j_x)}{i\omega + 1/(j_x, j_x)\left(\left[\hat{j}_x, \hat{H}\right], \left[\hat{H}, \hat{j}_x\right]\right)_{z \quad i\omega}}. \tag{11.71}$$

Since within the single-band approximation (11.35) (11.37) the current operator commutes with $\hat{H}_0$, one can replace $\left[\hat{j}_x, \hat{H}\right]$ by $\left[\hat{j}_x, \hat{H}'\right]$ in Eq. (11.71). As a result, Eq. (11.71) takes the form

$$\sigma_{xx}(\omega) = \frac{\beta(j_x, j_x)}{i\omega + 1/\tau(\omega)}, \tag{11.72}$$

where

$$\frac{1}{\tau(\omega)} = \frac{1}{(j_x, j_x)}\int_0^\infty dt \exp(i\omega t)\left(F_x(t \quad i\lambda), F_x^+\right) \tag{11.73}$$

and

$$F_x = \left[\hat{j}_x, \hat{H}'\right]. \tag{11.74}$$

To calculate (j_x, j_x) one can neglect the scattering operator $\hat{H}'$. Then, taking into account that $\left[\hat{j}_x, \hat{H}_0\right] = 0$, we have

$$(j_x, j_x) = \left\langle j_x^2 \right\rangle. \tag{11.75}$$

By substituting Eq. (11.38) into Eq. (11.75) and using Wick's theorem we find

$$\begin{aligned}(j_x, j_x) &= \sum_k e^2 v^2 \cos^2\varphi_k \left\langle \hat{\xi}^+_{k1}\hat{\xi}_{k1}\right\rangle\left\langle \hat{\xi}_{k1}\hat{\xi}^+_{k1}\right\rangle \\ &= \sum_k e^2 v^2 \cos^2\varphi_k\, f(\varepsilon_k)[1 \quad f(\varepsilon_k)] \\ &= \frac{1}{2\beta}\sum_k e^2 v^2 \left(\quad \frac{\partial f(\varepsilon_k)}{\partial \varepsilon_k}\right),\end{aligned} \tag{11.76}$$

where we average $\cos^2\varphi_k \to \frac{1}{2}$. At $T \ll |\varepsilon_F|$ the result is

$$\beta(j_x, j_x) = e^2 \frac{N(\varepsilon_F) v^2}{2}. \tag{11.77}$$

On comparing Eqs. (11.72) and (11.77) with Eq. (6.23) one can see that Eq. (11.72) is nothing other than the Drude formula, and $\tau(\omega = 0)$ given by Eq. (11.73) is nothing other than the mean-free-path time. At $\omega = 0$ it can be simplified, similarly to the transformation from Eq. (3.7) to Eq. (3.8):

$$\frac{1}{\tau} = \frac{1}{2\langle j_x^2 \rangle} \int_{\infty}^{\infty} dt \langle F_x(t) F_x^+ \rangle. \tag{11.78}$$

This, together with Eq. (6.23), gives us the *Kubo Nakano Mori formula* for the resistivity. As has already been mentioned it is equivalent to the solution of the semiclassical Boltzmann equation by the variational approach (Ziman, 2001).

By substituting Eqs. (11.36) and (11.37) into Eqs. (11.74) and (11.78) and calculating the average using Wick's theorem we find, finally (we restore here the Planck constant), the expression for the momentum relaxation rate of Dirac fermions:

$$\frac{1}{\tau} = \frac{2\pi}{hN(\varepsilon_F)} \sum_{\vec{k}\vec{k}'} \delta\left(\varepsilon_{\vec{k}} \quad \varepsilon_F\right) \delta\left(\varepsilon_{\vec{k}'} \quad \varepsilon_F\right) \left(\cos\varphi_{\vec{k}} \quad \cos\varphi_{\vec{k}'}\right)^2 \left|V^{\text{eff}}_{\vec{k}\vec{k}'}\right|^2 \tag{11.79}$$

Together with Eq. (11.34), this allows us to analyze various scattering mechanisms.

11.3 Scattering mechanisms in graphene on a substrate

There are two fundamental experimental facts about the conductivity of graphene on a substrate. First, the dependence of the conductivity on the charge-carrier concentration n typically has a V-shape (Novoselov *et al.*, 2004, 2005a; Zhang *et al.*, 2005). If we introduce the mobility μ via the relation

$$\sigma = ne\mu \tag{11.80}$$

this means that μ is weakly dependent on the concentration and $\sigma \sim n$ except in the close proximity of the neutrality point. Typical results (Novoselov *et al.*, 2005a) are shown in Fig. 11.1 (note that n is proportional to the gate voltage). This behaviour has been confirmed by numerous works by many experimental groups and seems to be universal. It does not depend on the type of substrate, but the value of μ does. Whereas for graphene on SiO_2 one

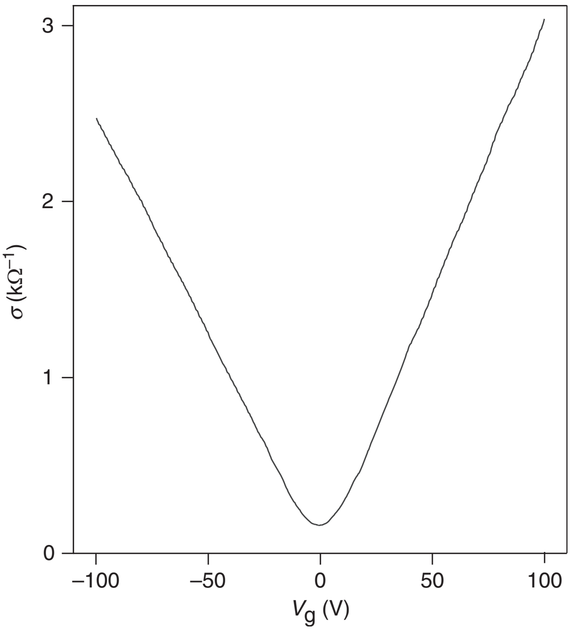

Fig. 11.1. The dependence of the conductivity of graphene on the gate voltage $V_g \sim n$. (Reproduced with permission from Novoselov *et al.*, 2005a.)

typically has $\mu \approx 10^4$ cm^2 V^{-1} s^{-1} (Novoselov *et al.*, 2004, 2005a; Zhang *et al.*, 2005), for graphene on hexagonal BN μ can be an order of magnitude higher (Dean *et al.*, 2010).

Second, for graphene on a substrate the temperature dependence of conductivity is extremely weak. If one tries to separate ‘extrinsic’ (due to defects) and ‘intrinsic’ (e.g., due to electron–phonon interaction) contributions to the mobility using Matthiessen’s rule (Ziman, 2001)

$$\frac{1}{\mu(T)} = \frac{1}{\mu_{\text{ext}}} + \frac{1}{\mu_{\text{int}}(T)} \tag{11.81}$$

assuming that μ_{ext} is temperature-independent and $\mu_{\text{int}}(T) \to 0$ at $T \to 0$, one finds $\mu_{\text{int}} \approx (2–4) \times 10^5$ cm^2 V^{-1} s^{-1} (Morozov *et al.*, 2008), which means that the difference in conductivity between $T \approx 0$ and room temperature is no more than a few per cent. We postpone the discussion of this temperature dependence until the next section and focus here on the origin of μ_{ext}.

Importantly, the concentration and temperature dependences of the conductivity for bilayer graphene are more or less the same as for single-layer graphene (Novoselov *et al.*, 2006). To discuss this case we will use the same semiclassical Boltzmann equation as for the case of single-layer graphene, the only differences being in the dispersion law and the transformation to electrons and holes ($\varphi_k \to 2\varphi_k$ in Eqs. (11.19) and (11.34)). In both cases, the inverse relaxation time (11.79) can be estimated as

$$\frac{1}{\tau} \approx \frac{2\pi}{h} N(\varepsilon_{\mathrm{F}}) |V(k_{\mathrm{F}})|^2, \tag{11.82}$$

where $V(k_{\mathrm{F}})$ is a typical value of $V^{\mathrm{eff}}_{\vec{k}\vec{k}'}$ at $\left|\vec{k}\right| \approx \left|\vec{k}'\right| \approx k_{\mathrm{F}}$. On substituting Eq. (11.82) into the Drude formula (11.72) and (11.77) we find

$$\sigma(n) \sim \frac{v_{\mathrm{F}}^2}{|V(k_{\mathrm{F}})|^2}, \tag{11.83}$$

where $v_{\mathrm{F}} = v =$ constant for the case of single-layer graphene and

$$v_{\mathrm{F}} = \frac{h k_{\mathrm{F}}}{m} \sim n^{1/2} \tag{11.84}$$

for the case of bilayer graphene. This means that, to explain the experimentally observed behaviour $\sigma(n)$, one needs to assume

$$|V(k_{\mathrm{F}})|^2 \approx \text{constant} \tag{11.85}$$

for the case of bilayer graphene and

$$|V(k_{\mathrm{F}})|^2 \sim \frac{1}{k_{\mathrm{F}}^2} \tag{11.86}$$

for the case of single-layer graphene.

For randomly distributed defects, one needs to use Eq. (11.14) (assuming the Born approximation) or the more accurate Eq. (11.15) (assuming only a low concentration of defects). In the latter case, the answer can be expressed in terms of scattering phases; see Eqs. (6.23) (6.26) for the case of single-layer graphene and Eq. (6.54) for the case of bilayer graphene.

Up to now we have not taken into account the screening effects (see Section 7.7). Within the RPA, the scalar potential $V^{(0)}_{\vec{k}\vec{k}'}$ in Eq. (11.34) is replaced by

$$V^{(\mathrm{s})}_{\vec{k}\vec{k}'} = \frac{V^{(0)}_{\vec{k}\vec{k}'}}{\varepsilon\left(q = \left|\vec{k}\quad \vec{k}'\right|, \omega = 0\right)}. \tag{11.87}$$

Beyond the RPA, so-called vertex corrections should be taken into account, but we will not discuss them here; just for estimations this simple theory will suffice. At the same time, there is no screening of the vector potential $\vec{V}_{\vec{k}\vec{k}'}$ (Gibertini *et al.*, 2010).

Let us restrict ourselves to the case of the scalar potential only and use Eq. (11.14). Thus, Eq. (11.79) will take the form (11.25), with the replacement

$u(q) = u(q)/\varepsilon(q)$. On introducing the new variable $x = \sin(\varphi/2)$ one can rewrite this equation as

$$\frac{1}{\tau(k_F)} = \frac{4k_F}{\pi\hbar v} n_{imp} \int_0^1 dx\, x^2 \sqrt{1} \quad x^2 \left| \frac{u(2k_F x)}{\varepsilon(2k_F x, 0)} \right|^2. \tag{11.88}$$

Note that only $\varepsilon(q, 0)$ with $q < 2k_F$ is involved in Eq. (11.88). In this regime, the RPA coincides with the Thomas Fermi approximation (see Eq. (7.107)), thus

$$\varepsilon(2k_F x, 0) = \varepsilon_{ext} + \frac{2e^2}{\hbar v} \frac{1}{x} \tag{11.89}$$

and does not depend on k_F.

The behaviour (11.86) is provided by Coulomb impurities, where

$$u(q) = \frac{2\pi Z e^2}{q}. \tag{11.90}$$

Moreover, it takes place also with the replacement of the potential u by the T-matrix, see Eqs. (8.18) and (8.19). Therefore it is very natural to assume that charge impurities determine the electron mobility in graphene on a substrate (Nomura & MacDonald, 2006; Ando, 2006; Adam *et al.*, 2007; Peres, 2010; Das Sarma *et al.*, 2011). Quantitative estimations for the case of graphene on SiO$_2$ ($\varepsilon_{ext} \approx 2.5$) give (Adam *et al.*, 2007)

$$\sigma(n) \approx \frac{20e^2}{h} \frac{n}{n_{imp}}, \tag{11.91}$$

where four current channels (two spins and two valleys) are taken into account.

Indeed, an intentional addition of charge impurities (potassium adatoms) to graphene leads to a decrease of the electron mobility, in good agreement with the theory described above (Chen *et al.*, 2008). At the same time, there is convincing experimental evidence that this is *not* the main factor restricting electron mobility in standard exfoliated graphene samples on a substrate.

The main argument is that the electron mobility is relatively weakly changed in an environment with a high dielectric constant and, thus, very large ε_{ext}, e.g., after covering graphene with water, ethanol or other polar liquids, or when using substrates with large ε (Ponomarenko *et al.*, 2009). In particular, the mobility in graphene on SrTiO$_3$ (which has a dielectric constant growing from $\varepsilon \approx 300$ at room temperature to $\varepsilon \approx 5000$ at liquid-helium temperature) is of the same magnitude as that for graphene on SiO$_2$ and very weakly dependent on temperature (Couto, Sacépé & Morpurgo, 2011). Of course, the screened Coulomb interaction in such a situation *should be* strongly suppressed and strongly temperature-dependent.

It was suggested by Katsnelson, Guinea & Geim (2009) that the reason why charged adsorbate adatoms on graphene can be not very important for the electron mobility is their strong tendency to form clusters. Indeed, density-functional calculations (Wehling, Katsnelson & Lichtenstein, 2009b) show that the more charged the adsorbate species the weaker its chemical bond with graphene and the lower its migration barriers. This means that strongly bonded and immobile adsorbates have very small charge transfer to graphene and, thus, small effective Z, whereas impurities with $Z \geq 1$ can be kept more or less randomly distributed only at low enough temperatures. This was found to be the case for potassium atoms by Chen *et al.* (2008). The clusterization suppresses the scattering cross-section per impurity by orders of magnitude (Katsnelson, Guinea & Geim, 2009).

The above effect was confirmed experimentally by McCreary *et al.* (2010). They deposited gold adatoms onto graphene and observed their clusterization, with a simultaneous growth of the electron mobility.

Before discussing other possible scattering mechanisms we need to say a few words about the case of bilayer graphene. Actually, for any isotopic two-dimensional case the density of states at the Fermi energy is

$$N(E_{\mathrm{F}}) = \frac{g_{\mathrm{v}} g_{\mathrm{s}}}{2\pi} \int_0^\infty dk\, k \delta(\varepsilon_{\mathrm{F}} \quad \varepsilon(k)) = \frac{g_{\mathrm{s}} g_{\mathrm{v}}}{2\pi} \frac{k_{\mathrm{F}}}{h v_{\mathrm{F}}} \tag{11.92}$$

where

$$v_{\mathrm{F}} = \frac{1}{h} \left(\frac{\partial \varepsilon}{\partial k} \right)_{k \;\; k_{\mathrm{F}}} \tag{11.93}$$

and we have restored the spin and valley degeneracy factors. As a result the inverse screening radius is, instead of being given by Eq. (7.108) for single-layer graphene,

$$\kappa = g_{\mathrm{s}} g_{\mathrm{v}} \frac{e^2 k_{\mathrm{F}}}{h v_{\mathrm{F}} \varepsilon_{\mathrm{ext}}} \tag{11.94}$$

and, thus,

$$\varepsilon(2k_{\mathrm{F}} x, 0) = \varepsilon_{\mathrm{ext}} + \frac{g_{\mathrm{s}} g_{\mathrm{v}} e^2}{h v_{\mathrm{F}}} \frac{1}{2x}. \tag{11.95}$$

For the case of bilayer graphene, $\kappa \gg \mathrm{k}_{\mathrm{F}}$ since $v_{\mathrm{F}} \to 0$ at $n \to 0$. Actually, this is the case even for single-layer graphene if $\varepsilon_{\mathrm{ext}}$ is not too large. Therefore, v_{F} is cancelled out from Eq. (11.83) and we have an estimation

$$\sigma(n) \sim \frac{1}{n_{\mathrm{imp}} |u(k_{\mathrm{F}})|^2}, \tag{11.96}$$

which is valid both for single-layer and for bilayer graphene. This means that for the same type of purely scalar potential scattering the concentration dependence of the conductivity is the same. Strictly speaking, this is true only within the Born approximation, and for the case of strong scatterers there will be some difference (see below). The numerical coefficients can be different since, in the case of bilayer graphene, one has to make the replacement $\varphi \to 2\varphi$ in Eq. (11.32) and, as a result, the factor $\cos^2(\varphi/2)$ is replaced by $\cos^2\varphi$. Thus, for the same electron concentration and the same scatterers, the ratio of the resistivity of single-layer graphene to that of bilayer graphene is

$$\frac{\rho_1}{\rho_2} = \frac{\Phi_1}{\Phi_2}, \tag{11.97}$$

where

$$\Phi_1 = \int_0^1 dx\, x^4 \sqrt{1 - x^2} |u(2k_F x)|^2,$$

$$\Phi_2 = \int_0^1 \frac{dx\, x^4 (1 - 2x^2)^2}{\sqrt{1 - x^2}} |u(2k_F x)|^2$$

(see Eqs. (11.88) and (11.95)).

Another potentially important source of electron scattering is ripples (see Chapter 10). They create both a random vector potential (10.7) and a random scalar potential (10.8). By substituting these expressions into Eq. (11.34) and following the analysis of Sections 10.2 and 10.3 one finds that

$$|V(k_F)|^2 \sim F(q \approx k_F), \tag{11.98}$$

where the correlation function F is given by Eq. (10.28). For intrinsic (thermally induced) ripples one needs to use Eq. (10.29). Thus, for the case of not too small doping, when

$$k_F \gg q^* \tag{11.99}$$

one has (Katsnelson & Geim, 2008)

$$\rho \approx \frac{h}{e^2} \left(\frac{T}{\kappa a} \right)^2 \frac{|\ln(q^* a)|}{n}. \tag{11.100}$$

At room temperature, this has the correct $1/n$ dependence and corresponds to the correct order of magnitude for the mobility, $\mu \sim 10^4\,\mathrm{cm^2\,V^{-1}\,s^{-1}}$. There are two problems, however. First, the mobility is weakly temperature-dependent. Katsnelson & Geim (2008) suggested therefore that there is a mechanism of freezing (quenching) of the ripples and hence that they keep the structure corresponding to some quenching temperature T_q. If one makes the replacement $T \rightarrow T_q$ of the order of room temperature in Eq. (11.100), it seems to explain μ_{ext} reasonably well. Moreover, if one assumes that the large-scale ripple structure is frozen but flexural phonons can be excited within the ripples, it can explain also the temperature dependence of μ_{int} (Morozov *et al.*, 2008).

The weak temperature dependence of the ripple structure for graphene on SiO_2 has been confirmed by STM experiments (Geringer *et al.*, 2009). However, the origin of this quenching is still unknown. It was suggested and confirmed by density-functional calculations (Boukhvalov & Katsnelson, 2009b) that ripples can be stabilized by covalently bonded adatoms and admolecules. San-José, González & Guinea (2011) proposed an intrinsic mechanism of ripple stabilization that is based on the interactions of ripples with conduction electrons. The absence of a detailed theory of the quenching seems to be the weakest point of the idea that the ripples can be the main limiting factor for electron mobility, whereas from the experimental point of view this possibility cannot be excluded. Anyway, as will be discussed in the next section, intrinsic ripples are probably the main limiting factor for the electron mobility in freely suspended graphene samples.

Another important question within this scenario is that of whether the frozen ripples on a substrate have the same structure as intrinsic ripples or not. The results from the first two scanning-probe studies for graphene on SiO_2 (Ishigami *et al.*, 2007; Stolyarova *et al.*, 2007) indicated that these ripples repeat approximately the roughness of the substrate, whereas in the later work by Geringer *et al.* (2009) for the same system two types of ripples were found: a first type following the roughness of the substrate and a second type similar to the intrinsic ripples.

It is important to note that the first type seems to be irrelevant for the electron mobility. Indeed, let us consider a general type of correlation function,

$$\left\langle [h(\vec{r}) \quad h(0)]^2 \right\rangle \sim r^{2H}. \tag{11.101}$$

Then,

$$\left\langle \left| h_{\vec{q}} \right|^2 \right\rangle \sim q^{\quad 2(1+H)} \tag{11.102}$$

and for $2H < 1$ the correlation function $F(q)$ in (10.28) has a finite limit at $q = 0$, thus,

$$\left\langle \left| V(q=0) \right|^2 \right\rangle \approx \left(\frac{hv}{a} \right)^2 \frac{z^4}{R^2}, \tag{11.103}$$

where z and R are the characteristic height and radius of ripples, respectively. This leads to a concentration-independent and very small contribution to the resistivity,

$$\rho \approx \frac{h}{4e^2} \frac{z^4}{R^2 a^2}. \tag{11.104}$$

For $2H > 1$,

$$\rho \sim n^{1-2H}; \tag{11.105}$$

and for $2H = 1$,

$$\rho \sim \ln^2(k_{\mathrm{F}} a) \tag{11.106}$$

(Katsnelson & Geim, 2008). For the roughness of the substrate, one could expect $2H \approx 1$ (Ishigami *et al.*, 2007). Only frozen ripples with $2H \approx 2$ (such as intrinsic ripples at not too large distances r) are interesting as a scattering mechanism.

Another important potential source of scattering is resonance scattering (see Sections 6.5 and 6.6). They give a concentration dependence of the conductivity that is very close to linear (see Eqs. (6.103)), that is, a weakly concentration-dependent mobility

$$\mu \sim \ln^2(k_{\mathrm{F}} a). \tag{11.107}$$

At least in some cases this reproduces the experimental data better than does just constant mobility (Wehling *et al.*, 2010a; Peres, 2010; Couto, Sacépé & Morpurgo, 2011). This is certainly the case when vacancies are created in graphene by ion bombardment (Chen *et al.*, 2009), but, as discussed in Section 6.5, it is very unlikely that there will be any vacancies in graphene if they are not created intentionally. It was suggested by Wehling *et al.* (2010a) that the resonant scatterers in real graphene samples could be due to the formation of chemical C–C bonds between graphene and organic pollutants on it. Even a very small concentration of such bonds, $<10^{-4}$, would be sufficient to explain the experimental data.

For the case of bilayer graphene, within the parabolic-band approximation one could expect $\sigma \sim n$ and $\mu = \text{constant}$ for the cases of both resonant and generic impurities (Katsnelson, 2007c); see Section 6.3. Straightforward numerical simulations (Yuan, De Raedt & Katsnelson, 2010b) show that for the case of resonant scatterers this is true only if their concentration is very small. When the width of the impurity band exceeds $2|t_\perp|$ there is a crossover to the behaviour typical for single-layer graphene, Eq. (11.107).

To conclude this section, we note that one can expect different main scattering mechanisms in different samples. Currently, it seems that for most situations the choice is between resonant scatterers and frozen ripples, but charge impurities can also be relevant if one protects their more or less random distribution and prevents their clusterization.

11.4 Intrinsic mobility and transport properties of suspended graphene flakes

In this section we will consider intrinsic mobility in graphene in relation to electron phonon interaction (Stauber, Peres & Guinea, 2007; Morozov *et al.*, 2008; Mariani & von Oppen, 2008, 2010; Castro *et al.*, 2010b; Ochoa *et al.*, 2011). We will follow here the last two papers.

The inelastic scattering processes should satisfy the momentum- and energy-conservation laws. For single-phonon processes this means

$$\varepsilon_{\vec{k}} = \varepsilon_{\vec{k}'} \pm h\omega_{\vec{q}}, \tag{11.108}$$

where

$$\vec{k}' = \vec{k} \pm \vec{q}$$

(see Fig. 11.2(a)). The maximum momentum transfer within a given valley is $q = 2k_F$, and both electron states, $\left|\vec{k}\right\rangle$ and $\left|\vec{k}'\right\rangle$, should lie within a layer of the order of T near the Fermi energy. Thus, if

$$T > h\omega_{2k_F} \tag{11.109}$$

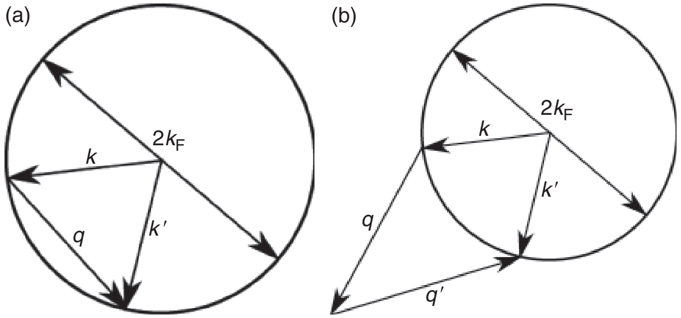

Fig. 11.2. Momentum transfer processes for single-phonon (a) and double-phonon (b) scattering processes.

the scattering processes can be considered almost elastic. The scattering probability is proportional to the number of thermally excited phonons (*virtual* phonons do not contribute to the resistivity, see Ziman (2001)) and is negligible at

$$h\omega_{2k_F} \gg T. \tag{11.110}$$

Up to room temperature, this excludes all optical phonons in graphene from our consideration. It also excludes intervalley scattering processes involving phonons with $\vec{q} \approx \vec{K}$ (see Section 9.7) since for all branches the condition (11.110) is satisfied at $\vec{q} = \vec{K}$ and $T \leq 300\,\mathrm{K}$ (see Fig. 9.1). Thus, we are interested only in acoustic phonons at $q \ll a^{-1}$ (in graphene, k_F is always much smaller than a^{-1}). There are three branches of such phonons, longitudinal (L) and transverse (T) in-plane phonons and flexural (F) out-of-plane phonons with the dispersion relations (see Section 9.2)

$$\omega_{\vec{q}}^{L} = v_L q, \quad v_L = \sqrt{\frac{\lambda + 2\mu}{\rho}}, \tag{11.111}$$

$$\omega_{\vec{q}}^{T} = v_T q, \quad v_T = \sqrt{\frac{\mu}{\rho}}, \tag{11.112}$$

$$\omega_{\vec{q}}^{F} = \sqrt{\frac{\kappa}{\rho}}q^2, \tag{11.113}$$

where ρ is the mass density. Keeping in mind real parameters for graphene, we can estimate the Bloch–Grüneisen temperature, $T_{BG} = h\omega_{2k_F}$, for the various branches:

$$T_{BG}^{L} = 57\sqrt{n}\ \mathrm{K}, \qquad T_{BG}^{T} = 38\sqrt{n}\ \mathrm{K}, \qquad T_{BG}^{F} = 0.1n\,\mathrm{K}, \tag{11.114}$$

where n is expressed in units of $10^{12}\,\mathrm{cm}^{-2}$. At $T > T_{BG}$ (Eq. (11.109)) phonons can be considered classically. One can see that for *flexural* phonons this is actually the case for any practically interesting temperatures.

The electron–phonon interaction in graphene originates from two sources: the electrostatic potential (10.8) which should be substituted into Eq. (11.17) and the vector potential (10.7) modulating the electron hopping. However, the deformation tensor $\hat{u}_{\alpha\beta}$ should be considered as an operator. It is given by Eq. (9.62), and the operators $\hat{u}_\alpha$ and $\hat{h}$ are expressed in terms of the corresponding phonon operators by Eq. (9.9). The resulting Hamiltonian takes the form (Ochoa *et al.*, 2011)

$$\begin{aligned}\hat{H}_{\mathrm{e\ \ ph}} = \sum_{\vec{k}\vec{k}'}\left(\hat{a}^{+}_{\vec{k}}\hat{a}_{\vec{k}'} + \hat{c}^{+}_{\vec{k}}\hat{c}_{\vec{k}'}\right)&\left\{\sum_{\upsilon\vec{q}} V^{\upsilon}_{1,\vec{q}}\left[\hat{b}^{\upsilon}_{\vec{q}} + \left(\hat{b}^{\upsilon}_{\ \ \vec{q}}\right)^{+}\right]\delta_{\vec{k}',\vec{k}\ \ \vec{q}}\right.\\ &\left.+\sum_{\vec{q}\vec{q}'} V^{\mathrm{F}}_{1,\vec{q}\vec{q}'}\left[\hat{b}^{\mathrm{F}}_{\vec{q}} + \left(\hat{b}^{\mathrm{F}}_{\ \ \vec{q}}\right)^{+}\right]\left[\hat{b}^{\mathrm{F}}_{\vec{q}'} + \left(\hat{b}^{\mathrm{F}}_{\ \ \vec{q}'}\right)^{+}\right]\delta_{\vec{k}',\vec{k}\ \ \vec{q}\ \ \vec{q}'}\right\}\\ +\sum_{\vec{k}\vec{k}'}&\left\{\sum_{\upsilon\vec{q}} V^{\upsilon}_{2,\vec{q}}\hat{a}^{+}_{\vec{k}}\hat{c}_{\vec{k}'}\left[\hat{b}^{\upsilon}_{\vec{q}} + \left(\hat{b}^{\upsilon}_{\ \ \vec{q}}\right)^{+}\right]\delta_{\vec{k}',\vec{k}\ \ \vec{q}}\right.\\ &\left.+\sum_{\vec{q}\vec{q}'} V^{\mathrm{F}}_{2,\vec{q}\vec{q}'}\hat{a}^{+}_{\vec{k}}\hat{c}_{\vec{k}'}\left[\hat{b}^{\mathrm{F}}_{\vec{q}} + \left(\hat{b}^{\mathrm{F}}_{\ \ \vec{q}}\right)^{+}\right]\left[\hat{b}^{\mathrm{F}}_{\vec{q}'} + \left(\hat{b}^{\mathrm{F}}_{\ \ \vec{q}'}\right)^{+}\right]\delta_{\vec{k}',\vec{k}\ \ \vec{q}\ \ \vec{q}'} + \mathrm{H.c.}\right\},\end{aligned} \tag{11.115}$$

where $\upsilon = \mathrm{L}, \mathrm{T}$, subscripts 1 and 2 label the terms originating from the scalar potential (10.8) and from the vector potential (10.7), respectively, and $\hat{a}_{\vec{k}}$ and $\hat{c}_{\vec{k}}$ are electron annihilation operators for sublattices A and B, respectively. The matrix elements are

$$\begin{aligned} V^{\mathrm{L}}_{1,\vec{q}} &= \frac{g}{\varepsilon(q,0)}iq\sqrt{\frac{h}{2\rho\Omega\omega^{\mathrm{L}}_{\vec{q}}}},\\ V^{\mathrm{T}}_{1,\vec{q}} &= 0,\\ V^{\mathrm{F}}_{1,\vec{q}\vec{q}'} &= \frac{g}{\varepsilon(|\vec{q}+\vec{q}'|,0)}qq'\cos\left(\varphi_{\vec{q}}\quad\varphi_{\vec{q}'}\right)\frac{h}{4\rho\Omega\sqrt{\omega^{\mathrm{F}}_{\vec{q}}\omega^{\mathrm{F}}_{\vec{q}'}}},\\ V^{\mathrm{L}}_{2,\vec{q}} &= \frac{hv\beta}{2a}iq\exp\left(2i\varphi_{\vec{q}}\right)\sqrt{\frac{h}{2\rho\Omega\omega^{\mathrm{L}}_{\vec{q}}}},\\ V^{\mathrm{T}}_{2,\vec{q}} &= \frac{hv\beta}{2a}q\exp\left(2i\varphi_{\vec{q}}\right)\sqrt{\frac{h}{2\rho\Omega\omega^{\mathrm{T}}_{\vec{q}}}},\\ V^{\mathrm{F}}_{2,\vec{q}\vec{q}'} &= \frac{hv\beta}{4a}qq'\exp\left[i\left(\varphi_{\vec{q}}\quad\varphi_{\vec{q}'}\right)\right]\frac{h}{2\rho\Omega\sqrt{\omega^{\mathrm{F}}_{\vec{q}}\omega^{\mathrm{F}}_{\vec{q}'}}},\end{aligned} \tag{11.116}$$

where Ω is the sample area and we take into account the screening of scalar potential by the static dielectric function (cf. Eq. (11.87)). Note that all matrix elements tend to zero at $q \to 0$ as usual for the interaction with acoustic phonons (Ziman, 2001).

One can see that the electron phonon interaction with flexural phonons does not involve single-phonon processes but only two-phonon ones. This follows from the structure of the deformation tensor (9.62). Single-flexural-phonon processes do arise in deformed samples with some external profile $h_0(x, y)$ (Castro *et al.*, 2010b; Ochoa *et al.*, 2011).

The resistivity can be found using the Kubo Nakano Mori formula (or, equivalently, by derivation and approximate solution of the Boltzmann equation). First, we have to substitute the operator $\hat{H}_{\mathrm{e\ ph}}$ instead of $\hat{H}'$ into Eqs. (11.74) and (11.78). The time dependence of the phonon operators is (Vonsovsky & Katsnelson, 1989)

$$\begin{aligned} \hat{b}_{\vec{q}}(t) &= \hat{b}_{\vec{q}} \exp(\ \ i\omega_{\vec{q}} t), \\ \hat{b}^{+}_{\vec{q}}(t) &= \hat{b}^{+}_{\vec{q}} \exp\left(i\omega_{\vec{q}} t\right). \end{aligned} \tag{11.117}$$

Next, we decouple the electron and phonon operators (this corresponds to the lowest-order approximation in $\hat{H}_{\mathrm{e\ ph}}$) and assume that the phonons are in equilibrium:

$$\begin{aligned} \left\langle \hat{b}^{+}_{\vec{q}} \hat{b}_{\vec{q}} \right\rangle &= N_{\vec{q}} = \frac{1}{\exp\left(h\omega_{\vec{q}}/T\right) \quad 1}, \\ \left\langle \hat{b}_{\vec{q}} \hat{b}^{+}_{\vec{q}} \right\rangle &= 1 + N_{\vec{q}}. \end{aligned} \tag{11.118}$$

This means that we neglect the effects of phonon drag, which makes the phonon system a nonequilibrium one in the presence of an electric current. It is known (Ziman, 2001) that this effect is usually not relevant for the resistivity but may be crucially important for the thermoelectric power. We will not consider it here.

At $T > T^{\mathrm{L,T}}_{\mathrm{BG}}$ the one-phonon scattering can be considered classically, that is, one can put

$$N_{\vec{q}} \approx 1 + N_{\vec{q}} \approx \frac{T}{h\omega_{\vec{q}}} \tag{11.119}$$

and neglect the phonon frequency in the energy-conservation law. The latter can be done, actually, at any temperature, since $\left| \varepsilon_{\vec{k}+\vec{q}} \quad \varepsilon_{\vec{k}} \right| \gg h\omega_{\vec{q}}$, except in the case $\vec{k} \perp \vec{q}$, which does not contribute to the integral characteristics.

In this case, we have just the same problem as for the scattering by static disorder, Eq. (11.79), with

$$\left| V^{\mathrm{eff}}_{\vec{k}\vec{k}'} \right|^2 \sim \left\langle \left| \vec{u}_{\vec{k}\vec{k}'} \right|^2 \right\rangle = \frac{T}{M\omega_{\vec{k}\ \ \vec{k}'}{}^2}. \tag{11.120}$$

An accurate calculation gives the result (Castro *et al.*, 2010b)

$$\frac{1}{\tau} \approx \left[\frac{g^2_{\mathrm{eff}}}{v^2_{\mathrm{L}}} + \frac{\beta^2 h^2 v^2}{a^2} \left(\frac{1}{v^2_{\mathrm{L}}} + \frac{1}{v^2_{\mathrm{T}}} \right) \right] \frac{k_{\mathrm{F}} T}{2\rho h^2 v}, \tag{11.121}$$

where

$$g_{\text{eff}} \approx \frac{g}{\varepsilon(q \approx k_{\text{F}}, 0)} \tag{11.122}$$

is the screened coupling constant. As will be shown below, this contribution is usually much smaller than that due to two-phonon processes (Morozov *et al.*, 2008). This situation is highly unusual; normally, both in a three-dimensional and in a two-dimensional electron gas, single-phonon processes are dominant. It is reminiscent of the case of electron–*magnon* scattering in half-metallic ferromagnets, where single-magnon processes are forbidden and the temperature dependence of the resistivity is determined by two-magnon processes (Irkhin & Katsnelson, 2002).

The energy and momentum conservation for the two-phonon scattering processes can involve phonons with large enough wave vectors (see Fig. 11.2(b)); thus, it is not clear a priori that even at $T > T_{\text{BG}}^{\text{F}}$ (which is, actually, always the case) the classical picture is correct. Nevertheless, as we will see below, this is true, and quantum-mechanical treatment of two-phonon scattering gives approximately the same answer (11.100) as the classical consideration of intrinsic ripples (Morozov *et al.*, 2008).

An accurate treatment of the two-phonon processes leads to the expression (Castro *et al.*, 2010b)

$$\begin{aligned} \frac{1}{\tau} = \frac{1}{32\pi^3 \rho^2 v k_{\text{F}}} \int_0^\infty dK \frac{[D(K)]^2 K^2}{\sqrt{k_F{}^2 - \frac{K^2}{4}}} \int_0^\infty dq \, \frac{q^3 N_q}{\omega_q} \\ \times \int_{|K-q|}^{K+q} dQ \frac{Q^3 (N_Q + 1)}{\omega_Q \sqrt{K^2 q^2 - \frac{\left(K^2 + q^2 - Q^2\right)^2}{4}}}, \end{aligned} \tag{11.123}$$

where we omit the superscript F for ω_q and N_q.

Here

$$[D(K)]^2 = \frac{g^2}{\varepsilon^2(K,0)} \left(1 - \frac{K^2}{4k_F^2}\right) + \left(\frac{\beta h v}{2c}\right)^2. \tag{11.124}$$

One can see that there is no backscattering ($K = 2k_{\text{F}}$) for the scalar potential, but there is backscattering for the vector potential, as there should be (see Chapters 4 and 6).

For the case $q^* \ll k_{\text{F}} \ll q_{\text{T}}$, where q^* is the 'Ginzburg' vector, as in Eq. (11.99), and q_{T} is determined by the condition

$$\omega_{q_{\text{T}}}^{\text{F}} = T \tag{11.125}$$

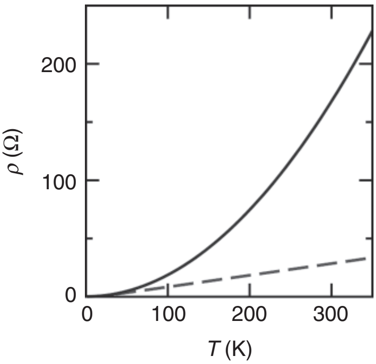

Fig. 11.3. Contributions to the resistivity of single-layer graphene from flexural phonons (solid line) and from in-plane phonons (dashed line). The electronic concentration is $n = 10^{12}\,\mathrm{cm}^{-2}$. (Reproduced with permission from Castro *et al.*, 2010b.)

the result is (Castro *et al.*, 2010b)

$$\frac{1}{\tau} = \frac{D^2 T^2}{64\pi h^2 \kappa^2 v k_{\mathrm{F}}} \ln\left(\frac{T}{h\omega^*}\right), \tag{11.126}$$

where $\omega^* = \omega^{\mathrm{F}}_{q^*}$ and D is some average value of $D(K)$. The cut-off at $q \approx q^*$ is necessary since, as we know, the harmonic approximation is not applied to the flexural phonons at $q \leq q^*$. Equation (11.126) agrees with the estimation (11.100). This justifies our statement that at $q_{\mathrm{T}} \gg k_{\mathrm{F}}$, which is equivalent to $T \gg T^{\mathrm{F}}_{\mathrm{BG}}$, 'two-flexural-phonon' scattering means the same as 'scattering by intrinsic ripples'. The case of low temperatures was studied in detail by Mariani & von Oppen (2008, 2010) and Castro *et al.* (2010b). We will not discuss it since it is not relevant for the current experimental situation.

By comparing Eqs. (11.121) and (11.126) one can estimate that the two-phonon processes dominate at

$$T > T_{\mathrm{c}}\,(\mathrm{K}) \approx 57n\left(10^{12}\,\mathrm{cm}^{-2}\right) \tag{11.127}$$

(Castro *et al.*, 2010b). A quantitative comparison of single-phonon and two-phonon contributions is shown in Fig. 11.3.

The theory for the case of bilayer graphene was developed by Ochoa *et al.* (2011). Both the temperature dependence and the concentration dependence of the resistivity are the same as for the case of single-layer graphene, accurately to within some numerical coefficients.

As has already been mentioned, for graphene on a substrate the intrinsic, temperature-dependent, contribution to the resistivity is negligible in comparison with the extrinsic one. The situation is dramatically different for suspended

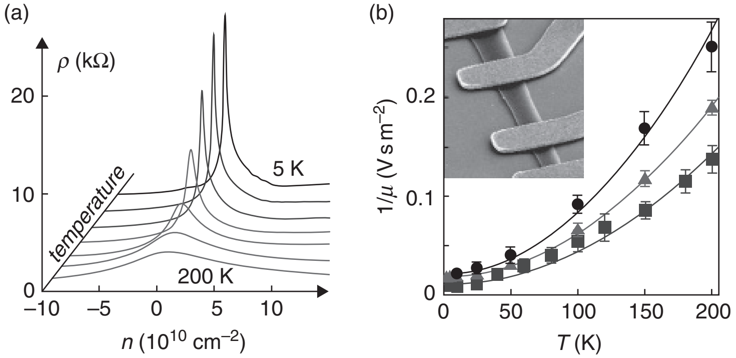

Fig. 11.4. (a) The resistivity of suspended single-layer graphene for $T = 5$, 10, 25, 50, 100, 150 and 200 K. (b) Examples of $\mu(T)$. The inset shows a scanning electron micrograph of one of the suspended devices. (Reproduced with permission from Castro *et al.*, 2010b.)

graphene flakes, for which, after annealing, the defects can be eliminated, and the mobility at liquid helium temperature can be of the order of 10^5–10^6 cm^2 V^{-1} s^{-1} (Du *et al.*, 2008; Bolotin *et al.*, 2008; Castro *et al.*, 2010b; Mayorov *et al.*, 2011). In this case, the intrinsic mobility dominates completely.

Typical experimental data are shown in Fig. 11.4. Comparison between theory and experiment shows (Castro *et al.*, 2010b) that two-flexural-phonon scattering (or, equivalently, scattering by intrinsic ripples) is probably the main limiting factor for the suspended samples. It restricts the mobility at room temperature to a value of the order of 10^4 cm^2 V^{-1} s^{-1} (see Eq. (11.100)). However, the mobility can be increased by expanding the samples. External deformation suppresses flexural phonons, making them stiffer:

$$\rho\omega^2 = \kappa q^4 + 2(\lambda + \mu)q^2 u \tag{11.128}$$

(cf. Eq. (9.148)). Estimations (Castro *et al.*, 2010b) demonstrate that even small deformations of $u \leq 1\%$ may be sufficient to increase the room-temperature mobility by an order of magnitude.

11.5 Nonlocal transport in magnetic fields

Graphene is unique, in the sense that one can pass continuously from electron conductivity to hole conductivity without crossing an insulator region. This means that by applying some small perturbations one can create two subsystems, an electron one and a hole one, differing by some intrinsic quantum number. The simplest case of such a perturbation is Zeeman splitting,

$$\delta = 2\mu_B B, \tag{11.129}$$

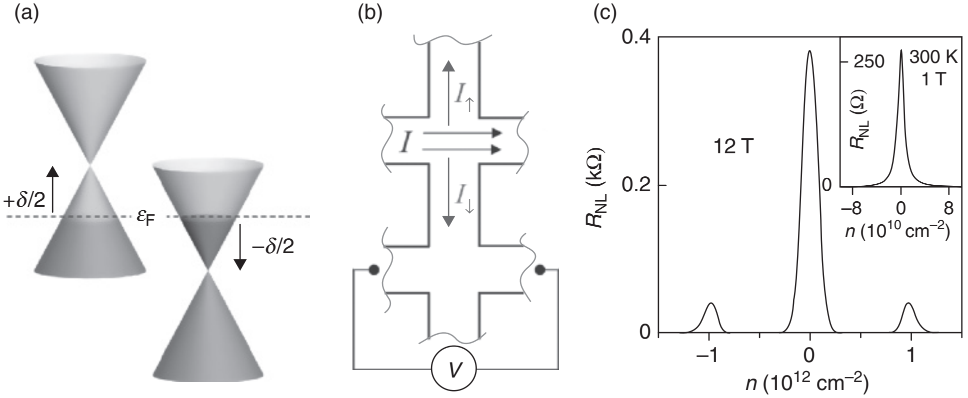

Fig. 11.5. (a) Zeeman splitting at the charge neutrality point. (b) Charge current and spin currents in the presence of the Lorentz force. (c) The nonlocal resistivity predicted by Eq. (11.159) for the quantum Hall regime (main panel) and for weak magnetic fields (inset). (Reproduced with permission from Abanin *et al.*, 2011.)

which makes the spin-up charge carriers be holes and the spin-down charge carriers be electrons (Fig. 11.5(a)). Similar effects can be brought about by valley polarization, but, for simplicity, we will discuss further the effects of spin splitting. Thus, we have a very strong coupling of spin and charge degrees of freedom: by changing the spin direction one can change the sign of charge! This peculiarity of graphene is probably responsible for one of its salient features, a giant nonlocal spin transport near the neutrality point (Abanin *et al.*, 2011).

The mechanism is the following. Suppose you create a charge current across the sample in the presence of an external magnetic field (it does not necessarily need to be strong enough for the system to be in the quantum Hall regime, since the effect under consideration is actually classical). This charge current consists of spin-up and spin-down components, which are, due to Zeeman splitting, electron and hole ones. In the magnetic field they will be deviated in opposite directions, leading to a *spin current* perpendicular to the original charge current. The spin current can propagate without decay for very large distances since the time of spin-flip scattering processes τ_s is normally several orders of magnitude larger than the Drude relaxation time τ. Then, due to an inverse mechanism, this spin current creates a voltage. Here we present a phenomenological theory of this effect (Abanin *et al.*, 2011). Previously similar physics had been discussed for the spin Hall effect in conventional semiconductors (Abanin *et al.*, 2009); however, for the case of graphene the effect is really huge, for the reasons mentioned above.

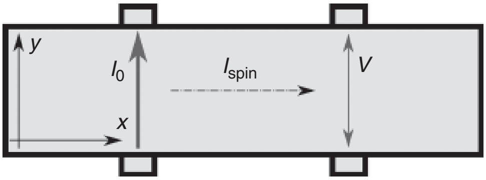

Fig. 11.6. A schematic representation of nonlinear transport (see the text).

Let us consider the geometry shown in Fig. 11.6. First, let us ignore the spin dependence of the conductivity. The relation between the current density and the electric field $\vec{E} = \ \vec{\nabla}\varphi$ is

$$\vec{j} = \ \hat{\sigma}\,\vec{\nabla}\varphi, \tag{11.130}$$

where

$$\hat{\sigma} = \begin{pmatrix} \sigma_{xx} & \sigma_{xy} \\ \sigma_{xy} & \sigma_{xx} \end{pmatrix} \tag{11.131}$$

is the conductivity tensor in the presence of a magnetic field, $\sigma_{xy} \sim B$. Equation (11.131) follows from Onsager's relations

$$\sigma_{\alpha\beta}(B) = \sigma_{\beta\alpha}(\ \ B) \tag{11.132}$$

and the isotropy of macroscopic properties in the xy-plane for the honeycomb lattice. Let us assume charge injection into the point $x = 0$, thus the boundary conditions are

$$j_y\left(y = \pm\frac{w}{2}\right) = I_0\delta(x), \tag{11.133}$$

where w is the sample width.

Owing to the structure of the tensor (11.131), the charge conservation law

$$\vec{\nabla}\vec{j} == 0 \tag{11.134}$$

is equivalent to the Laplace equation

$$\nabla^2\varphi(x, y) = 0 \tag{11.135}$$

with a general solution

$$\varphi(x, y) = \int_{\infty}^{\infty} \frac{dk}{2\pi}[a(k)\cosh(ky) + b(k)\sinh(ky)]\exp(ikx). \tag{11.136}$$

The coefficients $a(k)$ and $b(k)$ should be found from the boundary condition (11.133), that is,

$$\left(\sigma_{xy}\frac{\partial\varphi}{\partial x} - \sigma_{xx}\frac{\partial\varphi}{\partial y}\right)\Bigg|_{y=\pm w/2} = I_0\delta(x). \tag{11.137}$$

The solution is straightforward and gives us the voltage distribution

$$V(x) = \varphi\left(x, -\frac{w}{2}\right) - \varphi\left(x, \frac{w}{2}\right) = 2I_0\rho_{xx}\int_{-\infty}^{\infty}\frac{dk}{2\pi}\frac{\exp(ikx)}{k}\tanh\left(\frac{kw}{2}\right), \tag{11.138}$$

where $\hat{\rho} = \hat{\sigma}^{-1}$ is the resistivity tensor. On calculating the integral explicitly we have the final answer

$$V(x) = \frac{2I_0\rho_{xx}}{\pi}\ln\left(\coth\left(\frac{\pi x}{2w}\right)\right) \approx \frac{4I_0\rho_{xx}}{\pi}\exp\left(-\frac{\pi|x|}{w}\right), \tag{11.139}$$

where in the last equality we assume that $|x| \gg w$. Experimentally, in graphene a rather high nonlocal resistivity

$$R(x) = \frac{V(x)}{I_0} \tag{11.140}$$

is observed at $|x| \geq 5w$ and even $10w$, which cannot be explained by 'just' charge transport ($\exp(-5\pi) \approx 1.5 \times 10^{-7}$). It also cannot be explained by transport via edge states since it is observed beyond the quantum Hall regime as well.

So, let us come back to our original statement that the transport properties in graphene can be anomalously sensitive to the spin projection. In particular, in the situation shown in Fig. 11.5(a)

$$(\sigma_1)_{xy} = -(\sigma_2)_{xy}, \tag{11.141}$$

where subscripts 1 and 2 will be used for spin up and spin down, respectively.

Let us use, instead of Eq. (11.130), two separate Ohm laws for each spin projection:

$$\vec{j}_i = -\hat{\sigma}_i\vec{\nabla}\varphi_i, \tag{11.142}$$

where $\hat{\sigma}_i$ has the structure (11.131) and

$$\varphi_i = \phi + \frac{n_i}{D_i}, \tag{11.143}$$

where

$$D_i = \frac{dn_i}{d\mu} \tag{11.144}$$

is the thermodynamic density of states (note that here μ is the chemical potential, not the mobility, as in the greatest part of this chapter!) and ϕ is the electrostatic potential. The second term on the right-hand side of Eq. (11.143) describes diffusion processes in the situation in which spin-up and spin-down electron densities n_i are finite. We will assume the electroneutrality condition

$$n_1 = \quad n_2 = n \tag{11.145}$$

and separate the total current density $\vec{j}_0$ and the spin current density $\vec{j}'$:

$$\vec{j}_{1,2} = \vec{j}_0 \pm \vec{j}'. \tag{11.146}$$

The equation of spin diffusion reads

$$\vec{\nabla}\vec{j}' = \quad \gamma(n_1 \quad n_2) = \quad 2\gamma n, \tag{11.147}$$

where $\gamma = \tau_s^{\quad 1}$ is the rate of spin-flip processes. Then we have the following set of equations (together with Eq. (11.147)):

$$\vec{\nabla}\phi + \frac{1}{D_1}\vec{\nabla}n = \quad \hat{\rho}_1(\vec{j}_0 + \vec{j}'), \tag{11.148}$$

$$\vec{\nabla}\phi \quad \frac{1}{D_2}\vec{\nabla}n = \quad \hat{\rho}_2(\vec{j}_0 \quad \vec{j}'), \tag{11.149}$$

$$\vec{\nabla}\vec{j}_0 = 0, \tag{11.150}$$

where $\hat{\rho}_i = \hat{\sigma}_i^{\quad 1}$.

One can exclude $\vec{\nabla}\phi$ from these equations and express the spin current as

$$\vec{j}' = \quad \hat{\sigma}\left[\left(\frac{1}{D_1} + \frac{1}{D_2}\right)\vec{\nabla}n + (\hat{\rho}_1 \quad \hat{\rho}_2)\vec{j}_0\right], \tag{11.151}$$

where

$$\hat{\sigma} = \hat{\rho}^{\quad 1}, \qquad \hat{\rho} = \hat{\rho}_1 + \hat{\rho}_2. \tag{11.152}$$

On substituting Eq. (11.151) into Eq. (11.146) and taking into account Eq. (11.137) we find at last the closed equation for the spin density:

$$\nabla^2 n \quad \frac{1}{l_s^2} n = \quad \frac{D_1 D_2}{D_1 + D_2}\vec{\nabla}\left[(\hat{\rho}_1 \quad \hat{\rho}_2)\vec{j}_0\right], \tag{11.153}$$

where l_s is the spin-diffusion length:

$$\frac{1}{l_s^2} = \frac{2\gamma}{\sigma_{xx}} \frac{D_1 D_2}{D_1 + D_2}. \tag{11.154}$$

It follows from Eqs. (11.150) and (11.133) that $j_{0x} = 0$ and j_{0y} does not depend on y:

$$j_{0y} = I_0 \delta(x). \tag{11.155}$$

On substituting Eq. (11.155) into Eq. (11.153) we find a rigorous (within our model) equation:

$$\nabla^2 n - \frac{1}{l_s^2} n = -\frac{D_1 D_2}{D_1 + D_2} \left((\hat{\rho}_1)_{xy} - (\hat{\rho}_2)_{xy} \right) I_0 \frac{d\delta(x)}{dx}. \tag{11.156}$$

If we assume that $w \ll l_s$ we can neglect the y-dependence of n, and Eq. (11.156) is solved immediately:

$$n(x) = -\frac{D_1 D_2}{2(D_1 + D_2)} \left[\left((\rho_1)_{xy} - (\rho_2)_{xy} \right) \right] \cdot I_0 \operatorname{sgn} x \exp\left(-\frac{|x|}{l_s} \right). \tag{11.157}$$

Finally, taking into account that for the thin strip the current is assumed to be constant in the y-direction, we find

$$V(x) = w\left[(\rho_1)_{xy} j_{1x}(x) + (\rho_2)_{xy} j_{2x}(x) \right] = w\left[(\rho_1)_{xy} - (\rho_2)_{xy} \right] j'_x(x) \tag{11.158}$$

and use Eq. (11.151) for j'_x. The final answer for the nonlocal resistance (11.140) is

$$R(x) = \frac{w}{2l_s} \sigma_{xx} \left[(\rho_1)_{xy} - (\rho_2)_{xy} \right]^2 \exp\left(-\frac{|x|}{l_s} \right). \tag{11.159}$$

This formula seems to be in good agreement with the experimental data (Abanin *et al.*, 2011). Actually, this derivation is very general. The only peculiarity of graphene is that near the neutrality point the difference $(\rho_1)_{xy} - (\rho_2)_{xy}$ can be huge (see Fig. 11.5(c)).

11.6 Beyond the Boltzmann equation: localization and antilocalization

In general, the semiclassical Boltzmann equation does not suffice to describe the transport properties of a two-dimensional electron gas because of *weak localization* effects (Altshuler *et al.*, 1980). They originate from quantum interference effects between different trajectories passing in opposite

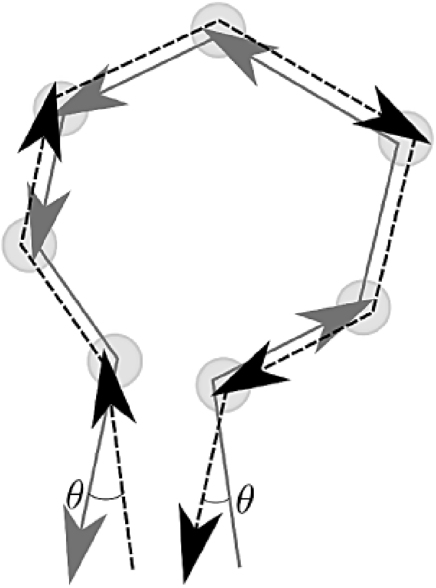

Fig. 11.7. Interference between trajectories with opposite directions of electron motion.

directions (Fig. 11.7). The corresponding correction to the conductivity is of the order of

$$\delta\sigma \sim \pm\frac{e^2}{h}\Lambda, \tag{11.160}$$

where Λ is a 'big logarithm': at $T=0$ it is $\ln(L/a)$. These interference effects are sensitive to the magnetic field (due to the Aharonov Bohm effect), which results in a large magnetoresistivity. Usually, $\delta\sigma<0$ and suppression of the interference by the magnetic field increases the conductivity (negative magnetoresistance). Inelastic scattering processes also destroy the interference, leading to a cut-off of the logarithm: $\Lambda \to \ln(\varepsilon_F/T)$. In graphene, the magnetoresistance related to the weak localization is strongly suppressed, in comparison with the case of a conventional electron gas. This was found by Morozov *et al.* (2006) and explained by them as the effect of random pseudomagnetic fields created by ripples (see Chapter 10). Later, these effects were observed and studied in detail (Tikhonenko *et al.*, 2008, 2009).

Actually, the physics of the weak localization in graphene (McCann *et al.*, 2006) is very complicated. First, the Berry phase π is involved in the interference processes, which changes the sign of localization corrections: instead of weak localization one can have weak *anti*localization. Second, the effects of trigonal warping break the time-reversal symmetry for a given valley, whereas the intervalley scattering processes restore it. Since the trajectories in Fig. 11.7 are related by time reversal, this symmetry is very important. As a result, depending on the types of defects in the sample, one can have either weak localization (and negative magnetoresistance) or weak antilocalization (and positive magnetoresistance). This prediction (McCann *et al.*, 2006) has been confirmed experimentally (Tikhonenko *et al.*, 2009).

Closer to the neutrality point, the localization corrections become of the order of the Boltzmann conductivity and the semiclassical approach fails completely. This happens in a relatively narrow concentration range that is quite difficult to probe experimentally. Theoretically, the situation also does not look very clear. Earlier works were reviewed by Evers & Mirlin (2008). Here we just mention some important, more recent papers: Bardarson *et al.* (2007, 2010), Titov *et al.* (2010) and Ostrovsky *et al.* (2010). The main results are the following.

If we do not take into account intervalley scattering (which means that all inhomogeneities are supposed to be smooth), we never have Anderson localization and the conductivity at the neutrality point remains of the order of minimal metallic conductivity (see Chapter 3) or grows slowly with the sample size (antilocalization). In particular, random pseudomagnetic fields have no effect on the value of the minimal conductivity since they can be eliminated by a gauge transformation similar to that discussed in Section 3.4 (Ostrovsky, Gornyi & Mirlin, 2008). The random mass term ($V_z\sigma_z$ in Eq. (11.33)) affects the value of the minimal conductivity very weakly, except when the average mass is not zero ($\langle V_z \rangle \neq 0$); in that case localization is possible (Bardarson *et al.*, 2010). For a random scalar potential, antilocalization seems to arise (Bardarson *et al.*, 2007).

In the presence of intervalley scattering, Anderson localization takes place, in the generic case. However, the most interesting case of resonant scatterers such as vacancies or covalently bonded adatoms (see Chapter 6) requires special consideration, due to the additional ‘chiral’ symmetry (Altland, 2002; Evers & Mirlin, 2008; Ostrovsky *et al.*, 2010; Titov *et al.*, 2010). It seems that in this case the localization radius diverges at the neutrality point and the conductivity at $n = 0$ remains at the level of the minimal conductivity. All these issues require further study, both theoretically and, especially, experimentally.

12

Spin effects and magnetism

12.1 General remarks on itinerant-electron magnetism

Up to now we have not discussed physical phenomena in graphene related to the spin of the electron (here we mean *real* spin and associated with it magnetic moment, rather than *pseudo*spin, or the sublattice index, which plays so essential a role throughout the book). The only exception was Zeeman splitting in an external magnetic field but, of course, this is just the simplest (and probably not the most interesting) of the spin effects. In this chapter we will discuss these spin phenomena.

First, due to exchange interactions of purely quantum-mechanical origin, various types of magnetic order can arise (Herring, 1966; Vonsovsky, 1974; Moriya, 1985; Yosida, 1996). The situation with possible magnetic ordering in graphene and other carbon-based materials is highly controversial (see Section 12.2) but, due to the huge interest in the field and its potential practical importance, this issue deserves some discussion. Before doing this, it is worth recalling some general concepts and models of itinerant-electron magnetism.

The simplest model used in the theory of itinerant-electron magnetism is the so-called *Hubbard model* (Hubbard, 1963; Kanamori, 1963; Gutzwiller, 1963). The Hamiltonian reads

$$\hat{H} = \sum_{ij\sigma} t_{ij} \hat{c}_{i\sigma}^{+} \hat{c}_{j\sigma} + U \sum_{i} \hat{n}_{i\uparrow} \hat{n}_{i\downarrow}, \tag{12.1}$$

where $\hat{c}_{i\sigma}^{+}$ and $\hat{c}_{i\sigma}$ are creation and annihilation operators, respectively, on site i with the spin projection $\sigma = \uparrow, \downarrow$, t_{ij} are the hopping parameters, $\hat{n}_{i\sigma} = \hat{c}_{i\sigma}^{+} \hat{c}_{i\sigma}$ are operators of electron number and U is the intra-site interaction parameter. The main approximation in the Hubbard model is that we neglect inter-site Coulomb interaction. The Hamiltonian (12.1) is a simplification of a more general ‘polar model’ (Schubin & Wonsowski, 1934). One can easily generalize the Hamiltonian (12.1) to the multiband case:

$$\hat{H} = \sum_{ij\sigma\lambda\lambda'} t_{i\lambda,j\lambda'} \hat{c}^{+}_{i\lambda\sigma} \hat{c}_{j\lambda'\sigma} + \frac{1}{2} \sum_{\substack{i\sigma\sigma' \\ \lambda_1\lambda_2\lambda_1'\lambda_2'}} \langle \lambda_1\lambda_2 | U | \lambda_1'\lambda_2' \rangle \hat{c}^{+}_{i\lambda_1\sigma} \hat{c}^{+}_{i\lambda_2\sigma'} \hat{c}_{i\lambda_2'\sigma'} \hat{c}_{i\lambda_1'\sigma}, \tag{12.2}$$

where λ is an orbital (band) quantum number.

The simplest theory of itinerant-electron magnetism was proposed by Stoner (1936). It is based just on the mean-field (Hartree Fock) approximation. Let us make the following replacement in the Hamiltonian (12.1):

$$\hat{n}_{i\uparrow}\hat{n}_{i\downarrow} \to \hat{n}_{i\uparrow} n_{\downarrow} + \hat{n}_{\uparrow} n_{\uparrow}, \tag{12.3}$$

where we assume also that the averages $\langle \hat{n}_{i\sigma} \rangle \equiv n_\sigma$ are not dependent on i (but can be spin-dependent). After the standard Fourier transformation, the Hamiltonian (12.1) with the replacement (12.3) takes the form

$$\hat{H} = \sum_{\vec{k}} t_\sigma\left(\vec{k}\right) \hat{c}^{+}_{\vec{k}\sigma} \hat{c}_{\vec{k}\sigma}, \tag{12.4}$$

where

$$\begin{aligned} t_\uparrow\left(\vec{k}\right) &= t\left(\vec{k}\right) + U n_\downarrow, \\ t_\downarrow\left(\vec{k}\right) &= t\left(\vec{k}\right) + U n_\uparrow. \end{aligned} \tag{12.5}$$

This is just a single-electron Hamiltonian, and one can easily find

$$n_\sigma = \sum_{\vec{k}} f_{\vec{k}\sigma}, \tag{12.6}$$

where

$$f_{\vec{k}\sigma} = f\left(t_\sigma\left(\vec{k}\right)\right) \tag{12.7}$$

is the Fermi distribution function. One can show straightforwardly that nontrivial solutions with $n_\uparrow \neq n_\downarrow$ corresponding to the ferromagnetic order exist if

$$\alpha \equiv U N(\varepsilon_{\mathrm{F}}) > 1, \tag{12.8}$$

where

$$N(\varepsilon) = \sum_{\vec{k}} \delta\left(\varepsilon \quad t\left(\vec{k}\right)\right) \tag{12.9}$$

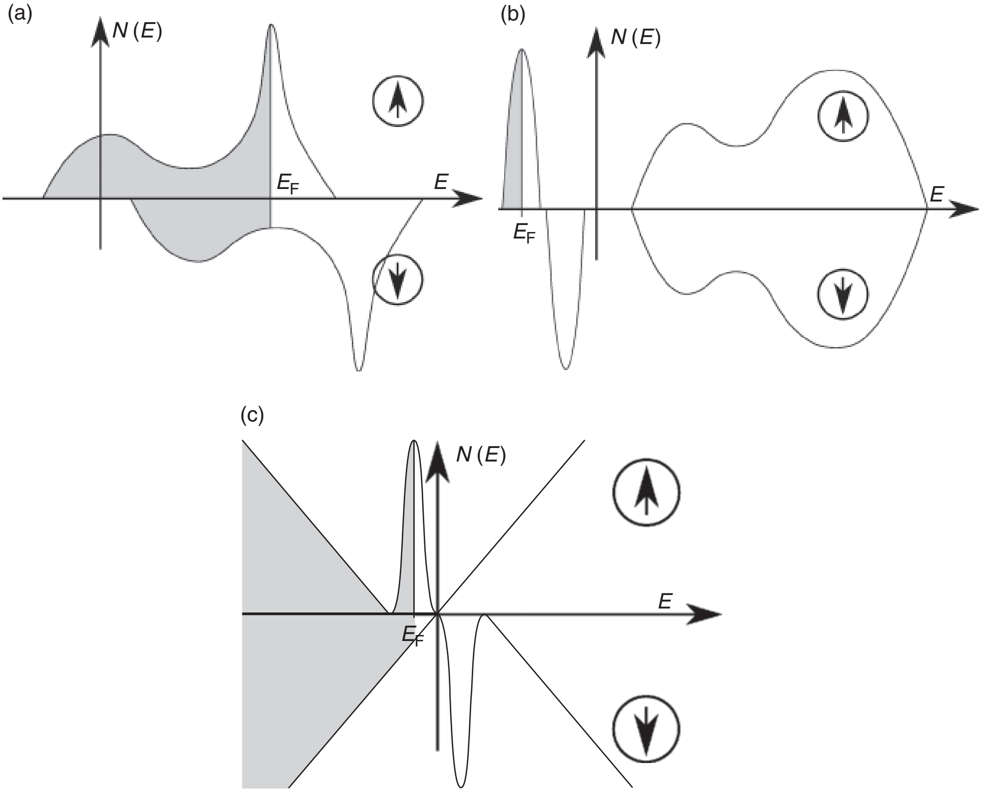

Fig. 12.1. A sketch of the electronic structures for various types of itinerant-electron ferromagnet: (a) the conventional case; (b) and (c) defect-induced half-metallic ferromagnetism in semiconductors and in graphene, respectively.

is the density of states (per spin projection). The inequality (12.8) is called the *Stoner criterion*. In the Stoner approximation (12.5) the densities of states for spin-up and spin-down electrons are related by just a rigid shift (see Fig. 12.1(a)). When $\alpha \to 1$, the saturation magnetization (in units of the Bohr magneton)

$$M(T=0) = n_{\uparrow}(T=0) - n_{\downarrow}(T=0) \sim \sqrt{\alpha - 1}. \qquad (12.10)$$

When the temperature increases the magnetization decreases, vanishing at the Curie temperature T_C determined by the condition

$$U \int d\varepsilon \left(-\frac{\partial f}{\partial \varepsilon} \right) N(\varepsilon) = 1. \qquad (12.11)$$

At $\alpha \to 1$,

$$T_C \sim \sqrt{\alpha - 1} \qquad (12.12)$$

in the Stoner approximation.

Using the identity $\hat{n}_{i\sigma}^2 = \hat{n}_{i\sigma}$ one can rewrite the interaction term in the Hubbard Hamiltonian (12.1) as

$$U\sum_i \hat{n}_{i\uparrow}\hat{n}_{i\downarrow} = \frac{U}{2}\sum_i \left(\hat{n}_{i\uparrow} + \hat{n}_{i\downarrow}\right) - \frac{U}{2}\sum_i \left(\hat{n}_{i\uparrow} - \hat{n}_{i\downarrow}\right)^2. \tag{12.13}$$

The first term is just a renormalization of the chemical potential and can therefore be neglected. The Stoner approximation is exact for some artificial model with infinitely long-range and infinitely weak interaction:

$$\hat{H} = \sum_{ij\sigma} t_{ij}\hat{c}_{i\sigma}^{+}\hat{c}_{j\sigma} - \frac{U}{4N_0}\left(\hat{N}_\uparrow - \hat{N}_\downarrow\right)^2, \tag{12.14}$$

where N_0 is the number of sites,

$$\hat{N}_\sigma = \sum_i \hat{n}_{i\sigma}. \tag{12.15}$$

Importantly, two terms on the right-hand side of Eq. (12.14) commute and (using for them the notations $\hat{H}_1$ and $\hat{H}_2$)

$$\exp(-\beta\hat{H}) = \exp(-\beta\hat{H}_1)\exp(-\beta\hat{H}_2). \tag{12.16}$$

Using further the Hubbard–Stratonovich transformation

$$\exp\left[\frac{\beta U}{4N_0}\left(\hat{N}_\uparrow - \hat{N}_\downarrow\right)^2\right] = \left(\frac{N_0\beta}{4\pi U}\right)^{1/2}\int_{-\infty}^{\infty} d\Delta \exp\left[-\frac{N_0\beta\Delta^2}{4U} - \frac{\beta\Delta}{2}\left(\hat{N}_\uparrow - \hat{N}_\downarrow\right)\right], \tag{12.17}$$

one can calculate the partition function by integrating over Δ by the saddle-point method, the latter being exact in the limit $N_0 \to \infty$. This leads *exactly* to Eqs. (12.5)–(12.7).

This allows us to understand the physical meaning of the Stoner criterion (12.8). Let us remove

$$\delta N = \frac{\left(\langle\hat{N}_\uparrow\rangle - \langle\hat{N}_\downarrow\rangle\right)}{2} \ll N \tag{12.18}$$

electrons (N is the total number of electrons) from the states with $\sigma = \downarrow$ below the Fermi energy to the states with $\sigma = \uparrow$ above the Fermi energy (see Fig. 12.2). Each of these electrons increases its band energy by

$$\delta\varepsilon = \delta N \cdot \Delta_1, \tag{12.19}$$

where

$$\Delta_1 = \frac{1}{N(\varepsilon_{\mathrm{F}})N_0} \tag{12.20}$$

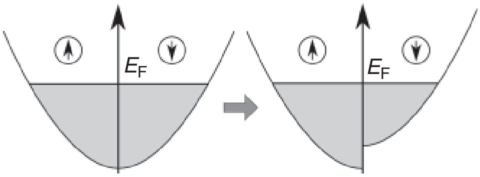

Fig. 12.2. Spontaneous spin polarization in itinerant-electron ferromagnets.

is the average distance between the single-particle energies near the Fermi energy ($N(\varepsilon_F)$ is the density of states *per site*, and the total density of states of the whole system is N_0 times larger). Thus, the increase of the total band energy is

$$\delta E_{\text{band}} = \delta N \, \delta\varepsilon \;\; = \frac{\left(\langle \hat{N}_\uparrow \rangle \quad \langle \hat{N}_\downarrow \rangle\right)^2}{4N(\varepsilon_F)N_0}. \tag{12.21}$$

At the same time, according to Eq. (12.14), the decrease of the interaction energy is

$$\delta E_{\text{int}} = \quad \frac{U\left(\langle \hat{N}_\uparrow \rangle \quad \langle \hat{N}_\downarrow \rangle\right)^2}{4N_0}. \tag{12.22}$$

The Stoner creation (12.8) is nothing but the condition that the spin polarization is energetically favourable,

$$\delta E_{\text{band}} + \delta E_{\text{int}} < 0. \tag{12.23}$$

Typically, itinerant-electron ferromagnetism in 3d metals and in their alloys and compounds is related to situations in which in the paramagnetic case the Fermi energy ε_F lies close to the peak of the density of states formed by a merging of Van Hove singularities; this is true for the prototype cases like Fe and Ni, as well as for weak itinerant-electron ferromagnets like $ZrZn_2$ (Irkhin, Katsnelson & Trefilov, 1992, 1993). Actually, this means *some* instability, not necessarily magnetic; it can also be a structural instability (Katsnelson, Naumov & Trefilov, 1994). This remark will be essential when we discuss the possibility of ferromagnetism in graphene with defects (see the next section).

In realistic models with a finite radius of inter-electron interaction the Stoner theory of ferromagnetism is not accurate. First, as was shown by Kanamori (1963), the bare Coulomb interaction U in the criterion (12.8) should be replaced by the T-matrix; this statement becomes accurate in the limit of a small concentration of electrons or holes (the gaseous approximation) (Galitskii, 1958a, 1958b). For the multiband Hubbard model (12.2) the T-matrix is determined by the equation (Edwards & Katsnelson, 2006)

$$\langle 13|T(E)|24\rangle = \langle 13|U|24\rangle + \sum_{5678} \langle 13|U|57\rangle\langle 57|P(E)|68\rangle\langle 68|T(E)|24\rangle, \quad (12.24)$$

where $|1\rangle = |i_1\lambda_1\rangle$ and

$$\langle 57|P(E)|68\rangle = \int_{\infty}^{\infty} dx \int_{\infty}^{\infty} dy \frac{1 \quad f(x) \quad f(y)}{E \quad x \quad y} \rho_{56}(x)\rho_{78}(y), \quad (12.25)$$

in which $\rho_{12}(x)$ is the corresponding site- and orbital-resolved spectral density and $f(x)$ is the Fermi distribution function. If we have a more or less structureless electron band of width W, $P(E) \sim 1/W$, and, in the limit of strong interaction $U \gg W$,

$$T(E) \approx W. \quad (12.26)$$

At the same time, $N(E) \approx 1/W$ and, in general, after the replacement $U \rightarrow T(\varepsilon_F)$, $\alpha \approx 1$, in clear contradiction with the original criterion (12.8). Thus, one can conclude that the Stoner theory overestimates the tendency towards ferromagnetism even at temperature $T = 0$.

The situation is essentially different in the cases in which the ferromagnetism is due to some defect-induced (e.g., by an impurity or vacancy) band in a gap, or pseudogap, of the main band (see Figs. 12.1(b) and (c)). This situation is relevant for graphene, as will be discussed in the next section. As was shown by Edwards & Katsnelson (2006), in such cases the T-matrix renormalization is less relevant, and the renormalized interaction $T(\varepsilon_F)$ is close to the bare one, U.

Even more serious problems with the Stoner theory arise at finite temperatures. One can demonstrate that, in general, the main suppression of magnetization is not due to the single-particle excitations but due to collective spin fluctuations (Moriya, 1985). As a result, the Curie temperature is strongly overestimated within the Stoner theory; if iron were a 'Stoner ferromagnet' it would have $T_C \approx 4000$ K instead of the real value of $T_C \approx 1043$ K (Liechtenstein, Katsnelson & Gubanov, 1985). For the case of weak itinerant-electron ferromagnets, $\alpha \rightarrow 1$, the true behaviour is (Moriya, 1985)

$$T_C \sim (\alpha \quad 1)^{3/4} \quad (12.27)$$

instead of Eq. (12.12).

At low temperatures, these spin fluctuations are nothing other than spin waves, as in localized (Heisenberg) magnets (Fig. 12.3). Typically, the energy of spin *rotations* is much smaller than that of electron hole (Stoner) excitations. However, the case of ferromagnetism in a narrow defect-induced band is special also in this sense (Edwards & Katsnelson, 2006).

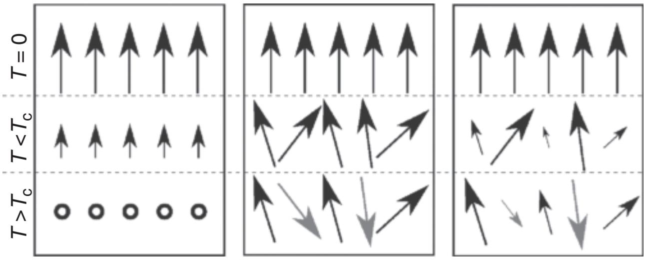

Fig. 12.3. The temperature evolution of ferromagnetic states in the Stoner model (left panel), in the Heisenberg model (middle panel) and in real itinerant-electron ferromagnets (right panel).

To explain this important point we need to describe first another basic model of itinerant-electron ferromagnets, the *s d exchange model* (Vonsovsky, 1946; Zener, 1951a, 1951b, 1951c; Vonsovsky & Turov, 1953). Nowadays this model is frequently called the *Kondo lattice model*, after the very important work of Kondo (1964) on a magnetic impurity in a metal. I think it is fairer historically to talk about the Kondo *effect* within the s d exchange (or Vonsovsky Zener) *model*.

Within this model it is postulated that there exist some local magnetic moments described by spin operators $\hat{\vec{S}}_i$ and that they interact locally with the spins of conduction electrons:

$$\hat{H} = \sum_{ij\sigma} t_{ij} \hat{c}^{+}_{i\sigma} \hat{c}_{j\sigma} \quad I \sum_i \hat{\vec{S}}_i \hat{\vec{s}}_i, \tag{12.28}$$

where

$$\hat{\vec{s}}_i = \frac{1}{2} \sum_{\sigma\sigma'} \hat{c}^{+}_{i\sigma} \hat{\vec{\sigma}}_{\sigma\sigma'} \hat{c}_{i\sigma'} \tag{12.29}$$

and I is the s d exchange interaction constant. Despite the fact that the Hamiltonian (12.28) does not contain the exchange interactions between the localized spins at different sites, it arises as an *indirect* interaction via conduction electrons known as *RKKY* (Ruderman Kittel Kasuya Yosida) *interaction* (Vonsovsky, 1974). Within the lowest order of the perturbation expansion in I, the effective Hamiltonian for localized spins is

$$\hat{H}_{\text{eff}} = \quad \sum_{i<j} J_{ij} \hat{\vec{S}}_i \hat{\vec{S}}_j, \tag{12.30}$$

where

$$J_{ij} = I^2 \chi_{ij} \tag{12.31}$$

and

$$\chi_{ij} = \frac{1}{4} T \sum_{\varepsilon_n} G^{(0)}_{ij}(i\varepsilon_n + \mu) G^{(0)}_{ji}(i\varepsilon_n + \mu) \tag{12.32}$$

is the inhomogeneous susceptibility of conduction electrons. Equation (12.32) is reminiscent of Eq. (6.135) for the interaction between adatoms and can be derived in a similar way. The RKKY interaction (12.31) for the case of graphene has some interesting properties, which will be discussed in the next section.

The criterion of applicability of the expressions (12.30) and (12.31) is the smallness of the spin polarization in the conduction-electron subsystem. For the case of systems with complete spin polarization, such as magnetic semiconductors (Nagaev, 1983, 2001) and half-metallic ferromagnets (Katsnelson *et al.*, 2008) the situation is totally different and, instead, the *double-exchange* mechanism is responsible for the ferromagnetism, with an essentially non-Heisenberg character of exchange interactions (Auslender & Katsnelson, 1982). In this case, typical spin-wave energies are of the order of

$$h\omega_{\mathrm{sw}} \approx \frac{n|t|}{M}, \tag{12.33}$$

where n is the charge-carrier concentration and M is the magnetization (Edwards, 1967; Irkhin & Katsnelson, 1985a, 1985b). This formula is valid both for s d exchange and for Hubbard models. In the first case, M is of the order of one and, for small enough n,

$$h\omega_{\mathrm{sw}} \ll \varepsilon_{\mathrm{F}} \tag{12.34}$$

since $\varepsilon_{\mathrm{F}} \sim n^{2/3}$ (for the three-dimensional case) and $\varepsilon_{\mathrm{F}} \sim n^{1/2}$ (for the two-dimensional case). If we have a strong polarization in the defect-induced band (see Figs. 12.1(b) and (c)) $M \sim n$ should hold and

$$h\omega_{\mathrm{sw}} \sim |t| \gg \varepsilon_{\mathrm{F}}. \tag{12.35}$$

Thus, we have a very unusual situation in which the spin rotations are more energetically expensive than the electron hole (Stoner) excitations. Also, as was mentioned above, the T-matrix renormalization of the Stoner criterion is not relevant here. As a result, one can conclude that, if it were possible to create ferromagnetism in the defect-induced band of itinerant electrons, this situation would be described by the Stoner model and one could expect much higher Curie temperatures than for conventional magnetic semiconductors (Edwards & Katsnelson, 2006). This is one of the strongest motivations for the search for ferromagnetism in sp-electron systems, including graphene.

12.2 Defect-induced magnetism in graphene

Experimentally, sp-electron magnetism, in particular in carbon-based materials, is one of the most controversial issues in modern materials science (for reviews, see Esquinazi & Höhne, 2005; Makarova & Palacio, 2006; Yazyev, 2010). Typically, the observed experimental magnetic moment (when there the existence of ferromagnetism has been claimed) is very small, $\mu \leq 10^{\ 3}\ \ 10^{\ 4}\mu_B$ per atom. Keeping in mind that magnetic iron is everywhere on this planet (dust contains a lot of ferrimagnetic magnetite, Fe_3O_4) the question of possible contamination is crucial, and it is very difficult to demonstrate convincingly that the observed magnetism is intrinsic (Nair *et al.*, 2011). To follow better the possible arguments and counterarguments see, e.g., reviews of the scientific literature on the magnetism of CaB_6 (Edwards & Katsnelson, 2006) and of polymerized fullerenes (Boukhvalov & Katsnelson, 2009c). Importantly, one can prove (Edwards & Katsnelson, 2006) that a Curie temperature of the order of room temperature is thermodynamically incompatible with $\mu \leq 10^{\ 2}\mu_B$; thus, if one observes ferromagnetic ordering with $\mu \approx 10^{\ 3}\ \ 10^{\ 4}\mu_B$ at room temperature it should be either a mistake or a strongly inhomogeneous situation, with ferromagnetic regions with local $\mu > 10^{\ 2}\mu_B$ in a nonmagnetic surrounding.

The first experimental study of magnetism of *graphene* (actually, graphene paper, a mixture of single-layer and multilayer graphene, was studied) did not reveal any magnetic ordering but, rather, a quite mysterious paramagnetism (Sepioni *et al.*, 2010).

It is natural to ask why we should discuss so controversial an issue at all. Well, first, it is a really hot subject. More importantly, some theoretical results seem to be reliable (actually, there are even some *theorems*, as will be discussed below) and worthy of consideration. They also give us a deeper understanding of the physics of defects (Chapter 6) and edge states (Chapter 5) in graphene.

Let us start with the case of vacancies (Section 6.5) or covalently bonded adsorbates (Section 6.6). As we have seen, their electronic structures are quite similar, so, in the simplest approximation, the vacancy can be considered as a model for the hydrogen adatom or some other 'resonant-scattering' centre. All these defects create mid-gap states within the graphene pseudogap (see Fig. 6.1). As was discussed in the previous section, a peak in the density of states near the Fermi energy can lead to a magnetic instability. This conclusion is confirmed by straightforward density-functional calculations: the periodic array of vacancies or hydrogen adatoms on graphene has a tendency to undergo spontaneous spin polarization (Yazyev & Helm, 2007). The corresponding electronic structure is shown in Fig. 12.4. For large enough distances between the defects, the magnetic moment per defect is close to the magnitude of the Bohr magneton, μ_B.

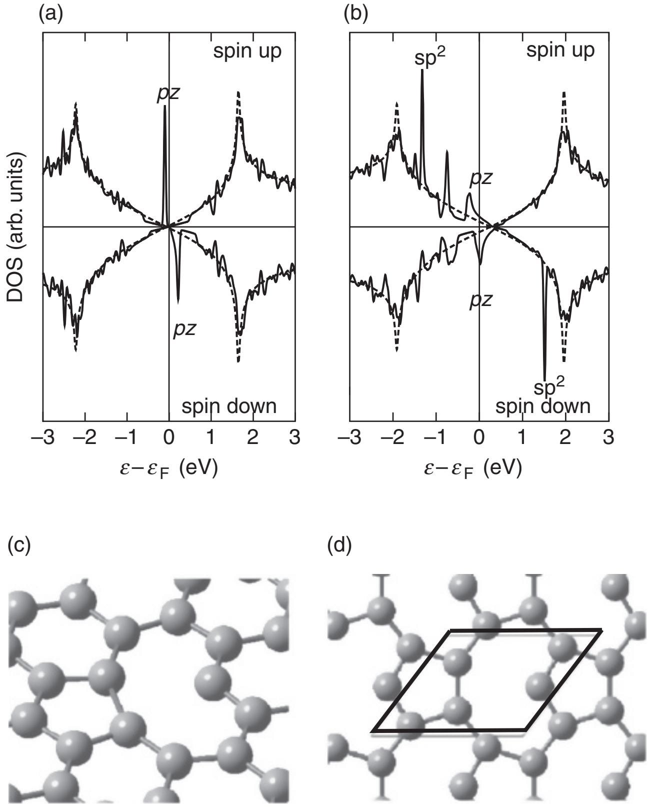

Fig. 12.4. Spin-polarized densities of states of (a) a hydrogen adatom and (b) a vacancy in graphene; (c) and (d) show the atomic structures for the case of a vacancy. (Reproduced with permission from Yazyev & Helm, 2007.)

Very recently, such magnetic moments have been observed experimentally in graphene with vacancies and in fluorinated graphene; no magnetic *ordering* has been found (Nair *et al.*, 2011). It is associated with dangling bonds but distributed over a rather large surrounding area. Bivacancies (Boukhvalov & Katsnelson, 2009c) or couples of neighbouring hydrogen atoms (Boukhvalov, Katsnelson & Lichtenstein, 2008) turn out to be nonmagnetic.

The real meaning of these results is clarified by the *Lieb theorem* (Lieb, 1989), one of the few rigorous results in the theory of itinerant-electron magnetism. The theorem is about the ground state of the single-band Hubbard model (12.1) on a bipartite lattice; the honeycomb lattice is just an example of this generic case. The most general definition of the bipartite lattice is that it consists of two sublattices, A and B, such that all hopping integrals within the same sublattice are zero:

$$\hat{t}_{\mathrm{AA}} = \hat{t}_{\mathrm{BB}} = 0. \qquad (12.36)$$

Therefore, the band part of the Hamiltonian for the bipartite lattice has the structure

$$\hat{H}_0 = \begin{pmatrix} 0 & \hat{t} \\ \hat{t}^+ & 0 \end{pmatrix} \tag{12.37}$$

with nonzero blocks only between two sublattices. Let us consider the case in which the numbers of sites within the sublattices A and B, N_A and N_B, can be different. This means that we have vacancies, and the numbers of vacancies belonging to A and to B are, in general, not the same. Thus, $\hat{t}$ is an $N_A \times N_B$ matrix.

Before discussing the effects of interactions, let us consider some properties of the single-particle spectrum of the Hamiltonian (12.37) (Inui, Trugman & Abrahams, 1994; Kogan, 2011). We will assume, to be specific, that $N_B \geq N_A$.

First, there are at least $N_B - N_A$ linearly independent eigenfunctions with the eigenvalue $E = 0$ and all components equal to zero on the sites of the A sublattice. This is the obvious consequence of the structure (12.37): the system of linear equations

$$\hat{t}\psi = 0 \tag{12.38}$$

has at least $N_B - N_A$ linearly independent solutions.

Second, for the eigenfunctions $\psi_n = \{\psi_n(i)\}$ corresponding to the nonzero eigenvalues E_n,

$$\begin{pmatrix} -E_n & \hat{t} \\ \hat{t}^+ & -E_n \end{pmatrix} \psi_n = 0, \tag{12.39}$$

there is a symmetry property,

$$\psi_{\bar{n}}(i) = \pm\psi_n(i), \tag{12.40}$$

where $\psi_{\bar{n}}$ are the eigenfunctions corresponding to $-E_n$ and the plus and minus signs on the right-hand side of Eq. (12.40) correspond to the cases in which i belongs to A and B, respectively.

Thus, the spectrum of the Hamiltonian (12.37) is symmetric (if E_n is an eigenvalue, $-E_n$ is an eigenvalue too) and contains at least $N_B - N_A$ solutions with $E = 0$. It turns out that the latter states are unstable with respect to spontaneous spin polarization at arbitrarily small $U > 0$ (Lieb, 1989).

Moreover, the Lieb theorem claims that the ground state of the Hubbard model (12.1) with $U > 0$, the single-particle Hamiltonian (12.37) and the number of electrons equal to the number of sites, $N = N_A + N_B$, is unique (apart from the trivial $(2S + 1)$-fold degeneracy) and has the spin

$$S = \frac{N_B - N_A}{2}. \tag{12.41}$$

The theorem can be proved in two steps. First, it is shown that the ground state is unique at any U, that is, that the states belonging to different multiplets with spins S and $S' \neq S$ cannot both be eigenstates with the minimal energy. The consequence is that the ground-state spin S cannot be dependent on U. In the opposite case there will unavoidably be a crossing of the minimal energies with a given spin, $E_0(S;U)$ and $E_0(S';U)$, at some $U = U_c$. Second, in the limit of large U and $N = N_0$ the Hubbard model (12.1) is equivalent to the Heisenberg model with the Hamiltonian

$$\hat{H}' = \sum_{i<j} \frac{2|t_{ij}|^2}{U} \left(\hat{\vec{s}}_i \hat{\vec{s}}_j \quad \frac{1}{4} \right) \tag{12.42}$$

(see, e.g., Yosida, 1996) and for the latter the result (12.41) can be proved quite straightforwardly and easily (Lieb & Mattis, 1962).

Importantly, the Lieb theorem does not assume the thermodynamic limit $N_0 \to \infty$ and is valid also for small systems. Its applications to the magnetic properties of finite graphene fragments have been discussed by Yazyev (2010).

It follows from the Lieb theorem that if all vacancies sit in the same sublattice their spins are parallel in the ground state. If, oppositely, $N_A = N_B$, the ground state is a singlet, with $S = 0$. This means that the interactions between vacancy-induced magnetic moments are ferromagnetic if the vacancies belong to the same sublattice and antiferromagnetic if they belong to different sublattices. As we see, this result is rigorous within the Hubbard model with half-filling ($N = N_0$). The same conclusion for the covalently bonded adatoms or vacancies follows from the density-functional calculations (Yazyev & Helm, 2007; Boukhvalov & Katsnelson, 2011).

It can be also proved for the RKKY interaction (12.31) within the s d exchange model (12.28) (Kogan, 2011). By Fourier transformation of Eq. (12.32) it can be represented as

$$\chi_{ij} = \quad \frac{1}{4} \int_0^\beta d\tau \, G_{ij}^{(0)}(\tau) G_{ji}^{(0)}(\quad \tau), \tag{12.43}$$

where $\beta = T^{\quad 1}$ and

$$G_{ij}^{(0)}(\tau\ ) = T \sum_{\varepsilon_n} G_{ij}^{(0)}(i\varepsilon_n + \mu) \exp(\quad i\varepsilon_n \tau) \tag{12.44}$$

(see also Cheianov *et al.*, 2009). It can be expressed in terms of the eigenfunctions and eigenenergies of the Hamiltonian $\hat{H}_0$ (Mahan, 1990),

$$G_{ij}^{(0)}(\tau) = \sum_n \psi_n^*(i)\psi_n(j)\exp(-\xi_n\tau)[f(\xi_n) - \theta(\tau)], \tag{12.45}$$

where $\xi_n = E_n - \mu$ and $\theta(\tau > 0) = 1$, $\theta(\tau < 0) = 0$.

For the case of an undoped bipartite lattice, $\mu = 0$, using Eq. (12.40) one finds

$$G_{ji}^{(0)}(-\tau) = \mp\left[G_{ij}^{(0)}(\tau)\right]^*, \tag{12.46}$$

where the minus and plus signs correspond to the cases in which *i* and *j* belong to the same sublattice and to different sublattices, respectively. As a result,

$$\chi_{ij} = \pm\frac{1}{4}\int_0^\beta d\tau\left|G_{ij}^{(0)}(\tau)\right|^2. \tag{12.47}$$

On substituting Eq. (12.47) into Eqs. (12.30) and (12.31) we come, again, to the conclusion that for the undoped (half-filled) case the exchange interactions are ferromagnetic within the same sublattice and antiferromagnetic between sites from different sublattices.

12.3 Magnetic edges

It is clear from the previous consideration that the possibility of ferromagnetism in graphene-like systems is related to zero-energy modes and other mid-gap states. As was discussed in Chapter 5 the zero-energy modes arise naturally for a generic boundary of a terminated honeycomb lattice (see Eq. (5.70)). One can conclude therefore that the edges should be magnetic (except in the case of armchair edges, for which there are no mid-gap states). This was first suggested by Fujita *et al.* (1996) and confirmed by numerous further calculations (e.g., Son, Cohen & Louie, 2006a; Yazyev & Katsnelson, 2008; for a review, see Yazyev, 2010). If we have nanoribbons with zigzag edges, the atoms at the opposite edges belong to different sublattices. Therefore, one can expect that the exchange interactions between the edges are antiferromagnetic and that the nanoribbon as a whole should have no magnetic moment. Within the framework of the Hubbard model this just follows from the Lieb theorem. The density-functional calculations by Son, Cohen & Louie (2006a) show that this interaction can be switched to the ferromagnetic one by applying an external electric field.

This result seems to be very interesting in the context of *spintronics* based on the coupling between electric and magnetic degrees of freedom of conducting materials (Žutić, Fabian & Das Sarma, 2004). Possible graphene spintronic devices have been studied theoretically by Kim & Kim (2008) and by Wimmer

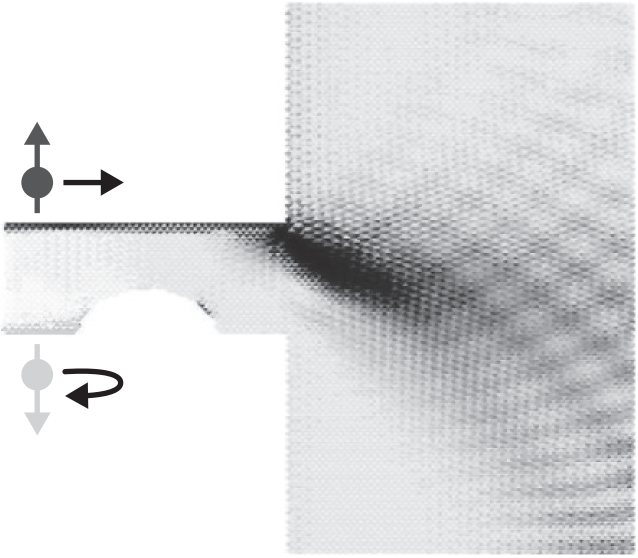

Fig. 12.5. The spin-injection profile of a graphene nanoribbon with a distorted edge for spin injection into a region of n-doped graphene. (Reproduced with permission from Wimmer *et al.*, 2008.)

et al. (2008). As an example, one can mention a simple and elegant way to produce a spin-polarized electric current due to a difference in shapes of the opposite zigzag edges suggested in the latter paper (Fig. 12.5).

However, there are several problems that should be discussed carefully before entertaining any such dreams about applications. First, the Mermin Wagner theorem (Mermin & Wagner, 1966; Ruelle, 1999) forbids long-range order in low-dimensional systems (such as one-dimensional graphene edges) at finite temperatures. The range of magnetic order is limited by the temperature-dependent spin correlation lengths $\xi^{\alpha}(\alpha = x, y, z)$ which define the decay law of the spin correlation

$$\left\langle \hat{s}_i^{\alpha} \hat{s}_{i+l}^{\alpha} \right\rangle = \left\langle \hat{s}_i^{\alpha} \hat{s}_i^{\alpha} \right\rangle \exp\left(\frac{l}{\xi_{\alpha}} \right). \tag{12.48}$$

In principle, the spin correlation length ξ imposes limitations on the device sizes. In order to establish this parameter one has to determine the energetics of spin fluctuations contributing to the breakdown of the ordered ground-state configuration and extract the exchange parameters. This has been done via density-functional calculations by Yazyev & Katsnelson (2008). The total energy of the spin-spiral state (Fig. 12.6) has been calculated and fitted to the classical Heisenberg model. The spin-wave stiffness constant $D \approx 2100$ meV Å^2 has been found to be several times higher than that in iron or nickel. This

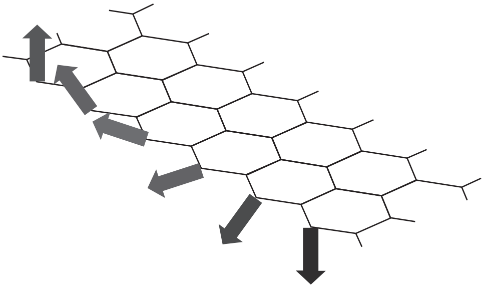

Fig. 12.6. The spin-spiral structure used for the calculation of the exchange coupling constant for a graphene zigzag edge. (Reproduced with permission from Yazyev & Katsnelson, 2008.)

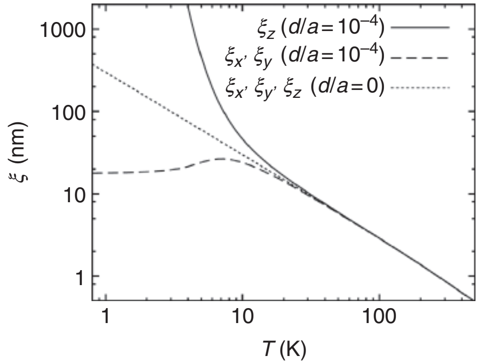

Fig. 12.7. The correlation length of magnetization vector components orthogonal (ξ_z) and parallel ($\xi_{x,y}$) to the graphene plane as a function of temperature for weakly anisotropic ($d/a = 10^{-4}$) and isotropic ($d = 0$) Heisenberg models. (Reproduced with permission from Yazyev & Katsnelson, 2008.)

confirms the general conclusion (Edwards & Katsnelson, 2006) that defect-induced sp-electron magnetism can be characterized by very high magnon energies (see Section 12.1).

The magnetic correlation length in the presence of spin-wave fluctuations was obtained with the help of the one-dimensional Heisenberg-model Hamiltonian

$$\hat{H} = -a\sum_i \hat{s}_i \hat{s}_{i+1} - d\sum_i \hat{s}_i^z \hat{s}_{i+1}^z, \tag{12.49}$$

where the Heisenberg coupling $a = 105$ meV was found from the fitting of the computational results. The estimated small anisotropy parameter $d/a \approx 10^{-4}$ originates from the weak spin orbit interaction in carbon (see the next section). This simple model Hamiltonian has known analytic solutions (Fisher, 1964). Figure 12.7 shows the spin correlation lengths calculated for our particular case. Above the crossover temperature $T_x \approx 10\,\mathrm{K}$, weak magnetic anisotropy does not play any role and the spin correlation length $\xi \propto T^{-1}$. However, below T_x the spin correlation length grows exponentially with decreasing temperature. At $T = 300\,\mathrm{K}$ the spin correlation length $\xi \approx 1\,\mathrm{nm}$.

From a practical point of view, this means that the sizes of spintronic devices based on the magnetic zigzag edges of graphene and operating under normal temperature conditions are limited to several nanometres. At present, such sizes are very difficult to achieve, which can be regarded as a pessimistic conclusion. Nevertheless, one has to keep in mind that the spin stiffness predicted for the magnetic graphene edges is still higher than the typical values for traditional magnetic materials. That is, graphene outperforms d-element-based magnetic materials, and there is room for improvement. Achieving control over the magnetic anisotropy d/a could possible raise the crossover temperature T_x above 300 K and thus significantly extend ξ. Possible approaches for reaching this goal include chemical functionalization of the edges with heavy-element functional groups or coupling graphene to a substrate.

Another serious problem is the possibility of reconstruction of zigzag edges to some nonmagnetic configuration (see Section 5.6). Theoretically, the result regarding ferromagnetism of zigzag edges at $T = 0$ looks very reliable, but the situation with real edges of real graphene is not so clear. Probably, some chemical protection of the edges can be used to keep the magnetic state stable enough.

Indirect evidence of possible magnetism of graphene edges has been found very recently by scanning tunnelling spectroscopy (STS), namely splitting of the edge mid-gap states has been observed (Tao *et al.*, 2011). Spin-polarized STS should be used to prove that this is *spin*-splitting, but this work has not yet been done.

12.4 Spin–orbit coupling

As we discussed above, spintronic applications due to an intrinsic magnetism of graphene are still very speculative. At the same time, one can inject spin-polarized current into graphene using ferromagnetic leads, e.g., cobalt, and then manipulate with this current. There is a huge amount of experimental activity in this field (Tombros *et al.*, 2007, 2008; Han *et al.*, 2009a, 2009b; Jo *et al.*, 2011). In this situation, the spin dynamics in graphene is determined by spin orbit coupling, leading to various spin-relaxation processes, such as Elliott Yafet, D'yakonov Perel, Bir Aronov Pikus and other mechanisms (Žutić, Fabian & Das Sarma, 2004). The main idea is that, in the presence of spin–orbit coupling, *some* of the scattering processes will be accompanied by spin-flips; this is the essential feature of the simplest and most general process, the Elliot–Yafet mechanism. A rough estimation for the spin-flip time, τ_s, is given by Elliot's formula (Elliot, 1954)

$$\frac{1}{\tau_s} \approx \frac{(\Delta g)^2}{\tau}, \tag{12.50}$$

where $\Delta g = g - 2$ is the contribution of the orbital moment to the conduction-electron g-factor and τ is the mean-free-path time (that is, the time taken for the relaxation of momentum). The first experiments (Tombros *et al.*, 2007) have already demonstrated that τ_s in graphene is orders of magnitude shorter than one would expect from a naïve estimation of the spin–orbit coupling in graphene. This observation initiated a serious theoretical activity (Huertas-Hernando, Guinea & Brataas, 2009; Castro Neto & Guinea, 2009; Jo *et al.*, 2011). Here we do not discuss the mechanisms of spin relaxation in graphene but focus on the quantum-mechanical part of the problem, that is, on the various contributions to spin–orbit coupling and their effects on the electron-energy spectrum.

Spin–orbit coupling is a relativistic effect following from the Dirac equation (we mean here the *real* Dirac equation rather than its analogue for graphene) as the second-order perturbation in the fine-structure constant $e^2/(hc)$ (Berestetskii, Lifshitz & Pitaevskii, 1971; Bjorken & Drell, 1964):

$$\hat{H}_{\text{s-o}} = \frac{h}{4m^2c^2}\left(\vec{\nabla}V \times \hat{\vec{p}}\right) \cdot \hat{\vec{\sigma}}, \tag{12.51}$$

where $\hat{\vec{p}} = -ih\vec{\nabla}$, V is the potential energy and $\hat{\vec{\sigma}}$ are the Pauli matrices acting on the real electron spin (not on the pseudospin, as in the greatest part of the book!). The main contribution originates from regions close to atomic nuclei where $\left|\vec{\nabla}V\right|$ is much larger than it is in interatomic space. As mentioned in Chapter 1, the order of magnitude of the intra-atomic spin–orbit coupling can be estimated from the energy difference of the multiplets $^3\text{P}_0$ and $^3\text{P}_1$ for the carbon atom (Radzig & Smirnov, 1985),

$$\Delta E_{\text{s-o}} \approx 2\,\text{meV}. \tag{12.52}$$

It is, roughly, 10^{-4} of the π-electron bandwidth, as it would be natural to expect for a quantity proportional to $\left(e^2/(hc)\right)^2$.

In the representation of valent (2s2p) states of carbon the Hamiltonian (12.51) can be represented as

$$\hat{H}_{\text{s-o}} = \xi \hat{\vec{L}} \cdot \hat{\vec{\sigma}}, \tag{12.53}$$

where

$$\hat{\vec{L}} = \hat{\vec{r}} \times \hat{\vec{p}} \tag{12.54}$$

is the orbital moment operator.

Our further analysis follows Huertas-Hernando, Guinea & Brataas (2006) and Yao *et al.* (2007). Within the basis of sp^3 states of the carbon atom (see Section 1.1) the Hamiltonian (12.53) can be rewritten as

$$\hat{H}_{\text{s-o}} = 2\xi \sum_j \Big(\hat{c}^+_{jz\uparrow}\hat{c}_{jx\downarrow} - \hat{c}^+_{jz\downarrow}\hat{c}_{jx\uparrow} + i\hat{c}^+_{jz\uparrow}\hat{c}_{jy\downarrow} - i\hat{c}^+_{jz\downarrow}\hat{c}_{jy\uparrow} + i\hat{c}^+_{jx\downarrow}\hat{c}_{jy\downarrow} - i\hat{c}^+_{jx\uparrow}\hat{c}_{jy\uparrow} + \text{H.c.}\Big), \tag{12.55}$$

where we take into account only intra-atomic matrix elements (j is the site label) and x, y and z label the $|p_x\rangle$, $|p_y\rangle$ and $|p_z\rangle$ orbitals. Of course, s-orbitals are not involved since $\hat{\vec{L}}|s\rangle = 0$.

Now we have to rewrite the Hamiltonian (12.55) in the representation of σ-orbitals (1.9) and π-orbitals ($|p_z\rangle$). Importantly, in the nearest-neighbour approximation $\left(\hat{H}_{\text{s-o}}\right)_{\pi\pi} = 0$, due to symmetry considerations. First, only the $\hat{L}_z\hat{\sigma}_z$ term survives, due to the mirror symmetry in the graphene plane. Second, there is an additional vertical reflection plane along the nearest-neighbour bonds. Under the reflection in this plane, $\hat{x}, \hat{p}_x \to \hat{x}, \hat{p}_x$ and $\hat{y}, \hat{p}_y \to -\hat{y}, -\hat{p}_y$ and, therefore, $\hat{L}_z \to -\hat{L}_z$ which finishes the proof.

Thus, we have to use second-order perturbation theory and the effective Hamiltonian of spin–orbit coupling is

$$\left(\hat{H}^{\text{eff}}_{\text{s-o}}\right)_{\pi\pi} = \left(\hat{H}_{\text{s-o}}\right)_{\pi\sigma} \frac{1}{\hat{H}^{(0)}_{\pi} - \hat{H}^{(0)}_{\sigma}} \left(\hat{H}_{\text{s-o}}\right)_{\sigma\pi}, \tag{12.56}$$

where $\hat{H}^{(0)}_{\pi,\sigma}$ are the corresponding band Hamiltonians without spin–orbital coupling. As a result, the effective Hamiltonians for the vicinities of the K and K′ points are (Yao *et al.*, 2007)

$$\hat{H}_{\mathrm{K,K'}}(\vec{q}) = \xi_1 + \begin{pmatrix} \mp\xi_1 & hv(q_x \mp iq_y) \\ hv(q_x \pm iq_y) & \pm\xi_1 \end{pmatrix} \tag{12.57}$$

instead of Eq. (1.19), where

$$\xi_1 = 2|\xi|^2 \frac{\varepsilon_{2\text{p}} - \varepsilon_{2\text{s}}}{9V^2_{\text{sp}\sigma}}, \tag{12.58}$$

where $\varepsilon_{2\text{p}}$ and $\varepsilon_{2\text{s}}$ are the atomic energy levels for 2p and 2s states and $V_{\text{sp}\sigma}$ is a matrix element of the hopping Hamiltonian for the σ-block, between s and p states. All these energies are of the order of 10 eV; thus the effective spin orbit coupling constant for the case of flat, defect-free graphene is $\xi_1 = 10^{\quad 3}$ meV (Huertas-Hernando, Guinea & Brataas, 2006; Yao *et al.*, 2007).

A special case of spin orbit coupling is associated with the external electric field perpendicular to the graphene plane (the Rashba effect) (Kane & Mele, 2005a; Huertas-Hernando, Guinea & Brataas, 2006; Min *et al.*, 2006; Rashba, 2009; Zarea & Sandler, 2009; Stauber & Schliemann, 2009). The potential of the external electric field

$$\hat{H}_E = eEz \tag{12.59}$$

has nonzero matrix elements only between $|s\rangle$ and $|p_z\rangle$ orbitals. In the secondary quantized form, Eq. (12.59) reads

$$\hat{H}_E = z_0 eE \sum_{j\sigma} \left(\hat{c}^{+}_{jz\sigma} \hat{c}_{js\sigma} + \hat{c}^{+}_{js\sigma} \hat{c}_{jz\sigma} \right), \tag{12.60}$$

where

$$z_0 = \langle p_z | z | s \rangle \tag{12.61}$$

is of the order of the radius of the carbon atom. The effective Hamiltonian of spin orbit coupling in the presence of the electric field, apart from Eq. (12.56), contains the cross-term

$$\left(\hat{H}_{\mathrm{R}}\right)_{\pi\pi} = \left(\hat{H}_E\right)_{\pi\sigma} \frac{1}{\hat{H}^{(0)}_{\pi} \quad \hat{H}^{(0)}_{\sigma}} \left(\hat{H}_{\text{s-o}}\right)_{\pi\pi} + \left(\hat{H}_{\text{s-o}}\right)_{\pi\sigma} \frac{1}{\hat{H}^{(0)}_{\pi} \quad \hat{H}^{(0)}_{\sigma}} \left(\hat{H}_E\right)_{\sigma\pi} \tag{12.62}$$

(cf. Eq. (10.70)). Taking into account this term, plus Eq. (12.57), we will find the spin orbit 8×8 Hamiltonian

$$\hat{H}_{\text{s-o}} = \quad \xi_1 \hat{\eta}_z \hat{\tau}_z \hat{\sigma}_z + \xi_{\mathrm{R}} \left(\hat{\eta}_x \hat{\tau}_z \hat{\sigma}_y \quad \hat{\eta}_y \hat{\sigma}_x \right), \tag{12.63}$$

where $\hat{\eta}$, $\hat{\tau}$ and $\hat{\sigma}$ are Pauli matrices acting on the pseudospin (that is, the sublattice index), valley index and real-spin projection, respectively. Note that in most of the book the Pauli matrix $\hat{\eta}$ has been written as $\hat{\sigma}$! The *Rashba coupling* ξ_{R} in Eq. (12.63) is given by (Huertas-Hernando, Guinea & Brataas, 2006; Min *et al.*, 2006)

$$\xi_{\mathrm{R}} = \frac{2eEz_0}{3V_{\mathrm{sp}\sigma}} \xi. \tag{12.64}$$

For the largest values of the electric field which can be created in graphene, $E \approx 1$ V nm $^{\quad 1}$, ξ_{R} is an order of magnitude larger than ξ_1.

There are many mechanisms that can dramatically increase the effective spin orbit coupling in graphene. First, it is very sensitive to the curvature which can be associated with the ripples (Huertas-Hernando, Guinea & Brataas, 2006). In curved graphene, there is no longer mirror symmetry in the vertical plane along the nearest-neighbour bonds, and the effective spin–orbit coupling for the π-block does not vanish to first order in ξ; this leads to Rashba-type coupling, with an effective coupling constant of the order of

$$\xi_{\mathrm{R}} \approx \xi a H, \tag{12.65}$$

where H is the mean curvature (9.77) and (9.78). For typical parameters of the ripples this spin–orbit coupling is an order of magnitude larger than the intrinsic one, of the order of 10^{-2}–10^{-1} meV (Huertas-Hernando, Guinea & Brataas, 2006).

Second, the effective spin–orbit coupling can be essentially increased by covalently bonded impurities, such as hydrogen adatoms, which change the state of carbon atoms locally from sp^2 to sp^3 (Castro Neto & Guinea, 2009). Again, this creates an effective spin–orbit coupling in the π-block already in the first order in ξ, making $\xi_1 \approx \xi$ locally. This makes 'resonant impurities' very efficient sources of spin-flip scattering. This conclusion seems to be in agreement with the recent experimental data (Jo *et al.*, 2011).

Finally, let us discuss the effect of the Hamiltonian (12.63) on the electron-energy spectrum of graphene (Kane & Mele, 2005b; Stauber & Schliemann, 2009). This Hamiltonian does not couple the valleys. For the valley K ($\tau_z = +1$) we have a 4 × 4 matrix (in the basis A↑, B↑, A↓, B↓) for the total Hamiltonian:

$$\hat{H} = \begin{pmatrix} \xi_1 & hv(q_x - iq_y) & 0 & 0 \\ hv(q_x + iq_y) & \xi_1 & 2i\xi_{\mathrm{R}} & 0 \\ 0 & 2i\xi_{\mathrm{R}} & \xi_1 & hv(q_x - iq_y) \\ 0 & 0 & hv(q_x + iq_y) & \xi_1 \end{pmatrix}, \tag{12.66}$$

where we skip the constant energy shift ξ_1 in Eq. (12.57). The equation for the eigenenergies takes the form

$$\det(\hat{H} - E) = \left(E^2 - \xi_1^2 - h^2v^2q^2\right)^2 - 4\xi_{\mathrm{R}}^2(E + \xi_1)^2 = 0. \tag{12.67}$$

At $\xi_{\mathrm{R}} = 0$, the spectrum is

$$E = \pm\sqrt{h^2v^2q^2 + \xi_1^2}, \tag{12.68}$$

with the gap $\Delta_{\text{s-o}} = 2|\xi_1|$. The existence of the gap does not contradict the proof given in Chapter 1 since, in the presence of spin–orbit coupling, the time-reversal operation does not have the form (1.39) but includes the spin reversal.

In the opposite case, $\xi_1 = 0$, the spectrum is

$$E^2 = h^2 v^2 q^2 + 2\xi_{\mathrm{R}}^2 \pm 2\xi_{\mathrm{R}} \sqrt{h^2 v^2 q^2 + {\xi_{\mathrm{R}}}^2}. \tag{12.69}$$

This is reminiscent of the spectrum of bilayer graphene in the parabolic-band approximation; see Chapter 1. Two bands have a gap, with the energy $\pm 2|\xi_{\mathrm{R}}|$ at $q = 0$, and two others are gapless, with the parabolic spectrum at $q \to 0$. In general, for finite ξ_1 and ξ_{R} the gap exists at $|\xi_1| > |\xi_{\mathrm{R}}|$ and its value is

$$\Delta_{\text{s-o}} = 2(|\xi_1| \quad |\xi_{\mathrm{R}}|). \tag{12.70}$$

In the regime in which the gap exists the mass term has opposite signs for the two valleys (see Eq. (12.57)). This results in a very interesting picture of the 'quantum spin Hall effect' (Kane & Mele, 2005a, 2005b). This phenomenon is not relevant for real graphene, due to the very small value of the gap. However, these two papers by Kane and Mele were very important in the development of a novel field, namely the physics of topological insulators (Moore, 2009; Qi & Zhang, 2010; Hasan & Kane, 2010; Qi & Zhang, 2011).

I think that this is a nice example, one of the many examples of the huge influence of graphene on our general understanding of physics, with which to finish this book.

References

Abanin, D. A., Lee, P. A. & Levitov, L. S. (2006). *Phys. Rev. Lett.* **96**, 176803

Abanin, D. A., Morozov, S. V., Ponomarenko, L. A., Gorbachev, R. V., Mayorov, A. S., Katsnelson, M. I., Watanabe, K., Taniguchi, T., Novoselov, K. S., Levitov, L. S. & Geim, A. K. (2011). *Science* **332**, 328

Abanin, D. A., Shytov, A. V., Levitov, L. S. & Halperin, B. I. (2009). *Phys. Rev. B* **79**, 035304

Abergel, D. S. L., Apalkov, V., Berashevich, J., Ziegler, K. & Chakraborty, T. (2010). *Adv. Phys.* **59**, 261

Abergel, D. S. L., Russel, A. & Falko, V. I. (2007). *Appl. Phys. Lett.* **91**, 063125

Abraham, F. F. & Nelson, D. R. (1990). *Science* **249**, 393

Abramowitz, M. & Stegun, I. A. (1964). *Handbook of Mathematical Functions*. New York: Dover

Abrikosov, A. A. (1988). *Fundamentals of the Theory of Metals*. Amsterdam: North Holland

Abrikosov, A. A. (1998). *Phys. Rev. B* **58**, 2788

Adam, S., Hwang, E., Galitski, V. M. & Das Sarma, S. (2007). *Proc. Natl Acad. Sci. USA* **104**, 18392

Adhikari, S. K. (1986). *Am. J. Phys.* **54**, 362

Aharonov, Y. & Bohm, D. (1959). *Phys. Rev.* **115**, 485

Aharonov, Y. & Casher, A. (1979). *Phys. Rev. A* **19**, 2461

Akhiezer, A. I. & Peletminskii, S. V. (1981). *Methods of Statistical Physics*. Oxford: Pergamon

Akhmerov, A. R. & Beenakker, C. W. J. (2008). *Phys. Rev. B* **77**, 085423

Aleiner, I. L. & Efetov, K. B. (2006). *Phys. Rev. Lett.* **97**, 236801

Altland, A. (2002). *Phys. Rev. B* **65**, 104525

Altshuler, B. L., Khmelnitskii, D., Larkin, A. I. & Lee, P. A. (1980). *Phys. Rev. B* **22**, 5142

Anderson, P. W. (1958) *Phys. Rev.* **112**, 900

Anderson, P. W. (1970). *J. Phys. C* **3**, 2346

Ando, T. (2006). *J. Phys. Soc. Japan* **75**, 074716

Ando, T., Fowler, A. B. & Stern, F. (1982). *Rev. Mod. Phys.* **54**, 437

Ando, T., Nakanishi, T. & Saito, R. (1998). *J. Phys. Soc. Japan* **67**, 2857

Ando, T., Zheng, Y. & Suzuura, H. (2002). *J. Phys. Soc. Japan* **71**, 1318

Aronovitz, J. A. & Lubensky, T. C. (1988). *Phys. Rev. Lett.* **60**, 2634

Atiyah, M. F. & Singer, I. M. (1968). *Ann. Math.* **87**, 484

Atiyah, M. F. & Singer, I. M. (1984). *Proc. Natl Acad. Sci. USA*, **81**, 2597

Auslender M. & Katsnelson, M. I. (2007). *Phys. Rev. B* **76**, 235425

Auslender, M. I. & Katsnelson, M. I. (1982). *Teor. Mat. Fiz.* **51**, 436

Balandin, A. A. (2011). *Nature Mater.* **10**, 569

Balandin, A. A., Chosh, S., Bao, W., Calizo, I., Teweldebrhan, D., Miao, F. & Lau, C. N. (2008). *Nano Lett.* **8**, 902

Balatsky, A. V., Vekhter, I. & Zhu, J.-X. (2006). *Rev. Mod. Phys.* **78**, 373

Balescu, R. (1975). *Equilibrium and Nonequilibrium Statistical Mechanics.* New York: Wiley

Bao, W., Miao, F., Chen, Z., Zhang, H., Jang, W., Dames, C. & Lau, C. N. (2009). *Nature Nanotech.* **4**, 562

Bardarson, J. H., Medvedeva, M. V., Tworzydlo, J., Akhmerov, A. R. & Beenakker, C. W. J. (2010). *Phys. Rev. B* **81**, 121414

Bardarson, J. H., Tworzydlo, J., Brower, P. W. & Beenakker, C. W. J. (2007). *Phys. Rev. Lett.* **99**, 106801

Basko, D. M. (2008). *Phys. Rev.* **78**, 115432

Bassani, F. & Pastori Parravicini, G. (1975). *Electronic States and Optical Transitions in Solids.* Oxford: Pergamon

Beenakker, C. W. J. (2008). *Rev. Mod. Phys.* **80**, 1337

Beenakker, C. W. J. & Büttiker, M. (1992). *Phys. Rev. B* **46**, 1889

Beenakker, C. W. J. & van Houten, H. (1991). *Solid State Phys.* **44**, 1

Belenkii, G. L., Salaev, E. Yu. & Suleimanov, R. A. (1988). *Usp. Fiz. Nauk* **155**, 89

Bellissard, J., van Elst, A. & Schulz-Baldes, H. (1994). *J. Math. Phys.* **35**, 5373

Bena, C. & Kivelson, S. A. (2005). *Phys. Rev. B* **72**, 125432

Berestetskii, V. B., Lifshitz, E. M. & Pitaevskii, L. P. (1971). *Relativistic Quantum Theory*, vol. 1. Oxford: Pergamon

Berry, M. V. (1984). *Proc. R. Soc. (London) A* **392**, 45

Berry, M. V. & Mondragon, R. J. (1987). *Proc. R. Soc. (London) A* **412**, 53

Bhandary, S., Eriksson, O., Sanyal, B. & Katsnelson, M. I. (2010). *Phys. Rev. B* **82**, 165405

Binnig, G. & Rohrer, H. (1987). *Rev. Mod. Phys.* **59**, 615

Biswas, R. R., Sachdev, S. & Son, D. T. (2007). *Phys. Rev. B* **76**, 205122

Bjorken, J. D. & Drell, S. D. (1964). *Relativistic Quantum Mechanics.* New York: McGraw-Hill

Blake, P., Hill, E. W., Castro Neto, A. H., Novoselov, K. S., Jiang, D., Yang, R., Booth, T. J. & Geim, A. K. (2007). *Appl. Phys. Lett.* **91**, 063124

Blanter, Ya. M. & Büttiker, M. (2000). *Phys. Rep.* **336**, 1

Blount, E. I. (1962). *Phys. Rev.* **126**, 1636

Bohr, A. & Mottelson, B. R. (1969). *Nuclear Structure*, vol. 1. New York: Benjamin

Bolotin, K. I., Ghahari, F., Shulman, M. D., Stormer, H. L. & Kim, P. (2009). *Nature* **462**, 196

Bolotin, K. I., Sikes, K. J., Jiang, Z., Klima, M., Fudenberg, G., Hone, J., Kim, P. & Stormer, H. L. (2008). *Solid State Commun.* **146**, 351

Booth, T. J., Blake, P., Nair, R. R., Jiang, D., Hill, E. W., Bangert, U., Bleloch, A., Gass, M., Novoselov, K. S., Katsnelson, M. I. & Geim, A. K. (2008). *Nano Lett.* **8**, 2442

Born, M. & Wolf, E. (1980). *Principles of Optics.* Oxford: Pergamon

Boukhvalov, D. W. & Katsnelson, M. I. (2008). *Nano Lett.* **8**, 4373

Boukhvalov, D. W. & Katsnelson, M. I. (2009a). *J. Phys.: Condens. Matter* **21**, 344205

Boukhvalov, D. W. & Katsnelson, M. I. (2009b). *J. Phys. Chem. C* **113**, 14176

Boukhvalov, D. W. & Katsnelson, M. I. (2009c). *Eur. Phys. J. B* **68**, 529

Boukhvalov, D. W. & Katsnelson, M. I. (2011). *ACS Nano* **5**, 2440

Boukhvalov, D. W., Katsnelson, M. I. & Lichtenstein, A. I. (2008). *Phys. Rev. B* **77**, 035427

Brandt, N. B., Chudinov, S. M. & Ponomarev, Ya. G. (1988). *Semimetals: Graphite and Its Compounds*. Amsterdam: North Holland

Brar, V. W., Decker, R., Solowan, H.-M., Wang, Y., Maserati, L., Chan, K. T., Loe, H., Girit, C. O., Zettl, A., Louie, S. G., Cohen, M. L. & Crommie, M. F. (2011). *Nature Phys.* **7**, 43

Brau, F., Vandeparre, H., Sabbah, A., Poulard, C., Boudaoud, A. & Damman, P. (2011). *Nature Phys.* **7**, 56

Bray, A. J. (1974). *Phys. Rev. Lett.* **32**, 1413

Brey, L. & Fertig, H. A. (2006). *Phys. Rev. B* **73**, 235411

Brey, L. & Fertig, H. A. (2009). *Phys. Rev. B* **80**, 035406

Briassoulis, D. (1986). *Computers Structures* **23**, 129

Calogeracos, A. & Dombey, N. (1999). *Contemp. Phys.* **40**, 313

Cangemi, D. & Dunne, G. (1996). *Ann. Phys.* **249**, 582

Castro, E. V., Novoselov, K. S., Morozov, S. V., Peres, N. M. R., Lopes dos Santos, J. M. B., Nilsson, J., Guinea, F., Geim, A. K. & Castro Neto, A. H. (2007). *Phys. Rev. Lett.* **99**, 216802

Castro, E. V., Novoselov, K. S., Morozov, S. V., Peres, N. M. R., Lopes dos Santos, J. M. B., Nilsson, J., Guinea, F., Geim, A. K. & Castro Neto, A. H. (2010a). *J. Phys.: Condens. Matter* **22**, 175503

Castro, E. V., Ochoa, H., Katsnelson, M. I., Gorbachev, R. V., Elias, D. C., Novoselov, K. S., Geim, A. K. & Guinea, F. (2010b). *Phys. Rev. Lett.* **105**, 266601

Castro Neto, A. H. & Guinea, F. (2009). *Phys. Rev. Lett.* **103**, 026804

Castro Neto, A. H., Guinea, F. & Peres, N. M. R. (2006). *Phys. Rev. B* **73**, 205408

Castro Neto, A. H., Guinea, F., Peres, N. M. R., Novoselov, K. S. & Geim, A. K. (2009). *Rev. Mod. Phys.* **81**, 109

Cerda, E. & Mahadevan, L. (2003). *Phys. Rev. Lett.* **90**, 074302

Chang, M.-C. & Niu, Q. (2008). *J. Phys.: Condens. Matter* **20**, 193202

Checkelsky, J. G., Li, L. & Ong, N. P. (2008). *Phys. Rev. Lett.* **100**, 20680

Cheianov, V. V. & Falko, V. I. (2006). *Phys. Rev. B* **74**, 041403

Cheianov, V. V., Falko, V. & Altshuler, B. L. (2007). *Science* **315**, 1252

Cheianov, V. V., Falko, V. I., Altshuler, B. L. & Aleiner, I. L. (2007). *Phys. Rev. Lett.* **99**, 176801

Cheianov, V. V., Syljuåsen, O., Altshuler, B. L. & Falko, V. (2009). *Phys. Rev. B* **80**, 233409

Chen, J.-H., Cullen, W. G., Jang, C., Fuhrer, M. S. & Williams, E. D. (2009). *Phys. Rev. Lett.* **102**, 236805

Chen, J.-H., Jang, C., Adam, S., Fuhrer, M. S., Williams, E. D. & Ishigami, M. (2008). *Nature Phys.* **4**, 377

Chico, L., Benedict, L. X., Louie, S. G. & Cohen, M. L. (1996). *Phys. Rev. B* **54**, 2600

Choi, S.-M., Jhi, S.-H. & Son, Y.-W. (2010). *Phys. Rev. B* **81**, 081407

Cocco, G., Cadelano, E. & Colombo, L. (2010). *Phys. Rev. B* **81**, 241412

Couto, N. J. G., Sacépé, B. & Morpurgo, A. F. (2011). *Phys. Rev. Lett.* **107**, 225501

Coxeter, H. S. M. (1989). *Introduction to Geometry*. New York: Wiley

Crassee, I., Levallois, J., Walter, A. L., Ostler, M., Bostwick, A., Rotenberg, E., Seyller, T., van der Marel, D. & Kuzmenko, A. B. (2011). *Nature Phys.* **7**, 48

Cserti, J., Csordás, A. & Dávid, G. (2007). *Phys. Rev. Lett.* **99**, 066802

Cserti, J. & Dávid, G. (2006). *Phys. Rev. B* **74**, 125419

Danneau, R., Wu, F., Craciun, M. F., Russo, S., Tomi, M. Y., Salmilehto, J., Morpurgo, A. F. & Hakonen, P. J. (2008). *Phys. Rev. Lett.* **100**, 196802

Das Sarma, S., Adam, S., Huang, E. H. & Rossi, E. (2011). *Rev. Mod. Phys.* **83**, 407

Davydov, A. S. (1976). *Quantum Mechanics*. Oxford: Pergamon

Dean, C. R., Young, A. F., Meric, I., Lee, C., Wang, L., Sorgenfrei, S., Watanabe, K., Taniguchi, T., Kim, P., Shepard, K. L. & Hone, J. (2010). *Nature Nanotech.* **5**, 722

De Juan, F., Grushin, A. G. & Vozmediano, M. A. H. (2010). *Phys. Rev. B* **82**, 125409

Delplace, P. & Montambaux, G. (2010). *Phys. Rev. B* **82**, 205412

De Raedt, H. & Katsnelson, M. I. (2008). *JETP Lett.* **88**, 607

DoCarmo, M. P. (1976). *Differential Geometry of Curves and Surfaces*. London: Prentice-Hall

Dombey, N. & Calogeracos, A. (1999). *Phys. Rep.* **315**, 41

Dresselhaus, G. (1974). *Phys. Rev. B* **10**, 3602

Dresselhaus, M. S. & Dresselhaus, G. (2002). *Adv. Phys.* **51**, 1

Du, X., Skachko, I., Barker, A. & Andrei, E. Y. (2008). *Nature Nanotech.* **3**, 491

Du, X., Skachko, I., Duerr, F., Cucian, A. & Andrei, E. Y. (2009). *Nature* **462**, 192

Edwards, D. M. (1967). *Phys. Lett. A* **24**, 350

Edwards, D. M. & Katsnelson, M. I. (2006). *J. Phys.: Condens. Matter* **18**, 7209

Efetov, K. B. (1997). *Supersymmetry in Disorder and Chaos*. Cambridge: Cambridge University Press

Elias, D. C., Gorbachev, R. V., Mayorov, A. S., Morozov, S. V., Zhukov, A. A., Blake, P., Novoselov, K. S., Geim, A. K. & Guinea, F. (2011). *Nature Phys.* **7**, 701

Elias, D. C., Nair, R. R., Mohiuddin, T. M. G., Morozov, S. V., Blake, P., Halsall, M. P., Ferrari, A. C., Boukhvalov, D. W., Katsnelson, M. I., Geim, A. K. & Novoselov, K. S. (2009). *Science* **323**, 610

Elliott, R. J. (1954). *Phys. Rev.* **96**, 266

Esaki, L. (1958). *Phys. Rev.* **109**, 603

Esquinazi, P. & Höhne, R. (2005). *J. Magn. Magn. Mater.* **290–291**, 20

Evers, F. & Mirlin, A. D. (2008). *Rev. Mod. Phys.* **80**, 1355

Eyring, H., Walter, J. & Kimball, G. E. (1946). *Quantum Chemistry*. Ithaca, NY: Cornell University Press

Faddeev, L. D. & Slavnov, A. A. (1980). *Gauge Fields: Introduction to a Quantum Theory*. Reading, MA: Benjamin

Falko, V. I. (2008). *Phil. Trans. R. Soc. A* **366**, 205

Fasolino, A., Los, J. H. & Katsnelson, M. I. (2007). *Nature Mater.* **6**, 858

Fedoryuk, M. V. (1977). *Method of Steepest Descent*. Moscow: Nauka

Ferrari, A. C., Meyer, J. C., Scardaci, V., Casiraghi, C., Lazzeri, M., Mauri, F., Piscanec, S., Jiang, D., Novoselov, K. S., Roth, S. & Geim, A. K. (2006). *Phys. Rev. Lett.* **97**, 187401

Fialkovsky, I. V. & Vassilevich, D. V. (2009). *J. Phys. A* **42**, 442001

Fisher, M. E. (1964). *Am. J. Phys.* **32**, 343

Fogler, M. M. (2009). *Phys. Rev. Lett.* **103**, 236801

Fogler, M. M., Guinea, F. & Katsnelson, M. I. (2008). *Phys. Rev. Lett.* **101**, 226804

Fogler, M. M., Novikov, D. S., Glazman, L. I. & Shklovskii, B. I. (2008). *Phys. Rev. B* **77**, 075420

Fowler, W. A. (1984). *Rev. Mod. Phys.* **56**, 149

Fradkin, E. (1986). *Phys. Rev. B* **33**, 3263

Friedel, J. (1952). *Phil. Mag.* **43**, 253

Fritz, L., Schmalian, J., Müller, M. & Sachdev, S. (2008). *Phys. Rev. B* **78**, 085416

Fujita, M., Wakabayashi, K., Nakada, K. & Kusakabe, K. (1996). *J. Phys. Soc. Japan* **65**, 1920

Galitskii, V. M. (1958a). *Zh. Éksp. Teor. Fiz.* **34**, 151

Galitskii, V. M. (1958b). *Zh. Éksp. Teor. Fiz.* **34**, 1011

Gangadharaiah, S., Farid, A. M. & Mishchenko, E. G. (2008). *Phys. Rev. Lett.* **100**, 166802

Gazit, D. (2009). *Phys. Rev. E* **80**, 041117

Geim, A. K. (2009). *Science* **324**, 1530

Geim, A. K. (2011). *Rev. Mod. Phys.* **83**, 851

Geim, A. K. & Novoselov, K. S. (2007). *Nature Mater.* **6**, 183

Geringer, V., Liebmann, M., Echtermeyer, T., Runte, S., Schmidt, M., Rückamp, R., Lemme, M. C. & Morgenstern, M. (2009). *Phys. Rev. Lett.* **102**, 076102

Gerritsma, R., Kirchmair, G., Zähringer, F., Solano, E., Blatt, R. & Roos, C. F. (2010). *Nature* **463**, 38

Ghosh, S., Bao, W., Nika, D. L., Subrina, S., Pokatilov, E. P., Lau, C. N. & Balandin, A. A. (2010). *Nature Mater.* **9**, 555

Gibertini, M., Tomadin, A., Polini, M., Fasolino, A. & Katsnelson, M. I. (2010). *Phys. Rev. B* **81**, 125437

Giesbers, A. J. M., Ponomarenko, L. A., Novoselov, K. S., Geim, A. K., Katsnelson, M. I., Maan, J. C. & Zeitler, U. (2009). *Phys. Rev. B* **80**, 201403

Giesbers, A. J. M., Zeitler, U., Katsnelson, M. I., Ponomarenko, L. A., Mohiuddin, T. M. & Maan, J. C. (2007). *Phys. Rev. Lett.* **99**, 206803

Giovannetti, G., Khomyakov, P. A., Brocks, G., Kelly, P. J. & van den Brink, J. (2007). *Phys. Rev. B* **76**, 073103

Giuliani, A., Mastropietro, V. & Porta, M. (2011). *Phys. Rev. B* **83**, 195401

Glazman, L. I., Lesovik, G. B., Khmelnitskii, D. E. & Shekhter, R. I. (1988). *Pis'ma ZhÉTF* **48**, 218

Goerbig, M. O. (2011). *Rev. Mod. Phys.* **83**, 1193

González, J., Guinea, F. & Vozmediano, M. A. H. (1994). *Nucl. Phys. B* **424**, 595

González, J., Guinea, F. & Vozmediano, M. A. H. (1999) *Phys. Rev. B* **59**, 2474

Gorbar, E. V., Gusynin, V. P., Miransky, V. A. & Shovkovy, I. A. (2002). *Phys. Rev. B* **66**, 045108

Greiner, W., Mueller, B. & Rafelski, J. (1985). *Quantum Electrodynamics of Strong Fields*. Berlin: Springer

Greiner, W. & Schramm, S. (2008). *Am. J. Phys.* **76**, 509

Grib, A. A., Mamaev, S. V. & Mostepanenko, V. M. (1994). *Vacuum Effects in Strong Fields*. St Petersburg: Friedmann

Guinea, F. (2008). *J. Low Temp. Phys.* **153**, 359

Guinea, F., Castro Neto, A. H. & Peres, N. M. R. (2006). *Phys. Rev. B* **73**, 245426

Guinea, F., Geim, A. K., Katsnelson, M. I. & Novoselov, K. S. (2010). *Phys. Rev. B* **81**, 035408

Guinea, F., Horovitz, B. & Le Doussal, P. (2008). *Phys. Rev. B* **77**, 205421

Guinea, F., Katsnelson, M. I. & Geim, A. K. (2010). *Nature Phys.* **6**, 30

Guinea, F., Katsnelson, M. I. & Vozmediano, M. A. H. (2008). *Phys. Rev. B* **77**, 075422

Güney, D. Ö. & Meyer, D. A. (2009). *Phys. Rev. A* **79**, 063834

Gusynin, V. P. & Sharapov, S. G. (2005). *Phys. Rev. Lett.* **95**, 146801

Gusynin, V. P., Sharapov, S. G. & Carbotte, J. P. (2006). *Phys. Rev. Lett.* **96**, 256802

Gusynin, V. P., Sharapov, S. G. & Carbotte, J. P. (2007a). *J. Phys.: Condens. Matter* **19**, 026222

Gusynin, V. P., Sharapov, S. G. & Carbotte, J. P. (2007b). *Phys. Rev. B* **75**, 165407

Gusynin, V. P., Sharapov, S. G. & Carbotte, J. P. (2009). *New J. Phys.* **11**, 095407

Güttinger, J., Stampfer, C., Libisch, F., Frey, T., Burgdörfer, J., Ihn, T. & Ensslin, K. (2009). *Phys. Rev. Lett.* **103**, 046810

Gutzwiller, M. C. (1963). *Phys. Rev. Lett.* **10**, 159

Halperin, B. I. (1982). *Phys. Rev. B* **25**, 2185

Halperin, W. (1986). *Rev. Mod. Phys.* **58**, 533

Han, M. Y., Brant, J. C. & Kim, P. (2010). *Phys. Rev. Lett.* **104**, 056801

Han, M. Y., Özyilmaz, B., Zhang, Y. & Kim, P. (2007). *Phys. Rev. Lett.* **98**, 206805

Han, W., Pi, K., Bao, W., McCreary, K. M., Li, Y., Wang, W. H., Lau, C. N. & Kawakami, R. K. (2009a). *Appl. Phys. Lett.* **94**, 222109

Han, W., Wang, W. H., Pi, K., McCreary, K. M., Bao, W., Li, Y., Miao, F., Lau, C. N. & Kawakami, R. K. (2009b). *Phys. Rev. Lett.* **102**, 137205

Hasan, M. Z. & Kane, C. L. (2010). *Rev. Mod. Phys.* **82**, 3045

Hasegawa, Y., Konno, R., Nakano, H. & Kohmoto, M. (2006). *Phys. Rev. B* **74**, 033413

Hatsugai, Y. (1993). *Phys. Rev. Lett.* **71**, 3697

Hatsugai, Y., Fukui, T. & Aoki, H. (2006). *Phys. Rev. B* **74**, 205414

Heeger, A. J., Kivelson, S., Schrieffer, J. R. & Su, W.-P. (1988). *Rev. Mod. Phys.* **60**, 781

Heine, V. (1960). *Group Theory in Quantum Mechanics*. Oxford: Pergamon

Helfrich, W. (1973). *Z. Naturforsch.* **28C**, 693

Hentschel, M. & Guinea, F. (2007). *Phys. Rev. B* **76**, 115407

Herbut, I. F., Juričić, V. & Vafek, O. (2008). *Phys. Rev. Lett.* **100**, 046403

Herring, C. (1966). *Exchange Interactions among Itinerant Electrons*. New York: Academic Press

Hewson, A. C. (1993). *The Kondo Problem to Heavy Fermions*. Cambridge: Cambridge University Press

Hill, A., Mikhailov, S. A. & Ziegler, K. (2009). *Europhys. Lett.* **87**, 27005

Hobson, J. P. & Nierenberg, W. A. (1953). *Phys. Rev.* **89**, 662

Huang, L., Lai, Y.-C. & Grebogi, C. (2010). *Phys. Rev. E* **81**, 055203

Hubbard, J. (1963). *Proc. R. Soc. (London) A* **276**, 238

Huefner, M., Molitor, F., Jacobsen, A., Pioda, A., Stampter, C., Ensslin, K. & Ihn, T. (2009). *Phys. Stat. Sol. (b)* **246**, 2756

Huertas-Hernando, D., Guinea, F. & Brataas, A. (2006). *Phys. Rev. B* **74**, 155426

Huertas-Hernando, D., Guinea, F. & Brataas, A. (2009). *Phys. Rev. Lett.* **103**, 146801

Hwang, E. H. & Das Sarma, S. (2007). *Phys. Rev. B* **75**, 205418

Inui, M., Trugman, S. A. & Abrahams, E. (1994). *Phys. Rev. B* **49**, 3190

Irkhin, V. Yu. & Katsnelson, M. I. (1985a). *J. Phys. C* **18**, 4173

Irkhin, V. Yu. & Katsnelson, M. I. (1985b). *Zh. Ěksp. Teor. Fiz.* **88**, 522

Irkhin, V. Yu. & Katsnelson, M. I. (1986). *Z. Phys. B* **62**, 201

Irkhin, V. Yu. & Katsnelson, M. I. (2002). *Eur. Phys. J. B* **30**, 481

Irkhin, V. Yu., Katsnelson, M. I. & Trefilov, A. V. (1992). *J. Magn. Magn. Mater.* **117**, 210

Irkhin, V. Yu., Katsnelson, M. I. & Trefilov, A. V. (1993). *J. Phys.: Condens. Mat.* **5**, 8763

Ishigami, M., Chen, J. H., Cullen, W. G., Fuhrer, M. S. & Williams, E. D. (2007). *Nano Lett.* **7**, 1643

Ishihara, A. (1971). *Statistical Physics*. New York: Academic Press

Jackiw, R., Milstein, A. I., Pi, S.-Y. & Terekhov, I. S. (2009). *Phys. Rev. B* **80**, 033413

Jackson, J. D. (1962). *Classical Electrodynamics*. New York: Wiley

Jiang, J., Saito, R., Samsonidge, G., Chou, S. G., Jorio, A., Dresselhaus, G. & Dresselhaus, M. S. (2005). *Phys. Rev. B* **72**, 235408

Jiang, Z., Henriksen, E. A., Tung, L. C., Wang, Y.-L., Schwartz, M. E., Han, M. Y., Kim, P. & Stormer, H. L. (2007a). *Phys. Rev. Lett.* **98**, 197403

Jiang, Z., Zhang, Y., Stormer, H. L. & Kim, P. (2007b). *Phys. Rev. Lett.* **99**, 106802

Jo, S., Ki, D.-K., Jeong, D., Lee, H.-J. & Kettermann, S. (2011). *Phys. Rev. B* **84**, 075453

John, D. L., Castro, L. C. & Pulfrey, D. L. (2004). *J. Appl. Phys.* **96**, 5180

Jones, R. A. (2002). *Soft Condensed Matter*. Oxford: Oxford University Press

Kadanoff, L. P. & Baym, G. (1962). *Quantum Statistical Mechanics*. New York: Benjamin

Kailasvuori, J. (2009). *Europhys. Lett.* **87**, 47008

Kailasvuori, J. & Lüffe, M. C. (2010). *J. Statist. Mech.: Theory Exp.* P06024

Kaku, M. (1988). *Introduction to Superstrings*. Berlin: Springer

Kalashnikov, V. P. & Auslender, M. (1979). *Fortschr. Phys.* **27**, 355

Kamenev, A. & Levchenko, A. (2009). *Adv. Phys.* **58**, 197

Kanamori, J. (1963). *Prog. Theor. Phys.* **30**, 276

Kane, C. L. & Mele, E. J. (2005a). *Phys. Rev. Lett.* **95**, 146802

Kane, C. L. & Mele, E. J. (2005b). *Phys. Rev. Lett.* **95**, 226801

Karssemeijer, L. J. & Fasolino, A. (2011). *Surface Sci.* **605**, 1611

Katsnelson, M. I. (2006a). *Eur. Phys. J. B* **51**, 157

Katsnelson, M. I. (2006b). *Eur. Phys. J. B* **52**, 151

Katsnelson, M. I. (2006c). *Phys. Rev. B* **74**, 201401

Katsnelson, M. I. (2007a). *Mater. Today* **10**, 20

Katsnelson, M. I. (2007b). *Eur. Phys. J. B* **57**, 225

Katsnelson, M. I. (2007c). *Phys. Rev. B* **76**, 073411

Katsnelson, M. I. (2008). *Europhys. Lett.* **84**, 37001

Katsnelson, M. I. (2010a). *Europhys. Lett.* **89**, 17001

Katsnelson, M. I. (2010b). *Phys. Rev. B* **82**, 205433

Katsnelson, M. I. & Geim, A. K. (2008). *Phil. Trans. R. Soc. A* **366**, 195

Katsnelson, M. I. & Guinea, F. (2008). *Phys. Rev. B* **78**, 075417

Katsnelson, M. I., Guinea, F. & Geim, A. K. (2009). *Phys. Rev. B* **79**, 195426

Katsnelson, M. I., Irkhin, V. Yu., Chioncel, L., Lichtenstein, A. I. & de Groot, R. A. (2008). *Rev. Mod. Phys.* **80**, 315

Katsnelson, M. I., Naumov, I. I. & Trefilov, A. V. (1994). *Phase Transitions* **49**, 143

Katsnelson, M. I. & Novoselov, K. S. (2007). *Solid State Commun.* **143**, 3

Katsnelson, M. I., Novoselov, K. S. & Geim, A. K. (2006). *Nature Phys.* **2**, 620

Katsnelson, M. I. & Prokhorova, M. F. (2008). *Phys. Rev. B* **77**, 205424

Katsnelson, M. I. & Trefilov, A. V. (2002). *Dynamics and Thermodynamics of Crystal Lattices*. Moscow: Atomizdat

Keldysh, L. V. (1964). *Zh. Éksp. Teor. Fiz.* **47**, 1515

Kellendonk, J. & Schulz-Baldes, H. (2004). *J. Funct. Anal.* **209**, 388

Kim, W. Y. & Kim, K. S. (2008). *Nature Nanotech.* **3**, 408

Kim, K. S., Zhao, Y., Jang, H., Lee, S. Y., Kim, J. M., Kim, K. S., Ahn, J.-H., Kim, P., Choi, J.-Y. & Hong, B. H. (2009). *Nature* **457**, 706

Klein, O. (1929). *Z. Phys.* **53**, 157

Kogan, E. (2011). *Phys. Rev. B* **84**, 115119

Kohmoto, M. (1985). *Ann. Phys.* **160**, 343

Kohmoto, M. (1989). *Phys. Rev. B* **39**, 11943

Kohn, W. (1959). *Phys. Rev.* **115**, 1460

Kohn, W. & Luttinger, J. M. (1957). *Phys. Rev.* **108**, 590

Kondo, J. (1964). *Prog. Theor. Phys.* **32**, 37

Kosevich, A. M. (1999). *Theory of Crystal Lattices*. New York: Wiley

Koshino, M. & Ando, T. (2006). *Phys. Rev. B* **73**, 245403

Koshino, M. & Ando, T. (2007). *Phys. Rev. B* **76**, 085425

Koshino, M. & Ando, T. (2010). *Phys. Rev. B* **81**, 195431

Koshino, M. & McCann, E. (2010). *Phys. Rev. B* **81**, 115315

Koskinen, P., Malola, S. & Häkkinen, H. (2008). *Phys. Rev. Lett.* **101**, 115502

Kotakoski, J., Krasheninnikov, A. V. & Nordlund, K. (2006). *Phys. Rev. B* **74**, 245420

Kotov, V. N., Uchoa, B., Pereira, V. M., Castro Neto, A. H. & Guinea, F. (2011). arXiv:1012.3484

Kouwenhoven, L. P., Markus, C. M. & McEuen, P. L. (1997). Electron transport in quantum dots, in *Mesoscopic Electron Transport* (ed. Sohn, L. L., Kouwenhoven, L. P. & Schön, G.). Dordrecht: Kluwer

Kownacki, J.-P. & Mouhanna, D. (2009). *Phys. Rev. E* **79**, 040101

Krekora, P., Su, Q. & Grobe, R. (2005). *Phys. Rev. A* **72**, 064103

Kroes, J. M. H., Akhukov, M. A., Los, J. H., Pineau, N. & Fasolino, A. (2011). *Phys. Rev. B* **83**, 165411

Kubo, R. (1957). *J. Phys. Soc. Japan* **12**, 570

Kubo, R., Hasegawa, H. & Hashitsume, N. (1959). *J. Phys. Soc. Japan* **14**, 56

Kuratsuji, H. & Iida, S. (1985). *Prog. Theor. Phys.* **74**, 439

Kuzemsky, A. L. (2005). *Int. J. Mod. Phys. B* **19**, 1029

Kuzmenko, A. B., van Heumen, E., Carbone, F. & van der Marel, D. (2008). *Phys. Rev. Lett.* **100**, 117401

Kuzmenko, A. B., van Heumen, E., van der Marel, D., Lerch, P., Blake, P., Novoselov, K. S. & Geim, A. K. (2009). *Phys. Rev. B* **79**, 115441

Landau, L. D. (1930). *Z. Phys.* **64**, 629

Landau, L. D. (1937). *Phys. Z. Sowjetunion* **11**, 26

Landau, L. D. (1956). *Zh. Éksp. Teor. Fiz.* **30**, 1058

Landau, L. D., Abrikosov, A. A. & Khalatnikov, I. M. (1956). *Nuovo Cimento*, Suppl. **3**, 80

Landau, L. D. & Lifshitz, E. M. (1970). *Theory of Elasticity*. Oxford: Pergamon

Landau, L. D. & Lifshitz, E. M. (1977). *Quantum Mechanics*. Oxford: Pergamon

Landau, L. D. & Lifshitz, E. M. (1980). *Statistical Physics*. Oxford: Pergamon

Landau, L. D. & Lifshitz, E. M. (1984). *Electrodynamics of Continuous Media*. Oxford: Pergamon

Landau, L. D. & Peierls, R. (1931). *Z. Phys.* **69**, 56

Landau, L. D. & Pomeranchuk, I. Y. (1955). *Dokl. AN SSSR* **102**, 489

Landsberg, G. & Mandelstam, L. (1928). *Naturwissenschaften* **16**, 557

Le Doussal, P. & Radzihovsky, L. (1992). *Phys. Rev. Lett.* **69**, 1209

Lee, C., Wei, X., Kysar, J. W. & Hone, J. (2008). *Science* **321**, 385

Lee, P. A. (1993). *Phys. Rev. Lett.* **71**, 1887

Levy, N., Burke, S. A., Meaker, K. L., Manlasigui, M., Zettl, A., Guinea, F., Castro Neto, A. H. & Crommie, M. F. (2010). *Science* **329**, 544

Li, J., Schneider, W.-D., Berndt, R. & Delley, D. (1998). *Phys. Rev. Lett.* **80**, 2893

Libisch, F., Stampfer, C. & Burgdörfer, J. (2009). *Phys. Rev. B* **79**, 115423

Lieb, E. H. (1981). *Rev. Mod. Phys.* **53**, 603

Lieb, E. H. (1989). *Phys. Rev. Lett.* **62**, 1201

Lieb, E. & Mattis, D. (1962). *J. Math. Phys.* **3**, 749

Liechtenstein, A. I., Katsnelson, M. I. & Gubanov, V. A. (1985). *Solid State Commun.* **54**, 327

Lifshitz, I. M. (1952). *Zh. Éksp. Teor. Fiz.* **22**, 475

Lifshitz, I. M., Azbel, M. Ya. & Kaganov, M. I. (1973). *Electron Theory of Metals.* New York: Plenum

Lifshitz, I. M., Gredeskul, S. A. & Pastur, L. A. (1988). *Introduction to the Theory of Disordered Systems.* New York: Wiley

Lin, D.-H. (2005). *Phys. Rev. A* **72**, 012701

Lin, D.-H. (2006). *Phys. Rev. A* **73**, 044701

Los, J. H. & Fasolino, A. (2003). *Phys. Rev. B* **68**, 024107

Los, J. H., Ghiringhelli, L. M., Meijer, E. J. & Fasolino, A. (2005). *Phys. Rev. B* **72**, 214102

Los, J. H., Katsnelson, M. I., Yazyev, O. V., Zakharchenko, K. V. & Fasolino, A. (2009). *Phys. Rev. B* **80**, 121405

Low, T., Guinea, F. & Katsnelson, M. I. (2011). *Phys. Rev. B* **83**, 195436

Ludwig, A. W. W., Fisher, M. P. A., Shankar, R. & Grinstein, G. (1994). *Phys. Rev. B* **50**, 7526

Lukose, V., Shankar, R. & Baskaran, G. (2007). *Phys. Rev. Lett.* **98**, 116802

Luttinger, J. M. & Kohn, W. (1958). *Phys. Rev.* **109**, 1892

Luzzi, R., Vasconcellos, A. R. & Ramos, J. G. (2000). *Int. J. Mod. Phys. B* **14**, 3189

Ma, S. K. (1976). *Modern Theory of Critical Phenomena.* Reading, MA: Benjamin

MacDonald, A. H. & Středa, P. (1984). *Phys. Rev. B* **29**, 1616

Madhavan, V., Chen, W., Jamneala, T., Crommie, M. F. & Wingreen, N. S. (1998). *Science* **280**, 567

Madhavan, V., Chen, W., Jamneala, T., Crommie, M. F. & Wingreen, N. S. (2001). *Phys. Rev. B* **64**, 165412

Mafra, D. L., Samsonidze, G., Malard, L. M., Elias, D. C., Brant, J. C., Plentz, F., Alves, E. S. & Pimenta, M. A. (2007). *Phys. Rev. B* **76**, 233407

Mahan, G. (1990). *Many-Particle Physics.* New York: Plenum

Makarova, T. & Palacio, F. (eds.) (2006). *Carbon Based Magnetism: An Overview of the Metal Free Carbon-Based Compounds and Materials.* Amsterdam: Elsevier

Malard, L. M., Pimenta, M. A., Dresselhaus, G. & Dresselhaus, M. S. (2009). *Phys. Rep.* **473**, 51

Mañes, J. L. (2007). *Phys. Rev. B* **76**, 045430

Mañes, J. L., Guinea, F. & Vozmediano, M. A. H. (2007). *Phys. Rev. B* **75**, 155424

Manyuhina, O. V., Hertzel, J. J., Katsnelson, M. I. & Fasolino, A. (2010). *Eur. Phys. J. E* **32**, 223

Mariani, E. & von Oppen, F. (2008). *Phys. Rev. Lett.* **100**, 076801

Mariani, E. & von Oppen, F. (2010). *Phys. Rev. B* **82**, 195403

Martin, I. & Blanter, Ya. M. (2009). *Phys. Rev. B* **79**, 235132

Martin, J., Akerman, N., Ulbricht, G., Lohmann, T., Smet, J. H., von Klitzing, K. & Yacoby, A. (2007). *Nature Phys.* **4**, 144

Maultzsch, J., Reich, S. & Thomsen, C. (2004). *Phys. Rev. B* **70**, 155403

Mayorov, A. S., Elias, D. C., Mucha-Kruczynski, M., Gorbachev, R. V., Tudorovskiy, T., Zhukov, A., Morozov, S. V., Katsnelson, M. I., Falko, V. I., Geim, A. K. & Novoselov, K. S. (2011). *Science* **333**, 860

McCann, E., Abergel, D. S. L. & Falko, V. I. (2007). *Solid State Commun.* **143**, 110

McCann, E. & Falko, V. I. (2004). *J. Phys.: Condens. Matter* **16**, 2371

McCann, E. & Falko, V. I. (2006). *Phys. Rev. Lett.* **96**, 086805

McCann, E., Kechedzhi, K., Falko, V. I., Suzuura, H., Ando, T. & Altshuler, B. L. (2006). *Phys. Rev. Lett.* **97**, 146805

McClure, J. W. (1956). *Phys. Rev.* **104**, 666

McClure, J. W. (1957). *Phys. Rev.* **108**, 612

McCreary, K. M., Pi, K., Swartz, A. G., Han, W., Bao, W., Lau, C. N., Guinea, F., Katsnelson, M. I. & Kawakami, R. K. (2010). *Phys. Rev. B* **81**, 115453

Mermin, N. D. (1968). *Phys. Rev.* **176**, 250

Mermin, N. D. & Wagner, H. (1966). *Phys. Rev. Lett.* **17**, 22

Meyer, J. C., Geim, A. K., Katsnelson, M. I., Novoselov, K. S., Booth, T. J. & Roth, S. (2007a). *Nature* **446**, 60

Meyer, J. C., Geim, A. K., Katsnelson, M. I., Novoselov, K. S., Obergfell, D., Roth, S., Girit, C. & Zettl, A. (2007b). *Solid State Commun.* **143**, 101

Meyer, J. R., Hoffman, C. A., Bartoli, F. J. & Rammohan, L. R. (1995). *Appl. Phys. Lett.* **67**, 757

Miao, F., Wijeratne, S., Zhang, Y., Coskun, U. C., Bao, W. & Lau, C. N. (2007). *Science* **317**, 1530

Migdal, A. B. (1977). *Qualitative Methods in Quantum Theory*. Reading, MA: Benjamin

Mikitik, G. P. & Sharlai, Yu. V. (1999). *Phys. Rev. Lett.* **82**, 2147

Mikitik, G. P. & Sharlai, Yu. V. (2008). *Phys. Rev. B* **77**, 113407

Min, H., Hill, J. E., Sinitsyn, N. A., Sahu, B. R., Kleinman, L. & MacDonald, A. H. (2006). *Phys. Rev. B* **74**, 165310

Mishchenko, E. G. (2008). *Europhys. Lett.* **83**, 17005

Moldovan, D. & Golubović, L. (1999). *Phys. Rev. E* **60**, 4377

Molitor, F., Knowles, H., Dröscher, S., Gasser, U., Choi, T., Roulleau, P., Güttinger, J., Jacobsen, A., Stampfer, C., Ensslin, K. & Inn, T. (2010). *Europhys. Lett.* **89**, 67005

Moore, J. (2009). *Nature Phys.* **5**, 378

Mori, H. (1965). *Prog. Theor. Phys.* **34**, 399

Moriya, T. (1985). *Spin Fluctuations in Itinerant Electron Magnetism*. Berlin: Springer

Morozov, S. V., Novoselov, K. S., Katsnelson, M. I., Schedin, F., Elias, D. C., Jaszczak, J. A. & Geim, A. K. (2008). *Phys. Rev. Lett.* **100**, 016602

Morozov, S. V., Novoselov, K. S., Katsnelson, M. I., Schedin, F., Ponomarenko, L. A., Jiang, D. & Geim, A. K. (2006). *Phys. Rev. Lett.* **97**, 016801

Morpurgo, A. F. & Guinea, F. (2006). *Phys. Rev. Lett.* **97**, 196804

Mott, N. F. (1974). *Metal–Insulator Transitions*. London: Taylor & Francis

Mott, N. F. & Davis, E. A. (1979). *Electron Processes in Non-Crystalline Materials*. Oxford: Clarendon

Mounet, N. & Marzari, N. (2005). *Phys. Rev. B* **71**, 205214

Muñoz-Rojas, F., Fernández-Rossier, J., Brey, L. & Palacios, J. J. (2008). *Phys. Rev. B* **77**, 045301

Nagaev, E. L. (1983). *Physics of Magnetic Semiconductors*. Moscow: Mir

Nagaev, E. L. (2001). *Phys. Rep.* **346**, 387

Nagaev, K. E. (1992). *Phys. Lett. A* **169**, 103

Nair, R. R., Blake, P., Grigorenko, A. N., Novoselov, K. S., Booth, T. J., Stauber, T., Peres, N. M. R. & Geim, A. K. (2008). *Science* **320**, 1308

Nair, R. R., Ren, W., Jalil, R., Riaz, I., Kravets, V. G., Britnell, L., Blake, P., Schedin, F., Mayorov, A. S., Yuan, S., Katsnelson, M. I., Cheng, H.-M., Stupinski, W., Bulusheva, L. G., Okotrub, A. V., Grigorieva, I. V., Grigorenko, A. N., Novoselov, K. S. & Geim, A. K. (2010). *Small* **6**, 2877

Nair, R. R., Sepioni, M., Tsai, I.-L., Lehtinen, O., Keinonen, J., Krasheninnikov, A.V., Thomson, T., Geim, A. K. & Grigorieva, I. V. (2011). arXiv: 1111.3775

Nakada, K., Fujita, M., Dresselhaus, G. & Dresselhaus, M. S. (1996). *Phys. Rev. B* **54**, 17954

Nakahara, N. (1990). *Geometry, Topology and Physics*. Bristol: IOP

Nakano, H. (1957). *Prog. Theor. Phys.* **17**, 145

Nelson, D. R. & Peliti, L. (1987). *J. Physique* **48**, 1085

Nelson, D. R., Piran, T. & Weinberg, S. (eds.) (2004). *Statistical Mechanics of Membranes and Surfaces*. Singapore: World Scientific

Nemanich, R. J. & Solin, S. A. (1977). *Solid State Commun.* **23**, 417

Nemanich, R. J. & Solin, S. A. (1979). *Phys. Rev. B* **20**, 392

Nersesyan, A. A., Tsvelik, A. M. & Wenger, F. (1994). *Phys. Rev. Lett.* **72**, 2628

Newton, R. G. (1966). *Scattering Theory of Waves and Particles*. New York: McGraw-Hill

Ni, Z. H., Ponomarenko, L. A., Nair, R. R., Yang, R., Anissimova, S., Grigorieva, I. V., Schedin, F., Blake, P., Shen, Z. X., Hill, E. H., Novoselov, K. S. & Geim, A. K. (2010). *Nano Lett.* **10**, 3868

Nomura, K. & MacDonald, A. H. (2006). *Phys. Rev. Lett.* **96**, 256602

Novikov, D. S. (2007). *Phys. Rev. B* **76**, 245435

Novoselov, K. S. (2011). *Rev. Mod. Phys.* **83**, 837

Novoselov, K. S., Geim, A. K., Morozov, S. V., Jiang, D., Katsnelson, M. I., Grigorieva, I. V., Dubonos, S. V. & Firsov, A. A. (2005a). *Nature* **438**, 197

Novoselov, K. S., Geim, A. K., Morozov, S. V., Jiang, D., Zhang, Y., Dubonos, S. V., Grigorieva, I. V. & Firsov, A. A. (2004). *Science* **306**, 666

Novoselov, K. S., Jiang, D., Schedin, F., Booth, T. J., Khotkevich, V. V., Morozov, S. V. & Geim, A. K. (2005b). *Proc. Natl Acad. Sci. USA* **102**, 10451

Novoselov, K. S., Jiang, Z., Zhang, Y., Morozov, S. V., Stormer, N. L., Zeitler, U., Maan, J. C., Boebinger, G. S., Kim, P. & Geim, A. K. (2007). *Science* **315**, 1379

Novoselov, K. S., McCann, E., Morozov, S. V., Falko, V. I., Katsnelson, M. I., Zeitler, U., Jiang, D., Schedin, F. & Geim, A. K. (2006). *Nature Phys.* **2**, 177

Ochoa, H., Castro, E. V., Katsnelson, M. I. & Guinea, F. (2011). *Phys. Rev. B* **83**, 235416

Olariu, S. & Popescu, I. (1985). *Rev. Mod. Phys.* **57**, 339

Ono, S. & Sugihara, K. (1966). *J. Phys. Soc. Japan* **21**, 861

Oostinga, K. B., Heersche, H. B., Liu, X., Morpurgo, A. F. & Vandersypen, L. M. K. (2008). *Nature Mater.* **7**, 151

Ostrovsky, P. M., Gornyi, I. V. & Mirlin, A. D. (2006). *Phys. Rev. B* **74**, 235443

Ostrovsky, P. M., Gornyi, I. V. & Mirlin, A. D. (2008). *Phys. Rev. B* **77**, 195430

Ostrovsky, P. M., Titov, M., Bera, S., Gornyi, I. V. & Mirlin, A. D. (2010). *Phys. Rev. Lett.* **105**, 266803

Park, C.-H., Giustino, F., Cohen, M. L. & Louie, S. G. (2008). *Nano Lett.* **8**, 4229

Partoens, B. & Peeters, F. M. (2006). *Phys. Rev. B* **74**, 075404

Patashinskii, A. Z. & Pokrovskii, V. L. (1979). *Fluctuation Theory of Phase Transitions*. New York: Pergamon

Pauling, L. (1960). *The Nature of the Chemical Bond*. Ithaca, NY: Cornell University Press

Peierls, R.E. (1933). *Z. Phys.* **80**, 763

Peierls, R. E. (1934). *Helv. Phys. Acta* **7**, 81

Peierls, R. E. (1935). *Ann. Inst. Henri Poincaré* **5**, 177

Peliti, L. & Leibler, S. (1985). *Phys. Rev. Lett.* **54**, 1690

Pellegrino, F. M. D., Angilella, G. G. N. & Pucci, R. (2010). *Phys. Rev. B* **81**, 035411
Pendry, J. B. (2004). *Contemp. Phys.* **45**, 191
Peng, L. X., Liew, K. M. & Kitipornchai, S. (2007). *Int. J. Mech. Science* **49**, 364
Pereira, J. M., Peeters, F. M. & Vasilopoulos, P. (2007) *Phys. Rev. B* **76**, 115419
Pereira, V. M. & Castro Neto, A. H. (2009). *Phys. Rev. Lett.* **103**, 046801
Pereira, V. M., Castro Neto, A. H. & Peres, N. M. R. (2009). *Phys. Rev. B* **80**, 045401
Pereira, V. M., Guinea, F., Lopes dos Santos, J. M. B., Peres, N. M. R. & Castro Neto, A. H. (2006). *Phys. Rev. Lett.* **96**, 036801
Pereira, V. M., Nilsson, J. & Castro Neto, A. H. (2007). *Phys. Rev. Lett.* **99**, 166802
Perenboom, J. A. A. J., Wyder, P. & Meier, F. (1981). *Phys. Rep.* **78**, 173
Peres, N. M. R. (2010). *Rev. Mod. Phys.* **82**, 2673
Peres, N. M. R., Castro Neto, A. H. & Guinea, F. (2006). *Phys. Rev. B* **73**, 195411
Peres, N. M. R., Guinea, F. & Castro Neto, A. H. (2006). *Phys. Rev. B* **73**, 125411
Platzman, P. M. & Wolf, P. A. (1973). *Waves and Interactions in Solid State Plasmas.* New York: Academic Press
Polini, M., Tomadin, A., Asgari, R. & MacDonald, A. H. (2008). *Phys. Rev. B* **78**, 115426
Pomeranchuk, I. & Smorodinsky, Y. (1945). *J. Phys. (USSR)* **9**, 97
Ponomarenko, L. A., Schedin, F., Katsnelson, M. I., Yang, R., Hill, E. W., Novoselov, K. S. & Geim, A. K. (2008). *Science* **320**, 356
Ponomarenko, L. A., Yang, R., Gorbachev, R. V., Blake, P., Mayorov, A. S., Novoselov, K. S., Katsnelson, M. I. & Geim, A. K. (2010). *Phys. Rev. Lett.* **105**, 136801
Ponomarenko, L. A., Yang, R., Mohiuddin, T. M., Katsnelson, M. I., Novoselov, K. S., Morozov, S. V., Zhukov, A. A., Schedin, F., Hill, E. W. & Geim, A. K. (2009). *Phys. Rev. Lett.* **102**, 206603
Prada, E., San-Jose, P., Wunsch, B. & Guinea, F. (2007). *Phys. Rev. B* **75**, 113407
Prange, R. E. & Girvin, S. M. (eds.) (1987). *The Quantum Hall Effect.* Berlin: Springer
Principi, A., Polini, M. & Vignale, G. (2009). *Phys. Rev. B* **80**, 075418
Principi, A., Polini, M., Vignale, G. & Katsnelson, M. I. (2010). *Phys. Rev. Lett.* **104**, 225503
Prodan, E. (2009). *J. Math. Phys.* **50**, 083517
Pyatkovskiy, P. K. (2009). *J. Phys.: Condens. Matter* **21**, 025506
Qi, X. & Zhang, S. (2010). *Phys. Today*, January, p. 33
Qi, X. & Zhang, S. (2011). *Rev. Mod. Phys.* **83**, 1057
Radzig, A. A. & Smirnov, B. M. (1985). *Reference Data on Atoms, Molecules and Ions.* Berlin: Springer
Raman, C. V. (1928). *Nature* **121**, 619
Raman, C. V. & Krishnan, K. S. (1928). *Nature* **121**, 501
Rammer, J. & Smith, H. (1986). *Rev. Mod. Phys.* **58**, 323
Rashba, E. I. (2009). *Phys. Rev. B* **79**, 161409
Recher, P., Trauzettel, B., Rycerz, A., Blanter, M. Ya., Beenakker, C. W. J. & Morpurgo, A. F. (2007). *Phys. Rev. B* **76**, 235404
Reich, S., Maultzsch, J., Thomsen, C. & Ordejón, P. (2002). *Phys. Rev. B* **66**, 035412
Robinson, J. R., Schomerus, H., Oroszlány, L. & Falko, V. I. (2008). *Phys. Rev. Lett.* **101**, 196803
Roldán, R., Fasolino, A., Zakharchenko, K. V. & Katsnelson, M. I. (2011). *Phys. Rev. B* **83**, 174104
Rossi, E. & Das Sarma, S. (2008). *Phys. Rev. Lett.* **101**, 166803
Ruelle, D. (1999). *Statistical Mechanics: Rigorous Results.* London: Imperial College Press & Singapore: World Scientific

Rusin, T. M. & Zawadski, W. (2008). *Phys. Rev. B* **78**, 125419

Rusin, T. M. & Zawadski, W. (2009). *Phys. Rev. B* **80**, 045416

Russo, S., Oostinga, J. B., Wehenkel, D., Heersche, H. B., Sobhani, S. S., Vandersypen, L. M. K. & Morpurgo, A. F. (2008). *Phys. Rev. B* **77**, 085413

Rycerz, A. (2010). *Phys. Rev. B* **81**, 121404

Rycerz, A., Recher, P. & Wimmer, M. (2009). *Phys. Rev. B* **80**, 125417

Ryu, S., Mudry, C., Furusaki, A. & Ludwig, A. W. W. (2007). *Phys. Rev. B* **75**, 205344

Sachs, B., Wehling, T. O., Katsnelson, M. I. & Lichtenstein, A. I. (2011). *Phys. Rev. B* **84**, 195444

Sadowski, M. L., Martinez, G., Potemski, M., Berger, C. & de Heer, W. A. (2006). *Phys. Rev. Lett.* **97**, 266405

Safran, S. A. & DiSalvo, F. J. (1979). *Phys. Rev. B* **20**, 4889

Saha, K., Paul, I. & Sengupta, K. (2010). *Phys. Rev. B* **81**, 165446

San-José, P., González, J. & Guinea, F. (2011). *Phys. Rev. Lett.* **106**, 045502

Sasaki, K., Kawazoe, Y. & Saito, R. (2005). *Prog. Theor. Phys.* **113**, 463

Schakel, A. M. J. (1991). *Phys. Rev. D* **43**, 1428

Schapere, A. & Wilczek, F. (eds.) (1989). *Geometric Phases in Physics*. Singapore: World Scientific

Schedin, F., Geim, A. K., Morozov, S. V., Hill, E. W., Blake, P., Katsnelson, M. I. & Novoselov, K. S. (2007). *Nature Mater.* **6**, 652

Schilfgaarde, M. & Katsnelson, M. I. (2011). *Phys. Rev. B* **83**, 081409

Schoenberg, D. (1984). *Magnetic Oscillations in Metals*. Cambridge: Cambridge University Press

Schrödinger, E. (1930). *Sitz. Preuß. Akad. Wiss. Phys.-Math.* **24**, 418

Schubin, S. & Wonsowski, S. (1934). *Proc. R. Soc. (London) A* **145**, 159

Schuessler, A., Ostrovsky, P. M., Gornyi, I. V. & Mirlin, A. D. (2009). *Phys. Rev. B* **79**, 075405

Schulman, L. S. (1981). *Techniques and Applications of Path Integration*. New York: Wiley

Sepioni, M., Nair, R. R., Rablen, S., Narayanan, J., Tuna, F., Winpenny, R., Geim, A. K. & Grigorieva, I. V. (2010). *Phys. Rev. Lett.* **105**, 207205

Sharapov, S. G., Gusynin, V. P. & Beck, H. (2004). *Phys. Rev. B* **69**, 075104

Sharma, M. P., Johnson, L. G. & McClure, J. W. (1974). *Phys. Rev. B* **9**, 2467

Sharon, E., Roman, B., Marder, M., Shin, G.-S. & Swinney, H. L. (2002). *Nature* **419**, 579

Sheehy, D. E. & Schmalian, J. (2009). *Phys. Rev. B* **80**, 193411

Shklovskii, B. I. & Efros, A. L. (1984). *Electronic Properties of Doped Semiconductors*. Berlin: Springer

Shon, N. H. & Ando, T. (1998). *J. Phys. Soc. Japan* **67**, 2421

Shytov, A. V., Abanin, D. A. & Levitov, L. S. (2009). *Phys. Rev. Lett.* **103**, 016806

Shytov, A. V., Gu, N. & Levitov, L. S. (2007). arXiv:0708.3081 (unpublished)

Shytov, A. V., Katsnelson, M. I. & Levitov, L. S. (2007a). *Phys. Rev. Lett.* **99**, 236801

Shytov, A. V., Katsnelson, M. I. & Levitov, L. S. (2007b). *Phys. Rev. Lett.* **99**, 246802

Shytov, A., Rudner, M., Gu, N., Katsnelson, M. & Levitov, L. (2009). *Solid State Commun.* **149**, 1087

Shytov, A. V., Rudner, M. S. & Levitov, L. S. (2008). *Phys. Rev. Lett.* **101**, 156804

Simon, B. (1983). *Phys. Rev. Lett.* **51**, 2167

Slonczewski, J. S. & Weiss, P. R. (1958). *Phys. Rev.* **109**, 272

Snyman, I. & Beenakker, C. W. J. (2007). *Phys. Rev. B* **75**, 045322

Son, Y.-W., Cohen, M. L. & Louie, S. (2006a). *Nature* **444**, 347

Son, Y.-W., Cohen, M. L. & Louie, S. (2006b). *Phys. Rev. Lett.* **97**, 216803

Stampfer, C., Schurtenberger, E., Molitor, F., Güttinger, J., Ihn, T. & Ensslin, K. (2008). *Nano Lett.* **8**, 2378

Stander, N., Huard, B. & Goldhaber-Gordon, D. (2009). *Phys. Rev. Lett.* **102**, 026807

Stauber, T., Peres, N. M. R. & Geim, A. K. (2008). *Phys. Rev. B* **78**, 085432

Stauber, T., Peres, N. M. R. & Guinea, F. (2007). *Phys. Rev. B* **76**, 205423

Stauber, T. & Schliemann, J. (2009). *New J. Phys.* **11**, 115003

Stauber, T., Schliemann, J. & Peres, N. M. R. (2010). *Phys. Rev. B* **81**, 085409

Stern, F. (1967). *Phys. Rev. Lett.* **18**, 546

Steward, E. G., Cook, B. P. & Kellert, E. A. (1960). *Nature* **187**, 1015

Stöckmann, H.-J. (2000). *Quantum Chaos: An Introduction.* Cambridge: Cambridge University Press

Stolyarova, E., Rim, K. T., Ryu, S., Maultzsch, J., Kim, P., Brus, L. E., Heinz, T. F., Hybertsen, M. S. & Flynn, G. W. (2007). *Proc. Natl Acad. Sci. USA* **104**, 9209

Stoner, E. C. (1936). *Proc. R. Soc. (London) A* **154**, 656

Su, R.-K., Siu, G. G. & Chou, X. (1993). *J. Phys. A* **26**, 1001

Sugihara, K. (1983). *Phys. Rev. B* **28**, 2157

Suzuura, H. & Ando, T. (2002). *Phys. Rev. B* **65**, 235412

Taimanov, I. A. (2006). *Russ. Math. Surveys* **61**, 79

Tao, C., Jiao, L., Yazyev, O. V., Chen, Y.-C., Feng, J., Zhang, X., Capaz, R. B., Tour, J. M., Zettl, A., Louie, S. G., Dai, H. & Crommie, M. F. (2011). *Nature Phys.* **7**, 616

Teissier, R., Finley, J. J., Skolnick, M. S., Cockburn, J. W., Pelouard, J.-L., Grey, R., Hill, G., Pate, M.-A. & Planel, R. (1996). *Phys. Rev. B* **54**, 8329

Tenjinbayashi, Y., Igarashi, H. & Fujiwara, T. (2007). *Ann. Phys.* **322**, 460

Tersoff, J. & Hamann, D. R. (1985). *Phys. Rev. B* **31**, 805

Thomsen, C. & Reich, S. (2000). *Phys. Rev. Lett.* **85**, 5214

Thouless, D. J., Kohmoto, M., Nightingale, M. P. & den Nijs, M. (1982). *Phys. Rev. Lett.* **49**, 405

Tian, W. & Datta, S. (1994). *Phys. Rev. B* **49**, 5097

Tikhonenko, F. V., Horsell, D. W., Gorbachev, R. V. & Savchenko, A. K. (2008). *Phys. Rev. Lett.* **100**, 056802

Tikhonenko, F. V., Kozikov, A. A., Savchenko, A. K. & Gorbachev, R. V. (2009). *Phys. Rev. Lett.* **103**, 226801

Timoshenko, S. P. & Woinowsky-Krieger, S. (1959). *Theory of Plates and Shells.* New York: McGraw-Hill

Titov, M., Ostrovsky, P. M., Gornyi, I. V., Schuessler, A. & Mirlin, A. D. (2010). *Phys. Rev. Lett.* **104**, 076802

Tombros, N., Jozsa, C., Popinciuc, M., Jonkman, H. T. & van Wees, B. J. (2007). *Nature* **448**, 571

Tombros, N., Tanabe, S., Veligura, A., Jozsa, C., Popinciuc, M., Jonkman, H. T. & van Wees, B. J. (2008). *Phys. Rev. Lett.* **101**, 046601

Trushin, M., Kailasvuori, J., Schliemann, J. & MacDonald, A. H. (2010). *Phys. Rev. B* **82**, 155308

Tsidilkovskii, I. M. (1982). *Band Structure of Semiconductors.* Oxford: Pergamon

Tsidilkovskii, I. M. (1996). *Electron Spectrum of Gapless Semiconductors.* Berlin: Springer

Tudorovskiy, T. & Mikhailov, S. A. (2010). *Phys. Rev. B* **82**, 073411

Tudorovskiy, T., Reijnders, K. J. A. & Katsnelson, M. I. (2012). *Phys Scr.* T146,014010.

Tuinstra, F. & Koenig, J. L. (1970). *J. Chem. Phys.* **53**, 1126

Tworzydlo, J., Trouzettel, B., Titov, M., Rycerz, A. & Beenakker, C. W. J. (2006). *Phys. Rev. Lett.* **96**, 246802

Uchoa, B., Yang, L., Tsai, S.-W., Peres, N. M. R. & Castro Neto, A. H. (2009). *Phys. Rev. Lett.* **103**, 206804

Ugeda, M. M., Brihuega, I., Guinea, F. & Gómez-Rodriguez, J. M. (2010). *Phys. Rev. Lett.* **104**, 096804

Ukraintsev, V. A. (1996). *Phys. Rev. B* **53**, 11176

Veselago, V. S. (1968). *Sov. Phys. Usp.* **10**, 509

Vlasov, K. B. & Ishmukhametov, B. Kh. (1964). *Zh. Éksp. Teor. Fiz.* **46**, 201

Vonsovsky, S. V. (1946). *Zh. Éksp. Teor. Fiz.* **16**, 981

Vonsovsky, S. V. (1974). *Magnetism.* New York: Wiley

Vonsovsky, S. V. & Katsnelson, M. I. (1989). *Quantum Solid State Physics.* Berlin: Springer

Vonsovsky, S. V. & Svirsky, M. S. (1993). *Usp. Fiz. Nauk* **163**, no. 5, 115

Vonsovsky, S. V. & Turov, E. A. (1953). *Zh. Éksp. Teor. Fiz.* **24**, 419

Vozmediano, M. A. H., Katsnelson, M. I. & Guinea, F. (2010). *Phys. Rep.* **496**, 109

Wagner, M. (1991). *Phys. Rev. B* **44**, 6104

Wallace, P. R. (1947). *Phys. Rev.* **71**, 622

Wang, X., Ouyang, Y., Li, X., Wang, H., Guo, J. & Dai, H. (2008). *Phys. Rev. Lett.* **100**, 206803

Wassmann, T., Seitsonen, A. P., Saitta, M., Lazzeri, M. & Mauri, F. (2008). *Phys. Rev. Lett.* **101**, 096402

Wehling, T. O., Balatsky, A. V., Katsnelson, M. I., Lichtenstein, A. I., Scharnberg, K. & Wiesendanger, R. (2007). *Phys. Rev. B* **75**, 125425

Wehling, T. O., Balatsky, A. V., Tsvelik, A. M., Katsnelson, M. I. & Lichtenstein, A. I. (2008a). *Europhys. Lett.* **84**, 17003

Wehling, T. O., Dahal, H. P., Lichtenstein, A. I., Katsnelson, M. I., Manoharan, H. C. & Balatsky, A. V. (2010b). *Phys. Rev. B* **81**, 085413

Wehling, T. O., Katsnelson, M. I. & Lichtenstein, A. I. (2009a). *Chem. Phys. Lett.* **476**, 125

Wehling, T. O., Katsnelson, M. I. & Lichtenstein, A. I. (2009b). *Phys. Rev. B* **80**, 085428

Wehling, T. O., Novoselov, K. S., Morozov, S. V., Vdovin, E. E., Katsnelson, M. I., Geim, A. K. & Lichtenstein, A. I. (2008b). *Nano Lett.* **8**, 173

Wehling, T. O., Yuan, S., Lichtenstein, A. I., Geim, A. K. & Katsnelson, M. I. (2010a). *Phys. Rev. Lett.* **105**, 056802

Whittaker, E. T. & Watson, G. N. (1927). *A Course of Modern Analysis.* Cambridge: Cambridge University Press

Wilson, A. H. (1965). *Theory of Metals.* Cambridge: Cambridge University Press

Wilson, K. G. & Kogut, J. (1974). *Phys. Rep.* **12**, 75

Wimmer, M., Adagideli, I., Berber, S., Tománek, D. & Richter, K. (2008). *Phys. Rev. Lett.* **100**, 177207

Wimmer, M., Akhmerov, A. R. & Guinea, F. (2010). *Phys. Rev. B* **82**, 045409

Witowski, A. M., Orlita, M., Stepniewski, R., Wysmolek, A., Baranowski, J. M., Stupinski, W., Faugeras, C., Martinez, G. & Potemski, M. (2010). *Phys. Rev. B* **82**, 165305

Wunsch, B., Stauber, T., Sols, F. & Guinea, F. (2006). *New J. Phys.* **8**, 318

Wurm, J., Rycerz, A., Adagideli, I., Wimmer, M., Richter, K. & Baranger, H. U. (2009). *Phys. Rev. Lett.* **102**, 056806

Wurm, J., Wimmer, M., Baranger, H. U. & Richter, K. (2010). *Semicond. Sci. Technol.* **25**, 034003

Xing, X., Mukhopadhyay, R., Lubensky, T. C. & Radzihovsky, L. (2003). *Phys. Rev. E* **68**, 021108

Yacoby, A. & Imry, Y. (1990). *Phys. Rev. B* **41**, 5341

Yang, L., Deslippe, J., Park, C.-H., Cohen, M. L. & Louie, S. G. (2009). *Phys. Rev. Lett.* **103**, 186802

Yang, X. & Nayak, C. (2002). *Phys. Rev. B* **65**, 064523

Yao, Y., Ye, F., Qi, X.-L., Zhang, S. C. & Fang, Z. (2007). *Phys. Rev. B* **75**, 041401

Yazyev, O. V. (2010). *Rep. Prog. Phys.* **73**, 056501

Yazyev, O. V. & Helm, L. (2007). *Phys. Rev. B* **75**, 125408

Yazyev, O. V. & Katsnelson, M. I. (2008). *Phys. Rev. Lett.* **100**, 047209

Yennie, D. R., Ravenhall, D. G. & Wilson, R. N. (1954). *Phys. Rev.* **95**, 500

Yoon, D., Son, Y.-W. & Cheong, H. (2011). *Nano Lett.* **11**, 3227

Yosida, K. (1996). *Theory of Magnetism.* Berlin: Springer

Young, A. F. & Kim, P. (2009). *Nature Phys.* **5**, 222

Yuan, S., De Raedt, H. & Katsnelson, M. I. (2010a). *Phys. Rev. B* **82**, 115448

Yuan, S., De Raedt, H. & Katsnelson, M. I. (2010b). *Phys. Rev. B* **82**, 235409

Yuan, S. Roldán, R. & Katsnelson, M. I. (2011). *Phys. Rev. B* **84**, 035439

Zak, J. (1989). *Phys. Rev. Lett.* **62**, 2747

Zakharchenko, K. V., Fasolino, A., Los, J. H. & Katsnelson, M. I. (2011). *J. Phys.: Condens. Matter* **23**, 202202

Zakharchenko, K. V., Katsnelson, M. I. & Fasolino, A. (2009). *Phys. Rev. Lett.* **102**, 046808

Zakharchenko, K. V., Los, J. H., Katsnelson, M. I. & Fasolino, A. (2010a). *Phys. Rev. B* **81**, 235439

Zakharchenko, K. V., Roldán, R., Fasolino, A. & Katsnelson, M. I. (2010b). *Phys. Rev. B* **82**, 125435

Zarea, M. & Sandler, N. (2009). *Phys. Rev. B* **79**, 165442

Zel'dovich, Y. B. & Popov, V. S. (1972). *Sov. Phys. Usp.* **14**, 673

Zener, C. (1951a). *Phys. Rev.* **81**, 440

Zener, C. (1951b). *Phys. Rev.* **82**, 403

Zener, C. (1951c). *Phys. Rev.* **83**, 299

Zhang, H. G., Hu, H., Pan, Y., Mao, J. H., Gao, M., Guo, H. M., Du, S. X., Greber, T. & Gao, H.-J. (2010). *J. Phys.: Condens. Matter* **22**, 302001

Zhang, Y., Jiang, Z., Small, J. P., Purewal, M. S., Tan, Y.-W., Fazlollahi, M., Chudow, J. D., Jaszczak, J. A., Stormer, H. L. & Kim, P. (2006). *Phys. Rev. Lett.* **96**, 136806

Zhang, Y., Tan, Y.-W., Stormer, H. L. & Kim, P. (2005). *Nature* **438**, 201

Ziegler, K. (1998). *Phys. Rev. Lett.* **80**, 3113

Ziman, J. M. (2001). *Electrons and Phonons. The Theory of Transport Phenomena in Solids.* Oxford: Oxford University Press

Zubarev, D. N. (1974). *Nonequilibrium Statistical Thermodynamics.* New York: Consultants Bureau

Žutić, I., Fabian, J. & Das Sarma, S. (2004). *Rev. Mod. Phys.* **76**, 323

Index